

THESES

6

2008

v.1

745

565

745

LIBRARY
Michigan State
University

This is to certify that the
dissertation entitled

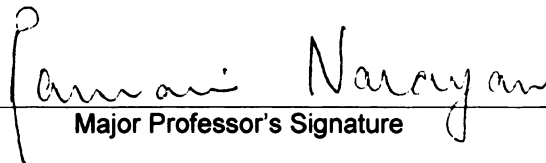
DESIGN AND ENGINEERING OF NOVEL STARCH-BASED
FOAM AND FILM PRODUCTS

presented by

YOGARAJ UMESH NABAR

has been accepted towards fulfillment
of the requirements for the

Ph.D. degree in CHEMICAL ENGINEERING
AND MATERIAL SCIENCE


Major Professor's Signature

December 4th, 2004

Date

PLACE IN RETURN BOX to remove this checkout from your record.
TO AVOID FINES return on or before date due.
MAY BE RECALLED with earlier due date if requested.

DATE DUE	DATE DUE	DATE DUE
APR 28 2009		

DESIGN AND

**DESIGN AND ENGINEERING OF NOVEL STARCH – BASED FOAM AND FILM
PRODUCTS**

VOLUME I

By

Yogaraj Umesh Nabar

A DISSERTATION

**Submitted to
Michigan State University
In partial fulfillment of the requirements
for the degree of**

DOCTOR OF PHILOSOPHY

Department of Chemical Engineering and Material Science

2004

Novel hydroxy

scale (~ 11-12

using water (as

(PHAE) as a fat

toughness, cell

optimum temper

density of the cy

> 92%. The dy

necessary for th

formulation deve

destabilizing var

the dynamics of

viscosity model

annular die, whic

twin-screw food

foam sheets was

insulation proper

characteristics. A

provided decent e

ABSTRACT

DESIGN AND ENGINEERING OF NOVEL STARCH – BASED FOAM AND FILM PRODUCTS

By

Yogaraj Umesh Nabar

Novel hydroxypropylated high amylose corn starch foams were produced on a small scale (~ 11-12 kg/hr) Werner Pfleiderer ZSK - 30 Twin Screw Extrusion (TSE) process using water (as a plasticizer as well as a blowing agent) and poly(hydroxyamino ether) (PHAE) as a functional aid. PHAE was successful in imparting mechanical strength and toughness, cell integrity, weather and water resistance to the foam structure. The optimum temperature, blowing agent content, and PHAE content were determined. The density of the cylindrical foam extrudates obtained was 22-25 kg/m³, with a resiliency of > 92%. The dynamics of the starch foam extrusion process were studied, which was necessary for the steady state operation of the starch foam process for the optimized formulation developed above. The moisture content and screw speed seem to be the most destabilizing variables since they induce rapid responses in the process variables. Once the dynamics of the starch-based foam process were investigated, a Power-law shear viscosity model developed using a dual-orifice die was further used in the design of an annular die, which was then successfully employed on an industrial scale (410-420 kg/hr) twin-screw food extruder, Wenger-80, to manufacture foam sheets. The density of the foam sheets was 27-30 kg/m³. The extruded starch foam sheets provided excellent insulation properties in terms of its R-values obtained suggested better insulation characteristics. Also, the dynamic cushioning data reveals that the starch foam sheets provided decent cushioning or shock absorption properties. Different models involving

finite difference
properties of t
simplified, sim
had been drast
greatly increas
biodegradable
new starch-bas
better) to those
poor compatibi
mechanical prop
and PBAT allow
and improved th
were carried ou
copolymer. TPS
maleate (MTPS
obtain PBAT-g
PBAT-g-MTPS
High performa
elongations (1-8
mechanical pro
These resins w
foams with de
cases.

finite difference and finite element techniques were employed to predict the cushioning properties of the starch-based foam sheets produced. The cushion design was greatly simplified, since the database required as input information on the cushion performance had been drastically reduced, while its applicability to various drop conditions had been greatly increased. Due to the discontinuation of the PHAE production, a new biodegradable aliphatic-aromatic co-polyester PBAT was used in an attempt to develop new starch-based foam formulations possessing properties that were equivalent (if not better) to those obtained using the starch-PHAE formulation. High levels of starch and its poor compatibility with the biodegradable polyesters lead to inferior physical and mechanical properties. The use of the maleated PBAT as a compatibilizer between starch and PBAT allowed the reduction of the density of resulting starch foams to $\sim 21 \text{ kg/m}^3$, and improved the resilience from 84% to as high as 95%. Transesterification reactions were carried out between thermoplastic starch (TPS) and PBAT to obtain PBAT-g-TPS copolymer. TPS was also reacted with maleic anhydride to obtain a thermoplastic starch maleate (MTPS) with a lower shear viscosity. This MTPS was also reacted with PBAT to obtain PBAT-g-MTPS copolymers. Nano-scale reinforcing clay was introduced in the PBAT-g-MTPS copolymer to improve its mechanical, thermal and barrier properties. High performance formulations having superior tensile strength (5000 psi) and break elongations ($>800\%$) were obtained. Compatibilized PBAT-talc blends having exemplary mechanical properties were also developed using transesterification catalytic systems. These resins when employed as functional aids in the starch-based foam process provided foams with densities as low as 17.5 kg/m^3 , and spring indices as high as 97% in certain cases.

**COPYRIGHT BY
YOGARAJ UMESH NABAR
2004**

Dedicated to

my parents, my sister, and my wife.

I would like

motivation. I

me attain m

advice and s

Dr. Gregory

Dr. Dan Gra

acknowledge

Ph.D. My co

Guoren Chen

This work w

my parents.

their prayers.

thesis. She h

work. never

to many ind

endeavor of

would like to

Goradia. Sac

Parulekar. Ve

me with supp

few names. th

like to extend

ACKNOWLEDGEMENTS

I would like to thank Dr. Ramani Narayan; my thesis advisor, guide and mentor. His motivation, resolute support and exemplary guidance have been instrumental in helping me attain my academic and professional goals. I would also like to acknowledge the advice and support offered by my Ph.D. committee: Dr. Carl Lira, Dr. Bruce Dale, and Dr. Gregory Baker during the course of my Ph.D. A special word of thanks should go to Dr. Dan Graiver and Ken Farminer, for his valuable inputs and encouragement. I wish to acknowledge the guidance and direction offered by Dr. Jean-Marie Raquez towards my Ph.D. My colleagues: Phuong Tran, Sunder Balakrishnan, Chisa Brookes, Laura Fisher, Guoren Cheng, Madhu Srinivasan, Tylisha Baber deserve special mention.

This work would not have been possible without the help and support from my family: my parents, my sister Mallika, and my wife Kanchan. This work was made possible by their prayers, support, motivation, and belief. Kanchan has been instrumental in my entire thesis. She has been a great encourager, provided tremendous support during my Ph.D. work, never complained about my long hours in the lab. My heartfelt gratitude goes out to many individuals who have influenced me and the choices I have made in this endeavor of mine: to name a few would be unfair; to name none would be penitent. I would like to thank Sharad Kumar, Adwait Telang, Priya Mani, Bhaskar Patham, Amit Goradia, Sachin Vaidya, Lavanya Parthasarthy, Prerna Sonthalia, Shirish Karande, Yash Parulekar, Venkata Giri Kolli, Kiran Misra, and Freddy Kharoliwalla who have provided me with support and help during the last four years. Although I have mentioned only a few names, there are many more people who have helped me in this venture and I would like to extend my appreciation to all the other people who I may have left out.

LIST OF T

LIST OF FI

TABLE OF

Chapter 1:

1.1 R

1.2 Pr

1.3 Sp

1.3.1

1.3.2

1.3.3

1.4 O

1.5 R

Chapter 2:

2.1 A

2.2 B

2.2.1

2.2.2

2.2.3

2.3 E

2.3.1

2.3.2

2.3.3

2.3.4

2.3.5

2.4 R

2.4.1

2.4.2

2.4.3

2.4.4

2.4.5

2.4.6

2.4.7

2.4.8

2.4.9

2.5 C

2.6 R

TABLE OF CONTENTS

LIST OF TABLES	xiii
LIST OF FIGURES	xviii
TABLE OF ABBREVIATIONS	xvii
Chapter 1: INTRODUCTION	1
1.1 Rationale	1
1.2 Proposed Goals	5
1.3 Specific Objectives	6
1.3.1 Goal.....	6
1.3.2 Problem Statement.....	6
1.3.3 Objectives of this research.....	7
1.4 Organization of the Thesis.....	11
1.5 References.....	13
Chapter 2: STARCH-PHAE FOAM TECHNOLOGY	16
2.1 Abstract.....	16
2.2 Background.....	17
2.2.1 Gelatinization.....	21
2.2.2 Destructurized Starch.....	22
2.2.3 Types of Starches and Modifications.....	23
2.3 Experimental	25
2.3.1 Materials	25
2.3.2 Experimental Setup.....	29
2.3.3 Procedure	29
2.3.4 Characterization and Analysis	31
2.3.5 Screw Configuration	33
2.4 Results and Discussion	40
2.4.1 Type of Corn Starch.....	40
2.4.2 Effect of the amount of water on the Expansion Ratio (ER).....	42
2.4.3 Effect of the processing (melt) temperature on the Expansion Ratio (ER):	44
2.4.4 Effect of PHAE on ER.....	47
2.4.5 Effect of nucleating agent (talc) content on ER:.....	49
2.4.6 Effect of screw speed on the expansion ratio (ER).....	55
2.4.7 Compressive Strength and Resiliency	59
2.4.8 Moisture Sorption Analysis	59
2.4.9 Cell size/structure.....	61
2.5 Conclusion	64
2.6 References.....	65

**Chapter 3:
DEVELOP**

- 3.1 Abst
- 3.2 Intro
- 3.3 Expe
 - 3.3.1
 - 3.3.2
 - 3.3.3
 - 3.3.4
- 3.4 Resu
 - 3.4.1
 - 3.4.2
 - 3.4.3
 - 3.4.4
 - 3.4.5
 - 3.4.6
 - 3.4.7
- 3.5 Cono
- 3.6 Refe

**Chapter 4:
FOAM EX**

- 4.1 A
- 4.2 In
- 4.3 TI
- 4.4 E
 - 4.4.1
 - 4.4.2
 - 4.4.3
 - 4.4.4
- 4.5 R
 - 4.5.1 on 'K'
 - 4.5.2
- 4.6 S
 - 4.6.1
 - 4.6.2
 - 4.6.3
 - 4.6.4
 - 4.6.5
 - 4.6.6
- 4.7 C
- 4.8 R

**Chapter 5:
5.1 B**

Chapter 3: TRANSIENT MODELING OF STARCH FOAM PROCESS TO DEVELOP CONTROL STRATEGIES	67
3.1 Abstract.....	67
3.2 Introduction.....	68
3.3 Experimental Section.....	70
3.3.1 Experimental Design.....	70
3.3.2 Linearity.....	73
3.3.3 Dynamic (Transient) Responses	73
3.3.4 Multiple Input Tests.....	74
3.4 Results and Discussion	77
3.4.1 Step-Input Variations in the Starch Feed Rate.....	77
3.4.2 Step-Input Variations in the Screw Speed	80
3.4.3 Step-Input Variations in the Moisture Content (% MC).....	82
3.4.4 Step-Input Variations in the PHAE Content.....	84
3.4.5 Linear Domains.....	86
3.4.6 Dynamic Responses	89
3.4.7 Multiple Input Tests.....	95
3.5 Conclusion	109
3.6 References.....	111
Chapter 4: ANNULAR DIE DESIGN AND SCALE-UP OF THE STARCH-PHAE FOAM EXTRUSION PROCESS	113
4.1 Abstract.....	113
4.2 Introduction.....	114
4.3 Theory	119
4.4 Experimental Section.....	120
4.4.1 Materials	120
4.4.2 Experimental Setup.....	121
4.4.3 Bifurcated Die.....	123
4.4.4 Procedure	125
4.5 Results and Discussion	127
4.5.1 Effect of Moisture Content, Temperature, PHAE content and Screw Speed on 'K' and 'n':	127
4.5.2 Annular Die Design for Foam Sheet Extrusion	142
4.6 Scale – Up of the Starch-PHAE Foam Extrusion Process.....	148
4.6.1 Feeding.....	148
4.6.2 Screw Design	150
4.6.3 Final conical screws.....	153
4.6.4 Thermal Resistance (R-value).....	162
4.6.5 Temperature Hold Time Test.....	163
4.6.6 Dynamic Cushion Curve testing	166
4.7 Conclusion	171
4.8 References.....	173
Chapter 5: PREDICTION OF CUSHION CURVES.....	176
5.1 Background.....	176

5.2 Meth
Curves.....
5.2.1
5.2.2
5.2.3
5.2.4
5.2.5
5.2.6
Differenc
5.2.7
5.2.8
5.2.9
5.2.10
5.2.11
5.3 Meth
5.3.1
5.3.2
5.4 Conc
5.5 Refer

**Chapter 6: PH
OF STARCH
POLYMERS.**

6.1 Abst
6.2 Intro
6.3 Expe
6.3.1
6.3.2
6.3.3
6.3.4
6.4 Resu
6.4.1
starch foa
6.4.2
6.4.3
of the star
6.5 Conc
6.6 Refer

**Chapter 7: EF
BETWEEN ST**

7.1 Abstr
7.2 Intro
7.2.1
7.2.2
7.3 Exper

5.2	Method I: Governing Differential Equations for the Prediction of Cushion Curves	181
5.2.1	Determination of material yield point stress, σ_y :	186
5.2.2	The Yield Pressure, σ :	189
5.2.3	The Total Cell Wall Surface Area, S:	191
5.2.4	The Convection Heat Transfer Coefficient, H:	191
5.2.5	The Total Air Mass, m:	193
5.2.6	Solving the Governing Differential Equations using the Forward Finite Difference Method:	195
5.2.7	The Polytropic Process	207
5.2.8	Force vs. Compression Results	211
5.2.9	The Finite Element Method (FEM):	214
5.2.10	The Finite Element Model:	215
5.2.11	Finite Element Program and Input:	217
5.3	Method II: The Dynamic Stress-Strain Curve	220
5.3.1	Analysis	220
5.3.2	Application	225
5.4	Conclusions	230
5.5	References	233

Chapter 6: PHYSICO – MECHANICAL AND HYDROPHOBIC PROPERTIES OF STARCH FOAMS EXTRUDED WITH DIFFERENT BIODEGRADABLE POLYMERS

		235
6.1	Abstract	235
6.2	Introduction	236
6.3	Experimental	239
6.3.1	Materials	239
6.3.2	Experimental Setup	242
6.3.3	Procedure	244
6.3.4	Characterization	245
6.4	Results and Discussion	247
6.4.1	Effect of Functional Aids on the Density and Expansion Ratio (ER) of the starch foams	247
6.4.2	Compressive Strength and Resiliency	257
6.4.3	Effect of Functional Aids on the Weight Gain and Dimensional Stability of the starch foams on Moisture Sorption	259
6.5	Conclusion	266
6.6	References	268

Chapter 7: EFFECT OF MALEATED PBAT AS A COMPATIBILIZER BETWEEN STARCH AND PBAT

		270
7.1	Abstract	270
7.2	Introduction	271
7.2.1	Incompatible Blends	271
7.2.2	Compatibilization Theory	273
7.3	Experimental Section	276

- 7.3.1
- 7.3.2
- 7.3.3
- 7.3.4
- 7.4 Res
- 7.4.1
- 7.4.2
- 7.4.3
- 7.4.4
- 7.4.5
- 7.4.6
- 7.4.7
- 7.5 Con
- 7.6 Refe

**Chapter 8: EL
COMPATIBI**

- 8.1 Abst
- 8.2 Intro
- 8.3 Expe
- 8.3.1
- 8.3.2
- 8.3.3
- 8.4 Resu
- 8.4.1
- 8.4.2
- 8.4.3
- 8.4.4
- 8.4.5
- 8.4.6
- 8.4.7
- 8.4.8
- 8.4.9
- 8.4.10
- 8.5 Conc
- 8.6 Refer

Chapter 9: RE

- 9.1 Intro
- 9.1.1
- 9.1.2
- 9.1.3
- 9.1.4

7.3.1	Materials	276
7.3.2	Experimental Setup.....	277
7.3.3	Procedure	278
7.3.4	Characterization and Analyses.....	280
7.4	Results and Discussion	285
7.4.1	Effect of MA and the Free Radical Initiator on the Properties of MA-g-PBAT	285
7.4.2	TGA	294
7.4.3	DSC.....	294
7.4.4	Density, Expansion Ratio (ER) and Specific length (SL) of Starch foams ..	297
7.4.5	Compressive Strength and Resiliency	300
7.4.6	Moisture Sorption Analysis	304
7.4.7	Wide Angle X-Ray Scattering	306
7.5	Conclusion	308
7.6	References.....	309

Chapter 8: EFFECT OF MALEATED CORN OIL-g-PBAT AS A COMPATIBILIZER BETWEEN STARCH AND PBAT 312

8.1	Abstract.....	312
8.2	Introduction.....	313
8.3	Experimental.....	316
8.3.1	Experimental Setup.....	316
8.3.2	Procedure	317
8.3.3	Characterization and Analysis	319
8.4	Results and Discussion	321
8.4.1	Iodine and Acid numbers for CO and MCO [25, 26]	321
8.4.2	Free Radical Initiated Reaction to form MCO-g-PBAT.....	323
8.4.3	Effect of the initiator on grafting percentage of MCO on the polyester.	326
8.4.4	Effect of the MCO on grafting percentage of MCO on the polyester	327
8.4.5	TGA	328
8.4.6	DSC.....	331
8.4.7	Density, Expansion Ratio (ER) and Specific length (SL) of Starch foams ..	332
8.4.8	Compressive Strength and Resiliency	334
8.4.9	ESEM.....	336
8.4.10	Moisture Sorption Analysis	336
8.5	Conclusions.....	338
8.6	References.....	339

Chapter 9: REACTIVE PBAT-G-TPS AND PBAT-G-MTPS BLENDS..... 341

9.1	Introduction.....	341
9.1.1	Starch blends with polyesters.....	342
9.1.2	Starch-Polyester Reactive Blends	344
9.1.3	Starch Derivatives.....	345
9.1.4	Starch – based Nano-Composites	349

9.2	Materials and Equipment	352
9.3	PBAT-Thermoplastic Starch (TPS) graft copolymers	353
9.3.1	Synthesis of PBAT-TPS graft copolymers by reactive extrusion processing	353
9.3.2	Soxhlet Extraction Studies	354
9.4	PBAT-Maleated thermoplastic starch graft copolymers.....	355
9.4.3	Soxhlet Extraction Studies	356
9.4.4	Fourier Transformed Infrared Spectroscopy (FTIR) Studies.....	356
9.4.5	Thermal Analysis Studies	357
9.4.6	Intrinsic Viscosity Studies	357
9.4.7	Nuclear Magnetic Resonance (NMR) Studies.....	358
9.4.8	Environmental Scanning Electron Microscopy (ESEM).....	358
9.4.9	Wide Angle X-ray Scattering.....	358
9.4.10	Blown Film Studies.....	359
9.4.11	Determination of the Mechanical Properties of the Films	359
9.5	Results and Discussion	360
9.5.1	PBAT-TPS graft copolymers.....	360
9.5.2	Maleated Thermoplastic Starch (MTPS)	368
9.5.3	PBAT-MTPS graft copolymers (unfilled & nano-clay filled).....	383
9.6	Density, Expansion Ratio (ER) and Specific length (SL) of Starch foams	413
9.6.1	Moisture Sorption Analysis	418
9.7	Conclusions.....	420
9.8	References.....	422

Chapter 10: REACTIVE EXTRUSION OF BIODEGRADABLE MA-G-PBAT-TALC COMPOSITES.....	426
10.1 Abstract.....	426
10.2 Introduction.....	427
10.3 Experimental Section	430
10.3.1 Materials	430
10.3.2 Experimental Procedure.....	430
10.4 Results and discussion	435
10.4.1 Preparation of compatibilized PBAT-talc composites.....	435
10.4.2 Mechanical properties of maleated PBAT-talc composites.....	442
10.4.3 <i>In situ</i> chemically modified PBAT-talc composites prepared through One-Step Reactive Extrusion Process.....	449
10.4.4 Tensile properties of compatibilized melt-blends prepared through a one-step reactive extrusion process.....	453
10.4.5 Thermal properties of <i>in situ</i> chemically modified PBAT-talc composites .	457
10.5 Starch Foam Extrusion using PBAT-talc blends	459
10.6 Conclusions.....	467
10.7 Current Research and Future Recommendations.....	469
10.7.1 Stabilizers.....	469
10.7.2 Experimental Protocol	471
10.7.3 Mechanical Properties as a Function of time	471

10.8 Re

Chapter 11:

Chapter 12:

12.1 PB

.....

12.1.1

12.1.2

12.1.3

12.1.4

12.2 The

12.3 Ret

10.8	References.....	476
Chapter 11:	SUMMARY AND CONCLUSIONS.....	479
Chapter 12:	RECOMMENDED PROJECTS	494
12.1	PBAT – Trimethoxy(vinyl)silane/Dimethoxy(vinylmethyl)silane – Talc blends	494
12.1.1	Introduction.....	494
12.1.2	Experimental Section.....	496
12.1.3	Results and Discussion	497
12.1.4	Recommendations for the PBAT-silane-talc composites	500
12.2	Thermoplastic Starch (TPS) – based Nano-Composites.....	502
12.3	References.....	505

Table 2.1: P

Table 2.2: F
Foams -----

Table 2.3: N
Starch - base

Table 3.1: S
Feed Rate. ---

Table 3.2: S
Screw Speed

Table 3.3: S
Content. -----

Table 3.4: S
Feed Rate. ---

Table 3.5: Ab

Table 3.6: Dy

Table 3.7: Dy

Table 3.8: Des

Table 4.1: Vis

Table 4.2: Val
various input c

Table 4.3: App

Table 4.4: Para
dies -----

Table 4.5: Scre

Table 4.6: Trou

LIST OF TABLES

Table 2.1: Physico-Mechanical Properties of Extruded Corn Starch Foams-----	40
Table 2.2: Effect of PHAE content on Physico-Mechanical Properties of Starch Foams -----	48
Table 2.3: Normalized Steady State Weight Gains, Diameters, Lengths of the Starch – based Foams with different PHAE contents -----	61
Table 3.1: Steady State Process Gains for Step-Input Variations in the Starch Feed Rate. -----	79
Table 3.2: Steady State Process Gains for Step-Input Variations in the Extrusion Screw Speed-----	81
Table 3.3: Steady State Process Gains for Step-Input Variations in the Moisture Content. -----	83
Table 3.4: Steady State Process Gains for Step-Input Variations in the PHAE Feed Rate. -----	85
Table 3.5: Absolute and Relative Linear Domains.-----	88
Table 3.6: Dynamic Properties (Pressure).-----	92
Table 3.7: Dynamic Properties (Torque). -----	93
Table 3.8: Design for Multiple Input Tests.-----	95
Table 4.1: Viscosity Models from Literature -----	116
Table 4.2: Values of Consistency Index ‘K’, and Flow-Behavior Index ‘n’ for various input conditions. -----	128
Table 4.3: Apparent and Actual shear rates for various input conditions -----	129
Table 4.4: Parameters for the determination of shape factors for annular/circular dies -----	144
Table 4.5: Screw Configuration for Wenger TX – 80 Twin-Screw Extruder---	151
Table 4.6: Troubleshooting Guide-----	156

Table 4.7: T

Table 4.8: T

Table 4.9: S

Table 4.10:

Table 5.1: D

Table 5.2: S

Table 5.3: E
thickness of

Table 5.4: E
thickness of 2

Table 5.5: V

Table 5.6: E
thickness of

Table 5.7: E
thickness of

Table 5.8: I

Table 5.9:

Table 6.1
Compressi
Aids-----

Table 6.2
Starch-bas

Table 7.1
Maleation

Table 7.2
MA-g-PI

Table 7.
Differen

Table 4.7: Typical Starch Foam Sheet Production Table -----	159
Table 4.8: Thermal Resistivity of Foam Sheets -----	163
Table 4.9: Suggested Drop Heights Based on Weight of Product -----	167
Table 4.10: Typical Fragility Levels for Different Products -----	168
Table 5.1: Data and Initial Conditions-----	197
Table 5.2: Solution to System of Differential Equations.-----	198
Table 5.3: Error table for the cushion curve with a drop height of 30 inches and thickness of 1 inch.-----	201
Table 5.4: Error table for the cushion curve with a drop height of 30 inches and thickness of 2 inches. -----	201
Table 5.5: Variability in Px^k at selected times from Table 5.2. -----	210
Table 5.6: Error table for the cushion curve with a drop height of 30 inches and thickness of 1 inch ($k = 1.059$). -----	218
Table 5.7: Error table for the cushion curve with a drop height of 30 inches and thickness of 2 inches ($k = 1.022$).-----	218
Table 5.8: Dynamic Stress-Strain Results for Starch Foam -----	225
Table 5.9: Predicted Values for $h = 30$ inches, $t = 2$ inches -----	229
Table 6.1: Unit Densities, Radial Expansion Ratios, Specific Lengths, Compressive Strengths and Spring Indices (Resilience) with different Functional Aids-----	248
Table 6.2: Normalized Steady State Weight Gains, Diameters, Lengths of the Starch-based Foams with different Functional Aids -----	260
Table 7.1: Maleation of PBAT: Torque %, MFI, Intrinsic Viscosity, Weight % Maleation and SEC Results-----	289
Table 7.2: Melting and Crystallization Enthalpies and Temperatures for different MA-g-PBAT -----	297
Table 7.3: Densities, Expansion Ratios, Specific Lengths of Starch Foams using Different Functional Aids. -----	299

Table 7.4:
Foams on M

Table 8.1: S

Table 8.2: M

Table 8.3:
MCO-g-PB

Table 8.4:
Foams on M

Table 9.1:
copolymers -

Table 9.2: S

Table 9.3: T
TPS Graft C

Table 9.4: T
TPS Graft C

Table 9.5: S

Table 9.6: T
PBAT-MTPS

Table 9.7: T
PBAT-MTPS

Table 9.8: T

Table 9.9: T
PBAT-g-MI

Table 9.10:

Table 9.11:
g-MTPS as c

Table 9.12:
Foams on M

Table 10.1:

Table 7.4: Normalized Steady State Weight Gains and Dimensions of Starch Foams on Moisture Sorption -----	305
Table 8.1: Some Properties of MCO-g-PBAT-----	325
Table 8.2: Melting and Crystallization Enthalpies & T for MCO-g-PBAT-----	331
Table 8.3: Physico-Mechanical Properties of Starch foams using PBAT and MCO-g-PBAT (BMCO).-----	333
Table 8.4: Normalized Steady State Weight Gains and Dimensions of Starch Foams on Moisture Sorption -----	337
Table 9.1: Blown Film Processing Conditions for Polyester-Starch graft copolymers -----	359
Table 9.2: Soxhlet Extraction results of PBAT-TPS graft copolymers -----	362
Table 9.3: Tensile Strength, Modulus of Elasticity, Break Elongation of PBAT-TPS Graft Copolymer (Machine Direction)-----	366
Table 9.4: Tensile Strength, Modulus of Elasticity, Break Elongation of PBAT-TPS Graft Copolymer (Transverse Direction) -----	367
Table 9.5: Soxhlet Extraction results of PBAT-MTPS graft copolymers -----	386
Table 9.6: Tensile Strength, Modulus of Elasticity (MoE), Break Elongation of PBAT-MTPS Graft Copolymer (Machine Direction) -----	392
Table 9.7: Tensile Strength, Modulus of Elasticity (MoE), Break Elongation of PBAT-MTPS Graft Copolymer (Transverse Direction)-----	393
Table 9.8: Tear and Puncture properties of PBAT-g-MTPS (70/30)-----	400
Table 9.9: Tensile Strength, Modulus of Elasticity (MoE), Break Elongation of PBAT-g-MTPS Copolymer using 1 wt% Nanoclay (Machine Direction)-----	401
Table 9.10: Physico-Mechanical Properties of Starch-based foams (Control).-	416
Table 9.11: Physico-Mechanical Properties of Starch-based foams (using PBAT-g-MTPS as compatibilizer).-----	417
Table 9.12: Normalized Steady State Weight Gains and Dimensions of Starch Foams on Moisture Sorption -----	419
Table 10.1: Temperature profile used for blown films -----	433

Table 10.2:
Melt-Flow I
number-aver
(M_w/M_n) of
reactive extr

Table 10.3:
the melt-blend

Table 10.4:
from the melt

Table 10.5:
direct reactive
and 0.5wt% i

Table 10.6:
PBAT-talc c
process (see c

Table 10.7:
from PBAT-
extrusion pro

Table 10.8:
loading. -----

Table 10.9:
blend. -----

Table 10.10:
chemically mo
extrusion proce

Table 10.11:
chemically mo
extrusion proce

Table 10.12:
(in situ chemica
PBAT mixed in

Table 12.1:
the PBAT-silane

Table 10.2: Effect of esterification catalysts (Sn(Oct) ₂ and 4-DMAP) on the Melt-Flow Index (MFI) of MA-g-PBAT-talc composites, and the weight fraction, number-average molecular weight (M _n), and molecular weight distribution (M _w /M _n) of their recovered polyester part, as prepared through a two-step reactive extrusion process. -----	439
Table 10.3: Tensile Properties (Machine Direction) of blown films derived from the melt-blends prepared containing 30 wt% in talc (see Table 10.2)-----	443
Table 10.4: Tensile Properties (Transverse Direction) of blown films derived from the melt-blends prepared containing 30 wt% in talc (see Table 10.2) -----	444
Table 10.5: Molecular Characteristics of PBAT-talc melt-blends prepared by direct reactive extrusion process – [One Step] (in the presence of 3.0 wt% MA and 0.5wt% in peroxide) -----	451
Table 10.6: Tensile Properties (Machine Direction) of Blown films derived from PBAT-talc composites compatibilized through the one-step reactive extrusion process (see entries 1-6 et 8, Table 5) -----	455
Table 10.7: Tensile Properties (Transverse Direction) of Blown films derived from PBAT-talc composites compatibilized through the one-step reactive extrusion process (see entries 1-6 et 8, Table 5)-----	456
Table 10.8: DSC data of plain PBAT matrix and composites at different talc loading. -----	458
Table 10.9: Physico-Mechanical Properties of Starch foams using PBAT-talc blend.-----	460
Table 10.10: Physico-Mechanical Properties of Starch foams using in situ chemically modified PBAT-talc composites (prepared through a one-step reactive extrusion process). -----	464
Table 10.11: Mechanical properties of the films obtained using the in situ chemically modified PBAT-talc composites prepared through a one-step reactive extrusion process, involving 30% talc-----	474
Table 10.12: Mechanical properties of the films obtained using the masterbatch (in situ chemically modified PBAT-talc composites with 60% talc) and the plain PBAT mixed in the ratio of 50:50.-----	475
Table 12.1: Tensile Properties (Machine Direction) of blown films derived from the PBAT-silane-talc blends -----	499

Table 12.2
from the PI

Table 12.2: Tensile Properties (Transverse Direction) of blown films derived from the PBAT-silane-talc blends ----- 500

Figure 2.1:

Figure 2.2:

Figure 2.3:

Figure 2.4:

Figure 2.5:

(MEA) react
Resorcinol --

Figure 2.6:

Figure 2.7:

Figure 2.8:

starch -----

Figure 2.9:

Figure 2.10:

expressed in

temperature c

Figure 2.11:

different amo

6% water (w

Figure 2.12:

amounts of b

(w w of starch

Figure 2.13:

expressed in

at a temperat

Figure 2.14:

Figure 2.15:

Figure 2.16:

LIST OF FIGURES

Figure 2.1: Molecular Structure of Amylose -----	19
Figure 2.2: Molecular Structure of Amylopectin -----	19
Figure 2.3: Swelling of Starch Granules -----	21
Figure 2.4: Destructurized Starch -----	23
Figure 2.5: Hydroquinone diglycidyl ether (HDGE) and Monoethanolamine (MEA) react to give PHAE thermoset. Bisphenol A could also be used instead of Resorcinol -----	27
Figure 2.6: Bisphenol A diglycidyl ether -----	28
Figure 2.7: The Twin-Screw Extrusion System. -----	30
Figure 2.8: Screw Configuration with the Pressure Profile for the plasticization of starch -----	34
Figure 2.9: Screw Configuration with the Pressure Profile for foaming of starch. -	35
Figure 2.10: Effect of the Amount of Water used on the degree of foaming, expressed in terms of ' ■ ' Expansion Ratio (ER), and ' ◇ ' density at a temperature of 105°C -----	43
Figure 2.11: Effect of the Process Temperature on the Degree of Foaming, at two different amounts of blowing agents: ' ◇ ' 7% water (w/w starch), ' ■ ' 6% water (w/w of starch).-----	45
Figure 2.12: Effect of the Process Temperature on the Density, at two different amounts of blowing agents: ' ◇ ' 7% water (w/w starch), ' ■ ' 6% water (w/w of starch)-----	46
Figure 2.13: Effect of the Amount of Talc used on the degree of foaming, expressed in terms of the ' ■ ' Expansion Ratio (ER), and ' ◇ ' density at a temperature of 105°C, and inlet water concentration of 7% (dry basis).-----	49
Figure 2.14: ESEM of the starch foam cross-section (0% talc)-----	50
Figure 2.15: ESEM of the starch foam cross-section (0.5% talc) -----	51
Figure 2.16: ESEM of the starch foam cross-section (1.0% talc) -----	52

Figure 2.17:

Figure 2.18:

Figure 2.19:

Figure 2.20:
terms of
105°C, inlet
7% (Starch.

Figure 2.21:
Energy; and
of 7% (Starch)

Figure 2.22:
density (kg m

Figure 2.23:

Figure 2.24:

Figure 3.1: C

Figure 3.2: h

Figure 3.3: I
Rate. (b) Scr

Figure 3.4:
the Moisture
10% Step Ch
Content (b):
(0% Step Ch
Content (e):
the Moisture

Figure 3.5: M
(from 'Princ
Variation Ru

Figure 3.6: M
(from 'Princ
Variation Ru

Figure 2.17: ESEM of the starch foam cross-section (2.0% talc) -----	53
Figure 2.18: Number of talc particles involved in forming a cell.-----	54
Figure 2.19: Unit Foam density as a function of Cell Density. -----	55
Figure 2.20: Effect of the Screw Speed on the degree of foaming, expressed in terms of ‘ ■ ’ Expansion Ratio (ER), and ‘ ◇ ’ density at a temperature of 105°C, inlet water concentration of 7% (Starch, wet basis), and PHAE content of 7% (Starch, wet basis) -----	57
Figure 2.21: Effect of the Screw Speed on the ‘ ■ ’ Specific Mechanical Energy; and ‘ ◇ ’ Density at a temperature of 105°C, inlet water concentration of 7% (Starch, wet basis), and PHAE content of 7% (Starch, wet basis). -----	58
Figure 2.22: Logarithmic plot of Compressive Strength (Pa) as a function of foam density (kg/m ³).-----	60
Figure 2.23: ESEM of the starch foam surface (0% PHAE) -----	62
Figure 2.24: ESEM of the starch foam surface (7.0% PHAE)-----	63
Figure 3.1: Control, Process and Product Variables of the Extrusion System. -----	71
Figure 3.2: Experimental Design-----	75
Figure 3.3: Linearity in Pressure with Step-Input Variations in the (a) Starch Feed Rate, (b) Screw Speed, (c) Moisture Content, (d) PHAE Feed Rate-----	87
Figure 3.4: Transient Response of Pressure to Different Step-Input Variations in the Moisture Content modeled as a First Order Process with a Dead Time (Lag): + 10% Step Change in the Moisture Content (a); + 8% Step Change in the Moisture Content (b); + 4% Step Change in the Moisture Content (c); Original Steady State (0% Step Change in the Moisture Content) (d); - 4% Step Change in the Moisture Content (e); - 8% Step Change in the Moisture Content (f); - 10% Step Change in the Moisture Content (g) -----	90
Figure 3.5: Measured (Recorded) Values of Pressure compared to the Calculated (from ‘Principle of Superposition’) Values for the different Multiple Step-Input Variation Runs-----	96
Figure 3.6: Measured (Recorded) Values of Torque compared to the Calculated (from ‘Principle of Superposition’) Values for the different Multiple Step-Input Variation Runs-----	97

Figure 3.7:
(from 'Pristine'
Variation R

Figure 3.8:

Figure 3.9:

Figure 3.10:

Figure 3.11:

Figure 3.12:

Figure 3.13:

Figure 4.1: Extruder. ----

Figure 4.2: F

Figure 4.3: E

Figure 4.4: D

Figure 4.5: D

Figure 4.6: D

Figure 4.7: R
SME and the I

Figure 4.8: R
Moisture Cont

Figure 4.9: R
SME and the I

Figure 4.10:
Moisture Cont

Figure 4.11:
Values of $\ln(t)$

Figure 4.12: C

Figure 3.7: Measured (Recorded) Values of SME compared to the Calculated (from 'Principle of Superposition') Values for the different Multiple Step-Input Variation Runs-----	98
Figure 3.8: Response surface of pressure for the various manipulated variables ---	100
Figure 3.9: Response surface of Torque for the various manipulated variables. ----	101
Figure 3.10: Response surface of SME for the various manipulated variables. -----	102
Figure 3.11: Predicted Versus Actual Values of Pressure. -----	103
Figure 3.12: Predicted Versus Actual Values of Torque. -----	104
Figure 3.13: Predicted Versus Actual Values of SME. -----	105
Figure 4.1: Foaming Screw Configuration for the Century ZSK – 30 Twin-Screw Extruder. -----	122
Figure 4.2: Bifurcated Die – Design. -----	124
Figure 4.3: Dependence of '◆: K' and '■: n' on Moisture Content-----	130
Figure 4.4: Dependence of '◆: K' and '■: n' on Die Temperature.-----	131
Figure 4.5: Dependence of '◆: K' and '■: n' on PHAE Content. -----	131
Figure 4.6: Dependence of '◆: K' and '■: n' on SME. -----	132
Figure 4.7: Response Surface of the Consistency Coefficient 'K' to variations in SME and the Die Temperature. -----	136
Figure 4.8: Response Surface of the Consistency Coefficient 'K' to variations in Moisture Content and the PHAE Content.-----	137
Figure 4.9: Response Surface of the Flow Behavior Index 'n' to variations in SME and the Die Temperature. -----	138
Figure 4.10: Response Surface of the Flow Behavior Index 'n' to variations in Moisture Content and the PHAE Content.-----	139
Figure 4.11: Comparison of the Predicted Values of 'ln(K)' with the Actual Values of 'ln(K)'. -----	140
Figure 4.12: Comparison of the Predicted Values with the Actual Values of 'n' ---	141

Figure 4.1

Figure 4.1

Figure 4.15

80 -----

Figure 4.16

Sheet Extrusion

Figure 4.17

· Δ · Polystyrene

Figure 4.18

sheet, at a

starch foam

Polystyrene

Figure 4.19

sheet, at a d

foam sheet.

sheet, · Δ ·

Figure 5.1

Figure 5.2

Figure 5.3

Figure 5.4

Figure 5.5

Figure 5.6

cells (con

Figure

determin

Figure

Figure

Differen

Figure

drop h

Figure 4.13: Schematic of the Annular Die. -----	143
Figure 4.14: Screw Configuration for Wenger TX-80 TSE -----	152
Figure 4.15: Starch Foam Extrusion Process Flow Diagram on the Wenger TX - 80 -----	154
Figure 4.16: Downstream Cutting and Laminating Operation for the Starch Foam Sheet Extrusion -----	155
Figure 4.17: Comparison of ‘◆’ Expanded Polystyrene (EPS), ‘□’ Starch, and ‘△’ Polyurethane foams as Insulation Materials, ‘■’ Ambient.-----	165
Figure 4.18: Dynamic Cushion Curves for a 2.5 cm and a 5 cm thick starch foam sheet, at a drop height of 0.75 m, as per ASTM D-1596: ‘____’ 2.5 cm thick starch foam sheet, ‘____’ 5 cm thick Starch foam sheet, ‘----’ 5 cm thick Polystyrene foam sheet -----	169
Figure 4.19: Dynamic Cushion Curves for a 2.5 cm and a 5 cm thick starch foam sheet, at a drop height of 0.75 m, as per ASTM D-4168: ‘■’ 2.5 cm thick starch foam sheet, ‘◆’ 5 cm thick starch foam sheet, ‘▲’ 5 cm thick polystyrene foam sheet, ‘▲’ 5 cm thick polyethylene foam sheet. -----	170
Figure 5.1: Real Cushion behavior compared to Hookean (Linear) cushion.-----	179
Figure 5.2: Schematic of a weight in a free fall onto a cushion. -----	181
Figure 5.3: Free body diagram of cushion and weight. -----	182
Figure 5.4: Determination of material yield point stress from foam yield stress. ---	186
Figure 5.5: Compressive Force/Stress vs. Compressive Strain Curves-----	187
Figure 5.6: Assumed Circular Cross-section of foam with hypothetical square cells (compression test). -----	188
Figure 5.7: Foam section with hypothetical array of square cells (for the determination of cushion curves).-----	189
Figure 5.8: Temperatures in the cell cross-section. -----	191
Figure 5.9: Comparison of Cushion Curves from Experiment and Finite Difference Solutions. -----	200
Figure 5.10: Comparison of Cushion Curves from Finite Difference Solution at a drop height of 30” and varying thicknesses.-----	203

Figure 5.1
thickness of

Figure 5.12
thickness of

Figure 5.13
thickness of

Figure 5.14
curve-----

Figure 5.15
Compression

Figure 5.16
and Finite El

Figure 5.17:

Figure 5.18:

Figure 5.19:

Figure 6.1:

Figure 6.2:

Figure 6.3:

Figure 6.4:

Figure 6.5:

Figure 6.6:

Figure 6.7:

Extruder----

Figure 6.8:

Figure 6.9:

Figure 6.10

Figure 6.11

Figure 5.11: Comparison of Cushion Curves from Finite Difference Solution at a thickness of 2” and varying drop heights. -----	204
Figure 5.12: Comparison of Cushion Curves from Finite Difference Solution at a thickness of 2” and varying cell sizes. -----	205
Figure 5.13: Comparison of Cushion Curves from Finite Difference Solution at a thickness of 2” and varying cell wall thicknesses.-----	206
Figure 5.14: The Effect of k (Different Drop Heights) on the Force-Compression curve-----	212
Figure 5.15: The Effect of k (Different Foam Thicknesses) on the Force-Compression curve. -----	213
Figure 5.16: Cushion Curves from Experiment, Finite Difference Formulation and Finite Element Method (Using Polytropic Constant). -----	219
Figure 5.17: The dynamic Stress-Strain Curve. -----	223
Figure 5.18: The Dynamic Stress-Strain Curve for Starch Foams. -----	227
Figure 5.19: The (sh / t) vs. (G + 1)s Curve.-----	228
Figure 6.1: Poly (caprolactone)-----	240
Figure 6.2: Poly (butylene adipate-co-terephthalate)-----	240
Figure 6.3: Poly (vinyl alcohol) -----	240
Figure 6.4: Cellulose Acetate -----	241
Figure 6.5: Glyoxal -----	241
Figure 6.6: Methylated Pectin -----	241
Figure 6.7: Foaming Screw Configuration for the Century ZSK – 30 Twin-Screw Extruder-----	243
Figure 6.8: ESEM of the surface of starch foams with 12% PVA-----	251
Figure 6.9: ESEM of the surface of starch foams with no functional aids. -----	254
Figure 6.10: ESEM of the surface of starch foams with 3% PCL. -----	255
Figure 6.11: ESEM of the surface of starch foams with 7% PBAT. -----	257

Figure 6.12:
of their densit

Figure 7.1: E

Figure 7.2: 2.

Figure 7.3: Pr

Figure 7.4: FT

Figure 7.5: β -

Figure 7.6: TC
and PBAT. Di
(3% MA, 0.0%
(3% MA, 0.25%

Figure 7.7: TC
and PBAT. Di
0.5% L101). (c
0.5% L101). an

Figure 7.8: Lo
density (kg/m^3)

Figure 7.9: ES
(120X).-----

Figure 7.10: E
(120X).-----

Figure 7.11: ES
MA-g-PBAT an

Figure 7.12: W
No additives (ii)

Figure 8.1: Mol

Figure 8.2: EXP
Reactor.-----

Figure 8.3: For
Reaction.-----

Figure 6.12: Compressive Strength (Pa) of the starch-based foams as a function of their density (kg/m^3)-----	258
Figure 7.1: Effect of composition and viscosity on phase morphology -----	273
Figure 7.2: 2,5-dimethyl-2,5-di-(tert-butylperoxy) hexane (Free Radical Initiator) -----	277
Figure 7.3: Proposed Free Radical Initiated Maleation Mechanism.-----	287
Figure 7.4: FTIR of MA-g-PBAT and PBAT. -----	288
Figure 7.5: β -scission on grafting of MA on the PBAT backbone. -----	293
Figure 7.6: TGA of the maleated samples MA-g-PBAT (different grafting levels) and PBAT. Different Peroxide (L 101) contents: (a) Pure PBAT, (b) MA-g-PBAT (3% MA, 0.0% L101), (c) MA-g-PBAT (3% MA, 0.1% L101), (d) MA-g-PBAT (3% MA, 0.25% L101), and (e) MA-g-PBAT (3% MA, 0.5% L101). -----	295
Figure 7.7: TGA of the maleated samples MA-g-PBAT (different grafting levels) and PBAT. Different MA contents: (a) Pure PBAT, (b) MA-g-PBAT (1% MA, 0.5% L101), (c) MA-g-PBAT (2% MA, 0.5% L101), (d) MA-g-PBAT (3% MA, 0.5% L101), and (e) MA-g-PBAT (5% MA, 0.5% L101) -----	296
Figure 7.8: Logarithmic plot of Compressive Strength (Pa) as a function of foam density (kg/m^3).-----	300
Figure 7.9: ESEM micrograph of the surface of starch foams with no additives (120X).-----	302
Figure 7.10: ESEM micrograph of the surface of starch foams with 5% PBAT (120X).-----	303
Figure 7.11: ESEM micrograph of the surface of starch foams blended with 0.5% MA-g-PBAT and 4.5% PBAT (400X). -----	304
Figure 7.12: Wide-Angle X-Ray Scattering of the Starch foam samples with (i) No additives (ii) 5% PBAT (iii) (0.5% MA-g-PBAT + 4.5% PBAT) blend -----	307
Figure 8.1: Molecular Structure of Corn oil. -----	313
Figure 8.2: Experimental Set-up for the Maleation of Corn Oil using a Parr Reactor. -----	316
Figure 8.3: Formation of Maleated Corn Oil (MCO) by 1, 4- Diels Alder Reaction.-----	322

Figure 8.4: FTIR

Figure 8.5: MCO-g

Figure 8.6: FTIR o

Figure 8.7: TGA
L101, 0% MCO: (---)
0.25% L101, 2% M

Figure 8.8: TGA
L101, 0% MCO: (---)
L101, 5% MCO: --

Figure 8.9: Logarithmic
density (kg/m^3)---

Figure 8.10: ESE

Figure 9.1: Starc

Figure 9.2: Meth

Figure 9.3: P
synthesis of PB

Figure 9.4: FTI

Figure 9.5: TC

Figure 9.6: Pr

Figure 9.7: F

Figure 9.8: F

Figure 9.9: I

Figure 9.10:

Figure 9.11:
maleic acid

Figure 9.12:

Figure 9.13:

Figure 8.4: FTIR for CO, MCO -----	323
Figure 8.5: MCO-g-PBAT polymer -----	324
Figure 8.6: FTIR on PBAT, MCO-g-PBAT -----	326
Figure 8.7: TGA for various MCO-g-PBAT (different MCO contents): (a) 0% L101, 0% MCO; (b) 0.25% L101, 0% MCO; (c) 0.25% L101, 1% MCO; (d) 0.25% L101, 2% MCO; (e) 0.25% L101, 5% MCO. -----	329
Figure 8.8: TGA for various MCO-g-PBAT (different L101 contents): (a) 0% L101, 0% MCO; (b) 0% L101, 5% MCO; (c) 0.25% L101, 5% MCO; (d) 0.5% L101, 5% MCO. -----	330
Figure 8.9: Logarithmic plot of Compressive Strength (Pa) as a function of foam density (kg/m^3)-----	334
Figure 8.10: ESEM on starch foam surface (5% MCO-g-PBAT)-----	336
Figure 9.1: Starch Reaction with half-esters of dicarboxylic acids-----	348
Figure 9.2: Methyl, tallow (T), bis-2-hydroxyethyl, quaternary ammonium -----	352
Figure 9.3: Proposed Acid-catalyzed trans-esterification chemistry in the synthesis of PBAT-TPS graft copolymers. -----	361
Figure 9.4: FTIR Spectrum of PBAT-TPS graft co-polymers -----	364
Figure 9.5: TGA Results of PBAT-TPS graft copolymers -----	365
Figure 9.6: Proposed Chemistry for Maleation of starch using maleic anhydride --	368
Figure 9.7: FTIR results of MTPS samples using maleic acid modifier-----	371
Figure 9.8: FTIR results of MTPS samples using maleic anhydride modifier-----	372
Figure 9.9: DSC Results of MTPS samples -----	374
Figure 9.10: TGA Results of MTPS samples-----	375
Figure 9.11: TGA Results of MTPS samples modified with 2.5%, 5% and 8% maleic acid -----	376
Figure 9.12: Intrinsic viscosity of regular corn starch-----	377
Figure 9.13: Intrinsic viscosity of TPS -----	378

Figure 9.14: Intri

Figure 9.15: Intri

Figure 9.16: Intri

Figure 9.17: Intri
101)-----

Figure 9.18: NMB

Figure 9.19: NMB
8% MA-----

Figure 9.20: Prop
PBAT-MTPS grafi

Figure 9.21: FTIR

Figure 9.22: DSC

Figure 9.23: TGA

Figure 9.24: Electr

Figure 9.25: Electr

Figure 9.26: Electr

Figure 9.27: Electr

Figure 9.28: Electr

Figure 9.29: X-Ray

Figure 9.30: X-Ray

Figure 9.31: X-Ray

Figure 9.32: X-Ray

Figure 9.33: X-Ray

Figure 9.34: X-Ray

Figure 9.35: ESEM c

Figure 9.14: Intrinsic viscosity of MTPS (2.5% Maleic anhydride) -----	378
Figure 9.15: Intrinsic viscosity of MTPS (5.0% Maleic anhydride) -----	379
Figure 9.16: Intrinsic viscosity of MTPS (8.0% Maleic anhydride) -----	379
Figure 9.17: Intrinsic viscosity of MTPS (2.5% Maleic anhydride and 0.1% L 101)-----	380
Figure 9.18: NMR Spectrum for Thermoplastic Starch (TPS)-----	381
Figure 9.19: NMR Spectrum for Maleated Thermoplastic Starch (MTPS) using 8% MA-----	382
Figure 9.20: Proposed Trans-esterification reaction chemistry in the synthesis of PBAT-MTPS graft copolymers. -----	384
Figure 9.21: FTIR Results of PBAT-MTPS graft copolymers-----	388
Figure 9.22: DSC Results of PBAT-MTPS graft copolymer-----	389
Figure 9.23: TGA Results of PBAT-MTPS graft copolymer -----	390
Figure 9.24: Electron Micrograph of the aliphatic-aromatic copolyester PBAT ----	396
Figure 9.25: Electron Micrograph of the PBAT-Granular Starch blend-----	396
Figure 9.26: Electron Micrograph of the PBAT-TPS blend-----	397
Figure 9.27: Electron Micrograph of PBAT-g-TPS (Maleic Acid catalyst) -----	397
Figure 9.28: Electron Micrograph of PBAT-g-MTPS -----	398
Figure 9.29: X-Ray diffractograms of starch, TPS, PBAT, and PBAT-TPS blend -	406
Figure 9.30: X-Ray diffractogram results of MTPS and PBAT-g-MTPS-----	407
Figure 9.31: X-Ray diffractogram results with Cloisite Na ⁺ -----	410
Figure 9.32: X-Ray diffractogram results with Cloisite 30B-----	411
Figure 9.33: X-Ray diffractogram results with Bentone 111-----	411
Figure 9.34: X-Ray diffractogram results with Bentone 166-----	412
Figure 9.35: ESEM on starch foam surface from Example 1. -----	418

Figure 10.1: Proposed mechanism for the esterification reaction between silanol coming from talc (R-OH) and grafted-maleic anhydride polyester chains catalyzed by tin octoate-----	437
Figure 10.2: Proposed mechanism for the esterification reaction between silanol coming from talc (R-OH) and grafted-maleic anhydride polyester chains catalyzed by 4-Dimethylamino pyridine (4 – DMAP). NB: the positive charge bore by 4-dimethylaminopyridine is stabilized by resonance-----	438
Figure 10.3: SEM Images of cryofractured surface of (a) a simple PBAT-talc melt-blend and (b) MA-g-PBAT-based composites prepared in the presence of 1wt% in Sn(Oct) ₂ (entries 1 and 4, Table 10.2). -----	446
Figure 10.4: SEM Images of ruptured films of (a) PBAT-talc melt-blend (b) MA-g-PBAT-based composites prepared in the presence of 1wt% in Sn(Oct) ₂ -----	448
Figure 10.5: Schematic representation the extruder using for the single-step process -----	449
Figure 10.6: SEM of the cross-section of starch foams using (a) – 5% PBAT, (b) – 5% PBAT-talc blend.-----	461
Figure 10.7: Logarithmic plot of Compressive Strength (Pa) as a function of foam density (kg/m ³).-----	466
Figure 10.8: Structural Formula for ULTRANOX 626 -----	470
Figure 12.1: X-Ray Patterns for alkali salt modified TPS-clay nano-composite ----	503

TABLE OF ABBREVIATIONS

<i>Chapter 1</i>	
PCL	Poly (ϵ -caprolactone)
PLA	Poly (D,L, or DL-lactide)
PBAT	Poly (butylene adipate-co-terephthalate)
PHE	Poly (hydroxyester)
PHEE	Poly (hydroxyesterether)
ISO	International Standards Organization
USDA	United States Department of Agriculture
PFR	Plug Flow Reactor
CSTR	Continuous Stirred Tank Reactor
RTD	Residence Time Distribution
PHAE	Poly (hydroxyaminoether)
PE	Polyethylene
T_m	Melting Temperature
SME	Specific Mechanical Energy
MA-g-PBAT	Maleated Poly (butylene adipate-co-terephthalate)
MCO	Maleated Corn Oil
MCO-g-PBAT	Maleated Corn Oil grafted Poly (butylene adipate-co-terephthalate)
TGA	Thermo-Gravimetric Analysis

DSC	Differential Scanning Calorimetry
FTIR	Fourier Transformed Infra Red Spectroscopy
SEC	Size Exclusion Chromatography
MTPS	Maleated Thermoplastic Starch
PBAT-g-MTPS	Poly (butylene adipate-co-terephthalate) grafted Maleated Thermoplastic Starch
NMR	Nuclear Magnetic Resonance
XPS	X-ray Photoelectron Spectroscopy
CA	Cellulose Acetate
MP	Methylated Pectin
PVA	Poly (vinylalcohol)
<i>Chapter 2</i>	
TSE	Twin-Screw Extruder/Extrusion
WAXS	Wide angle X-Ray Scattering
SAXS	Small angle X-Ray Scattering
MDS	Molecular Dispersion of Starch and Water
LER	Liquid Epoxy Resin
RDGE	Resorcinol Diglycidyl Ether
HDGE	Hydroquinone diglycidyl ether
MEA	Monoethanolamine
KB	Kneading Blocks
RH/LH	Right Handed/Left Handed

DS	Degree of Substitution
ER	Expansion Ratio
ESEM	Environmental Scanning Electron Microscopy/Micrograph
RPM	Revolutions per minute
<i>Chapter 3</i>	
MIMO	Multiple Input Multiple Output
K	Steady State Gain
K_R	Relative Steady State Gain
τ	Time Constant
t_d	Dead time
RSA	Response Surface Analysis
BIBO	Bounded Input Bounded Output
MC	Moisture Content
FODT	First Order Process with Dead Time
PID	Proportional-Integral-Derivative Control
ΔP	Pressure Drop
<i>Chapter 4</i>	
K	Consistency Coefficient
n	Flow Behavior Index
η	shear viscosity
ΔH	Molar “free energy of activation” in a stationary fluid

R	Universal Gas Constant
k_1	moisture content (MC) coefficient
$\dot{\gamma}$	Shear Rate
Q	volumetric flow rate
G	Dimensionless Shock Deceleration
<i>Chapter 5</i>	
FDM	Finite Difference Method/Model
FEM	Finite Element Method/Model
<i>Chapter 6</i>	
PEA	Poly (esteramide)
PHBV	Poly (hydroxybutyrate-co-valerate)
<i>Chapter 7</i>	
Lupersol/Luperox 101	2,5-dimethyl-2,5-di-(<i>tert</i> -butylperoxy)hexane
MA	Maleic Anhydride
PBS	Poly(butylene succinate)
PBSA	Poly(butylene succinate-co-adipate)
HPLC	High Performance Liquid Chromatography
SL	Specific Length
MFI	Melt Flow Index
THF	Tetrahydrofuran
LPBAT	Cross-linked Poly (butylene adipate-co-terephthalate)

<i>Chapter 8</i>	
CO	Corn Oil
KOH	Potassium Hydroxide
<i>Chapter 9</i>	
TPS	Thermoplastic Starch
EAA	Poly (ethylene-co-acrylic acid)
EVOH	Polyethylene-vinyl alcohol
LDPE	Low Density Polyethylene
MS	Molar Substitution
MMT	montmorillonite
HDT	Heat Distortion Temperature
CLTE	Coefficient of Linear Thermal Expansion
PBAT-g-TPS	Poly (butylene adipate-co-terephthalate) grafted Thermoplastic Starch
DCM	Dichloromethane
FPM	Feet per minute
<i>Chapter 10</i>	
4 - DMAP	4 – Dimethyl aminopyridine
HDPE	High Density Polyethylene
HCl	Hydrochloric acid

INTRODUCTION

1.1 Rationale

During the last century, a tremendous advance in the field of materials has been made with the introduction of plastics. In today's world, life without plastics is incomprehensible. While plastics are strong, lightweight, inexpensive and easily processable, they are not readily broken down by the natural elements in the environment. This is of particular concern when plastics are used in single-use disposable packaging and consumer goods. Thus, new products have to be designed and engineered from "conception to reincarnation" incorporating a holistic "life cycle thinking approach". The impacts of raw material resources used in the manufacture of a product and the ultimate fate (disposal) of the product when it enters the waste stream have to be factored in the design of the product. This has opened up new market opportunities for developing biodegradable and bio-based products from annually renewable resources, as the next generation of sustainable materials that meets ecological and economic requirements (1 – 5).

The use of annually renewable biomass as opposed to petrochemicals as the feedstocks for the production of polymers, chemicals and fuel needs to be understood from a global carbon cycle basis. Global warming is caused by an overabundance of carbon in the atmosphere, in the form of CO₂. Crude oil is pumped out of the ground and made into gasoline, diesel and synthetic materials by the chemical industry. These polymers, chemicals and fuels are used by manufacturers, cars and trucks, which release CO₂.

a
y
a
e
r
v
l
a
b
F
P
ra
fi
E
th
p
d
d
sy
la

Plants and trees capture CO₂ through photosynthesis. Plants are then fossilized over geological timeframes to give us new fossil fuels. This is your geological carbon cycling process. The rate at which the carbon is captured is in geological timeframes – millions of years – versus the timeframe the carbon is released, which is in biological timeframes – years, at best, decades. This is the cause of the global warming which the Kyoto protocols attempt to address. So the solution is to either reduce the use of fossil fuels via efficiencies and limited usage but there is only so much that can be attained using this methodology. Another approach is to use annually renewable crops like corn, soy, wheat, etc. to make polymers, chemicals and fuels by the growing biochemical industry. This approach will ensure that the rate of CO₂ capture is equal to the CO₂ release. This is a huge positive environmental attribute. It's important to note that even though it hasn't been ratified by the US, the Kyoto Protocols, or a reasonable facsimile, is in our future. Furthermore, if we manage our biomass resources effectively by making sure that we plant more biomass than we utilize, we can begin to start reversing the carbon dioxide rate equation and move towards a net balance between carbon dioxide fixation/sequestration and release due to consumption (4)).

Environmental regulations, societal concerns, and a growing environmental awareness throughout the world have triggered a paradigm shift in industry to develop products and processes compatible with the environment. In this regard, there is an interest in developing and evaluating materials based on recyclable polymers, natural polymers and degradable polymers. These include natural polymers like starch, cellulose, proteins, synthetic biodegradable polymers like poly (ϵ -caprolactone) (PCL), poly (D, L, or DL-lactide) (PLA), poly (butylene adipate-*co*-terephthalate) (PBAT), poly (hydroxy esters)

(PHE), poly (hydroxy ester ethers) (PHEE) and their modified versions. Along with the above mentioned polymers, the entire portfolio of biodegradable plastics are used in a variety of applications ranging from packaging films, cutlery items such as spoons, knives, forks etc., biodegradable packaging foams and many more. One such application that is the focus of this work is biodegradable thermoplastic foam, specifically, those used for insulation, surface protection, and cushioning.

Today's petroleum-based foam plastic protective packaging is a \$3 billion market in the United States and growing 12% annually. This market is experiencing growing pressure from existing and proposed environmental and disposal regulations, and market based sustainability initiatives. It presents a major disposal problem for companies and municipalities as it is lightweight and bulky and so does not lend itself to a viable economic and environmentally responsible recycling operation due to expensive handling and transportation costs. It is not biodegradable, which makes disposal in soil or composting operations untenable. Further, issues such as sustainability, industrial ecology, biodegradability, and recyclability are becoming major considerations in a company's product packaging design, especially with single use disposable packaging. ISO (International Standards Organization) 14000 environmental management standards are becoming a requirement in the market place and companies are actively positioning themselves to secure certification. ISO 14000 is a voluntary program wherein a company assesses the environmental impact of its products and processes and continuously strives for improvement. As of 2001, there were 2,700 companies in North America with ISO 14001 certification – triple the number from 1999; and over 31,000 companies worldwide.

The
pro
yea
ass
mi
its
Or
TW
ba
a.
di
P
D
fi
re
r
F
H
c
c
e
(
c

The U.S. Government has set the goal of tripling U.S. use of bioenergy and biobased products by the year 2010. Meeting this goal could create an additional \$15-20 billion a year in new income for farmers and rural America, and reduce the environmental impact associated with annual greenhouse gas emission by an amount equal to as much as 100 million metric tons of carbon (6). The U.S. Government has expressed the desire to use its buying power to promote usage of biobased materials, as evidenced in Presidential Orders 13101 and 13123 and the recently passed Farm Bill (7).

The U.S. Department of Agriculture (USDA) is developing guidelines to designate bio-based products that can be procured by Federal agencies. There is, thus, a market need for a, bio-based, biodegradable foam plastic packaging that can be safely and effectively disposed of in soil or in composting operations, but retains all of the current foam plastics performance requirements. Multinational companies, like Toyota, Sony, Nortel, General Dynamics and Herman Miller are actively seeking new, environmentally responsible foam packaging to replace existing petroleum based foams. In previous work, we have reported on the rationale, design, and engineering of bio-based, biodegradable polymer materials, specifically starch-based products (1-9).

Extruders are the most common machines in the Plastics Processing Industry. Extruders have been used, in the traditional sense, to transform solid plastic into uniform melt, for delivery to the next stage of processing. Various physical processes such as devolatilization and blending have been carried out in extruders, primarily twin-screw extruders involving commercial polymers like polyamides, polyolefins, and polyesters (10). Various reactors (Batch, PFR, CSTR or a combination of these) have been used to conduct chemical reactions that include polymerizations, polymer functionalization,

reactive grafting, etc. The concept of using extruders to perform the above mentioned chemical reactions is novel and unique and is termed as “*Reactive Extrusion*” (11 – 22). More specifically, *reactive extrusion* refers to the process of conducting chemical reactions during the melt extrusion process. Discrete processes can be carried out in specific modular segments of a twin-screw extruder whose screw configuration can be tailored to meet the desired objective. The reaction times needed to achieve near complete conversion need to be well within the residence times available in extrusion operations (typically less than 5 minutes). The advantage of using extruders to conduct reactions is as follows:

- Fast and continuous process.
- Solvent free, melt process.
- Control over residence time and residence time distribution (RTD).
- Integration of other extrusion ‘streams’ along with the polymerization process.
- Efficient devolatilization capability through the vent port.
- Modular in design and hence easy to scale up.

Interest in environmentally friendly materials has stimulated development of extruded starch-based foams, as replacements for poly (ethylene), poly (styrene) and poly (urethane) foams in packaging and insulation applications. Natural polymers like starch by themselves do not lend adequate performance properties. Extruded starch foams are generally water soluble, and their properties are sensitive to moisture content. However, the use of synthetic biodegradable polyesters in combination with starch is expected to be a viable alternative to providing fully degradable thermoplastic foam that has performance properties similar to that of polyethylene/polystyrene.

1.2 Proposed Goals

This study targeted the design and engineering of a scale-up process for the extrusion of starch-based foam sheets, for the reproduction of the results obtained on a laboratory scale. The target applications were cushion packaging and insulation. Poly (hydroxy amino ether) (PHAЕ), supplied by Dow Chemicals under the trade name BLOX 110, was used as the performance enhancer for the starch foams. It further deals with the design of new formulations involving a proprietary aliphatic-aromatic biodegradable co-polyester, poly (butylene adipate-*co*-terephthalate) (PBAT) from BASF Chemicals. The polyester exhibited phase separation from the starch and partially crystallized. PBAT was chemically modified using maleic anhydride, by grafting reactive groups (anhydride) on the polyester backbone in order to improve its compatibility with starch. It also targets the design of a reactive extrusion process to modify starch using maleic anhydride and the subsequent characterization of the modified thermoplastic starch. Finally, it deals with the synthesis of biodegradable blends based on the above-mentioned biodegradable polyester with modified starch and other inorganic fillers, and their use as performance enhancers in extruded starch foams.

1.3 Specific Objectives

1.3.1 Goal

“Design and engineer a thermoplastic starch product that can be foamed to provide a closed cell structure that is capable of good protective cushion packaging as substitute for Polyethylene (PE) based foam packaging – Additionally the product must have sufficient water resistance, flexibility, low density, resilience.”

1.3.2 Problem Statement

Starch, an anhydroglucose polymer from corn, offers a structural platform to manufacture sustainable, biodegradable foam packaging. Starch granules, however, exhibit hydrophilic properties and strong inter-molecular association via hydrogen bonding due to the hydroxyl groups on the granule surface. This strong hydrogen bonding association and crystallization leads to poor thermal processing since the melting temperature (T_m) is higher than the thermal decomposition temperature, and degradation sets in before thermal melting. The hydrophilicity and thermal sensitivity renders the starch molecule unsuitable for thermoplastic applications.

1.3.3 Objectives of this research

- I. Using water as a plasticizer and blowing agent to produce cylindrical foam shapes and sheets, employing a twin screw extruder as the reactor of choice. The polar molecule of water helps in breaking the hydrogen bonds involved in the starch macromolecule, due to the hydroxyl groups present, thus breaking down the granular, crystalline structure, and imparting flow properties.

II. Use functional aids to improve the physico-mechanical properties of the starch foams, such as lower densities, resilience (spring index), flexibility, humidity resistance, and an aesthetic appeal. The type of starch selected for this foams application was hydroxypropylated high amylose corn starch based on its superior physico-mechanical properties. The functional aid considered in this case was poly (hydroxy amino ether) (PHAE). PHAE offers the adhesion and durability of epoxy resins with the flexibility and processability of thermoplastic resins.

- A. Optimization of all processing parameters such as moisture content (plasticizing and blowing agent), temperature, PHAE (functional aid), talc (nucleating agent), and the screw speed (minimizing the mechanical energy input, though maintaining lower densities and good mechanical properties).
- B. Characterization of the starch foam products obtained on the lab- scale in terms of their density, expansion ratio, specific length, cell size and structure, and other mechanical properties.
- C. Black-box modeling of the starch foaming process, in order to develop process control strategies and also to determine the most influential variable on the stability of the process. Transient modeling of the starch foam extrusion process, using step tests on primary variables such as starch feed rate, moisture content, screw speed, and PHAE feed rate. To measure the response of the process through pressure and torque records.
- D. Development of a viscosity model necessary for the design of an annular die for the production of starch foam sheets on a manufacturing scale. The

variations in moisture content, temperature, PHAE content, and screw speed (Specific Mechanical Energy, SME) are considered in the determination of the viscosity model.

- E. Scale-up of the starch foam extrusion process to produce starch foam sheets using the above-designed annular die on a manufacturing scale twin-screw extruder.
- F. Determination of the cushioning and insulation properties of the starch foam sheets for the respective target applications.
- G. Numerical simulation of the drop test method for the prediction of the cushioning properties of the starch foam sheets using a finite difference formulation.

III. Development of functional aids which serve as alternatives to the current polymer PHAE. Preliminary studies were carried out using a few biodegradable polymers as functional aids. Poly (butylene adipate-*co*-terephthalate), a biodegradable aliphatic-aromatic co-polyester provided promising results.

- A. Reactive blends based on modified biodegradable polyesters and thermoplastic starch. The polymer needs to be modified due to its incompatibility with starch.
 - 1. Reactive modification of PBAT in a twin-screw extruder using maleic anhydride to form maleated poly (butylene adipate-*co*-terephthalate) (MA-*g*-PBAT).
 - 2. Reactive modification of corn oil in a 2 L Parr reactor using maleic anhydride to form maleated corn oil (MCO).

3. F

4.

B.

C.

3. Reactive modification of PBAT in a twin-screw extruder using maleated corn oil to form modified PBAT (MCO-g-PBAT).
 4. Characterization of the MA-g-PBAT and MCO-g-PBAT using Thermal analysis such as Thermo-Gravimetric Analysis (TGA) and Differential Scanning Calorimetry (DSC), Fourier transformed Infra Red Spectroscopy (FTIR), Size Exclusion Chromatography (SEC), and Intrinsic viscosity measurements.
 5. Foam extrusion studies using MA-g-PBAT and MCO-g-PBAT as compatibilizing agents between the polyester and starch.
 6. Characterization of the foams in terms of their density, expansion ratio, specific length and mechanical properties such as compressibility and resilience.
- B. Reactive modification of starch in a twin-screw extruder using maleic anhydride to form maleated thermoplastic starch (MTPS).
- C. Reactive blend of PBAT with MTPS in extruders, to give PBAT-g-MTPS.
1. Foam extrusion studies using PBAT-g-MTPS as a compatibilizing agent between the polyester and starch.
 2. Characterization of the MTPS and PBAT-g-MTPS using Thermal analysis such as Thermo-Gravimetric Analysis (TGA) and Differential Scanning Calorimetry (DSC), Fourier transformed Infra Red Spectroscopy (FTIR), Nuclear Magnetic Resonance (NMR), and Intrinsic viscosity measurements.

3. C

sp

r

D. Blen

effi

1.

2

1.4 Org

The thesis

work that h

Chapter 2 c

process vari

3. Characterization of the foams in terms of their density, expansion ratio, specific length and mechanical properties such as compressibility and resilience.
- D. Blends of PBAT with talc, and their use as functional aids in starch foams, for effective distribution of the nucleating agents in the starch matrix.
1. Modification of PBAT to improve compatibility (or grafting) with talc, and hence improve the mechanical properties (tensile strength and elongation).
 2. Characterization of the blends using Thermal analysis such as Thermo-Gravimetric Analysis (TGA) and Differential Scanning Calorimetry (DSC), Fourier transformed Infra Red Spectroscopy (FTIR), Size Exclusion Chromatography (SEC), X-Ray Photoelectron Spectroscopy (XPS), and Intrinsic viscosity measurements.
 3. Use of these reactive blends as functional aids in the production of starch foams for improved physico-mechanical properties.
 4. Characterization of the foams in terms of their density, expansion ratio, specific length and mechanical properties such as compressibility and resilience.

1.4 Organization of the Thesis

The thesis is composed of several chapters, each of which individually addresses the work that has been done in relation to the specific objectives outlined above.

Chapter 2 deals with the existing starch foam technology and the optimization of the process variables such as type of starch used, process temperature, plasticizing/blowing

agent content, PHAE content, nucleating agents, and the foaming screw configuration among others. It is crucial to operate this optimized process under the much needed steady state conditions. Chapter 3 deals with the development of control algorithms using step changes manipulated input variables such as the starch and PHAE feed rates, the moisture content, and the screw speed of the twin-screw extruder; and monitoring the response of various process variables such as the die pressure, motor load (torque) on the extruder, and the specific mechanical energy (SME) for the starch foam product. Chapter 4 deals with the development of a starch-PHAE blend shear viscosity model, which is essential in the design of an annular die for the scale-up of this existing technology to produce starch-based foam sheets using the optimized variables. In Chapter 5, the cushion curves for the starch foam sheets were predicted using finite difference and finite element methods, and were compared to the experimental data. Chapter 6 deals with the selection of a new performance enhancer, as a substitute to PHAE; resulting from the discontinued production of PHAE by Dow Chemical. Certain synthetic biodegradable polyesters such as PCL and PBAT, natural polymers such as Cellulose Acetate (CA) and Methylated Pectin (MP), poly (vinyl alcohol) (PVA), and cross-linkers like glyoxal were used, in an attempt to improve the physical, mechanical, and hydrophobic properties (dimensional stability and weight gain in the presence of moisture) of the starch foams. PBAT gave the best results in terms of physico-mechanical properties, and low densities. Chapters 7 and 8 involve modification of PBAT in an attempt to graft certain reactive groups on the polyester backbone and thus, improve the compatibility between the polyester and the starch for an enhancement in properties of starch-based foams. The modified polyester can be used as a compatibilizer. Chapter 9 deals with the synthesis of

MTPS by reactive extrusion and its subsequent characterization using Thermal analysis, Fourier transformed Infra Red Spectroscopy (FTIR), Nuclear Magnetic Resonance (NMR), and Intrinsic viscosity measurements. Chapter 9 also deals with synthesis and characterization of biodegradable compositions based on reactive blends of the above-discussed biodegradable polyester with MTPS and other optional inorganic fillers (nucleating agents). Also, nano-clay was incorporated in these blends for improved mechanical and barrier properties. These reactive blends are further used as compatibilizers between the starch and the polyester. Chapter 10 involves the study of compatibilization between the polyester PBAT and an inert filler such as talc, thus improving the mechanical properties (tensile strength and elongation). Summary and Conclusions are outlined in Chapter 11 and recommendations for future work are discussed in Chapter 12.

1.5 References

- 1) Bloembergen, S., David, J., Geyer, D., Gustafson, A., Snook, J., Narayan, R. Biodegradable Plastics and Polymers, 601, Elsevier, New York, 1994.
- 2) Narayan, R. Biomass (Renewable) Resources for Production of Materials, Chemicals, and Fuels -- A Paradigm Shift. Rowell, R. M., Schultz, T. P., Narayan, R., Eds; American Chemical Society Symposium Series, American Chemical Society, Washington, DC, 476, 1, 1992.
- 3) Narayan, R. Polymeric Materials from Agricultural Feedstocks, In: Polymers from Agricultural Coproducts, Ed., Fishman, M.L., Friedman, R.B. and Huang, S.J. American Chemical Society Symposium Series, American Chemical Society, Washington, DC, 575, 2, 1994.
- 4) Narayan, R. Biodegradable Plastics and Polymers, 261, Elsevier, New York 1994.
- 5) Narayan, R. Paradigm for Successful Utilization of Renewable Resources, Eds: Sessa, D.J. and Willett, J.L. AOCS Press, Champaign, Illinois, 1998, pp. 78.
- 6) The technology roadmap for plant/crop-based renewable resources 2020 (Feb, 1999) DOE/GO-10099-706. www.oit.doe.gov/agriculture
- 7) U.S. Farm Security and Rural Investment Act of 2002 (P. L. 107-171), Title IX Energy, Section 9002.
- 8) Narayan, R. Kunststoffe, 79, 1022, 1989.
- 9) Rowell, R., Schultz, T., Narayan, R. Emerging Technologies for Materials and Chemicals from Biomass, ACS Symposium, 467, 1991.
- 10) Brown, S. B. Annual Review of Materials Research, 21, 409 – 435, 1991.
- 11) Bouilloux, A., Druz, J., Lambla, M. Preprints of the 3rd International Polymer Conference on Reactive Processing of Polymers, 181, 1984.
- 12) Hocker, H., Michaeli, W., Berghaus, U., Frings, W. Journal of Applied Polymer Science, 48, 871, 1993.
- 13) Ishida, H., Huang, Z. Proceedings of the Annual Technical Conference of the Society of Plastics Engineers, 205, 1984.
- 14) Macosko, C. W., Bouilloux, A., Kotnour, T. Industrial Engineering Chemistry Research, 30, 2431, 1991.

- 15) Menges, G., Bartilla, T. Polymer Engineering and Science, 27, 1216, 1987.
- 16) Stuber, N. P., Tirrell, M. Processing of Polymers, 193, 1984.
- 17) Tzonagakis, C., Vlachopoulos, J., Hamielec, A. E. Polymer Engineering and Science, 28, 170, 1988.
- 18) Inata, H., Matsumara, S. Journal of Applied Polymer Science, 32, 1877, 1995.
- 19) Thomas, N.W., Berardinelli, F.M., Edelman, R. US Patent 4,128,599, 1978.
- 20) Carlson, D., Nie, L., Narayan, R., Dubois, P. Journal of Applied Polymer Science, 72, 477, 1999.
- 21) Bikaris, D., Panayiotou, C. Journal of Applied Polymer Science, 70, 1503, 1998.
- 22) Vaidya, U.R., Bhattacharya, M. Journal of Applied Polymer Science, 52, 617, 1994.

STARCH-PHAE FOAM TECHNOLOGY

2.1 Abstract

Cylindrical starch foam shapes were produced on a small scale (~ 11-12 kg/hr) Werner Pfleiderer ZSK - 30 Twin Screw Extrusion (TSE) process using water, which functions as a plasticizer as well as a blowing agent. The properties of the starch foams depend on the type of starch used (hydroxypropylated high amylose corn starch, 70% amylose), the amount of water and additives (poly (hydroxyamino ether)) (PHAE) used, and extrusion conditions such as temperature and the screw configuration. PHAE offers the adhesion and durability of epoxy resins with the flexibility and processability of thermoplastic resins. PHAE was successful in imparting mechanical strength and toughness, cell integrity, weather and water resistance to the foam structure. The purpose of this work was to study the effects of the extrusion (melt) temperature, amount of water added and the screw configuration on the density of starch foams. The water externally added was varied from 3% to 12%, while the poly (hydroxyamino ether) (PHAE) content was varied from 3% to 15% of the starch used (on a wet basis). The foaming was carried out at melt temperatures in the range from 85°C to 145°C. A match of material properties with process engineering conditions was achieved to facilitate the control of expansion to a structure with valuable commercial properties. The effects of processing conditions on the foaming process were studied using a Werner Pfleiderer ZSK - 30 Twin Screw Extruder (TSE). The optimum temperature, blowing agent content, and PHAE content were determined. The density of the cylindrical foam extrudates obtained was 22-25

kg/m³. The screw configuration, temperature and pressure profiles, additives affected the morphology, Expansion Ratio, resilience and compressibility of the product.

2.2 Background

Foaming consists of generating tiny gas bubbles in the polymer melt phase in order to produce lightweight materials without sacrificing mechanical and physical properties of the polymer. The final foam products usually possess better insulation properties, as well as higher degrees of impact resistance in the presence of gas bubbles in the polymer melt. Plastic foams are materials that comprise a cellular core structure created by the expansion of a blowing agent. A physical or chemical blowing agent can be used. When a physical blowing agent is used it dissolves in the polymer under high pressure. In contrast when a chemical blowing agent is used, it releases gas at a certain decomposition temperature, and the released gas dissolves in the polymer.

When cell nucleation takes place in the extrusion foaming die, the cells grow and the foam density decreases as the available blowing agent molecules diffuse into the cells. The growth rate of the cells is limited by the diffusion rate and the stiffness of the viscoelastic polymer/gas solution. In general, cell growth is affected primarily by the time allowed for the cell to grow, the temperature of the system, the state of super-saturation, the hydrostatic pressure or stress applied to the polymer matrix, and the viscoelastic properties of the polymer/gas solution.

We have developed technology to manufacture starch foam products having the resilience and compressibility of foam polystyrene, using water as the plasticizer and blowing agent. The polar molecule of water helps in breaking the hydrogen bonds

involved in the starch macromolecule, due to the hydroxyl groups present, thus breaking down the granular, crystalline structure, and imparting flow properties. In this project we are developing process engineering know how to make a portfolio of foam products with control of cell structure, and die shapes.

Starch is inexpensive, naturally occurring renewable polymer that is a potential raw material for the manufacture of plastic-like materials. In its granular form, starch has very few uses, and in order to release the polymer properties, granule disruption (plasticization) has to take place. Its use in plastic production would greatly reduce the demand for petroleum as well as alleviate the negative impact on the environment caused by discarded plastic products.

Starch is the second most abundant carbohydrate in the plant world after cellulose. It is the main storage polysaccharide in plants and is similar in structure and function to glycogen, which is the main storage polysaccharide in animals. Main sources of commercial starch are maize, potato, wheat, cassava and waxy maize (1). Starch, unlike cellulose, exists in a granular structure and is typically bimodal and polydispersed, both at the granular and molecular level. This underscores the uniqueness of starch. The molecular bimodal nature of starch refers to the major molecular components, namely the high molecular weight branched amylopectin, and the more linear material, amylose. Amylose is a linear or sparsely branched polymer of a molecular weight in the range of 10^5 to 10^6 g/mol linked primarily by $\alpha 1 \rightarrow 4$ bonds (Figure 2.1). The chains form a spiral-shaped single or double helix (2).

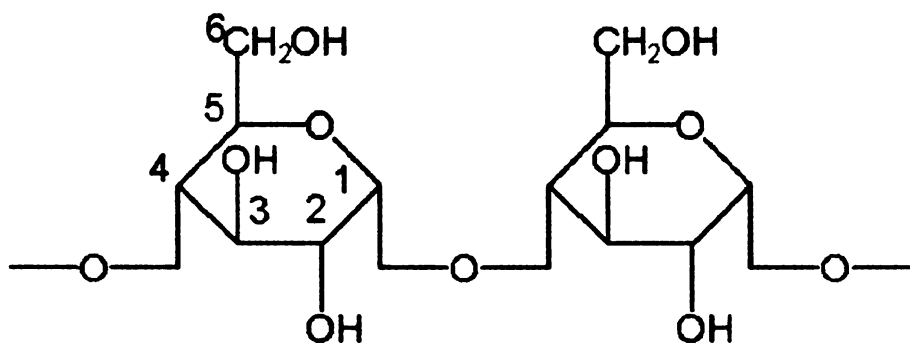


Figure 2.1 Molecular Structure of Amylose

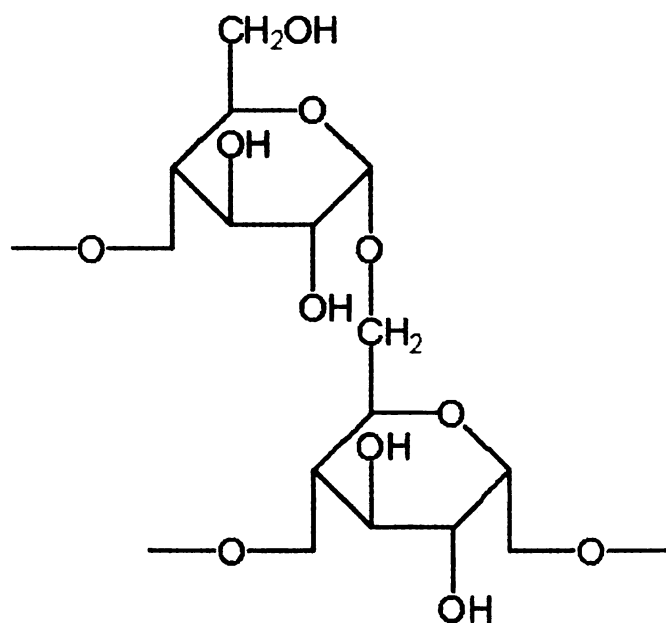


Figure 2.2 Molecular Structure of Amylopectin

In contrast, amylopectin is highly multiple branched with a molecular mass of 10^7 to 10^9 g/mol. Amylopectin also contains $\alpha 1 \rightarrow 4$ linked glucose units, but has in addition $\alpha 1 \rightarrow 6$ glucosidic branching points occurring every 25-30 glucose units. Figure 2.2 shows the structure of amylopectin.

The ratio of these two components varies depending upon the source of the starch and everything from 100% amylopectin to 100% amylose has been reported as occurring in nature or as a result of classical plant breeding. This is particularly the case with maize where the full range has been reported. The amylose contents of most starches, such as wheat, maize and potato starch, are all in the range of 20-30%. However, in waxy starches, the amylose content is as low as 1% (3).

Starch occurs naturally in granules. The granules vary in size and shape, depending upon species, and can range from approximately 1 micron to as large as 120 microns. The starch molecules are oriented radially in the granule to form roughly spherical shells, called 'micelles'. These micelles hold the granule together to permit swelling in heated water without the complete disruption and solubilization of the individual starch molecules (Figure 2.3).

These highly oriented and crystalline micellular areas explain the ability of ungelatinized starch granules to rotate a plane of polarized light to produce characteristic interference crosses. This bi-refrinct cross (Maltese cross) is one of the features used in identifying starch source. When the radial orientation of crystalline micelle is disturbed, the bi-refrinct cross disappears. Wide -angle and small-angle X-ray scattering (WAXS and SAXS) have shown that starch is partially crystalline. The overall crystallinity of the native starches is about 20-45% (4). The type of native, crystalline structure, labeled as A-, B- or C-type, depends on the starch source. Native A- and B-type crystal lattices consist of double helical, six-fold structures. The difference between the two types is the packing density of the double helices in the unit cell. The B-type structure is described as a more loosely packed hexagonal assembly of the helices with a column of water

molecules p
structure. th
thought of t

2.2.1 Gel

Gelatinizat
process is

are consid

noticed an

binding f

granule i

ruptured a

bound mic

As the granu
space is occup
iodine vapor.

molecules present in the center of the hexagonal arrangement, whereas in the A-type structure, this column of water is replaced by a double helix. The C-type structure is thought of to be an intermediate between the A and B type structures (5).

2.2.1 Gelatinization

Gelatinization of starch is a well-known process in the food and paper industries. This process is used to modify the rheology of various systems. Gelatinization temperatures are considered as ranges covering the temperatures at which loss of bi-refringence is first noticed and less than 10% remains. This temperature range is greatly influenced by the binding forces within the granule, which vary with starch source. When the starch granule is heated in water, the weaker hydrogen bonds in the amorphous areas are ruptured and the granule swells with progressive hydration (Figure 2.3). The more tightly bound micelles remain intact, holding the granule together. Bi-refringence is lost.

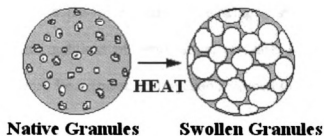


Figure 2.3 Swelling of Starch Granules

As the granule continues to expand, more water is imbibed, clarity is improved, more space is occupied, movement is restricted and viscosity increased. When stained with iodine vapor, one can see a "ghost" which indicates that the granule structure and/or

granule fragments can still be visible. With the swelling of amylose-containing granules such as corn, the amylose molecules are solubilized and leach out into solution. These molecules will then reassociate into aggregates and precipitate at low concentrations or set to a gel at higher amylose concentrations (6). This is referred to as "set back" or retrogradation. The congealed paste will become cloudy and opaque with time and will eventually release water to shrink into a rubbery consistency.

The gelatinization and melting process are dependent on the water content. A single peak, denoted as the gelatinization endotherm (G), is observed at water content above 66% (w/w). At water content below 66%, a shoulder appears at higher temperatures, denoted as a melting endotherm (M). At very low water contents, the G endotherm disappears and only the M endotherm is observed (7, 8).

2.2.2 Destructurized Starch

Starch gelatinization is not good enough to make a starch-based plastic material. Destructurizing starch is a pre-requirement for making a starch-based thermoplastic material. Under certain conditions of temperature, pressure, shear, limited water and sufficient time, starch may be extruded and injection molded to produce a thermoplastic material that can have mechanical properties suitable for particular applications as a structural material. This material is starch in an entirely new form, and is called a "molecular dispersion of starch and water" (MDS).

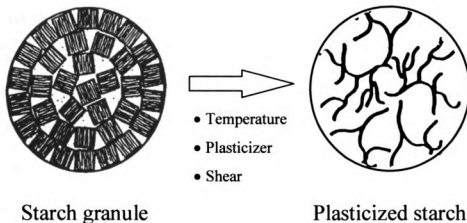


Figure 2.4 Destructurized Starch

MDS products are molecularly homogeneous (with both amylose and amylopectin dispersed uniformly throughout the material), are amorphous, have no granular structure (Figure 2.4), have relatively high molecular-weight amylopectin, are not brittle or friable and have superior mechanical properties. U.S. Patent No 5,095,054 to Lay et al. (9) discloses the use of water as a plasticizer for starch in order to make the material processable in for example an extruder.

2.2.3 Types of Starches and Modifications

High amylopectin maize, or waxy maize as it is known because of the reference to the waxy appearance of the kernel, has been available for nearly a century. High amylose versions of cornstarch are more recent, being developed in the last 40 years. Most common and commercially available are those hybrids, which contain either 50% or 70% amylose. Within the last 5 years, plant breeders have been able to develop a new hybrid, which is essentially free of amylopectin (< 5%).

For industrial applications, a wider range of chemical modifications has been developed including cationic, anionic, and amphoteric substitutions, as well as hydrophobic starches

l
e
s
P
T
P
c
q
T
in
is
fo
h
st
d
et
T
di
hy
ca
lin
de

and novel aldehyde chemistry, allowing wide applications in such industries as paper making, textiles and biodegradable/re-pulpable packaging products in response to environmental pressures. The biodegradable applications make use of high amylose starch from maize and are extruded to produce a material competitive with expanded polystyrene.

The dispersion stability and non-ionic character of the hydroxyalkyl ethers of starch are properties of commercial interest. Ready availability and low cost also provide commercial interest. Hydroxyethyl- and hydroxypropyl starches are produced in quantities of about 200 million pounds (91×10^6 kg) per year.

The use of starch and derivatives thereof to form various shaped articles has been shown in a number of patent publications (10 – 12). U.S. Pat. Nos. 5,035,930 and 5,043,196 issued on Jul. 30, 1991 and Aug. 27, 1991, respectively, disclose foamed shaped products formed from high amylose starch and particularly alkylene oxide modified starch. The high amylose starch used in this invention may be unmodified or modified and the term starch as used herein includes both types. By modified it is meant that the starch can be derivatized or modified by typical processes known in the art, e.g., esterification, etherification, oxidation, acid hydrolysis, cross-linking and enzyme conversion. Typically, modified starches include esters, such as the acetate and the half-esters of dicarboxylic acids, particularly the alkenylsuccinic acids; ethers, such as the hydroxyethyl- and hydroxypropyl starches and starches reacted with hydrophobic cationic epoxides; starches oxidized with hypochlorite; starches reacted with cross-linking agents such as phosphorus oxychloride, epichlorohydrin, and phosphate derivatives prepared by reaction with sodium or potassium orthophosphate or

tripolyphosphate and combinations thereof. These and other conventional modifications of starch are described in publications such as "Starch: Chemistry and Technology", Second Edition, edited by Roy L. Whistler et al., Chapter X (13); Starch Derivatives: Production and Uses by M. W. Rutenberg et al., Academic Press, Inc., 1984 (14). One modification of the high amylose starches used in this invention that is especially advantageous is the etherification with alkylene oxides, particularly those containing 2 to 6, preferably 2 to 4, carbon atoms. Ethylene oxide, propylene oxide and butylene oxide are exemplary compounds useful in etherifying the starting starch materials with propylene oxide being especially preferred. Varying amounts of such compounds may be used depending on the desired properties and economics. Generally, up to 15% or more and preferably, up to about 10%, by weight, based on the weight of starch will be used. Extruded starches modified in this manner, showed improved expansion, uniformity and resiliency.

2.3 Experimental

2.3.1 Materials

Regular un-modified cornstarch was obtained from Cargill-grade SMP 1100, with equilibrium moisture content of about 12 percent (w/w). Waxy cornstarch was obtained from Cargill-grade WP 1108, with equilibrium moisture content of about 12 percent (w/w). High Amylose cornstarch was obtained from National Starch and Chemicals (Indianapolis, IN), with equilibrium moisture content of about 11 percent (w/w). The hydroxypropylated high amylose cornstarch was purchased from National Starch and Chemicals (Indianapolis, IN), under the trade name of HYLON 7. The density of

HYLON 7 starch is 1.2 g/cm^3 . The inherent moisture content of the starch is 11.2% under ambient conditions. Water is used as the plasticizer as well as the blowing agent. Water content is maintained at 8-10% of the starch used. Talc (Magnesium Silicate), used as the nucleating agent, was obtained from Luzenac (Ontario, Canada). It has a specific gravity of 2.76 and a bulk density of 150 kg/m^3 . Poly (hydroxyamino ether) (PHAE) is an additive, which offers the adhesion and durability of epoxy resins with the flexibility and processability of thermoplastic resins.. PHAE was purchased from Dow Chemicals (Midland, MI), under the trade name BLOX 110. PHAE has a melt temperature of 75°C , and is produced by reacting liquid epoxy resin (LER) with hydroxy functional dinucleophilic amines and diglycidyl ethers of bisphenol-A, hydroquinone, or resorcinol (RDGE), as shown in Figures 2.5 and 2.6 (15). Winkler et al. (16) and Silvis et al. (17) extruded blends of starch-based thermoplastic hydroxy-functionalized polyetheramines, which were pelletized and formed into loose-fill packaging foams using a twin-screw or a single-screw extruder. PHAE was successful in imparting mechanical strength and toughness, cell integrity, weather and water resistance to the foam structure. The purpose of this work was to study the effects of the extrusion (melt) temperature, amount of water added and the screw configuration on the density of starch foams.

The water externally added was varied from 3% to 12%, while the poly (hydroxyamino ether) (PHAE) content was varied from 3% to 15% of the starch used (on a wet basis). The foaming was carried out at melt temperatures in the range from 85°C to 145°C . A match of material properties with process engineering conditions was achieved to facilitate the control of expansion to a structure with valuable commercial properties.

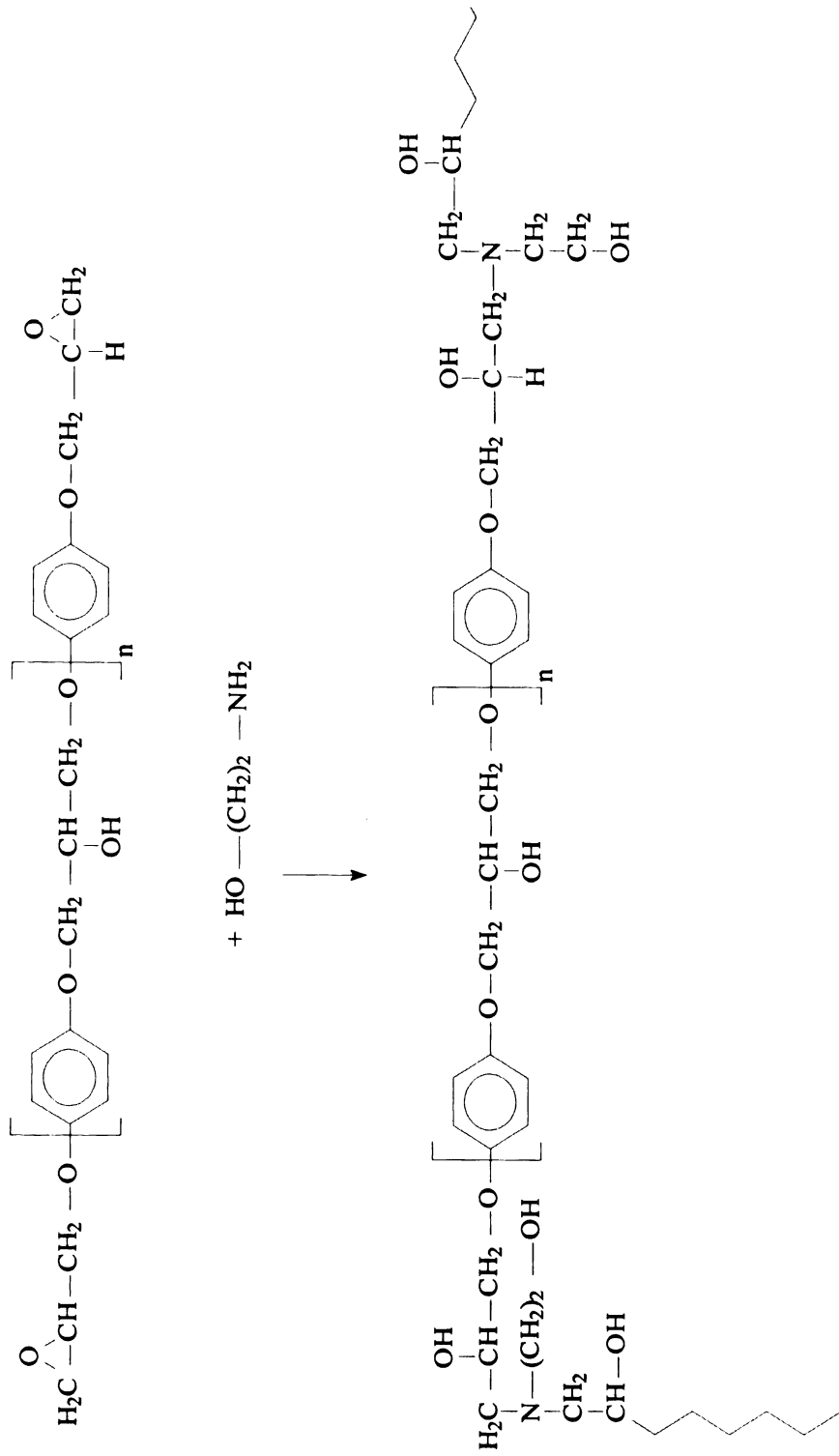


Figure 2.5 Hydroquinone diglycidyl ether (HDGE) and Monoethanolamine (MEA) react to give PHAE thermoset.

Bisphenol A could also be used instead of Resorcinol.

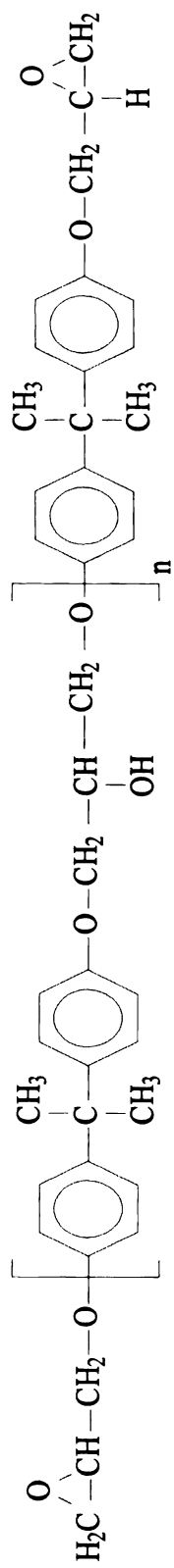
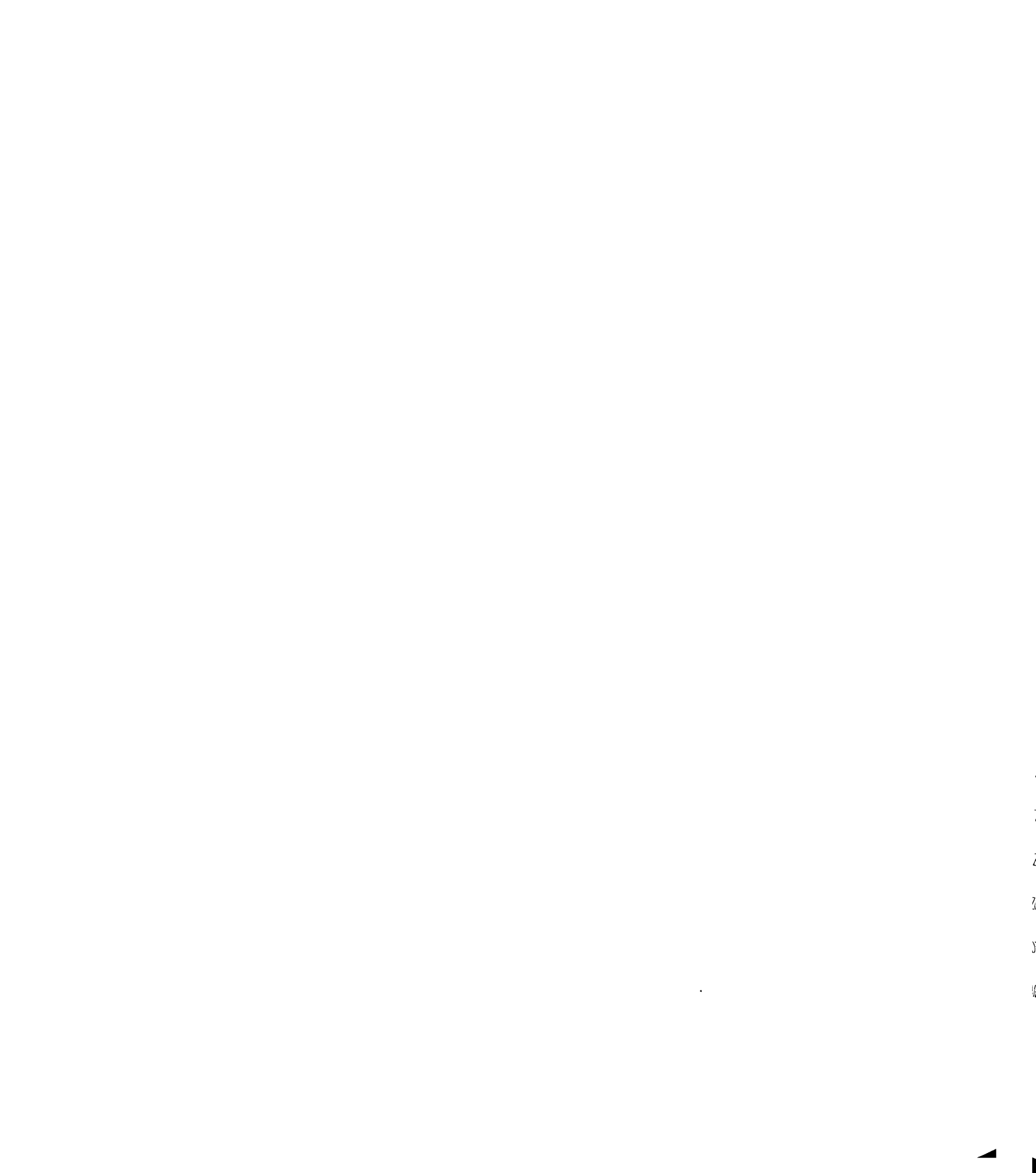


Figure 2.6 Bisphenol A diglycidyl ether



2.3.2 Experimental Setup

The experimental setup used in this study was a twin-screw extrusion system (Figure 2.7). The twin-screw extrusion system consists of an extruder driver with a speed control gearbox, a Werner Pfleiderer ZSK-30 twin-screw co-rotating extruder with a screw diameter of 30 mm, an L/D of 32, a positive displacement pump for injecting water into the extruder, accurate single-screw feeders for feeding starch, and PHAE and talc could be fed individually or as a mixture. A cylindrical filament die 2.7mm in diameter and 8.1 mm in length, with a cooling sleeve was assembled to the extruder. The sensors were mounted on the die to measure the temperature and pressure of the melt. A high-speed cutter was used to get cylindrical foam extrudates of required size.

2.3.3 Procedure

The temperatures in the ZSK-30 extruder zones were set up to reach the required temperatures. The temperature profile for the best product obtained was as follows:

Feed (Zone 1): 20°C (cold feed)

Zone 2: 100°C

Zone 3: 110°C

Zone 4: 120°C

Zone 5: 120°C

Zone 6: 110°C

Die: 105°C

Melt temperature: 105°C - 107°C.

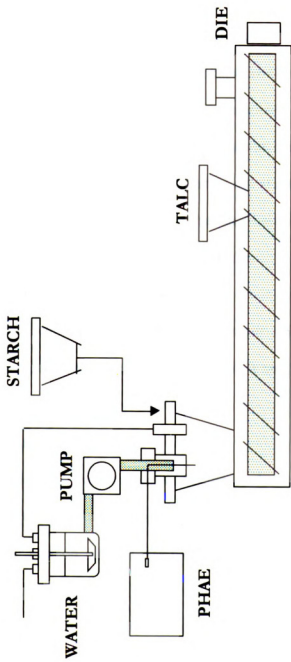


Figure 2.7 The Twin-Screw Extrusion System.

The feeder for starch was calibrated and set at a particular speed. The other feeder/feeders were calibrated and set at feeding rates accordingly. Initially, during start-up, water was pumped into the system immediately after the feed throat, at 15-20% of the starch fed, and later its flow rate was reduced to about 7-10% of starch. The inherent moisture present in starch (11.2%) also helped in plasticization of starch. The different parameters were varied one at a time while the other parameters remained those of the basic setting. When formulations were changed, extrusion was continued until the torque and the die pressure stabilized. Extrusions were carried out at a torque of 70-75%, and a pressure of 4.8-5.2 MPa. The foam was extruded at a rate of about 11-12 kg/hr, while the foam sheets were extruded at a throughput of 410-420 kg/hr.

2.3.4 Characterization and Analysis

The samples collected were conditioned as per ASTM D – 4332 (18), in a constant environment room at $23 \pm 1^\circ\text{C}$ ($73.4 \pm 3.6^\circ\text{F}$) and $50 \pm 2\%$ RH for at least 72 hours before testing.

2.3.4.1 Density

This test method covers the determination of density of foam by calculation from the mass and volume of a regularly shaped specimen. The test method ASTM D – 3575 (section 43, Method A) (19) was used. At least 10 specimens were measured for each formulation.

The dimensions of the sample were measured using a Vernier Calipers graduated to permit measurements accurate to 0.001 inches. Expansion ratio was calculated as the ratio of the cross-sectional area of the foam to that of the die.

2.

Co

Co

m

For

(0.

sur

thi

ma

Co

sec

60

Av

2.3.

Foa

grap

202

2.3.

10

envi

temp

samp

weigl

2.3.4.2 Compressive Strength and Resiliency

Compressive strength and resiliency describe the mechanical integrity of the foam. Compressive strength of the lab-scale specimens was measured according to the test method explained by Tatarka et al. (20), on a UTS SFM – 20 tensile testing machine. Foam specimens were securely fastened lengthwise and compressed by a steel probe (0.635 cm diameter) with a hemi-spherical end-cap. By lowering the piston to the foam surface, an initial load of 0.5 N was applied on the specimen for approximately 5 s. From this point, the probe was lowered at a rate of 30 mm/min for a distance of 3 mm. The maximum load was recorded. After 60 s had elapsed, a relaxation load was recorded. Compressive strength was determined by dividing the maximum load by the cross-sectional area of the probe. Resiliency is the percentage of the compressive force after the 60 s hold period divided by the maximum force required to compress the foam by 3 mm. Averages were calculated from five sets of starch foam specimens.

2.3.4.3 Environmental Scanning Electron Microscopy:

Foam samples were sectioned with a razor blade and mounted on aluminum stubs with graphite filled tape, sputter coated with gold and examined with a Phillips Electroscan 2020 environmental scanning electron microscope.

2.3.4.4 Moisture Sorption Analysis

10 blocks of each formulation, collected at different times were placed in an environmental humidity chamber, subject to a relative humidity of $95 \pm 5 \%$, and a temperature of $38 \pm 5 \text{ }^\circ\text{C}$. The weight and the dimensions (length and diameter) of the samples were monitored. They were measured at regular intervals using an accurate weighing balance and a pair of Vernier Calipers, to the third decimal place. The entities

measured at different time intervals were normalized using the value measured before placing the samples in the humidity chamber (time, $t = 0$). The weight and dimensions of the samples were recorded until a steady state value was reached (approximately 30 days). The results for a formulation were obtained as an average over the 10 samples used for that formulation.

2.3.5 Screw Configuration

The objective to be attained in an extruder was to ensure proper plasticization of granular starch, thus disrupting its crystalline structure, and complete dissolution of the blowing agent in the plasticized starch, by promoting convective diffusion under high processing pressure, to form a single-phase plastic.

The screw configuration played an important role in this foaming process, because, unlike conventional plastics, which require only temperature to form a melt phase, plasticization of starch required thermal energy as well as mechanical energy in the form of shear to form a thermoplastic melt. Hence, the screw configuration had to be so designed to achieve the afore-mentioned objective, and to build up enough pressure at the die, to cause uniform foaming. Figures 2.8 and 2.9 show the regular plasticization and foaming screw configurations on the small scale ZSK – 30 TSE. The plasticization screw configuration differed in the sense that the excess moisture in the thermoplastic melt was de-volatilized in the last conveying zone. It is worth noting that two other screw configurations (not reported) were used for the foaming operation. These screw configurations had low and medium levels of shearing through kneading blocks. Also, the left-handed elements were not used in these configurations to build up pressure within the extruder.

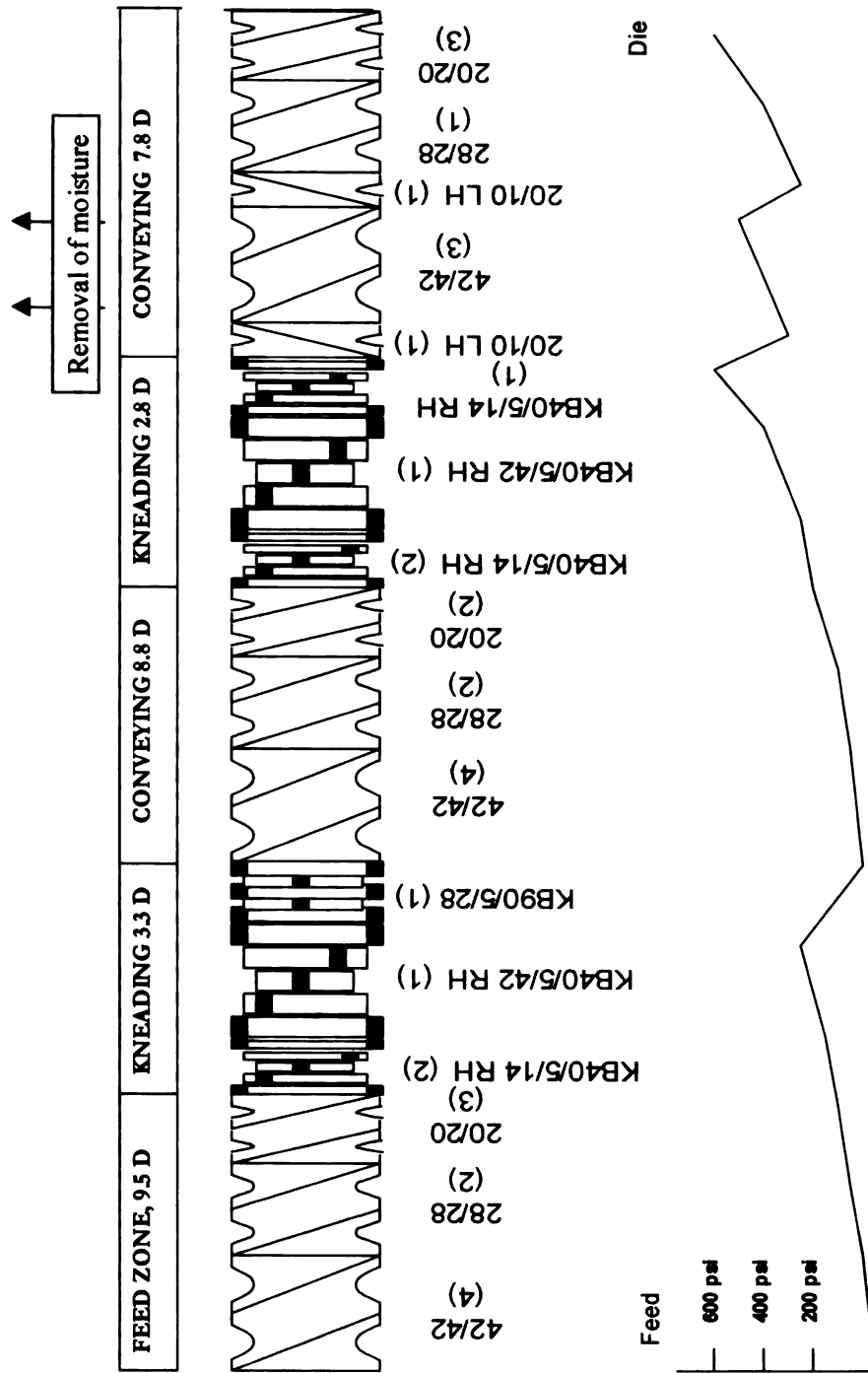


Figure 2.8 Screw Configuration with the Pressure Profile for the plasticization of starch.

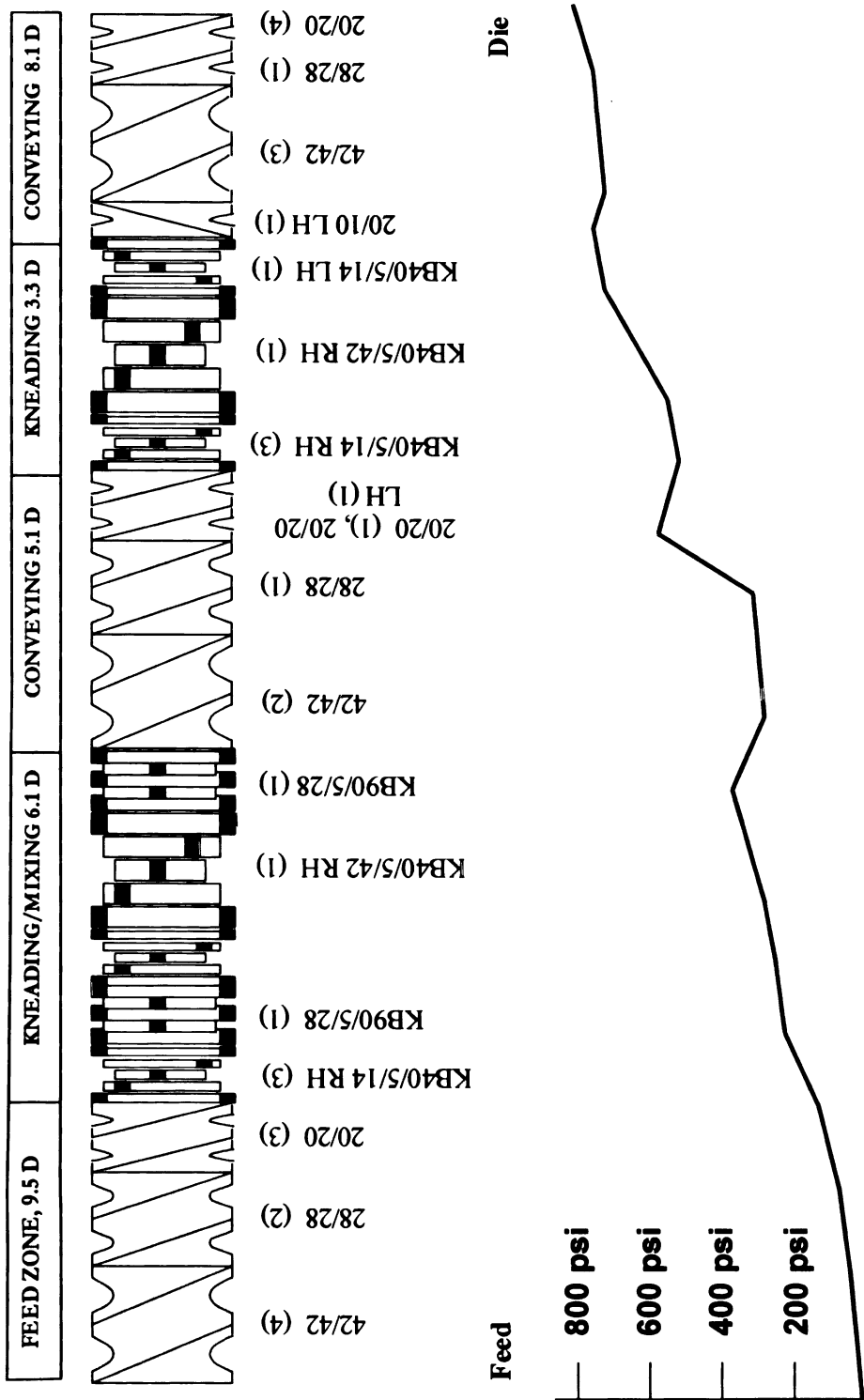


Figure 2.9 Screw Configuration with the Pressure Profile for foaming of starch.

The control starch foam density obtained using the low shear screw configuration was $52.2 \pm 2.3 \text{ kg/m}^3$, while it was $38.6 \pm 1.8 \text{ kg/m}^3$ using the medium shear screw configuration. These values were higher as compared to those reported later in the results and discussions section.

Manipulating the screw configuration is a tedious process. Hence, when a density $\sim 30 \text{ kg/m}^3$ was obtained for the control starch foams using the screw configuration reported (Figure 2.9), no further attempts were made to modify the screw configuration.

2.3.5.1 Foaming Screw Configuration

The foaming screw configuration is explained on the basis of the following zones:

2.3.5.1.1 Feed/Conveying zone

The feed zone consisted of all right-handed conveying screw elements, also called as right-handed bushings. Unlike plastic resin processing, starch tends to clog up the feed zone. Hence, four large pitch (42mm) right-handed conveying screw elements were used to quickly convey the starch and prevent build-up/clogging in the feed zone, which is a major issue in processes involving starch.

The starch, PHAE and talc were added to the feed hopper, while the water was injected through a side tube.

The elements were so arranged that their pitch reduced along the length of the screw. This was done to increase the pressure along the length of the screw, and it also helped in increasing the residence time. The increase in pressure would help in increasing the solubility of water in the thermoplastic starch melt. Density of the feed is low because of

the air trapped in the incoming granular raw material. The incoming material was compressed and the air was expelled. The water was injected in this feed zone to facilitate textural and viscosity development and to enhance conductive heat transfer. Decreasing the pitch increased the surface-to-volume ratio, thus increasing the conversion of mechanical energy to heat through friction. However, the positive pumping characteristic of these conveying elements limited the ability of the screws to effectively convert mechanical energy into heat through friction. Hence, kneading elements were added. These elements reduced the positive conveying feature and, thus, forced the extruder barrel to fill, which helps in building up pressure, which assists foaming at the die.

2.3.5.1.2 Kneading/Mixing zone

The wide-flighted dispersive kneading blocks helped break the starch granules into smaller particles. The shearing action of the wide-flighted elements, between the barrel and the flights was responsible for the break-up of the granules into finer particles. The narrow-flighted kneading blocks in this kneading zone provided better homogenizing properties, thus enhancing the blending of starch, water and the additives.

The next set of screw elements were the neutral kneading blocks, which held the material for longer and thus increased the residence time. This would further facilitate the dissolution of water in the melt, and ensure complete plasticization.

The kneading zone continued the compression started in the feeding zone, and the flow channels of the extruder achieved a higher degree of fill as a result of the compression of the extrudate. Basically, in the kneading zone, starch granules were broken down into finer particles, and the hydrogen bonds are broken down in the starch matrix by the water

molecules, resulting in a thermoplastic melt of plasticized starch. Within this zone of the extruder barrel, the extrudate began to lose its granular definition, the density began to increase and pressure began to develop in the barrel.

Within the kneading zone, the discrete particles of starch begin to agglomerate due to the increasing temperature resulting from conduction, and viscous energy dissipation.

The left-handed elements were mainly used for building up high pressures inside the extruder. They were included downstream, to build-up higher pressures than the solubility pressure.

2.3.5.1.3 Conveying Zone

This conveying zone released the built-up pressure slightly, and helped convey the plasticized starch to the next kneading zone, thus preventing a build up of material in the extruder. A left-handed bushing was introduced at the end of the conveying zone to increase the pressure, so that the resulting melt is supersaturated with water.

2.3.5.1.4 Kneading Zone

Another kneading zone was incorporated in the configuration to ensure complete homogenization of the materials, and dissolution of the water in the starch matrix. This zone was sealed on both sides by left-handed elements, thus ensuring complete mixing of the material held in the kneading zone. The extrudate formed a more integral flowing dough mass as it moved through this kneading zone and typically reached its maximum compaction. This is the zone of the extruder where the mass became amorphous and texturized. Temperature and pressure increased most rapidly in this region, as shear rates

were highest because of the screw configuration and maximum compression of the extrudate.

2.3.5.1.5 Final Conveying Zone

The last conveying zone forced the supersaturated melt through the die. Pressure, temperature, and the resulting fluid viscosity were such that the extrudate is forced from the extruder creating the desired final product texture, density and functional properties.

The nucleating sites were generated at the sudden drop in pressure at the die (21), and the supersaturated blowing agent diffuses out through the matrix, giving rise to a foamed structure.

2.4 Results and Discussion

2.4.1 Type of Corn Starch

Table 2.1 Physico-Mechanical Properties of Extruded Corn Starch Foams

No.	Type of Starch	Unit Density (kg/m ³)	Radial Expansion ratio	Specific Length (cm/gm)	Compressive Strength (Pa)	Resiliency (%)
1	Regular Corn Starch	45.8	23.3	16.4	7.6 E+05	21.9
2	Waxy Corn Starch	42.4	28.6	14.4	8.0 E+05	31.5
3	High Amylose Corn Starch	35.7	35.6	13.8	4.5 E+05	60.5
4	Hydroxy- propylated High Amylose Corn Starch	30.2	39.7	14.6	4.4 E+05	69.8

Table 2.1 shows the physico-mechanical properties of the foams obtained using different types of corn starches. The high amylose corn starch provided foam with lower density, higher expansion ratio and a higher spring index as compared to the foams obtained using the waxy corn starch and the regular corn starch (Table 2.1, Entries 1 – 3).

Due to the high level of co-operative hydrogen bonding that can occur between the essentially linear chains of amylose, little or no swelling of the granule occurs in water

and consequently, it is not possible to cook out the starch granule under normal conditions. The applications of amylose starches are rarely in the granular form, but in a dispersed state, generated by special cooking conditions using a combination of high temperature and shear. Under these conditions, the amylose chains can be separated and then allowed to re-associate under controlled conditions, finding applications as films, foams, barriers, adhesives, and a way to control the digestion of starch as a food ingredient.

In contrast, regular starch or the amylose free forms are more readily hydrated and the swollen granules provide a range of viscosity profiles, which find wide applications particularly in food.

The hydroxypropylated high amylose corn starch, however, provides foam with the best physico-mechanical properties (Table 2.1, Entries 4). Low degree of substitution (DS) hydroxyethyl- and hydroxypropyl starches behave like low-substituted starch acetates (13, 14). The effects generally increase with increasing DS; thus, the gelatinization temperature decreases. The rate of granule swelling and dispersion on cooking increases, clarity and cohesiveness of dispersion increase, and the tendency to increase in viscosity and gel on cooling and aging decreases. Hydroxyalkylation also improves the low-temperature stability and the clarity, solubility (14), and flexibility.

Further, the effect of process variables on the degree of foaming using hydroxypropylated high amylose corn starch was investigated. These process variables included the content of water, the temperature of the thermoplastic starch melt, the PHAE content, talc content, and the screw speed.

The effect of process variables on the degree of foaming was investigated. These process variables included the content of water, the temperature of the thermoplastic starch melt, the PHAE content, and the screw speed.

2.4.2 Effect of the amount of water on the Expansion Ratio (ER)

The expansion ratio and density were very sensitive functions of the amount of water injected. The ER increased with an increase in the amount of water, but beyond a certain amount, it decreased (Figure 2.10). The maximum expansion ratio was obtained when the water added is 7% of the starch used (wet basis). The inherent moisture content of the starch was 11.2%. Thus, the total moisture content of the starch in the process was 17.42%.

The maximum flow rate of water that can be injected to achieve a greater volume expansion ratio was limited by the solubility of the water in starch. When water did not completely dissolve in the starch matrix, it resulted in a non-uniform structure and much lower expansion ratio. The processing pressure should be higher than the solubility pressure to dissolve water in the starch matrix. The expansion ratio decreased with increase in amount of water, due to enhanced gas loss, as a result of increased plasticizing effect. When water dissolved in the starch matrix, the viscosity of the melt dropped as a result of the free volume increase.

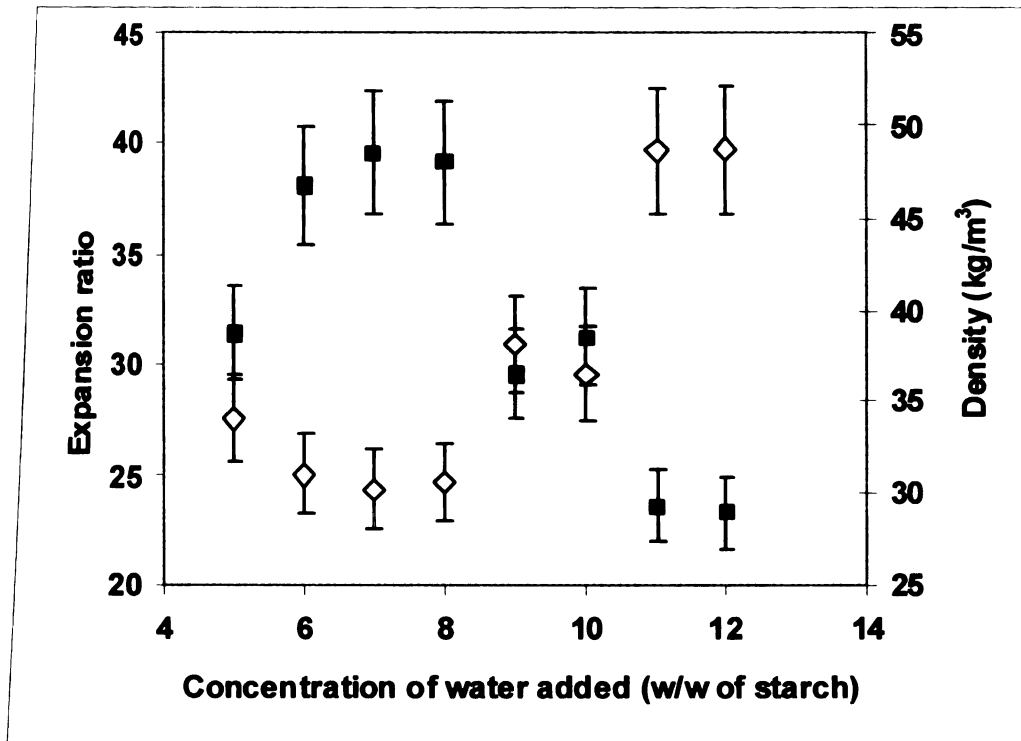


Figure 2.10 Effect of the Amount of Water used on the degree of foaming, expressed in terms of ‘ ■ ‘Expansion Ratio (ER), and ‘ ◇ ‘density at a temperature of 105°C.

The plasticizing effect increased with an increase in the amount of water injected. Similarly, the diffusivity of water in the starch matrix increased as well. Hence, the loss of moisture to the atmosphere by diffusion increased with an increase in the amount of water. Also, the use of high amount of water (>10%), led to high fluctuation of pressure in the barrel, due to which high processing pressures could not be achieved.

2.4.3 Effect of the processing (melt) temperature on the Expansion Ratio (ER):

When stabilized processing conditions were obtained by completely dissolving the injected water (blowing agent), well-expanded starch foams were achieved in a certain temperature range. The maximum expansion ratio was obtained when the melt temperature was in the range of 100°C to 110°C (Figure 2.11).

When the melt was overcooled below 90°C, the foam did not expand because the increased stiffness of the thermoplastic starch matrix was unfavorable for cell growth. Also, above 120°C, the expansion ratio was lower due to the escape of excess moisture to the environment during expansion. Thus, the foam product obtained was dry and brittle. The corresponding unit densities are shown in Figure 2.12.

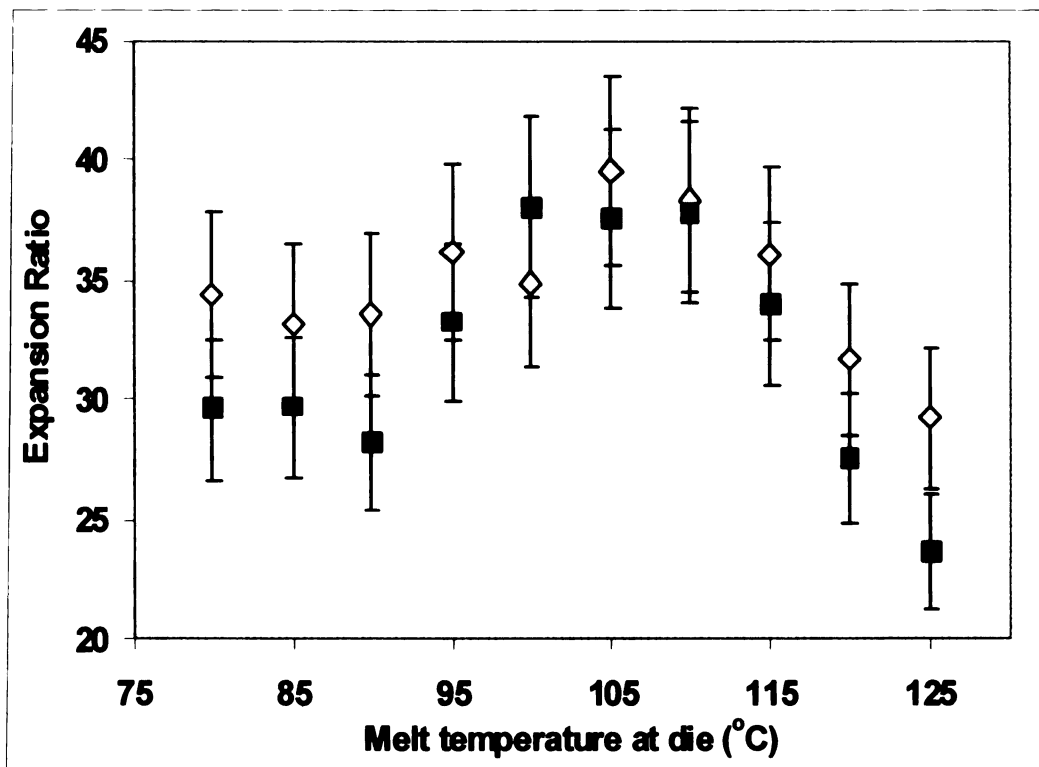


Figure 2.11 Effect of the Process Temperature on the Degree of Foaming, at two different amounts of blowing agents: ‘ \diamond ‘ 7% water (w/w starch), ‘ \blacksquare ‘ 6% water (w/w of starch).

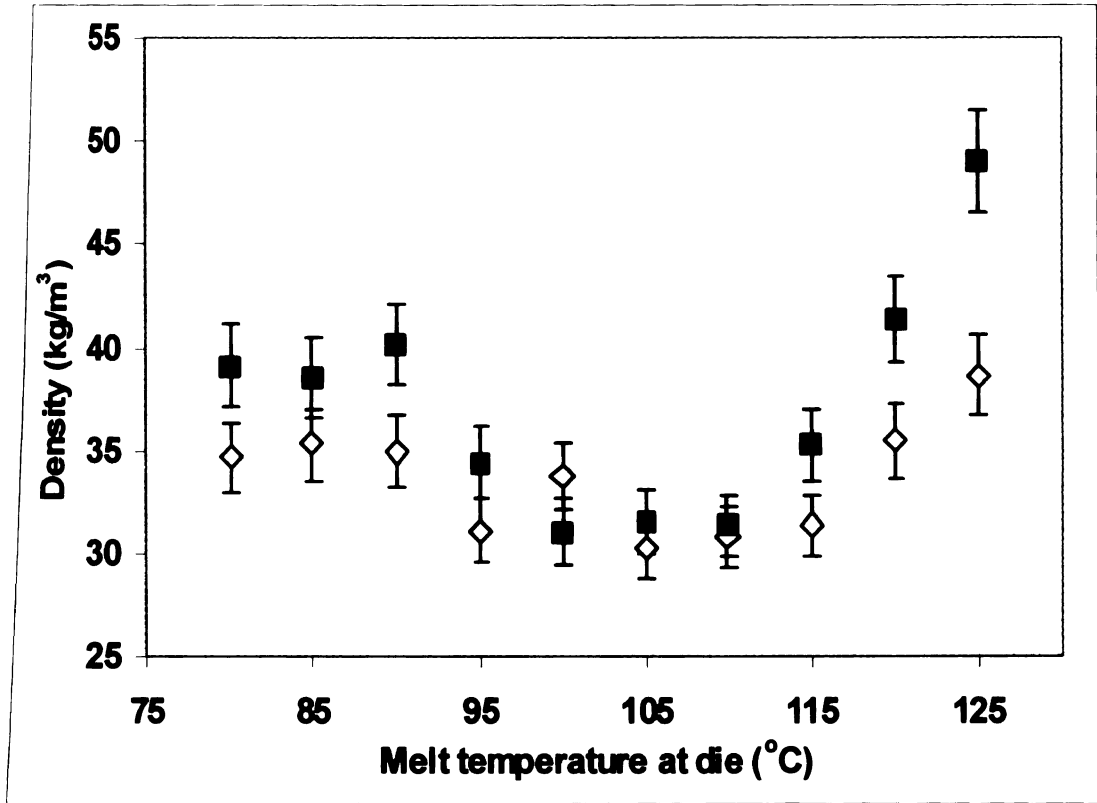


Figure 2.12 Effect of the Process Temperature on the Density, at two different amounts of blowing agents: ‘ \diamond ’ 7% water (w/w starch), ‘ \blacksquare ’ 6% water (w/w of starch).

2.4.4 Effect of PHAE on ER

PHAE is a thermoplastic epoxy based resin offered by Dow Chemicals. It offered the adhesion and durability of epoxy resins with the flexibility and processability of thermoplastic resins. When we included PHAE as an additive in our starch foam process, we obtained a foam structure with improved mechanical strength and toughness, weather and water resistance.

It was observed that the expansion ratio increased with an increase in the PHAE content, but just up to a certain level, and then decreased again. As shown in Table 2.2, the maximum ER and minimum density was obtained at a PHAE content of 7% of the starch used. The density of the starch foam was higher in the absence of PHAE. This is because thermoplastic starch did not have enough melt strength and flexibility to support the expansion. This led to the rupture of cell walls and the surface of starch foams leading to the loss of water. The presence of a flexible polymer like PHAE, which is compatible with starch helped support foam expansion, and gave rise to a uniform cell size and structure, and hence a lower density material. However, at a higher PHAE content (greater than 7% PHAE), the foam density increased marginally.

This was due to the fact that the pressure developed at the die was lower due to a reduction in melt viscosity of the extrudate. The die pressure was 5.4 ± 0.2 MPa in the absence of PHAE, while it was 5.0 ± 0.13 MPa and 4.4 ± 0.1 MPa in the presence of 7% and 15% PHAE, respectively.

Table 2.2 Effect of PHAE content on Physico-Mechanical Properties of Starch Foams.

Processing Aids	Unit Density (kg/m ³)	Radial Expansion ratio	Specific Length (cm/gm)	Compressive Strength (Pa)	Resiliency (%)
Control (Hydroxypropylated High Amylose Corn Starch)	30.19	39.65	14.59	4.36E+05	69.8
3.0 % PHAE	25.28	41.28	16.73	3.49E+05	90.9
5.0 % PHAE	24.23	41.76	17.25	3.39E+05	91.9
7.0 % PHAE	22.56	43.86	17.64	3.12E+05	93.5
10.0 % PHAE	24.31	39.60	18.14	3.35E+05	92.7
15.0 % PHAE	24.95	36.36	19.24	3.64E+05	92.9

A more detailed study on the shear viscosities of the starch-based melts using PHAE in the extruder, and its effect on foaming, will be reported later (Chapter 4). At higher PHAE concentrations, the expanded foams contracted after reaching a maximum radial expansion, leading to lower expansion ratios. This contraction resulted in higher densities. This contraction may be due to a cooling rate not rapid enough to prevent cell collapse, as suggested by Willett et al. (22). With an increase in PHAE concentration, the specific length (cm/gm) increased too, implying an improvement in flow properties.

2.4.5 Effect of nucleating agent (talc) content on ER:

The addition of talc gave rise to a compact and more uniform cell structure. The density increased slightly due to the compactness of the foam. The talc content was varied from 0.5% to 2% of the starch used. As shown in Figure 2.13, the maximum ER and minimum density is obtained at a talc content of 0% of the starch used. However, we have used 1% talc in our studies to obtain a more uniform cross-section of foams, and with a higher percentage of closed-cells.

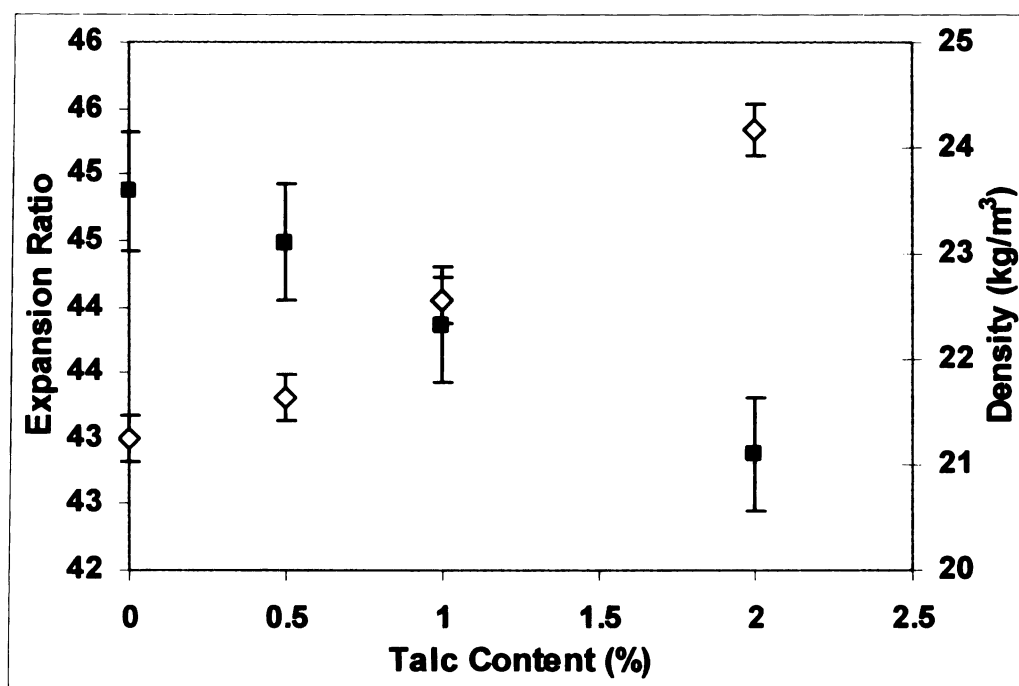


Figure 2.13 Effect of the Amount of Talc used on the degree of foaming, expressed in terms of the ' ■ ' Expansion Ratio (ER), and ' ◇ ' density at a temperature of 105°C, and inlet water concentration of 7% (dry basis).

Figures 2.14 – 2.17 show the scanning electron micrographs of the foam cross-section at various talc contents. The cell size decreases from about 500 μm to about 200 μm , as the talc content is increased from 0% to 2%.

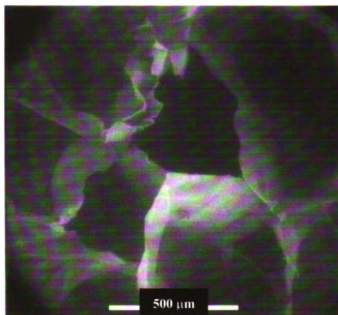


Figure 2.14 ESEM of the starch foam cross-section (0% talc)

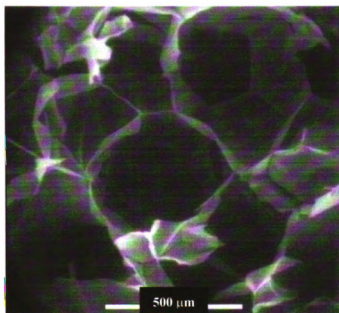


Figure 2.15 ESEM of the starch foam cross-section (0.5% talc)

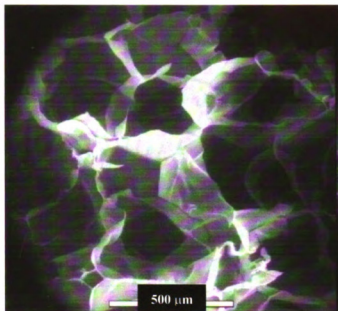


Figure 2.16 ESEM of the starch foam cross-section (1.0% talc)

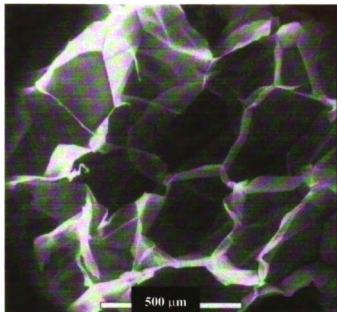


Figure 2.17 ESEM of the starch foam cross-section (2.0% talc)

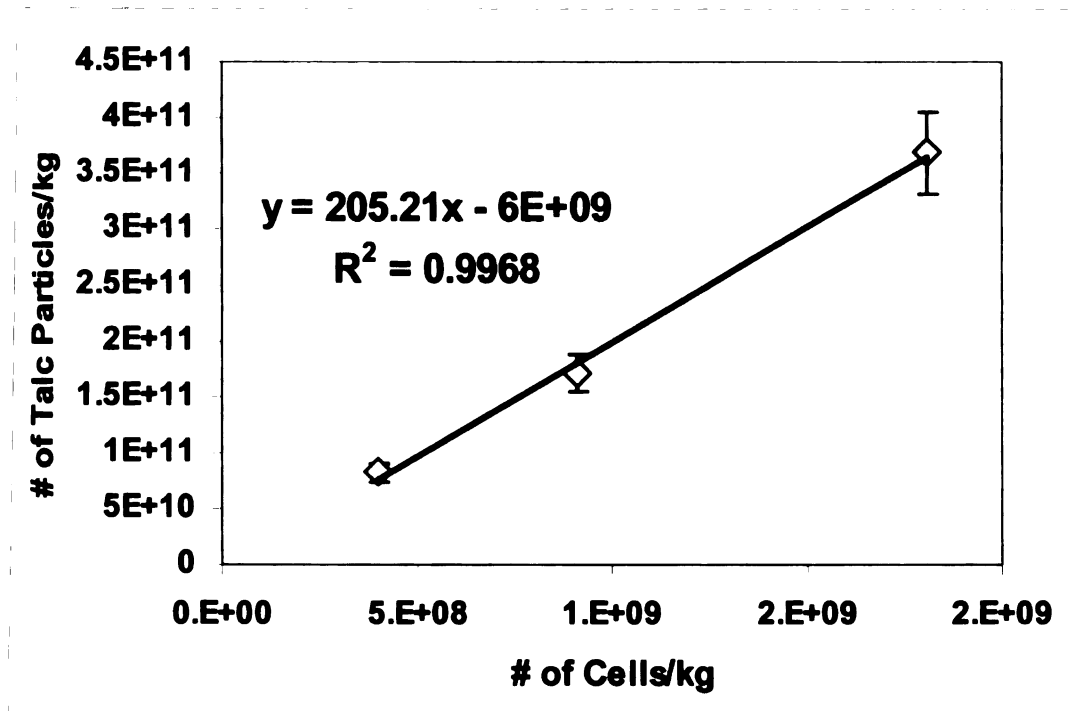


Figure 2.18 Number of talc particles involved in forming a cell.

Figure 2.18 shows that a strong linear function exists between the number of talc particles present per kg of the foam sample to the number of cells formed in the same amount of foam. Each talc particle would form a nucleating site, and it suggests that approximately 200 such nucleating sites formed coalesce to form a single cell in the foam.

Figure 2.19 shows that the calculated unit foam density (kg/m^3) is also a strong linear function of the cell density (Number of cells/ m^3), which in turn is a function of the talc content added.

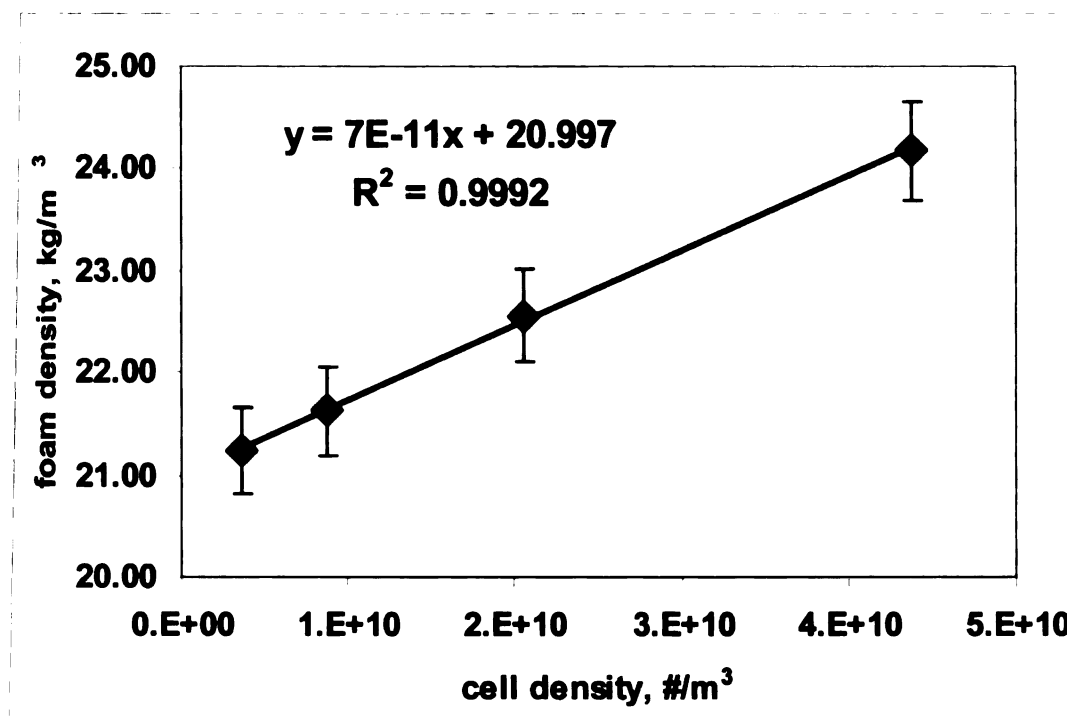


Figure 2.19 Unit Foam density as a function of Cell Density.

2.4.6 Effect of screw speed on the expansion ratio (ER)

Screw speed directly affected the degree of barrel fill, and hence the residence time distribution and the shear stress on the material being extruded. From Figure 2.20 below, it was observed that there was no significant variation in the densities and the expansion ratios of the starch foams at screw speeds varying from 200 rpm to 250 rpm. There was a marginal decrease in density at higher screw speeds. However at screw speeds lower than 175 rpm, the density increased considerably. Thus, screw speeds in excess of 175 rpm were normal. Figure 2.20 also shows that at higher screw speeds, the expansion ratio decreased too with a reduction in density. This implied a substantial increase in the

specifi

creatin

factors

At the

speed

by the

not ch

starve

Howe

comp

with

the so

also

specific length of the product. At these speeds, significant frictional heat was generated creating starch-melting phenomena with a reduction in the viscoelastic nature. One of the factors in determining the maximum volumetric output of the extruder is the screw speed. At the same starch feed rate, the torque loading on the motor is higher at lower screw speeds. Thus, the volumetric output at which we can process the starch foams is limited by the screw speed used. It is worth noting that a change in screw speed, however, would not change the volumetric throughput of the extruder since the twin-screw extruders are starve-fed. Also, the pressure developed at the die was lower at lower screw speeds. However, at higher screw speeds, there was an increase in wear rate of mechanical components such as screws and barrels. The specific mechanical energy also, increased with an increase in screw speed, and leveled off at higher screw speeds (Figure 2.21). As the screw speed increased, the apparent melt viscosity can be assumed to decrease, which also decreased the net power input via viscous dissipation.

Expansion Ratio

F
te
W

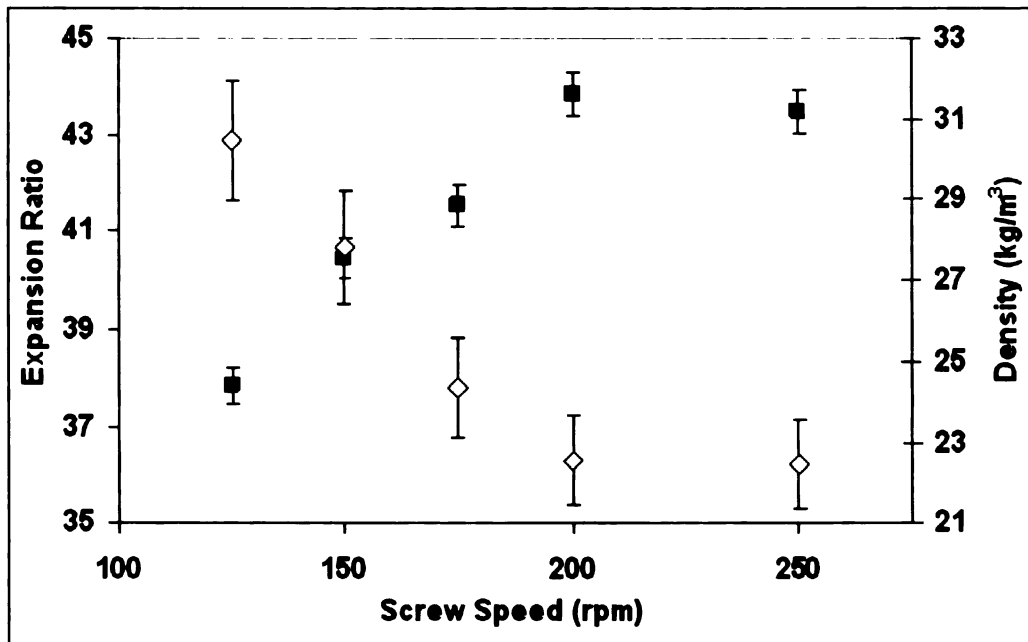


Figure 2.20 Effect of the Screw Speed on the degree of foaming, expressed in terms of ‘ ■ ’ Expansion Ratio (ER), and ‘ ◇ ’ density at a temperature of 105°C, inlet water concentration of 7% (Starch, wet basis), and PHAE content of 7% (Starch, wet basis).

A
S
E
V
C

Fig

a

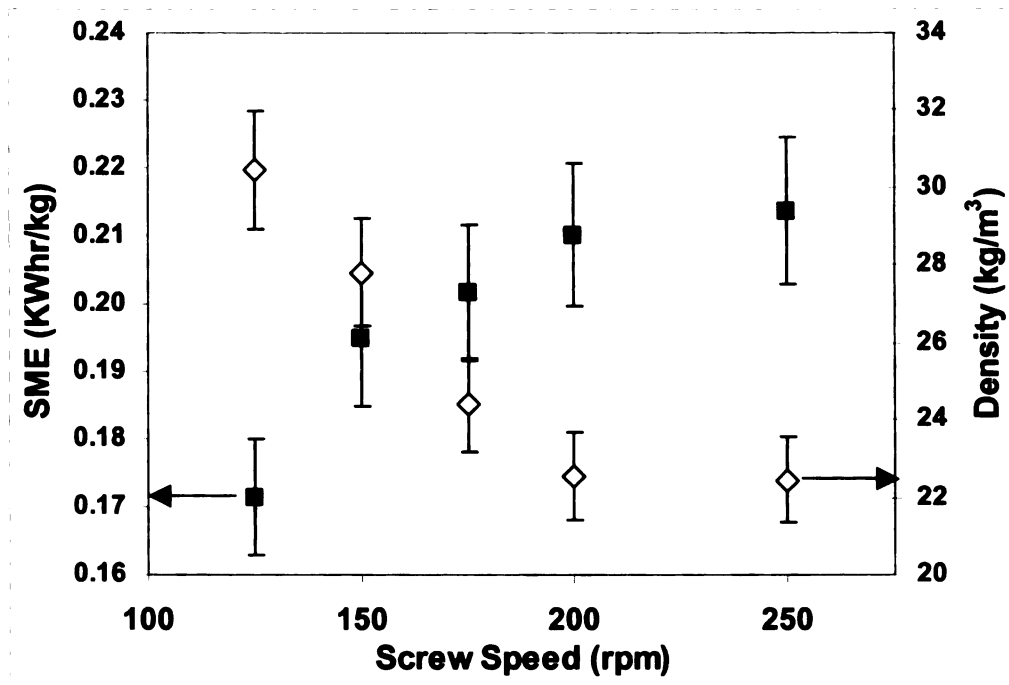


Figure 2.21 Effect of the Screw Speed on the ‘ ■ ’ Specific Mechanical Energy; and ‘ ◇ ’ Density at a temperature of 105°C, inlet water concentration of 7% (Starch, wet basis), and PHAE content of 7% (Starch, wet basis).

2.4.7 Compressive Strength and Resiliency

The compressive strength and resiliency of the foam samples is listed in Table 2.2. Typically, a power-law relationship is observed between compressive strength σ_c and foam density ρ ($\sigma_c \sim \rho^n$). Denser foams tend to have thicker cell walls and hence resist deformation better than lower density foams with thinner cell walls. A strong relation existed between foam density and compressive strength (Figure 2.22). The regression line in Figure 2.22 was drawn using the data from Table 2.2, and a slope of 1.15 was obtained ($n = 1.15$). A value of $n = 0.92$ was obtained by Willett et al. (22), while Hutchinson and co-workers (23) reported exponents of 1.5 – 1.6 for compressive strengths of foams prepared from maize grits.

The addition of PHAE improved the resiliency considerably from 69.7% (Control) to 93.5% at a PHAE content of 7% of the starch used.

2.4.8 Moisture Sorption Analysis

Starch foams gain weight as well as shrink in the presence of moisture. This gain in weight and the dimensional stability of the starch-based foams is important in packaging applications. The lower the loss in dimensions, the better is the dimensional stability. Table 2.3 shows the normalized steady state weight gains and dimensions of the starch foams (varying PHAE content) respectively. The hydrophobic behavior of the starch-based foams improved with an increase in the PHAE content. The hydroxypropylated high amylose starch foams gained about 13% of their original weight (time, $t = 0$), while shrinking by about 50% of their original length and diameter in the absence of PHAE. At the optimum PHAE content of 7%, the starch foams gained about 8% of the original

weight, while shrinking by about 20% of their original dimensions. This was as a result of the high water-barrier properties of PHAE.

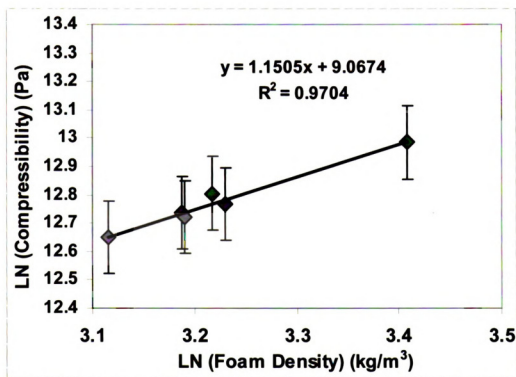


Figure 2.22 Logarithmic plot of Compressive Strength (Pa) as a function of foam density (kg/m³).

Table 2.3 Normalized Steady State Weight Gains, Diameters, Lengths of the Starch-based Foams with different PHAE contents

PHAE Content (%)	Normalized Steady State Weight Gain $\left[\frac{W - W_0}{W_0} \right]$ (± 0.024)	Normalized Steady State Diameter $\left[\frac{D}{D_0} \right]$ (± 0.034)	Normalized Steady State Length $\left[\frac{L}{L_0} \right]$ (± 0.038)
0.0 %	0.128	0.564	0.498
3.0 %	0.109	0.731	0.702
5.0 %	0.092	0.780	0.746
7.0 %	0.078	0.844	0.811
10.0 %	0.058	0.887	0.861
15.0 %	0.036	0.936	0.921

2.4.9 Cell size/structure

Figures 2.23 and 2.24 show the surface of the starch foam sheets without and with 7% PHAE respectively. PHAE provided a finer and a more stable surface preventing the rapid loss of moisture through the surface. This is probably due to the surface migration of a fraction of PHAE added during the production of starch foams, which is in good agreement with the results obtained with PHEE (22).

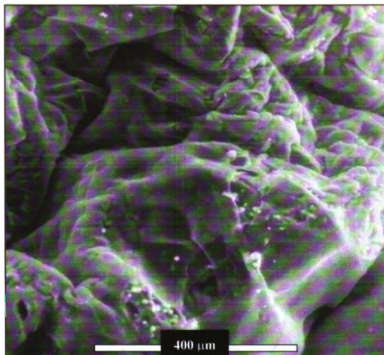


Figure 2.23 ESEM of the starch foam surface (0% PHAE)

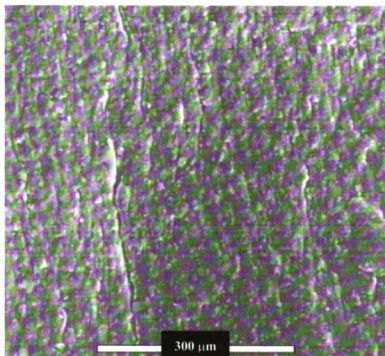


Figure 2.24 ESEM of the starch foam surface (7.0% PHAE)

2.5 Conclusion

Cylindrical starch foam shapes were produced on a small scale (~ 11-12 kg/hr) Werner Pfleiderer ZSK - 30 Twin Screw Extrusion (TSE) process using water, which functions as a plasticizer as well as a blowing agent. The properties of the starch foams depend on the type of starch used (hydroxypropylated high amylose corn starch, 70% amylose), the amount of water and additives (poly (hydroxy aminoether)) (PHAE) used, and extrusion conditions such as temperature and the screw configuration. PHAE offered the adhesion and durability of epoxy resins with the flexibility and processability of thermoplastic resins. PHAE was successful in imparting mechanical strength and toughness, cell integrity, weather and water resistance to the foam structure. The purpose of this work was to study the effects of the extrusion (melt) temperature, amount of water added and the screw configuration on the density of starch foams. A match of material properties with process engineering conditions was achieved to facilitate the control of expansion to a structure with valuable commercial properties. The effects of processing conditions on the foaming process were studied using a Werner Pfleiderer ZSK - 30 Twin Screw Extruder (TSE). The optimum temperature, blowing agent content, and PHAE content were determined. The density of the cylindrical foam extrudates obtained was 22-25 kg/m³. The screw configuration, temperature and pressure profiles, additives affected the morphology, Expansion Ratio, resilience and compressibility of the product. The following Chapter 3 deals with the study of the influence of input variables such as the starch feed rate, screw speed, moisture content, and the PHAE feed rate on the process variables such as pressure, torque and the specific mechanical energy of the system.

2.6 References

- 1) <http://www.opta-food.com/access/starch2.html>
- 2) Manners, D.J. Carbohydrate Polymers, 11, 87, 1989.
- 3) Morrison, W.R., Tester, R.F., Gidley, M.J., Karkalas, J. Carbohydrate Research, 245, 289, 1993.
- 4) Zobel, H. F. Starch, 40, 44, 1988.
- 5) Van Soest, J. J. G., Hulleman, S. H. D., D. de Witt, Vliiegenthart, J. F. G., Industrial Crops and Products, 5, 11, 1996.
- 6) Evans, I. D., Haisman, D. R. Starch, 34, 224, 1982.
- 7) Donovan, J. W. Biopolymers, 18, 263, 1979.
- 8) Van Soest, J. J. G., D. de Witt, Tournois, H., Vliiegenthart, J. F. G. Carbohydrate Research, 1995.
- 9) Lay, G., Rehm, J., Stepto, R. F., Thoma, M., Sachetto, J-P., Lentz, D. J., Silbiger, J. US Patent 5,095,054, 1992.
- 10) Lacourse, N. L.; Altieri, P. A. US Patent 4,863,655, 1989.
- 11) Lacourse, N. L.; Altieri, P. A. US Patent 5,035,930, 1991.
- 12) Lacourse, N. L.; Altieri, P. A. US Patent 5,043,196, 1991.
- 13) Whistler, R. L. Starch: Chemistry and Technology; Second Edition, Whistler, R. L, Ed., Academic Press, Chapter X, 1984.
- 14) Rutenberg, M. W. Starch Derivatives: Production and Uses, Rutenberg, M. W., Ed., Academic Press, New York, 1984.
- 15) Heinemeyer, B. W., Tatum, S. D. US Patent 4,612,156, 1986.
- 16) Winkler, M. S., Berry, T. S., Kirkpatrick, D. E. US Patent 6,365,079, 2002.
- 17) Silvis, C. H., White, J. E. US Patent 5,275,853, 1986.
- 18) American Standard Test Methods, 2002. Standard Practice for Conditioning Containers, Packages, or Packaging Components for Testing. In: Annual Book of ASTM Standards. D – 4332, 15.09, Philadelphia, PA.

- 19) American Standard Test Methods, 2002. Standard Test Methods for Flexible Cellular Materials Made From Olefin Polymers. In: Annual Book of ASTM Standards. D – 3575, 8.02, Philadelphia, PA.
- 20) Tatarka, P. D.; Cunningham, R. L. Journal of Applied Polymer Science, 67, 1157, 1998.
- 21) Coleman, E. A. Proceedings of SPE Foams 1999 Conference, New Jersey, 173-183, 1999.
- 22) Willett, J. L.; Shogren, R. L. Polymer, 43, 5935, 2002.
- 23) Hutchinson, R. J., Siodlak, G. D. E., Smith, A. C. Journal of Materials Science, 22, 3956-3962, 1987.

TRANSIENT MODELING OF STARCH FOAM PROCESS TO DEVELOP CONTROL STRATEGIES

3.1 Abstract

The starch foam extrusion process was modeled as a Multiple Input Multiple Output (MIMO) process, and the dynamics of the process were studied as a response to step changes in the input variables such as starch feed rate, screw speed, moisture content and poly(hydroxy aminoether) (PHAЕ) feed rate. The responses were modeled as first order responses with a time delay. The linearity of the process was determined over a range around the set-point, and the parameters defining the first order system such as Gain ' K ', Time Constant ' τ ', and Dead time ' t_d ' were determined in the linear range. The transfer function models can then be used in a predictive computer control system for on-line fine-tuning of the operating conditions. This could ensure a consistently high quality product even when low frequency disturbances are present in the system. It was observed that the time constants and the dead times recorded for both the pressure and torque responses did not exhibit significant variation within each manipulated or input variable tested, indicating a dynamic linearity with respect to each manipulated variable. It was also observed that for the same step-input variations in the manipulated variables, the torque loading on the twin-screw extruder exhibited a faster response (lower dead time), and also reached a steady state sooner (lower time constant). The moisture content and screw speed seem to be the most destabilizing variables since they induce rapid responses

in the process variables. The moisture content in the extruder was, hence, determined to be the most influential factor in the stability of the process followed by screw speed and starch feed rate. PHAE feed rate was the least significant variable.

Multiple step-input tests were carried out in order to determine the validity of the principle of superposition. The validity of the principle of superposition implied the linearity of the process in the domain tested.

3.2 Introduction

Starch extrusion processes are multiple input, multiple output (MIMO) complex systems. Harper (1) gave a detailed description on the mechanics of extrusion. The phenomenon of starch foaming involves the physicochemical properties of starch, which are modified during extrusion. The rheological properties of the starch plastic are in turn reliant on these physicochemical properties (2), which affect the quality attributes of the foamed product.

Emphasis in starch extrusion research has focused on developing models to describe the complex processes in an extruder, predict some of the changes that occur, and aid in new process development (3). The control of such processes is directly linked to economic, qualitative and scientific interests. As far as control is concerned, the process has to be modeled. Different approaches, which are roughly of two types, have been used to model extrusion processing: white-box modeling, and black-box modeling (4). White-box modeling requires as much knowledge as possible in order to incorporate all the internal laws (physical, chemical, biological), which rule the system. The result is that all the coefficients of the model may have a physical significance. However, a complete description, including temperature effects, non-Newtonian rheology, and dynamics, is

indeed complicated and therefore, simplifying assumptions are usually made. Also, to truly simulate the extrusion process, thermal and physical model parameters must be determined for each particular product and extruder-die combination. On the other hand, black-box modeling means that the model is empirical, reduced to a simple mathematical relationship between the inputs and outputs of the process. Such models are valid only over a definite range of experimental conditions, but they are often adequate to develop process control strategies. Concerning food extrusion, three different techniques of black-box modeling have been implemented: Residence Time Distribution (RTD), Response Surface Analysis (RSA) and Dynamical Identification (5). Janssen (6) and Martelli (7) presented engineering analyses of a twin-screw extrusion process, including discussions on residence time distribution (RTD), melting mechanisms, power consumption, and operating characteristics of twin-screw extruders. RSA has been used by several researchers (8 – 12) for the optimization of extrusion processing. This approach enabled correlation of the important processing variables to product quality without an engineering model. Results were generally limited to the experimental conditions because of the non-linear response of the internal state of the extruder to externally manipulated variables such as screw speed, moisture and feed rate. They have especially been used to establish static relationships.

A basic modeling technique applied to extrusion processing is transfer function modeling from input/output data. Several researchers have studied the dynamic modeling and control of extrusion processes, based on their gross dynamic input-output behavior (13 – 20).

In the previous chapter, we have reported on the twin-screw extrusion production of starch foams using poly(hydroxy aminoether) (PHAE) as the functional aid, as well as on the optimization of the process (21). In this chapter, the dynamic response of various process variables of a twin-screw extrusion starch foaming process or the sensitivity of the process parameters to the change in inputs were studied, both of which must be known for the implementation of process control. The dynamic characteristics are obtained with step tests on four independent extrusion operating variables: starch feed rate, moisture content, screw speed and PHAE feed rate. The response is monitored on the following outputs: melt pressure; melt temperature and specific mechanical energy (SME). The corresponding system and its relevant manipulated, process and product variables are shown in Figure 3.1.

3.3 Experimental Section

3.3.1 Experimental Design

The experimental setup used in this study was a twin-screw extrusion system. The twin-screw extrusion system consisted of an extruder driver with a speed control gearbox, a ZSK-30 twin-screw co-rotating extruder with a screw diameter of 30 mm, an L/D of 32, a positive displacement pump for injecting water into the extruder, accurate single-screw feeders for feeding starch and PHAE. This specific screw configuration was selected to get the best physico-mechanical properties based on our previous work (21), and is reported in the Chapter 2. A cylindrical filament die 2.7 mm in diameter and 8.1 mm in length, with a cooling sleeve was assembled to the extruder. The sensors were mounted on the die to measure the temperature and pressure of the melt.

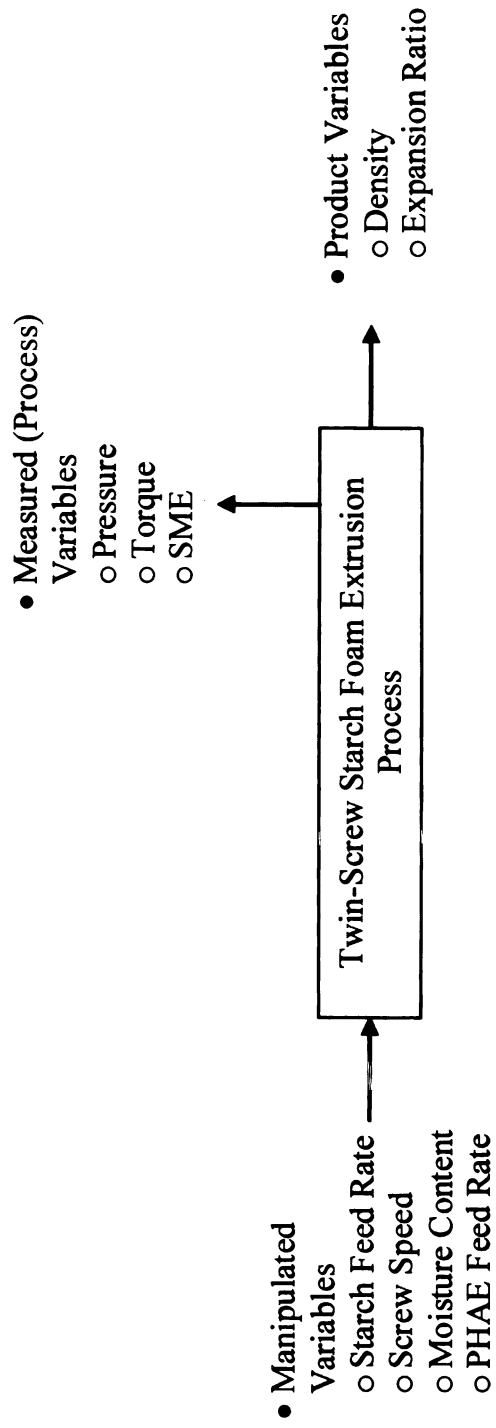


Figure 3.1 Control, Process and Product Variables of the Extrusion System.

The dynamical behavior of the process was studied through the following outputs: melt pressure (P) and melt temperature (T). The Specific Mechanical Energy (SME) was calculated using the following formula:

$$SME = \frac{kW \times Torque \times \frac{RPM_a}{RPM_r}}{\dot{m}} \quad (3.1)$$

SME = Specific Mechanical Energy (kW-hr/kg)

kW = Rated motor power (kW)

Torque = Motor Load (decimal)

RPM_a = actual screw speed

RPM_r = rated screw speed

m = Mass flow rate (kg/s)

The experiments consisted of different sequential variations around the following central set point²⁵: starch feed = 11.16 kg/hr, moisture content = 17.42% (w/w) on an overall basis, screw speed = 200 rpm, PHAE feed = 0.78 kg/hr. Its corresponding response variables are process temperature, T = 105°C, pressure at the die, P = 720 psi, SME = 0.21 kW-hr/kg (Torque loading = 72%). The experimental design for the single input variation runs is shown in Figure 3.2.

Each ‘forward step test’ for always succeeded by a ‘back step test’ in order to let the process return to its original set point. The forward and back steps gave approximately the same results suggesting that probably there is negligible hysteresis.

In order to get significant and comparable outputs, the overall range of stimulation imposed on each control variable was set according to the pre-estimated gain of that variable. At steady state (set point), a step test was performed on either one or multiple

input variables. Once the output variables reached a steady value, the study was reduced to a static comparison between the output $Y(t)$ and the input $U(t)$, i.e., to the gain K .

$$K = \frac{DY(t)}{DU(t)} \quad (3.2)$$

To compare the different steady state gains, it is possible to define a relative steady state gain K_R , where:

$$K_R = \frac{\left[\frac{DY(t)}{Y(t)} \right]}{\left[\frac{DU(t)}{U(t)} \right]} \quad (3.3)$$

3.3.2 Linearity

It is important to assess the linearity or non-linearity of a process, as it helps to understand and predict its response to any variation in input. The hypothesis of linearity is an implicit and necessary prerequisite to most of the classical techniques of process control. A linear system must exhibit a constant steady state gain, whatever the magnitude of step test applied.

3.3.3 Dynamic (Transient) Responses

Once a step-input variation in the starch feed rate, screw speed, moisture content and PHAE feed rate was made (time, $t = 0$), the Pressure and Torque readings were manually recorded every 5 seconds until a steady state was reached. A common assumption in many time series techniques is that the data are stationary. A stationary process has the property that the mean, variance and autocorrelation structure do not change over time. These conditions were too drastic for these experiments as the measurements of process variables were very noisy. It was assumed that the process would become stationary and,

by graphical estimation, the time required to reach each steady state was calculated approximately.

3.3.4 Multiple Input Tests

Some multi-input experiments were carried out by performing step tests simultaneously on multiple manipulative variables. The principle of superposition was verified for multiple step input tests, within the linear domain. If the principle of superposition is satisfied, it implies that the system is linear within the domain tested. The variation of the process variables, namely, pressure, torque and the SME in response to the multi-variable input step tests were measured at steady state. Pressure, Torque and SME were also calculated theoretically, using a linear combination (principle of superposition) of the steady state gains previously determined by single input step tests. The following formula was used:

$$DY = K_{Starch\ Feed}D(Starch\ Feed) + K_{Screw\ Speed}D(Screw\ Speed) + K_{MC}D(MC) + K_{PHAЕ}D(PHAE) \quad (3.4)$$

Where:

Y – Pressure/Torque/SME.

These experiments were conducted to verify if the linearity observed on each variable could be extrapolated through an additive law to a multivariate control. The values of Pressure, Torque, and SME obtained for the multiple-input tests were fit to a model deemed appropriate, using STAT-EASE ‘Design of Experiments 6.0’ modeling software.

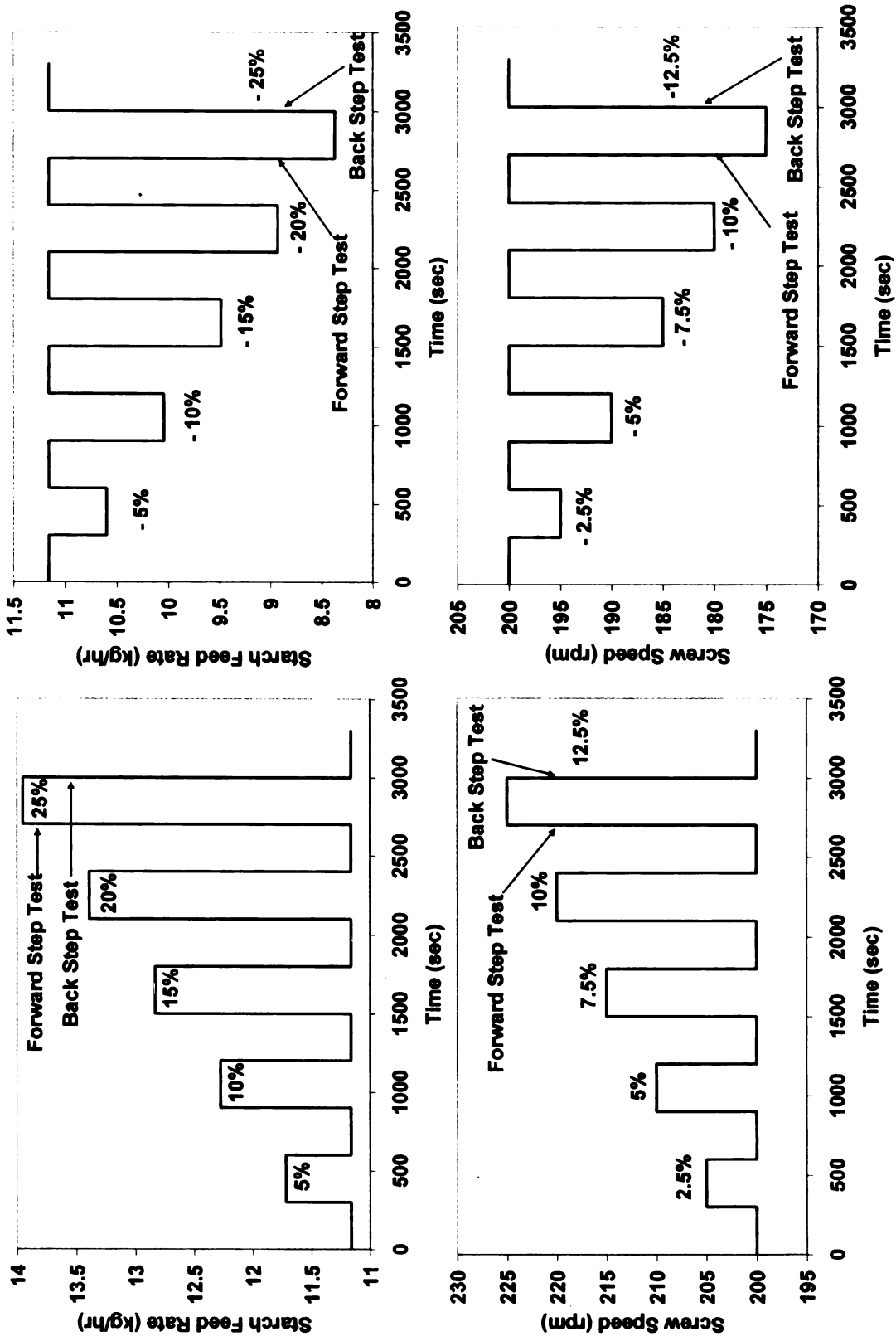


Figure 3.2 Experimental Design

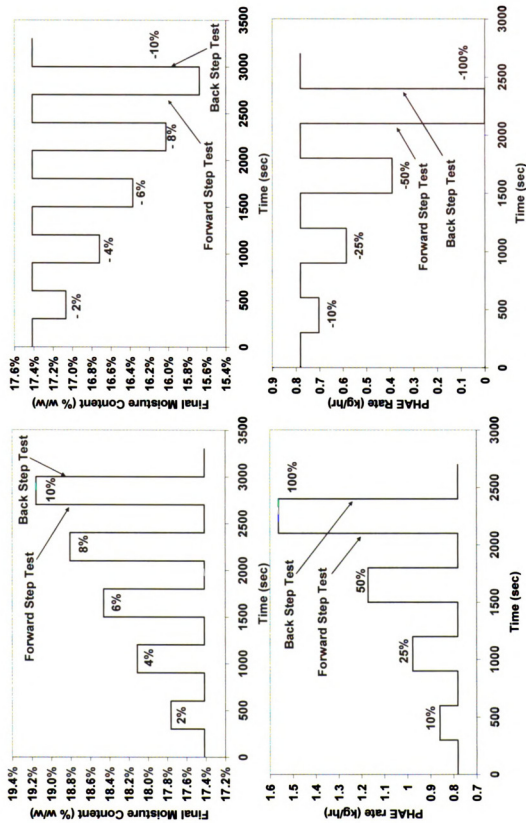


Figure 3.2 Experimental Design (Continued)

A central composite Response Surface experimental design (22) was employed to investigate the influence of step-changes in the starch feed rate, screw speed, moisture content and the PHAE feed rate on the process variables (pressure, torque and SME), which further govern the foam product functionalities (density, expansion ratio and resilience). Regression analyses were employed to fit the experimental data to linear polynomials (23). In these experiments conducted, the extruder almost always verified the conditions, which postulate that a bounded variation of the input induces a bounded variation of the output (BIBO stability). This means that, for and around the set point selected, the extruder remains far away from any uncontrollable change that could lead to an over-torque, or an over-pressure, and consecutively to a blockage of the screws (shutdown).

3.4 Results and Discussion

3.4.1 Step-Input Variations in the Starch Feed Rate

The absolute (K) and relative (K_R) steady state process gains for step-input variations in the starch feed rate are shown in Table 3.1. For the range of the tested set points, the melt temperature T was hardly sensitive to the variations in starch feed rate because feed variations induce tiny variations in self-heating. The self-heating would be as a result of the shear imposed on the extruding material (viscous dissipation). The set temperature at the die was 105°C. The maximum temperature rise was 2°C for a 25% increase in starch feed. Similarly, the temperature decreased with a decrease in starch feed rate (though

negligible). Hence, the values of G_R for this variable were positive. The temperature decreased by just 1°C for a 25% decrease in starch feed.

The melt pressure P , however, displayed significant variations due to an increase/decrease in the starch feed rate. The increase in P with the starch feed would be basically due to an increase in the filling ratio, and vice-versa. Thus, the values of K_R for this variable were positive. It was observed that the relative gains varied with the magnitude of the step test, and they increased as the size of the step change increased. Also, the values of the gains were different for the positive tests and the negative tests.

An increase in the starch feed rate lead to an increase in the motor load (torque) on the extruder drive, since a larger amount of material was being processed. The SME increases with an increase in the torque on the motor, while decreases with an increase in the starch feed rate. The net result was a decrease in the value of SME. On the other hand, a decrease in the starch feed rate gave lower values of torque, and finally a higher value of SME. Thus, the values of K_R for this variable were negative. Also, it was observed that the relative gains decreased with an increase in the magnitude of the step size.

Table 3.1 Steady State Process Gains for Step-Input Variations in the Starch Feed Rate.

No.	Step	K_T	K_{RT}	K_P	K_{RP}	K_{Torque}	K_{RTorque}	K_{SME}	K_{RSME}
	Change in								
	Starch Feed								
	Rate								
1	- 25.00 %	0.4	0.04	62.7	0.97	0.06	0.93	0.000	-0.01
2	- 20.00 %	0.4	0.05	57.3	0.89	0.06	0.93	0.000	-0.01
3	- 15.00 %	0	0	50.8	0.79	0.06	0.89	-0.001	-0.06
4	- 10.00 %	0	0	38.5	0.60	0.06	0.88	-0.001	-0.07
5	- 5.00 %	0	0	32.3	0.50	0.06	0.86	-0.002	-0.08
6	+ 5.00 %	0	0	17.9	0.28	0.06	0.89	-0.001	-0.05
7	+ 10.00 %	0	0	39.4	0.61	0.06	0.89	-0.001	-0.05
8	+ 15.00 %	0.6	0.06	47.8	0.74	0.06	0.93	0.000	-0.01
9	+ 20.00 %	0.9	0.1	60.5	0.94	0.06	0.92	0.000	-0.01
10	+ 25.00 %	0.7	0.08	68.1	1.06	0.06	0.93	0.000	-0.01

3.4.2 Step-Input Variations in the Screw Speed

The absolute (K) and relative (K_R) steady state process gains for step-input variations in the screw speed are shown in Table 3.2. Similar to the results observed for changes in the starch feed rate, the changes in temperature due to changes in screw speed were negligible, with the T changing by $\pm 1^\circ\text{C}$ with an increase/decrease in screw speed respectively. These changes were due to an increase/decrease in the viscous dissipation associated with material being worked between the screws and the barrel.

An increase in screw speed lead to a decrease in pressure due a decrease in the viscosity of the melt due to increased shear (equation), and vice versa. Thus, the values of K_R for this variable were negative. Also, it was observed that the values of the relative gains were almost constant over the range studied, indicating the possibility of linearity. Unlike the trend observed earlier in step changes in the starch feed rate, the values of K_R decreased with an increase in the magnitude of step size.

An increase in the screw speed decreased the torque, while both have opposing effects on the SME. The net result was a decrease in the SME, giving a negative value for K_R . Similarly, the torque increased with a decrease in the screw speed, finally resulting in an increase in the SME, giving negative values for K_R again.

**Table 3.2 Steady State Process Gains for Step-Input Variations in the Extrusion
Screw Speed.**

No.	Step Change in Screw Speed	K_T	K_{RT}	K_P	K_{RP}	K_{Torque}	K_{RTorque}	K_{SME}	K_{RSME}
1	-12.50%	0.04	0.08	-2.9	-0.80	-0.005	-1.47	0.000	-0.28
2	-10.00%	0.00	0	-2.8	-0.78	-0.006	-1.54	0.000	-0.39
3	-7.50%	0.00	0	-2.8	-0.78	-0.005	-1.52	0.000	-0.40
4	-5.00%	0.00	0	-2.9	-0.81	-0.005	-1.50	0.000	-0.43
5	-2.50%	0.00	0	-3.2	-0.89	-0.006	-1.56	-0.001	-0.52
6	+ 2.50%	0.00	0	-3.8	-1.06	-0.006	-1.67	-0.001	-0.71
7	+ 5.00%	0.00	0	-3.5	-0.97	-0.006	-1.56	-0.001	-0.63
8	+ 7.50%	0.07	0.13	-3.5	-0.98	-0.005	-1.46	-0.001	-0.57
9	+ 10.00%	0.05	0.10	-3.3	-0.92	-0.005	-1.31	0.000	-0.44
10	+ 12.50%	0.04	0.08	-3.2	-0.88	-0.004	-1.21	0.000	-0.36

3.4.3 Step-Input Variations in the Moisture Content (% MC)

The absolute (K) and relative (K_R) steady state process gains for step-input variations in the % MC are shown in Table 3.3. For the three process variables, T, P and SME; the variations in moisture content induced greater responses than the variations in starch feed rate and the screw speed.

It was observed that the temperature decreased by 3°C with only a 10% increase in the moisture content, and it increased by 2°C with a 10% decrease in MC. This resulted in higher values of K_R as compared to those reported earlier for the step tests in screw speed and the starch feed rate.

Also, the pressure and SME values varied inversely with step changes in the moisture content. A decrease in MC lead to an increase in the viscosity of the melt, leading to an increase in the melt pressure and the torque (and thus SME). It was observed that the values for the relative gain with respect to MC were almost constant implying a linear system. It was also observed that the step changes in MC influenced the SME input more than it affected the melt pressure, contradictory to the effects of changes in screw speed and the starch feed rate. A decrease in MC lead to an increase in the viscosity of the melt, leading to an increase in the melt pressure and the torque.

Table 3.3 Steady State Process Gains for Step-Input Variations in the Moisture Content.

No	Step	K_T	K_{RT}	K_P	K_{RP}	K_{Torque}	$K_{RTorque}$	K_{SME}	K_{RSME}
	Change in Moisture Content								
1	-10.00%	-114.8	-0.19	-3789.6	-0.92	-5.2	-1.25	-1.78	-1.47
2	-8.00%	-143.6	-0.24	-3588.7	-0.87	-5.2	-1.27	-1.79	-1.49
3	-6.00%	-95.7	-0.16	-3445.1	-0.83	-5.4	-1.30	-1.82	-1.51
4	-4.00%	-143.6	-0.24	-3445.1	-0.83	-5.6	-1.35	-1.88	-1.56
5	-2.00%	0	0.00	-3732.2	-0.90	-6.3	-1.53	-2.09	-1.73
6	+ 2.00%	0	0.00	-5167.7	-1.25	-5.5	-1.32	-1.82	-1.51
7	+ 4.00%	-143.6	-0.24	-4449.9	-1.08	-5.3	-1.28	-1.78	-1.47
8	+ 6.00%	-191.4	-0.32	-4402.1	-1.06	-5.1	-1.23	-1.70	-1.41
9	+ 8.00%	-143.6	-0.24	-4234.6	-1.02	-5.0	-1.20	-1.66	-1.38
10	+ 10.00%	-172.3	-0.29	-4191.6	-1.01	-4.7	-1.14	-1.59	-1.31

3.4.4 Step-Input Variations in the PHAE Content

The absolute (K) and relative (K_R) steady state process gains for step-input variations in the PHAE feed rate are shown in Table 3.4.

It was observed that the changes in PHAE content did not affect the temperature of the melt, except a change of $\pm 1^\circ\text{C}$ at a step change of $-/+ 100\%$ in the PHAE content respectively. Also, the step changes in the magnitude of PHAE content marginally affected the pressure giving low values of relative gain K_R as compared to those obtained by step changes in starch feed, screw speed and the MC. A positive step change in the PHAE content lead to a decrease in pressure, and vice-versa. Thus, the values of K_R for this variable were negative. However, the controlled variable that PHAE content influenced maximum is the SME input to the process. The SME decreased with an increase in the PHAE content and vice-versa. The value of the relative gain for this variable K_R was maximum near the set point and decreased as the magnitude of the step change increased.

Table 3.4 Steady State Process Gains for Step-Input Variations in the PHAE Feed Rate.

No.	Step Change	K_T	K_{RT}	K_P	K_{RP}	K_{Torque}	$K_{RTorque}$	K_{SME}	K_{RSME}
	in PHAE								
	Feed Rate								
1	-100.00%	-1.3	-0.01	-84.5	-0.09	-0.14	-0.15	-0.06	-0.22
2	-50.00%	0	0.00	-81.9	-0.09	-0.19	-0.21	-0.08	-0.28
3	-25.00%	0	0.00	-66.6	-0.07	-0.25	-0.27	-0.09	-0.34
4	-10.00%	0	0.00	-76.8	-0.08	-0.26	-0.28	-0.09	-0.34
5	+ 10.00%	0	0.00	-64.0	-0.07	-0.29	-0.32	-0.10	-0.38
6	+ 25.00%	0	0.00	-61.4	-0.07	-0.31	-0.33	-0.10	-0.39
7	+ 50.00%	0	0.00	-79.4	-0.09	-0.20	-0.22	-0.07	-0.27
8	+ 100.00%	-1.3	-0.01	-93.4	-0.10	-0.15	-0.17	-0.06	-0.21

Thus, from the results above, it can be seen that the temperature was the least affected output, while pressure and SME were the most affected outputs for the present screw profile and operating conditions. For extruder control, moisture content seemed to be the most influencing variable, followed by screw speed, the starch feed rate and PHAE feed rate.

3.4.5 Linear Domains

From the relative steady state gains above, it can be seen that the system was typically non-linear. However, it was possible to determine the minimal domain around the central set-point, within which the process could be assumed linear. It is possible that the process could be controlled within this domain using linear control algorithms. It was possible to identify a linear domain by plotting the absolute variation of the output variable versus the absolute variation of the input variable. Figures 3.3 (a), (b), (c), and (d) show the variations in pressure with different step variations in the starch feed rate, screw speed, moisture content, and PHAE feed rate respectively. The variations in torque and SME with step-changes in these manipulated variables were plotted likewise, and are not shown.

The absolute and relative linear domains for the various response variables to step-input variations in the manipulated variables are shown in Table 3.5 (Entries 1 – 12). In the case of pressure as the response variable (Entries 1 – 4, Table 3.5), the moisture content possibly had the smallest linear domain of the system, and therefore, seemed to be the most destabilizing variable of the system. PHAE feed rate, on the other hand, was the least destabilizing variable. Under the present operating conditions, the starch feed rate and the screw speed provided equivalent relative linear domains. Mulvaney et al. (13) stimulated the food extrusion process by step tests on screw speed, moisture content and feed rate and followed the process response through pressure records. They implicitly made the hypothesis that the process is linear.

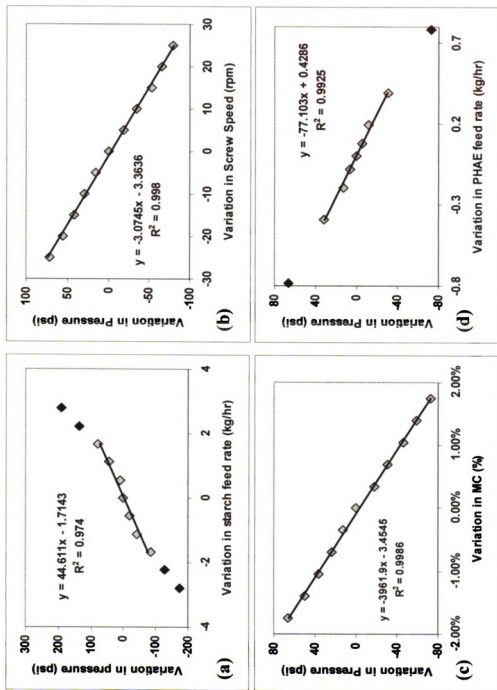


Figure 3.3 Linearity in Pressure with Step-Input Variations in the (a) Starch Feed Rate, (b) Screw Speed, (c) Moisture Content, (d) PHAF Feed Rate

Table 3.5 Absolute and Relative Linear Domains.

No.	Process Variables	Control Variables	Absolute Linear Domain	Relative Linear Domain
1	Pressure	Starch Feed Rate	± 1.67 kg/hr	$\pm 15.00\%$
2		Screw Speed	± 25 rpm	$\pm 12.50\%$
3		Moisture Content	$\pm 1.74\%$	$\pm 10.00\%$
4		PHAE Feed Rate	± 0.39 kg/hr	$\pm 50.00\%$
5	Torque	Starch Feed Rate	± 2.8 kg/hr	$\pm 25.00\%$
6		Screw Speed	± 25 rpm	$\pm 12.50\%$
7		Moisture Content	$\pm 1.74\%$	$\pm 10.00\%$
8		PHAE Feed Rate	± 0.20 kg/hr	$\pm 25.00\%$
9	SME	Starch Feed Rate	± 1.67 kg/hr	$\pm 15.00\%$
10		Screw Speed	± 15 rpm	$\pm 7.50\%$
11		Moisture Content	$\pm 1.74\%$	$\pm 10.00\%$
12		PHAE Feed Rate	± 0.39 kg/hr	$\pm 50.00\%$

For torque as the process response variable (Entries 5 – 8, Table 3.5), moisture content and screw speed provided narrow linear domains of $\pm 10\%$ and $\pm 12.5\%$ respectively. However, with respect to the variations in starch and PHAE feed rate, the process variations in torque loading were linear in a relatively wider range of $\pm 25\%$. With SME as the response variable (Entries 9 – 12, Table 3.5), the screw speed seemed to be the most destabilizing variable, since it governed the load (torque) on the extruder drive. The moisture content had significant influence too, since it affected the viscosity of the extrudate, which in turn governed the torque on the motor. Sanei (14) observed the

change in viscosity (with an online rheometer) as a consequence of variations of screw speed. The author concluded that the process is linear under the range of screw speeds tested. Moreira et al. (15) used step tests on screw speed and moisture content to study the dynamical behavior of the extruder through pressure. They performed step tests of medium magnitude, and also back steps to return to the initial set point. They suggested that the process might be non-linear.

Since, the temperature was not affected considerably, the linear domains were not determined. The variation in temperature was characterized by small jumps ($\pm 1 - 2^\circ\text{C}$), and hence, no particular trend was observed. Onwulata et al. (16), and Lu et al. (17) undertook fairly complete studies by adding temperature as an input variable and by following the effect of step tests both on product variables (like expansion ratio) and on process variables (like melt pressure). The authors used step tests of great amplitude and did not pronounce on the linearity of the system.

3.4.6 Dynamic Responses

Figure 3.4 shows the transient response of pressure to some step-input variations in the moisture content. These transient responses of Pressure (P) and Torque to step-input variations in the manipulated variables were modeled as first order processes (process gain, K ; time constant, τ) with a dead time, t_d (lag) (FODT Model). Many processes are higher than first order (contain more than one lag term) and so any first order model will only be an approximation. However, the approximation is sufficient in most cases and many of the Proportional-Integral-Derivative (PID) tuning procedures use a FODT process model.

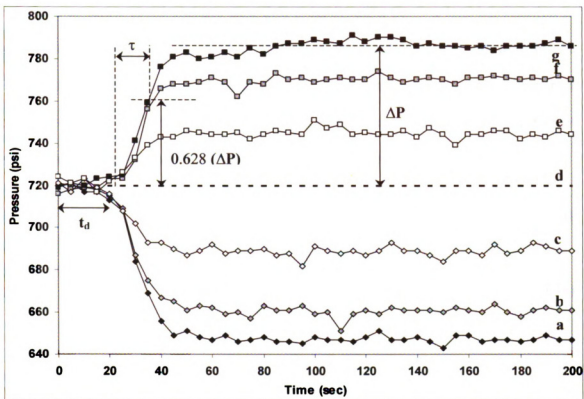


Figure 3.4 Transient Response of Pressure to Different Step-Input Variations in the Moisture Content modeled as a First Order Process with a Dead Time (Lag): + 10% Step Change in the Moisture Content (a); + 8% Step Change in the Moisture Content (b); + 4% Step Change in the Moisture Content (c); Original Steady State (0% Step Change in the Moisture Content) (d); - 4% Step Change in the Moisture Content (e); - 8% Step Change in the Moisture Content (f); - 10% Step Change in the Moisture Content (g)

Costin et al. (18) critically reviewed dynamic modeling and control of plasticating extruders, and concluded that the gross dynamic input/output behavior may be generally described by simple first/second order models. Chan et al. (19) studied the pressure

responses to screw speed changes as a first order function times a lead-lag function to effectively model responses with an initial increase or decrease followed by an exponential decay to the final steady state value. Equation (3.5a) represents a first order process with a dead time in the time domain, while Equation (3.5b) represents that process in the Laplace domain, using 's' as the Laplace operator.

$$P(t) = K_p [1 - e^{-(t-t_d)/\tau}] \cdot A_X \quad (3.5a)$$

$$P(s) = \frac{K_p e^{-t_d}}{\tau s + 1} \cdot X(s) \quad (3.5b)$$

Where:

K_p – Steady State Process Gain for Pressure as the Response Variable

t – Time Constant for the First Order Process

t_d – Dead Time (Lag)

X – Manipulated Variable (Starch Feed Rate/Screw Speed/Moisture Content/PHAЕ Feed Rate)

A_X – Amplitude of the Step-Input Change in the Manipulated Variable

The steady state process gain, apparent time constant, and apparent dead time were determined graphically based on the procedure developed by Ziegler and Nichols (24). Table 3.6 provides the first order time constants and the dead times in addition to the steady state process gains for the transient responses of pressure with step input variations in the starch feed rate, screw speed, moisture content and PHAE feed rate, while Table 3.7 provides the parameters for the transient responses of the torque loading.

Table 3.6 Dynamic Properties (Pressure).

Step Changes in Starch Feed Rate	Process Steady State Gain, K_p	τ, Time Constant (sec)	t_d, Dead Time (sec)
+ 5.00%	17.9	23	28
+ 15.00 %	47.8	25	32
+ 20.00 %	60.5	24	32
- 5.00%	32.3	24	29
- 15.00 %	50.8	31	35
- 20.00 %	57.4	31	36

Step Changes in Screw Speed	Process Steady State Gain, K_p	τ, Time Constant (sec)	t_d, Dead Time (sec)
+ 5.00%	-3.5	16	12
+ 10.00 %	-3.3	15	13
+ 12.50 %	-3.2	17	12
- 5.00%	-2.9	16	11
- 10.00 %	-2.8	10	16
- 12.50 %	-2.9	9	18

Step Changes in Moisture Content	Process Steady State Gain, K_p	τ, Time Constant (sec)	t_d, Dead Time (sec)
+ 4.00 %	-4449.9	12	18
+ 8.00 %	-4234.6	10	21
+ 10.00 %	-4191.6	13	20
- 4.00 %	-3445.1	12	19
- 8.00 %	-3588.7	10	24
- 10.00 %	-3789.6	13	23

Step Changes in PHAE Feed Rate	Process Steady State Gain, K_p	τ, Time Constant (sec)	t_d, Dead Time (sec)
+ 25.00 %	-61.4	24	22
+ 50.00 %	-79.4	29	24
+ 100.00 %	-93.5	38	26
- 25.00 %	-66.6	27	20
- 50.00 %	-81.9	32	23
- 100.00 %	-84.5	35	18

Table 3.7 Dynamic Properties (Torque).

Step Changes in Starch Feed Rate	Process Steady State Gain, K_{Torque}	τ, Time Constant (sec)	t_d, Dead Time (sec)
+ 5.00%	0.06	21	16
+ 15.00 %	0.06	26	15
+ 20.00 %	0.06	23	15
- 5.00%	0.06	19	20
- 15.00 %	0.06	22	18
- 20.00 %	0.06	19	19
Step Changes in Screw Speed	Process Steady State Gain, K_{Torque}	τ, Time Constant (sec)	t_d, Dead Time (sec)
+ 5.00%	-0.006	13	10
+ 10.00 %	-0.005	12	12
+ 12.50 %	-0.004	15	10
- 5.00%	-0.005	9	11
- 10.00 %	-0.006	14	10
- 12.50 %	-0.005	12	8
Step Changes in Moisture Content	Process Steady State Gain, K_{Torque}	τ, Time Constant (sec)	t_d, Dead Time (sec)
+ 4.00 %	-5.3	10	12
+ 8.00 %	-5.0	11	10
+ 10.00 %	-4.7	7	15
- 4.00 %	-5.6	11	12
- 8.00 %	-5.2	11	14
- 10.00 %	-5.2	9	13
Step Changes in PHAE Feed Rate	Process Steady State Gain, K_{Torque}	τ, Time Constant (sec)	t_d, Dead Time (sec)
+ 25.00 %	-0.31	22	19
+ 50.00 %	-0.21	26	16
+ 100.00 %	-0.15	25	23
- 25.00 %	-0.25	16	20
- 50.00 %	-0.20	20	21
- 100.00 %	-0.14	32	22

The process gains have been discussed earlier in this section. The data for characterization of the process were easily obtained in the laboratory, and subsequent modeling and determination of parameters was straightforward. These models would be suitable for dynamic simulation of the process using commercially available computer software, which would enable optimization of the process via simulation. The individual transfer functions could be combined to give a complete multivariable description of the starch foam extrusion process.

It was observed that the time constants and the dead times recorded for both the pressure and torque responses did not exhibit significant variation within each manipulated or control variable tested. Thus, the system displayed linear dynamic characteristics with respect to each manipulated variable. It was also observed that for the same step-input variations in the manipulated variables, the torque loading on the twin-screw extruder exhibited a faster response (lower dead time), and also reached a steady state sooner (lower time constant). For example, for step-input variations in moisture content, the dead time in the pressure response was ~ 20-22 seconds and the time constant was ~ 10-13 seconds. However, the dead time in the torque response was ~ 11-13 seconds, while the time constant was ~ 8-10 seconds.

Also, the response in pressure was fastest to step-input variations in the moisture content followed by the screw speed and the starch and PHAE feed rates. The response in torque loading was also fastest to step-input variations in the moisture content as well as the screw speed followed by the starch and PHAE feed rates. Thus, the moisture content and screw speed seem to be the most destabilizing variables since they induce rapid responses in the process variables.

3.4.7 Multiple Input Tests

The experimental design shown in Table 3.8 was implemented for the multiple input step tests.

Table 3.8 Design for Multiple Input Tests.

Run	Starch Feed Rate	Screw Speed	Moisture Content	PHAE Feed Rate
1	+ 10%	+ 10%	+ 10%	+ 10%
2	+ 10%	+ 10%	+ 10%	0%
3	+ 10%	+ 10%	0%	+ 10%
4	+ 10%	0%	+ 10%	+ 10%
5	0%	+ 10%	+ 10%	+ 10%
6	+ 10%	+ 10%	0%	0%
7	0%	+ 10%	+ 10%	0%
8	0%	0%	+ 10%	+ 10%
9	+ 10%	0%	0%	+ 10%
10	+ 10%	0%	+ 10%	0%
11	0%	+ 10%	0%	+ 10%
12	-10%	-10%	-10%	-10%
13	-10%	-10%	-10%	0%
14	-10%	-10%	0%	-10%
15	-10%	0%	-10%	-10%
16	0%	-10%	-10%	-10%
17	-10%	-10%	0%	0%
18	0%	-10%	-10%	0%
19	0%	0%	-10%	-10%
20	-10%	0%	0%	-10%
21	-10%	0%	-10%	0%
22	0%	-10%	0%	-10%

The experimental (measured) and calculated values (from Principle of Superposition) of pressure, torque and SME are shown in the Figures 3.5, 3.6, 3.7 respectively.

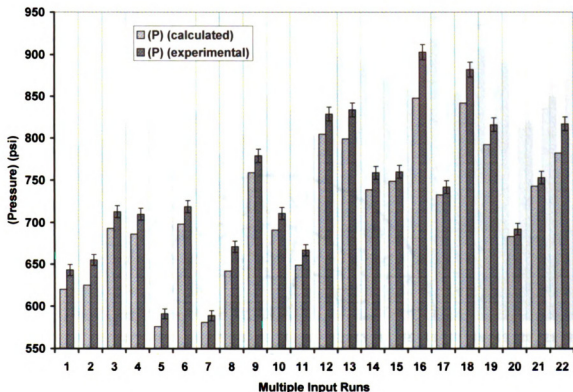


Figure 3.5 Measured (Recorded) Values of Pressure compared to the Calculated (from 'Principle of Superposition') Values for the different Multiple Step-Input Variation Runs

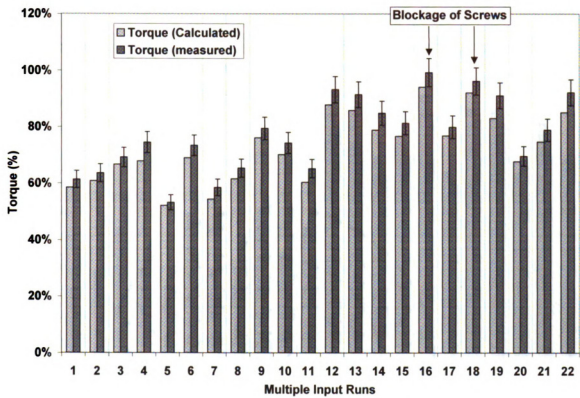


Figure 3.6 Measured (Recorded) Values of Torque compared to the Calculated (from 'Principle of Superposition') Values for the different Multiple Step-Input Variation Runs

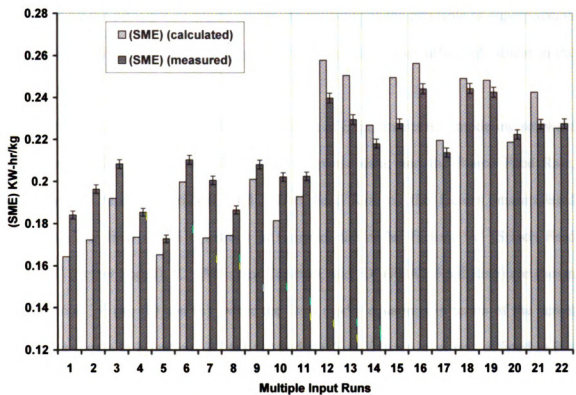


Figure 3.7 Measured (Recorded) Values of SME compared to the Calculated (from 'Principle of Superposition') Values for the different Multiple Step-Input Variation Runs

The principle of superposition was fairly satisfied in the control variables, the error margin being low, especially in the case of the pressure readings. It was also observed that the pressure readings obtained from the experiment were always higher than those calculated by the principle of superposition. The validity of the principle of superposition in the above multiple input tests suggested that the process was sufficiently linear in the domain tested.

A linear model was fit using STATEASE 'Design of Experiments 6.0' modeling software with Pressure (P), Torque and SME as the response data; and the Starch Feed Rate, Screw Speed, Moisture Content, and PHAE Feed Rate as the factors (manipulated variables). The final model equations in terms of the coded factors 'A' (Starch Feed Rate), 'B' (Screw Speed), 'C' (Moisture Content), and 'D' (PHAE Feed Rate) are shown in Equations 3.6 (a), (b) and (c); while the final model equations in terms of the actual factors are shown in Equations 3.7 (a), (b) and (c). Significance level was defined as $P < 0.05$.

$$P = 738.03 + 54.45A - 70.55B - 73.56C - 6.05D \quad (3.6a)$$

$$Torque = 0.73 + 0.078A - 0.082B - 0.064C - 0.023D \quad (3.6b)$$

$$SME = 0.21 + 5.432E - 03A - 4.28E - 03B - 0.018C - 9.655E - 03D \quad (3.6c)$$

$$P = 1693.75 + 48.79 (\text{Starch Feed Rate}) - 3.528 (\text{Screw Speed}) - 4215.37 (\text{Moisture Content}) - 77.58 (\text{PHAE Feed Rate}) \quad (3.7a)$$

$$Torque = 1.648 + 0.0695 (\text{Starch Feed Rate}) - 4.115 E - 03 (\text{Screw Speed}) - 3.684 (\text{Moisture Content}) - 0.29 (\text{PHAE Feed Rate}) \quad (3.7b)$$

$$SME = 0.483 + 4.87E - 03 (\text{Starch Feed Rate}) - 2.14 E - 04 (\text{Screw Speed}) - 1.058 (\text{Moisture Content}) - 0.124 (\text{PHAE Feed Rate}) \quad (3.7c)$$

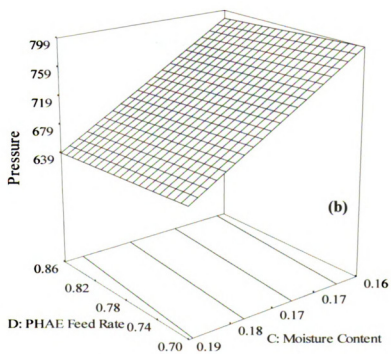
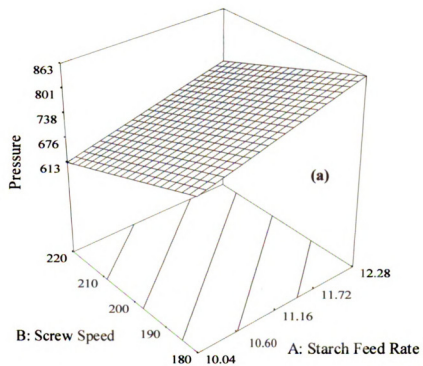


Figure 3.8 Response surface of pressure for the various manipulated variables

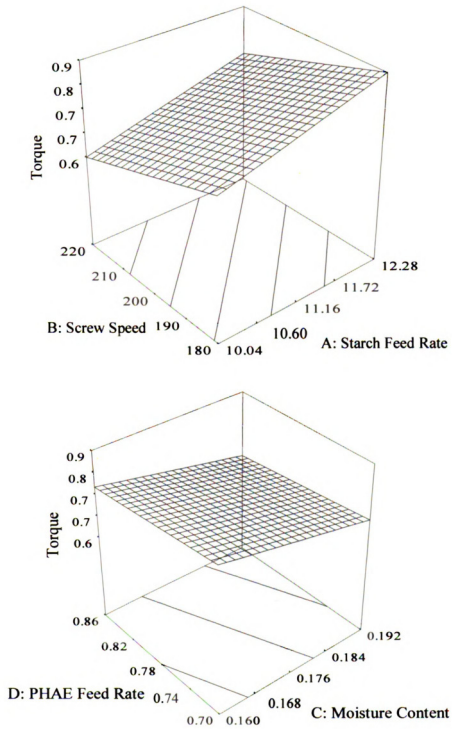


Figure 3.9 Response surface of Torque for the various manipulated variables.

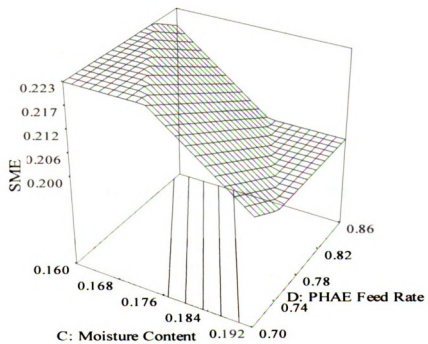
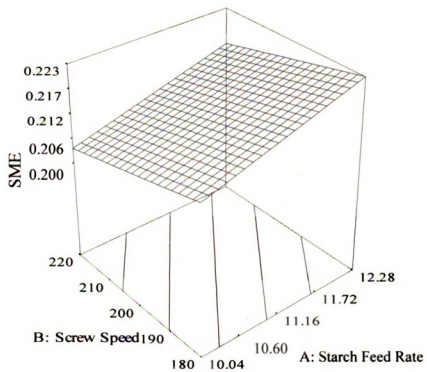


Figure 3.10 Response surface of SME for the various manipulated variables.

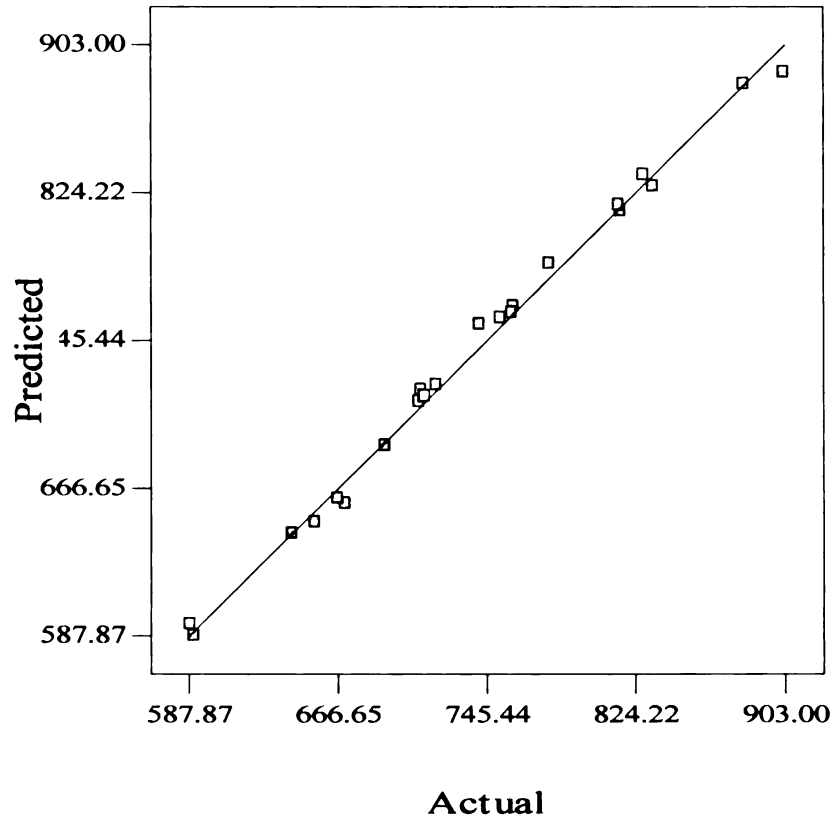


Figure 3.11 Predicted Versus Actual Values of Pressure.

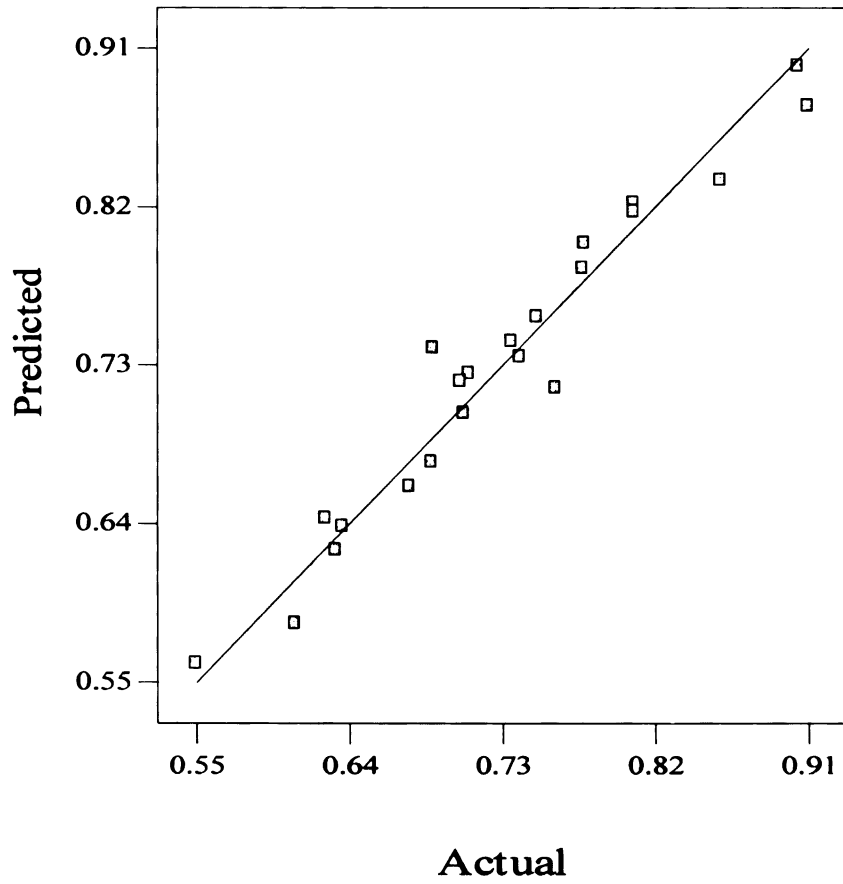


Figure 3.12 Predicted Versus Actual Values of Torque.

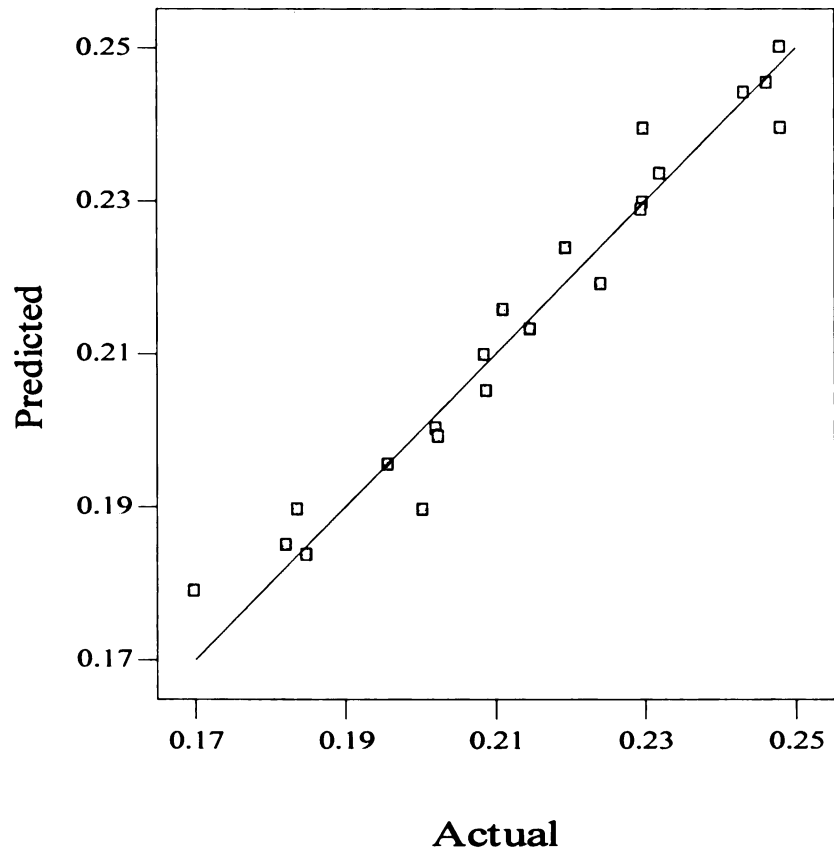


Figure 3.13 Predicted Versus Actual Values of SME.

Figure 3.8 (a) shows the response surface of pressure for the starch feed rate and screw speed as manipulated variables, while Figure 3.8 (b) shows its response surface for the moisture content and PHAE feed rate as input variables. Thus, figure 3.8 shows that variations in the moisture content, screw speed and the starch feed rate induced significant variations in pressure as compared to those due to step-changes in the PHAE feed rate. Similarly, Figures 3.9 and 3.10 show the response surface for torque and SME respectively. Figures 3.11, 3.12, 3.13 show the comparison between the actual values of pressure, torque and SME obtained and the values from the linear model developed respectively. The variance analysis for these data revealed a determination coefficient (R^2) of 0.9943 ($P < 0.0001$). Similarly, the R^2 values for torque and SME were 0.9502 ($P < 0.0001$) and 0.9533 ($P < 0.0001$) respectively. Thus, multiple regression analyses showed a significant linear effect of the manipulated variables on the response variables. The coefficients of the manipulated (input) variables in Equations 7 (a), (b) and (c) are similar to the values of the steady state process gains for the corresponding single step-input tests performed earlier, suggesting the linearity of the process within the domain tested.

The non-linearity of the process was demonstrated by Cayot et al. (20) by the observation of the transient responses. Majority of the responses were reported to be of first order with a delay. Second order responses were also recorded by Cayot et al. (20) but no correlation was developed between the response and the manipulated variables.

The decision of whether automation is cost-effective really depends on the skill of the operator and the frequency of start-up and shutdown. In many instances, the feed material dictates the feasibility of a fast start-up or shutdown. For example, start-up can be as

quick as 2 – 3 minutes for extruding pet food cereals with feedstock at 20% moisture and at 2000 kg/hr, while it took 25-30 minutes for the start-up of starch foam sheets with the feed at 11.2% inherent moisture and at about 400 kg/hr. The production of the starch foam sheets on a manufacturing scale will be discussed in the following Chapter 4. Start-up may take only a short time but, more importantly, stable production took considerably longer. As the machine size increased, the time taken to achieve thermal stability usually increased. The Wenger TX – 80 twin-screw extruder producing 400 – 420 kg/hr of starch foam sheets took 40 – 60 minutes for the product quality to stabilize. During this time, the product bulk density, texture, etc. changed as the die-block and screw temperature increased. Hence, the water addition, screw speed, barrel temperature, and sometimes starch feed-rate had to be varied to keep the quality within specification. Operators not conversant with extruder effects on product quality will find this difficult. This is where process control can help. Simple closed feedback control loops can be superimposed to be effective.

The main controlling parameters were the specific mechanical energy input (SME) and die pressure. The SME value is a function of the measured screw torque, and if the screw speed and feed-rate are kept constant, then the torque can be directly adjusted using water addition. This was carried out manually like most other extruder operations. The water adjustment was made to allow for moisture variability in the starch. It was correlated to the bulk density and the texture of the product. The manual operation could be eliminated by using a servomotor pump system, with feedback control from the torque measurement. Barrel temperature could be simply linked to the measured product temperature, which is normally measured within the die housing.

Die-pressure adjustment on-the-run is not a common facility on extruders, but a type of throttle valve could be used to give variable gaps between the end of the screw and the die entrance.

Although process control can help production and quality consistency, natural raw materials like starch do vary in physical composition. Determining the reasons why torque, die-pressure or temperatures fluctuate between batches or over a time-span is complicated. Strict quality control of raw materials and data acquisition during production can help in piecing together the whole story.

Sensors have been used to quantify moisture distribution and viscoelastic properties of the material within die assemblies. In recording data, it is important not to rely on one single measurement. Pressure transducers are known for their temperature sensitivity and if positioned in the barrel within a dead space, material can plug the space and give an artificial pressure reading. Having more than one probe is more reliable, but costs more.

3.5 Conclusion

The starch foam extrusion process was modeled as a Multiple Input Multiple Output (MIMO) process, and the dynamics of the process were studied as a response to step changes in the input variables such as starch feed rate, screw speed, moisture content and PHAE feed rate. The responses were modeled as first order responses with a time delay. The linearity of the process was determined over a range around the set-point, and the parameters defining the first order system such as Gain 'K', Time Constant ' τ ', and Dead time ' t_d ' were determined in the linear range. The transfer function models can then be used in a predictive computer control system for on-line fine-tuning of the operating conditions. This could ensure a consistently high quality product even when low frequency disturbances are present in the system. It was observed that the time constants and the dead times recorded for both the pressure and torque responses did not exhibit significant variation within each manipulated or control variable tested. Thus, the system displayed linear dynamic characteristics with respect to each manipulated variable. It was also observed that for the same step-input variations in the manipulated variables, the torque loading on the twin-screw extruder exhibited a faster response (lower dead time), and also reached a steady state sooner (lower time constant). The response in pressure was fastest to step-input variations in the moisture content followed by the screw speed and the starch and PHAE feed rates. The response in torque loading was also fastest to step-input variations in the moisture content as well as the screw speed followed by the starch and PHAE feed rates. Thus, the moisture content and screw speed were the most destabilizing variables since they induce rapid responses in the process variables. The moisture content in the extruder was, hence, determined to be the most influential factor

in the stability of the process followed by screw speed and starch feed rate. PHAE feed rate was the least significant variable.

Multiple step-input tests were carried out in order to determine the validity of the principle of superposition. The validity of the principle of superposition implied the linearity of the process in the domain tested. The hypothesis of linearity is an implicit and necessary prerequisite to most of the classical techniques of process control. A linear model was fit using STATEASE 'Design of Experiments 6.0' modeling software with Pressure (P), Torque and SME as the response data; and the Starch Feed Rate, Screw Speed, Moisture Content, and PHAE Feed Rate as the factors (manipulated variables). Multiple regression analyses showed a significant linear effect of the manipulated variables on the response variables.

Once the dynamics of the starch-based foam process, and the influence of the manipulated variables on the process and product variables were studied, it was necessary to determine the melt viscosity of the starch-PHAE plastic, which showed immense promise for the large-scale manufacture of starch-based foam sheets from the previously developed optimized formulation. The subsequent Chapter 4 deals with the development of such a viscosity model for the starch-PHAE blend, and its dependence on the aforementioned variables. This viscosity model was further used in the design of an annular die for the production of starch-PHAE foam sheets to be targeted for cushioning and insulation applications.

3.6 References

- 1) Harper, J. M., CRC Critical Reviews in Food Science and Nutrition, 11(2), 155, 1979.
- 2) Eerikainen, T., Linko, P. Extrusion cooking modeling, control and optimization. In Extrusion Cooking, Mercier, C., Ed., American Association of Cereal Chemists, St Paul, USA, 157, 1989.
- 3) Janssen, L. P. B. M. Models for Extrusion Cooking, In Food Engineering and Process Applications, Vol. II, Unit Operations, M. Le Maguer and P. Jelen, Eds., Elsevier Applied Science Publishers, London, 115, 1986.
- 4) Della Valle, G., Tayeb, J. Proceedings of Agoral, Dijon, 16-17 April 1991.
- 5) Cayot, N. Contribution à la Modélisation du Procédé de Cuisson-Extrusion. Etude de la Non-linéarité du Système. In: Doctoral Thesis, Université de Bourgogne, 1992.
- 6) Janssen, L. P. B. M. Twin Screw Extrusion, Elsevier North-Holland, New York, 1978.
- 7) Martelli, F. G. Twin Screw Extruders: A Basic Understanding. Van Nostrand Reinhold, New York, 1983.
- 8) El-Dash, A., Gonzales, R., Ciol, M. Response Surface Methodology in the Control of Thermoplastic Extrusion of Starch, In Extrusion Cooking Technology, R. Jowitt, Ed., Elsevier Applied Science Publishers, London, 51, 1983.
- 9) Frazier, P. J., Crawshaw, A., Daniels, N. W. R., Eggitt, P. W. R. Optimization of Process Variables in Extrusion Texturing of Soy, In Extrusion Cooking Technology, R. Jowitt, Ed., Elsevier Applied Science Publishers, London, 1, 1983.
- 10) Olkku, J., Hagqvist, A. Steady State Modeling of Extrusion Cooking employing Response Surface Methodology, In Extrusion Cooking Technology, R. Jowitt, Ed., Elsevier Applied Science Publishers, London, 27, 1983.
- 11) Owusu-Ansah, J., Van de Voort, F. R., Stanley, D. W. Textural and Microstructural Changes in Corn Starch as a Function of Extrusion Variables, Canadian Institute of Food Science and Technology, 17(2), 65 – 70, 1984.
- 12) Richburg, L. L., Garcia, A., III. Response Surface Modeling of a Twin Screw Extruder, Paper 88-6016, Presented at the Summer Meeting of the American Society of Agricultural Engineers, June 26-29, Rapid City, SD, 1988.

- 13) Mulvaney, S. J., Hsieh, F., Onwulata, C. Brent Jr., J., Huff, H.E. Computer control and modeling of an extruder: dynamics, Paper No. 88-6517, In: International Winter Meeting of the American Society of Agricultural Engineers, 13–16 December, Chicago, 1988.
- 14) Sanei, A. Reproductibilité et Instrumentation en Cuisson-Extrusion. Etude de l'Aptitude Technologique des Farines de Blé. In: Doctoral-Engineer Thesis, Université de Technologie de Compiègne, 1990.
- 15) Moreira, R.G., Srivastava A.K., Gerrish, J.B. Food Control, 1(3), 179–184, 1990.
- 16) Onwulata, C.I., Mulvaney, S.J., Hsieh, F., Heymann, H. Journal of Food Science, 57(2), 512–515, 1992.
- 17) Lu, Q., Hsieh, F., Mulvaney, S.J., Tan J., Huff, M.E. Lebensmittel Wissenschaft und Technologie, 25, 261–270, 1992.
- 18) Costin, M. H., Taylor, P. A., Wright, J. D. Polymer Engineering and Science, 22, 393, 1982.
- 19) Chan, D., Nelson, R. W., Lee, L. J. Polymer Engineering and Science, 26(2), 152, 1986.
- 20) Cayot, N., Bounie, D., Baussart, H. Journal of Food Engineering, 25, 245-260, 1995.
- 21) Nabar, Y. U., Schindler, M., Narayan, R. Polymer Engineering and Science, In Press.
- 22) Myers, R. H. In: Response Surface Methodology, Allan and Bacon, Boston, 1971.
- 23) Chavez-Jauregui, R. N., Silva, M. E. M. P., Areas, J. A. G. Journal of Food Science, 65, 1009-1015, 2000.
- 24) Ziegler, J., Nichols, N. Transactions of the American Society of Mechanical Engineers, 64, 759-769, 1942.

ANNULAR DIE DESIGN AND SCALE-UP OF THE STARCH-PHAE FOAM EXTRUSION PROCESS

4.1 Abstract

Cylindrical starch foam shapes were produced on a small scale (~ 11-12 kg/hr) Century ZSK - 30 Twin Screw Extrusion (TSE) process using water as a plasticizer as well as a blowing agent, and poly(hydroxy aminoether) (PHAE) as a functional aid to improve the physico-mechanical properties of the starch foams. A bifurcated die was used for the determination of the viscosity model for the earlier optimized starch- PHAE based foam formulation to be scaled up for the production of starch foam sheets. A Power Law behavior was assumed, and the parameters in the Power Law model such as Consistency Coefficient 'K', and Flow Behavior Index 'n' were obtained as functions of temperature, moisture content, PHAE content and the Specific Mechanical Energy (SME) input to the extruder. The flow behavior index varied between a minimum of 0.11 (MC = 17.52%, T = 110°C, PHAE = 7%, Screw Speed = 250 rpm) to a maximum of 0.52 (MC = 50.15%, T = 110°C, PHAE = 7%, Screw Speed = 200 rpm). The variation in the flow behavior index was considerable with variations in moisture content (0.17 – 0.52 with MC = 17.5% - 50.15% respectively), while temperature, screw speed, and the PHAE content did not affect the value of 'n' significantly. The Consistency Coefficient varied between a minimum of 3208 Pa.sⁿ (MC = 50.15%, T = 110°C, PHAE = 7%, Screw Speed = 200 rpm) to a maximum of 140965 Pa.sⁿ (MC = 17.52%, T = 110°C, PHAE = 0%, Screw

Speed = 200 rpm). The variation in the Consistency Coefficient was also substantial with variations in moisture content (107880 Pa.sⁿ – 3208 Pa.sⁿ with MC = 17.5% - 50.15% respectively), while temperature, screw speed, and the PHAE content did not affect the value of 'K' appreciably. An annular die was designed for the manufacture of starch foam sheets using the viscosity model developed for the starch-PHAE formulation (K=107880 Pa.sⁿ & n=0.17 at MC = 17.52%, T = 110°C, PHAE = 7%, Screw Speed = 200 rpm), which provided the best physico-mechanical properties. The density of the cylindrical foam extrudates obtained on the Century ZSK – 30 was 22-23 kg/m³. This annular die was then successfully employed on an industrial scale (410-420 kg/hr) twin-screw food extruder, Wenger-80, to manufacture foam sheets. The density of the foam sheets was 27-30 kg/m³.

These results were then employed on an industrial scale (410-420 kg/hr) twin-screw food extruder, Wenger-80, to manufacture foam sheets. The density of the foam sheets was 27-30 kg/m³. The cushioning and insulation properties were studied and are reported.

4.2 Introduction

Common rheological models that are used to describe the viscosity of starch plastics as a function of shear rate are the Power Law or the Ostwalde - de Waele model (1), Casson model (2), Bingham (3), and Herschel-Bulkley model (4). Of these, the model that is widely used is the Power Law model. In a Power-Law model, $\tau = K\dot{\gamma}^n$, the Consistency Index 'K', and the Flow Behavior index 'n' are determined by plotting the shear stress (ΔP) against the shear rate (flow rate) on a logarithmic plot. The slope gives the value of 'n', while the y-intercept gives the value of 'K'. The drawbacks, however, are that the viscosity approaches a value of zero as the shear rate increases to infinity, and vice-versa.

Starch plastics may exhibit a yield stress. The models developed by Casson (2), Bingham (3), Herschel-Bulkley (4) (generalized Power Law model, with a yield stress added), and Mizrahi-Berk (5) incorporate terms defining the yield stress. Ofoli et al. (6) proposed another model that allowed for a yield stress, variable shear thinning and limiting viscosity at high shear rates. Disadvantages are the mathematical complexity of the model and the difficulty in obtaining model parameters without sophisticated computer programs. The Cross (7), Reiner – Philippoff (8), Van Wazer (9) and Powell – Eyring (10), Carreau (11) are useful in modeling pseudoplastic behavior over low, middle, and high shear rate ranges.

Table 4.1 (6, 12) lists these models available in the literature. The Power law model has found extensive use as a constitutive equation describing starch plastics because of its simplicity and ease of parameter estimation, and for extrusion operations (higher shear rates), it is more than adequate.

Several rheological models for extrusion of starch or protein doughs have been reported in the literature. Harper et al. (13) modeled the viscosity as a power law dependence on shear rate, an Arrhenius dependence on temperature, and an exponential dependence on moisture:

$$\eta(\dot{\gamma}) = K\dot{\gamma}^{n-1} \exp\left(\frac{\Delta H}{RT}\right) \exp(-k_1 MC) \quad (4.1)$$

Where η is the shear viscosity; K , the Consistency Coefficient; n , the flow behavior index; ΔH , the molar “free energy of activation” in a stationary fluid, which is related to the amount of energy required for a molecule to escape its surroundings and move into an adjoining site; R , the universal gas constant; and k_1 , the moisture content (MC) coefficient.

Table 4.1 Viscosity Models from Literature

Model	Shear Stress	Apparent Viscosity
Newtonian	$\tau = \mu\dot{\gamma}$	$\eta = \mu$
Power Law	$\tau = K\dot{\gamma}^n$	$\eta = K\dot{\gamma}^{n-1}$
Bingham Plastic	$\tau = \tau_0 + \mu_0\dot{\gamma}$	$\eta = \tau_0\dot{\gamma}^{-1} + \mu_0$
Herschel - Bulkley	$\tau = \tau_0 + K\dot{\gamma}^n$	$\eta = \frac{\tau_0}{\dot{\gamma}} + K\dot{\gamma}^{n-1}$
Casson	$\tau^{0.5} = \tau_0^{0.5} + (\mu_\infty\dot{\gamma})^{0.5}$	$\eta = \left[\left[\frac{\tau_0}{\dot{\gamma}} \right]^{0.5} + \mu_\infty^{0.5} \right]^2$
Mizrahi - Berk	$\tau^{0.5} = K_0M + K_c\dot{\gamma}^m$	$\eta = (K_0M\dot{\gamma}^{-0.5} + K_c\dot{\gamma}^{m-0.5})^2$
Heinz - Casson	$\tau^n = \tau_0^n + (\mu_0\dot{\gamma})^n$	$\eta = \left[\left[\frac{\tau_0}{\dot{\gamma}} \right]^n + \mu_0^n \right]^{1/n}$
Ofoli	$\tau^{n_1} = \tau_0^{n_1} + \mu_\infty\dot{\gamma}^{n_2}$	$\eta = \left[\left[\frac{\tau_0}{\dot{\gamma}} \right]^{n_1} + \mu_\infty\dot{\gamma}^{n_2-n_1} \right]^{1/n_1}$
Cross		$\eta = \eta_\infty + \frac{\eta_0 - \eta_\infty}{1 + K_1\dot{\gamma}^n}$
Reiner - Philippoff	$\tau = \left(\eta_\infty + \frac{\eta_0 - \eta_\infty}{1 + (\tau^2/K_1)} \right) \dot{\gamma}$	
Van Wazer		$\eta = \frac{\eta_0 - \eta_\infty}{1 + K_1\dot{\gamma} + K_2\dot{\gamma}^{n_1}} + \eta_\infty$
Powell - Eyring	$\tau = K_1\dot{\gamma} + \left(\frac{1}{K_2} \right) \sinh^{-1}(K_3\dot{\gamma})$	
Carreau		$\eta = \eta_\infty + (\eta_0 - \eta_\infty) \left[1 + (K_1\dot{\gamma})^2 \right]^{(n-1)/2}$

Online measurements are typically used to characterize the viscosity of starch plastics, to determine the power law relationship between the viscosity and shear rate. The extruder can be effectively used as a rheometer by attaching a capillary/slit die to the extruder (14). Online measurements using extruders are preferred to offline measurements using a capillary rheometer, since the conditions in the extruder are not possible to replicate in the offline techniques. A problem associated with this method to measure the power law coefficients is how to vary the extruder conditions to get different shear rates without changing material properties. At least three different shear rates are required. In a starve-fed extruder, this can be done by varying the flow rates. Apart from parameters such as moisture content, temperature, screw speed, the rheological properties of starch plastics are also dependent on molecular transformations such as gelatinization, melting and fragmentation (15). This molecular degradation, which is affected by shear rate, temperature and residence time (16, 17) resulted in a wide variation in power law values, and sometimes negative values (18, 19). Changing the flow rate to get different shear rates resulted in different processing histories and, hence, changed rheological properties. Empirical terms for molecular degradation have been accounted for in several proposed models to correct for these effects of physico-chemical changes (16, 19-21). The approach was to modify Harper's equation to include additional terms related to degree of gelatinization, screw speed and mechanical energy input. However, these models could not be generalized for other systems, since they were developed through empirical studies and statistically fitted.

The flow diversion method (use of a side-stream valve) was developed to avoid changing processing conditions in a single-screw extruder (22, 23). Flow rate through the die was

varied by diverting a part of the starch melt through a valve at the end of the barrel, before it entered the die. Thus, all the material experienced the same processing history, while different flow rates were achieved in the die leading to different shear rates.

Vergnes et al. (24) and Della Valle et al. (25) used a specially designed slit die called 'Rheopac' to study cornstarches with different amylose contents. Using this die the flow was split into two slit channels, and the flow was varied in each channel by adjusting a piston. Thus, the entrance pressures and the overall flow rate are kept constant, and the flow through the primary channel is varied to get a range of shear rates. This method still required several measurements to determine the flow behavior index.

Drozdek et al. (26) used a dual orifice die to measure flow behavior index values during extrusion of food materials. The two orifices had different radii, and different lengths resulting in different flow rates for a material, which has undergone the same processing history in the extruder. The dual orifice die simplifies the determination of flow behavior index by using only one condition, thus minimizing experiments, and also removes the need for entrance and exit conditions. However, in this study, the consistency coefficient was not determined or studied, since pressure transducers at the entrance to the bifurcated flow channels were not installed due to geometry restrictions. Also, no specific relationships were determined between the flow behavior index and the parameters involved such as temperature, moisture content, screw speed and the mechanical energy input.

In our previous paper (27), a comprehensive explanation on the twin-screw extrusion production of starch foams using PHAE as the functional aid, as well as on the optimization of the process has been provided. This research aims at determining the flow

behavior index, as well as the consistency coefficient using a bifurcated die. The effect of temperature, moisture content, screw speed, PHAE content, and the Specific Mechanical Energy (SME) on the consistency coefficient and flow behavior index was also studied. Further, the specific viscosity model developed for the optimized formulation for producing resilient low-density Starch-PHAE foams was used to design the annular die to be used in the large scale production of starch foam sheets on a Wenger TX-80 twin-screw extruder.

4.3 Theory

The volumetric flow rate (Q) through a capillary of length 'L' and radius 'R' has been derived using fundamental momentum balances (12):

$$\frac{Q}{\pi R^3} = \frac{1}{\tau_w^3} \int_0^{\tau_w} \tau^2 f(\tau) d\tau \dots (4.2)$$

For a power law fluid, this integral is solved by inserting $\dot{\gamma} = f(\tau) = (\tau/K)^{1/n}$ into the equation. Integration and substitution of $\tau_w = (\delta P)R/(2L)$ gives:

$$Q = \pi \left(\frac{\Delta P}{2LK} \right)^{1/n} \left(\frac{n}{3n+1} \right) R^{(3n+1)/n} \dots (4.3)$$

If the product is extruded simultaneously through two capillaries (as in a dual orifice die), with different radii and lengths, the pressure drop through each capillary is the same.

Therefore, the ratio of flow rates of the large (Q_L) and the small (Q_S) capillaries is:

$$\frac{Q_L}{Q_S} = \left(\frac{R_L}{R_S} \right)^{(3n+1)/n} \left(\frac{L_S}{L_L} \right)^{1/n} \dots (4.4)$$

The consistency index ‘K’ and the flow behavior index ‘n’ are assumed constant since the product through each capillary has experienced identical extrusion environment. The flow behavior index is calculated using measured values of the flow rate through each die orifice, and the dimensions of each capillary.

$$n = \frac{\log\left(\frac{L_s}{L_L}\right) + \log\left(\frac{R_L}{R_s}\right)}{\log\left(\frac{Q_L}{Q_s}\right) - 3\log\left(\frac{R_L}{R_s}\right)} \dots (4.5)$$

The value of ‘n’ obtained can be re-substituted in the above equation for the flow rate, and knowing Q and ΔP, the value for ‘K’ can be calculated. The pressure transducer measures the pressure just before the material enters the die. The assumption made here is that the pressure drop is entirely due to the die.

4.4 Experimental Section

4.4.1 Materials

The type of starch used was hydroxypropylated high amylose cornstarch (70% amylose content). The starch was purchased from National Starch and Chemicals (Indianapolis, IN), under the trade name of HYLON 7. The inherent moisture content of the starch was 11.2% under ambient conditions. Water was used as the plasticizer as well as the blowing agent. Water content was maintained at 8-10% of the starch used. PHAE is an additive, which offers the adhesion and durability of epoxy resins with the flexibility and processability of thermoplastic resins. PHAE was purchased from Dow Chemicals (Midland, MI), under the trade name BLOX 110. PHAE has a melt temperature of 75°C, and is produced by reacting liquid epoxy resin (LER) with hydroxy functional

dinucleophilic amines and diglycidyl ethers of bisphenol-A, hydroquinone, or resorcinol (RDGE) (28, 29).

4.4.2 Experimental Setup

The experimental setup used in this study was a twin-screw extrusion system. The twin-screw extrusion system consisted of an extruder driver with a speed control gearbox, a Century ZSK-30 twin-screw co-rotating extruder with a screw diameter of 30 mm, an L/D of 42, a positive displacement pump for injecting water into the extruder, accurate single-screw feeders for feeding starch and PHAE. The screw configuration employed in this study is shown in Figure 4.1, and was based on our previous work.

A cylindrical filament die 2.7 mm in diameter and 8.1 mm in length, with a cooling sleeve was assembled to the extruder. The sensors were mounted on the die to measure the temperature and pressure of the melt. A high-speed cutter was used to get cylindrical foam samples of required size.

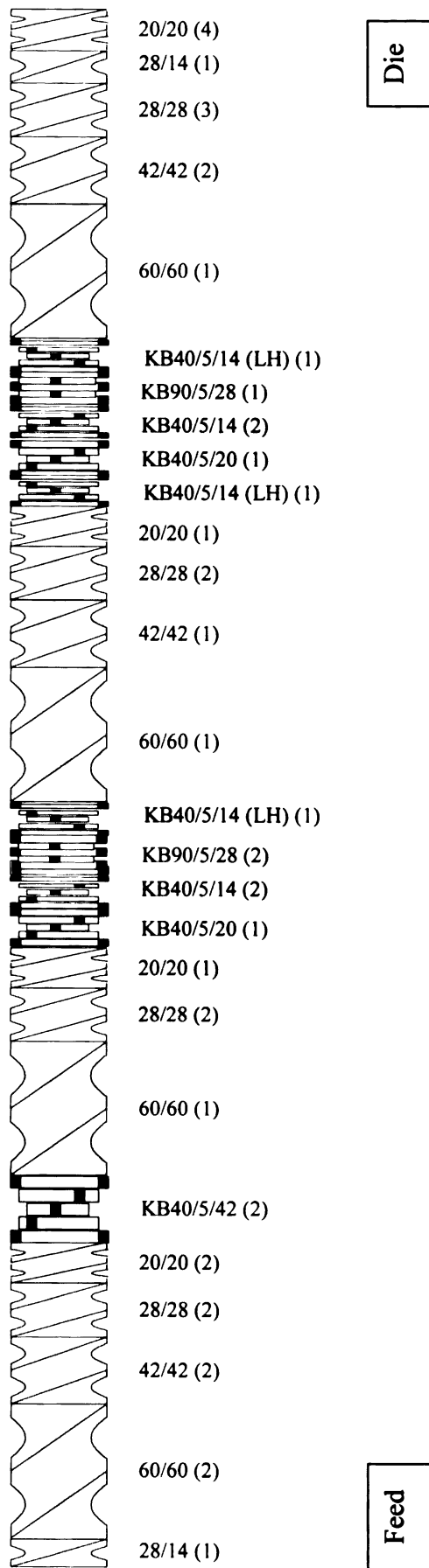


Figure 4.1 Foaming Screw Configuration for the Century ZSK – 30 Twin-Screw Extruder.

4.4.3 Bifurcated Die

The bifurcated die design is shown in Figure 4.2. The smaller filament die was 3 mm in diameter and 12 mm in length ($L/D = 4$), while the larger capillary die was 5.6 mm in diameter with a length of 19.6 mm ($L/D = 3.5$). Thus, each filament die was sufficiently long ($L > 2D$) to ensure fully developed flow through the die. An appreciable part of the pressure drop (ΔP), which occurs across the die, can be due to the pressure drops, which occur due to the constriction at the entrance of the die, and expansion losses at the exit. The constriction losses at the entrance were minimized by tapering the entrance, rather than an abrupt change in the cross-sectional area of the channel of flow. The die could be maintained at the set temperatures due to good temperature controllers on the extruder. The pressure transducer and the thermocouple were positioned as shown Figure 4.2. The viscosity model developed for the optimized formulation (27) was used for the design of an annular die to be used on the Wenger TX- 80 twin-screw manufacturing scale extruder, for the production of Starch-PHAE based foam sheets. The Wenger TX- 80 twin-screw manufacturing scale extruder had a screw diameter of 80 mm and an L/D of 16. An annular die of width 2 mm was used.

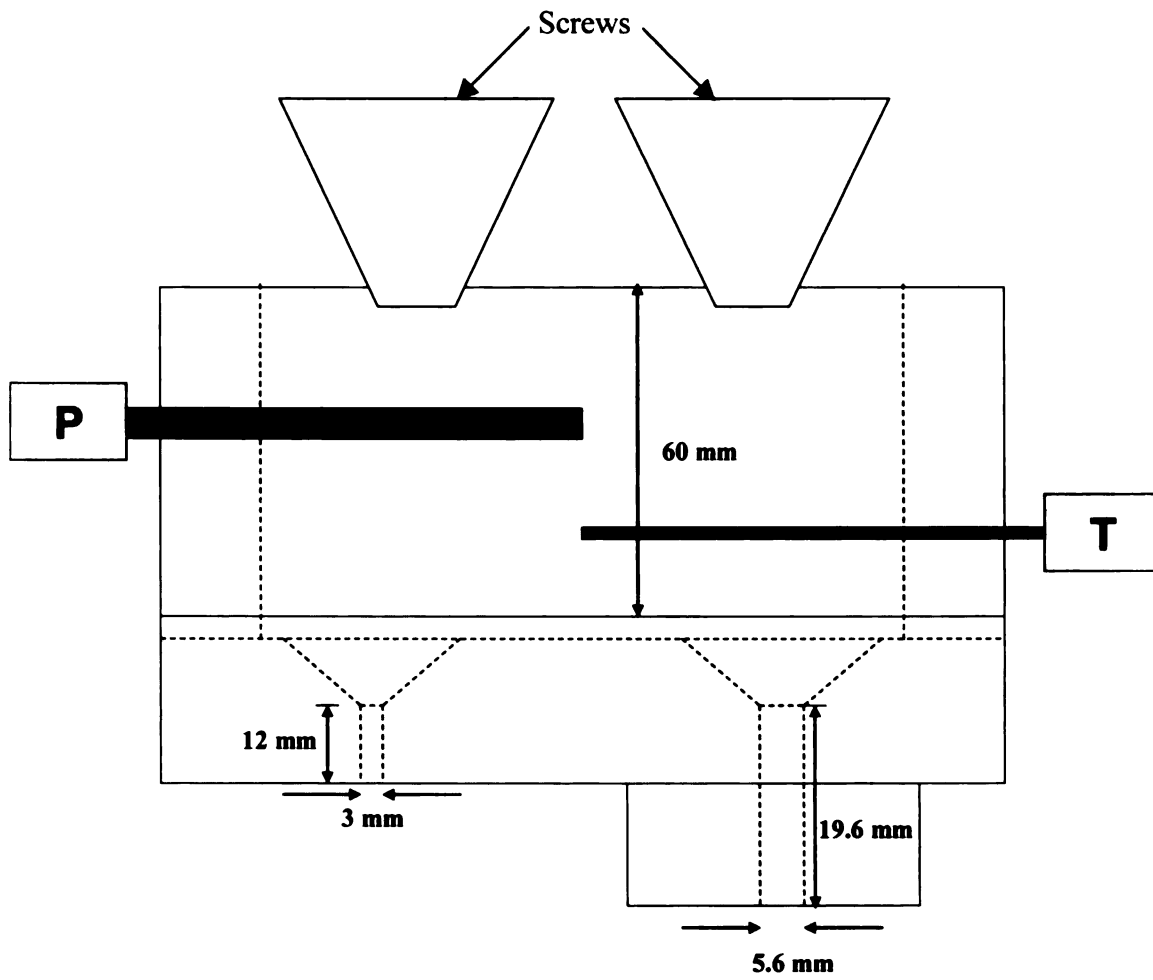


Figure 4.2 Bifurcated Die – Design.

4.4.4 Procedure

The temperatures in the extruder zones were set up to reach the required temperatures.

The temperature profile is as follows:

Zone 1: 20°C (cold feed)

Zone 2: 100°C

Zone 3: 115°C

Zone 4: 120°C

Zone 5: 125°C

Zone 6: 125°C

Zone 7: 120°C

Zone 8: 120°C

Zone 9: 115°C

Die: 110°C

Melt Temperature: 110-112°C

The feeder for starch was calibrated and set at a particular speed to feed at 11.2 kg/hr (~ 25 lb/hr). The other feeder/feeders were calibrated and set at feeding rates accordingly. Initially, during start-up, water was pumped into the system at 15-20% of the starch fed, and later its flow rate was reduced to about 8-10% of starch. The inherent moisture (11.2%) present in starch also helped in plasticization of starch. Thus, the total moisture content was 17.5%. The screw speed was maintained at 200 rpm.

Each extrusion trial was characterized by different parameters, changing one parameter value at each time within the following ranges: screw speed: 150 – 250 rpm, total moisture content: 17.5 % - 50.15% w/w (total weight basis), process temperature

(temperature at the die): 110°C - 120°C, PHAE content: 0% - 14% w/w (total weight basis). When the operating conditions were changed, extrusion was continued until the torque and the die pressure stabilized. The Specific Mechanical Energy (SME) was determined using the following equation (4.6) to quantify the thermo-mechanical treatment:

$$SME = \frac{kW \times Torque \times \frac{RPM_a}{RPM_r}}{\dot{m}} \quad (4.6)$$

SME = Specific Mechanical Energy (kW-hr/kg)

kW = Rated motor power (kW)

Torque = Motor Load (decimal)

RPM_a = actual screw speed

RPM_r = rated screw speed

m = Mass flow rate (kg/s)

The SME value remained sufficiently constant during and extrusion experiment with $\pm 2\%$. The extrudate was collected from each capillary simultaneously for at least a minute, and weighed to determine the mass flow rate. The density of the hydroxypropylated high amylose corn starch was 1410 kg/m³, while that of PHAE was 1340 kg/m³. The density of the extrudate within the die was determined using conservation of mass, and assuming the simple additivity of volumes. The mass flow rates were then converted into the volumetric flow rates, which were further used to determine ‘n’ and then ‘K’ using Equations (4.5) and (4.3) respectively.

The values of ‘K’ and ‘n’ obtained for the varying conditions of temperature, moisture content, PHAE content, and specific mechanical energy were fit to a model deemed

appropriate, using STAT-EASE ‘Design of Experiments 6.0’ modeling software. A central composite Response Surface experimental design (30) was employed to investigate the influence of temperature, moisture content, PHAE content, and specific mechanical energy on the consistency coefficient ‘K’ and flow behavior index ‘n’. Regression analyses were employed to fit the experimental data to linear polynomials (31).

4.5 Results and Discussion

4.5.1 Effect of Moisture Content, Temperature, PHAE content and Screw Speed on ‘K’ and ‘n’:

Table 4.2 shows the values of the consistency coefficient ‘K’ and flow behavior index ‘n’ obtained under varying conditions, while Table 4.3 provides the values for the apparent and actual shear rates through the smaller and larger filament dies for the different processing conditions used for the determination of ‘K’ and ‘n’. The apparent and actual shear rates (12) were calculated from the following equations (4.7) and (4.8):

$$\dot{\gamma}_{app} = \frac{32Q}{\pi D^3} \quad (4.7)$$

$$\dot{\gamma}_{act} = \frac{3n+1}{4n} \cdot \dot{\gamma}_{app} \quad (4.8)$$

The apparent shear rate in the filament dies varied from a minimum of 28.5 s⁻¹ to a maximum of 139.8 s⁻¹ for the smaller capillary, while it varied from 88 s⁻¹ to 181.1 s⁻¹ for the larger capillary die. The influence of each variable of the thermo-mechanical treatment was analyzed by maintaining the other variables constant, which is sometimes difficult due to the close interactions between the variables.

Table 4.2 Values of Consistency Index 'K', and Flow-Behavior Index 'n' for various input conditions.

No	MC (%)	PHAE (%)	T (K)	SS (rpm)	Torque (%)	SME (KW/hr/kg)	Throughput (Kg/hr)	K (Pa.s ²)	n	shear rate (1/s)	η (Pa.s)
1	17.52%	7.0%	383.16	200	67.0%	0.267	9.36	107880.2	0.17	200	2.69E+05
2	25.39%	7.0%	383.16	200	64.0%	0.232	10.28	30177.6	0.28	200	1.31E+05
3	30.98%	7.0%	383.16	200	62.0%	0.209	11.07	13146.5	0.37	200	9.29E+04
4	41.10%	7.0%	383.16	200	59.5%	0.173	12.86	4643.2	0.48	200	5.81E+04
5	50.15%	7.0%	383.16	200	57.0%	0.141	15.09	3208.1	0.52	200	4.93E+04
6	17.52%	0.0%	383.16	200	70.5%	0.300	8.75	140964.6	0.14	200	2.90E+05
7	17.52%	3.5%	383.16	200	68.6%	0.283	9.04	124996.0	0.15	200	2.79E+05
8	17.52%	10.5%	383.16	200	66.5%	0.256	9.70	95785.7	0.19	200	2.63E+05
9	17.52%	14.0%	383.16	200	66.2%	0.245	10.07	85988.3	0.21	200	2.56E+05
10	17.52%	7.0%	393.16	200	66.3%	0.264	9.36	92614.9	0.19	200	2.55E+05
11	17.52%	7.0%	403.16	200	65.2%	0.260	9.36	71608.3	0.23	200	2.39E+05
12	17.52%	7.0%	413.16	200	64.2%	0.256	9.36	57066.8	0.26	200	2.25E+05
13	17.52%	7.0%	433.16	200	62.6%	0.249	9.36	45882.2	0.29	200	2.09E+05
14	17.52%	7.0%	383.16	150	80.8%	0.241	9.36	74188.6	0.29	200	3.48E+05
15	17.52%	7.0%	383.16	175	74.2%	0.259	9.36	85932.1	0.24	200	3.04E+05
16	17.52%	7.0%	383.16	225	63.1%	0.283	9.36	116092.2	0.15	200	2.51E+05
17	17.52%	7.0%	383.16	250	58.2%	0.290	9.36	121882.0	0.11	200	2.17E+05

Table 4.3 Values of apparent and actual shear rates for various input conditions.

No	MC	PHAE	T	SS	Small Die Capillary		Large Die Capillary	
					(D = 3 mm, L/D = 4)		(D = 5.6 mm, L/D = 3.5)	
	(%)	(%)	°C	rpm	$\dot{\gamma}_{app}$	$\dot{\gamma}_{act}$	$\dot{\gamma}_{app}$	$\dot{\gamma}_{act}$
					(1/s)	(1/s)	(1/s)	(1/s)
1	17.52%	7.0%	383.16	200	43.6	95.9	94.5	208.0
2	25.39%	7.0%	383.16	200	69.2	114.5	112.2	185.6
3	30.98%	7.0%	383.16	200	85.8	122.5	123.2	175.9
4	41.10%	7.0%	383.16	200	112.4	143.2	148.7	189.5
5	50.15%	7.0%	383.16	200	139.8	172.6	181.1	223.7
6	17.52%	0.0%	383.16	200	33.1	85.4	88.0	227.6
7	17.52%	3.5%	383.16	200	37.9	90.8	91.3	218.9
8	17.52%	10.5%	383.16	200	48.7	100.5	98.2	202.5
9	17.52%	14.0%	383.16	200	53.4	105.0	102.3	201.0
10	17.52%	7.0%	393.16	200	46.8	96.2	94.0	193.4
11	17.52%	7.0%	403.16	200	51.9	95.8	93.2	172.2
12	17.52%	7.0%	413.16	200	55.3	94.9	92.7	159.0
13	17.52%	7.0%	433.16	200	57.7	93.7	92.0	149.5
14	17.52%	7.0%	383.16	150	58.3	93.7	92.1	148.0
15	17.52%	7.0%	383.16	175	53.1	95.5	92.9	167.2
16	17.52%	7.0%	383.16	225	38.1	93.9	95.3	235.1
17	17.52%	7.0%	383.16	250	28.5	86.7	97.0	295.4

Figures 4.3 – 4.6 below show the individual dependence of the Consistency Coefficient ‘K’ and Flow-Behavior Index ‘n’ on each of the variables such as Moisture Content, Temperature, PHAE content, and the Specific Mechanical Energy (SME) input respectively. Figures 4.3 – 4.6 show that ‘K’ shows an inverse and a direct power-law dependence on the moisture content (Figure 4.3) and the SME (Figure 4.6) of the system respectively, while it decreases exponentially with the die temperature (Figure 4.4); also, ‘K’ decreases linearly with an increase in the PHAE content (Figure 4.5). On the other hand, ‘n’ shows a linear decrease with an increase in SME (Figure 4.6), while a linear increase with an increase in the PHAE content (Figure 4.5). Also, ‘n’ increases logarithmically with increments in the moisture content (Figure 4.3) of the extrudate and the die temperature (Figure 4.4).

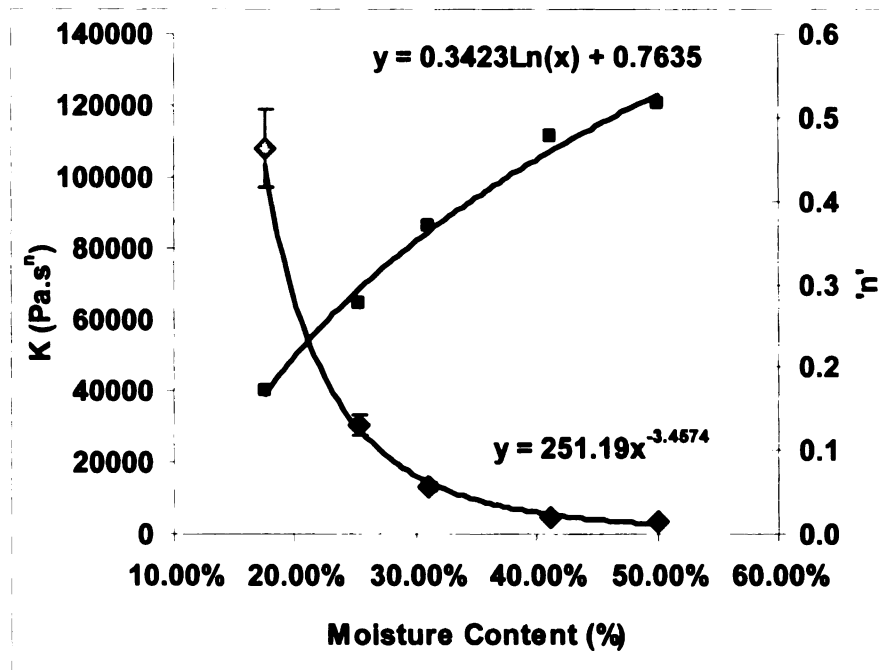


Figure 4.3 ‘◇: K’ and ‘■: n’ as functions of Moisture Content.

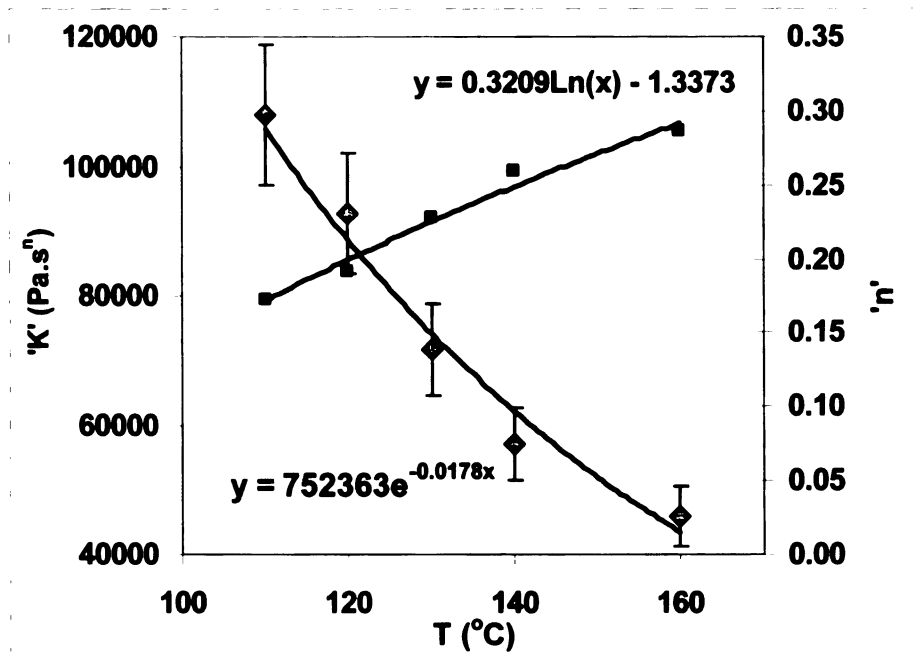


Figure 4.4 '◇: K' and '■: n' as functions of of Die Temperature.

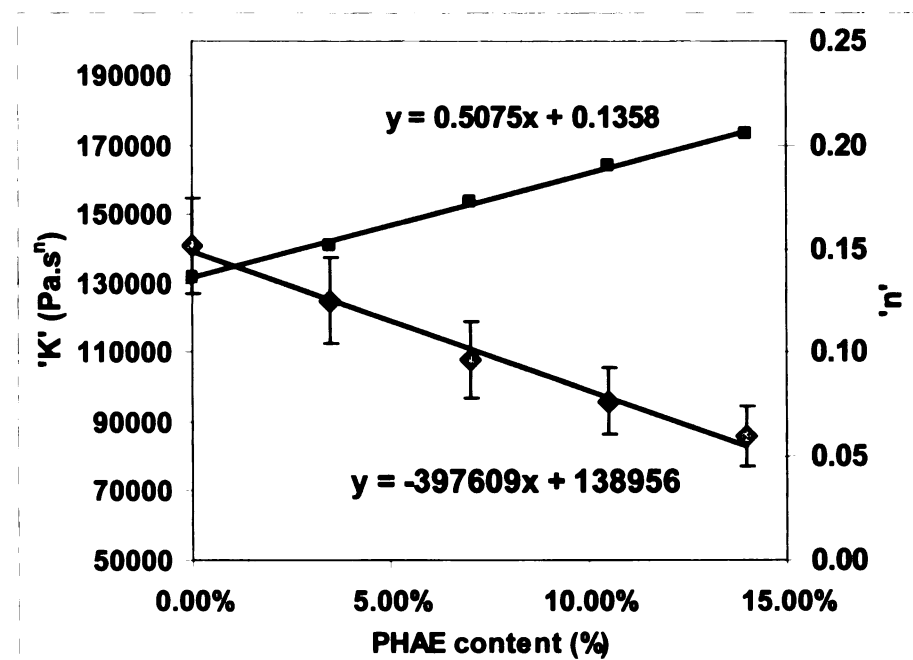


Figure 4.5 '◇: K' and '■: n' as functions of of PHAE Content.

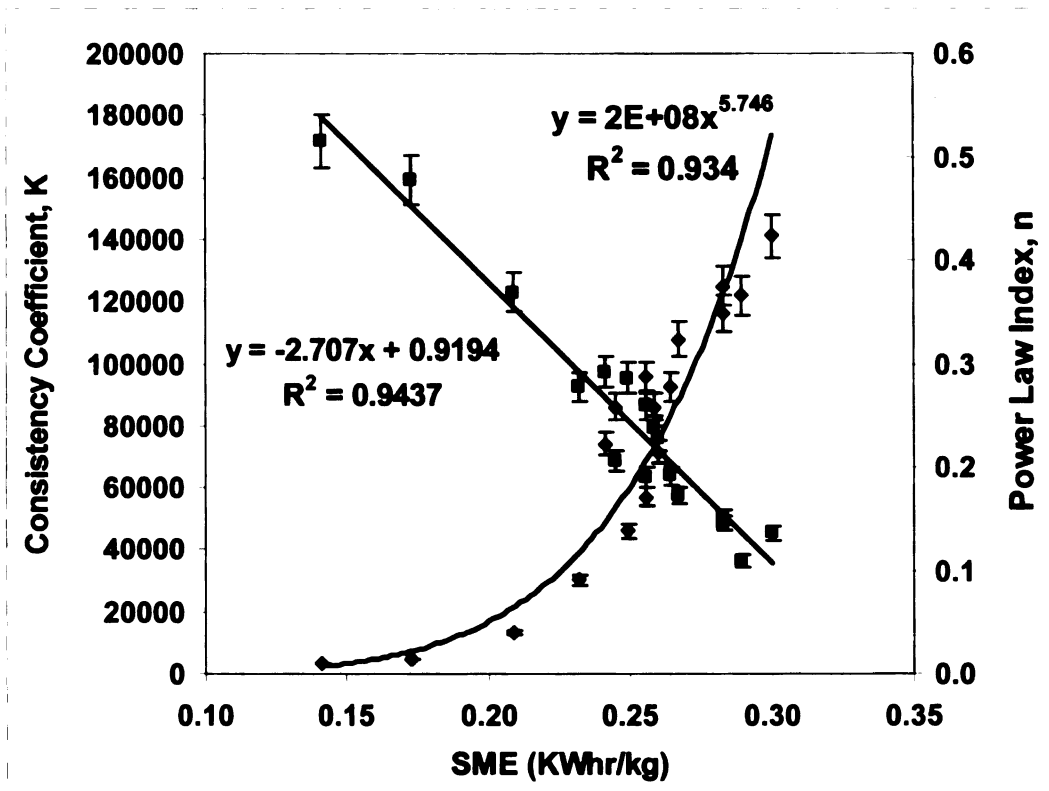


Figure 4.6 \diamond : K' and \blacksquare : n' as functions of of SME.

The flow behavior index varied between a minimum of 0.11 (MC = 17.52%, T = 110°C, PHAE = 7%, Screw Speed = 250 rpm) to a maximum of 0.52 (MC = 50.15%, T = 110°C, PHAE = 7%, Screw Speed = 200 rpm). The variation in the flow behavior index was considerable with variations in moisture content (0.17 – 0.52 with MC = 17.5% - 50.15% respectively), while temperature, screw speed, and the PHAE content did not affect the value of 'n' significantly. The Consistency Coefficient varied between a minimum of 3208 Pa.sⁿ (MC = 50.15%, T = 110°C, PHAE = 7%, Screw Speed = 200 rpm) to a maximum of 140965 Pa.sⁿ (MC = 17.52%, T = 110°C, PHAE = 0%, Screw Speed = 200 rpm). The variation in the Consistency Coefficient was also substantial with variations in

moisture content ($107880 \text{ Pa}\cdot\text{s}^n - 3208 \text{ Pa}\cdot\text{s}^n$ with MC = 17.5% - 50.15% respectively), while temperature, screw speed, and the PHAE content did not affect the value of 'K' appreciably.

The flow behavior index 'n' increased with an increase in the moisture content, while the consistency coefficient 'K' decreased. Similarly, 'n' increased and 'K' decreased with an increase in the die temperature, increase in the PHAE content, and a decrease in screw speeds. However, temperature, screw speed, and the PHAE content did not affect the value of 'n' significantly. This trend was similar to that obtained by Della Valle et al (25). However, the values of 'n' obtained were slightly lower, while the values of 'K' were considerably higher. Flow behavior index values were obtained in the range from 0.10 – 0.66 (25) for high amylose corn starch (70% amylose) for moisture contents of 20.5 – 36%, die temperatures of 105 - 190°C, and screw speeds of 130 – 240 rpm. Flow behavior index values were obtained in the range from 0.296 – 0.443 (22, 23) for corn meal for moisture contents of 25 – 35%, die temperatures of 160 - 180°C, and screw speeds of 160 – 240 rpm. However, several negative values were obtained too.

The viscosities were determined at a random shear rate of 200 sec^{-1} , which is typical in extrusion dies (32), under foaming conditions. It was observed that the viscosity of the starch plastics decreases with an increase in moisture content, increase in PHAE content, increase in temperature, and an increase in screw speeds. Clark (33) has discussed the reasons for the acceptance of the power law model for describing the rheological behavior of intermediate and low moisture starch plastics. It does not account for a yield stress, which are not particularly important in extrusion work.

The power law viscosity model so obtained is used to calculate the actual shear rate and shear stress, and thus used in the following protocol to determine the land length of the annular die for that particular formulation and that particular pressure drop. This annular die would be used in the manufacturing of the Starch-PHAE foam sheets on the Wenger TX – 80 TSE. It is to be noted, however, that ‘K’ and ‘n’ are functions of temperature, moisture content, PHAE content, and the mechanical energy input. Thus, the final model can be considered as:

$$\tau = K(MC, T, PHAE, SME) \dot{\gamma}^{n(MC, T, PHAE, SME)} \dots (4.9)$$

The model obtained for the optimized formulation in the production of starch foam sheets (hydroxypropylated high amylose cornstarch with 17.5% moisture content, 7% PHAE content, at 110°C, and at 200 rpm) is:

$$\begin{aligned} \tau &= 107880 \dot{\gamma}^{0.17} \\ \eta &= 107880 \dot{\gamma}^{-0.83} \dots (4.10) \end{aligned}$$

A linear model was fit using STATEASE ‘Design of Experiments 6.0’ modeling software with the Consistency Coefficient (K), and flow behavior index (n) as the response data; and the die temperature, SME, Moisture Content, and PHAE Feed Rate as the factors. The final model equations in terms of the coded factors ‘A’ (Die Temperature), ‘B’ (SME), ‘C’ (Moisture Content), and ‘D’ (PHAE Feed Rate) are shown in Equations 4.11 (a), and (b); while the final model equations in terms of the actual factors are shown in Equations 4.12 (a), and (b). Significance level was defined as $P < 0.05$.

$$\ln(K) = 9.56 - 0.26A + 1.11B - 1.01C + 0.13D \quad (4.11a)$$

$$n = 0.31 + 0.015A - 0.30B - 0.068C - 0.07D \quad (4.11b)$$

$$\ln(K) = 12.65 - 0.01 (\text{Die Temperature}) + 13.95 (\text{SME}) - 6.20 (\text{Moisture Content}) + 1.92 (\text{PHAE Content}) \quad (4.12a)$$

$$n = 1.126 + 5.85 \times 10^{-4} (\text{Die Temperature}) - 3.81 (\text{SME}) - 0.415 (\text{Moisture Content}) - 0.995 (\text{PHAE Content}) \quad (4.12b)$$

The die temperature is expressed in the absolute scale K, the moisture content and PHAE content are normalized values (between 0 and 1), SME is expressed in KW-hr/kg. Figure 4.7 shows the response surface of 'K' for the die temperature and SME as factors, while Figure 4.8 shows its response surface for the moisture content and PHAE feed rate as independent variables. The response surface of 'n' for die temperature, SME and for moisture content, PHAE content has been shown in Figures 4.9 and 4.10. Thus, Figures 4.9 – 4.10 show that variations in the moisture content and SME induced significant variations in the consistency coefficient 'K' and the flow behavior index 'n' as compared to those due to changes in the die temperature and the PHAE content. Figures 4.11 and 4.12 respectively show the comparison between the actual values of 'K' and 'n' obtained and the values from the models developed. The variance analysis for these data for 'K' revealed a determination coefficient (R^2) of 0.9793 ($P < 0.0001$). Similarly, the R^2 value for 'n' was 0.9865 ($P < 0.0001$). Thus, multiple regression analyses showed a significant linear effect of the independent variables on the flow behavior index, while an exponential effect on the Consistency Coefficient.

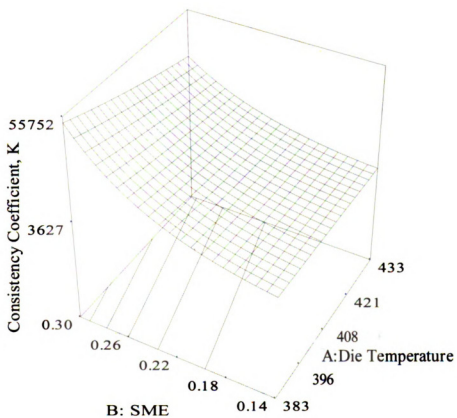


Figure 4.7 Response Surface of the Consistency Coefficient 'K' to variations in SME and the Die Temperature.

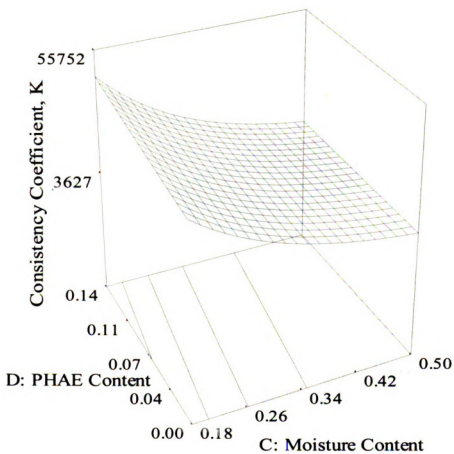


Figure 4.8 Response Surface of the Consistency Coefficient 'K' to variations in Moisture Content and the PHAE Content.

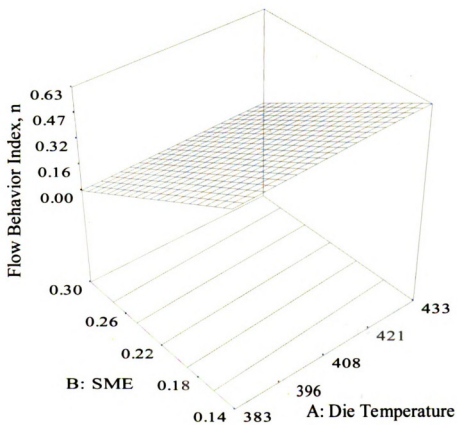


Figure 4.9 Response Surface of the Flow Behavior Index 'n' to variations in SME and the Die Temperature.

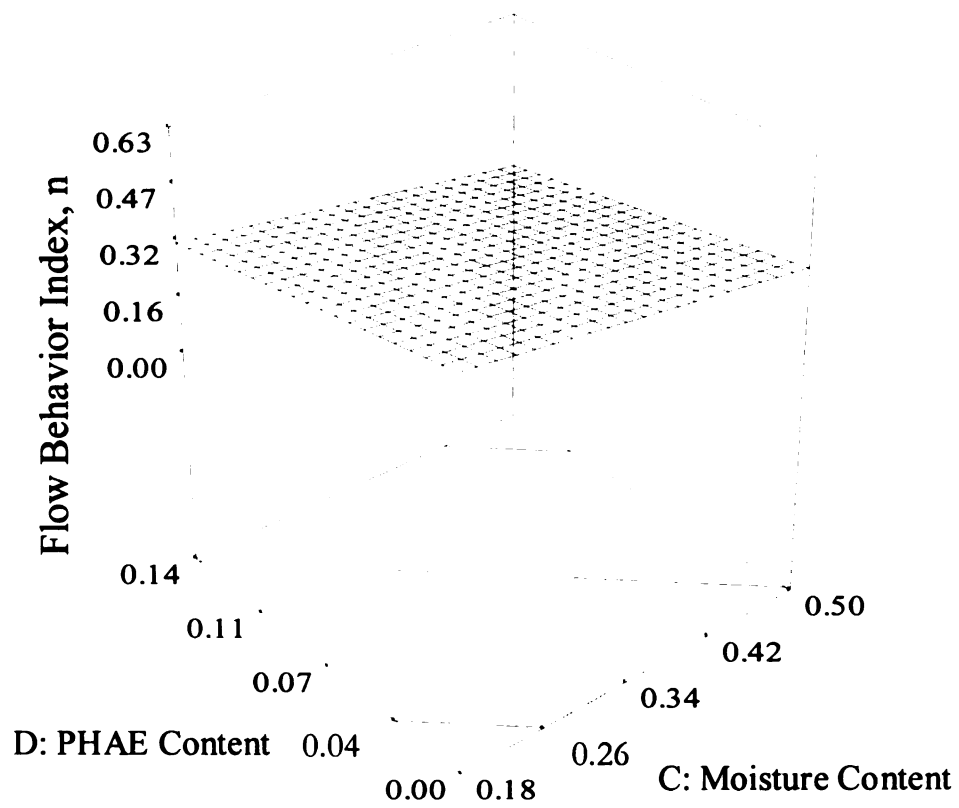


Figure 4.10 Response Surface of the Flow Behavior Index ‘n’ to variations in Moisture Content and the PHAE Content.

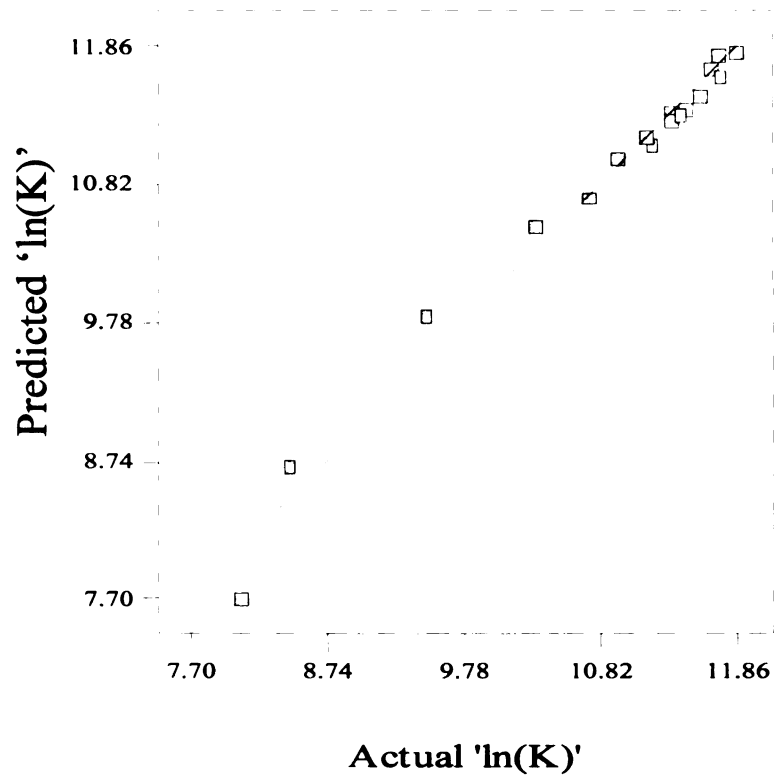


Figure 4.11 Comparison of the Predicted Values of 'ln(K)' with the Actual Values of 'ln(K)'.

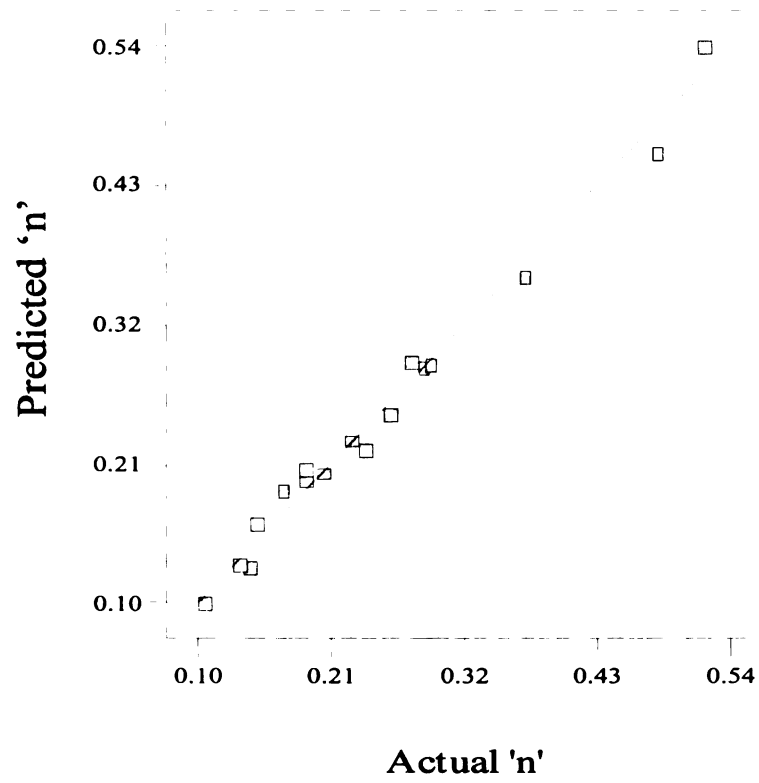


Figure 4.12 Comparison of the Predicted Values of 'n' with the Actual Values of 'n'.

4.5.2 Annular Die Design for Foam Sheet Extrusion

The primary function of the die is to impart shape to the extruded product. The secondary function of the die is to provide optimum pressure at the screw tip to assure that the extruder properly mixes the polymer and delivers it to the die at a uniform rate. The design is optimized by maximizing the pressure drop in the orifice region and minimizing the pressure drop in the other regions. The region having the highest pressure drop has the greatest influence on the flow distribution.

The pressure drop in the orifice region was controlled by setting the land length in order to provide a sufficient pressure drop. The viscous properties of the starch-PHAE blend determined above were considered for the design of this annular die. The pressure gradient and the flow rate through the die must be great enough to prevent premature foam formation within the die. If the extrusion rate is too low or the temperature is too high, foam will form within the die, cells will be ruptured by the shearing action, and the structure will collapse.

4.5.2.1 Using a viscosity model for Shear Stress, τ , and Shear rate, $\dot{\gamma}$ calculations:

The Power Law model as obtained in Equation (4.10) for the optimized formulation in the production of starch foam sheets (hydroxypropylated high amylose cornstarch with 17.5% moisture content, 7% PHAE content, at 110°C, and at 200 rpm), was used for the design of the annular die as shown in Figure 4.13. In this design, land length of the die is determined when the die-gap width (2 mm) is fixed. This is essential to generate enough pressure at the die to cause foaming. This annular die was used in the large-scale manufacturing of starch foam sheets using the Wenger TX – 80 twin-screw extruder.

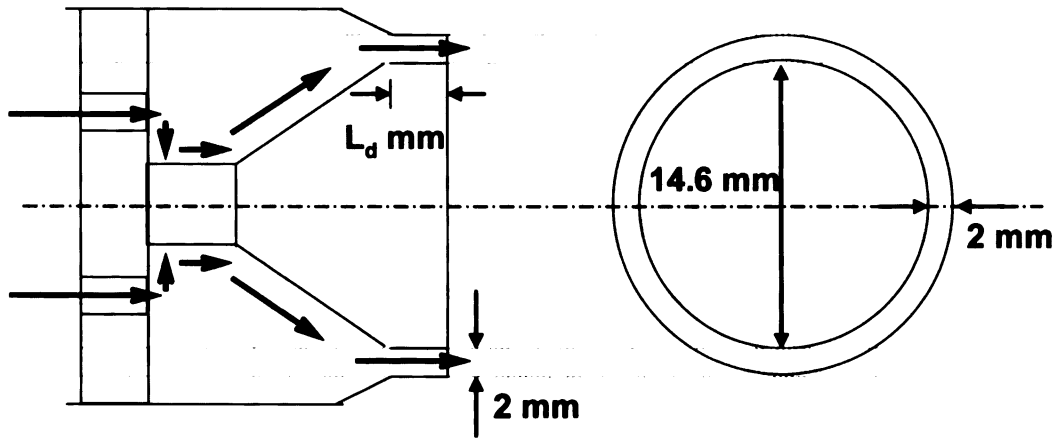


Figure 4.13 Schematic of the Annular Die.

The mass production rate on the Wenger TX-80 was approximately 410 – 415 kg/hr (900 – 910 lbs/hr). Thus, $\dot{m} = 415 \text{ kg/hr}$ and the density of the extrudate within the die was determined to be $\rho = 1360 \text{ kg/m}^3$ using conservation of mass, and assuming the simple additivity of volumes. Thus, the volumetric throughput was:

$$Q = \frac{\dot{m}}{\rho} = 8.5 \times 10^{-5} \frac{\text{m}^3}{\text{sec}} \dots (4.13)$$

For the annular die, the inner and outer radii were fixed to be 0.073 m and 0.075 m respectively to obtain a die gap width of 2 mm. The outer radius was fixed based on the geometry of the equipment.

$$\begin{aligned} R_i &= 0.073\text{m}; R_o = 0.075\text{m} \\ R_o - R_i &= 0.002\text{m} (\text{die gap}) \dots (4.14) \end{aligned}$$

The cross-sectional area ‘A’ and the hydraulic radius ‘R_h’, which is the ratio of the flow area to the perimeter, were determined as per their definitions.

$$R_h = \frac{A}{2\pi(R_o + R_i)} = \frac{\pi(R_o^2 - R_i^2)}{2\pi(R_o + R_i)} \dots (4.15)$$

Actual shear rate ($\dot{\gamma}_{act}$) and shear stress (τ) were calculated using the following equations (4.16) and (4.17) (33):

$$\dot{\gamma}_{act} = \frac{2Q(a + bn)}{R_h An} \dots (4.16)$$

$$\tau = \eta \dot{\gamma}_{act} \dots (4.17)$$

Equations (4.18) and (4.19) were used for the determination of the shape factors ‘a’ and ‘b’ using the aspect ratio (‘e’) and the coefficients A₀ – A₆ and B₀ – B₆ provided in Table 4.4 (33).

Table 4.4 Parameters for the determination of shape factors for annular/circular dies.

Annular Die			
A ₀	0.250	B ₀	0.750
A ₁	3.525716	B ₁	3.590286
A ₂	-20.943061	B ₂	-21.350268
A ₃	61.164339	B ₃	62.083357
A ₄	-92.305040	B ₄	-93.253366
A ₅	69.031394	B ₅	69.480584
A ₆	-20.224675	B ₆	-20.302289

$$a = A_0 + A_1e + A_2e^2 + A_3e^3 + A_4e^4 + A_5e^5 + A_6e^6 \dots (4.18)$$

$$b = B_0 + A_1e + B_2e^2 + B_3e^3 + B_4e^4 + B_5e^5 + B_6e^6 \dots (4.19)$$

$$e = \frac{R_i}{R_o}, \text{ for an annular die} \dots (4.20)$$

$$e = 0, \text{ for a circular die}$$

Hence, in this case, the shape factors were determined as shown in Equation (4.21).

$$\begin{aligned} e &= 0.9733 \\ a &= 0.4998 \dots (4.21) \\ b &= 1.0032 \end{aligned}$$

The flow behavior index 'n', which is the exponent of the shear rate ($\dot{\gamma}$) in the Power Law model was $n = 0.17$ (Equation 4.10).

The actual shear rate was determined using Equation (4.16) given above:

$$\dot{\gamma}_{act} = \frac{2Q(a + bn)}{R_h An} = 702.8 \text{ sec}^{-1} \dots (4.22)$$

The viscosity of the starch melt, ' η ' was determined using the above Power Law model (Equation 4.10) at the above calculated shear rate, $\dot{\gamma}$ (Equation 4.22).

$$\eta = 475.2 \text{ Pa} \cdot \text{sec} \dots (4.23)$$

The Shear Stress at the wall was calculated as the product of the viscosity of the starch melt and the shear rate at the wall.

$$\tau = 3.34 \times 10^5 \text{ Pa} \dots (4.24)$$

From the laboratory-scale experiments, the pressure developed at the die was 720 psi.

Thus, the pressure drop through the die was:

$$\Delta P = \frac{720}{14.7} = 49 \text{ atm} = 4.96 \times 10^6 \text{ Pa} \dots (4.25)$$

Thus, the land length of the die, ‘ L_d ’ was determined from the following equation for the wall shear stress:

$$\tau_w = \left(\frac{R_o - R_i}{2} \right) \frac{\Delta P}{L_d} \quad \dots (4.26)$$

$$L_d = 14.9 \text{ mm} \sim 15 \text{ mm}$$

An appreciable part of the ΔP , which occurs across the die, can be due to the pressure drops, which occur due to the constriction at the entrance of the die, and expansion losses at the exit. The constriction losses at the entrance were minimized by tapering the entrance, rather than an abrupt change in the cross-sectional area of the channel of flow.

Bagley (34) proposed the flowing formula to account for end-effects:

Where,

$$\tau_w = \frac{\Delta P}{\left(\frac{L_d}{\frac{R_o - R_i}{2}} + \frac{L^*}{\frac{R_o - R_i}{2}} \right)} \quad \dots (4.27)$$

L^* is the equivalent length of the die, which would increase ΔP by an amount accounting

for end-effects, mm. The value of $\frac{L^*}{(R_o - R_i)/2}$ was assumed to be equal to 2; and, thus,

the value of L was determined to be:

$$L_d = 12.9 \text{ mm} \sim 13 \text{ mm} \quad \dots (4.28)$$

Thus, without considering end-effects, the die would have been 15% too long.

The same protocol as above was used to determine the length of the known filament die ($D = 2.7 \text{ mm}$, $L_d = 8.1 \text{ mm}$, $L_d/D = 3$) on which all the lab-scale experiments were performed, and the optimization of the starch-PHAE foam process was carried out. Using

the above viscosity model, and the appropriate equations for the determination of the shear rate, shear stress, at the same pressure drop, a land length ' L_d ' of 8.0 mm was obtained after considering the end-effects. Thus, the error was 1.2%.

Thus, this model was considered fairly accurate, though some assumptions were made in the determination of the consistency coefficient.

Since foaming is a three dimensional expansion process, the expansion of width and height could be expected to be in direct proportion to the orifice size. However, it was observed that the edges of the die orifice had a tendency to restrain the width expansion, causing corrugation of the resulting foam sheets. In addition, residual elastic stresses and molecular orientation may cause further distortion. Corrugation could be prevented by using rolls to level the surface of the foam extrudates as described by Carlson (35) and Aykanian (36).

The foam sheets thus obtained were targeted to apply to cushion packaging and insulation cooler applications. The following section deals with the determination of insulation and cushioning properties of the starch foam sheets. The ability to provide insulation was measured in terms of the R-value, while the ability to perform as cushion packaging was measured in terms of cushion curves.

4.6 Scale – Up of the Starch-PHAE Foam Extrusion Process

The stability of the extrusion system, output and product quality is an optimization of machine process variables and feed ingredients. The main process variables such as the feed compositions, screw design and configuration, screw speed, barrel temperatures are directly controlled by the extruder operator, and were optimized earlier. The feed rate depends on the capacity of the pilot scale extruder, and the die design depends on the final product desired.

4.6.1 Feeding

Co-rotating extruders are in general starve fed, i.e. the conveying capacity of the extruder exceeds the rate at which the material is fed into it. The stable, consistent introduction of feed into the extruder is important. Inconsistent feed-rate results in varied product rate (inconsistent densities) and non-uniform texture. The required degree of accuracy of the feeder, however, depends on the tolerance of the extrusion process. Pulsations generated by the feeder can be smoothed out by good extruder configuration design. The foaming screw configuration described earlier accounts for the irregularities in feed rates. Also, raw materials can greatly influence the design of the feeder. Granulated starch is prone to aerate or hold pockets of air, and thus, has density variation within holding vessels. Hence, the design of agitators/activators within the feed hopper of the gravimetric (loss-in-weight, LIW) feeder is critical.

The feed material is pumped from a hopper into a live bin-feeder, from where it is screwed into the extruder barrel vertically. A holding/live bin provides a buffer of raw material at the inlet, so the extruder can operate continuously and without interruption. The bin-feeder also has a pair of butterfly agitators (in addition to the feeding screws),

which keep the fines and the granules in the chilsenated starch well mixed. The fines in the feed are low bulk density powders, which could cause 'sloughing' within the feed chute during vertical feeding. This is a phenomenon in which air tries to escape back up the feed chute, and can result in the dust particulates choking the feed entry port, giving a potentially unstable feed situation.

As the material is fed in to the extruder, the two intermeshing screws rapidly take it into the main body of the machine. The material is then subjected to mechanical and thermal stress by successive sections of restrictive screws or elements.

As the feed zone is not normally full, the injection of water into the barrel under atmospheric pressure is facilitated. The type of water pump is important since any fluctuations in water feed are disastrous. It is important to check the water pump's positive displacement efficiency before starting up. Any air entrainment or badly seated valve arrangements invariably cause a premature shutdown when the water entry port becomes partially blocked.

Typically peristaltic, gear and mono-pumps are unreliable against pressures generated in the extruder feed zone. Piston pumps are the most positive displacement type, and if used as a multihead system, any pulsation is reduced. The main disadvantage of the piston pump is in the valve and ball arrangement where any solid matter, either as a foreign body or natural in the feedstock, will prevent the ball seating in the valve. This drastically reduces the positive nature of the pump, and although it may be apparent that the pump is functioning well under atmospheric pressure, any backpressure caused by partial blockage in the feed pipe is disastrous.

4.6.2 Screw Design

The twin-screw extrusion system used for the production of starch-based foam sheets consisted of an extruder driver with a speed control gearbox, a Wenger TX-80 twin-screw co-rotating extruder with a screw diameter of 80 mm, an L/D of 16, a positive displacement pump for injecting water into the extruder, an accurate single-screw feeder for feeding PHAE. Talc was not used in the production of starch foam sheets in order to get the minimum density product. Also, the addition of talc rendered the product more brittle.

The L/D for the Wenger TX – 80 was half of that of the ZSK – 30 twin-screw extruder used earlier. Food extruders typically use a lower L/D ratio (10–18), as compared to a plastics extruder, to minimize degradation of starches extruded. The screw configuration for TX – 80 was designed corresponding to the configuration for ZSK – 30 discussed earlier. The L/D for each conveying and kneading zones on the ZSK – 30 were calculated as a fraction of the total L/D. These fractions were then used to determine the screw configuration of the Wenger TX – 80. A set of screw elements was available (limited), and the best possible screw configuration (Figure 4.14) was designed using the available screw elements. Following is the tabulated screw configuration (Table 4.5).

Table 4.5 Screw Configuration for Wenger TX – 80 Twin-Screw Extruder

	L/D	Type	Dimension per element	Number of Elements per Screw
A	3.00 D	Conveying	80/120 (Pitch/Length)	2
B	1.50 D	Conveying	60/120	1
C	0.75 D	Conveying	30/60	1
D	1.00 D	Kneading	4 Paddles each (10 mm width/paddle)	2
E	0.50 D	Kneading	3 Paddles each (13.3 mm width/paddle)	1
F	1.34 D	Kneading	1 Paddle each (13.3 mm width/paddle)	8
G	1.50 D	Conveying	20/120	1
H	1.50 D	Conveying	20/120	1
I	1.50 D	Kneading	1 Paddle each (13.3 mm width/paddle)	9
J	0.50 D	Kneading	1 Paddle each (10 mm width/paddle)	4
K	1.50 D	Conveying	20/120	1
L	1.50 D	Conveying (Discharge element)	20/120 (Conical)	1

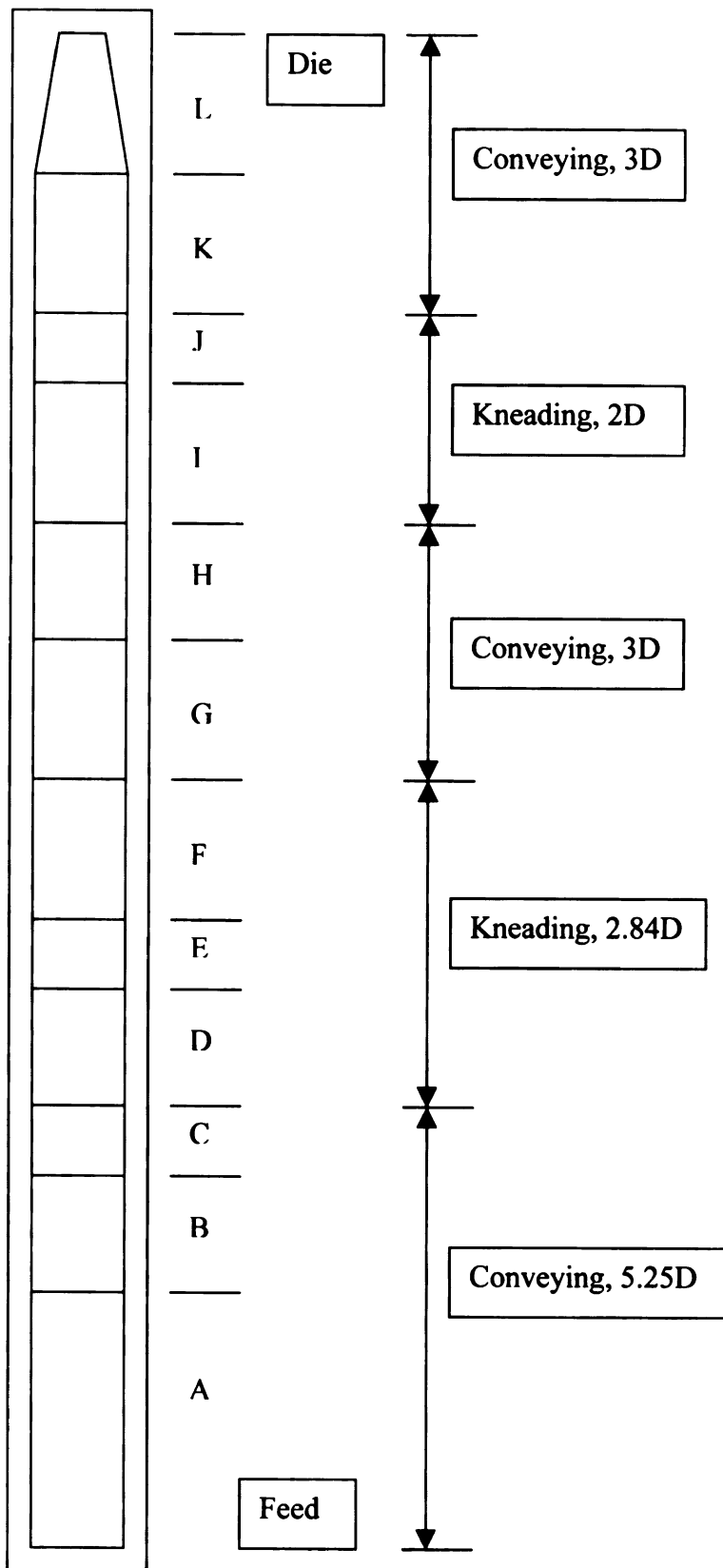


Figure 4.14 Screw Configuration for Wenger TX-80 TSE

4.6.3 Final conical screws

The final screws are conical. These conical screw elements cause a rapid pressure increase, a uniform pressure distribution around the screw periphery, and dampening of any pulsations, which may be present in the final section of the extruder. Special attention should be given to the use of two conical sections at the discharge of the extruder barrel to separate the product flow channel into two isolated flow channels. This design feature permits a uniform and rapid increase in pressure and temperature just prior to the discharge of the extruder.

This concept contributes to unique product textures, increased flexibility, and also minimizes screw and barrel wear, which is problematic and expensive in twin-screw extrusion systems. Wear is minimized because the two isolated channels distribute the product uniformly around the periphery of each extruder shaft. By forcing circumferential pressure symmetry in the highest-pressure region of the barrel, those extreme screw separating forces that exist in more conventional twin-screw extruders are eliminated. This uniform product distribution centers each shaft or screw within its respective flow channel, and functions much like an internal bearing. Due to the cone-angle relative to the extruder shaft axis, the two complementing conical screws gradually lose intermesh, while they maintain a constant flight depth and uniform flight profile.

Figures 4.15 and 4.16 show the entire scaled-up production unit for the manufacturing of the starch-PHAE foam sheets. Figure 4.15 displays the actual foam sheet extrusion process, while figure 4.16 depicts the downstream cutting and lamination process to obtain foam planks of required dimensions. Table 4.6 provides the troubleshooting guide typically followed.

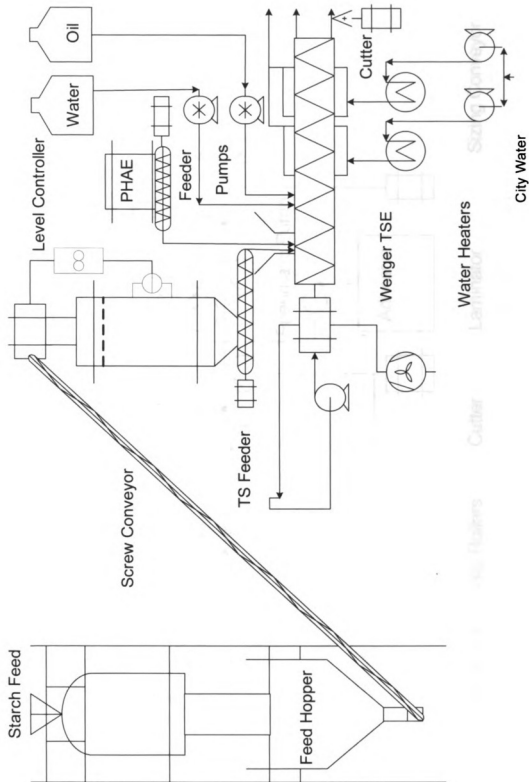


Figure 4.15 Starch Foam Extrusion Process Flow Diagram on the Wenger TX - 80

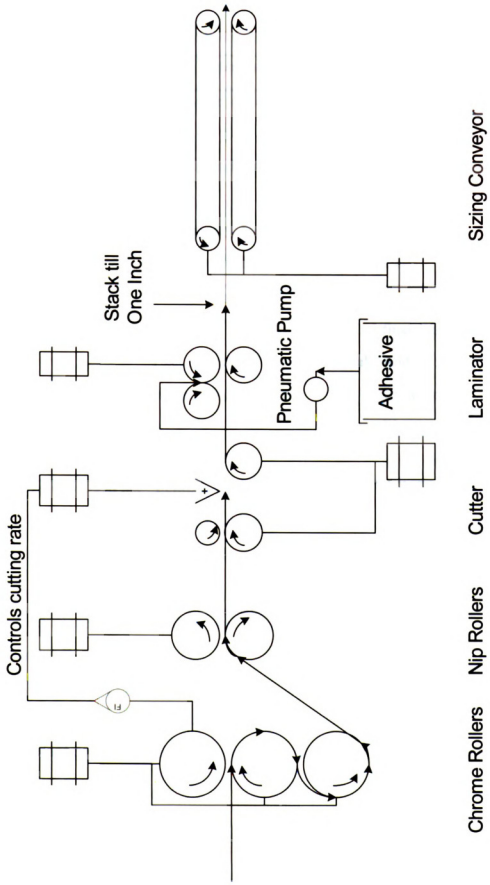


Figure 4.16 Downstream Cutting and Laminating Operation for the Starch Foam Sheet Extrusion

Table 4.6 Troubleshooting Guide

Problem	Extruder Solution	Mechanical Solution
Density too light	Add water to the extruder barrel.	Barrel Temperature must be constant.
	Cool down Extruder Heads.	Change water injection location.
	Reduce dry feed rate based on open area in the die.	Increase open area in the final die.
Density too heavy	Reduce water to the extruder barrel.	Decrease open area in the final die.
	Heat the extruder heads – normal range 120-140°C.	Add 0.25 – 0.5% Sodium Bicarbonate (Chemical Blowing Agent).
	Increase rate.	
Rough Surface of the Product	Extruder Heads may be too hot – Try cooling the Heads.	Increase open area in the final die.
	Extruder water injection too low.	Check wear of screws and the sleeve
Texture too hard, Large cell structure, Crunchy texture	Reduce water to the extruder barrel.	Decrease open area in the final die.
	Heat the extruder heads.	
Hard Spots	Heat extruder heads	Check extruder for proper screw configuration.

Table 4.6 (Contd.) Trouble-shooting Guide

	Pre-moisten metal.	Too much clearance in the die.
	Reduce size of raw material particle size.	Measure extruder parts for wear.
Surging or Extruder Instability	Check for build – up of raw material in the inlet head. Temperature too high in the extruder – cool heads.	Measure extruder barrel for wear. Product build – up in die from improper start – up procedure. Product build – up on cone screw. Barrel temperature must be constant. Change water injection location.
Cutter blades, Uneven edges, Tails		Make sure cutters are sharp and set tight. Check the clearance between the rollers.
Extruder Start – up	Heat Extruder cone – heads. Start extruder water injection at least 50 – 80% higher than running condition.	

Table 4.6 (Contd.) Trouble-shooting Guide

Start the starch lower than running feed rate.

Increase feed rate gradually after extrudate is flowing from the extruder die (let the torque stabilize after every step change in the feed rate).

Adjust head temperature to cool if necessary.

Reduce water injected to get desired product (let the torque stabilize after every step change in the feed rate).

Shutdown Procedure Cool down extruder barrel.

Add extruder water.

Decrease dry feed rate.

Stop feed.

Stop water.

Remove die.

Flush extruder.

Table 4.7 Typical Starch Foam Sheet Production Table

No	Screw Speed (rpm)	Starch feed rate (kg/hr)	Water injection rate (kg/hr)	PHAЕ (kg/hr)	SME (KWhr/kg) (± 0.007)	Barrel temperature profile		Density (Kg/m ³)
						(°C)	(°C)	
1	400	356.1	28.6	27.8	0.135	96	99	34.6 (± 0.7)
2^a	400	356.1	28.5	27.8	0.129	112	115	28.3 (± 0.4)
3	400	356.1	28.9	27.8	0.123	121	127	28.4 (± 1.7)
4	450	356.1	28.5	27.8	0.132	114	118	26.3 (± 1.3)
5	375	356.1	28.4	27.8	0.129	111	114	29.2 (± 0.6)
6	400	338.3	28.8	27.8	0.119	112	115	29.7 (± 0.7)
7	400	356.1	39.2	27.8	0.107	112	113	31.2 (± 0.4)
8	400	356.1	25.1	27.8	0.136	114	116	33.9 (± 1.6)
9	400	356.1	28.5	0.0	0.141	113	116	32.1 (± 1.1)
10	400	356.1	28.7	40.1	0.119	112	115	30.2 (± 0.2)

a – Regular Production Run.

The starch formulation developed and optimized for extrusion foam processing in the ZSK-30 was successfully employed on the large-scale Wenger TX-80. Table 4.7 shows the results obtained on the foam sheet line. The process was given sufficient time to reach a steady state, when any input parameters such as starch and PHAE feed rates, moisture

content and temperature were changed. Once the steady state was attained, samples were collected every 2 minutes for 10 minutes, and the corresponding temperatures and torque readings were recorded. The results were consistent with the results obtained on the laboratory scale extruder.

Entries 1 – 3 show the effect of temperature on the process. Lower temperatures (entry 1) resulted in a denser product, and higher torques. Also the product obtained was hard and brittle. At higher temperatures (entry 3), though the product had a similar density, it was brittle with cracks developing on the surface. Also, surging of the product was observed at higher temperatures, leading to inconsistencies in the downstream cutting and laminating operations. In the higher temperature zones, the shear viscosity of the localized melt in those zones was lower as compared to the viscosity of the starch melt in the other zones. Thus, this surging was due to process instabilities resulting from inconsistent viscosities within the extruder.

Entries 4 and 5 show the effect of screw speed on the final product. At a screw speed of 450 rpm (entry 4), a lower density product was obtained, however, in the presence of surging. This was due to a lower degree of fill in the barrel, resulting in an inconsistent flow. At lower screw speeds, the viscosity of the material in the extruder was higher due to lower work, resulting in a slower, though stable throughput from the extruder.

Entry 6 shows an extrusion run with a lower starch feed rate, which resulted in lower torque and reduced pressure at the die. This resulted in a higher density product, which turned brittle over time due to the presence of excess moisture.

Entries 7 and 8 exhibit the effect of moisture content within the extruder. At a higher water content (entry 7), an effect similar to entry 6 was observed. The product seemed

moist as it exited the extruder die, and showed low resiliency. The product hardened and became brittle over time, due to the presence of excess moisture. At low levels of moisture (entry 8), the torque was extremely high due to the highly viscous material in the extruder, and the product was dense in the absence of enough water (blowing agent). Also, the product had a rough texture (cracks on the surface), and the presence of hard spots in the foam implied incomplete gelatinization of the starch.

Entries 9 and 10 show the effect of PHAE content on the starch foams. As observed previously, the density of the starch foam was higher in the absence of PHAE (entry 9). The density of the starch foams reduced with the introduction of PHAE (Entry 2). However, at a higher PHAE content (entry 10), the foam density increased marginally. This was due to the fact that the pressure developed at the die was lower due to a reduction in melt viscosity of the extrudate. This was obvious from the torque readings for the run. The product obtained, though high density, was sellable because of its high flexibility.

The foam sheets thus obtained were targeted to apply to cushion packaging and insulation cooler applications. The following section deals with the determination of insulation and cushioning properties of the starch foam sheets. The ability to provide insulation was measured in terms of the R-value, while the ability to perform as cushion packaging was measured in terms of cushion curves.

4.6.4 Thermal Resistance (R-value)

It is a measure of resistance to heat flow. The ability of insulation to slow the transfer of heat is measured in R-values. The higher the R-value, the better is the insulation material's ability to resist the flow of heat through it. The C-value (C) is a measure of the Thermal Conductance of the material and is the reciprocal of R, or

$$C = \frac{1}{R} \quad (4.29)$$

C is determined only when the Thermal Conductivity (k) of a material is known.

$$C = \frac{k}{\text{Thickness}} \quad (4.30)$$

The test method ASTM C 177-97 (37) was used to determine the thermal conductivity of the foam sheet samples. The thicknesses used were 2.5 cm, 5 cm and 7.5 cm. Three samples of each thickness were run and the average was reported.

All samples had an R-value ranging from 616.4 to 669.2 K-m²/kW (Table 4.8). The overall average R-value of the samples tested was 634 K-m²/kW. This was in the same class of performance as low-density polystyrene foam bead board, while provided much better insulation properties as compared to polyethylene. However, polyurethane exhibited the best insulation properties.

Table 4.8 Thermal Resistivity of Foam Sheets

Entry	Sample	Average R/m K-m ² /kW (± 35.2)
1	Starch Foam Sheet (1.17" thick)	634.0
2	Starch Foam Sheet (2.08" thick)	616.4
3	Starch Foam Sheet (3.41" thick)	669.2
4	Polystyrene Bead Board	634.0
5	Polystyrene Composite Board	581.1
6	Expanded Polystyrene (EPS)	686.8
7	Extruded Polystyrene (XEPS)	880.5
8	Sprayed Polyurethane Foam	1215.1
9	Polyethylene (73°F)	352.2
10	Polyethylene (23°F)	422.6

4.6.5 Temperature Hold Time Test

A Temperature Hold Time Test was carried out to compare Expanded Polystyrene (EPS), Polyurethane (PUR), and Starch foams as insulation materials. The test was intended to be a qualitative test to compare the performance of multiple cases. Case configurations (sizing, insulation, amount of refrigerant) were determined by product requirements. Product considerations such as temperature requirements and product size and thermal

properties mean that a hold time for one product may be different from another unique product. The purpose of this test was to compare hold times for identical case configurations in different cases, not to establish a “case hold time”.

As this was a comparative test, there was some flexibility in testing procedure. The temperature probes were placed in direct contact with the product. The cases were lined with plastic bags to prevent water damage from condensation or possible leakage. Since the cases were all set up in the same method, the test produced useful results. All cases were taped closed with clear packaging tape. A 1000 ml Nalgene bottle with a water fill was used as the product, and was staged for 24 hours prior to testing. The refrigerant consisted of two large packs of 1 kg of gel-ice (Freez Pak brand item no. 4984) per case. One package of gel ice was placed below the product and one above. The temperature probe was fed through a hole in the bottle so that it was in direct contact with its contents. The EPS, PUR and starch foam cases were all 28 cm X 21.5 cm X 18 cm with a thickness of 5 cm at the wall. The temperatures were recorded over a length of 84 hours. The ambient is always maintained at 22°C. Our criterion for comparison was the length of time the product stays under 8°C.

As shown in Figure 4.17, it was observed that the starch foam sheets maintained the product under 8°C for 56.5 hours as compared to 51.5 hours for polystyrene and 83.5 hours for polyurethane foams. Thus, it proved to be a better insulator than polystyrene foam, polyurethane foams providing the best insulation. These results are also evident from the R-values obtained, polyurethane having the maximum R-value.

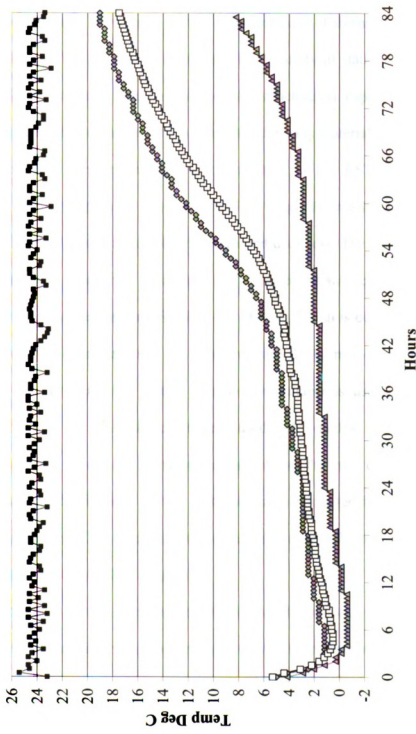


Figure 4.17 Comparison of '◇' Expanded Polystyrene (EPS), '□' Starch, and '△' Polyurethane foams as Insulation Materials, '■' Ambient.

4.6.6 Dynamic Cushion Curve testing

A dynamic cushion curve is a graphic representation of dynamic shock cushioning or transmitted shock in G's (dimensionless) over a variety of static loading conditions (psi or kPa) for a cushioning material thickness (or structure) at a specific equivalent free fall drop height. One cushion curve was generated for each material type, material thickness and drop height combination. The test procedure, as per ASTM D – 1596 (38), was basically one of dropping a platen of specified weight from a known drop height onto a foam cushion of predetermined bearing area and thickness. The deceleration experienced by the platen at impact was monitored and recorded by an accelerometer. Also cushion curves were generated as per ASTM D – 4168 (39), which is designed to evaluate foam-in-place cushioning materials in a manner in which the foam-in-place packaging material is used. In particular, the method included simultaneous use of the foam (cushion sample), and the box with other accessories used in this method of packaging. A platen of specified weight was placed in the box in contact with the foam cushion of predetermined bearing area and thickness. In this test, the entire packaged box was dropped from a known drop height. The accelerometer was in contact with the platen, which recorded the deceleration experienced by the platen.

It is important to identify the drop height from which the package will be expected to fall. There is, however, a certain inherent variability with the manner in which packages are handled. Generally, low level drops occur frequently, while very high-level drops are rare. The drop heights are assumed based on the weight of the product being handled and are presented in Table 4.9 (40). Typical fragility levels for different products are also discussed in Table 4.10 (40). Extremely fragile products such as missile guidance

systems, precision aligned test instruments, etc. have fragility levels in the range of 15 – 25 Gs, while rugged products such as industrial machinery have a fragility level greater than about 120 Gs. In this case, the drop height used was 0.75 m assuming the product to be packaged would be in the range of 25 – 50 kg (40).

Table 4.9 Suggested Drop Heights Based on Weight of Product

Package Weight (pounds)	Type of Handling	Suggested Drop Test Heights (inches)
0-20	One man throwing	42
21-50	one man carrying	36
51-250	Two men carrying	30
251-500	Light equipment	24
501-1000	light equipment	18
1001-up	Heavy equipment	12

Table 4.10 Typical Fragility Levels for Different Products

Extremely fragile	Missile guidance systems, precision aligned test instruments.	15-25 G's
Very delicate	Mechanically shock mounted instruments and electronic equipment, Disk drives.	25-40 G's
Delicate	Aircraft accessories, Computers, Laptops, Flat Panel monitors, Standard Monitors, Printers, Scanners.	40-60 G's
Moderately Delicate	Television Receivers, Aircraft accessories	60-85 G's
Moderately Rugged	Major Appliances	85-115 G's
Rugged	Industrial Machinery	115 G's and above

The cushion curves generated by ASTM D-1596 are shown in Figure 4.18. It was observed that the cushion curves shifted downward with an increase in the thickness of the foam sheet, under identical conditions of static loading and drop height. The cushion curves indicated that the starch foam sheets tested (thickness of 2.5 cm and 5 cm) would provide enough protection for products having fragility levels of greater than 70 G's, classified as moderately delicate, moderately rugged and rugged products. Foam sheets

with thickness greater than 5 cm would be required for more delicate products having fragility levels of less than 70 G's.

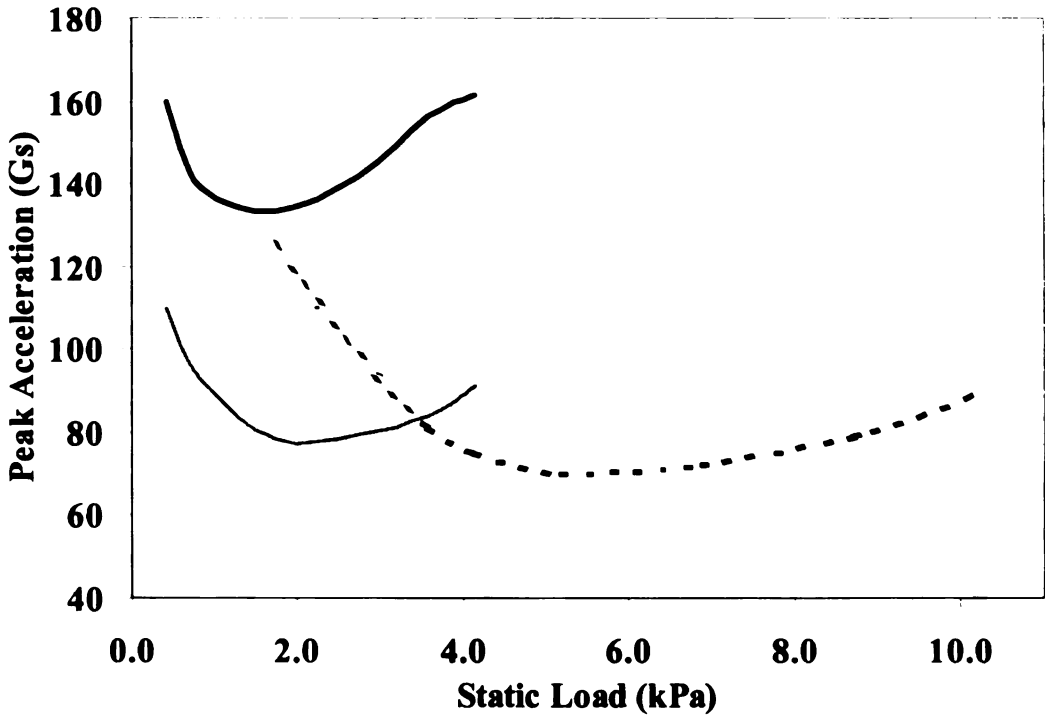


Figure 4.18 Dynamic Cushion Curves for a 2.5 cm and a 5 cm thick starch foam sheet, at a drop height of 0.75 m, as per ASTM D-1596: ‘—’ 2.5 cm thick starch foam sheet, ‘- - -’ 5 cm thick Starch foam sheet, ‘· · ·’ 5 cm thick Polystyrene foam sheet

A similar trend was observed in the cushion curves generated from the testing standard ASTM D-4168 (Figure 4.19). However, the peak deceleration values (G's) generated were expected to be lower than those generated from ASTM D-1596. This is because the box and other accessories, apart from the foam cushion, take a part of the shock in the drop tests. More work needs to be done to correlate the thickness and foam cell structure with the cushioning properties.

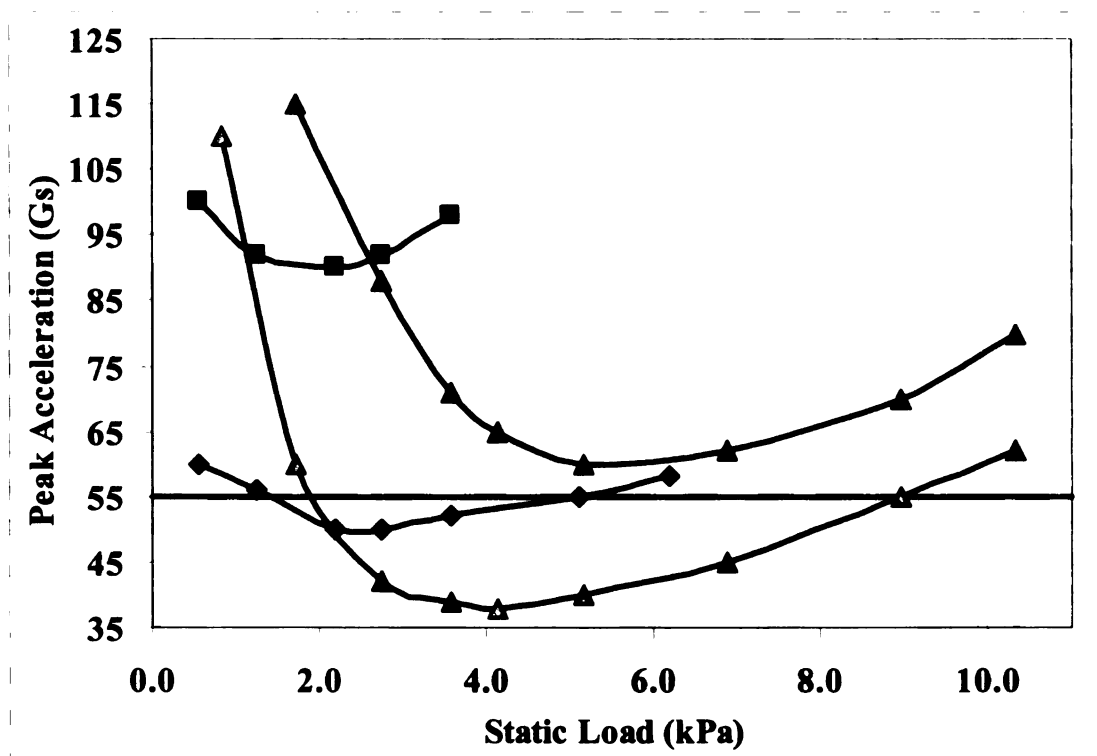


Figure 4.19 Dynamic Cushion Curves for a 2.5 cm and a 5 cm thick starch foam sheet, at a drop height of 0.75 m, as per ASTM D-4168: ‘■’ 2.5 cm thick starch foam sheet, ‘◆’ 5 cm thick starch foam sheet, ‘▲’ 5 cm thick polystyrene foam sheet, ‘△’ 5 cm thick polyethylene foam sheet.

4.7 Conclusion

Cylindrical starch foam shapes were produced on a small scale (~ 11-12 kg/hr) Century ZSK - 30 Twin Screw Extrusion (TSE) process using water as a plasticizer as well as a blowing agent, and poly(hydroxy aminoether) (PHAE) as a functional aid to improve the physico-mechanical properties of the starch foams. A bifurcated die was used for the determination of the viscosity model for the earlier optimized starch- PHAE based foam formulation to be scaled up for the production of starch foam sheets. A Power Law behavior was assumed, and the parameters in the Power Law model such as Consistency Coefficient 'K', and Flow Behavior Index 'n' were obtained as functions of temperature, moisture content, PHAE content and the Specific Mechanical Energy (SME) input to the extruder. The flow behavior index varied between a minimum of 0.11 (MC = 17.52%, T = 110°C, PHAE = 7%, Screw Speed = 250 rpm) to a maximum of 0.52 (MC = 50.15%, T = 110°C, PHAE = 7%, Screw Speed = 200 rpm). The variation in the flow behavior index was considerable with variations in moisture content (0.17 – 0.52 with MC = 17.5% - 50.15% respectively), while temperature, screw speed, and the PHAE content did not affect the value of 'n' significantly. The Consistency Coefficient varied between a minimum of 3208 Pa.sⁿ (MC = 50.15%, T = 110°C, PHAE = 7%, Screw Speed = 200 rpm) to a maximum of 140965 Pa.sⁿ (MC = 17.52%, T = 110°C, PHAE = 0%, Screw Speed = 200 rpm). The variation in the Consistency Coefficient was also substantial with variations in moisture content (107880 Pa.sⁿ – 3208 Pa.sⁿ with MC = 17.5% - 50.15% respectively), while temperature, screw speed, and the PHAE content did not affect the value of 'K' appreciably. An annular die was designed for the manufacture of starch foam sheets using the viscosity model developed for the starch-PHAE formulation

($K=107880 \text{ Pa}\cdot\text{s}^n$ & $n=0.17$ at $MC = 17.52\%$, $T = 110^\circ\text{C}$, $PHAE = 7\%$, Screw Speed = 200 rpm), which provided the best physico-mechanical properties. The density of the cylindrical foam extrudates obtained on the Century ZSK – 30 was 22-23 kg/m^3 . This annular die was then successfully employed on an industrial scale (410-420 kg/hr) twin-screw food extruder, Wenger-80, to manufacture foam sheets. The density of the foam sheets was 27-30 kg/m^3 .

The results obtained on the Wenger TX – 80 were consistent with the results obtained on the laboratory scale ZSK – 30 twin-screw extruder (27). The extruded starch foam sheets provided excellent insulation properties. The R-values obtained suggested better insulation characteristics, as compared to expanded polystyrene, and efforts are in progress to enhance their thermal resistivity to make them comparable to polyurethane foams. Also, the dynamic cushioning data reveals that the starch foam sheets provided decent cushioning or shock absorption properties.

Due to the many types of cushions available and the parameters, which determine their behavior, the number of cushion curves required for a thorough account of the subject is immense. It was natural, therefore, to try to reduce the database to descriptive equations either by curve fitting or by solving the dynamics problem using a model of the cushion. The succeeding Chapter 5 deals with the development of different models involving finite difference and finite element techniques to predict the cushioning properties of the starch-based foam sheets produced as described in the above sections.

4.8 References

- 1) Holdsworth, S. D. Journal of Texture Studies, 2, 393, 1971.
- 2) Casson, N. In Rheology of Dispersed Systems, Mill, C. C., Ed.; Pergamon Press: New York, 84 – 104, 1959.
- 3) Bingham, E. C. Fluidity and Plasticity; McGraw Hill: New York, 1922.
- 4) Herschel, W. H.; Bulkley, R. Proceedings of the American Society of Testing Materials, 26, 621 – 633, 1926.
- 5) Mizrahi, S.; Berk, Z. Journal of Texture Studies, 3, 69 – 79, 1972.
- 6) Ofoli, R. Y.; Morgan, R. G.; Steffe, J. F. Journal of Texture Studies, 18, 213 – 230, 1987.
- 7) Cross, M. M. Journal of Colloidal Science, 20, 417 – 437, 1965.
- 8) Philippoff, W. Kolloid – Zeit, 71, 1 – 16, 1935. Cited in: Brodkey, R. S. The Phenomena of Fluid Motions, Addison-Wesley Publishing Co.: Menlo Park, California, 1971.
- 9) Van Wazer, J. R. Viscosity and Flow Measurement, Interscience Publishers: New York, 1963.
- 10) Powell, R. E.; Eyring, H. J. Nature, 154, 427 – 428, 1944.
- 11) Carreau, P. J. PhD Dissertation, Department of Chemical Engineering, University of Wisconsin, Madison, 1968.
- 12) Steffe, J.F. Rheological Methods in Food Process Engineering, Freeman Press: East Lansing, MI, 1996.
- 13) Harper, J. M.; Rhodes, T. P.; Wanniger, L. A. AIChE Symposium Series, 67 (108), 40 – 43, 1971.
- 14) Han, C. D. Rheology in Polymer Processing, Academic Press: New York, 1976.
- 15) Lai, L.S.; Kokini, J.L. Biotechnology Progress, 7, 251 – 266, 1991.
- 16) Vergnes, B.; Villemaire, J.P. Rheologica Acta, 26, 570 – 576, 1987.
- 17) Wen, L.; Rodis, P.; Wasserman, B. P. Cereal Chemistry, 67, 268 – 275, 1990.

- 18) Bhattacharya, M.; Padmanabhan, M.; Seethamraju, K. Journal of Food Science, 59, 221 – 226, 1994.
- 19) Padmanabhan, M.; Bhattacharya, M. Journal of Rheology, 35, 315 – 343, 1991.
- 20) Lai, L.S.; Kokini, J.L. Journal of Rheology, 34, 1245 – 1266, 1990.
- 21) Senouci, A.; Smith, A. C. Rheologica Acta, 27, 546 – 554, 1988.
- 22) Padmanabhan, M.; Bhattacharya, M. Journal of Food Engineering, 18, 335 – 349, 1993.
- 23) Seethamraju, K.; Bhattacharya, M. Journal of Rheology, 38, 1029 – 1044, 1994.
- 24) Vergnes, B.; Della Valle, G.; Tayeb, J. Rheologica Acta, 32, 465 – 476, 1993.
- 25) Della Valle, G.; Colonna, P.; Patria, A.; Vergnes, B. Journal of Rheology, 40, 347 – 362, 1996.
- 26) Drozdek, K. D. MS Thesis, Urbana-Champaign, Urbana, IL: University of Illinois, 2000.
- 27) Nabar, Y. U.; Schindler, M.; Narayan, R. Polymer Engineering and Science, In Press.
- 28) Winkler, M. S.; Berry, T. S.; Kirkpatrick, D. E. US Patent 6,365,079, 2002.
- 29) Silvis, C. H.; White, J. E. US Patent 5,275,853, 1986.
- 30) Myers, R. H. In: Response Surface Methodology, Allan and Bacon, Boston, 1971.
- 31) Chavez-Jauregui, R. N., Silva, M. E. M. P., Areas, J. A. G. Journal of Food Science, 65, 1009-1015, 2000.
- 32) Rossen, J. L.; Miller, R. C. Food Extrusion, Food Technology (Chicago), 27 (8), 46, 1973.
- 33) Sansone, L. F. In Foam Extrusion – Principles and Practice, Lee, S.T., Ed.; Technomic Publishing Company: Lancaster, Pennsylvania, Chap. 7, 165 – 188, 2000.
- 34) Bagley, E. B. Journal of Applied Physics, 28, 624, 1957.
- 35) Carlson, F. A. US Patent 2,857,265, 1958.
- 36) Aykanian, A. A. US Patent 2,945,261, 1960.

- 37) American Standard Test Methods, 2002. Standard Test Method for Steady-State Thermal Transmission Properties by Means of the Heat-Flow Meter Apparatus. In: Annual Book of ASTM Standards. C-518, 4.06, Philadelphia, PA.
- 38) American Standard Test Methods, 2002. Standard Test Methods for Dynamic Shock Cushioning of Packaging Materials. In: Annual Book of ASTM Standards. D – 1596, 15.09, Philadelphia, PA.
- 39) American Standard Test Methods, 2002. Standard Test Methods for Transmitted Shock Characteristics of Foam-in-Place Cushioning Materials. In: Annual Book of ASTM Standards. D – 4168, 15.09, Philadelphia, PA.
- 40) American Standard Test Methods, 2002. Standard Test Methods for Mechanical-Shock Fragility of Products, Using Shock Machines. In: Annual Book of ASTM Standards. D – 3332, 15.09, Philadelphia, PA.

PREDICTION OF CUSHION CURVES

5.1 Background

Polymer foams have been classified by their cellular morphology, mechanical behavior and composition. Structurally the material can be described as open or closed cell (1). With closed cell materials the gas is dispersed in the form of discrete gas bubbles and the polymer matrix forms a continuous phase. In open cell foams the voids coalesce so that both the solid and fluid phases are continuous. With open cell structures, the fluid is able to flow through the polymer matrix under the action of some driving potential, whereas in closed cell structures, gas transport takes place by diffusion through the cell walls. The ease of movement of the fluid phase through the matrix is one of the factors governing the physical and mechanical properties of the cellular polymer. Closed cell foams are widely used in the packaging industry for cushioning fragile items. Open cell foams in which the air is able to circulate freely within the foam structure behave differently because the air flows freely rather than compresses (2, 3). In practice, the two cellular morphologies can co-exist so that the polymer foam is not always completely open or closed cell. The volume fraction of closed cell has a considerable influence on the mechanical behavior of these systems so it is an important structural characteristic.

The shock transmission properties of most commercially available cushions are published in the form of cushion curves (4). Cushion curves relate the peak deceleration of an object dropped on the cushion to the object's weight, the drop height, the impact area,

and the cushion thickness. The cushion curve diagram shows the maximum acceleration occurring during the shock as a function of cushioning area related to the item's mass. The diagram contains a number of curves with the parameter distinguishing them being the relation of drop height to cushion thickness. Using the diagram, the cushion's thickness and area, which will limit maximum acceleration on the item, can be easily determined. Because of the many types of cushions available and the parameters, which determine their behavior, the number of cushion curves required for a thorough account of the subject is immense. It was natural, therefore, to try to reduce the database to descriptive equations either by curve fitting or by solving the dynamics problem using a model of the cushion (1, 3, 5 – 8).

The simplest approach towards modeling cushion behavior would be to relate the cushion compression to the force the cushion exerts upon the resting product. The resulting solid mechanics problem must consider (9)

- Equation of motion
- Geometry
- Material Constitutive relations (Stress-Strain behavior)

Hooke's law (10) is an idealized model (linear stress-strain relationship), which some physical systems obey. The cushion behavior, however, is known to be non-linear, visco-elastic, time and temperature dependent. Despite these dependencies, there are models that try to "fit" foam cushions into the Hookean model (1, 3, 7).

The compression of a foam cannot be accurately modeled by the Hookean equation. This can be observed from the following prediction for the peak G-level to a mass dropped onto a cushion using Hooke's law, and comparing it to experimental data (2).

Stress = modulus X strain (Hooke's Law)

$$\sigma = E\varepsilon \quad (5.1)$$

σ = stress (psi)

E = Elastic Modulus (psi)

ε = strain

Energy absorbed by cushion = energy density X cushion volume

$$U = \frac{\sigma^2 At}{2E} \quad (5.2)$$

A = cushion bearing area

t = cushion thickness

Energy absorbed = Potential Energy

$$U = Wh \quad (5.3)$$

W = weight dropped

h = drop height

Combining Equations 5.1, 5.2, 5.3 and solving for the peak stress and using

$$\sigma = \frac{F}{A} \quad (5.4)$$

F = force,

$$F = \left(\frac{2hWEA}{t} \right)^{0.5} \quad (5.5)$$

Force = mass X acceleration

= Weight X G

$$F = WG \quad (5.6)$$

Solving for peak deceleration,

$$G = \left(\frac{2hE}{tS} \right)^{0.5} \quad (5.7)$$

Where static loading,

$$S = \frac{W}{A} \quad (5.8)$$

According to equation 5.7, G should continue to decrease as the static loading increases.

This is shown in figure 5.1 under linear cushion behavior.

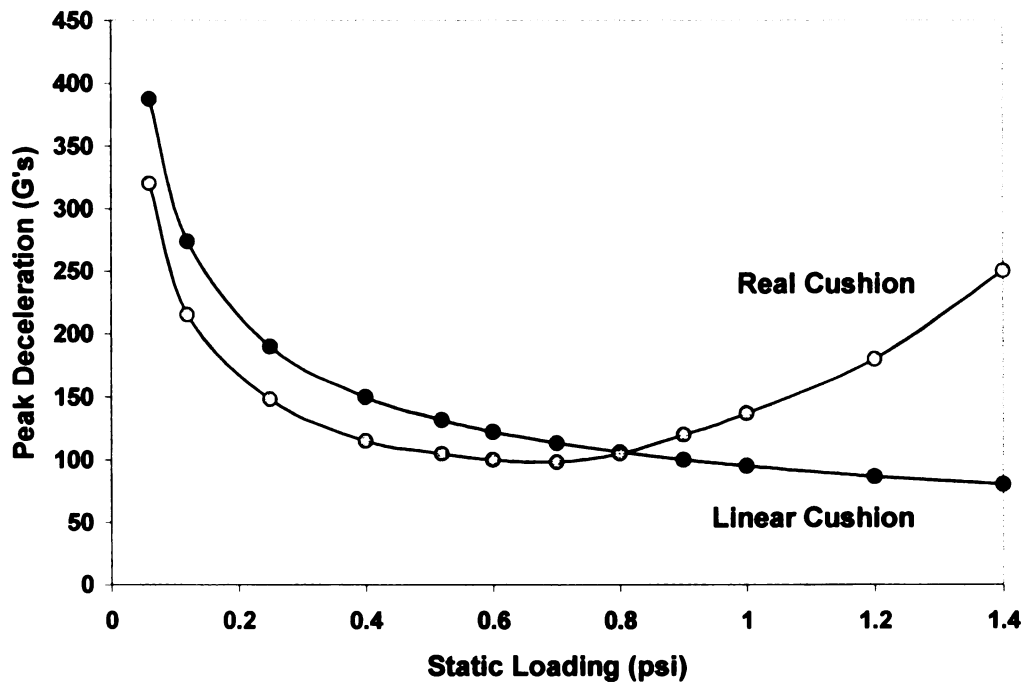


Figure 5.1 Real Cushion behavior compared to Hookean (Linear) cushion.

This agrees with known cushion performance, but only up to a certain point. It fails to predict the rise in deceleration as static loading increases. Since the only assumption involved in the analysis is Hooke's law, it could be implied that equation 5.1 gives rise to the error (3).

To model the cushion accurately, one needs to develop more realistic constitutive equations. To develop the constitutive equations, one must first consider the nature of the compression process. This leads to considering heat transfer.

As a closed-cell cushion compresses, the air volume decreases and the pressure and temperature increases. Since the air temperature is now higher than the cell wall temperature, heat is transferred from the air to the cell walls. This raises the wall temperature only slightly due to its large heat capacity so that the walls can be considered as a nearly constant temperature heat sink. During the entire compression and expansion process, energy is extracted from air and therefore not given back to the weight. As a consequence, the stress depends not only on strain, but strain rate as well (11). It was also shown that the heat transfer process cannot be adiabatic due to the large rise in temperature of the enclosed air, and also the large surface area of the cells available for heat transfer (2).

5.2 Method I: Governing Differential Equations for the Prediction of Cushion Curves

The compression of a cushion involved three time-dependent variables (12). The variables were the thickness of the cushion denoted by ' x ', the air pressure ' P ' within the cells, and the air temperature ' T '. Thus, in the modeling of a closed-cell foam, three differential equations must be solved simultaneously. These three equations were derived from the Newton's second law of motion, the ideal gas law, and the first law of thermodynamics.

Figure 5.2 shows a weight ' W ' in a free fall from a height ' h ' onto a block of closed-cell cushion of thickness ' x_0 ' with a bearing area ' A '.

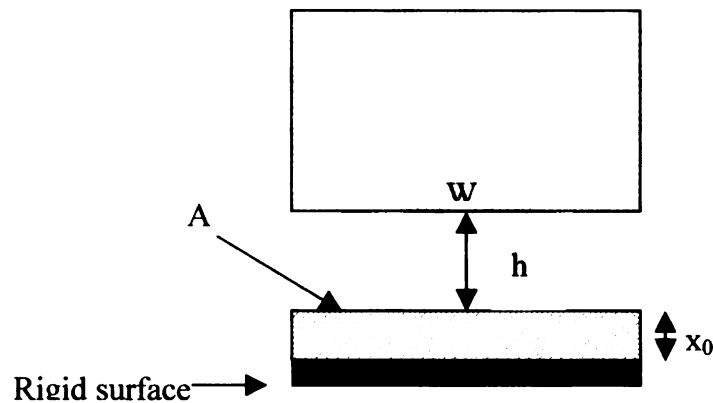


Figure 5.2 Schematic of a weight in a free fall onto a cushion.

Newton's second law was now applied and the first governing equation was derived. In order to solve for the deceleration of the weight, a force balance was performed on the weight. The free-body diagram in figure 5.3 shows the weight and a cut away portion of the cushion.

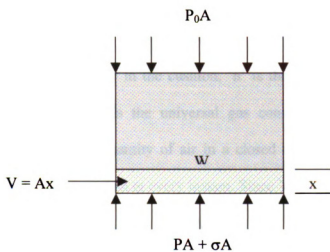


Figure 5.3 Free body diagram of cushion and weight.

Newton's second law states that:

$$\Sigma F = \frac{W}{g} \frac{d^2x}{dt^2} \quad (5.9)$$

$$PA + \sigma A - P_0A - W = \frac{W}{g} \frac{d^2x}{dt^2} \quad (5.10)$$

where ' σ ' is the yield pressure required to compress the foam structure (less the air), ' P_0 ' is the normal atmospheric pressure, ' P ' is the cell air pressure during compression (assumed to be the same for each cell), and ' g ' is the acceleration due to gravitational pull.

Solving for acceleration and rearranging equation (5.9) gave:

$$\frac{d^2x}{dt^2} = g \left[\frac{\sigma + P - P_0}{s} - 1 \right] \quad (5.11)$$

Equation (5.11) could not be solved since the variable 'P' is a function of time, 't'.

The second governing equation, which related the air pressure to the other variables, was the ideal gas law (13):

$$PV = nRT \quad (5.12)$$

where 'V' is the volume of air in the cushion, 'n' is the fixed number of moles of air trapped in the cushion, 'R' is the universal gas constant, and 'T' is the absolute temperature. Given that the quantity of air in a closed cell foam is constant, equation (5.12) states that PV/T is constant at every instant. Since $V = Ax$, we have:

$$P = P_0 \left(\frac{x_0}{x} \right) \left(\frac{T}{T_0} \right) \quad (5.13)$$

Equation (5.13) relates the pressure to the position, but a new variable 'T' has appeared. Consequently, another relation must be derived. The third equation required to solve the system of equations was the energy equation. The energy equation was applied to the fixed quantity of air within the foam using the first law of thermodynamics applied to the closed system (13):

$$\text{Work done} + \text{heat added} = \text{change in internal energy}$$

During the compression and expansion of the cells surrounding the air, there is work done on the air. This is known as simple boundary work. Heat is added to the air as a result of compression, and heat exchange takes place through convection heat transfer to the cell walls. The change in internal energy of the air is the direct result of a change in temperature (13, 14). Mathematically, the first law of thermodynamics is written as:

$$\partial q + \partial w = \partial u \quad (5.14)$$

For a closed system over a small time period, the work done, the heat exchanged, and the change in internal energy could be expressed as:

$$\partial w = -PdV \quad (5.14a)$$

$$\partial q = -HS(T - T_0)dt \quad (5.14b)$$

Where 'H' is the convection heat transfer coefficient, 'S' is the total surface area of the cells in the foam matrix, 'T' is the instantaneous air temperature, and 'T₀' is the ambient air temperature. Also,

$$\partial u = mC_v dT \quad (5.14c)$$

Where 'm' is the total mass of the air, C_v is the constant volume specific heat for air. Substituting equations (5.14a), (5.14b), (5.14c) into equation (5.14):

$$- PdV - HS(T - T_0)dt = mC_v dT \quad (5.15)$$

Rearranging with dV = Adx, and dividing by dt, the third governing equation became:

$$\frac{dT}{dt} = -\left(\frac{PA}{mC_v}\right)\frac{dx}{dt} - \left(\frac{HS}{mC_v}\right)(T - T_0) \quad (5.16)$$

In summary, the three governing equations were:

$$\text{Newton's Second Law: } \frac{d^2 x}{dt^2} = g\left[\frac{\sigma + P - P_0}{s} - 1\right] \quad (5.11)$$

$$\text{The Ideal Gas Law: } P = P_0\left(\frac{x_0}{x}\right)\left(\frac{T}{T_0}\right) \quad (5.13)$$

$$\text{Energy Balance: } \frac{dT}{dt} = -\left(\frac{PA}{mC_v}\right)\frac{dx}{dt} - \left(\frac{HS}{mC_v}\right)(T - T_0) \quad (5.16)$$

The three coupled equations may be reduced to two differential equations, since; equation (5.13) was not a differential equation. Substituting 'P' in equation (5.13) into equations (5.11) and (5.16) yielded:

$$\frac{d^2x}{dt^2} = g\left(\frac{\sigma - P_0}{s} - 1\right) + \left(\frac{gP_0x_0}{sT_0}\right)\frac{T}{x} \quad (5.17)$$

$$\frac{dT}{dt} = -\left(\frac{A}{mC_v} \frac{P_0x_0}{T_0}\right)\frac{T}{x} \frac{dx}{dt} + \left(\frac{HS}{mC_v}\right)T_0 - \left(\frac{HS}{mC_v}\right)T \quad (5.18)$$

Since the terms in parentheses were constants for a particular cushion, the above two equations could be written as:

$$\frac{d^2x}{dt^2} = K_1 + K_2 \frac{T}{x} \quad (5.17a)$$

$$\frac{dT}{dt} = -K_3 \frac{T}{x} \frac{dx}{dt} + K_4 - K_5 T \quad (5.18a)$$

Where:

$$K_1 = g\left(\frac{\sigma - P_0}{s} - 1\right) \quad (5.19a)$$

$$K_2 = \left(\frac{gP_0x_0}{sT_0}\right) \quad (5.19b)$$

$$K_3 = \left(\frac{AP_0x_0}{mC_vT_0}\right) \quad (5.19c)$$

$$K_4 = \left(\frac{HS}{mC_v}\right)T_0 \quad (5.19d)$$

$$K_5 = \left(\frac{HS}{mC_v}\right) \quad (5.19e)$$

In order to examine the effect of cushion geometry and cell dimensions on the constants K_1 through K_5 , certain terms in the above expressions needed to be examined. Specifically, they were σ , s , m , and H .

5.2.1 Determination of material yield point stress, σ_y :

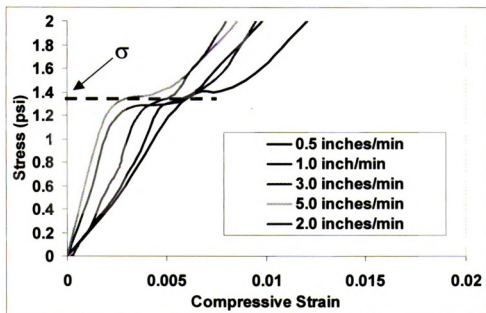
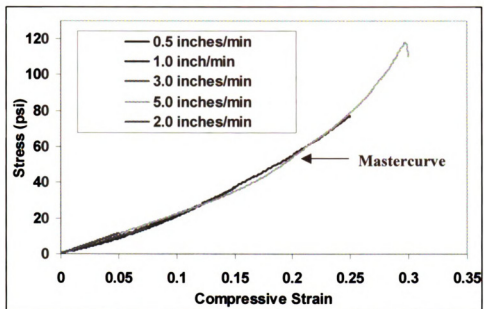


Figure 5.4 Determination of material yield point stress from foam yield stress.

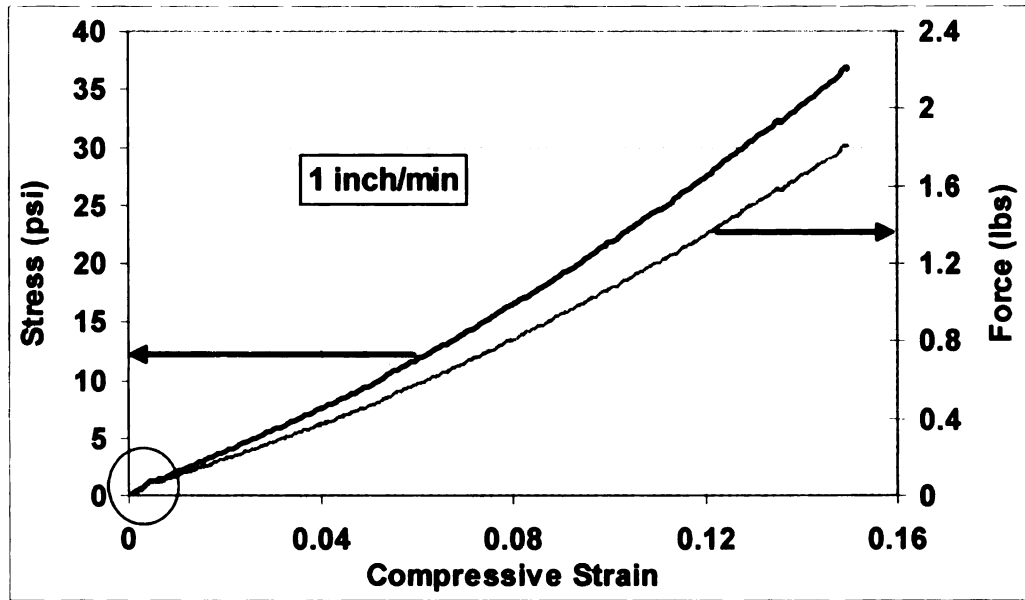


Figure 5.5 Compressive Force/Stress vs. Compressive Strain Curves

The yield stress determined from the above experiment was $\sigma = 1.4$ psi, and the diameter of the cylindrical probe used for compression testing was, 'd' = 0.25 inches.

The figure 5.6 below shows the hypothetical cross-section of the closed cell cushion (cells with square cross-section) under the compression test. The yield pressure, σ , is defined as the vertical surface pressure, which causes the cell walls to yield. A simple force balance yielded:

$$\sigma = \sigma_y \left(\frac{A_w}{A} \right) \quad (5.20)$$

Where:

σ_y – material yield point stress

A_w – total cross-sectional area of only the walls.

A - apparent bearing area ($\pi d^2/4$)

The yield pressure, σ , is the stress required to compress the cell matrix alone, and contributes significantly to decelerating the product. The polymer matrix could be considered as a thin wall membrane, which supports no bending moments (3, 7, 8). The cell could be assumed to undergo both buckling and yielding (1). Modeling of the cell matrix was difficult due to the variability in cell size and the complexity of the geometry. Many geometries have been proposed such as the spherical cell connected by a cylindrical strut model, the pentagonal dodecahedron cell and the tetrakidecahedral cell (1, 7). The geometry will vary depending on the material and the foaming process. Matonis (15) has proposed an equivalent model to simplify the analysis of the cell structure. The model proposed was a cubical plate model, which consisted of layered cubical arrays as in figures 5.6, 5.7.

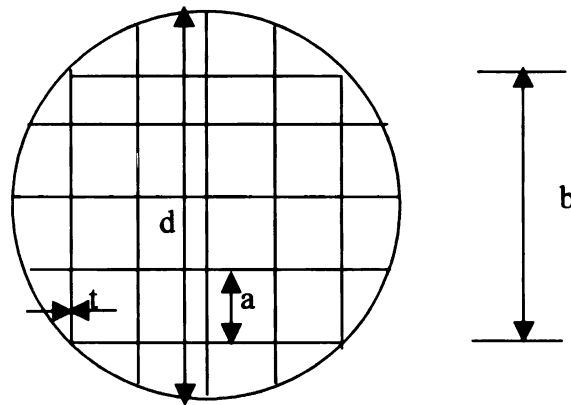


Figure 5.6 Assumed Circular Cross-section of foam with hypothetical square cells (compression test).

The total amount of wall support area in figure 5.6 was:

$$A_w = \left[b \frac{b+a}{a} + b \frac{b+a}{a} \right] t + \pi dt + 4 \left[\frac{b}{a} - 1 \right] at \quad (5.20a)$$

Rearranging and substituting results in:

$$A_w = 2t \left[\frac{b^2}{a} + b \right] + \pi dt + 4 \left[\frac{b}{a} - 1 \right] at \quad (5.20b)$$

Thus, equation (5.20) applied gave a material yield point stress of $\sigma_y = 1780$ psi.

5.2.2 The Yield Pressure, σ :

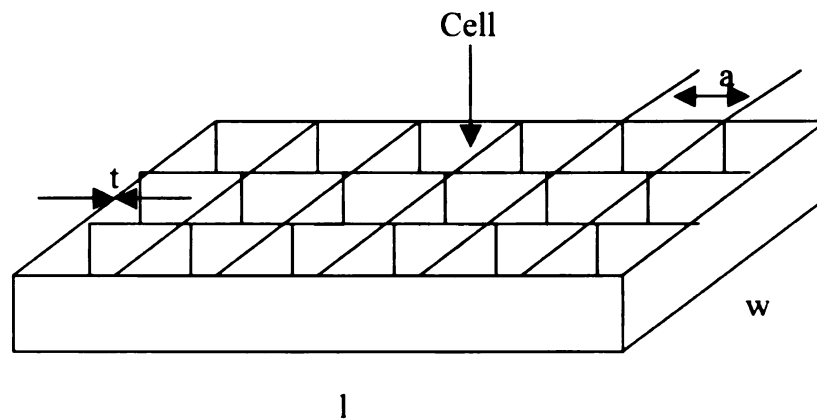


Figure 5.7 Foam section with hypothetical array of square cells (for the determination of cushion curves).

The above figure shows a hypothetical section from a closed cell cushion. The yield pressure, σ , is defined as the vertical surface pressure which causes the cell walls to yield.

A simple force balance yields:

$$\sigma = \sigma_y \left(\frac{A_w}{A} \right) \quad (5.20)$$

Where:

σ_y – material yield point stress

A_w – total cross-sectional area of only the walls.

A - Apparent bearing area ($l \times w$)

The total amount of wall support area in figure 5.7 was:

$$A_w = \left[l \frac{w+a}{a} + w \frac{l+a}{a} \right] t \quad (5.21)$$

Rearranging and substituting results in:

$$A_w = \left[\frac{2lw}{a} + l + w \right] t \quad (5.22)$$

Substituting equation (5.22) in equation (5.20) yielded:

$$\sigma = \sigma_y \left[\frac{2}{a} + \frac{1}{w} + \frac{1}{l} \right] t \quad (5.23)$$

Typical values for the cell dimensions for the starch foam sheets were (16):

$a \sim 0.03 - 0.04$ inches = 700 – 1000 μm .

$t \sim 0.00001$ inches = 0. 254 μm .

$\sigma_y \sim 1780$ psi, determined from compression tests.

Thus, equation (5.23) applied gave a yield pressure of $\sigma = 1.19$ psi.

5.2.3 The Total Cell Wall Surface Area, S:

The total cell wall surface area could be calculated by considering the average surface area of one cell and multiplying by the number of cells in a volume of cushioning material (2).

$$S = (6a^2) \left(\frac{l}{a} \frac{w}{a} \frac{x_0}{a} \right) = 6 \frac{lw x_0}{a} = 6 \frac{V_0}{a} \quad (5.24)$$

Where V_0 is the original volume of the cushioning material.

5.2.4 The Convection Heat Transfer Coefficient, H:

The heat transfer rate is related to the overall temperature difference between the gas in the encapsulated cell and the cell wall by the convection heat transfer coefficient, H. The estimate for 'H' considers the convection process to be a hybrid of the parent conduction process (2). A cross-section of the cell is shown in figure 5.8.

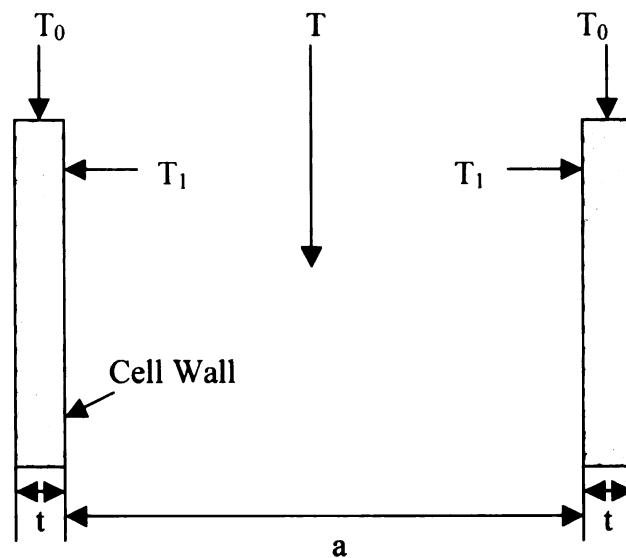


Figure 5.8 Temperatures in the cell cross-section.

Let T_0 be the temperature at the center of the cell wall, T_1 the temperature at the cell-air interface, and T the temperature of the air at the center of the cell. The basic conduction equation is (17):

$$q = -k \frac{dT}{dx} \quad (5.25)$$

where:

k – thermal conductivity

dT/dx – temperature gradient

q – heat flow rate through area S .

Since q through the air to the interface must equal q through the cell wall from the interface:

$$-\frac{q}{S} = k_a \left(\frac{T - T_1}{a/2} \right) = k_s \left(\frac{T_1 - T_0}{t/2} \right) \quad (5.26)$$

Where k_a and k_s are the thermal conductivities for air and the foam material. Solving for T_1 and reinserting into either of the two equalities above yields:

$$-q = HS(T - T_0) \quad (5.27)$$

with

$$H = \frac{2k_a k_s}{k_a t + k_s a} \quad (5.27a)$$

Now the thermal conductivity for air at 70°F is $k_a = 0.0148$ BTU/hr/ft/°F [79] and for a starch foam of 2” thickness was $k = 0.597$ BTU/hr/ft/°F (16).

The thermal conductivity of the foam material, k_s , was determined from the following equation, which related ‘ k ’ to ‘ k_a ’ and ‘ k_s ’ (18):

$$k = k_a + \frac{2}{3} k_s v_s \quad (5.27b)$$

v_s – volume fraction of the solid (foam material) phase.

$$v_s = \frac{\rho_{foam}}{\rho_{foam\ material}} \quad (5.27c)$$

Thus, k_s was determined to be 39.59 BTU/hr/ft/°F.

From equation (5.27a),

$$H = 11.84 \text{ BTU / hr / ft}^2 \text{ /}^\circ \text{ F} \quad (5.28)$$

Which was seen to be almost entirely dependent on the air component alone since $t \ll a$.

5.2.5 The Total Air Mass, m:

The mass of air was estimated to be the volume of the cushion times the density of the air. The foam itself contributed very little to the volume of the cushion. This could be realized by taking an open cell cushion and compressing the cushion. The open cell cushion could be made to flatten out completely. Thus, the mass is:

$$m = \rho(l \times w \times x_0)(1 - v_s) \quad (5.29)$$

where the air density is $\rho = 0.0000466 \text{ lb/in}^3 = 0.08057 \text{ lb/ft}^3$.

Substituting the results for σ , S, m, and H into the expressions for K_1 through K_5 gave:

$$K_1 = \frac{g}{s} \left(\sigma_y \left(\frac{2}{a} + \frac{1}{l} + \frac{1}{w} \right) - P_0 - s \right) \quad (5.30a)$$

$$K_2 = \left(\frac{g P_0 x_0}{T_0} \right) \left(\frac{1}{s} \right) \quad (5.30b)$$

$$K_3 = \left(\frac{P_0}{C_v \rho T_0} \right) \quad (5.30c)$$

$$K_4 = \left(\frac{6HT_0}{C_v \rho} \right) \left(\frac{1}{a} \right) \quad (5.30d)$$

$$K_5 = \left(\frac{6H}{C_v \rho} \right) \left(\frac{1}{a} \right) \quad (5.30e)$$

The terms on the right hand side of equations (5.30a) through (5.30e) have been grouped using parentheses in order to illustrate the effects of material properties, cell dimensions, cushion dimensions, and environmental terms on the constants. Without this simplification, one cannot deduce the effects of modifying the cell or cushion structure. The constants K_1 and K_2 depended on air properties, cell dimensions, cushion dimensions, and static loading, which in turn depended on weight of the falling mass. K_3 depended on air properties alone, whereas, K_4 and K_5 depended on cell dimensions and foam material properties.

At this point, it was evident that only K_1 and K_2 depended on types of variables normally associated with cushion design: the static loading, s ; and the cushion thickness, x_0 respectively. An additional parameter not contained in K_1 and K_2 , but important to cushion design, was the drop height information. The drop height parameter would enter the analysis through the governing equations as an initial condition on velocity. Specifically, the initial or impact velocity is (19):

$$v_i = \sqrt{2gh} \quad (5.31)$$

The gas related constants are given below:

$P_0 = 14.7$ psi (initial air pressure in the cells)

$T_0 = 70^\circ\text{F} = 529.6^\circ\text{R}$ (initial cell air temperature)

$C_v = 0.2398$ BTU/lb/ $^\circ\text{F}$ (Constant volume specific heat of air)

$$\rho = 0.0000466 \text{ lb/in}^3 = 0.08057 \text{ lb/ft}^3 \text{ (density of air at } 529.6^\circ\text{R)}$$

Now, once the weight (static load), drop height, and the original cushion thickness were known, the constants K1 – K5 were known, and the differential equations could be solved numerically for the pressure, P; temperature, T; and cushion thickness, x. The procedure for doing this is outlined in the next section. A computer program based on this procedure was written to accept drop data (W, w, l, x₀, and h) and generate the shock pulse.

5.2.6 Solving the Governing Differential Equations using the Forward Finite Difference Method:

From the three governing equations, a series of values for thickness, temperature and pressure could be generated. The forward finite difference method was used to generate these values. The technique involved initializing the variables and stepping the equations forward in time with an increment of Δt . Referring back to the summary of the differential equations, notice that only pressure could be found from the three equations (5.11), (5.13) and (5.16). The thickness and temperature variables were in differential form. In order to calculate the thickness and temperature, equations that relate position to acceleration, and temperature to temperature rate were required.

The equations that related position and velocity to acceleration were equations derived from kinematics in one dimension (20 – 22). These equations were only valid for uniformly accelerated motion. For some differential time dt , these equations hold true; and for some finite time Δt , they were only approximate.

$$x = x_0 + \frac{dx}{dt_0} \Delta t + \frac{1}{2} \frac{d^2x}{dt_0^2} \Delta t^2 \quad (5.32)$$

$$\frac{dx}{dt} = \frac{dx}{dt_0} + \frac{d^2x}{dt_0^2} \Delta t \quad (5.33)$$

$\frac{d^2x}{dt^2}$ - Represents the acceleration of the mass on the cushion

$\frac{dx}{dt}$ - Represents the velocity of the mass at an instant in time.

In a similar manner, the new temperature will depend on the rate of temperature change.

$$T = T_0 + \frac{dT}{dt_0} \Delta t \quad (5.34)$$

$\frac{dT}{dt}$ - Represents the rate of change in temperature.

The three governing equations (5.11), (5.13) and (5.16) coupled with the three finite difference equations (5.32), (5.33) and (5.34) were the six equations necessary to solve the finite difference problem. The drop data, material constants, environmental constants and gas related constants are shown in Table 5.1.

The procedure used in the forward finite difference program in EXCEL involved initialization of all the variables at time $t = 0$.

'G' is the dimensionless unit of acceleration, defined as the acceleration at a particular time interval divided by the gravitational acceleration. This variable was needed to specify the severity of the shock. When the pressure 'P' returned to its initial value of 14.7 psi, the weight was leaving the cushion and the finite difference calculation was completed. An example with the calculation is shown in Table 5.2.

For the particular run in Table 5.2, the peak deceleration was seen to be 107.3 G's and the shock duration was approximately 10.8 ms. The rebound velocity was 140.48 in/sec, which gave the coefficient of restitution (19) to be $e = 0.923$.

Table 5.1 Data and Initial Conditions

Density of Air, ρ	4.66042E-05 lb/in ³
Heat Transfer Coefficient, H	2.28395E-05 BTU/sec/in ² /°F
Surface Area, S	25,600 in ²
Initial temperature, T ₀	529.6 °R
Initial Thickness, x ₀	2 inches
Atmospheric (Initial) Pressure, P ₀	14.7 psi
Drop Height, h	30 inches
Length, l	8 inches
Width, w	8 inches
Weight, W	3.84 lbs
Static Loading, s	0.06 psi
Specific Heat of Air at Constant Volume, C _v	0.2398 BTU/lb/°F
Mass of Air, m	0.005965338 lb
Cross-Sectional (Bearing) Area, A	64 in ²
Gravitational Acceleration, g	386.4 in/sec ²
Cell Size, a	0.03 inches
Cell Wall Thickness, t	1.0 E-05 inches
Material Yield Point Stress, σ_y	1780 psi
Stress Required to compress Cell Matrix, σ	1.19 psi
Time Increment, Δt	0.0001 sec
Initial Velocity, v _i	-152.263 in/sec
K ₁	-87385.05642
K ₂	357.5075529
K ₃	0.265959317
K ₄	216466.3756
K ₅	408.7356034

Table 5.2 Solution to System of Differential Equations.

Δt	T (°R)	x (")	P (psi)	dx/dt	G	dT/dt	d ² x/dt ²
0.0000	529.60	2.00	14.70	-152.3	18.8	10723.3	7282.9
0.0001	530.67	1.98	14.84	-151.5	21.2	10327.2	8200.6
0.0002	531.71	1.97	14.99	-150.7	23.6	9940.5	9121.4
0.0003	532.70	1.95	15.13	-149.8	26.0	9562.5	10045.1
0.0004	533.66	1.94	15.27	-148.8	28.4	9192.6	10971.2
0.0005	534.57	1.92	15.42	-147.7	30.8	8830.1	11899.5
0.0006	535.46	1.91	15.56	-146.5	33.2	8474.5	12829.3
0.0007	536.31	1.90	15.71	-145.2	35.6	8125.2	13760.3
0.0008	537.12	1.88	15.85	-143.9	38.0	7781.8	14691.9
0.0009	537.90	1.87	16.00	-142.4	40.4	7443.6	15623.4
0.0010	538.64	1.85	16.14	-140.8	42.8	7110.3	16554.4
0.0011	539.35	1.84	16.28	-139.2	45.2	6781.4	17484.0
0.0012	540.03	1.82	16.43	-137.4	47.6	6456.4	18411.6
0.0013	540.67	1.81	16.57	-135.6	50.0	6134.9	19336.3
0.0014	541.29	1.80	16.71	-133.6	52.4	5816.5	20257.4
0.0015	541.87	1.78	16.86	-131.6	54.8	5501.0	21173.9
0.0016	542.42	1.77	17.00	-129.5	57.2	5187.8	22085.1
0.0017	542.94	1.76	17.14	-127.3	59.5	4876.8	22989.8
0.0018	543.43	1.75	17.28	-125.0	61.8	4567.6	23887.0
0.0019	543.88	1.73	17.42	-122.6	64.1	4260.1	24775.8
0.0020	544.31	1.72	17.55	-120.1	66.4	3953.8	25655.0
0.0021	544.70	1.71	17.69	-117.6	68.6	3648.8	26523.5
0.0022	545.07	1.70	17.82	-114.9	70.9	3344.8	27380.1
0.0023	545.40	1.69	17.95	-112.2	73.0	3041.6	28223.6
0.0024	545.71	1.68	18.08	-109.3	75.2	2739.2	29052.7
0.0025	545.98	1.66	18.21	-106.4	77.3	2437.4	29866.1
0.0026	546.23	1.65	18.33	-103.5	79.4	2136.4	30662.7
0.0027	546.44	1.64	18.45	-100.4	81.4	1835.9	31441.0
0.0028	546.62	1.63	18.57	-97.2	83.3	1536.1	32199.7
0.0029	546.78	1.62	18.68	-94.0	85.2	1237.1	32937.4
0.0030	546.90	1.62	18.79	-90.7	87.1	938.8	33652.9
0.0031	546.99	1.61	18.90	-87.4	88.9	641.5	34344.7
0.0032	547.06	1.60	19.01	-83.9	90.6	345.4	35011.5
0.0033	547.09	1.59	19.11	-80.4	92.3	50.4	35652.0
0.0034	547.10	1.58	19.20	-76.9	93.9	-242.9	36264.9
0.0035	547.07	1.57	19.29	-73.2	95.4	-534.6	36848.9
0.0036	547.02	1.57	19.38	-69.6	96.8	-824.1	37402.6
0.0037	546.94	1.56	19.46	-65.8	98.1	-1111.3	37925.0
0.0038	546.83	1.55	19.53	-62.0	99.4	-1395.8	38414.9
0.0039	546.69	1.55	19.60	-58.2	100.6	-1677.2	38871.0
0.0040	546.52	1.54	19.67	-54.3	101.7	-1955.2	39292.5
0.0041	546.32	1.54	19.73	-50.4	102.7	-2229.3	39678.2
0.0042	546.10	1.53	19.78	-46.4	103.6	-2499.2	40027.4
0.0043	545.85	1.53	19.83	-42.4	104.4	-2764.3	40339.1
0.0044	545.57	1.52	19.88	-38.4	105.1	-3024.2	40612.7
0.0045	545.27	1.52	19.91	-34.3	105.7	-3278.6	40847.4
0.0046	544.94	1.52	19.94	-30.2	106.2	-3526.8	41042.8
0.0047	544.59	1.51	19.97	-26.1	106.6	-3768.5	41198.4
0.0048	544.21	1.51	19.98	-22.0	106.9	-4003.2	41313.8
0.0049	543.81	1.51	20.00	-17.9	107.1	-4230.4	41388.8
0.0050	543.39	1.51	20.00	-13.7	107.2	-4449.8	41423.4
0.0051	542.95	1.51	20.00	-9.6	107.2	-4660.8	41417.3
0.0052	542.48	1.51	19.99	-5.4	107.1	-4863.0	41370.9
0.0053	541.99	1.51	19.98	-1.3	106.8	-5056.1	41284.2
0.0054	541.49	1.51	19.96	2.8	106.5	-5239.7	41157.6
0.0055	540.96	1.51	19.93	6.9	106.1	-5413.4	40991.6

Table 5.2 (contd.) Solution to System of Differential Equations

0.0056	540.42	1.51	19.90	11.0	105.6	-5577.0	40786.6
0.0057	539.87	1.51	19.86	15.1	104.9	-5730.0	40543.2
0.0058	539.29	1.51	19.82	19.2	104.2	-5872.4	40262.3
0.0059	538.71	1.51	19.77	23.2	103.4	-6003.8	39944.7
0.0060	538.10	1.52	19.72	27.2	102.5	-6124.1	39591.2
0.0061	537.49	1.52	19.66	31.2	101.5	-6233.1	39202.9
0.0062	536.87	1.52	19.59	35.1	100.4	-6330.8	38780.8
0.0063	536.24	1.52	19.52	39.0	99.2	-6417.0	38326.1
0.0064	535.59	1.53	19.44	42.8	97.9	-6491.7	37840.0
0.0065	534.95	1.53	19.36	46.6	96.6	-6555.0	37323.8
0.0066	534.29	1.54	19.28	50.3	95.2	-6606.9	36778.8
0.0067	533.63	1.54	19.19	54.0	93.7	-6647.5	36206.4
0.0068	532.96	1.55	19.10	57.6	92.2	-6676.9	35607.8
0.0069	532.30	1.56	19.00	61.2	90.5	-6695.3	34984.7
0.0070	531.63	1.56	18.90	64.7	88.9	-6702.9	34338.3
0.0071	530.96	1.57	18.80	68.1	87.1	-6699.8	33670.2
0.0072	530.29	1.58	18.69	71.5	85.4	-6686.4	32981.7
0.0073	529.62	1.58	18.58	74.8	83.5	-6662.9	32274.5
0.0074	528.95	1.59	18.47	78.0	81.7	-6629.7	31549.9
0.0075	528.29	1.60	18.35	81.1	79.7	-6587.1	30809.3
0.0076	527.63	1.61	18.24	84.2	77.8	-6535.3	30054.3
0.0077	526.98	1.61	18.12	87.2	75.8	-6474.9	29286.1
0.0078	526.33	1.62	18.00	90.2	73.8	-6406.2	28506.1
0.0079	525.69	1.63	17.87	93.0	71.7	-6329.5	27715.8
0.0080	525.06	1.64	17.75	95.8	69.7	-6245.3	26916.4
0.0081	524.43	1.65	17.62	98.5	67.6	-6154.0	26109.2
0.0082	523.82	1.66	17.50	101.1	65.5	-6056.1	25295.4
0.0083	523.21	1.67	17.37	103.6	63.3	-5951.8	24476.3
0.0084	522.61	1.68	17.24	106.1	61.2	-5841.8	23652.8
0.0085	522.03	1.69	17.11	108.4	59.1	-5726.3	22826.3
0.0086	521.46	1.70	16.98	110.7	56.9	-5605.9	21997.6
0.0087	520.90	1.72	16.86	112.9	54.8	-5480.9	21167.9
0.0088	520.35	1.73	16.73	115.0	52.6	-5351.8	20338.0
0.0089	519.81	1.74	16.60	117.1	50.5	-5218.9	19508.9
0.0090	519.29	1.75	16.47	119.0	48.3	-5082.6	18681.5
0.0091	518.78	1.76	16.34	120.9	46.2	-4943.4	17856.5
0.0092	518.29	1.77	16.21	122.7	44.1	-4801.6	17034.7
0.0093	517.81	1.79	16.09	124.4	42.0	-4657.6	16216.8
0.0094	517.34	1.80	15.96	126.0	39.9	-4511.7	15403.5
0.0095	516.89	1.81	15.84	127.5	37.8	-4364.2	14595.4
0.0096	516.46	1.82	15.71	129.0	35.7	-4215.6	13793.1
0.0097	516.03	1.84	15.59	130.4	33.6	-4066.0	12997.2
0.0098	515.63	1.85	15.46	131.7	31.6	-3915.8	12208.1
0.0099	515.24	1.86	15.34	132.9	29.6	-3765.3	11426.3
0.0100	514.86	1.88	15.22	134.0	27.6	-3614.7	10652.2
0.0101	514.50	1.89	15.10	135.1	25.6	-3464.4	9886.2
0.0102	514.15	1.90	14.99	136.1	23.6	-3314.4	9128.7
0.0103	513.82	1.92	14.87	137.0	21.7	-3165.1	8379.9
0.0104	513.50	1.93	14.76	137.8	19.8	-3016.7	7640.1
0.0105	513.20	1.95	14.64	138.6	17.9	-2869.3	6909.7
0.0106	512.92	1.96	14.53	139.3	16.0	-2723.1	6188.7
0.0107	512.64	1.97	14.42	139.9	14.2	-2578.4	5477.5
0.0108	512.39	1.99	14.31	140.5	12.4	-2435.2	4776.2

The solution over the duration of the shock pulse seemed to produce reasonable results. For example, the velocities and accelerations had magnitudes that were reasonable. The value of G increased at first and then decreased, and the coefficient of restitution was less than 1.

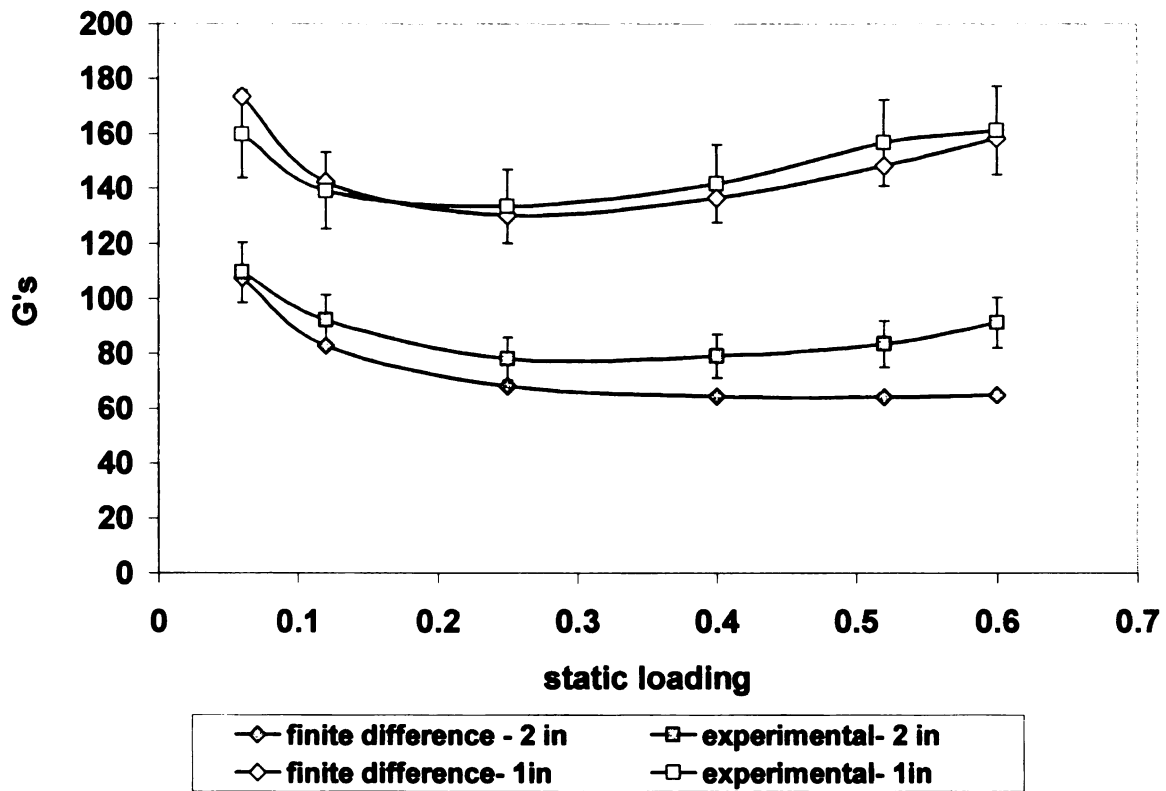


Figure 5.9 Comparison of Cushion Curves from Experiment and Finite Difference Solutions.

To check the validity of the model and the solution obtained from finite difference, the results of the finite difference solution for the 2 inch and 1 inch thick cushions were compared to the published cushion curves (16). Figure 5.9 shows that the finite difference equations predict the concavity of the curve.

Table 5.3 Error table for the cushion curve with a drop height of 30 inches and thickness of 1 inch.

Static Loading, s (psi)	G (Experimental)	G (Predicted)	Error (%)
0.06	159.8	173.6	8.6
0.12	139.2	142.4	2.3
0.25	133.4	130.1	-2.5
0.40	141.7	136.6	-3.6
0.52	156.6	148.2	-5.4
0.60	161.2	158.3	-1.8

Table 5.4 Error table for the cushion curve with a drop height of 30 inches and thickness of 2 inches.

Static Loading, s (psi)	G (Experimental)	G (Predicted)	Error (%)
0.06	109.5	107.6	-1.8
0.12	92.2	82.9	-10.1
0.25	78.1	68.2	-12.7
0.40	79.2	64.3	-18.8
0.52	83.6	64.2	-23.2
0.60	91.4	67.0	-26.7

Assuming that the finite difference method solves the system of differential equations accurately, the model seemed to consistently overestimate the G's for the 1" thick cushion. Also, for a 2" thick cushion, the model seemed to overestimate G's for low static loadings, and underestimate the deceleration for high loads.

The probable sources of error could be:

- i. The actual experimental cushion curves are in error by 10-15% (23) on average.
- ii. The 1-inch and 2-inch thick foams were actually 4 and 8 quarter inch corrugated sheets laminated together. Thus, the presence of voids between the laminated sheets might have added to the error.
- iii. The assumption made was that the foams under consideration were closed-cell foams. Thus, the possibility of mass transfer of air between the cushion and the surroundings was not considered. Starch foams are not completely closed-celled foams.
- iv. Also, at higher static loadings, it was possible that the some cell walls rupture increasing the open cell content, and thus deteriorating the cushioning performance. This leads to an underestimation of G-shock values by the finite difference formulation.
- v. Constant values for air properties were used.
- vi. The heat transfer coefficient, H , is known to be a function of temperature difference (13, 14). However, a constant value of $H = 11.84 \text{ BTU/hr/ft}^2/\text{°F}$ was used. H is also known to be accurate to within $\pm 50\%$.
- vii. The experimental error in reading the cushion curve must also be included in assessing the accuracy of the finite difference method.

Figure 5.10 shows the cushion curves developed by the finite difference formulation on foams with thicknesses of one through four inches respectively, at a drop height of 30 inches.

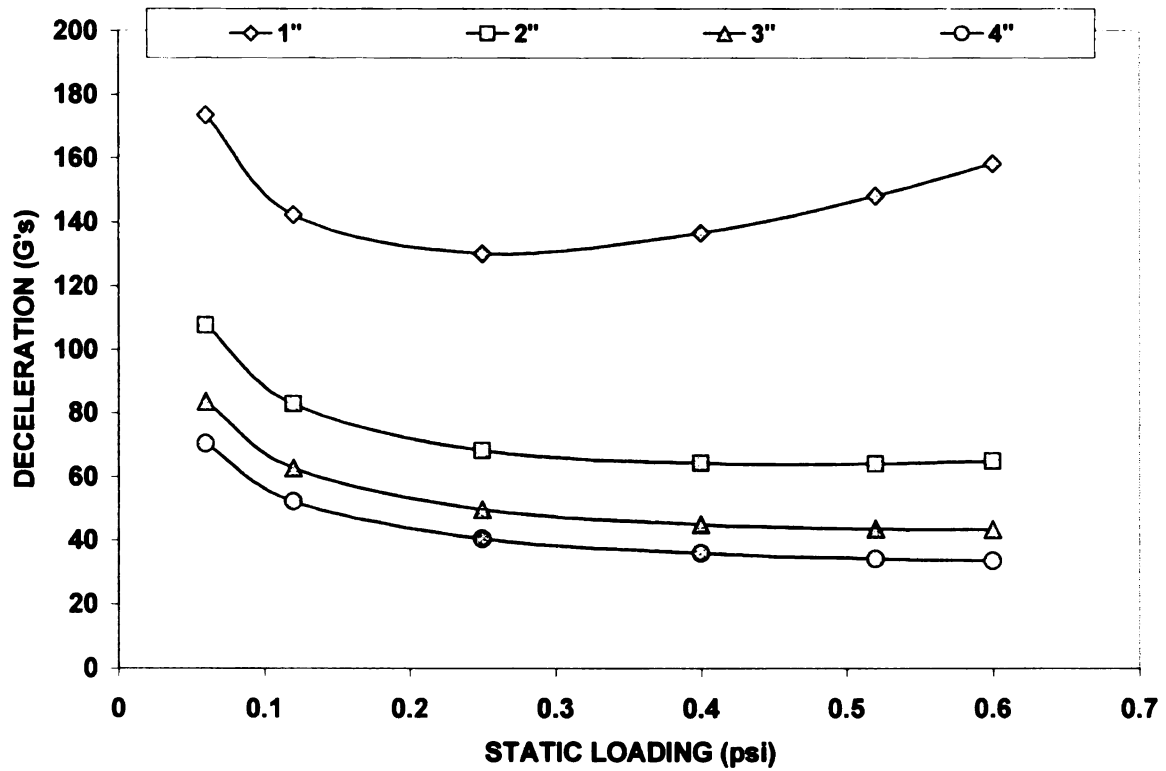


Figure 5.10 Comparison of Cushion Curves from Finite Difference Solution at a drop height of 30" and varying thicknesses.

Figure 5.11 shows the cushion curves for a 2-inch thick starch foam sheet for drop heights varying from 6 inches to 36 inches. It could be seen that the peak G-values decreased with decreasing drop height. This was because the impact velocity was lower at lower drop heights. It was also seen that, at lower drop heights, the starch foam could protect products of a particular fragility level over a wider static loading range.

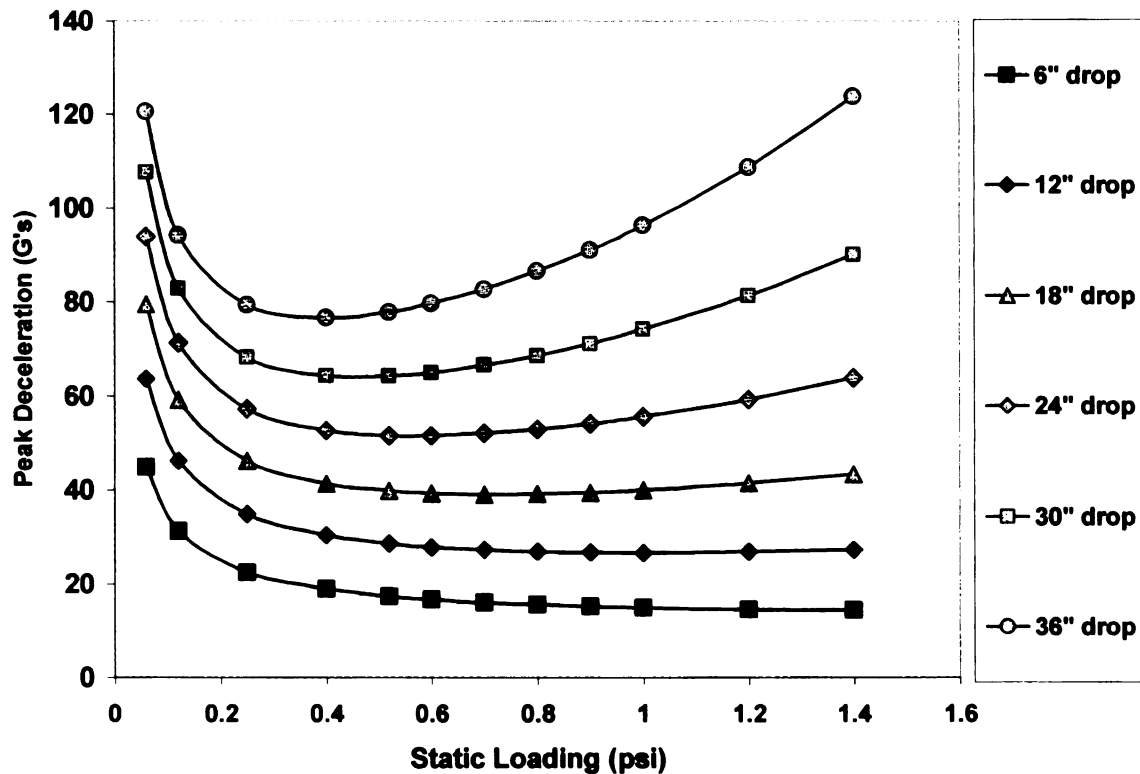


Figure 5.11 Comparison of Cushion Curves from Finite Difference Solution at a thickness of 2" and varying drop heights.

Figures 5.12 and 5.13 depict the cushion curves for a 2-inch thick starch foam sheet at a 30-inch drop height, at varying cell sizes and varying cell wall thicknesses respectively. The starch foam sheets currently made have a cell size of approximately 0.03 inches (~750 μm). It could be seen that with reducing cell size, the foam cushion provided lower peak decelerations (lower G-values). A lower and more uniform cell-size could be obtained by using nucleating agents such as talc, at the expense of an increase in density. Also, the use of nucleating agents increased the closed-cell content of the foam.

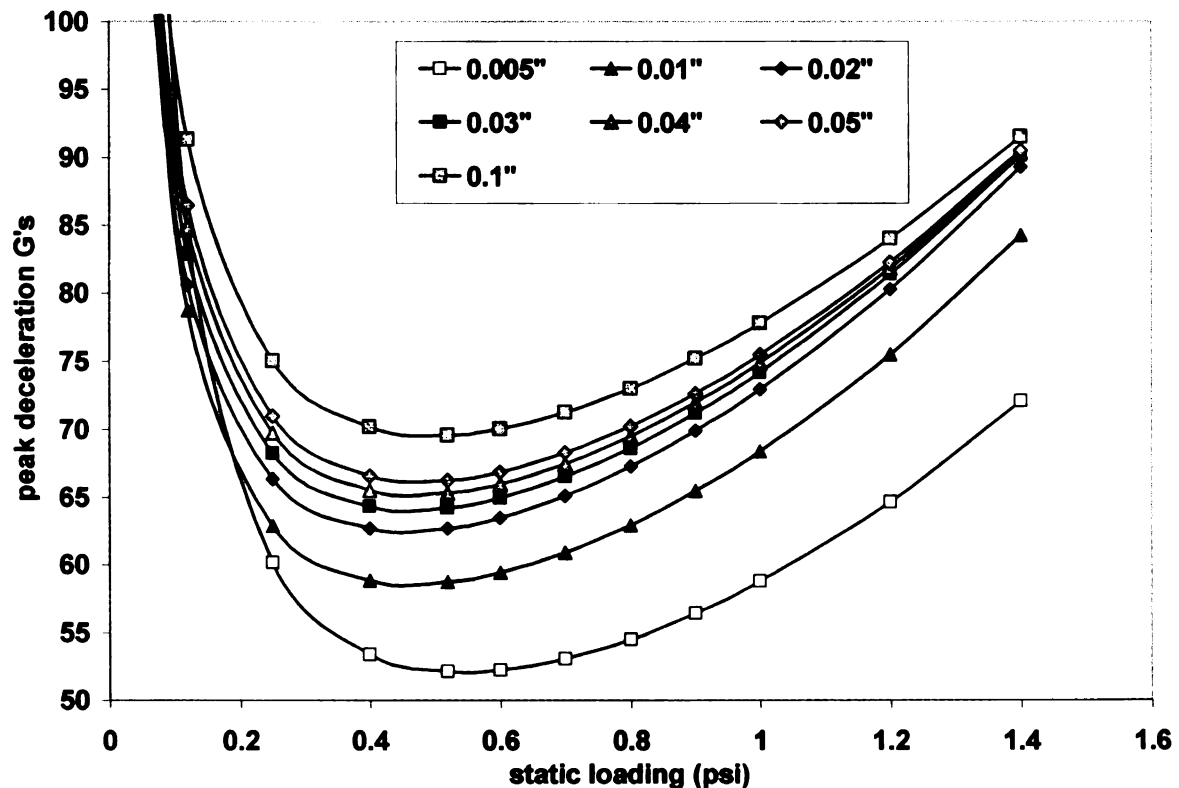


Figure 5.12 Comparison of Cushion Curves from Finite Difference Solution at a thickness of 2" and varying cell sizes.

The starch foam sheets have a cell wall thickness of 10^{-5} inches. It could be seen that as the cell wall thickness increased, the G-values dropped indicating better cushion performance, implying a better quality flexible foam. However, at lower static loadings, the foams with thicker cell walls (10^{-4} inches) acted as a rigid foam instead of a flexible foam leading to high G-shock values. Thus, it would finally depend on the size and the weight of the product to be protected. It was also seen that the G-values did not change considerably for foams with thinner cell walls (10^{-7} inches).

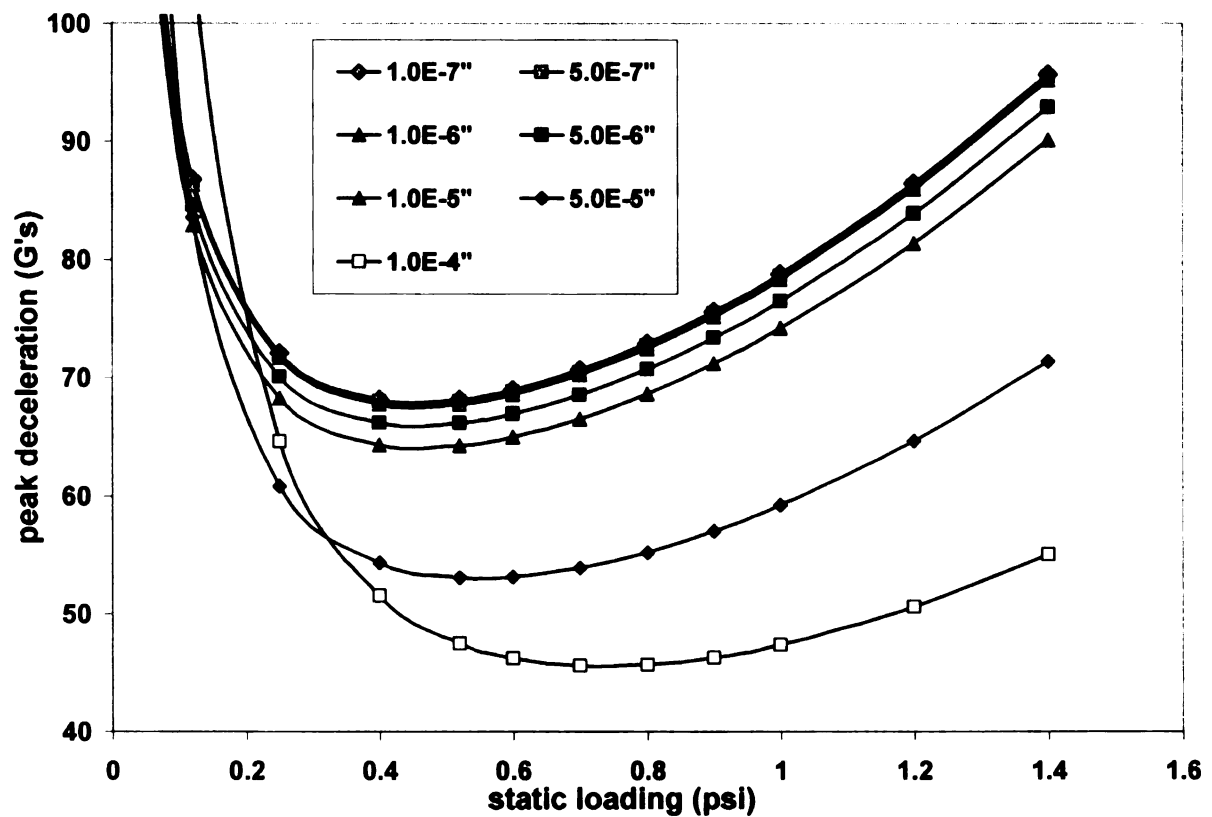


Figure 5.13 Comparison of Cushion Curves from Finite Difference Solution at a thickness of 2" and varying cell wall thicknesses.

5.2.7 The Polytropic Process

The solution process so far had been tedious and complicated because the generation of G's required lengthy calculations. An alternative method to generate G's was to model the compression of air as a polytropic process (12, 24).

$$PV^k = Const \quad (5.35)$$

This model explicitly excluded the heat transfer and the thermodynamic terms. Implicitly, all of these terms were included in the polytropic constant, k (24). The motivation for using the polytropic model was to simplify the stress-strain analysis so that cushion geometries, which were more complicated than a simple block, may be analyzed. This then allowed for techniques such as finite element method (FEM) to be used. It also simplified the model considerably by requiring only one physical constant, k, instead of the many thermodynamic terms previously involved.

As a result of the finite difference calculations, values of position (thickness) and pressure at specific times were known. When the complete table had been generated, the material constant 'k' in equation (5.35) could be determined by fitting the known data to the polytropic equation. The value of 'k' determined the amount of heat transfer that occurred within the cushion. The value of 'k' is 1.0 for an isothermal process: in an isothermal process, compression is assumed to occur so slowly relative to the heat transfer rate that the air remains at constant temperature as it is compressed. The value of 'k' is 1.4 for an adiabatic process (it is the ratio of specific heats for air): in an adiabatic process, compression is assumed to occur so quickly that no heat is transferred to the walls.

An adiabatic process would result if H or S were extremely small or if the cushion was compressed quickly as in a drop. If H or S were very large, or if the cushion was compressed slowly, then the process would approach isothermal conditions. Since, H and S were both finite in reality, the compression process would neither be isothermal nor adiabatic. Thus, the expected result was $1.0 < k < 1.4$.

Predicting the polytropic constant involved fitting equation (5.35) to the data in the finite difference table. Since $PV^k = \text{constant}$, and the bearing area was constant, we could fit the data to $Px^k = \text{constant}$ instead. Since the pressure and thickness were P_0 and x_0 initially, this yielded:

$$\left(\frac{P}{P_0}\right)\left(\frac{x}{x_0}\right)^k = 1 \quad (5.36)$$

The objective now was to assume that equation (5.36) is true and to choose 'k' to "best fit" the data in the table. This was a necessary step in order to develop the constitutive equations for a closed cell foam.

Because the air compression is not truly a polytropic process, equation (5.36) would not be satisfied exactly, and, k was chosen to best fit all the data points for pressure and position (25). As a result, there would be an error between the actual value and the expected value.

Instead of using equation (5.36) in its present form, take the natural log of both sides:

$$\ln\left(\frac{P}{P_0}\right) + k \ln\left(\frac{x}{x_0}\right) = 0 \quad (5.37)$$

Defining the error at any instant 'i':

$$\ln\left(\frac{P}{P_0}\right) + k \ln\left(\frac{x}{x_0}\right) = \varepsilon_i \quad (5.38)$$

The Sum of Squares of Errors (SSE) becomes:

$$SSE = \sum_{i=1}^N \varepsilon_i^2 = \sum_{i=1}^N \left(\ln \left(\frac{P_i}{P_0} \right) + k \ln \left(\frac{x_i}{x_0} \right) \right)^2 \quad (5.39)$$

Taking the first derivative of equation (5.39) and setting the result equal to zero gives:

$$\frac{d}{dk}(SSE) = \sum_{i=1}^N 2 \left[\ln \frac{P_i}{P_0} + k \ln \frac{x_i}{x_0} \right] \ln \left(\frac{x_i}{x_0} \right) = 0 \quad (5.40)$$

$$\sum_{i=1}^N \left(\ln \frac{P_i}{P_0} \ln \frac{x_i}{x_0} \right) + k \sum_{i=1}^N \left(\ln \frac{x_i}{x_0} \right)^2 = 0 \quad (5.41)$$

$$k = - \frac{\sum_{i=1}^N \left(\ln \frac{P_i}{P_0} \ln \frac{x_i}{x_0} \right)}{\sum_{i=1}^N \left(\ln \frac{x_i}{x_0} \right)^2} \quad (5.42)$$

The result for ‘k’ using equation (5.42) and the data in table was $k = 1.022$. Using this k, the values of Px^k for several points in table were generated. The results are shown in Table 5.5. Even though Px^k was not constant, it appeared to vary by no more than 5.2%. Next, a series of tables were generated similar to Table 5.2 for six different drop heights, and the same initial conditions. This was done to examine the effect of drop parameters on ‘k’. Using equation (5.42), the results ranged from $k = 1.011$ for a 6” drop height to $k = 1.024$ for a 36” drop height. These results showed that cushion compression was closer to being isothermal than adiabatic, and that k was relatively insensitive to drop conditions.

Table 5.5 Variability in Px^k at selected times from Table 5.2.

$k = 1.022$ (drop height =30 inches, foam thickness = 2 inches)	
Time (ms)	Px^k
5	31.62
10	30.93
15	28.65
20	27.76
25	28.80
30	29.95
35	30.85
40	31.50
45	31.99
50	32.35
Average Px^k	30.44
Standard deviation	1.57 (5.17%)

5.2.8 Force vs. Compression Results

Figure 5.14 shows the force-compression results for a 2-inch thick block cushion. These results were obtained using the polytropic equation using the following definitions of force and compression:

$$\text{Force, } F = (P - P_0)A \quad (5.43)$$

$$\text{Compression, } u = x_0 - x \quad (5.44)$$

Substituting the expression for P from equation (5.36), the force vs. compression relation for a polytropic process becomes:

$$F = P_0 A \left[\left(\frac{x_0}{x_0 - u} \right)^k - 1 \right] \quad (5.45)$$

The force vs. compression curves in the figure 5.14 were obtained using the polytropic constants for different drop heights (different k's, along with the values $A = 64 \text{ in}^2$ and $x_0 = 2$ inches. The results showed that the force vs. compression curve was fairly insensitive to the variance in k. The important part to note here is that the constants in the three differential equations could now be lumped into one polytropic constant, and the equations of elasticity may be developed from this.

The force vs. compression curves in the figure 5.15 were obtained using the polytropic constants for different foam thicknesses (different ks, along with the values $A = 64 \text{ in}^2$ and $h = 30$ inches.

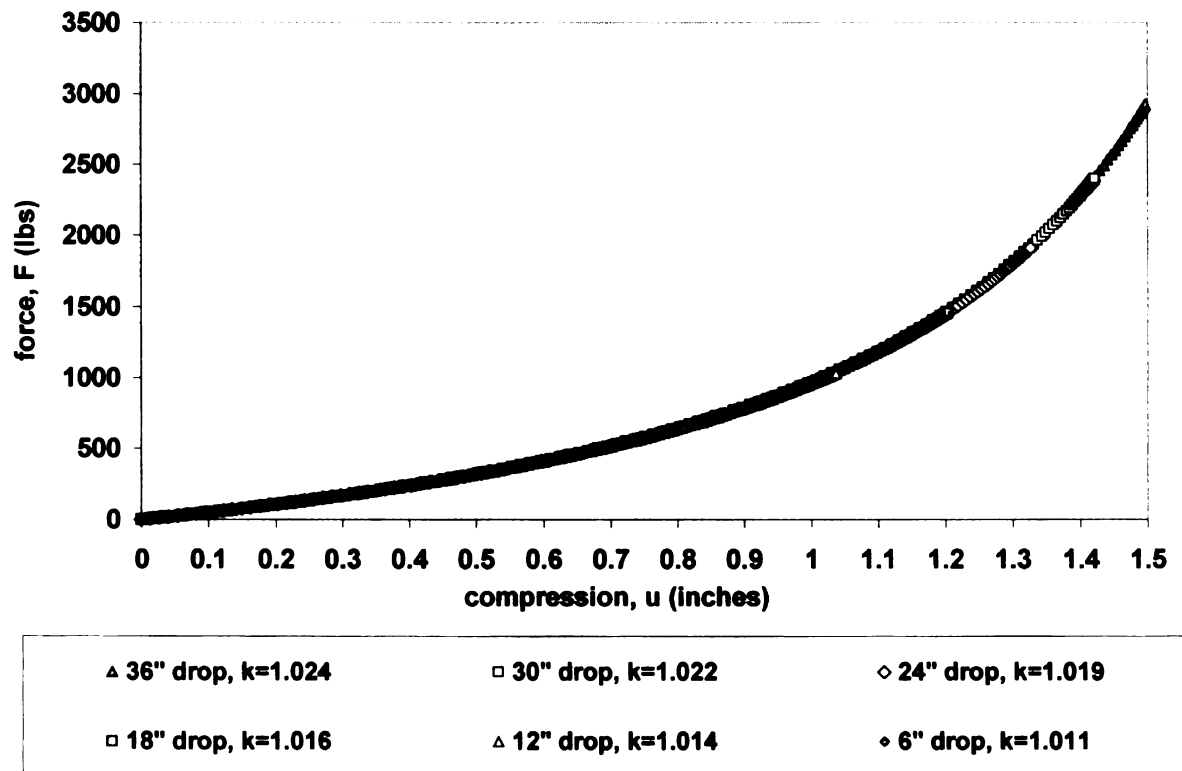


Figure 5.14 The Effect of k (Different Drop Heights) on the Force-Compression curve

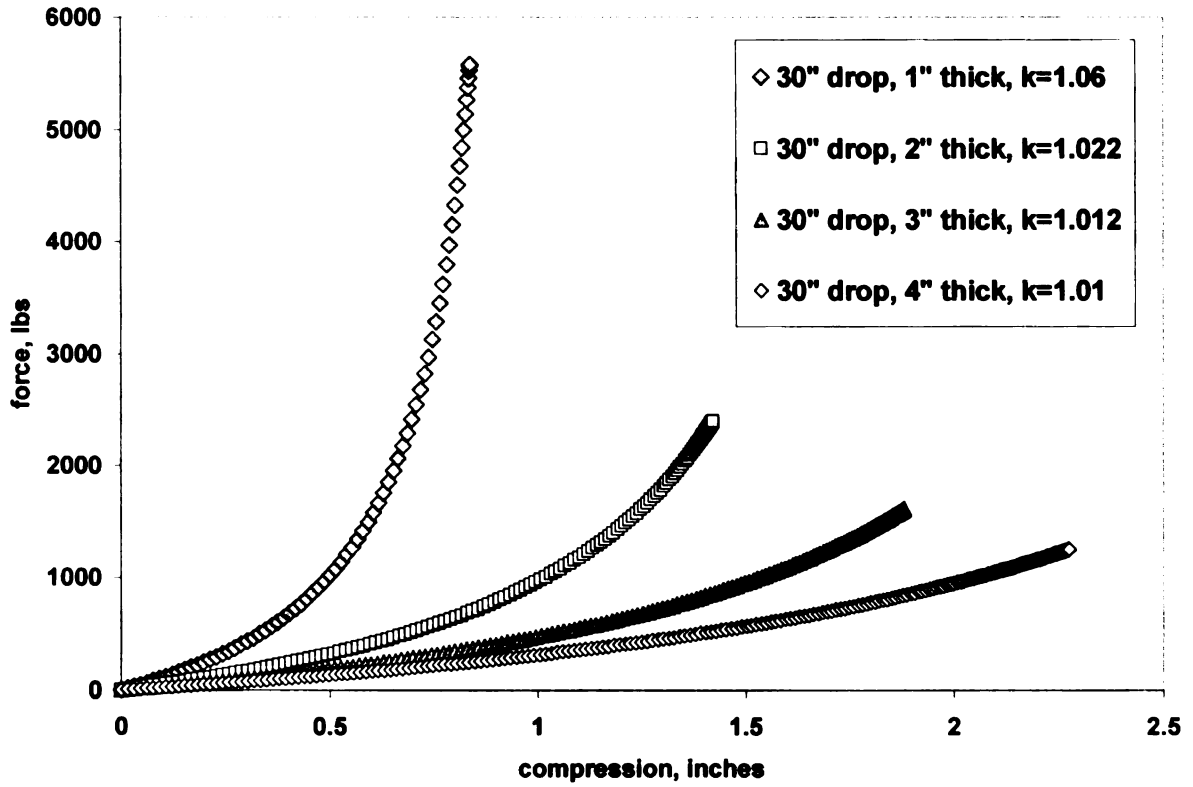


Figure 5.15 The Effect of k (Different Foam Thicknesses) on the Force-Compression curve.

5.2.9 The Finite Element Method (FEM):

The finite element method is a powerful tool that models a complex domain as a collection of geometrically simple sub-domains. The FEM can be interpreted as a piecewise application of the variational method to solve differential equations, in which the approximation functions are algebraic polynomials, and the undetermined parameters represent the values of the solution at a finite number of pre-selected points called nodes (26). The variational method is a technique used to solve a differential equation approximately by putting the differential equation into a variational form and taking the approximate solution to be a combination of shape functions.

The accuracy of the FEM depends upon the element used to model the complex domain. Elements can have nodes that have one, two, or three degrees of freedom. The numbers of nodes in the element (p-refinement), as well as the number of elements in the domain (h-refinement) contribute to the accuracy of the approximation. The type of element and mesh used will generally require some knowledge of the physical system to be modeled.

When one looks at a typical cushion, especially a block cushion with a square bearing area, lines of symmetry become noticeable. A 3-D problem can be reduced to a 1-D problem, and expect a reasonable degree of accuracy, because the depth dimension is much greater than the side dimensions. The objective was to show that an impact on a closed cell cushion could be accurately modeled by the polytropic equation and analyzed accurately by the FEM. The results were compared to existing experimental data.

5.2.10 The Finite Element Model:

Since the material constant has already been determined, and the problem has been reduced to a 1-D problem, the closed cell cushion may now be viewed as an elastic solid (12), whose modulus of elasticity was a function of strain. The governing equation became:

$$P(x) = \left(\sigma + E(x) \frac{du}{dx} \right) A(x) \quad (5.46)$$

$$\frac{dP}{dx} = \sigma \frac{dA(x)}{dx} + \frac{d}{dx} \left(A(x) E(x) \frac{du}{dx} \right) \quad (5.47)$$

Where 'x' is the co-ordinate variable along the thickness, E(x) is the material modulus at x, u is the displacement of a node during compression, P(x) is the compressive force, σ is the yield pressure, and A(x) is the cross-sectional area at x. The finite element model is able to solve the governing differential equation (equation 5.47) for a variable material modulus and a variable cross-sectional area. The way in which the area varies with the depth is determined by the geometry of the cushion. The variation in the material modulus with the depth of the cushion is not obvious, and hence must be determined by performing a force balance on an element of cushion, and using the polytropic compression model. During compression, the stress applied to the cushion must overcome the build-up in air pressure over and above the atmospheric pressure.

$$\sigma = P - P_0 \quad (5.48)$$

Using the polytropic relation for P:

$$\sigma = \frac{P_0 V_0^k}{V^k} - P_0 \quad (5.49)$$

For a particular element, $V_0 = At_0$, and $V = At$, where A is the cross-sectional area of the element, V_0 is the volume of the uncompressed element, V is the volume of the compressed element, t_0 is the original thickness before the stress σ is applied, and t is the thickness after. Substituting into equation (5.49) and solving for σ gives:

$$\sigma = P_0 \left[\left(\frac{t_0}{t} \right)^k - 1 \right] \quad (5.50)$$

Now, since $t = t_0 - u$, u is the compression:

$$\frac{t_0}{t} = \frac{t_0}{t_0 - u} = \frac{1}{1 - \frac{u}{t_0}} = \frac{1}{1 - \varepsilon} \quad (5.51)$$

Where ε is the strain. Substituting yields:

$$\sigma = P_0 \left[\left(\frac{1}{1 - \varepsilon} \right)^k - 1 \right] \quad (5.52)$$

Equation (5.52) is the stress vs. strain relation for the cushion element. Dividing both sides by ε , and noting that by definition, the modulus is the ratio of stress to strain:

$$E = \frac{P_0}{\varepsilon} \left[\left(\frac{1}{1 - \varepsilon} \right)^k - 1 \right] \quad (5.53)$$

In the small strain limit, E approached kP_0 psi, and steadily increased for larger strains. Both the material modulus and cross-sectional area were now a function of x . The area was an explicit function of x , because it varied directly with position as the geometry of the cushion dictates. The modulus was an implicit function of x because it varied with the strain and strain varied with position. Because the modulus was a function of strain, and the strain distribution was not known before hand, the material modulus was initially

guessed. A reasonable guess would be the value, $E = 14.7$ psi for small strains. The problem could then be solved with each element having this modulus. The resulting strain field could then be used to correct the modulus for each element using equation (5.53) and the process was repeated. The program iterated until the material modulus converged upon a value for each element. Upon convergence, the results were eventually used to calculate the peak G delivered to a product in a drop.

5.2.11 Finite Element Program and Input:

The method to solve equation (5.47), along with the auxiliary equations (5.52-5.53) involved the implementation of a computer algorithm in a Fortran computing environment. The computer code was developed by Chen (12) and it was written to model each element in a closed cell cushion according to equation (5.53). The program contained some computational as well as syntax errors. Also, better approximations as compared to those in (12) were used for $E(x)$.

Tables 5.6 and 5.7 give the G-shock values for the 1-inch thick and 2-inch thick starch foam sheets respectively. These results were similar to those obtained from the finite difference formulation. This seems obvious since the polytropic constant was determined using the finite difference method itself. Based upon the error, it seemed that the constitutive equations derived earlier, modeled the cushioning properties of the starch foams satisfactorily at low static loadings, while the error maximized at higher loadings probably due to the brittleness of the starch foams. Figure 5.16 compares the cushion curves obtained from experiment, the finite difference formulation and the finite element method.

Table 5.6 Error table for the cushion curve with a drop height of 30 inches and thickness of 1 inch ($k = 1.059$).

Static Loading, s (psi)	G (Experimental)	G (Predicted)	Error (%)
0.06	159.8	156.7	-1.9
0.12	139.2	140.3	0.8
0.25	133.4	142.4	6.7
0.40	141.7	153.1	8.0
0.52	156.6	162.3	3.7
0.60	161.2	168.3	4.4

Table 5.7 Error table for the cushion curve with a drop height of 30 inches and thickness of 2 inches ($k = 1.022$).

Static Loading, s (psi)	G (Experimental)	G (Predicted)	Error (%)
0.06	109.5	103.5	-5.5
0.12	92.2	87.5	-5.1
0.25	78.1	75.2	-3.7
0.40	79.2	71.0	-10.4
0.52	83.6	71.4	-14.5
0.60	91.4	73.2	-19.9

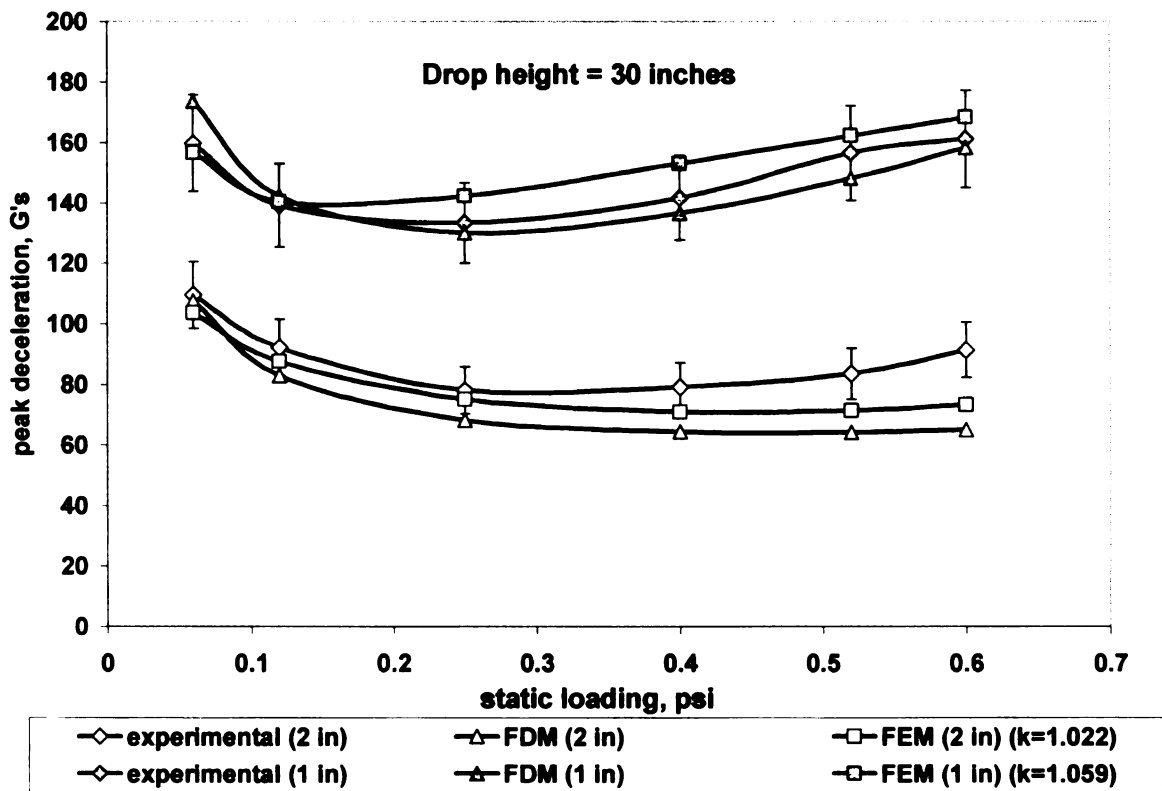


Figure 5.16 Cushion Curves from Experiment, Finite Difference Formulation and Finite Element Method (Using Polytropic Constant).

5.3 Method II: The Dynamic Stress-Strain Curve

Even though several cushion curves for different thicknesses are graphed on one set of 'G vs. s' axes for a given drop height, a large collection of these graphs for various drop heights are required for a reasonably complete description of cushion performance. Yet even with this amount of information, the set of curves is still incomplete in the sense that they do not directly provide data for other drop heights and cushion thicknesses. The practical procedure for the consolidation of all the cushion curves for a particular type of cushion (Arcel ® 512, a 2 lb/ft³ closed-cell moldable Polyethylene copolymer made by ARCO Chemical Co.) into a single relationship was discussed by Burgess (11). The validity of such a procedure was determined for the starch foam sheets.

5.3.1 Analysis

It is possible to predict the peak deceleration of an object dropped on to a cushion using force and energy balances if the dynamic stress-strain curve for the cushion material is known (8). The dynamic stress-strain curve, however, is usually not known beforehand and is very difficult to obtain experimentally. The static stress-strain curve obtained from standard compression tests overlooks the substantial contribution of strain-rate dependent effects on the overall dynamic stress. The dynamic stress-strain curve was deduced directly from the cushion curve information. The dynamic stress was taken as a function of the strain ϵ and the strain rate $d\epsilon/dt$.

$$\sigma = f\left(\epsilon, \frac{d\epsilon}{dt}\right) \quad (5.54)$$

Which may be written as:

$$\sigma = f(\epsilon) \quad (5.55)$$

Equation (5.54) is a property of the material alone and equation (5.55) depends on the particular strain history encountered in the impact. Thus, the function in equation (5.54) would be fixed; while the function in equation (5.55) would vary depending on the way strain behaves with time during the impact. Equation (5.55) may be used as the dynamic stress-strain curve for the material only if its functional form was not too dependent on the variations in strain history, that were likely to occur as the cushion thickness and drop height were altered.

For closed-cell cushions, the function in equation (5.55) was expected to remain relatively stable since the dominant factor in the dynamic stress-strain relationship was the strain itself and not the strain rate (5, 6, 8, 11). Also, the initial strain rate upon impact was simply the impact velocity divided by the cushion thickness, and since the impact velocity depends on the square root of the drop height, the strain rate must also. This meant that the drop height must be quadrupled in order to double the strain rate, which meant that large changes in drop height were required to significantly alter the strain rate. Both the relatively weak dependence of the stress on the strain rate and the strain rate on the drop height taken together suggested that the dynamic stress-strain curve for the material may be taken in the form of equation (5.55).

Using equation (5.55) it was now possible to perform the force and energy balances that would lead to the consolidation of all cushion curves for a given material into a single relationship valid for all drop heights and cushion thicknesses.

The area under the dynamic stress-strain curve up to a certain value of strain is the energy absorbed per unit volume of the material (8). The energy absorbed by the cushion in a drop is the product of the weight of the object dropped (W) and the drop height (h). The

volume of the cushion is the product of the cross-sectional area (A) and the cushion thickness (t). Thus, the energy absorbed per unit volume is (Wh) / (At) = (sh / t), where s is the conventional static loading (s = W / A). Thus,

$$\frac{sh}{t} = \int_0^{\epsilon_m} \sigma \cdot d\epsilon = f(\epsilon_m) \quad (5.56)$$

The integral in equation (5.56) is the expression for the area under the stress-strain curve, which from equation (5.55), would now be a function of ϵ_m only. The shock G transmitted may be deduced from Newton's Law by applying a force balance in the vertical direction to the weight at maximum cushion compression.

$$\sigma_m A - W = WG \quad (5.57)$$

Where σ_m is the maximum compressive stress corresponding to the maximum compressive strain ϵ_m .

$$\therefore \sigma_m - s = sG \quad (5.58)$$

$$\therefore \sigma_m = s(G + 1) = f(\epsilon_m) \quad (5.59)$$

Hence, from equations (5.56) and (5.59), it is apparent that '(sh / t)' and '(G + 1) s' were related to each other in the same way for every drop since they were both related to the quantity ϵ_m through a material property, the dynamic stress-strain curve. This formed the basis for the consolidation procedure (11):

$$(G + 1)s = f\left(\frac{sh}{t}\right) \quad (5.60)$$

Equation (5.60) could be explained geometrically using the following dynamic stress-strain curve as shown in figure 5.17. The numerical value of (sh / t) corresponds to the

area under the curve up to the strain value ' ϵ_m ' and ' $(G + 1)s$ ' is the height of the curve at that point.

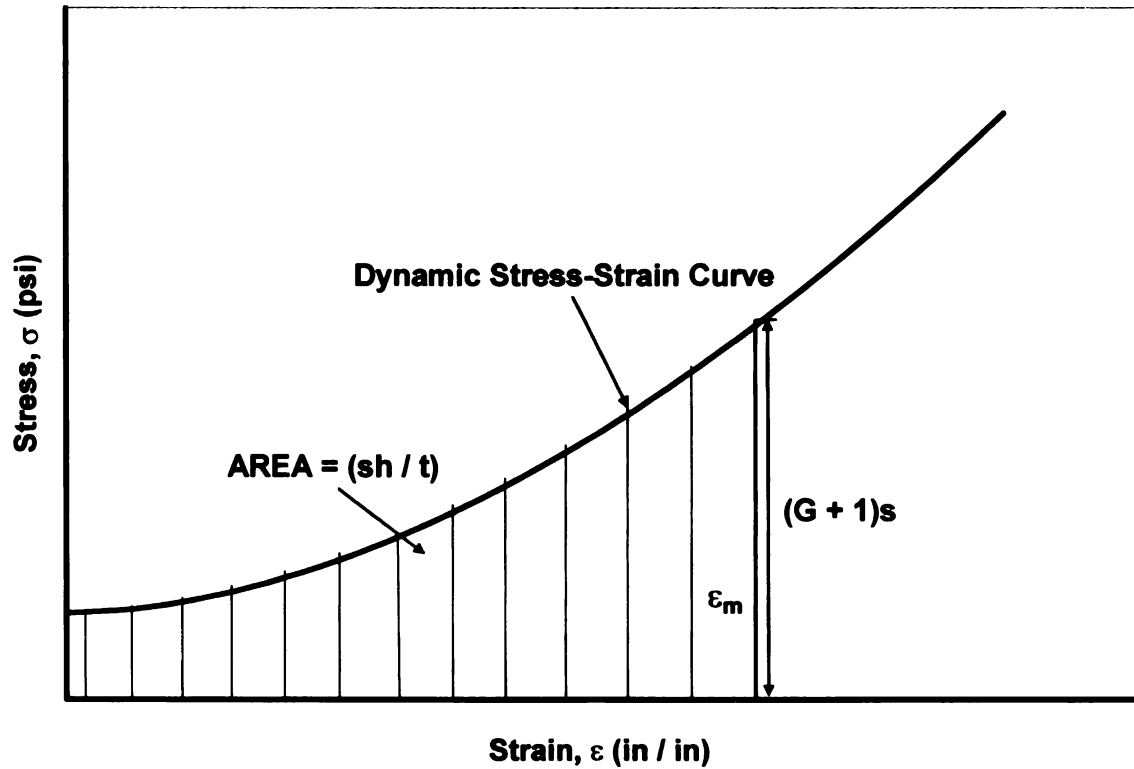


Figure 5.17 The dynamic Stress-Strain Curve.

In order to obtain the relationship between the two, it was only necessary to arbitrarily choose any one of the 'G vs. s' cushion curves for a specific drop height and cushion thickness, and then tabulate $(G + 1)s$ values against (sh / t) values. The fact that the relationship obtained corresponded to a property of the material, meant that the same relationship must be obtained independent of the particular cushion curve used, and therefore, represented the sought after consolidation of all the cushion curves for this material.

Since the maximum cushion strain incurred in the drop, ϵ_m , is also a geometric property of the stress-strain curve, it was possible to obtain information about it. Since the area (sh / t) under the curve and the corresponding height $(G + 1)s$ are now assumed known at every point on the curve, the strain was determined incrementally by considering the small change in area ($\Delta sh/t$), associated with an increase in strain ($\Delta\epsilon$). Equating this change in area to the area of the thin vertical rectangle with height $(G + 1)s$ and base $\Delta\epsilon$ yielded:

$$\Delta\left(\frac{sh}{t}\right) = (G + 1)s \cdot \Delta\epsilon \quad (5.61)$$

so that the incremental strain was:

$$\Delta\epsilon = \frac{\Delta\left(\frac{sh}{t}\right)}{(G + 1)s} \quad (5.62)$$

The maximum cushion strain ϵ_m was now tabulated against (sh / t) , along with $(G + 1)s$, with the initial condition that $\epsilon_m = 0$, when $s = 0$, and by using equation (5.62). The consolidation procedure was now applied to a set of cushion curves.

5.3.2 Application

The dynamic stress-strain curve was generated using the cushion curve for a 1-inch thick starch foam with a 30-inch drop height. The predictions generated from this data were validated using the experimental data available for a 2-inch thick starch foam with a 30-inch drop height. The experimentally obtained values for the cushion curves have been shown earlier in Figure 5.9.

The first step was to gather 'G vs. s' information from the 1-inch thick, 30-inch drop height cushion curve. This information is tabulated in the first two columns of the following Table 5.8.

Table 5.8 Dynamic Stress-Strain Results for Starch Foam

s	G	(sh / t)	(G + 1)s	ε
Static loading	Peak Deceleration	Area under the curve	Dynamic Stress	Strain
(psi)	(g)	(psi)	(psi)	(%)
0.06	159.8	1.8	9.65	19
0.12	139.2	3.6	18.82	28
0.25	133.4	7.5	37.60	39
0.40	141.7	12.0	63.08	46
0.52	156.6	15.6	89.95	50
0.60	161.2	18.0	105.32	52

The stress-strain curve information was then determined directly from the first two columns of the Table 5.8, with $h = 30$ inches and $t = 1$ inch. The results for the area (sh / t) and the height $(G + 1)s$ are shown in the third and fourth columns in Table 5.8 respectively. The strain was then determined step-wise using the third and fourth columns in equation (5.62), and the initial condition that $\varepsilon = 0$ when $s = 0$. For example, the entry in the first row for ε (%) was derived from:

$$\varepsilon = 0 + \Delta\varepsilon = 0 + \frac{1.8 - 0}{9.65} = 0.187 = 18.7\% \quad (5.63)$$

The strain increment for the second entry was:

$$\begin{aligned} \varepsilon &= 0.187 + \Delta\varepsilon \\ \therefore \varepsilon &= 0.187 + \frac{3.6 - 1.8}{18.82} \\ \therefore \varepsilon &= 0.282 = 28.2\% \end{aligned} \quad (5.64)$$

The strain increment for the third entry was:

$$\begin{aligned} \varepsilon &= 0.282 + \Delta\varepsilon \\ \therefore \varepsilon &= 0.282 + \frac{7.5 - 3.6}{37.6} \\ \therefore \varepsilon &= 0.386 = 38.6\% \end{aligned} \quad (5.65)$$

The process was continued by adding the strain increment to the previous strain each time.

The first and the second columns of Table 5.8 could be discarded, since their use was limited to a single cushion curve, in this case for $h = 30$ inches and $t = 1$ inch. The last three columns are the area under the curve, stress and strain values, respectively, for the dynamic stress-strain curve, and should therefore apply to all of the first impact cushion curves for the starch foam sheets. The dynamic stress-strain curve is shown in Figure 5.18, and the (sh / t) vs. $(G + 1)s$ curve is shown in Figure 5.19.

The area and stress columns of Table 5.8 were used to predict the shock values for the other cushion curve in figure 5.9. Assume $h = 30$ inches, $t = 2$ inches, and $s = 0.25$ psi. Then $(sh / t) = 3.75$ psi, and from Figure 5.19, the corresponding value for $(G + 1)s$ was 19.5. Therefore, the predicted shock was:

$$G = (19.5 / 0.25) - 1$$

$$G = 77$$

The actual value of G from experiment was 78.14, which implied an error of 1.46%. The error was maximum at higher static loadings. The error was 15.39% at a static loading of 0.6 psi and 1.98% at a static loading of 0.06 psi.

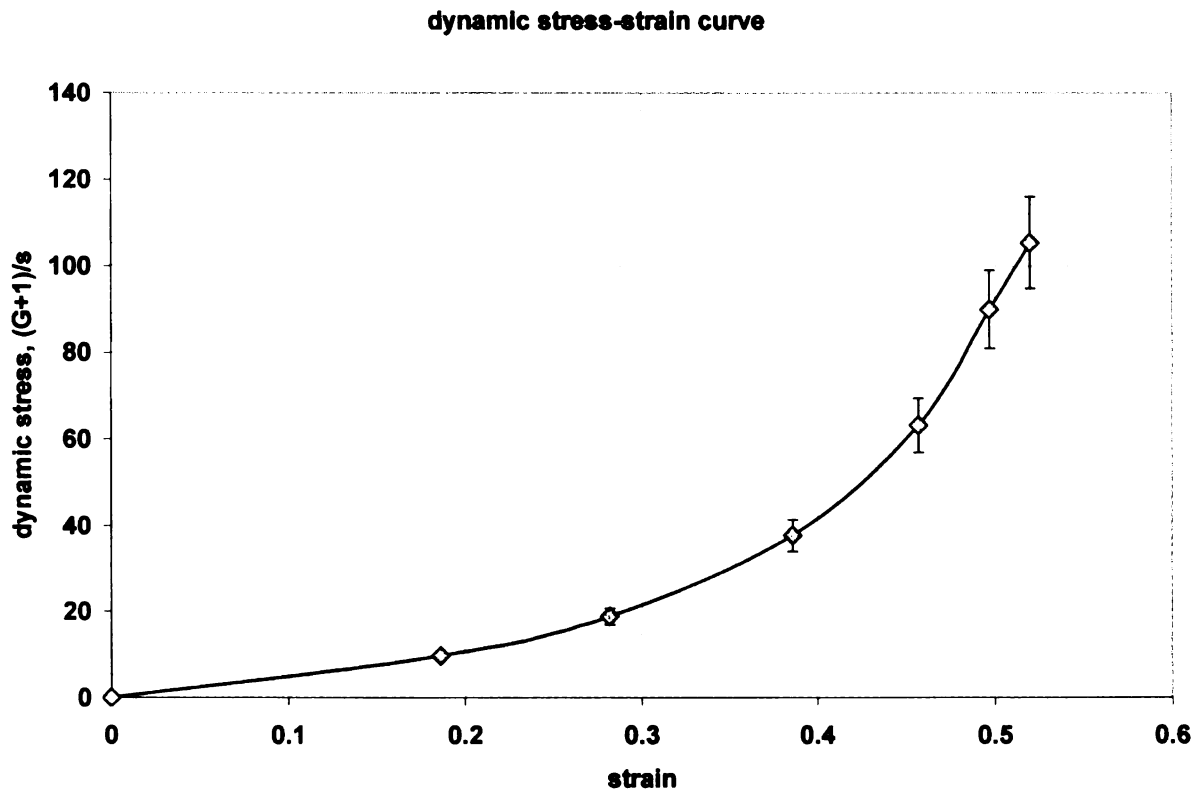


Figure 5.18 The Dynamic Stress-Strain Curve for Starch Foams.

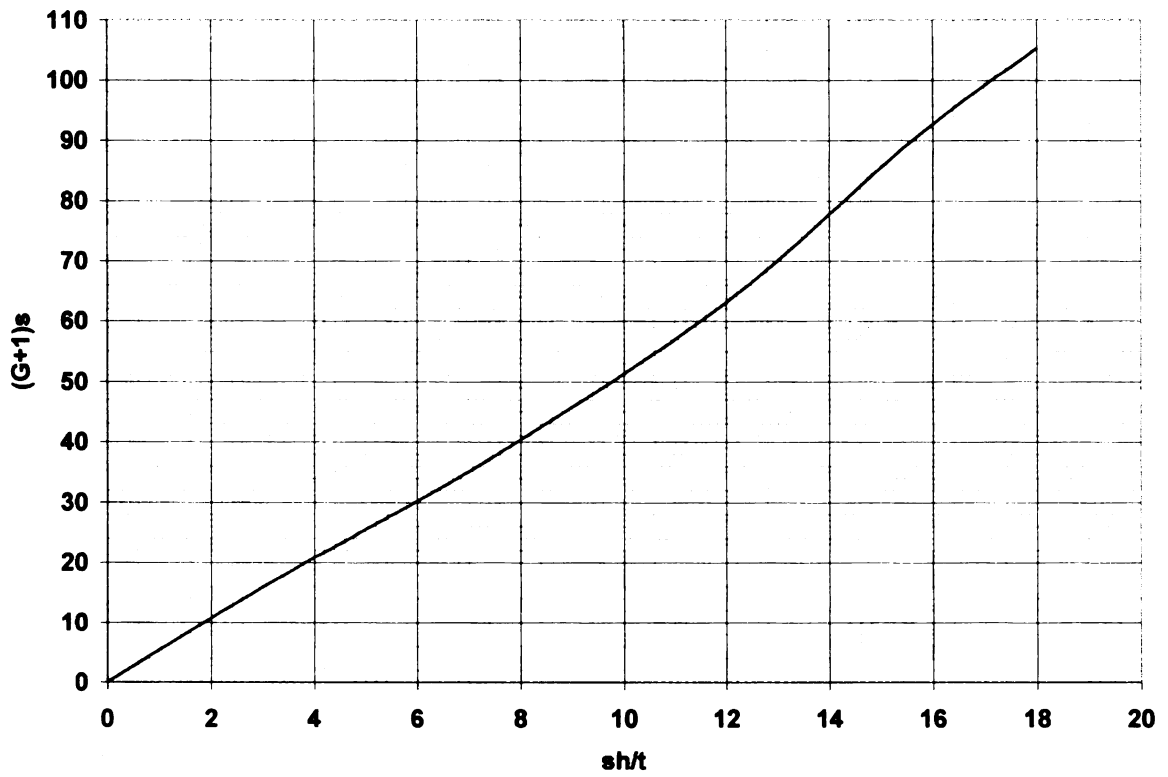


Figure 5.19 The (sh / t) vs. $(G + 1)s$ Curve.

Table 5.9 Predicted Values for h = 30 inches, t = 2 inches

s	(sh / t)	(G + 1)s	G	G	Error	Cushion
Static		From	Predicted	Experimental		Strain
Loading		Curve				ϵ
psi	psi	psi			(%)	(%)
0.06	0.90	6.5	107.3	109.5	1.98	13.85
0.12	1.80	11	90.7	92.2	1.64	22.03
0.25	3.75	19.5	77.0	78.1	1.46	32.03
0.40	6.00	30	74.0	79.2	6.57	39.53
0.52	7.80	40	75.9	83.6	9.18	44.03
0.60	9.00	47	77.3	91.4	15.39	46.58

Table 5.9 gives the experimental and predicted values for the cushion curve for the 2-inch thick foam. The error was found to be greatest for large values of (sh / t), which correspond to drop situations requiring large amounts of energy to be absorbed. This was probably due to the fact that the starch foams were comparatively brittle as compared to the other closed-cell foams, and therefore, tends to rupture at high strains. In such cases, the dynamic stress-strain relationship becomes extremely complicated (11), and the arguments leading to equation (5.60) evidently break down.

Similar situation occurs when an attempt is made to apply this consolidation procedure to open-cell foams. For such foams, the strain rate is the dominant factor, not the strain, so that the transition from equation (5.54) to (5.55), and ultimately equation (5.60) does not

hold true. This consolidation procedure applied to open-cell foams does not, in general, produce acceptable results (11).

The consolidation procedure was simple to apply, and utilized only one of the conventional 'G vs. s' cushion curves for a specific drop height and cushion thickness. There were many advantages in having a single relationship for cushion performance compared with many conventional cushion curves normally required.

1. Compactness of information.
2. The results may be used for a continuous range of drop heights and cushion thicknesses, whereas, the conventional cushion curves are limited to only those values published.
3. The results also provided information on the maximum cushion strain incurred in the impact, whereas, the conventional curves do not.
4. The cushion design was greatly simplified, since the database required as input information on the cushion performance had been drastically reduced, while its applicability to various drop conditions had been greatly increased.
5. It was no longer necessary to perform nearly as many drop tests on a new material to evaluate its dynamic performance since; a single G vs. s cushion curve was all that was required to generate all other cushion curves.

5.4 Conclusions

Due to the many types of cushions available and the parameters, which determine their behavior, the number of cushion curves required for a thorough account of the subject is immense. It was natural, therefore, to try to reduce the database to descriptive equations

either by curve fitting or by solving the dynamics problem using a model of the cushion. Different models involving finite difference and finite element techniques were developed to predict the cushioning properties of the starch-based foam sheets produced. The solution to the three equations governing the drop/impact test, viz., force balance, energy balance, and the ideal gas law, was obtained using the finite difference method. Assuming that the finite difference method solves the system of differential equations accurately, the model seemed to consistently overestimate the G's for the 1" thick cushion. Also, for a 2" thick cushion, the model seemed to overestimate G's for low static loadings, and underestimate the deceleration for high loads.

The finite element method used was based on the finite difference method and, hence, provided results similar to those obtained using the finite difference method.

A different type of consolidation procedure was employed to predict the cushion curves of foam sheets, which utilized one of the conventional (experimentally determined) 'G vs. s' cushion curves for a specific drop height and cushion thickness. There were many advantages in having a single relationship for cushion performance compared with many conventional cushion curves normally required.

The cushion design was greatly simplified, since the database required as input information on the cushion performance had been drastically reduced, while its applicability to various drop conditions had been greatly increased. It was no longer necessary to perform nearly as many drop tests on a new material to evaluate its dynamic performance since; a single G vs. s cushion curve was all that was required to generate all other cushion curves.

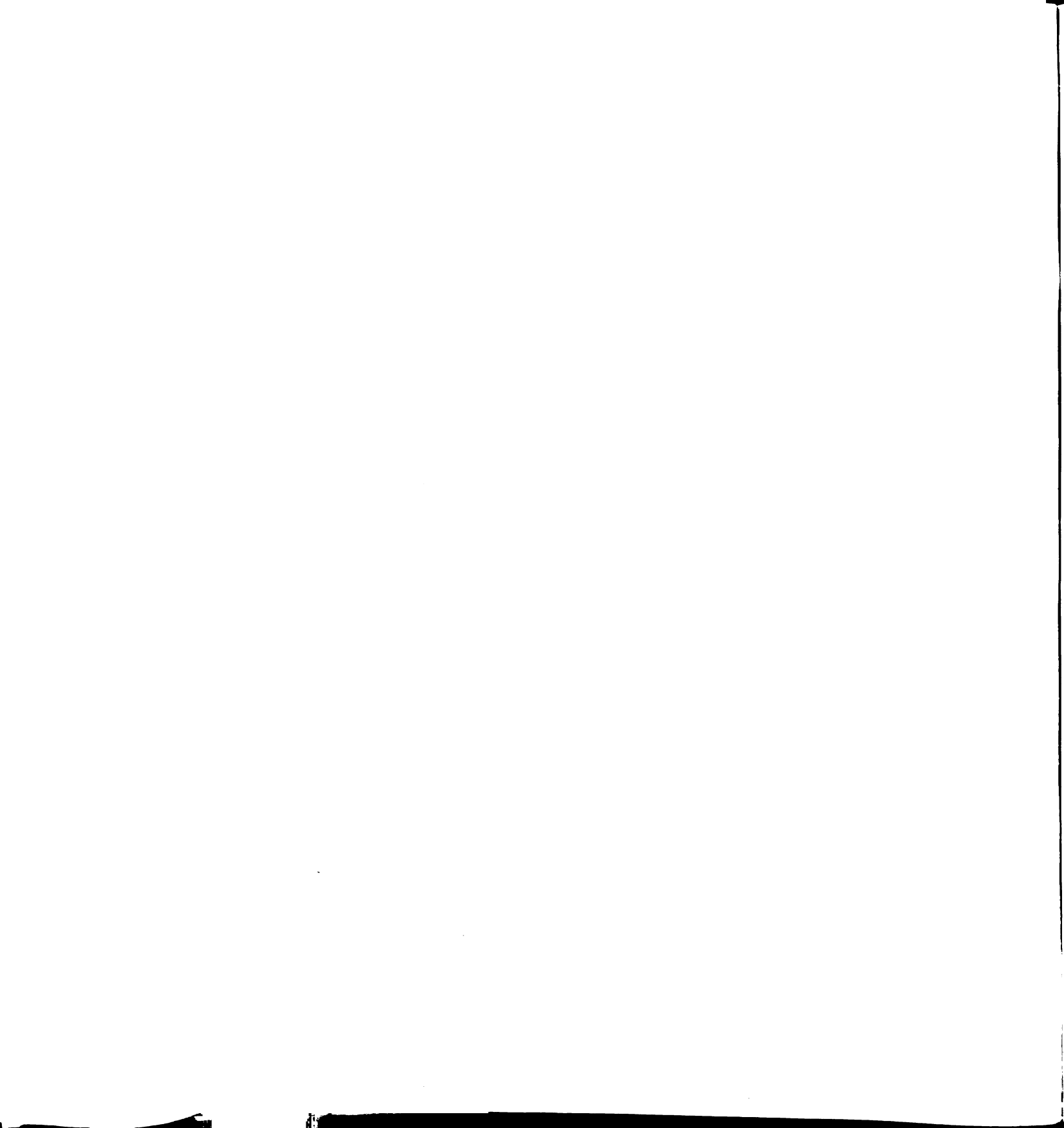
This chapter concludes the study of starch-based foams using PHAE as the functional aid for imparting mechanical strength and toughness, cell integrity, weather and water resistance to the foam structure. As a summary, this study involved the development and optimization of the starch-based foams using PHAE on the laboratory-scale ZSK-30 twin-screw extruder (Chapter 2) followed by the investigation of the dynamics of the starch foam process (chapter 3). A power-law shear viscosity model was developed for the starch plastic as a function of the moisture content, PHAE content, process temperature, and the specific mechanical energy input. This viscosity model was further used in the design of an annular die to be used on a manufacturing-scale Wenger TX-80 twin-screw extruder to produce starch-PHAE foam sheets. These foam sheets were evaluated for their cushioning and insulation properties (Chapter 4), and a numerical simulation was developed in the sections above for the prediction of these cushioning properties of the starch foam sheets (Chapter 5). These starch-based foam sheets using PHAE that were developed and evaluated, have been commercialized by a local Michigan-based company, KTM Industries, and is currently used as protective packaging by Toyota for automotive parts such as windshields and bumpers, and by Sony for entertainment systems.

The subsequent Chapter 6 deals with the selection of a new biodegradable polymer, as an alternative to the currently used PHAE to develop new starch-based foam formulations. The objective was to develop new starch-based foam formulations possessing properties that were equivalent (if not better) to those obtained using the starch-PHAE formulation.

5.5 References

- 1) Hilyard, M. C. Mechanics of Cellular Plastics. Applied Science Publishers, New York, 1982.
- 2) Burgess, G. J. Journal of Cellular Plastics, 24, 57-69, 1988.
- 3) Throne, J., Progelhof, R. Journal of Cellular Plastics, 21 (1), 43 – 50, 1985.
- 4) Military Standardization Handbook. 'Package Cushioning Design', MIL – HDBK – 304B, U. S. Department of Defense, 1978.
- 5) Gent, N., Thomas, A. G. Rubber Chemistry and technology, 36, 597-610, 1963.
- 6) Skockdopole, R. E., Rubens, L. C. Journal of Cellular Plastics, 1, 91-96, 1965.
- 7) J. Throne, R. Progelhof, Journal of Cellular Plastics, 20 (6), 437 – 442, 1984.
- 8) Shuttleworth, R., Shestopal, V., Goss, P. Journal of Applied Polymer Science, 30, 333-343, 1985.
- 9) Chen-Wai-Fah, Saleeb, A. F. Constitutive Equations for Engineering Materials. Volume 1: Elasticity and Modeling. New York: John Wiley and Sons, 1982.
- 10) Popov, E. P. Engineering Mechanics of Solids. Englewood Cliffs, NJ: Prentice Hall, 1990.
- 11) Burgess, G. Packaging Technology and Science, 3, 189-194, 1990.
- 12) Chen, A. W. Finite Difference and Finite Element Modeling of Closed Cell Cushions with Block and Ribbed Geometries based on Strain Dependent Terms. MS Thesis, Michigan State University, 1993.
- 13) Elliott, J. R., Lira, C. T. Introductory Chemical Engineering Thermodynamics. Prentice-Hall, New Jersey, 1999.
- 14) Holman, J. P. Heat Transfer, Sixth Edition. McGraw-Hill Book Company, New York, 1986.
- 15) Matonis, V. SPE Journal, 20, 1024, 1964.
- 16) Nabar, Y. U., Schindler, M., Narayan, R. Polymer Engineering and Science, In Press.
- 17) Kreith, F. Principles of Heat Transfer. Intext Educational Publishers, New York, 1973.

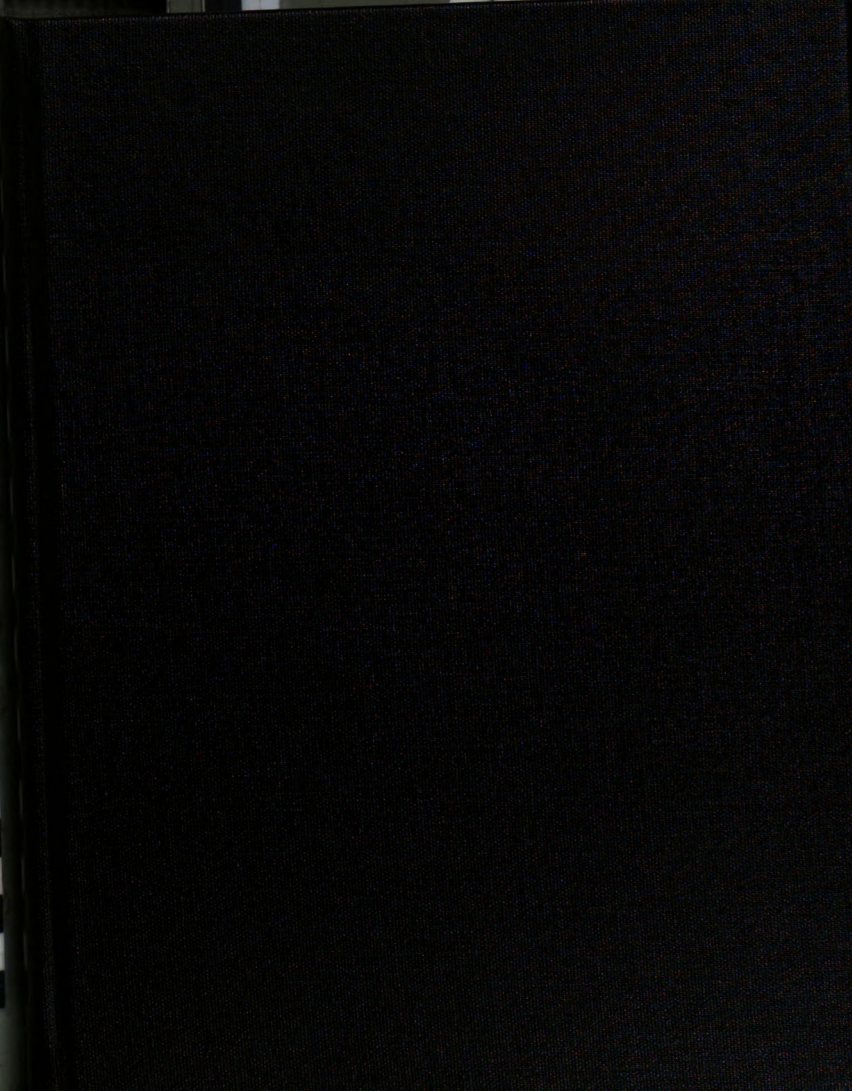
- 18) Leach, A. G. Journal of Physics, D: Applied Physics, 26, 733-739, 1993.
- 19) Branenburg, R., Lee, J. Fundamentals of Packaging Dynamics, L. A. B., Skaneateles, New York, 1991.
- 20) Kreyszig, E. Advanced Engineering Mathematics, Fourth Edition. John Wiley and Sons, New York, 1979.
- 21) Larson, R. E., Hostetler, R. P. Calculus with Analytic Geometry, D. C. Health Company, Lexington, MA, 1982.
- 22) Tipler, P. A. Physics, Second Edition. Worth Publishers Inc., New York, 1982.
- 23) American Standard Test Methods, 2002. Standard Test Methods for Dynamic Shock Cushioning of Packaging Materials. In: Annual Book of ASTM Standards. D - 1596, 15.09, Philadelphia, PA.
- 24) Wark, K. Jr. Thermodynamics, Fifth Edition. McGraw-Hill Book Company, New York, 1988.
- 25) Devore, J. L. Probability and Statistics for Engineering and Sciences, Second edition. Brooks/Cole Publishing Company, Monterey, CA, 1987.
- 26) Reddy, J. N. An Introduction to Finite Element Method, McGraw-Hill Book Company, New York, 1984.



MICHIGAN STATE UNIVERSITY LIBRARIES



3 1293 02956 2869



THESIS

6

2008

V.2

140

565

THS

LIBRARY
Michigan State
University

PLACE IN RETURN BOX to remove this checkout from your record.
TO AVOID FINES return on or before date due.
MAY BE RECALLED with earlier due date if requested.

DATE DUE	DATE DUE	DATE DUE

DESIGN AND I

Dep

**DESIGN AND ENGINEERING OF NOVEL STARCH – BASED FOAM AND FILM
PRODUCTS**

VOLUME II

By

Yogaraj Umesh Nabar

A DISSERTATION

**Submitted to
Michigan State University
In partial fulfillment of the requirements
for the degree of**

DOCTOR OF PHILOSOPHY

Department of Chemical Engineering and Material Science

2004

6.1 Abstract

Blends of hydro
below were extru
hydrophobic char
using other biode
adipate-co-tereph
Polyvinyl alcohol
improved in term
dimensional stab
moisture sorption
by reduction of un
and other proces
polyesters like PC
lower than 25 kg m
content, but the d
radial and longitu
polyesters as comp

**PHYSICO – MECHANICAL AND HYDROPHOBIC PROPERTIES
OF STARCH FOAMS EXTRUDED WITH DIFFERENT
BIODEGRADABLE POLYMERS**

6.1 Abstract

Blends of hydroxypropylated high amylose starch and various functional aids listed below were extruded into foams using a twin-screw extruder ZSK - 30. In this study, the hydrophobic character and mechanical properties of starch foams were improved by using other biodegradable polymers such as Poly-Caprolactone (PCL), Poly (butylene adipate-*co*-terephthalate) (PBAT), Cellulose Acetate (CA), Methylated Pectin (MP), Polyvinyl alcohol (PVA), and cross-linkers like glyoxal. The hydrophobic character was improved in terms of a reduction in steady state weight gain, and an increase in dimensional stability (reduction in loss of radial and longitudinal dimensions) on moisture sorption. At the same time, efforts were made to maximize the expansion ratios by reduction of unit densities. Formulations of these foams (in terms of additive content, and other processing parameters) were optimized. Particular formulations with PVA, polyesters like PCL and PBAT, and glyoxal with PVA gave foams with unit densities lower than 25 kg/m³. The dimensional stability increased with an increase in the polyester content, but the density increased beyond an optimum polyester content too. The loss in radial and longitudinal dimensions under steady state conditions was 12-20% with polyesters as compared to about 50-55% for control starch. Addition of these processing

aids did decrease
methylated pectin
densities, and slight

6.2 Introduction

Starch, an anhydrous
sustainable, biodegradable
alcohol (PVA) which
exhibit hydrophobic
bonding due to
thermal sensitivity
To impart hydrophobicity
blending of the
polystyrene, polyethylene
U.S and Australia
polystyrene. The
plastic and resin
and Hanna (1985)
methacrylate)
densities in the
40.1. Cha et al.
expansion ratio
(polystyrene)
used in addition

aids did decrease the water sensitivity of the starch foams. Foams with CA and methylated pectin, in the presence/absence of glyoxal had marginally lower unit densities, and slightly higher expansion ratios, as compared to those of control starch.

6.2 Introduction

Starch, an anhydroglucose polymer from corn, offers a structural platform to manufacture sustainable, biodegradable foam packaging. Extruded starch foams with polyvinyl alcohol (PVA) were first patented by Lacourse et al. (1, 2). Starch granules, however, exhibit hydrophilic properties and strong inter-molecular association via hydrogen bonding due to the hydroxyl groups on the granule surface. The hydrophilicity and thermal sensitivity renders the starch molecule unsuitable for thermoplastic applications.

To impart hydrophobicity to the starch foams, some researchers have reported the melt blending of thermoplastic starch with non-biodegradable hydrophobic polymers such as polystyrene, poly(methyl acrylate), etc. For example, Chinnaswamy and Hanna (3, 4) hold U.S and Australian patents on manufacturing loose-fill foams made of 70% starch and 30% polystyrene. The combination of polystyrene with starch reduced the use of petroleum-based plastic and rendered the material disintegrable, while providing water resistance. Bhatnagar and Hanna (5) extruded regular cornstarch with either polystyrene or poly (methyl methacrylate) at a 70:30 ratio with other additives in a single screw extruder. Foam densities in the range of 29.5-132 kg/m³ were obtained, with radial expansions of 8.8 - 40.1. Cha et al. (6) studied the moisture adsorption isotherms, bulk densities and expansion ratios of the starch-based foams involving about 33% synthetic polymers (polystyrene), which reduces its biodegradability. Also, chemical blowing agents were used in addition to water as the physical blowing agent. Cha et al (7, 8) conducted

extrusions to
moisture cont
starches, poly
agents. Howe
The followin
poly(caprolac
the starch-ba
foams from
from blends
cellulose ac
Neumann an
foams using
hydroxy fun
processing c
the range of
blended with
(talc), blowin
polycaprolac
and extrusion
Results indic
existed betw
PLA (19). Ea
21) or a con

extrusions to study the rheological properties of blend melts and effects of temperature and moisture contents on mechanical properties of starch-based foams containing wheat and corn starches, polyethylene-*co*-vinyl alcohol, polystyrene, plasticizers, and nucleating and blowing agents. However, the resultant starch-based foams were not completely biodegradable.

The following authors report the use of hydrophobic biodegradable polymers such as poly(caprolactone) (PCL), cellulose acetate (CA), aliphatic-aromatic co-polyesters, etc. in the starch-based foam formulations. Altieri and Tessler (9) patented the water-resistant foams from blends of starch with starch esters. Bastioli et al. (10 – 13) patented foams from blends of starch with 10-30% of polymers such as PVA, poly (caprolactone), cellulose acetate, poly (ethylene vinyl alcohol), and poly (ethylene-*co*-acrylic acid). Neumann and Seib (14, 15) patented the technology to make biodegradable starch-based foams using polyalkylene glycols. Xu and Doane (16, 17) prepared starch foams using hydroxy functional polyesters as a processing aid. Depending on the formulation and processing conditions, the foams reported in the patents cited above had bulk densities in the range of approximately 3-100 kg/m³. Wang and Shogren (18) extruded cornstarch blended with biodegradable polymers to make loose-fill foams. Effects of nucleating agent (talc), blowing agents (water, ethanol, and propanol) and different polymers (polylactic acid, polycaprolactone, polyvinyl alcohol, polybutylene succinate-adipate, and polyester-amide) and extrusion conditions on foam density, resilience, and compressibility were examined. Results indicated that 0.5-1% talc addition was the optimum range. No significant differences existed between the blowing agents. Hanna and co-workers reported that the addition of PLA (19), Eastar Bio co-polyester (poly (butylene adipate-*co*-terephthalate)) (PBAT) (20, 21) or a commercial starch-based material (Mater-Bi from Novamont) (22) increased

radial expansion
contents. These f
Shogren (23) ext
wheat starch and
biodegradable po
(PHEE), poly (ca
valerate) among o
Some reactive m
hydrophobicity. E
with methyl acry
high amylose star
Starch-based foa
sorption in a hu
dimensions. Stu
starch-based foa
performed earli
polymers such
of these starch
the loss in dim
mechanical pr
Weight gain
adversely aff
critical. The

radial expansions for the starch-based foams for particular compositions and moisture contents. These foams also showed improved flexibility and water resistance. Willett and Shogren (23) extruded blends of normal cornstarch as well as high amylose cornstarch, wheat starch and potato starch with resins such as PVA, cellulose acetate, and several biodegradable polyesters such as poly (lactic acid) (PLA), poly (hydroxy ester ether) (PHEE), poly (caprolactone), poly (ester amide) (PEA), and poly (hydroxybutyrate-*co*-valerate) among others.

Some reactive modifications of starch itself have also been performed to impart hydrophobicity. Boehmer et al. (24) patented foams based on graft copolymers of starch with methyl acrylate. Shogren (25) reported that extruded foams made from acetylated high amylose starch had higher water resistance, but high bulk densities of 40-60 kg/m³.

Starch-based foams due to their hygroscopic nature tend to gain weight on moisture sorption in a humid environment. This is also accompanied by shrinkage in the foam dimensions. Studies on determining the weight gain and the dimensional stability of the starch-based foams, which are critical for cushion packaging applications, have not been performed earlier. The objective of this study was to use water-resistant biodegradable polymers such as PCL, PBAT, PVA, CA, and MP to improve the hydrophobic character of these starch foams. Hydrophobicity was imparted by decreasing the weight gain and the loss in dimensions by shrinkage on moisture sorption, without sacrificing the physico-mechanical properties such as lower densities and higher resilience (spring indices). Weight gain and shrinkage (loss in dimensions) in starch foams on moisture sorption adversely affects its performance in cushioning as well as the insulation, and hence, is critical. The best formulations were determined based on their lower weight gains, high

dimensional stability
compressibility and
In this study, the
Physical properties
dimensional stability

6.3 Experiment

6.3.1 Materials

The type of starch
content). The starch
IN), under the trade
The inherent moisture
was used as the plasticizer
8-10% of the starch
obtained from Luzern
density of 150 kg m⁻³
Semi-crystalline polyethylene
name Tone 787, was
Charleston, WV). Polyethylene
51.100, and PDI of 2.0
BASF Chemicals (Ludwigshafen)
Substitution = 2.0) (Huls)
It had a weight-average molecular weight
191°C, and a melting

dimensional stability, low densities and improved mechanical properties such as compressibility and resilience.

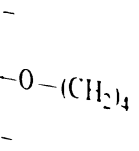
In this study, the operating conditions were almost fixed, based on preliminary studies. Physical properties, such as unit densities, expansion ratios, equilibrium weight gains and dimensional stability on moisture sorption were studied.

6.3 Experimental

6.3.1 Materials

The type of starch used was hydroxypropylated high amylose cornstarch (70% amylose content). The starch was purchased from National Starch and Chemicals (Indianapolis, IN), under the trade name of HYLON 7. The density of HYLON 7 starch is 1.2 g/cm^3 . The inherent moisture content of the starch is 11.2% under ambient conditions. Water was used as the plasticizer as well as the blowing agent. Water content was maintained at 8-10% of the starch used. Talc (Magnesium Silicate), used as the nucleating agent, was obtained from Luzenac (Ontario, Canada). It has a specific gravity of 2.76 and a bulk density of 150 kg/m^3 . The talc content was maintained at 1% for all the experiments. Semi-crystalline polycaprolactone (PCL) resin (Figure 6.1) of M_n 80,000, under the trade name Tone 787, was purchased from Union Carbide Chemicals and Plastics (South Charleston, WV). Poly (butylene adipate-*co*-terephthalate) (PBAT) resin (Figure 6.2) of M_n 51,100, and PDI of 2.214, under the trade name Ecoflex FBX 7011, was purchased from BASF Chemicals (Ludwigshafen, Germany). Cellulose Acetate (grade JLF-68) (Degree of Substitution = 2.0) (Figure 6.3) was acquired from Hoechst Celanese Corp (Somerville, NJ). It had a weight-average molecular weight, M_w of $\sim 55,100$, an M_n of $\sim 11,800$, T_g of 191°C , and a melting temperature of 230°C . The melting endotherm started at 218°C .

PVA (Figure 6.
under the trade
146.000). Glyox
from Sigma - A



F

PVA (Figure 6.5) was purchased from Air Products and Chemicals (Allentown, PA), under the trade name Airvol 325 (degree of hydrolysis of 98.3%, $M_w \sim 85,000 - 146,000$). Glyoxal (Figure 6.6) and methylated pectin (93% methylated) (Figure 6.7) were from Sigma – Aldrich Chemical Co. (St. Louis, MO).

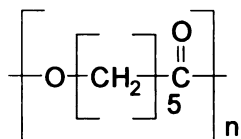


Figure 6.1 Poly (caprolactone)

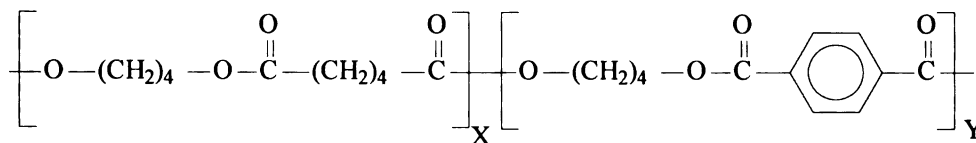


Figure 6.2 Poly (butylene adipate-co-terephthalate)

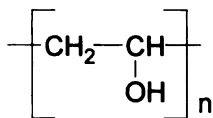


Figure 6.3 Poly (vinyl alcohol)

linkages to
cellulose gro

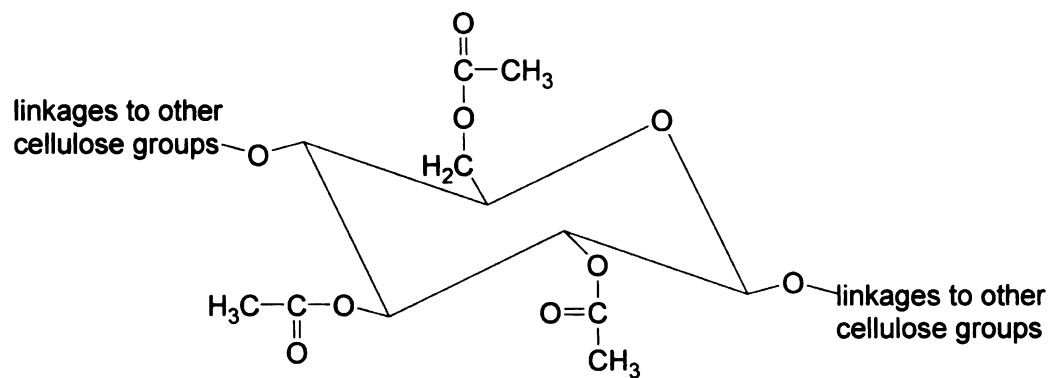


Figure 6.4 Cellulose Acetate

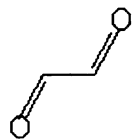


Figure 6.5 Glyoxal

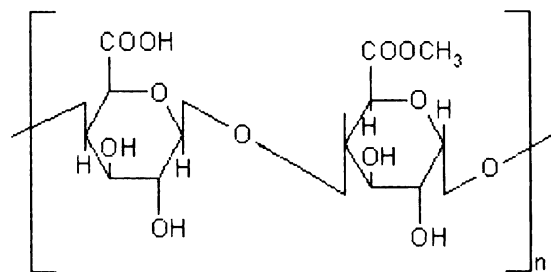


Figure 6.6 Methylated Pectin

6.3.2 Experiment

The experiment

screw extrusion

ZSK-30 twin-screw

positive displacement

feeders for feeding

screw configuration

selected to get the

A cylindrical filament

sleeve was assembled

the temperature and

foam extrudates of

6.3.2 Experimental Setup

The experimental setup used in this study was a twin-screw extrusion system. The twin-screw extrusion system consisted of an extruder driver with a speed control gearbox, a ZSK-30 twin-screw co-rotating extruder with a screw diameter of 30 mm, an L/D of 42, a positive displacement pump for injecting water into the extruder, accurate single-screw feeders for feeding starch, and the processing aids and talc were fed individually. The screw configuration is shown below in Figure 6.7. This specific screw configuration was selected to get the best physico-mechanical properties based on our previous work (26). A cylindrical filament die 2.7 mm in diameter and 8.1 mm in length, with a cooling sleeve was assembled to the extruder. The sensors were mounted on the die to measure the temperature and pressure of the melt. A high-speed cutter was used to get cylindrical foam extrudates of required size.

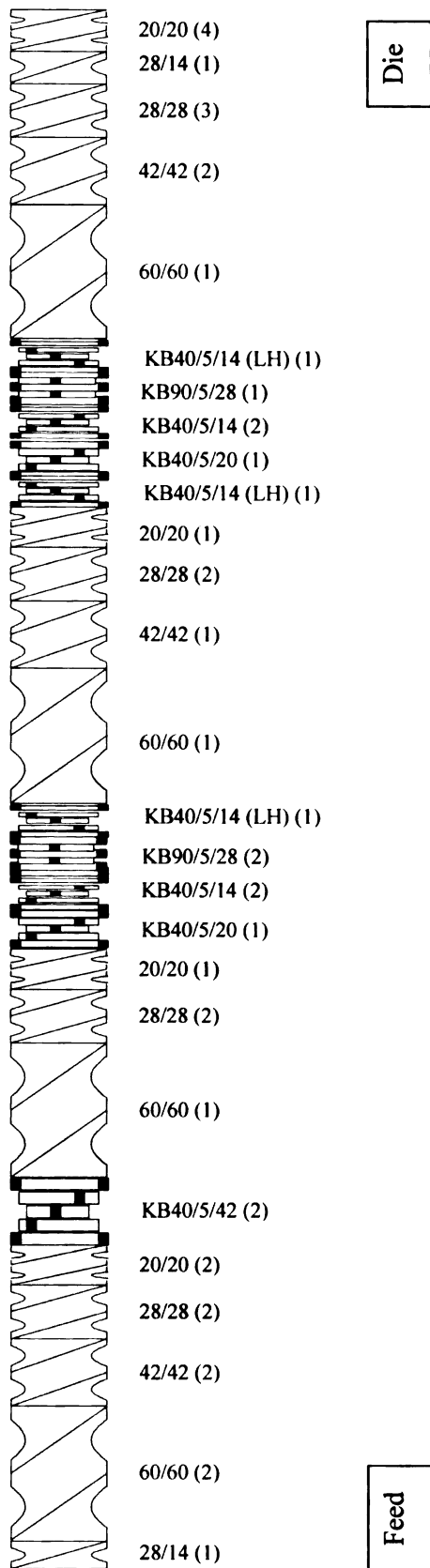


Figure 6.7 Foaming Screw Configuration for the Century ZSK – 30 Twin-Screw Extruder

6.3.3 Procedure

The temperature

The temperature

Zone 1: 20°C (0

Zone 2: 100°C

Zone 3: 115°C

Zone 4: 120°C

Zone 5: 125°C

Zone 6: 125°C

Zone 7: 120°C

Zone 8: 120°C

Zone 9: 115°C

Die: 115°C

Melt Temper

The feeder fo

25 lb/hr). Th

Initially, dur

and later its

(11.2%) pres

content was

used individu

6.3.3 Procedure

The temperatures in the extruder zones were set up to reach the required temperatures.

The temperature profile is as follows:

Zone 1: 20°C (cold feed)

Zone 2: 100°C

Zone 3: 115°C

Zone 4: 120°C

Zone 5: 125°C

Zone 6: 125°C

Zone 7: 120°C

Zone 8: 120°C

Zone 9: 115°C

Die: 115°C

Melt Temperature: 112-115°C

The feeder for starch was calibrated and set at a particular speed to feed at 11.2 kg/hr (~ 25 lb/hr). The other feeder/feeders were calibrated and set at feeding rates accordingly. Initially, during start-up, water was pumped into the system at 15-20% of the starch fed, and later its flow rate was reduced to about 8-10% of starch. The inherent moisture (11.2%) present in starch also helped in plasticization of starch. Thus, the total moisture content was 18%. The screw speed was maintained at 200 rpm. The processing aids were used individually, or in combination with each other. When formulations were changed,

extrusion was c
carried out at a

6.3.4 Charac

The samples ob
The samples co
environment ro
before testing.

6.3.4.1 Density

The density of t
specimen accor
samples were m
The dimensions
permit measure

as the ratio of the

6.3.4.2 Compr

Compressive str
Compressive stre
machine. Foam s
probe (0.635 cm
foam surface, an
From this point, t
The maximum loa
Compressive stre

extrusion was continued until the torque and the die pressure stabilized. Extrusions were carried out at a torque of 70-75%, and a pressure of 700-1000 psi.

6.3.4 Characterization

The samples obtained were in the form of cylindrical blocks of a length of about 3 cm. The samples collected were conditioned as per ASTM D – 4332 (27), in a constant environment room at $23 \pm 1^\circ\text{C}$ ($73.4 \pm 3.6^\circ\text{F}$) and $50 \pm 2\%$ RH for at least 72 hours before testing.

6.3.4.1 Density

The density of the foam was calculated from the mass and volume of a regularly shaped specimen according to the test method ASTM D – 3575 (section 43, Method A) (28). 10 samples were measured for each formulation.

The dimensions of the sample were measured using a Vernier Calipers graduated to permit measurements accurate to 0.001 inches. The Expansion Ratio (ER) was calculated as the ratio of the cross-sectional area of the foam to that of the die.

6.3.4.2 Compressive Strength and Resiliency (1, 29)

Compressive strength and resiliency describe the mechanical integrity of the foam. Compressive strength of the lab-scale specimens was measured on a UTS tensile testing machine. Foam specimens were securely fastened lengthwise and compressed by a steel probe (0.635 cm diameter) with a hemi-spherical end-cap. By lowering the piston to the foam surface, an initial load of 0.5 N was applied on the specimen for approximately 5 s. From this point, the probe was lowered at a rate of 30 mm/min for a distance of 3 mm. The maximum load was recorded. After 60 s had elapsed, a relaxation load was recorded. Compressive strength was determined by dividing the maximum load by the cross-

sectional area of the

60 s hold period d

Averages were cal

6.3.4.3 Moisture

10 blocks of ea

environmental hu

temperature of 38

samples were mo

weighing balance

measured at differ

placing the sample

and length were as

samples were reco

The steady state v

respectively. The

samples used for th

6.3.4.4 Environm

Foam samples wer

graphite filled tape

2020 environment.

with polyesters as p

sectional area of the probe. Resiliency is the percentage of the compressive force after the 60 s hold period divided by the maximum force required to compress the foam by 3 mm. Averages were calculated from five sets of starch foam specimens.

6.3.4.3 Moisture Sorption Analysis

10 blocks of each formulation, collected at different times were placed in an environmental humidity chamber, subject to a relative humidity of $95 \pm 5 \%$, and a temperature of $38 \pm 5 \text{ }^\circ\text{C}$. The weight and the dimensions (length and diameter) of the samples were monitored. They were measured at regular intervals using an accurate weighing balance and a pair of Vernier Calipers, to the third decimal place. The entities measured at different time intervals were normalized using the value measured before placing the samples in the humidity chamber (time, $t = 0$). The initial weight, diameter and length were assigned W_0 , D_0 , and L_0 respectively. The weight and dimensions of the samples were recorded until a steady state value was reached (approximately 30 days). The steady state weights and dimensions of the samples were assigned W , D , and L respectively. The results for a formulation were obtained as an average over the 10 samples used for that formulation.

6.3.4.4 Environmental Scanning Electron Microscopy (ESEM)

Foam samples were sectioned with a razor blade and mounted on aluminum stubs with graphite filled tape, sputter coated with gold and examined with a Phillips Electroscan 2020 environmental scanning electron microscope. The surfaces of the foam samples with polyesters as processing aids were used.

6.4 Results and Discussion

An optimum for the hydrophobic force densities and the polymers as functions of the obtained for some

6.4.1 Effect of starch

In the case of the the PVA content (Entries 2 – 6) ρ (kg m^{-3}) was obtained reduced its melt, and the melt, and the Mechanical Properties Willett et al. compared to soluble in water and the increase in the PVA deviation was

6.4 Results and Discussion

An optimum formulation had to be reached with each functional aid, to get the most hydrophobic foam without sacrificing the physico-mechanical properties. The unit densities and the expansion ratios for the foam formulations using the biodegradable polymers as functional aids are reported in Table 6.1. Densities lower than 25 kg/m^3 were obtained for some formulations.

6.4.1 Effect of Functional Aids on the Density and Expansion Ratio (ER) of the starch foams

In the case of PVA, it was observed that the expansion ratio increased with an increase in the PVA content, but just up to a certain level, and then decreased again (Table 6.1, Entries 2 – 6)). The maximum expansion ratio of 45.1 and minimum unit density of 24.5 kg/m^3 was obtained at a PVA content of 3% of the starch used. Addition of PVA to starch reduced its melt flow index (MFI) value (30), indicating an increase in the viscosity of the melt, indicated by a rise in the torque on the extruder, and thus the Specific Mechanical Energy (SME). This was in accordance with the behavior observed by Willett et al. (23), that an increase in SME was observed in the starch/PVA blend as compared to the starch control. Also, PVA, a high molecular weight molecule, being soluble in water, would decrease its diffusivity. This lead to a more controlled expansion, and the increased stiffness of the starch matrix supported this expansion. With an increase in the PVA content, there was a lowering effect on the flow behavior. This negative deviation was due to a phase separation in the system.

**Table 6.1 Unit Densities, Radial Expansion Ratios, Specific Lengths, Compressive Strengths and Spring Indices
(Resilience) with different Functional Aids**

Table 6.1 Unit Densities, Radial Expansion Ratios, Specific Lengths, Compressive Strengths and Spring Indices (Resilience) with different Functional Aids

Entry	Processing Aids	Unit Density (kg/m ³)	Radial Expansion ratio	Specific Length (cm/gm)	Resiliency (%)
1	None (Control)	30.2 (± 0.8)	39.6 (± 1.1)	14.6 (± 0.6)	69.8 (± 2.1)
2	3% PVA	24.5 (± 0.5)	45.1 (± 1.0)	15.8 (± 0.5)	72.8 (± 1.8)
3	6% PVA	29.2 (± 0.6)	39.7 (± 0.9)	15.1 (± 0.8)	72.4 (± 1.2)
4	9% PVA	32.2 (± 0.9)	36.7 (± 0.9)	14.8 (± 0.4)	71.0 (± 1.2)
5	12% PVA	34.2 (± 1.3)	34.2 (± 0.6)	14.9 (± 0.5)	71.6 (± 1.3)
6	15% PVA	36.4 (± 1.6)	31.8 (± 0.9)	15.1 (± 0.3)	71.2 (± 0.8)
7	0.1% Glyoxal + 3% PVA	24.4 (± 0.4)	44.9 (± 1.8)	15.9 (± 0.6)	66.2 (± 3.9)
8	0.2% Glyoxal + 3% PVA	24.1 (± 0.4)	46.8 (± 2.3)	15.5 (± 0.6)	66.6 (± 4.2)
9	0.3% Glyoxal + 3% PVA	23.5 (± 0.6)	48.5 (± 1.7)	15.3 (± 0.5)	66.3 (± 3.7)
10	0.4% Glyoxal + 3% PVA	25.8 (± 0.3)	44.8 (± 2.1)	15.1 (± 0.9)	66.4 (± 3.1)
11	1.0% Glyoxal + 3% PVA	30.5 (± 1.3)	39.1 (± 1.4)	14.6 (± 0.8)	65.4 (± 5.1)

Table 6.1 (Cont'd.) Unit Densities, Specific Lengths, Compressive Strengths and Spring Indices (Resilience)

12	3% CA	30.2 (± 1.2)	39.6 (± 2.1)	14.6 (± 0.9)	74.7 (± 3.2)
13	6% CA	29.7 (± 1.0)	40.4 (± 1.6)	14.6 (± 1.1)	76.7 (± 2.7)
14	10% CA	29.6 (± 1.3)	40.5 (± 2.2)	14.6 (± 1.4)	77.5 (± 3.5)

Table 6.1 (Cont'd.) Unit Densities, Specific Lengths, Compressive Strengths and Spring Indices (Resilience)

12	3% CA	30.2 (± 1.2)	39.6 (± 2.1)	14.6 (± 0.9)	74.7 (± 3.2)
13	6% CA	29.7 (± 1.0)	40.4 (± 1.6)	14.6 (± 1.1)	76.7 (± 2.7)
14	10% CA	29.6 (± 1.3)	40.5 (± 2.2)	14.6 (± 1.4)	77.5 (± 3.5)
15	3% Methylated Pectin	30.1 (± 1.9)	39.7 (± 2.6)	14.6 (± 1.3)	71.0 (± 2.8)
16	6% Methylated Pectin	29.9 (± 1.6)	40.2 (± 1.9)	14.6 (± 1.1)	70.0 (± 2.3)
17	10% Methylated Pectin	29.8 (± 1.5)	40.3 (± 2.1)	14.6 (± 1.6)	70.9 (± 3.2)
18	0.1% Glyoxal + 10% CA	30.1 (± 0.6)	39.7 (± 1.3)	14.6 (± 0.9)	73.1 (± 2.1)
19	0.2% Glyoxal + 10% CA	29.7 (± 0.5)	40.5 (± 1.1)	14.6 (± 0.7)	74.3 (± 2.3)
20	0.3% Glyoxal + 10% CA	28.6 (± 0.5)	42.3 (± 0.8)	14.4 (± 0.9)	74.4 (± 2.8)
21	0.4% Glyoxal + 10% CA	31.1 (± 0.8)	38.3 (± 0.9)	14.7 (± 1.1)	71.6 (± 2.4)
22	1.0% Glyoxal + 10% CA	32.7 (± 1.4)	36.0 (± 1.7)	14.8 (± 1.5)	67.5 (± 3.8)
23	0.1% Glyoxal + 10% Methylated Pectin	29.9 (± 0.8)	40.0 (± 1.5)	14.6 (± 0.8)	66.2 (± 3.9)
24	0.2% Glyoxal + 10% Methylated Pectin	29.6 (± 0.7)	40.5 (± 1.5)	14.6 (± 1.0)	67.5 (± 3.6)
25	0.3% Glyoxal + 10% Methylated Pectin	28.8 (± 0.5)	42.0 (± 1.2)	14.5 (± 0.9)	66.9 (± 4.1)
26	0.4% Glyoxal + 10% Methylated Pectin	32.1 (± 1.1)	36.9 (± 1.4)	14.8 (± 1.3)	68.4 (± 4.3)
27	1.0% Glyoxal + 10% Methylated Pectin	34.8 (± 1.9)	33.5 (± 2.4)	15.0 (± 2.1)	66.8 (± 4.9)

Table 6.1 (Cont'd.) Unit Densities, Specific Lengths, Compressive Strengths and Spring Indices (Resilience)

28	1% PCI.	27.4 (± 0.5)	41.0 (± 0.6)	15.5 (± 0.4)	75.3 (± 1.2)
29	3% PCI.	26.2 (± 0.3)	42.7 (± 0.4)	15.6 (± 0.2)	78.2 (± 1.3)
30	7% PCI.				

Table 6.1 (Cont'd.) Unit Densities, Specific Lengths, Compressive Strengths and Spring Indices (Resilience)

28	1% PCL	27.4 (± 0.5)	41.0 (± 0.6)	15.5 (± 0.4)	75.3 (± 1.2)
29	3% PCL	26.2 (± 0.3)	42.7 (± 0.4)	15.6 (± 0.2)	78.2 (± 1.3)
30	7% PCL	37.4 (± 1.1)	28.2 (± 0.9)	16.6 (± 0.7)	75.7 (± 0.8)
31	10% PCL	47.1 (± 1.5)	19.3 (± 1.5)	19.2 (± 0.9)	73.6 (± 1.1)
32	1% PBAT	26.2 (± 0.3)	45.3 (± 0.4)	14.7 (± 0.5)	80.3 (± 0.8)
33	3% PBAT	24.5 (± 0.3)	46.5 (± 0.3)	14.8 (± 0.3)	83.6 (± 1.2)
34	5% PBAT	24.2 (± 0.2)	46.7 (± 0.5)	15.5 (± 0.4)	84.2 (± 1.1)
35	7% PBAT	24.7 (± 0.4)	46.0 (± 0.4)	14.8 (± 0.6)	85.9 (± 0.8)
36	10% PBAT	28.7 (± 0.2)	41.1 (± 0.3)	14.8 (± 0.5)	83.1 (± 0.7)

An improvement
adhesion between
increase in the
agent) considera

Figure 6.

Glyoxal has found
glues and adhesive
used as a cross-link

An improvement in mechanical properties was not realized due to the poor interface adhesion between the fibrous PVA structure and the starch matrix (Figure 6.8). Also, an increase in the PVA content may have reduced the diffusivity of water (the blowing agent) considerably resulting in lower values of the ER.

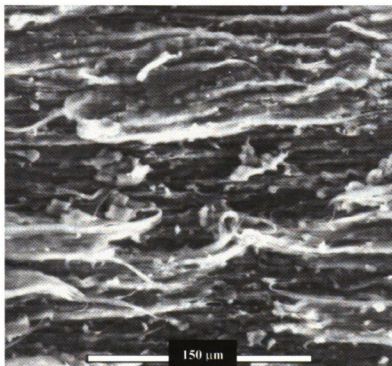


Figure 6.8 ESEM of the surface of starch foams with 12% PVA

Glyoxal has found applications as a cross-linker in the production of moisture resistant glues and adhesives as well as moisture resistant foundry binders. Hence, glyoxal was used as a cross-linker for starch to improve its hydrophobic character. 3% PVA was used

in the formulation
(Entries 7 - 11).
content, but beyond
maximum ER of
content of 0.3%.
The increase in ER
starch and with
making it stiffer.
Also, an increase
to cell rupture. At
restricting the ex
(0.3%) was requi
some hydrophobic
Cellulose acetate
and the expansion
density of 29.6 kg
the formulation c
maximum expansi
glyoxal was used
one obtained by us
When PCL was us
and reached a maxi
density of the corre

in the formulations to obtain a product with lower unit density. As seen in Table 6.1 (Entries 7 – 11), the ER increased while the density decreased with an increase in glyoxal content, but beyond a certain amount the ER decreased and the unit density increased. A maximum ER of 48.5 and a minimum density of 23.5 kg/m^3 were obtained at a glyoxal content of 0.3%.

The increase in ER can be attributed to the fact that glyoxal acted as a cross-linker within starch and with PVA, and increased the molecular weight of the starch matrix, thus making it stiffer. This helped in preventing the loss of the moisture through the surface. Also, an increase in melt strength due to cross-linking prevented the loss of moisture due to cell rupture. At higher glyoxal contents, however, the stiffness increased considerably, restricting the expansion due to loss of flexibility. Thus an optimum amount of glyoxal (0.3%) was required to give maximum ER and a minimum unit density in addition to some hydrophobic character.

Cellulose acetate and Methylated Pectin did not have a significant effect on the density and the expansion ratio of the starch foams (Table 6.1, Entries 12 – 17). A minimum unit density of 29.6 kg/m^3 and a maximum expansion ratio (ER) of 40.5 were obtained with the formulation containing 10% CA. A minimum unit density of 29.8 kg/m^3 and a maximum expansion ratio of 40.4 were obtained with 10% methylated pectin. When glyoxal was used as a cross-linker between CA and MP, the response was similar to the one obtained by using glyoxal with PVA (Table 6.1, Entries 18 - 27).

When PCL was used in the starch-based foam formulations, the ER increased initially and reached a maximum of 42.7 at a PCL content of about 3% (Table 6.1, Entry 29). The density of the corresponding formulation was 26.2 kg/m^3 . The density increased to 47.1

kg m³ with an i

6.1. Entry 31). I

migrated to the

lower surface t

dynes/cm) (31) I

overall energy is

6.9 (also, Figure

foam surface in t

6.10 showed the

compared to the

6.9).

kg/m³ with an increase in PCL content to 10%, with a low expansion ratio of 19.3 (Table 6.1, Entry 31). PCL was not compatible with starch, and phase separated, and most of it migrated to the surface into the skin. The polyester migrated to the surface because of the lower surface tension in the melt, thus forming a hydrophobic coating. PCL (39.6 dynes/cm) (31) has a lower surface energy than starch (53.7 dynes/cm) (32), and thus the overall energy is minimized by the migration of the polymer to the foam surface. Figures 6.9 (also, Figure 2.21) and 6.10 show the scanning electron micrographs of the starch foam surface in the absence of any functional aids, and with 3% PCL respectively. Figure 6.10 showed the presence of a smooth skin on the surface of the starch foams, as compared to the surface of the control starch foam without any processing aids (Figure 6.9).

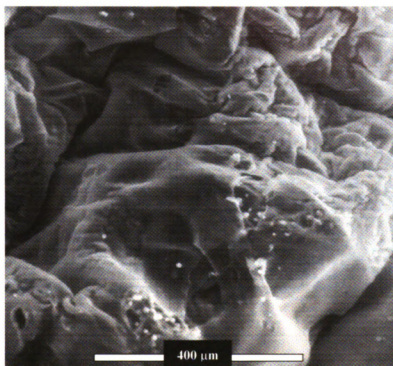


Figure 6.9 ESEM of the surface of starch foams with no functional aids.

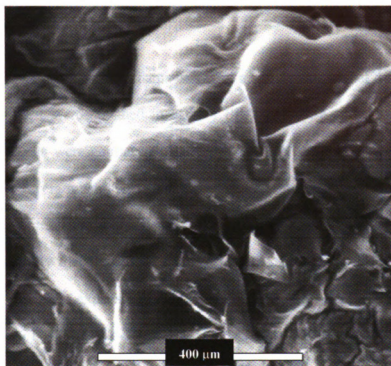


Figure 6.10 ESEM of the surface of starch foams with 3% PCL.

This finding was consistent with the results seen by Willett et al. (23) where X-ray Photoelectron Spectroscopy was used to show the manifestation of the polyester on the surface of starch foams. This prevented the loss of water (blowing agent) through the skin resulting in an increase in the ER, and a reduction in unit density.

However, further increase in the PCL content led to poorer densities and expansion ratios due to a non-homogeneous melt phase involving the starch plastic and the PCL. This resulted in much denser foam, since water did not function as a blowing agent for PCL.

Thus, the un-
Chemically mo
increase the co
which is hydro
The effect of PB
higher values of
PBAT. These re
densities obtaine
5% PBAT were
There is a possi
starch matrix. M
shown in Table 6
migrated to the s
starch foam surf
preventing the rap
a lower surface e
minimized by the
PBAT on the sur
higher elasticity a
contents, slightly
agent for PBAT. r
lower than that me

Thus, the un-foamed PCL phase separated resulting in an increase in the density. Chemically modifying either starch or PCL, and grafting one onto the other could increase the compatibility between starch and PCL. This could result in a molecule, which is hydrophobic by itself.

The effect of PBAT on the starch foams was very much similar to that due to PCL. But, higher values of ER were obtained in case of PBAT, because of higher flexibility of PBAT. These results were contrary to those observed by Willett et al. (23). Also, the densities obtained were much lower than those reported by Fang et al. (20). Foams with 5% PBAT were extruded at a unit density of 24.2 kg/m^3 at an expansion ratio of 46.7. There is a possibility that the PBAT showed higher compatibility than PCL with the starch matrix. Maximum expansion ratios were obtained at a PBAT content of 3-7% as shown in Table 6.1 (Entries 32 – 36). The ER was higher in this range because PBAT migrated to the surface, which was evident from the scanning electron micrograph of the starch foam surface in Figure 6.11, thus providing a finer and a more stable surface preventing the rapid loss of moisture through the surface. PBAT (44.2 dynes/cm) (31) has a lower surface energy than starch (53.7 dynes/cm) (32), and thus the overall energy is minimized by the migration of the polymer to the foam surface.

PBAT on the surface resisted tears and formation of holes on the surface, as it has a higher elasticity as compared to thermoplastic starch. Similar to PCL, at higher PBAT contents, slightly denser foam was obtained, since water did not function as a blowing agent for PBAT, resulting in lower values of the ER. However, the densities were still lower than that measured for the control.

Efforts are on
between the two
also exhibits b

Figure

6.4.2 Compress

Typically, a pow
foam density ρ (c
deformation better
existed between fo
in Figure 6.12 was

Efforts are on to chemically modify either PBAT or starch for better compatibility between the two, thus that the resulting entity (molecule) is hydrophobic by itself and also exhibits better mechanical properties.

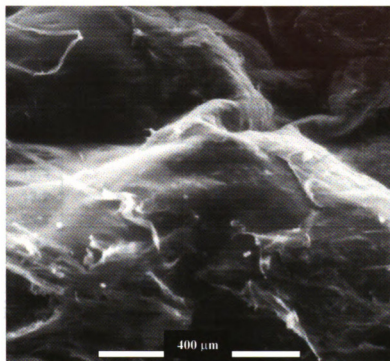


Figure 6.11 ESEM of the surface of starch foams with 7% PBAT.

6.4.2 Compressive Strength and Resiliency

Typically, a power-law relationship is observed between compressive strength σ_c and foam density ρ ($\sigma_c \sim \rho^n$). Denser foams tend to have thicker cell walls and hence resist deformation better than lower density foams with thinner cell walls. A strong relation existed between foam density and compressive strength (Figure 6.12). The regression line in Figure 6.12 was drawn and a slope of 0.82 was obtained ($n = 0.82$). A value of $n =$

0.92 was obtained
exponents of 1.1
variation in the
due to a difference
twin-screw extruder

LN (Compressibility) (Pa)

Figure 6.12 C

The resiliency of
provided a resiliency
resiliency considered
PCL and CA helped

0.92 was obtained by Willett et al. (23), while Hutchinson and co-workers (33) report exponents of 1.5 – 1.6 for compressive strengths of foams prepared from maize grits. The variation in the value of the slope obtained (0.82) and the values reported in literature was due to a different type of starch used, and probably also due to a different experimental twin-screw extrusion configuration.

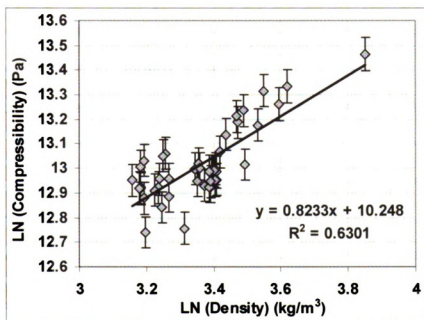


Figure 6.12 Compressive Strength (Pa) of the starch-based foams as a function of their density (kg/m³)

The resiliency of the foam samples is listed in Table 6.1. The control starch foams provided a resiliency (spring index) of 69.7%. The addition of PBAT improved the resiliency considerably from 69.7% to 85.9% at a PBAT content of 7% of the starch used. PCL and CA helped increase the spring index up to ~ 78%, while PVA and Methylated

Pectin barely in
linker, it increa
decreased by ~
Thus, PBAT p
kg m³), better h

6.4.3 Effect of the starch

Table 6.2 below
to a humid env
character. It was
PVA concentrati
a PVA content o
as compared to th
Starch foams shr
is important in pa
dimensional stabi
Results indicated
dimensional stabi

Pectin barely increased the resiliency to ~71 - 72%. When glyoxal was added as a cross-linker, it increased the rigidity of the starch foams and, thus, the resiliency of the foams decreased by ~ 3%.

Thus, PBAT provided the best properties in terms of its lower densities (~ 24 – 25 kg/m³), better hydrophobic properties, and spring indices as high as 85%.

6.4.3 Effect of Functional Aids on the Weight Gain and Dimensional Stability of the starch foams on Moisture Sorption

Table 6.2 below (Entries 2 – 6) exhibits the response of the PVA modified starch foams to a humid environment. A lower final weight gain value implies more hydrophobic character. It was observed that the hydrophobic character increased with an increase in PVA concentration, but just up to a certain extent. Minimum weight gain was observed at a PVA content of 12%. The samples with 15% PVA showed higher moisture absorption as compared to those with 12%.

Starch foams shrink in the presence of moisture. The dimensional stability of the product is important in packaging applications. The lower the loss in dimensions, the better is the dimensional stability. Thus, a higher ordinate value indicates better dimensional stability. Results indicated that the samples with 6% polyvinyl alcohol exhibited maximum dimensional stability (minimum radial and longitudinal shrinkage).

..... Steady State Weight Gains, Diameters, Lengths of the Starch-based Foams with different

Functional Aids

Entry /	Processing Aids	Normalized Steady	Normalized Steady
---------	-----------------	-------------------	-------------------

Table 6.2 Normalized Steady State Weight Gains, Diameters, Lengths of the Starch-based Foams with different

Functional Aids

Entry	Processing Aids	Normalized Steady State Weight Gain $\left[\frac{W - W_0}{W_0} \right]$ (± 0.032)	Normalized Steady State Diameter $\left[\frac{D}{D_0} \right]$ (± 0.041)	Normalized Steady State Length $\left[\frac{L}{L_0} \right]$ (± 0.046)
1	None (Control)	0.128	0.564	0.498
2	3% PVA	0.122	0.682	0.655
3	6% PVA	0.122	0.769	0.743
4	9% PVA	0.120	0.740	0.682
5	12% PVA	0.113	0.717	0.659
6	15% PVA	0.114	0.697	0.631
7	0.1% Glyoxal + 3% PVA	0.117	0.715	0.718
8	0.2% Glyoxal + 3% PVA	0.117	0.721	0.729
9	0.3% Glyoxal + 3% PVA	0.114	0.738	0.774
10	0.4% Glyoxal + 3% PVA	0.118	0.670	0.726

Table 6.2 (Cont'd.) Normalized Steady State Weight Gains, Diameters, Lengths of the Starch-based Foams

	1.0% Glyoxal + 3% PVA			
11		0.123	0.657	0.738
12	3% CA	0.119	0.614	0.525
13	6% CA			

Table 6.2 (Cont'd.) Normalized Steady State Weight Gains, Diameters, Lengths of the Starch-based Foams

11	1.0% Glyoxal + 3% PVA	0.123	0.657	0.738
12	3% CA	0.119	0.614	0.525
13	6% CA	0.112	0.651	0.566
14	10% CA	0.105	0.691	0.632
15	0.1% Glyoxal + 10% CA	0.099	0.725	0.636
16	0.2% Glyoxal + 10% CA	0.094	0.714	0.638
17	0.3% Glyoxal + 10% CA	0.093	0.751	0.658
18	0.4% Glyoxal + 10% CA	0.100	0.683	0.641
19	1.0% Glyoxal + 10% CA	0.110	0.679	0.587
20	3% Methylated Pectin	0.124	0.610	0.515
21	6% Methylated Pectin	0.116	0.637	0.541
22	10% Methylated Pectin	0.110	0.678	0.614
23	0.1% Glyoxal + 10% Methylated Pectin	0.106	0.697	0.619
24	0.2% Glyoxal + 10% Methylated Pectin	0.105	0.719	0.628
25	0.3% Glyoxal + 10% Methylated Pectin	0.104	0.734	0.642
26	0.4% Glyoxal + 10% Methylated Pectin	0.108	0.653	0.620

Table 6.2 (Cont'd.) Normalized Steady State Weight Gains, Diameters, Lengths of the Starch-based Foams

27	1.0% Cilyoxal + 10% Methylated Pectin	0.114	0.621	0.573
28	1% PCL	0.096	0.581	0.672

Table 6.2 (Cont'd.) Normalized Steady State Weight Gains, Diameters, Lengths of the Starch-based Foams

27	1.0% Glyoxal + 10% Methylated Pectin	0.114	0.621	0.573
28	1% PCL	0.096	0.581	0.672
29	3% PCL	0.094	0.638	0.736
30	7% PCL	0.092	0.654	0.798
31	10% PCL	0.090	0.752	0.869
32	1% PBAT	0.095	0.689	0.696
33	3% PBAT	0.094	0.743	0.752
34	5% PBAT	0.094	0.788	0.808
35	7% PBAT	0.094	0.826	0.829
36	10% PBAT	0.091	0.855	0.876

The steady state
as compared to
dimensions at 6
was 25% as com
starch.

The free hydro
surrounding mo

alcohol, hydrog

PVA and those

excess of PVA

absorbing moist

resulted in high

When glyoxal v

starch by glyox

reduced from a

0% up to 0.3%

11).

These results

samples. The s

dimensions. a

dimensional s

glyoxal and

content of 0.3

The steady state weight gain by samples containing 6% PVA was not considerably higher as compared to those by 12% PVA (12.2% as compared to 11.2%). The loss in radial dimensions at 6% PVA was about 20% while the shrinkage in the longitudinal direction was 25%, as compared to 35% for samples containing 12% PVA and 50% for control starch.

The free hydroxyl groups from starch were capable of forming hydrogen bonds with surrounding moisture resulting in its hygroscopic nature. In the presence of polyvinyl alcohol, hydrogen bonding may have taken place between the free hydroxyl groups of PVA and those on starch, thus reducing the absorption of moisture. However, addition of excess of PVA led to a large number of free hydroxyl groups, which were capable of absorbing moisture themselves. This increased the hydrophilicity of the foam, and hence resulted in higher weight gains.

When glyoxal was used in combination with 3% PVA, as a result of the cross-linking of starch by glyoxal, the moisture sorption decreased. Thus, the steady state weight gain reduced from about 12.2% to about 11.4% with an increase in the glyoxal content from 0% up to 0.3%, but beyond that moisture sorption increased again (Table 6.2, Entries 7 – 11).

These results were consistent with those showing the dimensional stability of these samples. The samples with 0.3% glyoxal showed minimum loss of radial and longitudinal dimensions, as well as lowest gain in weight under steady state conditions. The dimensional stability improved from 40% (at 0% glyoxal and 3% PVA) to 25% (at 0.3% glyoxal and 3% PVA). Also, the maximum expansion ratio is obtained at a glyoxal content of 0.3%. Thus, an optimum amount of glyoxal to be used would be 0.3%.

Cellulose Ace

weight gain da

an increase in

Hence, further

glyoxal. The n

PVA (Table 6)

suggesting that

cellulose acetat

though margina

The loss of ra

compared to 50-

dimensional stab

maximum dimer

19). The loss in n

The carboxylate

their charge. Me

which take up a

would also impa

gain decreased w

glyoxal was used

improve the hydro

6.2 (Entries 23 - 2

Cellulose Acetate imparted some hydrophobic character evident from the steady state weight gain data (Table 6.2, Entries 12 – 14). The steady state weight gain decreased with an increase in the cellulose acetate content, due to the hydrophobic character of CA. Hence, further efforts were made to cross-link cellulose acetate (10%) with starch using glyoxal. The nature of the response was similar to that obtained using glyoxal with 3% PVA (Table 6.2, Entries 15 – 19). However, the steady state weight gain was lower, suggesting that some hydroxyl groups on starch were used up in cross-linking with the cellulose acetate molecules, due to which the moisture sorption would have been lower, though marginally.

The loss of radial and longitudinal dimensions was about 35-40% at 10% CA as compared to 50-55% in the case of control starch foams (Table 6.2, Entries 12 – 14). The dimensional stability was maximum at a CA content of 10%. In the presence of glyoxal, maximum dimensional stability was obtained at 0.3% glyoxal (Table 6.2, Entries 15 – 19). The loss in radial dimensions was improved to 25%.

The carboxylate groups in the pectin molecule tend to expand its structure as a result of their charge. Methylation of these carboxylic acid groups forms their methyl esters, which take up a similar space but are much more hydrophobic. Thus, esterified pectin would also impart hydrophobic character to the starch foams. The steady state weight gain decreased with an increase in the pectin content (Table 6.2, Entries 20 – 22). Hence glyoxal was used as a cross-linking agent between starch and pectin. Glyoxal helped improve the hydrophobic character, though not considerably, which is evident from Table 6.2 (Entries 23 – 27).

The steady state

foam formulation

6.2. Entries 20

The addition of

starch foams. The

of the sample.

Table 6.2 (Entry

stability of the

(Table 2. Entries

10% PCL). with

The PCL migration

32). thus forming

micrographs of

there was a limit

and minimum of

compromise has

Like PCL, the p

water endurance

similar to those of

As shown in Tab

9.5% of the origi

stability increased

The steady state loss of radial and longitudinal dimensions when MP was used in the foam formulations was similar to the response in the presence of CA and is shown (Table 6.2, Entries 20 – 27).

The addition of PCL did have a slight advantage in decreasing the weight gain of these starch foams. The equilibrium weight gains were about 8.8 – 9.5% of the original weight of the sample, as compared to ~ 13% in the case of the control starch foams, as shown in Table 6.2 (Entries 28 – 31). Also, the addition of PCL helped increase the dimensional stability of the starch foams considerably. The loss of radial and longitudinal dimensions (Table 2, Entries 28 – 31) decreased from 50% to about 25% and 13% respectively (at 10% PCL), with an increase in the PCL content.

The PCL migrated to the surface because of the lower surface tension in the melt (31, 32), thus forming a hydrophobic coating. This was evident from the scanning electron micrographs of the surface of the foams in figures 6.9 and 6.10 as seen earlier. However, there was a limitation involved in the addition of PCL. The maximum expansion ratio and minimum density for the foams was obtained at a PCL content of 3%. Hence, a compromise has to be reached in adding PCL to the formulation.

Like PCL, the purpose of adding PBAT was to improve the hydrophobic character and water endurance of the starch foams. The results obtained by using PBAT were very similar to those obtained by using PCL.

As shown in Table 6.2 (Entries 32 – 36), the steady state weight gain was about 8.5 – 9.5% of the original weight of the foam samples on addition of PBAT, but dimensional stability increased significantly.

The loss of rate
from 50% to 3
most of the PB
the core. Thus,
to.

The aliphatic-
densities, high
gain and high d

6.5 Conclusion

Hydroxypropyl la
functional aids
different formul
Some formulatio
The starch foam
 38 ± 5 °C to de
functional aids
significantly aff
be reduced fro
formulations in
dimensions cou
certain formula
formulations inv
a possibility tha

The loss of radial and longitudinal dimensions (Table 6.2, Entries 32 – 36) decreased from 50% to about 12% with an increase in the PBAT content. This could imply that most of the PBAT in the foam samples manifested at the surface (Figure 6.11), and not in the core. Thus, the core of these samples continued to absorb as much moisture as it used to.

The aliphatic-aromatic co-polyester PBAT provided the best properties in terms of low densities, higher resilience and better hydrophobic properties (low steady state weight gain and high dimensional stability).

6.5 Conclusion

Hydroxypropylated high amylose cornstarch was extruded into foams using various functional aids such as PCL, PBAT, PVA, CA, Glyoxal and methylated pectin. The different formulations were successfully optimized to give foams with lowest densities. Some formulations with PVA and PBAT gave foams with densities lower than 25 kg/m^3 . The starch foams were subjected to a relative humidity of $95 \pm 5 \%$, and a temperature of $38 \pm 5 \text{ }^\circ\text{C}$ to determine the change in weight and dimensions on moisture sorption. The functional aids such as PVA, CA, MP and their combinations with glyoxal did not significantly affect the weight gain on moisture sorption. However, the weight gain could be reduced from about 13% for control starch to a minimum of about 9% for formulations involving PCL and PBAT. Also, the shrinkage in radial and longitudinal dimensions could be reduced from about 50% for control starch to about 12-20% for certain formulations involving biodegradable polyesters, and to about 25-40% in formulations involving PVA, glyoxal, CA and pectin and combinations thereof. There is a possibility that most of the polyester migrates to the surface of the foams restricting the

shrinkage of t

Thus, the hydr

dimensional st

The aliphatic-a

densities, high

gain and high

compatibility b

well as the hyd

reactive extrus

chemically mod

polyester.

shrinkage of the starch foams, while the core continues to absorb as much moisture. Thus, the hydrophobic character of the starch-based foams in terms of its weight gain and dimensional stability on moisture sorption was improved considerably.

The aliphatic-aromatic co-polyester PBAT provided the best properties in terms of low densities, higher resilience and better hydrophobic properties (low steady state weight gain and high dimensional stability). Chapters 7, 8 and 9 focus on improving the compatibility between the starch and polyesters to improve the physico-mechanical as well as the hydrophobic properties of the starch-based foams. This would be done using reactive extrusion as a tool to chemically modify the starch or the polyester. The chemically modified entities would act as compatibilizers between the starch and the polyester.

6.6 Referend

- 1) Lacos
- 2) Lacou
- 3) Chinn
- 4) Chinn
- 5) Bhatn
Agric
- 6) Cha. J
Crops
- 7) Cha. J
Agric
- 8) Cha. J
Agric
- 9) Altieri.
- 10) Bastiol
Montin
- 11) Bastiol
5,360,8
- 12) Bastiol
5,736,5
- 13) Bastiol
- 14) Neuman
- 15) Neuman
- 16) Xu. W.
- 17) Xu. W.
- 18) Wang.
BioF.nv
1997.

6.6 References

- 1) Lacourse, N. L., Altieri, P. A. US Patent 4,863,655, 1989.
- 2) Lacourse, N. L., Altieri, P. A. US Patent 5,043,196, 1991.
- 3) Chinnaswamy, R., Hanna, M. A. US Patent 5,496,895, 1996.
- 4) Chinnaswamy, R., Hanna, M. A. Australian Patent AU-B-63333/90, 1996.
- 5) Bhatnagar, S., Hanna, M. A. Transactions of the American Society of Agricultural Engineers, 38, 567, 1995.
- 6) Cha, J. Y., Chung, D. S., Seib, P. A., Flores, R. A., Hanna, M. A. Industrial Crops and Products, 2001, 14, 23.
- 7) Cha, J. Y., Chung, D. S., Seib, P. A. Transactions of the American Society of Agricultural Engineers, 42, 1765, 1999.
- 8) Cha, J. Y., Chung, D. S., Seib, P. A. Transactions of the American Society of Agricultural Engineers, 42, 1801, 1999.
- 9) Altieri, P. A., Tessler, M. M. US Patent 5,554,660, 1996.
- 10) Bastioli, C., Bellotti, V., Del Giudice, L., Lombi, R., Rallis, A., Del Tredici, G., Montino, A., Ponti, R. US Patent 5,288,765, 1994.
- 11) Bastioli, C., Bellotti, V., Del Giudice, L., Lombi, R., Rallis, A. US Patent 5,360,830, 1994.
- 12) Bastioli, C., Bellotti, V., Del Tredici, G., Montino, A., Ponti, R. US Patent 5,736,586, 1998.
- 13) Bastioli, C., Bellotti, V., Del Tredici, G., Rallis, A. US Patent 5,801,207, 1998.
- 14) Neumann, P. E., Seib, P. A. US Patent 5,185,382, 1993.
- 15) Neumann, P. E., Seib, P. A. US Patent 5,208,267, 1993.
- 16) Xu, W., Doane, W. M. US Patent 5,665,786, 1997.
- 17) Xu, W., Doane, W. M. US Patent 5,854,345, 1998.
- 18) Wang, L., Shogren, R. L. Proceedings 6th Annual Meeting of the BioEnvironmental Degradable Polymer Society, The Society: St. Paul, MN; 1997.

- 19) Fang
- 20) Fang
- 21) Biby.
- 22) Fang.
- 23) Wille
- 24) Boehr
- 25) Shogr
- 26) Nabar
Press.
- 27) Ameri
Contai
of AS
- 28) Americ
Cellula
Standa
- 29) Tatarka
1157. 1
- 30) Zhiqian
1999.
- 31) Biresaw
Physics
- 32) Lawton
McKee.
- 33) Hutchin
22. 3950

- 19) Fang, Q., Hanna, M. A. Cereal Chemistry, 77 (6), 779, 2000.
- 20) Fang, Q., Hanna, M. A. Bioresource Technology, 78, 115, 2001.
- 21) Biby, G., Hanna, M. A.; Fang, Q. US Patent 6,184,261, 2001.
- 22) Fang, Q., Hanna, M. A. Industrial Crops and Products, 13, 219, 2001.
- 23) Willett, J. L., Shogren, R. L. Polymer, 43, 5935, 2002.
- 24) Boehmer, E. W., Hanlon, D. L. US Patent 5,272,181, 1993.
- 25) Shogren, R. L. Carbohydrate Polymers, 29(1), 57, 1996.
- 26) Nabar, Y. U., Schindler, M., Narayan, R. Polymer Engineering and Science, In Press.
- 27) American Standard Test Methods, 1997. Standard Practice for Conditioning Containers, Packages, or Packaging Components for Testing. In: Annual Book of ASTM Standards. D – 4332, 15.09, Philadelphia, PA.
- 28) American Standard Test Methods, 1997. Standard Test Methods for Flexible Cellular Materials Made From Olefin Polymers. In: Annual Book of ASTM Standards. D – 3575, 8.02, Philadelphia, PA.
- 29) Tatarka, P. D., Cunningham, R. L. Journal of Applied Polymer Science, 67, 1157, 1998.
- 30) Zhiqiang, L., Yi, F., Xiao-Su, Y. Journal of Applied Polymer Science, 74, 2667, 1999.
- 31) Biresaw, G., Carriere, C. J. Journal of Polymer Science, Part B: Polymer Physics, 39, 920 – 930, 2000.
- 32) Lawton, J. W. Cereal: Novel Uses and Processes. Campbell, G. M.; Webb, C.; McKee, S. L. Editors. Plenum Press, New York, 43, 1997.
- 33) Hutchinson, R. J., Siodlak, G. D. E., Smith, A. C. Journal of Materials Science, 22, 3956, 1987.

7.1 Abstract

Free-radical-in
terephthalate).
reactive extrus
radical initiator
wt% MA conce
wt% peroxide c
experiments. U
the polyester b
viscosity meas
calorimetry wer
concentration at
of MA, while de
feed MA conce
polyester proved
amylose cornsta
maleated co-pol-

EFFECT OF MALEATED PBAT AS A COMPATIBILIZER

BETWEEN STARCH AND PBAT

7.1 Abstract

Free-radical-initiated grafting of maleic anhydride (MA) onto poly(butylene adipate-*co*-terephthalate), a biodegradable aliphatic-aromatic co-polyester, was performed by reactive extrusion. 2,5-dimethyl-2,5-di-(*tert*-butylperoxy)hexane was used as the free-radical initiator. The peroxide concentration was varied between 0.0 and 0.5 wt% at 3.0 wt% MA concentration, as well as the MA concentration between 1.0 and 5.0 wt% at 0.5 wt% peroxide concentration. The reaction temperature was maintained at 185°C for all experiments. Under these conditions, between 0.194% and 0.691% MA was grafted onto the polyester backbone. Size-exclusion chromatography, melt flow index, intrinsic viscosity measurements, thermal gravimetric analysis, and differential scanning calorimetry were used to characterize the maleated copolyester. Increasing the initiator concentration at a constant MA concentration of 3% resulted in an increase in the grafting of MA, while decreasing the molecular weight of the resulting polymer. Increasing the feed MA concentration also increased the grafting percentage. The maleation of the polyester proved to be very efficient in promoting strong interfacial adhesion with high amylose cornstarch in starch foams as prepared by melt blending. Thus, the use of maleated co-polyester as a compatibilizer between starch and PBAT allowed the

reduction of
resilience from
improved hydro
stability on mo

7.2 Introduction

High levels of
poorer physical
flexibility.

7.2.1 Incompatibility

Polymer blends
years because of
types of polymer
heterogeneous
blends. this miscibility
(T_g), for the blend
relationship for

Here T_{g1} and T_{g2}
respectively, and
respectively.

reduction of the density of resulting starch foams to $\sim 21 \text{ kg/m}^3$, and improved the resilience from 84% to as high as 95%. Also, the resulting starch foams exhibited improved hydrophobic properties in terms of lower weight gain and higher dimensional stability on moisture sorption.

7.2 Introduction

High levels of starch and its poor compatibility with the biodegradable polyesters lead to poorer physical and mechanical properties such as density, compressibility, resilience and flexibility.

7.2.1 Incompatible Blends

Polymer blends have become an important subject of scientific investigation in recent years because of their growing commercial importance (1). Broadly classified, the two types of polymer blends are homogeneous (i.e., miscible or compatible) blends and heterogeneous (i.e., immiscible or incompatible) blends. In the case of homogeneous blends, this miscibility of the two polymers results in a single glass transition temperature (T_g), for the blend, which is composition dependent, as per the Fox-Flory theory. The Fox relationship for a two-component blend (2) is explained in equation (7.1) as follows:

$$\frac{1}{T_g} = \frac{\phi_1}{T_{g1}} + \frac{\phi_2}{T_{g2}} \quad (7.1)$$

Here T_{g1} and T_{g2} are the glass transition temperatures of the components 1 and 2 respectively, and ϕ_1 and ϕ_2 are the volume fractions of components 1 and 2 in the blend respectively.

Heterogeneous
affect their rhe
of the finished
morphology of
the dispersed p
the blend. On
processing con
Most of the p
different phase
interface, which
produces very l
hinders the for
polymer pairs at
Incompatible po
properties, and
arrangement of t
in this case the m
phases to contrib
blend, but this is
may represent a
phase. Most inco
however, vary in

Heterogeneous polymer blends, on the other hand, have many interrelated variables that affect their rheological behavior, processability, and the mechanical/physical properties of the finished product. For instance, the method of blend preparation controls the morphology of the blend (e.g., the state of dispersion, the size of the dispersed phase, and the dispersed phase size distribution), which in turn controls the rheological properties of the blend. On the other hand, the rheological properties strongly dictate the choice of processing conditions, which in turn strongly influence the morphology.

Most of the polymer pairs are not thermodynamically miscible and so exist in two different phases in the polymer blend. This breakdown into two phases creates an interface, which might lead to poor performance of the blend system. Poor adhesion also produces very low mechanical properties due to poor stress transfer between phases and hinders the formation of highly structured morphologies. The interaction between the polymer pairs at the molecular level has been defined by the term “*compatibility*”.

Incompatible polymer blends can be organized into a variety of morphologies. Many properties, and subsequently uses, of a blend depend critically on the nature of this arrangement of the two phases. One phase may be dispersed in a matrix of the other, and in this case the matrix phase dominates the properties. A parallel arrangement allows both phases to contribute to many properties in direct proportion to their composition in the blend, but this is a nonisotropic structure since perpendicular to this direction the system may represent a series arrangement with properties that disproportionately favor one phase. Most incompatible blends investigated to date show phase separation. The phases, however, vary in amount, size, sharpness of their interfaces, and degree of continuity.

Figure

The type of mixture
composition and
two parameters
proportion or is

7.2.2 Compati

Simple blending
characteristics. H
This leads to the

- Poor inte
- Difficult

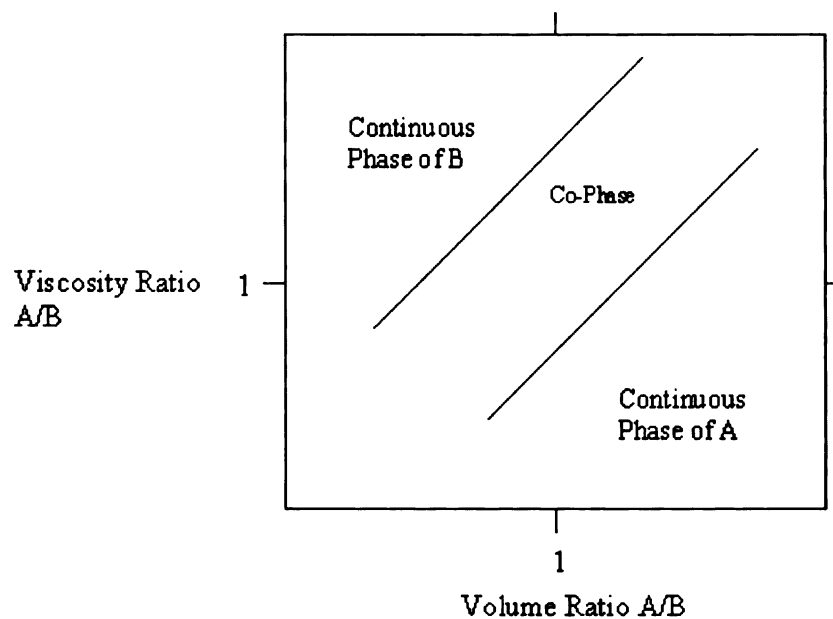


Figure 7.1 Effect of composition and viscosity on phase morphology

The type of morphology depends upon several factors, the most important being the composition and the viscosities of each component. Figure 7.1 shows the effect of those two parameters on the morphology of the blend. The component, which is in higher proportion or is less viscous, tends to form the continuous phase (3).

7.2.2 Compatibilization Theory

Simple blending of immiscible blends does not generally give a material with desired characteristics, because of the high interfacial tension existing between the two phases.

This leads to the following conditions:

- Poor interfacial adhesion
- Difficulty of attaining the desired degree of dispersion

- Poor

In general, tw

(7.2).

In equation (7

components, w

excess term, χ

equals zero, th

arithmetic ave

compatibilizati

modulus of the

constituents' P

compatibilizati

Developing a bi

ability to contro

interfacial adhes

effective way to

functionalize the

reactive function

bonds; and thus,

adhesion. The re

blending. Most c

groups should rea

- Poor mechanical properties.

In general, two component polymer mixtures can be described by the following equation (7.2).

$$P = P_1 w_1 + P_2 w_2 + \Delta P^E (w) \quad (7.2)$$

In equation (7.2), P is the property of the blend, P_1 and P_2 are the property values of the components, w_1 and w_2 are the mass fractions of components 1 and 2 and $\Delta P^E (w)$ is an excess term, which is dependent on the composition under consideration. If $\Delta P^E (w)$ equals zero, there is an additive result, and the property of the blend is the weighted arithmetic average of the constituents' properties. For polymer alloys, however, the compatibilization achieved results in positive values of $\Delta P^E (w)$, which means that the modulus of the polymer combination is better than the weighted arithmetic average of the constituents' properties (4). There are various routes for obtaining this effect of compatibilization.

Developing a blend with satisfactory overall physico-mechanical behavior depends on the ability to control interfacial tension to generate a small dispersed phase size and strong interfacial adhesion to improve the stress transfer between the component phases (5). An effective way to improve the compatibility between starch and the polyester matrix is to functionalize the polyester matrix by grafting highly reactive functions. These grafted reactive functions can react with the hydroxyl groups of the starch to form covalent bonds; and thus, they provide better control of the size of phase and strong interfacial adhesion. The reactivity of the functional groups is an important parameter in reactive blending. Most of the blends are commercially prepared in an extruder. The functional groups should react to form the required concentration of graft or block copolymer in the

short residence
anhydride gro
reactivity. A
copolymerizat
between the
tremendously.
greater than th
the component
incorporated o
methods report
8). solid-state
aqueous (13) o
an effective wa
polymers (15.
biodegradable p
18). Earlier resu
maleation of b
(PBS) and Eas
maleation of PI.
lead to product
polyester based
attempted earlier
melt-blending w

short residence times typical of extrusion processes. From this point of view, a cyclic anhydride group may react more quickly than the carboxylic group because of its higher reactivity. Anhydride functionality can be incorporated into a polymer chain by copolymerization or grafting of anhydrides like maleic anhydride. If a reaction occurs between the compatibilizer and the blend components, it will improve adhesion tremendously. The adhesive strength resulting from chemical bonding is about 35 times greater than that resulting from Van Der Waals attraction. In order for a reaction to occur, the components of the blend need to be functionalized, i.e. specific segments need to be incorporated on the polymer chain that can react with the copolymer. There are different methods reported in the literature to produce a graft polymer such as melt grafting (6 – 8), solid-state grafting (9, 10), solution grafting (11, 12), and suspension grafting in aqueous (13) or organic solvents (14). The reactive extrusion technique has proved to be an effective way to introduce a variety of functional groups onto the surface of natural polymers (15, 16). Maleic anhydride was first used as a monomer to graft onto non-biodegradable polymers such as polyethylene, polypropylene and other polymers (17, 18). Earlier results from research conducted by Bhattacharya and co-workers (19 – 29) on maleation of biodegradable polymers such as PCL, PBSA, poly(butylene succinate) (PBS) and Eastar Bio[®] co-polyester; and by Narayan and co-workers (30, 31) on maleation of PLA indicate that blends of anhydride functional polymers and starch could lead to products with useful end properties. However, efforts to improve the starch-polyester based foam properties using these kinds of compatibilizers have not been attempted earlier. Recently, we have shown that PBAT could be a good candidate for melt-blending with starch to produce foams, by providing better physico-mechanical

properties su

properties suc

Hence, the of

PBAT with

anhydride gra

The effect of

molecular p

chromatograp

differential sc

properties. Fin

indices on usir

PBAT is repor

ray diffraction

properties of th

stability on mo

7.3 Experi

7.3.1 Materia

The type of star

content). The st

(N), under the tr

The inherent mo

used as the plasti

of the starch use

properties such as lower densities, better spring indices; and better hydrophobic properties such as improved dimensional stability on moisture sorption (32).

Hence, the objective of this study was to manufacture starch foams in the presence of PBAT with better physico-mechanical and hydrophobic properties, wherein maleic anhydride grafted PBAT was used as a compatibilizer between pristine PBAT and starch. The effect of maleic anhydride and free-radical initiator was first studied on the molecular parameters of the resulting maleated-PBAT using size-exclusion chromatography, intrinsic viscometry, and melt-flow index. Thermogravimetric and differential scanning calorimetry analyses were also used to investigate their thermal properties. Finally, the foam performance, in terms of lower densities and better spring indices on using maleated PBAT (MA-g-PBAT) as a compatibilizer between starch and PBAT is reported in this paper, and related to the scanning electron micrographs and X-ray diffraction patterns of the resulting starch foam surfaces. Also, the hydrophobic properties of the starch foams in terms of lower weight gains and improved dimensional stability on moisture sorption are reported.

7.3 Experimental Section

7.3.1 Materials

The type of starch used was hydroxypropylated high amylose cornstarch (70% amylose content). The starch was purchased from National Starch and Chemicals (Indianapolis, IN), under the trade name of HYLON 7. The density of HYLON 7 starch is 1.2 g/cm³. The inherent moisture content of the starch is 11.2% under ambient conditions. Water is used as the plasticizer as well as the blowing agent. Water content is maintained at 8-10% of the starch used. Talc (Magnesium Silicate), used as the nucleating agent, was obtained

from Luzen

150 kg m³.

adipate-co-ter

trade name

benzenedicar

important bi

applications.

Figure 7.2

2,5-dimethyl-2

anhydride (M)

Sigma-Aldrich

7.3.2 Experim

The experimen

system. The tw

control gearbo

diameter of 30

from Luzenac (Englewood, CO). It has a specific gravity of 2.76 and a bulk density of 150 kg/m³. The talc content was maintained at 1% for all the experiments. Poly(butylene adipate-*co*-terephthalate) (PBAT) was purchased from BASF Corporation, under the trade name Ecoflex (F). PBAT is made by condensing 1,4-butanediol with 1,4-benzenedicarboxylic acid (terephthalic acid) and hexanedioic acid (adipic acid). It is an important biodegradable polymer, which has been used in established blown-film applications.

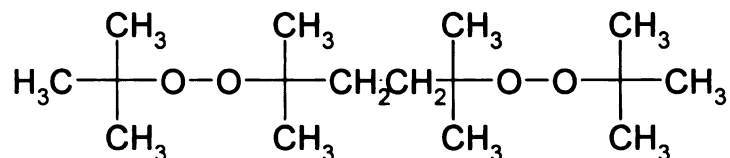


Figure 7.2 2,5-dimethyl-2,5-di-(*tert*-butylperoxy) hexane (Free Radical Initiator)

2,5-dimethyl-2,5-di-(*tert*-butylperoxy) hexane (Lupersol 101) (Figure 7.2) and maleic anhydride (MA) were purchased from Elf Atochem (King of Prussia, PA) and from Sigma-Aldrich Chemical Company (St. Louis, MO), respectively.

7.3.2 Experimental Setup

The experimental setup used in the maleation of the polyester was a twin-screw extrusion system. The twin-screw extrusion system consists of an extruder driver with a speed control gearbox, a Century ZSK-30 twin-screw co-rotating extruder with a screw diameter of 30 mm, an L/D of 40, accurate single-screw feeders for feeding PBAT and

MA. MA gra

A Masterflex

filament die

assembled to

cooling water

heated zones

pressure of th

water-bath. be

The experimen

was the same

feeding the pu

carrying it thro

the functional e

The experimen

system. Accura

aid and talc w

displacement p

die 2.7 mm in d

extruder. A high

7.3.3 Procedu

The temperature

the maleation o

20 125 145 165

MA. MA granules were finely powdered using a mortar and a pestle for uniform feeding. A Masterflex pump was used to feed Lupersol 101, the organic peroxide. A cylindrical filament die 2.7mm in diameter and 8.1 mm in length, with a cooling sleeve was assembled to the extruder. The barrel could be cooled by adjusting the flow rate of the cooling water supply, which was manually controlled using valves for each of the nine heated zones. The sensors were mounted on the die to measure the temperature and pressure of the melt. The MA-g-PBAT product was cooled by carrying it through a water-bath, before pelletizing it downstream. It was further used as a compatibilizer.

The experimental setup used in the blending of the maleated polyester with the polyester was the same twin-screw extrusion system. Accurate single-screw feeders were used for feeding the pure co-polyester and the maleated co-polyester. The blend was cooled by carrying it through a water-bath, before pelletizing it downstream. This blend was used as the functional aid in the production of starch foams.

The experimental setup used in the foaming of starch was the above twin-screw extrusion system. Accurate single-screw feeders were used for feeding starch, and the processing aid and talc were fed individually or they could be fed as a mixture. A positive displacement pump is used for injecting water into the extruder. A cylindrical filament die 2.7 mm in diameter and 8.1 mm in length, with a cooling sleeve was assembled to the extruder. A high-speed cutter was used to get cylindrical foam shapes of required size.

7.3.3 Procedure

The temperatures in the extruder zones were set up to reach the required temperatures for the maleation of the co-polyester. The temperature profile during extrusion was 20/125/145/165/185/185/185/185/185/180°C from the barrel section just after the feed

throat to the
calibrated and
MA and the
The screw sp
45-60°, and
nitrogen in or
of maleic anhi
then blended
processing ai
extrusion was
after the feed t
carried out at
maintained at
98-100 psi.
The polyester
as functional a
and set at a p
(was) were ca
is pumped into
about 8-9% of
starch. T
20 85 115 125
throat to the

throat to the die, with a melt temperature of 184°C-188°C. The feeder for PBAT was calibrated and set at a particular speed to feed at 11.2 kg/hr (~25 lb/hr). The feeder for MA and the pump for Lupersol 101 were calibrated and set at feeding rates accordingly. The screw speed was maintained at 200 rpm. Extrusions were carried out at a torque of 45-60%, and a pressure of 98-105 psi. The extrusions were carried out under a blanket of nitrogen in order to prevent unwanted side reactions. The maximum grafting percentage of maleic anhydride on the polyester was determined, and that particular formulation was then blended with the pure polyester in ratios of 5:95 to 50:50. These blends were used as processing aids in the production of starch foams. The temperature profile during extrusion was 20/85/125/135/145/150/150/150/150/145 °C from the barrel section just after the feed throat to the die, with a melt temperature of 146°C -150°C. Extrusions were carried out at a throughput of 9.1-11.2 kg/hr (~ 20-25 lbs/hr). The screw speed was maintained at 200 rpm. Extrusions were carried out at a torque of 60%, and a pressure of 98-100 psi.

The polyester, maleated polyesters and their blends with the original polyester were used as functional aids in the extrusion of starch foams. The feeder for starch was calibrated and set at a particular speed to feed at 11.2 kg/hr (~ 25 lb/hr). The other feeder/feeders (was) were calibrated and set at feeding rates accordingly. Initially, during start-up, water is pumped into the system at 15-20% of the starch fed, and later its flow rate is reduced to about 8-9% of starch. The inherent moisture present in starch also aids in plasticization of starch. The temperature profile during extrusion was 20/85/115/125/130/130/130/125/125/115 °C from the barrel section just after the feed throat to the die, with a melt temperature of 115°C -118°C. The screw speed was

maintained at
the torque at
75%, and a p

7.3.4 Char

7.3.4.1 Ext

The extent of

was a modifi

removed by c

dried sample

added to hyd

vigorously st

selectively re

vacuum ove

dissolved in

using potass

completely s

calculated fr

9

Where V_{KOH}

KOH solutio

maintained at 200 rpm. When formulations were changed, extrusion was continued until the torque and the die pressure stabilized. Extrusions were carried out at a torque of 70-75%, and a pressure of 700-750 psi.

7.3.4 Characterization and Analyses

7.3.4.1 Extent of maleation

The extent of maleation for samples grafted with MA was determined by titration, which was a modification of the procedure developed by Li et al. (33). The unreacted MA was removed by drying the samples at 85°C under vacuum. After dissolution of 1g of the dried sample in 100 mL of chloroform, 1 mL of hydrochloric solution in water (1 M) was added to hydrolyze anhydride functions into carboxylic acid functions. The solution was vigorously stirred for 30 minutes. Then, PBAT grafted with maleic acid moiety was selectively recovered by precipitation into methanol, filtration and drying at 85°C in a vacuum oven overnight. The resulting dried and so-purified MA-g-PBAT was then dissolved in chloroform, and the solution was titrated to a phenolphthalein end point using potassium hydroxide in methanol. Under these conditions, the MA-g-PBAT was completely soluble, and did not precipitate during the titration. The MA content was calculated from the following equation:

$$\% MA \text{ grafted} = \frac{N_{KOH} \times V_{KOH}}{2 \times W_{sample}} \times 98.06 \times 100 \quad (7.3)$$

Where V_{KOH} and N_{KOH} are the volume (liters) and the normality (mol/equivalent) of the KOH solution; and W_{sample} is the weight of MA-g-PBAT in grams.

7.3.4.2 Me

A Ray-Ran t

MA-g-PBA T

a 1.00 kg loa

MFI of PBA

7.3.4.3 Four

The FTIR spe

4000 cm^{-1} usi

dichlorometh

then dried in e

spectra.

7.3.4.4 Intrin

The intrinsic v

(Cannon CT-1

PBAT and M

required conce

7.3.4.5 Size E

Size Exclusion

99%) at 35°C u

PL - DG802 de

7.3.4.2 Melt Flow Index (MFI)

A Ray-Ran melt flow indexer was used to characterize the melt viscosity of PBAT and MA-g-PBAT. ASTM standard test D-1238 (34) was used at the conditions of 130°C and a 1.00 kg load in an attempt to get the MFIs in the stipulated range of 0.15-50 g/10 min. MFI of PBAT was also determined at standard conditions of 190°C and a 2.16 kg load.

7.3.4.3 Fourier Transform Infrared Spectroscopy (FTIR)

The FTIR spectra of PBAT and MA-g-PBAT thin films were scanned from 400 cm^{-1} to 4000 cm^{-1} using a Perkin Elmer Model 2000 FTIR. Polymer samples were dissolved in dichloromethane and cast onto a potassium bromide disc to obtain a thin film. They were then dried in a chamber with a current of nitrogen before they were scanned to obtain the spectra.

7.3.4.4 Intrinsic Viscosity (IV)

The intrinsic viscosity measurements were carried out at 24.5°C in a constant temperature (Cannon CT-1000, Cannon Instrument Co., PA) bath using a Ubbelohde viscometer. PBAT and MA-g-PBAT samples were dissolved in dichloromethane and diluted to required concentrations.

7.3.4.5 Size Exclusion Chromatography (SEC)

Size Exclusion Chromatography of PBAT samples was performed in THF (Labscan, 99%) at 35°C using a Polymer Laboratories (PL) liquid chromatograph equipped with a PL – DG802 degazer, an isocratic HPLC pump LC 1120 (flow rate = 1ml/min), a Basic-

Marathon A
column PL g
molecular w
reference to p

7.3.4.6 The

A high resolu
used to deter
Nitrogen wa
balance purg
min.

7.3.4.7 Di

Differential
MA-g-PBA
experimen
at 50 ml m
any prior
determine
to determi

Marathon Autosampler, a PL-RI refractive index detector and three columns: a guard column PL gel 10 μm and two columns PL gel mixed-B 10 μm . Molecular weights and molecular weight distribution of PBAT and MA-g-PBAT samples were calculated with reference to polystyrene standards.

7.3.4.6 Thermogravimetric Analysis (TGA)

A high resolution Thermal Gravimetric Analyzer (TGA) 2950 from TA Instruments was used to determine the degradation temperature of the original PBAT and MA-g-PBAT. Nitrogen was used as the purge gas with the sample purge being 60 ml/min and the balance purge being 40 ml/min. The sample was heated to 550°C at the rate of 10 K per min.

7.3.4.7 Differential Scanning Calorimetry (DSC)

Differential Scanning Calorimetry was used to determine the melting temperature of the MA-g-PBAT polymers. A modulated DSC 2920 from TA Instruments was used. The experiment was conducted in an inert atmosphere of nitrogen with the nitrogen flow rate at 50 ml/min. The sample was heated to 190°C at the rate of 20 K per minute to remove any prior history, and then cooled back to -50°C at the rate of 5 K per minute to determine the crystallization peaks. It was reheated to 190°C at the rate of 5 K per minute to determine the melting of the polymer and the maleated products.

Foam samp

The foam sa

environment

7.3.4.8 Den

The density of

specimen acc

least 10 speci

The dimension

permit measu

ratio of the c

determined by

for the density

7.3.4.9 Com

Compressive s

Compressive s

Systems SFM

lengthwise and

end-cap. By lo

on the specime

of 30 mm/min

elapsed. a rela

Foam samples

The foam samples collected were conditioned as per ASTM D-4332 (35), in a constant environment room at $23 \pm 1^\circ\text{C}$ and $50 \pm 2\%$ RH for at least 72 hours before testing.

7.3.4.8 Density, Expansion Ratio (ER), Specific Length (SL)

The density of the foam was calculated from the mass and volume of a regularly shaped specimen according to the test method ASTM D-3575 (section 43, Method A) (36). At least 10 specimens were measured for each formulation.

The dimensions of the sample were measured using a Vernier Calipers graduated to permit measurements accurate to 0.001 inches. Expansion ratio was calculated as the ratio of the cross-sectional area of the foam to that of the die. The specific length is determined by the ratio of the length of the specimen to the mass of the specimen used for the density measurement, in terms of cm/g.

7.3.4.9 Compressive Strength and Resiliency (37)

Compressive strength and resiliency describe the mechanical integrity of the foam. Compressive strength of the lab-scale specimens was measured on a United Testing Systems SFM-20 tensile testing machine. Foam specimens were securely fastened lengthwise and compressed by a steel probe (0.635 cm diameter) with a hemi-spherical end-cap. By lowering the piston to the foam surface, an initial load of 0.5 N was applied on the specimen for approximately 5 s. From this point, the probe was lowered at a rate of 30 mm/min for a distance of 3 mm. The maximum load was recorded. After 60 s had elapsed, a relaxation load was recorded. Compressive strength was determined by

dividing

percenta

force req

starch fo

7.3.4.10

10 bloc

environn

temperat

samples

weighing

measure

placing t

and leng

samples

The stea

respectiv

samples

7.3.4.11

An enviro

observe t

razor bla

dividing the maximum load by the cross-sectional area of the probe. Resiliency is the percentage of the compressive force after the 60 s hold period divided by the maximum force required to compress the foam by 3 mm. Averages were calculated from five sets of starch foam specimens.

7.3.4.10 Moisture Sorption Analysis

10 blocks of each formulation, collected at different times were placed in an environmental humidity chamber, subject to a relative humidity of $95 \pm 5 \%$, and a temperature of $38 \pm 5 \text{ }^\circ\text{C}$. The weight and the dimensions (length and diameter) of the samples were monitored. They were measured at regular intervals using an accurate weighing balance and a pair of Vernier Calipers, to the third decimal place. The entities measured at different time intervals were normalized using the value measured before placing the samples in the humidity chamber (time, $t = 0$). The initial weight, diameter and length were assigned W_0 , D_0 , and L_0 respectively. The weight and dimensions of the samples were recorded until a steady state value was reached (approximately 30 days). The steady state weights and dimensions of the samples were assigned W , D , and L respectively. The results for a formulation were obtained as an average over the 10 samples used for that formulation.

7.3.4.11 Environmental Scanning Electron Microscopy (ESEM)

An environmental scanning electron microscope (Phillips Electroscan 2020) was used to observe the surface morphology of the starch foams. The samples were sectioned by a razor blade and mounted on aluminum stubs.

73.
X-ra
diff
con
wit
the
72

7.4
7.4
Th
(P
im
ra
th
in
m
hi
th
Pe
m
a

7.3.4.12 Wide Angle X-ray Scattering

X-ray diffraction analysis was performed with a Rigaku Rotaflex Ru-200BH X-ray diffractometer operated at 40 KV, 40 mA with a nickel filtered Cu K_α radiation and a θ compensating slit. Data was acquired in 0.1° 2 θ , 10 s steps. Foam samples were mixed with liquid nitrogen, and ground to powder using a mortar and pestle. The samples were then equilibrated in a constant environment room at 23 ± 1°C and 50 ± 2% RH for at least 72 hours before testing.

7.4 Results and Discussion

7.4.1 Effect of MA and the Free Radical Initiator on the Properties of MA-*g*-PBAT

The grafting of maleic anhydride (MA) onto poly(butylene adipate-*co*-terephthalate) (PBAT) was performed in an attempt to produce reactive functional groups, which would improve the interfacial adhesion between starch and the polyester. The proposed free radical initiated maleation mechanism (31) is depicted in Figure 7.3. It is worth noting that some authors have proposed an end-chain grafting mechanism, involving the insertion through the aliphatic dicarboxylic acid units of the copolyesters (29). The maleation of PBAT was carried out at only one temperature, i.e. 185°C, a temperature high enough to avoid the homopolymerization of maleic anhydride. It is worth noting that the temperature does not significantly affect the grafting percentage of MA on the polyester backbone, as observed by our earlier studies (30, 31). Table 7.1 reports the molecular parameters of the resulting maleated PBAT by changing the initiator content and MA content on the grafting of MA on the polyester.

The
(Fig
the
obs
for

The grafting of MA onto the aliphatic-aromatic copolyester has been attested by FTIR (Figure 7.4). By comparison to the FTIR spectrum of pure copolyester and focusing on the carbonyl absorption peaks, two extra absorption peaks at 1787 and 1861 cm^{-1} were observed for the grafted polyester, assigned to the symmetric and asymmetric stretching for the carbonyl functions of MA, respectively (38, 39).

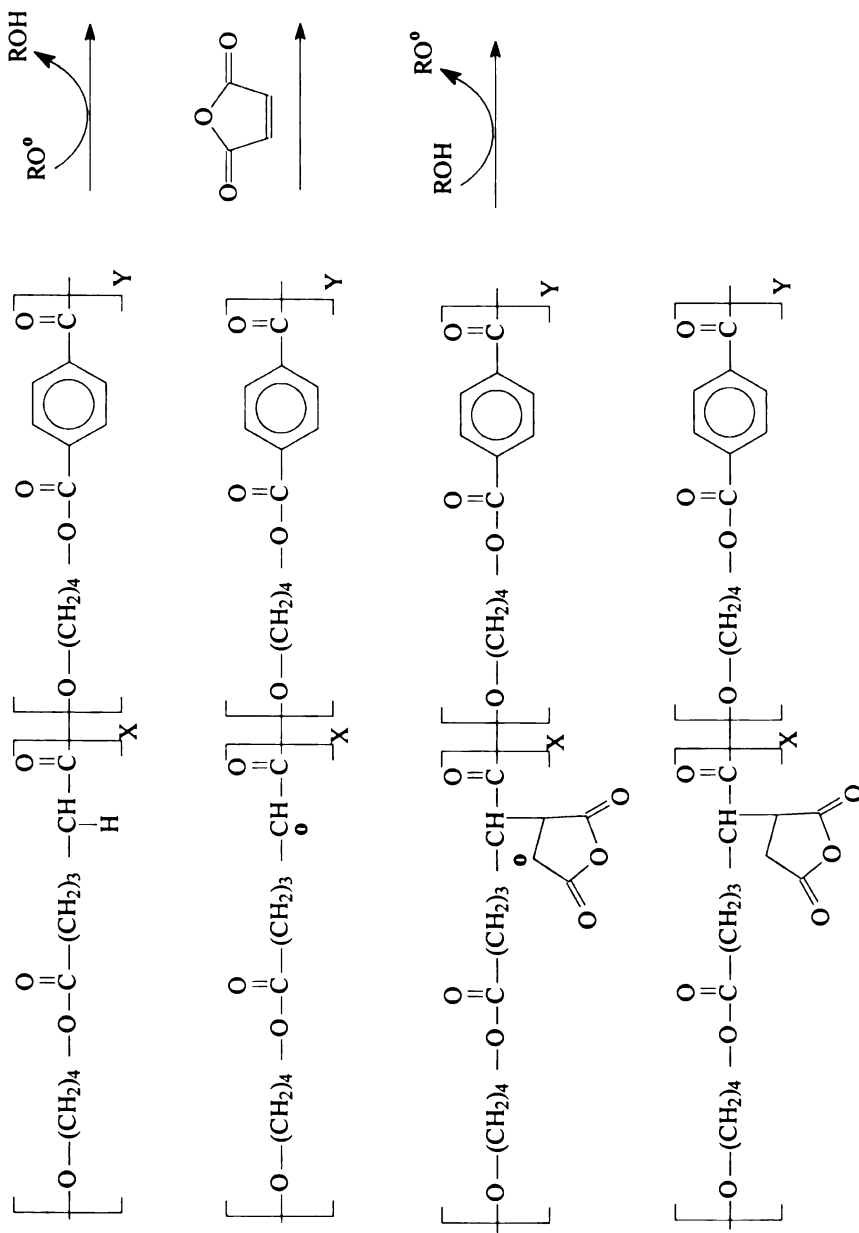


Figure 7.3 Proposed Free Radical Initiated Maleation Mechanism.

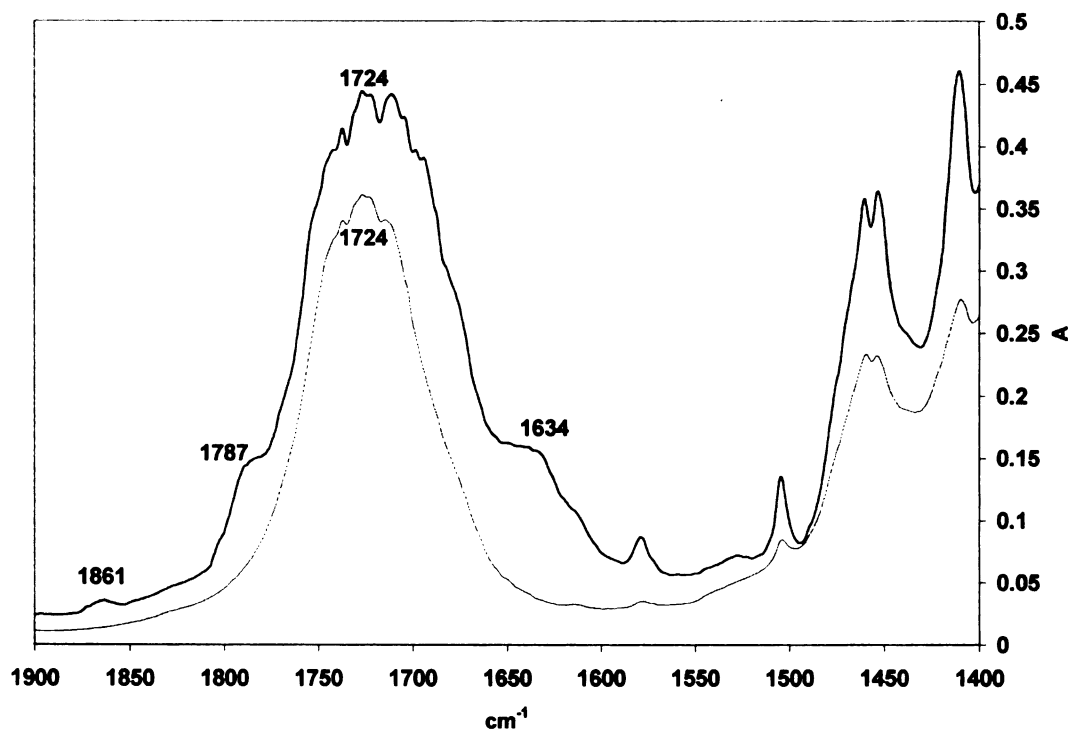


Figure 7.4 FTIR of MA-g-PBAT and PBAT.

Table 7.1 Maleation of PBAT: Torque %, MFI, Intrinsic Viscosity, Weight % Maleation and SEC Results

No.	Wt % MA	Wt % L101	Torque Load %	MFI g/10min	IV _w dl/gm	Wt % Maleation	M _n (first) ^(e) (g/mol)	M _w /M _n ^(e)	M _n (second)-M _w /M _n ^(f) (g/mol) ^(f)
1 ^a	0.0	0.00	-	5.8	1.02	-	51,100	2.23	-
2 ^b	0.0	0.0	70-72	13.2	0.92	-	39,780	4.1	-
3	3.0	0.00	69-73	34.3	0.72	0.194	28,560	2.9	-
4	3.0	0.10	70-74	36.5	0.74	0.250	26,410	2.39	-
5	3.0	0.25	65-67	40.6	0.60	0.325	24,200	2.99	-
6	3.0	0.50	59-62	42.9	0.40	0.526	28,990	2.61	386,300 – 2.61 ^f
7	1.0	0.50	72-76	1.5	1.05	0.323	32,730	3.48	1.51 X 10 ⁶ – 4.43 ^f
8	2.0	0.50	69-71	12.7	0.95	0.408	29,400	2.71	679,440 – 3.91 ^f
9	5.0	0.50	52-54	56.9	0.30	0.691	23,660	2.55	-
10	0.0	0.25	74-78	- ^c	- ^d	-	- ^d	- ^d	-

Fr
te
an
(M
w
7.
co
th
g
b
co
th
M
m
b
in

- a. Not Extruded
- b. Extruded (0% MA, 0% L101)
- c. MFI could not be determined since sample did not melt.
- d. Sample was insoluble in THF.
- e. M_n and M_w/M_n were determined by reference to a PS calibration (THF, 35°C, Elution flow = 1 mL/min)
- f. The M_n and M_w/M_n of a second population that can be observed from the SEC chromatogram, were determined by reference to a PS calibration (THF, 35°C, Elution flow = 1 mL/min)

From Table 7.1, it was observed that while keeping the MA concentration constant (entries 3-6, Table 7.1), an increase in the free-radical initiator concentration resulted in an increase in the grafted MA moieties onto the copolyester aliphatic-aromatic backbone (MA-g-PBAT). For instance, the amount of MA grafted improved from 0.194 to 0.526-wt% when the free-radical initiator increased from 0 to 0.5 wt% (entries 3 and 6, Table 7.1). The content of grafted MA also increased with an increase in the MA added at constant free-radical initiator content (entries 6-9, Table 7.1). However, by comparison to the number-average molecular weight of the extruded PBAT (entry 2, Table 7.1), the grafting of MA appears to cause the chain scission of the polyester backbone as indicated by the decrease in molecular weight and intrinsic viscosity of the MA-g-PBAT, as the concentration of the free radical initiator was increased. The MFI values also indicated that at a given amount of MA (3%), higher concentrations of initiator result in higher MFIs, which implies a reduction in melt viscosity. This drop in molecular weight and melt-viscosity could be due to the β -scission (Figure 7.5) taking place along the polymer backbone during the free-radical reaction, as reported by Carlson et al (30). The most interesting feature is that the molecular weight of resulting MA-g-PBAT may be

in
m
g
co
38
te
co
P
re
w
co
M
T
at
te
st
ex
7.
th
d
w
hi
th

increased at higher free-radical initiator concentration. For instance, the number-average molecular weight of MA-g-PBAT decreased from 26,410 (0.1 wt% L101) to 24,200 g/mol (0.25 wt% L101), and then increased to 28,990 g/mol (0.5 wt% L101) at a MA content of 3-wt% (entries 4-6, Table 7.1). To such extent, a second population with $M_n = 386,300$ g/mol could be also observed when 0.5 wt% of free-radical initiator was added (entry 6, Table 7.1). This can be adequately explained by the presence of another concomitant reaction, i.e. branching reactions, taking place during the maleation of PBAT. These branching reactions can also dominate during the maleation process resulting in an increase in the molecular weights, as observed for MA-g-PBAT prepared with lower MA content, i.e. at 1 and 2wt% in MA, while keeping the free-radical initiator constant at 0.5 wt% (entries 7-8, Table 7.1). This is well attested by the sharp decrease in MFI values, i.e. higher melt-viscosity of MA-g-PBAT, when the MA content decreased. This can be explained by the grafting efficiency of MA on the polyester, which decreased at low MA concentrations and higher L101 concentration possibly due to faster termination rate of free radicals. This is more likely due to radical consuming reactions such as radical recombination much favored at higher concentrations of free radicals. The experiment carried out in the exclusive presence of free-radical initiator (entry 10, Table 7.1) supported this observation as evidenced by the insolubility of the resulting sample in the SEC solvent, i.e. THF, as well as the incapability of melting in the MFI determination. Thus, the effect of the concentration of MA on the grafting percentage was not as pronounced as the initiator concentration. This could be due to the relatively high MA concentration, which may only improve the grafting efficiency by decreasing the probability of radical termination reactions before the grafting of MA, whereas, the

initiator concentration directly affects the total free radical concentration, which in turn affects the termination rate.

It is worth noting that, by comparing PBAT after and before extrusion (entries 1-2, Table 7.1), the size exclusion chromatography results indicate that the molecular weight of PBAT deteriorated significantly during extrusion. For instance, the average-number of PBAT passes from 51,100 to 39,780 g/mol after extrusion. This decrease of molecular weight could be due to the presence of thermal hydrolysis during the extrusion process.

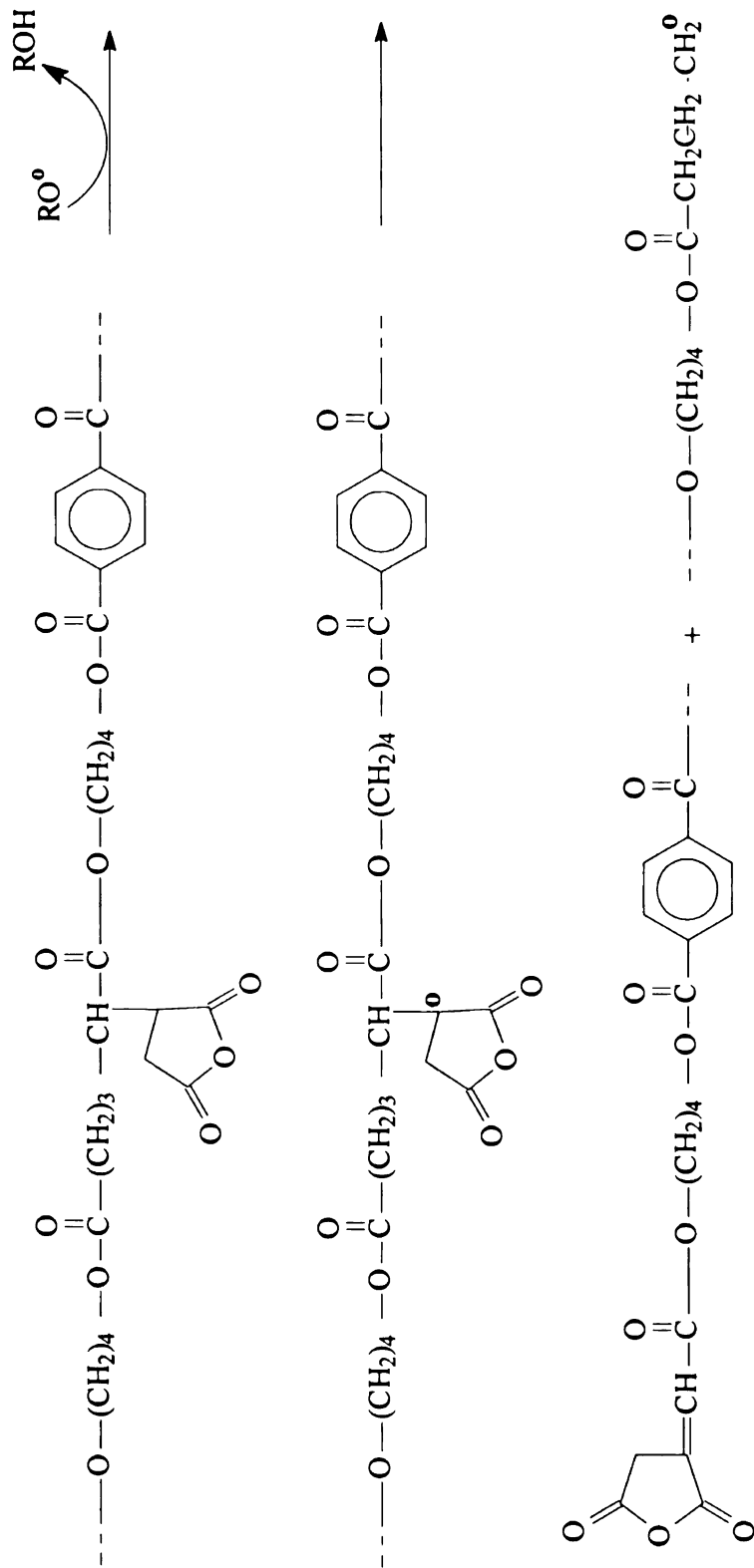


Figure 7.5 β -scission on grafting of MA on the PBAT backbone.

7.4.2 TGA

The thermogravimetric analyses of the maleated samples show that decomposition temperatures are lower than the pure polyester implying a less thermally stable product (Figures 7.6, 7.7). Thus, the maleated PBAT samples obtained exhibit lower thermal stability as compared to the original polyester. The maximum difference was about 25°C for the samples involving 5% MA and 0.5% L101. This was to be expected as the maleated polyester samples were, in general, of lower molecular weight.

7.4.3 DSC

Table 7.2 shows the melting (ΔH_m) and crystallization enthalpies (ΔH_c) and temperatures of the maleated polyesters as compared to PBAT. Both the enthalpies were lower than that for PBAT resulting from lower molecular weights of the maleated polyesters. The melting point (T_m) did not change significantly. The crystallization temperatures (T_c) were higher than that for PBAT suggesting that the polyester chains tend to crystallize faster during the cooling cycle (likely due to their lower molecular weights).

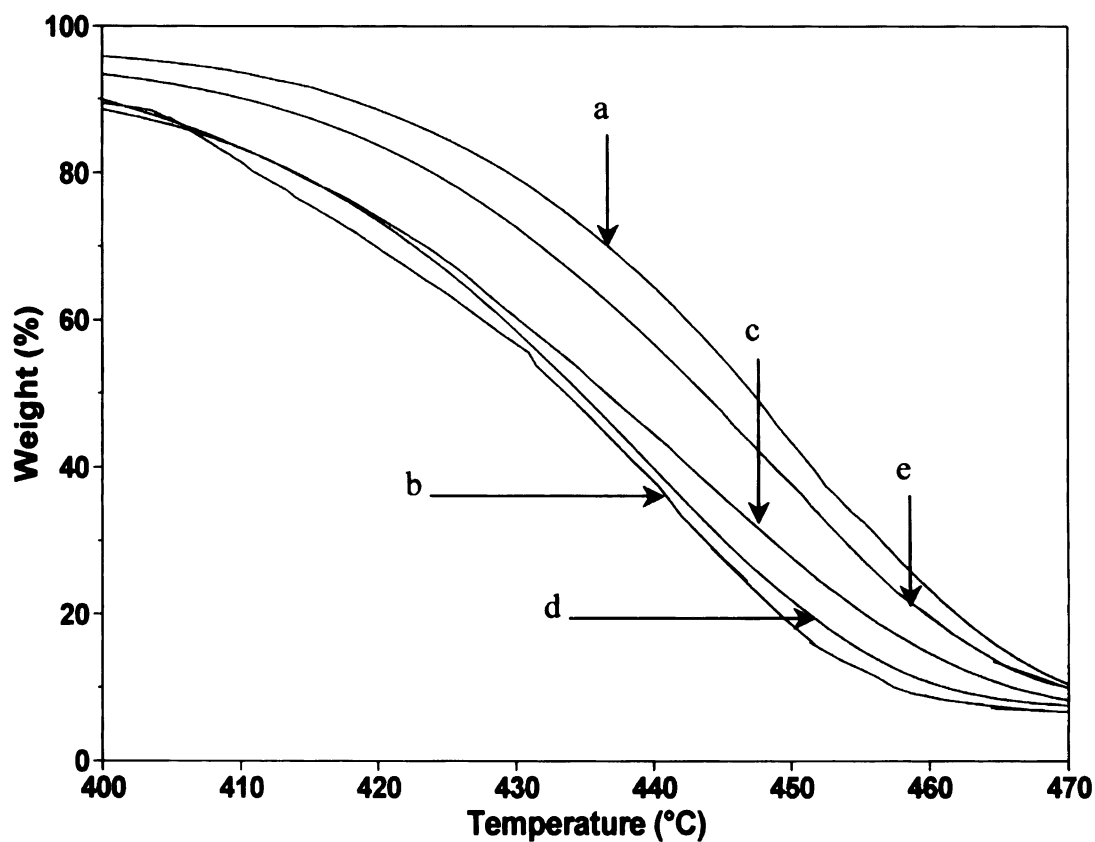


Figure 7.6 TGA of the maleated samples MA-*g*-PBAT (different grafting levels) and PBAT. Different Peroxide (L 101) contents: (a) Pure PBAT, (b) MA-*g*-PBAT (3% MA, 0.0% L101), (c) MA-*g*-PBAT (3% MA, 0.1% L101), (d) MA-*g*-PBAT (3% MA, 0.25% L101), and (e) MA-*g*-PBAT (3% MA, 0.5% L101).

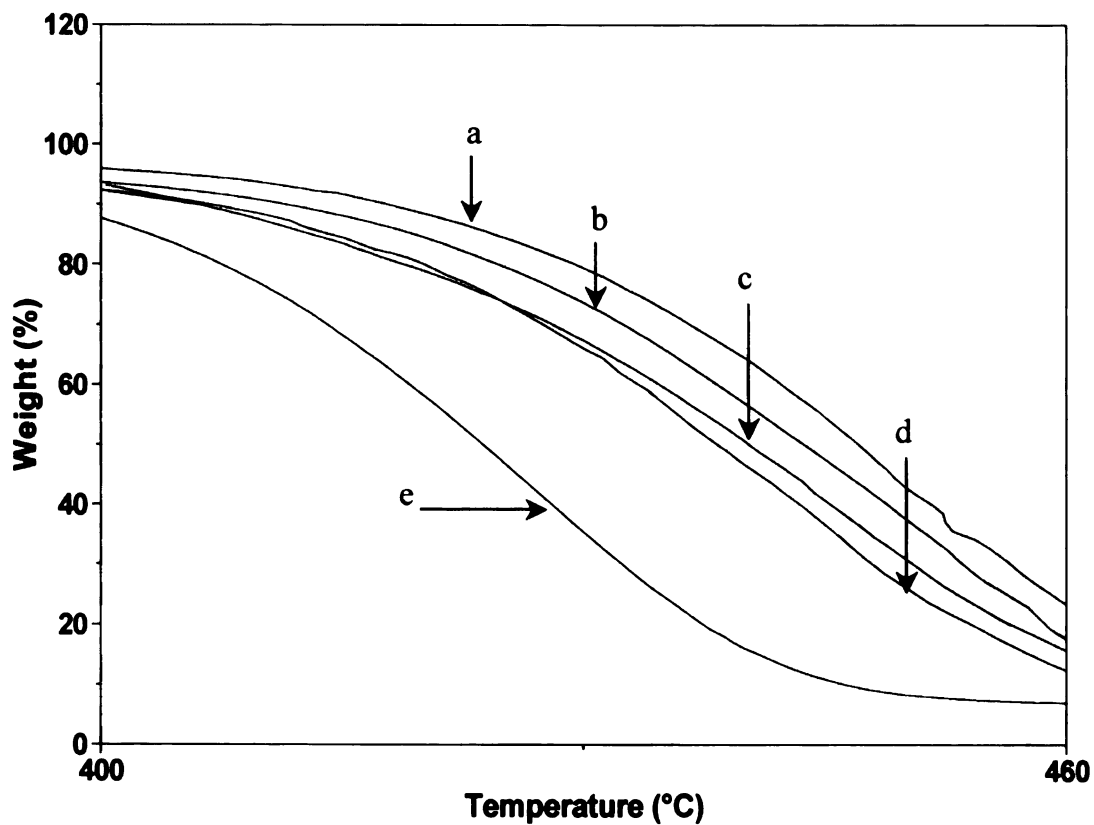


Figure 7.7 TGA of the maleated samples MA-*g*-PBAT (different grafting levels) and PBAT. Different MA contents: (a) Pure PBAT, (b) MA-*g*-PBAT (1% MA, 0.5% L101), (c) MA-*g*-PBAT (2% MA, 0.5% L101), (d) MA-*g*-PBAT (3% MA, 0.5% L101), and (e) MA-*g*-PBAT (5% MA, 0.5% L101)

Table 7.2 Melting and Crystallization Enthalpies and Temperatures for different MA-g-PBAT

No.	Wt % MA	Wt % L101	ΔH_c (J/g)	T_c (°C)	ΔH_m (J/g)	T_m (°C)
1	0.0	0.00	15.13	40.88	15.59	123.25
2	3.0	0.00	11.24	78.84	11.47	125.87
3	3.0	0.10	11.08	72.50	11.70	124.50
4	3.0	0.25	10.15	81.19	10.66	126.90
5	3.0	0.50	9.09	73.86	9.95	123.16
6	1.0	0.50	11.80	79.05	12.84	125.69
7	2.0	0.50	12.09	67.53	12.53	123.30
8	3.0	0.50	9.09	73.86	9.95	123.16
9	5.0	0.50	8.57	79.98	8.97	124.03

7.4.4 Density, Expansion Ratio (ER) and Specific length (SL) of Starch foams

The densities, expansion ratios and the specific lengths of the starch foams using the pristine PBAT as well as the maleated PBAT samples as functional aids are shown in Table 7.3. The density of the control starch foams was 30.2 kg/m³ while the expansion ratio was 39.7. It was observed that the pure maleated polyesters gave higher densities and lower expansion ratios (Table 7.3, entries 4-10), as compared to the foams obtained using the original PBAT (24.2 kg/m³, 46.7) respectively. This was due to the fact that some maleated PBAT samples had lower melt strengths as compared to PBAT (Table

7.3, Entries 4 – 7, 10), which was not enough to support cell expansion. However, the maleated PBAT samples made using low MA content and high peroxide amount resulted in stiff, highly branched materials, which also did not support cell growth in the starch foams. Hence, the MA-g-PBAT having maximum MA grafting percentage (see Table 7.1, Entry 9) was used as a compatibilizer between the starch and PBAT. This particular MA-g-PBAT was melt blended with PBAT in different proportions and these blends were used as functional aids in starch foams. A minimum density of 21.2 kg/m^3 was obtained with a maximum expansion ratio of 49.4 when a blend of 0.5% maleated polyester (Table 7.1, Entry 9) and 4.5% pure polyester was used as the processing aid in the production of starch foams. In general, the density decreased with a decrease in the compatibilizer content (Table 7.3, entries 11-14). At higher contents of the compatibilizer, the expanded foams contracted after exiting the die. This contraction resulted in increased densities and lower expansion ratios. This was observed possibly due to the lower melt strength of the maleated polyester, which was not sufficient to support cell expansion. Thus, the maleated PBAT proved efficient as a compatibilizer between starch and PBAT. The compatibilization of the melt resulted in improved densities (as low as 21 kg/m^3) and better spring indices as follows.

Table 7.3 Densities, Expansion Ratios, Specific Lengths of Starch Foams using Different Functional Aids.

	Processing Aids	Unit Density (kg/m ³)	Radial Expansion ratio	Specific Length (cm/g)	Resiliency (%)
1	None	30.2 (± 0.8)	39.7 (± 1.1)	14.6 (± 0.6)	69.8 (± 2.1)
2	5% pure polyester (PBAT)	24.2 (± 0.4)	46.7 (± 0.9)	15.5 (± 0.2)	84.2 (± 1.1)
3	5% LPBAT (0% MA, 0.25% L101)	26.7 (± 0.7)	42.6 (± 0.9)	15.3 (± 0.3)	85.6 (± 1.6)
4	5% MA-g-PBAT (3% MA, 0% L101)	26.2 (± 0.7)	44.9 (± 0.7)	14.9 (± 0.5)	79.2 (± 0.7)
5	5% MA-g-PBAT (3% MA, 0.1% L101)	26.4 (± 1.1)	44.4 (± 1.3)	14.9 (± 0.6)	81.0 (± 0.7)
6	5% MA-g-PBAT (3% MA, 0.25% L101)	26.2 (± 0.9)	44.2 (± 0.9)	15.0 (± 0.5)	80.2 (± 0.4)
7	5% MA-g-PBAT (3% MA, 0.5% L101)	26.8 (± 1.1)	43.5 (± 1.4)	15.0 (± 0.7)	80.0 (± 0.6)
8	5% MA-g-PBAT (1% MA, 0.5% L101)	29.9 (± 1.4)	44.1 (± 1.7)	13.2 (± 0.8)	78.8 (± 1.3)
9	5% MA-g-PBAT (2% MA, 0.5% L101)	26.0 (± 0.5)	45.4 (± 0.6)	14.8 (± 0.4)	81.5 (± 1.0)
10	5% MA-g-PBAT (5% MA, 0.5% L101)	27.9 (± 0.8)	41.6 (± 0.6)	15.0 (± 0.5)	77.0 (± 1.7)
11	(2.5% MA-g-PBAT + 2.5% PBAT) blend	26.2 (± 0.8)	42.9 (± 0.6)	15.5 (± 0.5)	86.0 (± 0.5)
12	(1.0% MA-g-PBAT + 4.0% PBAT) blend	23.7 (± 0.3)	45.3 (± 0.6)	16.3 (± 0.3)	89.0 (± 0.4)
13	(0.5% MA-g-PBAT + 4.5% PBAT) blend	21.2 (± 0.3)	49.4 (± 0.5)	16.7 (± 0.3)	94.9 (± 0.4)
14	(0.25% MA-g-PBAT + 4.75% PBAT) blend	22.2 (± 0.2)	47.9 (± 0.4)	16.4 (± 0.2)	93.3 (± 0.5)

7.4.5 Compressive Strength and Resiliency

Typically, a power-law relationship is observed between compressive strength σ_c and foam density ρ ($\sigma_c \sim \rho^n$). Denser foams tend to have thicker cell walls and hence resist deformation better than lower density foams with thinner cell walls. A strong relation existed between foam density and compressive strength (Figure 7.8). The regression line in Figure 7.8 was drawn and a slope of 0.92 was obtained ($n = 0.92$). A value of $n = 0.92$ was obtained by Willett et al. (40), while Hutchinson and co-workers (41) report exponents of 1.5 – 1.6 for compressive strengths of foams prepared from maize grits. The value of ‘n’ obtained was thus in agreement with the value reported by Willett et al. However, this value is specific to the type of materials used as well as the extrusion system used for foaming.

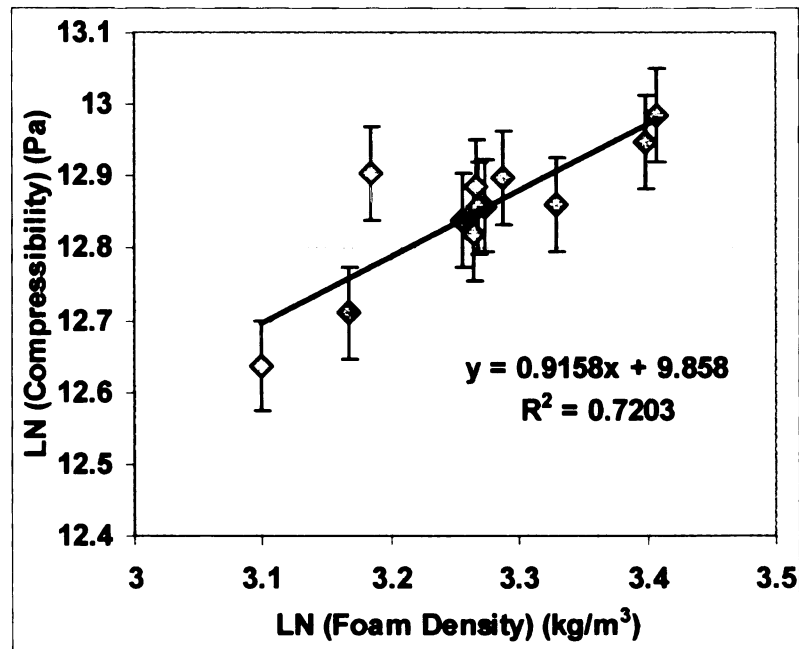


Figure 7.8 Logarithmic plot of Compressive Strength (Pa) as a function of foam density (kg/m³).

The resiliency of the foam samples is listed in Table 7.3. The addition of PBAT improved the resiliency considerably from 69.7% to 84.2% at a PBAT content of 5% of the starch used. The maleated polyester samples, though compatible with starch, did not help improve the resiliency of the starch foams, when used by them. The spring indices obtained were in the range of 77 – 81% using maleated polyesters with different grafting percentages (Table 7.3, Entries 4 – 10). The resilience provided by MA-g-PBAT using 5% MA and 0.5% L101 was minimum (~ 77%), probably due to its low melt strength. The maleated polyester samples with 3% MA all imparted resiliency ~ 80% to the foam samples. It can be observed from Table 7.1 that these maleated samples have similar melt flow indices (similar melt strengths).

The maleated polyester sample with maximum grafting percentage of MA (5% MA, 0.5% L101) was used as the compatibilizer between the starch and PBAT. This particular MA-g-PBAT was melt blended with PBAT in different proportions and these blends were used as functional aids in starch foams. The spring index obtained by using 5% of this blend containing 10% MA-g-PBAT and 90% PBAT was 94.9%. This further confirms that a small amount of MA-g-PBAT performs efficiently as a compatibilizer to provide starch foams with maximum resiliency and minimum density.

Scanning electron micrographs of the foam surfaces are shown in Figures 7.9, 7.10, and 7.11, which further attest that MA-g-PBAT did act as a compatibilizer between starch and PBAT. The surface of the starch foams containing no added polymer generally had some holes in them, suggesting that the skin of the foams may have burst during foaming (Figure 7.9 (2.21, 6.9)).

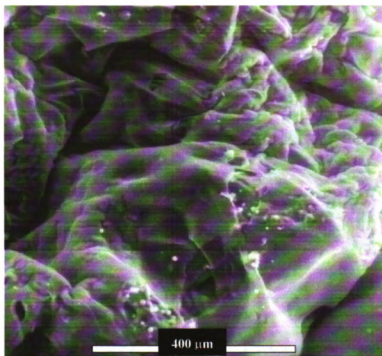


Figure 7.9 ESEM micrograph of the surface of starch foams with no additives (120X).

This was possibly due to the lower melt strength of starch melts. The surface of the starch foams with the polyester had minimal or no holes on the surface (Figure 7.10 (6.11)), and thus exhibited lower densities and higher expansions. This implies that these foams had higher melt strength and hence they resist bubble rupture. However, some incompatibilities between the polyester and thermoplastic starch were obvious from the

phase separation observed. This phase separation was absent in the presence of a small amount of the maleated polyester, as seen in the micrograph (Figure 7.11).

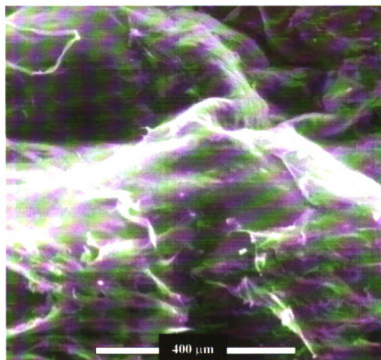


Figure 7.10 ESEM micrograph of the surface of starch foams with 5% PBAT (120X).

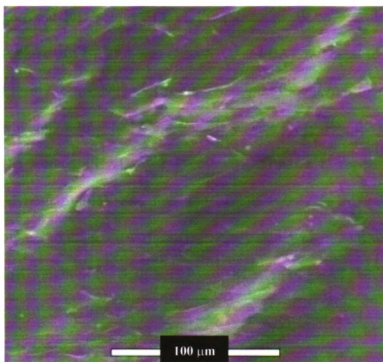


Figure 7.11 ESEM micrograph of the surface of starch foams blended with 0.5% MA-g-PBAT and 4.5% PBAT (400X).

7.4.6 Moisture Sorption Analysis

Starch-based foams due to their hygroscopic nature tend to gain weight on moisture sorption in a humid environment. This is also accompanied by shrinkage in the foam dimensions. Weight gain and shrinkage (loss in dimensions) in starch foams on moisture sorption adversely affect their performance in cushioning as well as the insulation, and hence, are critical. The normalized steady state weight gains and dimensions of the starch foam samples on moisture sorption are listed in Table 7.4. The hydrophobic properties of the starch foams using PBAT as a functional aid have been reported in our previous work

(31). The control hydroxypropylated high amylose cornstarch foams gained up to 13% of their original weight, and lost about 50% of their dimensions on moisture sorption. However, in the presence of PBAT, it was observed that PBAT migrated to the surface, which was evident from the scanning electron micrograph of the starch foam surface in Figure 7.10, thus providing a finer and a more stable surface preventing the rapid loss of moisture through the surface. PBAT (44.2 dynes/cm) (42) has a lower surface energy than starch (53.7 dynes/cm) (43), and thus the overall energy is minimized by the migration of the polymer to the foam surface. The steady state weight gain was about 9.3 – 9.5% of the original weight of the foam samples on addition of PBAT, but dimensional stability increased significantly.

Table 7.4 Normalized Steady State Weight Gains and Dimensions of Starch Foams on Moisture Sorption

No.	Processing Aids	Normalized Steady State Weight Gain, $\left[\frac{W - W_0}{W_0} \right]$ (± 0.032)	Normalized Steady State Diameter, $\left[\frac{D}{D_0} \right]$ (± 0.041)	Normalized Steady State Length, $\left[\frac{L}{L_0} \right]$ (± 0.046)
1	None	0.128	0.564	0.498
2	5% pure polyester (PBAT)	0.094	0.788	0.808
3	(0.5% MA-g-PBAT + 4.5% PBAT) blend	0.059	0.826	0.810

The loss of radial and longitudinal dimensions decreased from 50% to about 20% with an increase in the PBAT content. This could imply that most of the PBAT in the foam samples manifested at the surface (32) (Figure 7.10 (6.11)), and not in the core. Thus, the core of these samples continued to absorb as much moisture as it used to.

The results from Table 7.4 indicated that the foams using MA-g-PBAT as a compatibilizer did not affect the dimensional stability of the starch foams significantly (as compared to the starch foams using PBAT). However, the normalized equilibrium weight gain reduces from $\sim 9.3 - 9.5\%$ to $\sim 5.5 - 5.7\%$. This suggested that the compatibility between starch and PBAT might have been improved, since most of the polymer does not manifest at the surface as it did earlier on phase separation.

7.4.7 Wide Angle X-Ray Scattering

Wide Angle X-ray diffraction powder diffraction patterns for ground starch-polymer foams are shown in Figure 7.12. Starch foams containing no polymer showed reflection peaks at 2θ of approximately 12.2° , 13° and 17.7° . This pattern observed for starch extruded at moisture contents lower than 19%, was termed 'E' type starch and was thought to result from helical inclusion complexes of amylose with native starch lipids (44). This pattern was similar to the V6 hydrate pattern generally seen in amylose/fatty acid complexes (45), except that the peaks were shifted to lower angle implying larger interhelical spacing. Peaks at 9.4° and 28.6° 2θ are due to the talc, which was used as the nucleating agent in the foams. The foams made using the polyester also showed the diffraction peaks due to the amylose-lipid complexes. Additional reflection peaks were obtained at 18.9° , 19.7° , 22.5° and 23.8° 2θ corresponding to PBAT.

Fig

The

the p

poly

with

resu

MA

were

bette

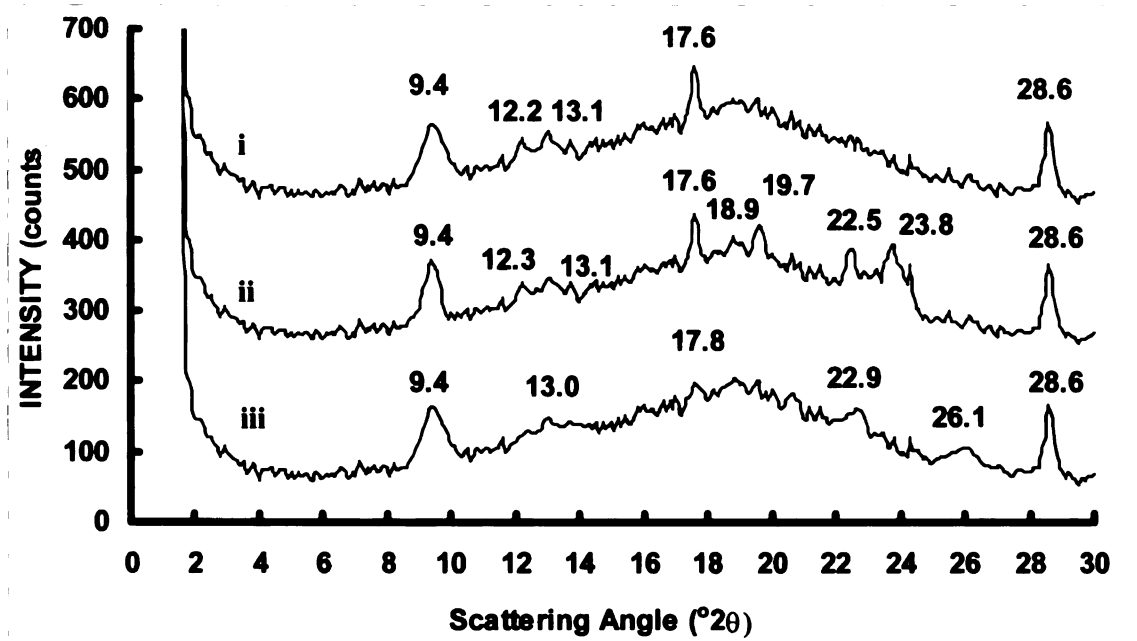


Figure 7.12 Wide-Angle X-Ray Scattering of the Starch foam samples with (i) No additives (ii) 5% PBAT (iii) (0.5% MA-g-PBAT + 4.5% PBAT) blend

These reflections occurred at similar scattering angles to the X-ray diffraction peaks of the pure polyester film prepared by casting from dichloromethane. This indicated that the polyester had phase separated from starch and partially crystallized. This was consistent with the results obtained from the micrograph (Figure 7.10). Earlier microscopy and DSC results also show that starch is incompatible with the polyester (44, 45). In contrast, when MA-g-PBAT was used as a compatibilizer, the characteristic peaks due to the PBAT were broadened and tended to vanish. This suggested that maleated PBAT provided a better dispersion of PBAT within the starch matrix.

7.5 Conclusion

Free-radical-initiated grafting of maleic anhydride (MA) onto poly (butylene adipate-*co*-terephthalate) (PBAT) backbone was achieved by reactive extrusion. The amount of MA grafted on the PBAT backbone was as high as 0.691% by weight. This grafted MA was sufficient to successfully compatibilize the polyester and starch. The maleation of the polyester proved to be very efficient in promoting strong interfacial adhesion with high amylose cornstarch in starch foams by melt blending. The maleated polyesters had lower molecular weights as compared to the original polyester, resulting in their lower melt strengths. Hence, MA-*g*-PBAT by itself did not prove effective as a functional aid in the production of starch foams. However, when MA-*g*-PBAT was used as a compatibilizer between starch and PBAT, it reduced the density of starch foams (using PBAT) to ~ 21 kg/m³, and improved the resilience from 84% to as high as 95%. Also, the starch foams in the presence of PBAT, wherein MA-*g*-PBAT was used as the compatibilizer, exhibited improved hydrophobic properties in terms of lower weight gains on moisture sorption.

The maleation of vegetable oils has been studied in detail in some of our previous work (46). Free-radical-initiated grafting of maleated corn oil (MCO) onto PBAT to give MCO-*g*-PBAT was performed with a motive to reduce the chain scission in PBAT due to acid hydrolysis and, hence, prevent the reduction in melt strength due to degradation of the backbone. The maleation of the polyester using Maleated Corn Oil (MCO) to give MCO-*g*-PBAT was carried out in an attempt to improve the compatibility between PBAT and starch, without reducing the melt strength of the polyester. The use of MCO-*g*-PBAT as a functional aid for starch foams has been studied in the subsequent Chapter 8.

7.6 References

- 1) Rudin, A. The Elements of Polymer Science and Engineering, Academic Press: New York, 1982.
- 2) MacKnight, W. J., Karasz F. E., Fried, J. R. Polymer Blends- Vol 1, Academic Press, 185, 1978.
- 3) Argyropoulos, D. C. Master Thesis, Michigan State University, 1992.
- 4) Snook, J. B. Master Thesis, Michigan State University, 1994.
- 5) Barlow, J. W., Paul, D. R. Polymer Engineering and Science, 24, 525-534, 1984.
- 6) Ruggeri, G., Aglietto, M., Petramani A., Ciardelli, F., European Polymer Journal, 19, 863-866, 1983.
- 7) Bratawidjaja, A. S., Gitopadmoyo, I., Watanabe, Y., Hatakeyama, T. Journal of Applied Polymer Science, 37, 1141-1145, 1989.
- 8) Ho, R. M., Su, A. C., Wu, C. H., Chen, S. I. Polymer, 34, 3264-3269, 1993.
- 9) Rengarajan, R., Parameshwar, V. R., Lee, S., Rinaldi, P. L. Polymer, 31, 1703-1706, 1990.
- 10) Singh, R. P. Progress in Polymer Science, 17, 251-281, 1992.
- 11) Minoura, Y., Ueda, M., Mizunuma, S., Oba, M. Journal of Applied Polymer Science, 13, 1625-1640, 1969.
- 12) Vijayakumar, M. T., Reddy, C. R., Joseph, K. T. European Polymer Journal, 21, 415-419, 1985.
- 13) Grigo, U., Merten, J., Binsack, R. US Patent 4,370,450, 1983.
- 14) Rengarajan, R., Vicic, M., Lee, S. Polymer, 30, 933-935, 1989.
- 15) Doane, W. M., Swanson, C. L., Fanta, G. F. Emerging Technologies for Materials and Chemicals from Biomass. Rowell, R. M., Schultz, T. P., Narayan, R., Eds; American Chemical Society Symposium Series, American Chemical Society, Washington, DC, 476, 197, 1992.
- 16) Glassner, W. G. Wood Processing and Utilization, Kennedy, J. F., Phillips, G. O., Williams, P. A. Eds, Ellis Horwood Ltd., West Sussex, 163, 1989.

- 17) Sathe, S. N., Rao, G. S. S., Devi, S. Journal of Applied Polymer Science, 53, 239-245, 1994.
- 18) Vermesch, L., Groeninckx, G. Journal of Applied Polymer Science, 53, 1365-1373, 1994.
- 19) Vaidya, U. R., Bhattacharya, M. Journal of Applied Polymer Science, 52, 617-628, 1994.
- 20) Vaidya, U. R., Bhattacharya, M., Zhang, D. Polymer, 36, 1179-1188, 1995.
- 21) Bhattacharya, M., Vaidya, U. R., Zhang, D., Narayan, R. Journal of Applied Polymer Science, 57, 539-554, 1995.
- 22) Ramkumar, D. H. S., Bhattacharya, M., Vaidya, U. R., Hakkainen, M., Albertsson, A. C., Karlsson, S. European Polymer Journal, 32, 999-1010, 1996.
- 23) Ramkumar, D. H. S., Bhattacharya, M., Vaidya, U. R. European Polymer Journal, 33, 729-742, 1997.
- 24) John, J., Tang, J., Yang, Z., Bhattacharya, M. Journal of Polymer Science: Part A: Polymer Chemistry, 35, 1139-1148, 1997.
- 25) Mani, R., Bhattacharya, M. European Polymer Journal, 34, 1467-1475, 1998.
- 26) Mani, R., Bhattacharya, M. European Polymer Journal, 34, 1477-1487, 1998.
- 27) Mani, R., Tang, J., Bhattacharya, M. Macromolecular Rapid Communications, 19, 283-286, 1998.
- 28) Mani, R., Bhattacharya, M. European Polymer Journal, 37, 515-526, 2001.
- 29) Mani, R., Bhattacharya, M., Tang, J. Journal of Polymer Science: Part A: Polymer Chemistry, 37, 1693-1702, 1999.
- 30) Carlson, D. L. Dubois, P. Nie, L. Narayan, R. Polymer Engineering and Science, 38, 311, 1998.
- 31) Carlson, D. L., Nie, L., Narayan, R., Dubois, P. Journal of Applied Polymer Science, 72, 477-485, 1999.
- 32) Nabar, Y., Draybuck, D., Narayan, R., Journal of Applied Polymer Science, In Review.
- 33) Li, H.-M., Chen, H.-B., Shen, Z.-G., Lin, S. Polymer, 43, 5455, 2002.

- 34) American Standard Test Methods, 2002. Standard Test Method for Melt Flow Rates of Thermoplastics by Extrusion Plastometer. In: Annual Book of ASTM Standards. D – 1238, 08.01, Philadelphia, PA.
- 35) American Standard Test Methods, 2002. Standard Practice for Conditioning Containers, Packages, or Packaging Components for Testing. In: Annual Book of ASTM Standards. D – 4332, 15.09, Philadelphia, PA.
- 36) American Standard Test Methods, 2002. Standard Test Methods for Flexible Cellular Materials Made From Olefin Polymers. In: Annual Book of ASTM Standards. D – 3575, 08.02, Philadelphia, PA.
- 37) Tatarka, P. D., Cunningham, R. L. Journal of Applied Polymer Science, 67, 1157-1176, 1998.
- 38) Bellamy, L. J. The Infra-Red Spectra of Complex Molecules, Wiley, New York, 1964.
- 39) Pouchert, C. J. The Aldrich Library of Infra-Red Spectra, Aldrich Chemical Company, Milwaukee, WI, 1970.
- 40) Willett, J. L., Shogren, R. L. Polymer, 43, 5935, 2002.
- 41) Hutchinson, R. J., Siodlak, G. D. E., Smith, A. C. Journal of Materials Science, 22, 3956-3962, 1987.
- 42) Biresaw, G., Carriere, C. J. Journal of Polymer Science, Part B: Polymer Physics, 39, 920 – 930, 2000.
- 43) Lawton, J. W. Biodegradable Coatings for Thermoplastic Starch. In: Cereal: Novel Uses and Processes. Campbell, G. M.; Webb, C.; McKee, S. L. Editors. Plenum Press, New York, 43, 1997.
- 44) Walia, P. S., Lawton, J. W., Shogren, R. L., Felker, F. C., Polymer, 41, 8083-8093, 2000.
- 45) Averous, L., Fauconnier, N., Moro, L., Fringant, C., Journal of Applied Polymer Science, 76, 1117-1128, 2000.
- 46) K. Seybold, MS Thesis, 'Design and Economic Analysis of Maleated Soybean Oil and Ester Production Facility.' Michigan State University, (1997).

EFFECT OF MALEATED CORN OIL-g-PBAT AS A COMPATIBILIZER BETWEEN STARCH AND PBAT

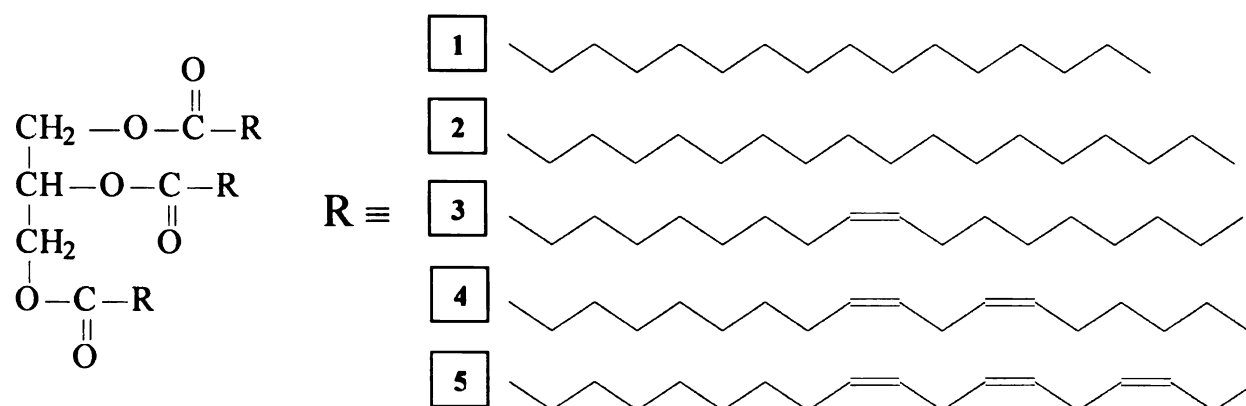
8.1 Abstract

Free-radical-initiated grafting of maleic anhydride (MA) onto corn oil was performed in a 2 liter Parr reactor. The organic peroxide 2, 5-dimethyl-2, 5-di-(*tert*-butylperoxy) hexane (Lupersol 101) was used as the free-radical initiator. The maleated corn oil (MCO) was characterized in terms of iodine number and acid number. Free-radical-initiated grafting of maleated corn oil (MCO) onto poly(butylene adipate-*co*-terephthalate), a biodegradable aliphatic-aromatic co-polyester, was performed by reactive extrusion using the same organic peroxide used earlier. The peroxide concentration was varied between 0.0 and 0.5 wt% at 5.0 wt% MCO concentration, as well as the MCO concentration between 1.0 and 5.0 wt% at 0.25 wt% peroxide concentration. The reaction temperature was maintained at 185°C for all experiments. Under these conditions, between 0.07% and 0.42% MCO was grafted onto the polyester backbone. Melt flow index, intrinsic viscosity measurements, thermal gravimetric analysis, and differential scanning calorimetry were used to characterize the modified copolyester. Increasing the initiator concentration at a constant MCO content of 5% resulted in an increase in the grafting of MCO. Increasing the feed MCO concentration also increased the grafting percentage. The maleation of the polyester using MCO was carried out in an attempt to improve the compatibility between the polyester and starch, without reducing the melt strength of the

polyester. This modification of the polyester proved to be very efficient in promoting strong interfacial adhesion with high amylose cornstarch in starch foams as prepared by melt blending. Thus, the use of MCO-g-PBAT as a functional aid allowed the reduction of the density of resulting starch foams to $\sim 21 \text{ kg/m}^3$, and improved the resilience from 84% to as high as 95%. Also, the resulting starch foams exhibited improved hydrophobic properties in terms of lower weight gain and higher dimensional stability on moisture sorption.

8.2 Introduction

A potential agriculture feedstock is corn oil (CO), which is a mixture of triglycerides containing long chain fatty acids (1) (Figure 8.1). Typically, corn oil contains 4.0 – 4.1 double bonds per mole depending on the origin of the seed.



1 ~ Palmitic (16:0) (10.9%)

2 ~ Stearic (18:0) (2.0%)

3 ~ Oleic (18:1) (25.4%)

4 ~ Linoleic (18:2) (59.6%)

5 ~ Linolenic (18:3) (1.2%)

Figure 8.1 Molecular Structure of Corn oil.

The presence of unsaturation on the fatty acid chains allows for chemical modifications through specific reactions with these double bonds and the introduction of reactive carbonyl functional groups.

There is a great deal of literature on functionalization of vegetable oils using maleic anhydride (MA) to enhance their reactivity. Morrel and Samuels (2) studied the reaction between maleic anhydride and conjugated oil systems using oils from china wood and oiticica containing fatty acids with conjugated double bonds. The reaction was found to follow a typical Diels-Alder addition. Root (3) investigated the functionalization of soybean oil with maleic anhydride and described the use of benzoyl peroxide in the maleation reaction. He concluded that the use of benzoyl peroxide as a catalyst was advantageous as it allowed the reaction to proceed at a lower reaction temperature of 110°C as compared 160-190°C when benzoyl peroxide was not used. Root hypothesized that the presence of a peroxide leads to electron delocalization resulting in conjugation of the double bonds within the unsaturated fatty acids in the vegetable oil to form a conjugated system. However, the mechanism of MA addition to vegetable oil and the products of this reaction are still ill defined and are the subject of a great deal of debate in the literature. Clocker (4) postulated a cyclobutane structure for oleic acid adducts. Bickford and coworkers (5) studied the reaction between maleic anhydride with methyl oleate and suggested that MA was added at the eighth or eleventh carbon atom. The results of Teeter (6) and Kappelmeier (7) also support succinic type structure on the basis of model compounds studies using methyl linoleate and methyl linolenate. Accordingly, the reactions with di-unsaturated, nonconjugated double bonds proceeded by the 'ene' reaction mechanism and the succinic type addition occurs at the eighth, eleventh, and

fourteenth carbon atoms, with a major addition product at the eleventh carbon. Based on these results, Kappelmeier and Van Den Nuet (7) postulated that conjugation might occur simultaneously with an attack at the methylene carbon by which a second mole of maleic anhydride can be added by a Diels-Alder addition. Somewhat similarly, Plimmer (8) suggested a second mole of maleic anhydride could be added to the hexene ring. Nagakura and Yoshitomi (9), however, suggested the presence of free radicals leads to copolymerization of maleic anhydride with the triglyceride and based their conclusion on the increase in the viscosity of the reaction product.

It is apparent that although, maleation of soybean oil has been reported previously, most of the work was focused on the mechanism of this reaction and almost no attention was given to process optimization of this free radical initiated reaction. Seybold (10) carried out the process optimization of this free radical initiated reaction to assess the process and determine the usefulness of this reaction. Uniquely, the study focussed on maleation within a closed system under elevated temperatures and pressures. The closed system synthesis prevented premature sublimation of the MA, which was a recurring problem in the past and caused lower yields.

In this particular study, free-radical-initiated grafting of maleic anhydride (MA) onto corn oil was performed in a 2 liter Parr reactor. The organic peroxide 2, 5-dimethyl-2, 5-di-(*tert*-butylperoxy) hexane (Lupersol 101) was used as the free-radical initiator. The maleated corn oil (MCO) was characterized in terms of iodine number and acid number. The maleation of the polyester using Maleated Corn Oil (MCO) to give MCO-*g*-PBAT was carried out in an attempt to improve the compatibility between PBAT and starch, without reducing the melt strength of the polyester. The MCO-*g*-PBAT was then used as

an additive in the manufacture of starch foams. The maleation of the polyester proved to be very efficient in promoting strong interfacial adhesion with high amylose cornstarch in starch foams by melt blending.

8.3 Experimental

8.3.1 Experimental Setup

The experimental setup used in the maleation of corn oil was as shown in figure 8.2. It consists of a 2 L Parr reactor, equipped with a mechanical agitator and an electrically heated coil.

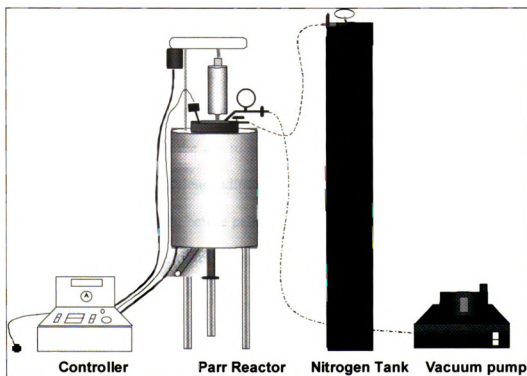


Figure 8.2 Experimental Set-up for the Maleation of Corn Oil using a Parr Reactor.

It also has vacuum ports and an outlet to drain the product (maleated corn oil). The Parr reactor is connected to a controller unit, used to control the temperature of the reaction mixture and the speed of the pitched-blade turbine impeller, which is used for mechanical agitation.

The experimental setup used in the reaction of MCO with the polyester was a twin-screw extrusion system. The twin-screw extrusion system consists of an extruder driver with a speed control gearbox, a Century ZSK-30 twin-screw co-rotating extruder with a screw diameter of 30 mm, an L/D of 42, accurate single-screw feeder for feeding PBAT. Masterflex pumps were used to feed Lupersol 101 and the MCO. A cylindrical filament die 2.7 mm in diameter and 8.1 mm in length, with a cooling sleeve was assembled to the extruder. The barrel could be cooled by adjusting the flow rate of the cooling water supply, which was manually controlled using valves for each of the nine heated zones. The sensors were mounted on the die to measure the temperature and pressure of the melt. The modified poly (butylene adipate-*co*-terephthalate) product was cooled by carrying it through a water-bath, before pelletizing it downstream. It was further used as an additive in the production of starch foams.

8.3.2 Procedure

Synthesis of maleated corn oil was performed in a 2 L Parr reactor. The reaction times, temperatures and stoichiometries chosen were optimums based on previous work (10). Approximately 950g (1.0919 mol) of corn oil were combined with 125g (1.2755 mol) of maleic anhydride and 10 ml of Lupersol 101 in the reactor. MA granules were finely powdered using a mortar and a pestle, for maximum surface area for reaction. The

organic peroxide used as an initiator in the maleation of corn oil possesses a half-life of 1 minute at 180°C and 13 seconds at 200°C. The reactor was sealed and then purged with nitrogen to create an inert atmosphere. Reaction time was 30 minutes and the reaction temperature was 150°C. The initial reaction time was taken when the reactor temperature reached a set temperature. At the end of each reaction, the reactor was connected to a vacuum pump for 30 minutes and any volatile contents (excess maleic anhydride and initiator) were collected in a solvent trap immersed in isopropanol dry ice bath. The above reaction was performed under a nitrogen atmosphere.

The temperatures in the extruder zones were set up to reach the required temperatures for the modification of the polyester using MCO. The temperature profile during extrusion was 20/125/145/165/185/185/185/185/185/180°C from the barrel section just after the feed throat to the die, with a melt temperature of 184°C -188°C. The feeder for PBAT was calibrated and set at a particular speed to feed at 11.36 kg/hr (25 lb/hr). The pumps for Lupersol 101 and MCO were calibrated and set at feeding rates accordingly. The screw speed was maintained at 100 rpm. Extrusions were carried out at a torque of 15-25%, and a pressure of 250-450 psi. The extrusions were carried out under a blanket of nitrogen in order to prevent unwanted side reactions.

The maximum grafting percentage of maleated corn oil on the polyester was determined. The modified PBAT (MCO-g-PBAT) formulations were used as processing aids in the production of starch foams. The MCO-g-PBAT which gave the lowest density of starch foams was blended with the pure polyester in ratios of 20:80 to 80:20. The temperature profile during extrusion from the barrel section just after the feed throat to the die was 20/125/145/165/185/185/185/185/175/170°C, with a melt temperature of 174°C -176°C.

Extrusions were carried out at a throughput of 9.1-11.36 kg/hr (20-25 lbs/hr). The screw speed was maintained at 150 rpm. Extrusions were carried out at a torque of ~35%, and a pressure of 100-120 psi.

The polyester, modified polyester and their blends were used as processing aids in the extrusion of starch foams. Starch foams were also run using corn oil (CO), and MCO as processing aids.

8.3.3 Characterization and Analysis

8.3.3.1 Iodine number for CO and MCO (11)

The iodine value is a measure of the unsaturation of fats and oils and is expressed in terms of the number of centigrams of iodine absorbed per gram of sample. This test is applicable to all fats and oils that do not contain conjugated double bonds as per ASTM D – 1959 standard. This is because in conjugated systems, the result is not a measure of total unsaturation, but rather is an empirical value indicative of the amount of unsaturation present.

Since one mole of Iodine (I_2) reacts per double bond, the number of double bonds can be calculated from the following equation:

$$\text{Number of Double Bonds} = \frac{\text{Iodine Number} \times 870.03 \text{ gms Corn Oil}}{100 \text{ centigrams} \times 253.8 \text{ gms } I_2 \times 1 \text{ gm Corn Oil}} \quad (8.1)$$

8.3.3.2 Acid number for CO and MCO (12)

The acid value is the number of milligrams of potassium hydroxide necessary to neutralize the free acids in 1 gram of sample. With samples that contain virtually no free acids other than fatty acids, the acid value may be directly converted by means of a suitable factor to percent free fatty acids. The percent maleation was determined by measuring acid numbers as per ASTM D – 1980 standard.

Since 2 moles of potassium hydroxide (KOH) are required to neutralize one mole of maleic anhydride, the number of moles of MA per mole of corn oil can be determined from the following equation:

$$\frac{\text{Moles of MA}}{\text{Moles of CO}} = \frac{\text{Acid Number} \times 870.03 \text{ gms Corn Oil}}{1000 \text{ milligrams} \times 112 \text{ gms KOH} \times 1 \text{ gm Corn Oil}} \quad (8.2)$$

8.3.3.3 Determination of the grafting percentage of MCO on the polyester

The extent of grafting for samples grafted with MCO can be determined by a Soxhlet extraction. Since the initial percent of MCO is very low (1-5% by weight), the grafted percentages obtained are very small. Soxhlet extraction systems were used to extract soluble components (MCO) from a solid sample into an organic solvent (carbon tetrachloride) for MCO but not for the polyester. The MCO-g-PBAT prepared was nicely ground into a fine powder under liquid nitrogen and kept for Soxhlet extraction in carbon tetrachloride as the solvent to determine the percent maleated corn oil reacted by removing the un-reacted MCO. The sample was placed in the cellulose extraction thimble in the Soxhlet and the round-bottomed flask containing the solvent is heated using a heating mantle. Boiling chips were used to prevent local hot spots. Solvent vapors rise (passing through the extraction thimble), enter the water-cooled condenser, and reliquify.

When the liquid level in the extractor reaches the top of the siphon tube, siphoning action returns the extract-enriched solvent to the flask. This extraction was carried out continuously for 24 hours. After the extraction, the thimble with the sample was kept for drying. The weight of the sample was taken at regular intervals till a constant weight was reached. This suggested complete removal of the solvent.

The product stripped off the maleated corn oil was further characterized for MFI, DSC, TGA, FTIR, and intrinsic viscosities. This MCO-g-PBAT could be used as a compatibilizer between the polyester and the starch.

8.4 Results and Discussion

8.4.1 Iodine and Acid numbers for CO and MCO (11, 12)

The unmodified corn oil had an acid number of zero, and iodine number of 117.4. The process was optimized to give acid values in the range of 120-125, and Iodine numbers around 85-90 (measure of unsaturation in fats and oils) (10). This suggests that the operating mechanism is via Diels-Alder addition chemistry as shown in Figure 8.3. It is hypothesized that reactions without catalyst at 150°C favor the grafting of maleic anhydride through “ene chemistry” since Diels-Alder is a sigma-tropic addition product. Thus, conjugation is expected to occur only in the presence of a catalyst as presented in Figure 8.3. The high temperature tends to favor a conjugated structure necessary for a Diels-Alder adduct. Free radical addition of the maleic anhydride on the labile hydrogen adjacent to the double bond would result in a succinic acid adduct, with no change to the percent unsaturation (retain same number of double bonds). However, Iodine value measurements (measure of double bonds in a structure) show a decrease on maleation.

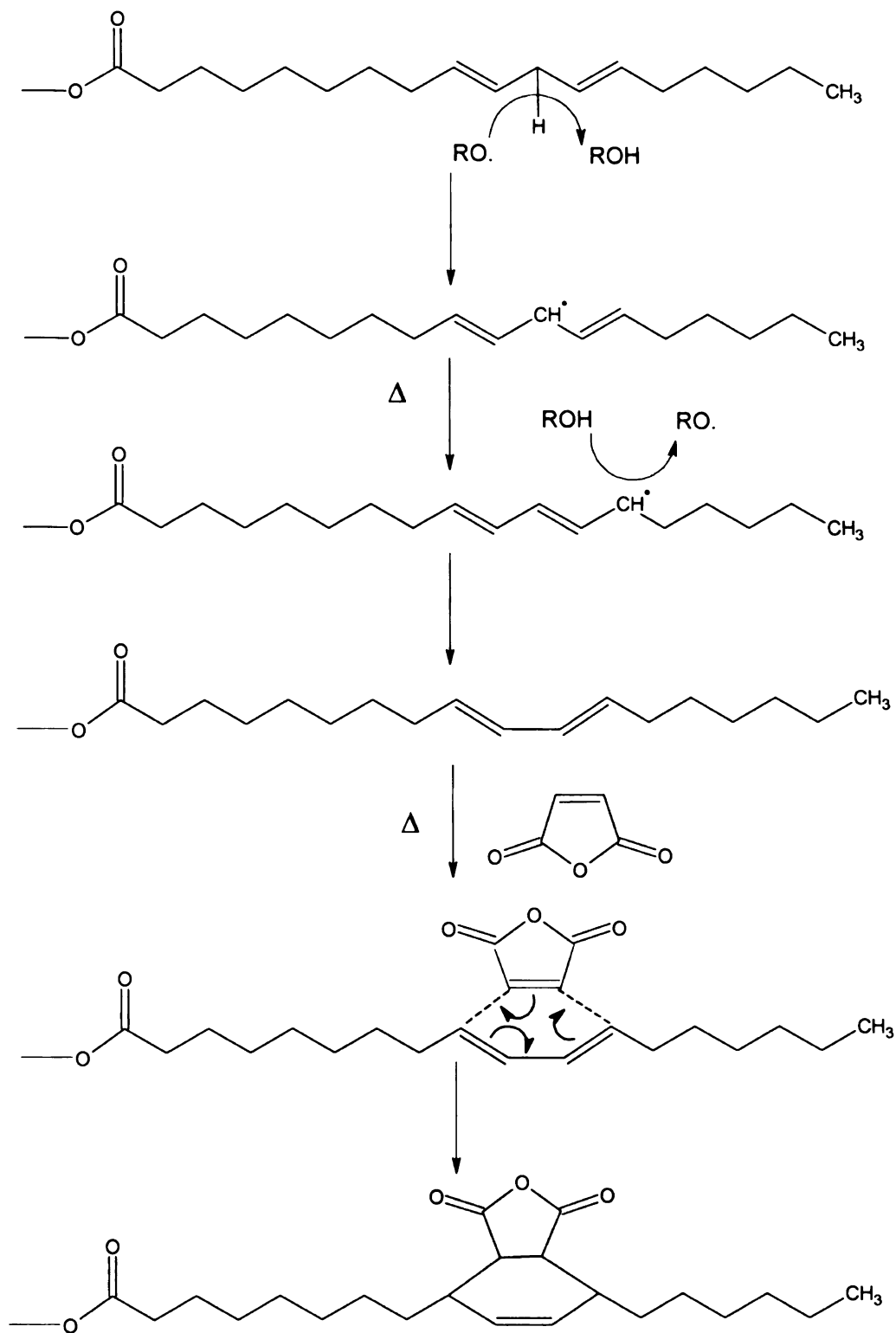


Figure 8.3 Formation of Maleated Corn Oil (MCO) by 1, 4- Diels Alder Reaction.

This supports the formation of the Diels-Alder adduct structure shown in Figure 8.3. The resultant product possesses approximately 1 mole of maleic anhydride (MA) per mole of soybean oil. The maleation of corn oil is believed to be a Diels-Alder reaction. The iodine number supports this conclusion. Corn oil has ~ 4.02 double bonds, while the maleated product has ~ 2.98 double bonds per mole. The reduction of 1 double bond supports the proposed structure. The acid number is also consistent with the structure presented. The acid number correlates ~ 0.97 mole of maleic anhydride per mole of soybean oil.

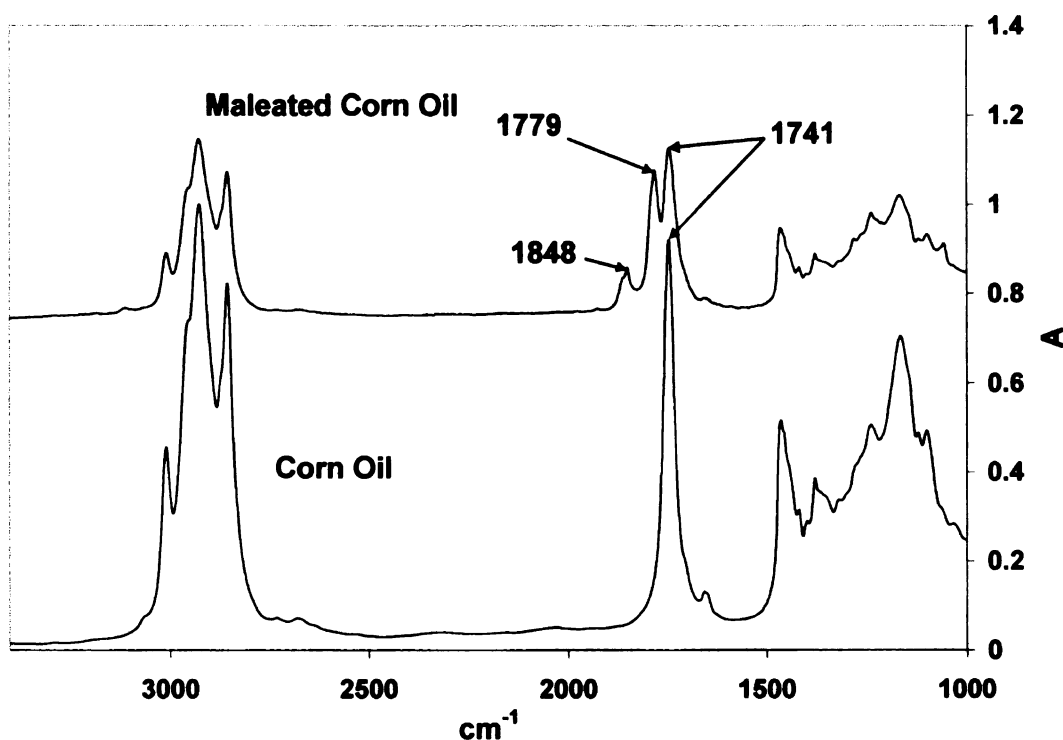


Figure 8.4 FTIR for CO, MCO

The FT-IR of MCO shows peaks at $\sim 1779 \text{ cm}^{-1}$ and 1848 cm^{-1} , which are not present in the case of corn oil (Figure 8.4). The cyclic anhydrides exhibit an intensive absorption band near 1780 cm^{-1} and a weak band near 1850 cm^{-1} , due to the symmetric and asymmetric stretching of C=O respectively (13, 14).

8.4.2 Free Radical Initiated Reaction to form MCO-g-PBAT

The grafting of MCO onto PBAT was performed in an attempt to produce reactive functional groups, which would improve the interfacial adhesion between starch and the polyester, without reducing the melt strength of the polyester. The proposed MCO-g-PBAT product obtained from the free radical initiated maleation mechanism (15) is depicted in Figure 8.5, and the free radical reaction is similar to the maleation mechanism shown in Figure 7.2. It is worth noting that some authors have proposed an end-chain grafting mechanism, involving the insertion through the aliphatic dicarboxylic acid units of the copolyesters (16).

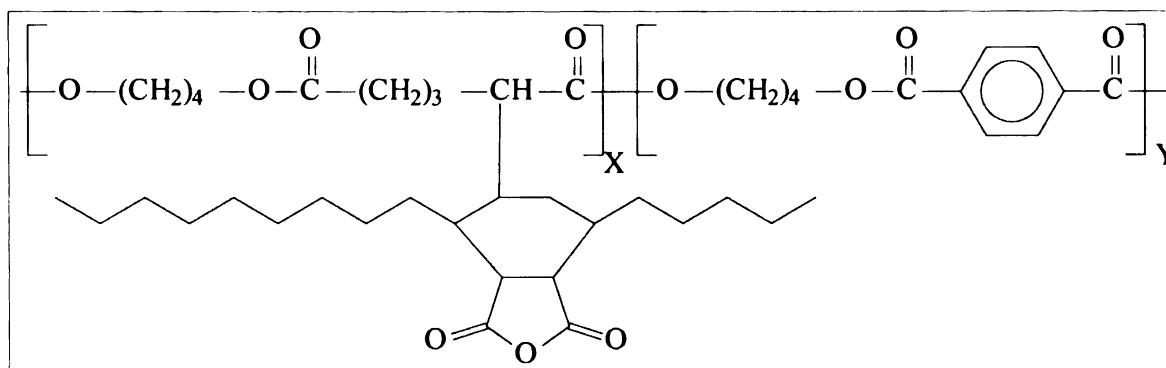


Figure 8.5 MCO-g-PBAT polymer

The grafting of MCO onto the aliphatic-aromatic copolyester has been attested by FTIR (Figure 8.6). By comparison to the FTIR spectrum of pure copolyester and focusing on the carbonyl absorption peaks, two extra absorption peaks at 1773 and 1856 cm⁻¹ were observed for the grafted polyester, assigned to the symmetric and asymmetric stretching for the carbonyl functions of MA, respectively (13, 14).

Table 8.1 reports the molecular parameters of the resulting MCO-g-PBAT by changing the initiator content and MCO content.

Table 8.1 Some Properties of MCO-g-PBAT

No	Wt % MCO	Wt % L101	MP Load %	MFI g/10min	IV _w dl/gm	Wt % Grafted
1 ^a	0.0	0.00	-	5.76	1.0156	-
2 ^b	0.0	0.00	70-72	13.24	0.9217	-
3	0.0	0.25	74-78	-	-	-
4	2.0	0.00	13-18	16.48	0.8702	0.0661
5	5.0	0.00	11-14	21.92	0.7311	0.0968
6	1.0	0.25	22-28	1.51	1.0466	0.1175
7	2.0	0.25	18-22	4.81	1.0335	0.1875
8	5.0	0.25	14-18	12.71	0.9658	0.3019
9	5.0	0.50	16-19	11.28	0.9203	0.4174

a- Not Extruded

b- Extruded (0% MCO, 0% L101)

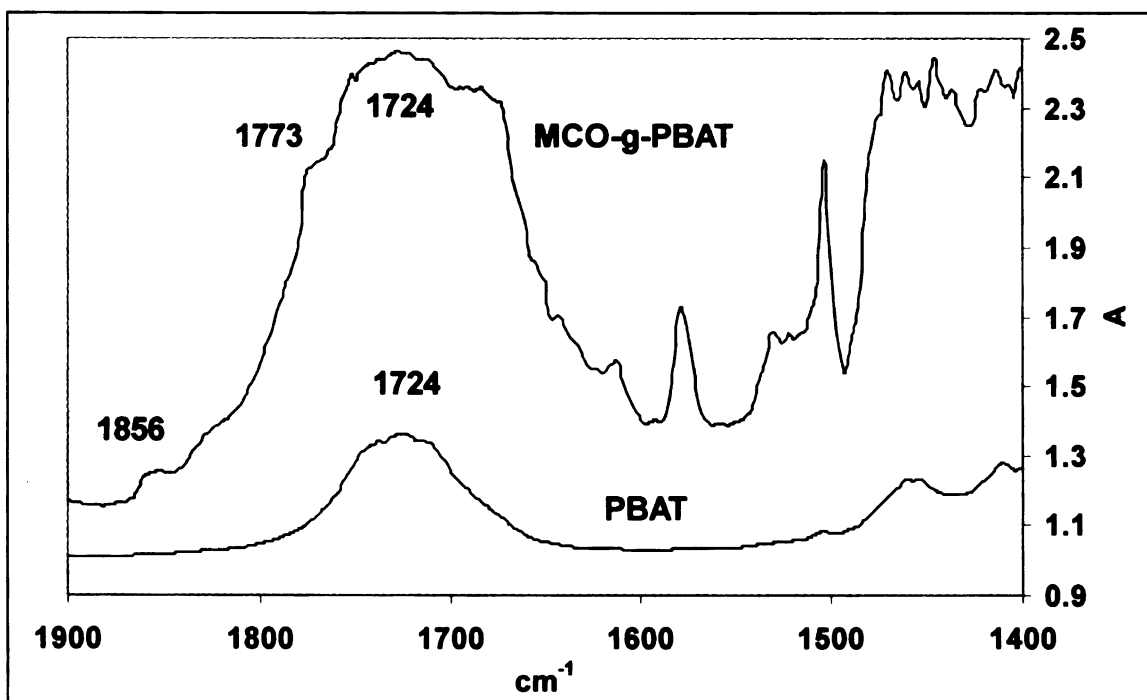


Figure 8.6 FTIR on PBAT, MCO-g-PBAT

8.4.3 Effect of the initiator on grafting percentage of MCO on the polyester

An increase in the free-radical concentration initiator results in an increase in the percent of MCO that is grafted, as indicated by percent grafted in Table 8.1 (entries 5, 8-9). The MCO concentration was kept constant at 5%. The increase in graft content with initiator concentration is due to the increase in number of radicals formed on decomposition of the initiator. The higher the radical concentration, the higher is the chain-transfer to the polymer backbone and higher the grafting. In this case, Table 8.1, however, shows an increase in torque load % at increasing amounts of peroxide. The chain scission of the polyester backbone due to grafting of MCO is not as pronounced as seen in the previous chapter (grafting of MA on the PBAT backbone). An increase in the addition of L101

increased the intrinsic viscosity indicating an increase in molecular weight of the samples. This suggests that the degradation of the polymer backbone due to acid hydrolysis (as in reaction of MA with PBAT) is minimized, probably due to the bulky molecule of MCO. Thus, the melt strength of the base polymer is retained in this case. The MFI values indicate that at a given amount of MCO (5%), the addition of increasing quantities of initiator result in lower MFIs, which implies an increase in melt viscosity. In the presence of both MCO and peroxide, there may be a competition between branching, which increases with an increase in peroxide concentration, thus increasing molecular weight, and the grafting of MCO, which increases with an increase in peroxide concentration but probably does not affect the molecular weight significantly, unlike in the presence of MA, which appears to cause the chain scission of the polyester.

8.4.4 Effect of the MCO on grafting percentage of MCO on the polyester

The MCO concentration was increased from 0% to 5% w/w while the initiator concentration and the temperature were kept constant at 0.25% w/w and 185°C respectively. An increase in the MCO concentration initiator results in an increase in the percent of MCO that is grafted, as indicated by percent maleation in Table 8.1 (entries 3, 6-8). There is also a reduction in torque load % at increasing amounts of MCO, which is mainly due to lubrication, which the oil provides. It was observed that the intrinsic viscosity for samples with 1% and 2% MCO in the presence of 0.25% L101 was higher than the pure polyester. This could imply an increase in molecular weight, possibly due to branching or cross-linking in the presence of peroxide, which dominates over the grafting reaction of MCO on the polyester chain. As the MCO content increased from 1% to 5%,

there was a reduction in melt strength and melt viscosity. Also, the lower intrinsic viscosities in Table 8.1 (entries 7 and 10) indicate a lower molecular weight. However, this reduction is not as drastic as was seen in the case of the grafting reaction of MA with PBAT. This is also probably due to the bulky MCO molecule (as compared to MA) that free anhydride is not able to lead to the acid hydrolysis of the PBAT backbone. This reduction is probably due to more radicals taking part in the grafting reaction as compared to the cross-linking reaction.

Also the content of MCO has less influence on the grafting percentage than the initiator concentration. This could be due to high MCO concentration and may only improve the grafting efficiency by decreasing the probability of radical termination reactions before the grafting of MCO, whereas the L101 concentration directly affects the total free radical concentration, which affects the termination rate.

8.4.5 TGA

The thermogravimetric analyses of the MCO-*g*-PBAT samples show that decomposition temperatures are similar to that of the pure polyester implying an equally thermally stable product (Figures 8.7, 8.8). Thus, the MCO-*g*-PBAT samples obtained exhibit similar thermal stability as compared to the original polyester. The maximum difference was about 4°C for the samples involving 5% MCO and 0.25% L101. This showed that the MCO-*g*-PBAT samples, in general, did not undergo a significant loss in molecular weight due to β -scission or acid hydrolysis of the polymer backbone.

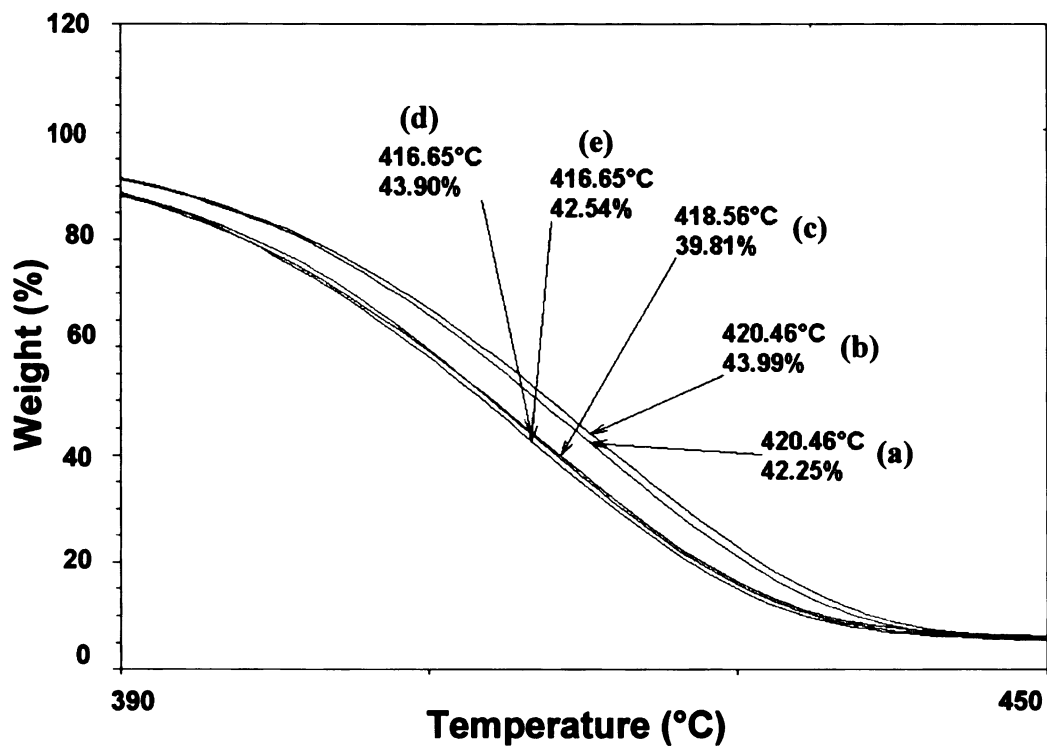


Figure 8.7 TGA for various MCO-g-PBAT (different MCO contents): (a) 0% L101, 0% MCO; (b) 0.25% L101, 0% MCO; (c) 0.25% L101, 1% MCO; (d) 0.25% L101, 2% MCO; (e) 0.25% L101, 5% MCO.

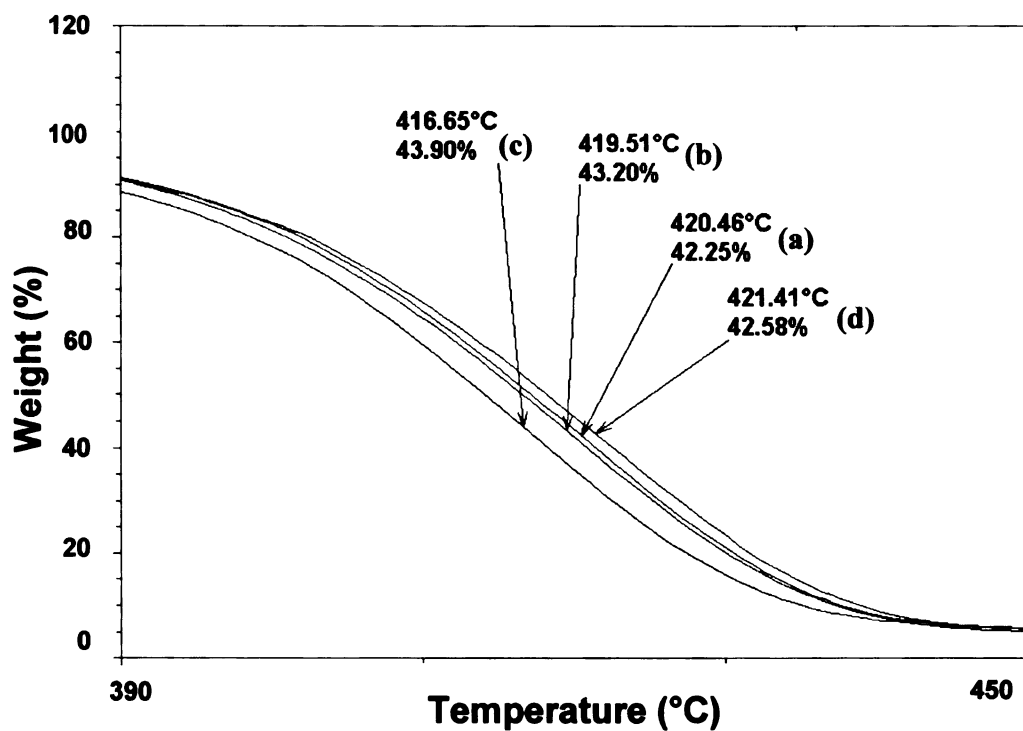


Figure 8.8 TGA for various MCO-g-PBAT (different L101 contents): (a) 0% L101, 0% MCO; (b) 0% L101, 5% MCO; (c) 0.25% L101, 5% MCO; (d) 0.5% L101, 5% MCO.

8.4.6 DSC

Table 8.2 shows the melting (ΔH_m) and crystallization enthalpies (ΔH_c) and temperatures of the maleated polyesters as compared to PBAT. Both the enthalpies were slightly lower than that for PBAT resulting from probably the slightly lower molecular weights of the MCO-g-PBAT samples. The melting point (T_m) did not change significantly. The crystallization temperatures (T_c) were higher than that for PBAT suggesting that the polyester chains tend to crystallize faster during the cooling cycle.

Table 8.2 Melting and Crystallization Enthalpies & T for MCO-g-PBAT

No.	Wt % MCO	Wt % L101	ΔH_m W/g	T_m °C	ΔH_c W/g	T_c °C
1	0.0	0.00	15.59	123.25	15.13	40.88
2	0.0	0.25	12.71	121.29	10.25	86.03
3	1.0	0.25	12.93	124.55	11.55	76.58
4	2.0	0.25	12.62	125.87	11.89	81.96
5	5.0	0.25	12.81	125.54	11.90	75.73
6	2.0	0.00	12.50	123.60	11.83	62.81
7	5.0	0.00	13.64	122.61	12.24	60.26
8	5.0	0.25	12.81	125.54	11.90	75.73
9	5.0	0.50	14.18	124.53	12.73	77.91

8.4.7 Density, Expansion Ratio (ER) and Specific length (SL) of Starch foams

The densities, expansion ratios and the specific lengths of the starch foams using different amounts of the MCO-g-PBAT as a compatibilizer between starch and the polyester, and also by itself are shown in Table 8.3. These values reported are the average of three separate extrusion runs. The density of the control starch foams was 30.2 kg/m^3 while the expansion ratio was 39.7. The foams obtained using the pure polyester had a density and expansion ratio of 24.2 kg/m^3 and 46.7 respectively (Table 8.3, Entry 2), while, it was observed that the pure modified polyester (5% MCO, 0.25% L101) gave the lowest density (21.7 kg/m^3) and the maximum expansion ratio (51.3) (Table 8.3, Entry 10). Also, the other MCO-g-PBAT samples with different grafting levels of MCO provided starch foams with densities lower than the starch-PBAT foams (Table 8.3, Entries 6 – 11). This was due to the fact that while MCO-g-PBAT samples had better compatibility with the starch, they also maintained the melt strength of the pristine PBAT, which was sufficient to support cell expansion.

The starch foams obtained using blends of MCO-g-PBAT [5% MCO, 0.5% L101] and PBAT as functional aids (Table 8.3, Entries 12 – 16) had densities and expansion ratios intermediate to those using the original PBAT and the MCO-g-PBAT [5% MCO, 0.5% L101]. In general, the density decreased with an increase in the compatibilizer content. This is probably because the modified polymer had a higher molecular weight and better compatibility with starch. The higher molecular weight results in higher melt strength, which would support cell expansion. The expansion ratio also increased with an increase in the MCO-g-PBAT content in the additive.

Table 8.3 Physico-Mechanical Properties of Starch foams using PBAT and MCO-g-PBAT (BMCO).

No	Processing Aids	Unit Density (kg/m ³)	Radial Expansion ratio	Specific Length (cm/gm)	Compressive Strength (Pa)	Resiliency (%)
1	None	30.2	39.7	14.6	4.36E+05	69.8
2	5% pure polyester (PBAT)	24.2	46.7	15.5	4.02E+05	84.3
3	2% corn oil (CO)	29.6	41.4	14.3	4.03E+05	75.4
4	2% Maleated corn oil (MCO)	27.9	41.1	15.2	3.93E+05	77.9
5	5% LPBAT [0% MCO, 0.25% L101]	26.7	42.6	15.3	3.77E+05	85.6
6	5% MCO-g-PBAT [2% MCO, 0.00% L101]	23.6	48.3	15.3	3.09E+05	91.7
7	5% MCO-g-PBAT [5% MCO, 0.00% L101]	23.4	49.0	15.2	3.11E+05	92.1
8	5% MCO-g-PBAT [1% MCO, 0.25% L101]	23.4	49.3	15.2	3.07E+05	87.9
9	5% MCO-g-PBAT [2% MCO, 0.25% L101]	22.4	50.1	15.6	3.04E+05	88.5
10	5% MCO-g-PBAT [5% MCO, 0.25% L101]	21.7	51.3	15.7	2.95E+05	94.1
11	5% MCO-g-PBAT [5% MCO, 0.50% L101]	22.6	49.7	15.6	3.06E+05	93.8
12	5% MCO-g-PBAT: PBAT::90:10	22.8	49.3	15.6	3.11E+05	92.6
13	5% MCO-g-PBAT: PBAT::80:20	23.4	48.2	15.5	3.13E+05	90.9
14	5% MCO-g-PBAT: PBAT::60:40	23.7	47.8	15.4	3.20E+05	89.2
15	5% MCO-g-PBAT: PBAT::40:60	23.8	47.7	15.4	3.32E+05	86.5
16	5% MCO-g-PBAT: PBAT::20:80	23.9	47.6	15.4	3.20E+05	86.3

8.4.8 Compressive Strength and Resiliency

The compressive strength and resiliency of the foam samples is listed in Table 8.3. Typically, a power-law relationship was observed between compressive strength σ_c and foam density ρ ($\sigma_c \sim \rho^n$). Denser foams tend to have thicker cell walls and hence resist deformation better than lower density foams with thinner cell walls. A strong relation exists between foam density and compressive strength. The regression line is drawn using the data from Table 8.3, and a slope of 1.16 is obtained ($n = 1.16$) (Figure 8.9). A value of $n = 0.92$ was obtained by Willett et al. (17), while Smith and co-workers (18) report exponents of 1.5 – 1.6 for compressive strengths of foams prepared from maize grits. However, this value is specific to the type of materials used as well as the extrusion system used for foaming.

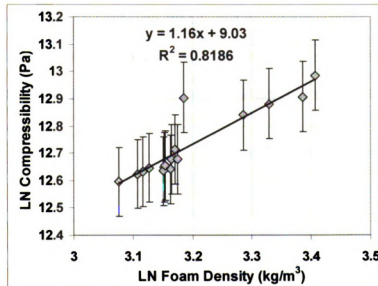


Figure 8.9 Logarithmic plot of Compressive Strength (Pa) as a function of foam density (kg/m^3)

The addition of PBAT improves the resiliency considerably from 69.7% to 84.24% at a PBAT content of 5% of the starch used. The MCO-*g*-PBAT samples were compatible with starch and helped improve the resiliency of the starch foams further. The spring indices obtained were in the range of 87 – 94% using MCO-*g*-PBAT with different grafting percentages (Table 8.3, Entries 6 – 11). The resilience provided by MCO-*g*-PBAT using 5% MCO and 0.25% L101 was maximum (94%), probably due to its grafting level and good melt strength (Table 8.1). The graft polymers have sufficient melt strength to support expansion, since the amount of degradation is lower as compared to MA-*g*-PBAT. This is due to the presence of a lower number of anhydride groups, which result in the degradation of the PBAT backbone.

The MCO-*g*-PBAT sample with sufficient grafting percentage of MA (5% MA, 0.25% L101) was used as the compatibilizer between the starch and PBAT. This particular MCO-*g*-PBAT was melt blended with PBAT in different proportions and these blends were used as additives in starch foams. The densities and spring indices obtained by using these blends were intermediate to the values obtained by using PBAT and MCO-*g*-PBAT by themselves.

8.4.9 ESEM

Scanning electron micrograph of the foam surface is shown in Figure 8.10. The surface of the starch foams with the polyester had minimal or no holes on the surface (figure 6.11), and thus exhibit lower densities and higher expansions. This implies that these foams have higher melt strength and hence they resist bubble rupture. However, some incompatibilities between the polyester and thermoplastic starch were obvious from the

pha
am

8.4.

The

mo

usin

PB.

hyd

wei

pres

evid

phase separation observed. This phase separation is absent in the presence of a small amount of the MCO-g-PBAT, as seen in the micrograph (Figure 8.10).

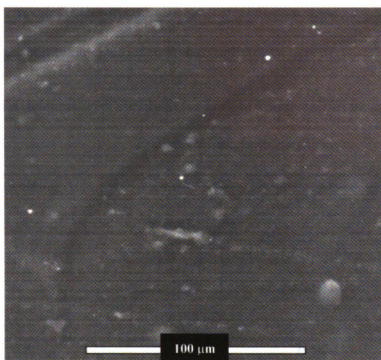


Figure 8.10 ESEM on starch foam surface (5% MCO-g-PBAT)

8.4.10 Moisture Sorption Analysis

The normalized steady state weight gains and dimensions of the starch foam samples on moisture sorption are listed in Table 8.4. The hydrophobic properties of the starch foams using PBAT as a functional aid (19), and using MA-g-PBAT as a compatibilizer between PBAT and starch (20) have been reported in our previous work. The control hydroxypropylated high amylose cornstarch foams gained up to 13% of their original weight, and lost about 50% of their dimensions on moisture sorption. However, in the presence of PBAT, it was observed that PBAT migrated to the surface, which was evident from the scanning electron micrograph of the starch foam surface in Figure 7.10,

thus providing a finer and a more stable surface preventing the rapid loss of moisture through the surface, as discussed in Chapter 7, Section 7.4.6. The steady state weight gain was about 9.3 – 9.5% of the original weight of the foam samples on addition of PBAT, but dimensional stability increased significantly.

Table 8.4 Normalized Steady State Weight Gains and Dimensions of Starch Foams on Moisture Sorption

No.	Processing Aids	Normalized Steady State Weight Gain, $\left[\frac{W - W_0}{W_0} \right]$ (± 0.032)	Normalized Steady State Diameter, $\left[\frac{D}{D_0} \right]$ (± 0.041)	Normalized Steady State Length, $\left[\frac{L}{L_0} \right]$ (± 0.046)
1	None	0.13	0.56	0.50
2	5% pure polyester (PBAT)	0.094	0.79	0.81
3	(0.5% MA-g-PBAT + 4.5% PBAT) blend	0.052	0.87	0.85

The loss of radial and longitudinal dimensions decreased from 50% to about 20% respectively with an increase in the PBAT content. This could imply that most of the PBAT in the foam samples manifested at the surface and not in the core. Thus, the core of these samples continued to absorb as much moisture as it used to.

The results from Table 8.4 indicated that the foams using MCO-g-PBAT as a functional aid affected the longitudinal stability of the starch foams slightly (as compared to the starch foams using PBAT). But the loss in radial dimensions was improved to just 13%

using MCO-*g*-PBAT, from about 20% for PBAT. Also, the normalized equilibrium weight gain reduces from ~ 9.3 – 9.5% to ~ 5.2 %. This suggested that the compatibility between starch and PBAT might have been improved, since most of the polymer does not manifest at the surface as it did earlier on phase separation.

8.5 Conclusions

Free-radical-initiated grafting of maleated corn oil (MCO) onto PBAT was performed with a motive to reduce the chain scission in PBAT due to acid hydrolysis and, hence, prevent the reduction in melt strength due to degradation of the backbone. The amount of MCO grafted on the PBAT backbone was as high as 0.42% by weight. The MCO-*g*-PBAT samples were compatible with starch and helped improve the resiliency of the starch foams. The spring indices obtained were in the range of 87 – 94% using MCO-*g*-PBAT with different grafting percentages. The resilience provided by MCO-*g*-PBAT using 5% MCO and 0.25% L101 was maximum (94%), probably due to its grafting level and good mechanical strength. The graft polymers have sufficient melt strength to support expansion, since the amount of degradation is lower as compared to MPBAT. This is due to the presence of a lower number of anhydride groups, which result in the degradation of the PBAT backbone.

The following Chapter 9 deals with the modification of starch in order to improve the compatibility between the starch and PBAT. Transesterification reactions were carried out between thermoplastic starch (TPS) and PBAT to obtain PBAT-*g*-TPS copolymer. TPS was also reacted with maleic anhydride to obtain a thermoplastic starch maleate (MTPS) with a lower shear viscosity. This MTPS was also reacted with PBAT to obtain PBAT-*g*-MTPS copolymers.

8.6 Refer

- 1) [http](#)
- 2) Mor
225
- 3) Roo
- 4) Clo
- 5) Bick
Cher
- 6) Teet
Soci
- 7) Kap
113.
- 8) Plim
- 9) Naga
- 10) K. Se
and F
- 11) AST
Acid
- 12) AST
Polym
(200
- 13) Bella
(196
- 14) Pou
Com
- 15) Carls
Scier
- 16) Mani
Cher

8.6 References

- 1) <http://www.scientificpsychic.com/fitness/fattyacids.html>
- 2) Morrel R.S., Samuels H., Journal of Chemical Society Abstracts, 2251-2254,1932.
- 3) Root F.B., U.S. Patent 2374381, 1945.
- 4) Clocker E.T., U.S. Patent 2188882, 1940.
- 5) Bickford W.G., Fisher G.S., Kyame L., Swift C.E., Journal of American Oil Chemists Society, 25, 254-257, 1948.
- 6) Teeter H.M., Geerts M.J., and Cowan J.C., Journal of American Oil Chemists Society, 25, 158-162, 1948.
- 7) Kappelmeier C.P.A., Van Der Nuet J.H., Van Goor W.R., Paint Oil Chem. Rev., 113, 11-18, 1950.
- 8) Plimmer H. and Robinson E.B., British Patent 565432, 1944.
- 9) Nagakura M. and Yoshitomi K., Yukagaku ,21, 83-91, 1972.
- 10) K. Seybold, MS Thesis, 'Design and Economic Analysis of Maleated Soybean Oil and Ester Production Facility.' Michigan State University, (1997).
- 11) ASTM D1959, Standard Test Method for Iodine Value of Drying Oils and Fatty Acids, Annual Book of ASTM Standards 06.03: 399-401 (2000)
- 12) ASTM D1980, Standard Test Method for Acid Value of Fatty Acids and Polymerized Fatty Acids, Annual Book of ASTM Standards 06.03: 418-419 (2000)
- 13) Bellamy L.J., The Infra-Red Spectra of Complex Molecules, Wiley: New York, (1964).
- 14) Pouchert C.J., The Aldrich Library of Infra-Red Spectra, Aldrich Chemical Company; Milwaukee, WI, (1970).
- 15) Carlson, D. L., Nie, L., Narayan, R., Dubois, P. Journal of Applied Polymer Science, 72, 477-485, 1999.
- 16) Mani, R., Bhattacharya, M., Tang, J. Journal of Polymer Science: Part A: Polymer Chemistry, 37, 1693-1702, 1999.

17) Will

18) Hut
22.

19) Nab
Rev

20) Nab

- 17) Willett, J. L., Shogren, R. L. Polymer, 43, 5935, 2002.
- 18) Hutchinson, R. J., Siodlak, G. D. E., Smith, A. C. Journal of Materials Science, 22, 3956-3962, 1987.
- 19) Nabar, Y., Draybuck, D., Narayan, R., Journal of Applied Polymer Science, In Review.
- 20) Nabar, Y., Raquez, J-M., Dubois, P., Narayan, R., Biomacromolecules, In Press.

9.1 Introd

The gelatin

gelatinizatio

applicability

temperatures

pressure and

and decomp

destructurize

water or othe

Thermoplast

produced fro

of several pl

temperatures

glycol, polyo

between dest

also entitled

processes suc

into shaped fo

REACTIVE PBAT-*g*-TPS AND PBAT-*g*-MTPS BLENDS

9.1 Introduction

The gelatinization and deconstructurization (plasticization) of starch using water as the gelatinization/plasticization agent has been briefly discussed in Chapter 2. The applicability of this starch is limited because of degradation due to water loss at elevated temperatures. At higher water content, the vapor pressure of water exceeds atmospheric pressure and water escapes leaving a brittle foamy material with a T_g above processing and decomposition temperatures with bad thermoplastic properties. The behavior of deconstructurized starch is glassy, and materials can only be processed by the addition of water or other plasticizers.

Thermoplastic starch (TPS) is described as substantially amorphous starch. TPS is produced from granular starch by employing heat and mechanical energy in the presence of several plasticizers, which do not evaporate substantially during processing at high temperatures and pressure. Some of the common plasticizers used are glycerol, ethylene glycol, polyols etc. From the description above, it has to be concluded that the difference between deconstructurized starch and TPS is still not well defined. Deconstructurized starch is also entitled as TPS when it can be processed by any of the known thermoplastic processes such as extrusion, injection molding, blow molding and compression molding into shaped forms without the addition of extra plasticizers.

Plasticization
hydrogen bonding
amorphous

9.1.1 Starch

Due to the
incorporate
desirability
2), typically
material. Ra
inclusion of
strength of a
granular starch
the poor adhesion
normally be
terms of
thermodynamic
performance
dried, and the
starch may
have been
constituent
itself. While

Plasticization of starch in an extruder using glycerol as the plasticizer breaks the hydrogen bonds, and disrupts the granular crystalline organization. It further releases the amorphous polymer chains with $\alpha 1 \rightarrow 4$ and $\alpha 1 \rightarrow 6$ linkages.

9.1.1 Starch blends with polyesters

Due to the biodegradable nature of starch, many researchers have attempted to incorporate starch into a variety of materials in order to improve the environmental desirability and reduce the cost of such materials. Starch may be added as inert filler (1, 2), typically in its native, unmodified state, which is generally water insoluble, granular material. Ramsay et al. (3) studied blends of granular starch with P (HB-co-HV). The inclusion of 25-wt% granular starch was reported to result in a composition with a tensile strength of about 60% the original. The authors acknowledged that the use of unmodified granular starch as a particulate filler did not offer any appreciable reinforcement due to the poor adhesion of the polymer granule interface. In such cases, the starch granules will normally behave as any other solid particulate filler and will contribute little, if any, in terms of improving the mechanical properties of the resulting material. The thermodynamic incompatibility between starch and synthetic polymers leads to the poor performance properties of these blends. Alternatively, starch that has been gelatinized, dried, and then ground into a powder may also be added as particulate filler. Although starch may be added as filler, its more interesting and technologically challenging uses have been in the area of using starch as a binder, as a thermoplastically processable constituent within thermoplastic polymer blends, and as a thermoplastic material by itself. While native starch does not typically behave as a thermoplastic material by itself,

it is thermo
patents tha
destructuriz
(4); U.S. Pa
U.S. Patent
et al (8, 9).
starch (TPS
manufacture
a small quat
starch melts
in order to
include U.S.
Bastoli et al
starch polym
same time, f
difficult to a
optimal poly
"optimize" th
polymers and
which tends
Another draw
mechanical P
science persp

it is thermoplastic in the presence of a plasticizer when heated and sheared. Examples of patents that disclose the manufacture of “destructured starch” and blends of destructurized starch and other polymers include U.S. Patent 4,673,438 to Wittwer et al. (4); U.S. Patent 4,095,054 to Lay et al. (5); U.S. Patent 5,256,711 to Tokiwa et al. (6); U.S. Patent 5,275,774 to Bahr et al. (7); U.S. Patents 5,382,611 and 5,405,564 to Stepto et al (8, 9). Lately, there have been considerable publications in the use of thermoplastic starch (TPS) as a component in multi phase blends (10 – 14). Still others have manufactured thermoplastic starch blends in which native starch is initially blended with a small quantity of water and a less volatile plasticizer such as glycerin in order to form starch melts that are subjected to a degassing procedure prior to cooling and solidification in order to remove substantially all of the water therefrom. Examples of such patents include U.S. Patents 5,412,005, 5,288,765, 5,262,458, 5,462,980 and 5,512,378 to Bastioli et al (15 – 19). Although many have attempted for years to discover the “perfect” starch/polymer blend that would yield an environmentally sound polymer while, at the same time, fulfilling desired mechanical and cost criteria, such a combination has been difficult to achieve. The reason for this is that the emphasis has been on finding the optimal polymer or mixture of polymers and other admixtures in order to thereby “optimize” the properties of the starch/polymer blend. One drawback is that most of the polymers and other admixtures are themselves significantly more expensive than starch, which tends to increase the cost of such polymer blends compared to starch melts. Another drawback is that such additives will only be able to marginally alter the mechanical properties of the starch/polymer blends when viewed from a materials science perspective. Hence the thermodynamic incompatibility between the starch and

the polyester

materials.

Chapter 7 (

methods ne

Previously

reactively g

to achieve c

were emplo

method was

backbone us

to form mal

copolymers

derivatization

9.1.2 Starch

As explained

the polyester

drawback, gr

modify starch

applications o

poly (ethyle

formation of

group in starch

the polyester at the molecular level leads to the poor performance properties of such materials. The theory underlining incompatible blends is discussed in more detail in Chapter 7 (Section 7.1.1). There is also considerable discussion related to processes and methods needed to achieve efficient compatibilization.

Previously in Chapters 7 and 8, poly(butylene adipate-*co*-terephthalate) (PBAT) was reactively grafted with Maleic Anhydride (MA) and Maleated Corn Oil (MCO) in order to achieve compatibilization between starch and PBAT. In this study, two novel methods were employed to achieve this compatibilization between starch and PBAT. The first method was to reactively graft a hydrophilic polymer such as starch onto the PBAT backbone using trans-esterification chemistry. The second method was to maleate starch to form maleated thermoplastic starch and then use the new maleated starch to form graft copolymers with PBAT. Prior work in the areas of reactive blending and starch derivatization is explained in sections [9.1.2](#) and [9.1.3](#) respectively.

9.1.2 Starch-Polyester Reactive Blends

As explained in the Chapter 7, the thermodynamic incompatibility between the starch and the polyester often leads to poor performance of these blends. In order to improve this drawback, graft copolymerization of vinyl monomer on the starch backbone was used to modify starch. Fanta and Bagley have reviewed the synthesis and discussed some applications of starch graft copolymers (20, 21). Otey et al. (22 – 24) blended starch with poly (ethylene-*co*-acrylic acid) (EAA). In these papers, the authors suggested the formation of hydrogen bonds between the carboxylic group in EAA and the hydroxyl group in starch. Increasing the level of starch decreased the percentage elongation of the

film and in

formed with

They report

OH groups

containing

Tomka et al

of thermop

esterification

with free hy

with proper

discloses a

fiber form,

synthetic th

compound s

aliphatic po

surface grafi

freely availa

9.1.3 Star

The term "s

structure of s

is generally

granular stan

film and increased the diffusion rate of water. Similar complexes like EAA can also be formed with the hydroxyl groups of the polyethylene-vinyl alcohol (EVOH) copolymer. They report a reaction between the anhydride group in the synthetic polymer with the –OH groups of starch. Bloembergen et al. (25) have reported on blends and alloys containing lignocelluloses like starch, cellulose acetate etc. U.S. Patent 5,314,934 to Tomka et al. (26) provides a process to produce a polymer mixture essentially consisting of thermoplastically processable starch (up to 70 wt %). During this mixing process, an esterification reaction takes place between the maleic anhydride groups in the terpolymer with free hydroxyl groups in the starch. These reactive blends can be blown into film with properties comparable to LDPE. U.S. Patent 5,234,977 to Bastioli et al. (27) discloses a material used for the production of biodegradable articles in film, sheet or fiber form, which can be produced by extrusion from a molten mass that includes a synthetic thermoplastic polymer and a destructured starch to which a boron containing compound such as boric acid has been added. Narayan et al. (28) have grafted starch onto aliphatic polyesters. They report on the fact that when starch is not plasticized, only surface grafting is possible. However, when starch is plasticized, the hydroxyl groups are freely available for reaction, thus enhancing the reactivity.

9.1.3 Starch Derivatives

The term “starch derivative” includes those modifications, which change the chemical structure of some of the D-glucopyranosyl units in the molecule. Derivatization of starch is generally conducted to modify the gelatinization and cooking characteristics of granular starch, to decrease the retrogradation and gelling tendencies of amylose-

containing starches and to enhance hydrophilic or hydrophobic characteristics. Starch can also be derivatized to increase its reactive capability in further downstream blending operations with other biodegradable polyesters. A starch derivative is fully defined by a number of factors: plant source (corn, waxy maize, potato); amylose to amylopectin ratio; Degree of Polymerization; type of derivative (ester, ether etc.); nature of the substituent group (acetate etc.); Degree of Substitution (DS) or molar substitution (MS) and physical form (granular, pregelatinized).

Most commercially produced derivatives have a DS, generally less than 0.2. The DS is a measure of the average number of hydroxyl groups on each D-glucopyranosyl unit, which is derivatized by substituent groups. DS is expressed as moles of substituent per D-glucopyranosyl unit. Since the majority of the glucose units in starch have three hydroxyl groups available for substitution, the maximum possible DS is three. DS can be expressed using the equation (9.1) as shown below; where W is the weight-% of the substituent (based on the total weight) and M is the molecular weight of the substituent.

$$DS = \frac{162 \times W}{100M - (M - 1)W} \quad (9.1)$$

Modified starch products have low DS levels. They were primarily designed to alter their solution properties for food applications or adhesion to paper. Acetylated starches, for example, have been known for more than 100 years. Starch triacetates were prepared earlier by carrying out the acetylation in acetic-anhydride-pyridine solution. This procedure was impractical to scale up due to the high costs involved with pretreatment and recovery of pyridine (29). More recently (30), cornstarch was fully acetylated by reacting with fourfold quantities of acetic anhydride at 123⁰C for 5 hours. The reaction was carried out in an alkaline medium of sodium hydroxide. The solubility of these starch

acetates

the ester

soluble i

Acetyl c

transpare

with tensi

Highly ac

solvent so

thermopla

not been c

derivatives

their crysta

Cyclic diba

free carbox

same chem

The reactio

with a cyc

yields prod

Most of th

intermediat

for 2 hours

acetates is dependent upon the acetyl value, the degree of degradation, polymerization of the ester, the type of starch and the nature of the solvent. Undegraded starch acetates are soluble in relatively few solvents, although many reagents cause the formation of gels. Acetyl derivatives of starch give molded products, which are brittle, clear and transparent. Dispersions of triacetates in dichloromethane gave clear and flexible films with tensile strengths in the range of 3500 psi.

Highly acetylated starches, historically, were of some interest because of their organic solvent solubility and their thermoplasticity for film and fiber applications analogous to thermoplastic cellulose esters. In spite of this development, high DS starch esters have not been developed commercially because they could not compete with similar cellulose derivatives in terms of strength and cost. Such high DS starch esters are characterized by their crystalline properties exhibiting clear melt transitions (25).

Cyclic dibasic acid anhydrides such as succinic anhydride yield starch esters containing a free carboxylate group that increases the water-holding capacity of the product (31). The same chemistry could be carried out with maleic anhydride to yield the maleate half ester. The reaction schemes are depicted below in Figure 9.1. Treatment of a starch suspension with a cyclic dicarboxylic acid anhydride containing a hydrophobic substituent group yields products with emulsion stabilizing properties (32).

Most of the modification of starch using cyclic anhydrides is buried into patents. This intermediate reaction product was further heated, after the addition of succinic anhydride, for 2 hours at the same temperature to give starch propionate succinate.

Starch

These sta

available

production

155 °C in t

(DS) 0.02 t

While all o

can be acyl

to yield th

extruders co

and phthali

during extr

alkaline m

hydrophobi

method ap

the chemist

clean, wast

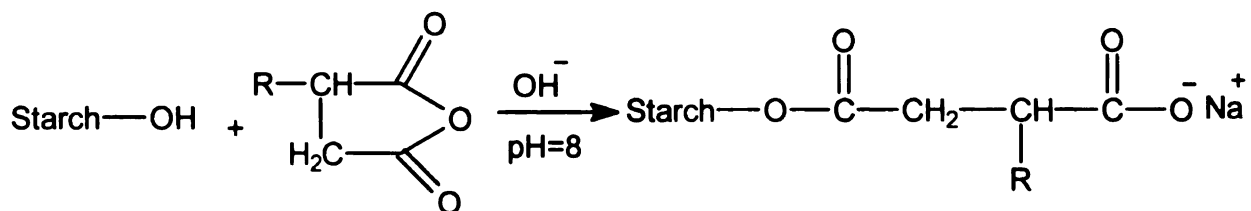


Figure 9.1 Starch Reaction with half-esters of dicarboxylic acids

These starch esters have value as dispersants in coatings replacing commercially available paint containing dispersants. U.S. Patent 3,732,207 (33) discusses the production of starch esters by heating starch with maleic or succinic anhydride at 100-155 °C in the presence of 0.5-15% moisture to give a product with degree of substitution (DS) 0.02 to 0.04.

While all of the above work is related to the production of starch esters in batch, starches can be acylated on extrusion with cyclic anhydrides in the presence of carbonate buffers to yield the corresponding starch esters. Tomasik et al. (34) reacted corn starches in extruders containing varying amounts of moisture (18, 20 and 30%) with succinic, maleic and phthalic anhydrides. Carbonate buffer, either pH 8 or pH 9 was added as a medium during extrusion. It is demonstrated that extrusion of starch with cyclic anhydrides in alkaline medium presents a facile method of preparation of anionic starches of hydrophobic character based. However, based on up-to-date collected experiences, this method apart from some advantages seems to have several limitations. They result from the chemistry of the process as well as from construction of extruder. The fast, cheap, clean, waste less process together with a possibility of a large production of such kind

starches is an advantage of this method. However, due to the high viscosity of the thermoplastic (TPS) melt, it is extremely difficult to extrude samples containing less than 25% moisture at temperatures of around 130°C. In all of the above studies, grafting of reactive moieties onto the starch backbone in melt phase has not been conducted.

In this study, starch was maleated in the melt phase using maleic anhydride/maleic acid in a twin-screw co-rotating extruder in the presence of glycerol plasticizer. These starch maleates were further reactively blended with PBAT aliphatic aromatic copolyester in the melt phase to form PBAT-Maleated Thermoplastic Starch graft copolymers to be used in blown film applications.

Biodegradable polymer nano-composites have received very little attention in the open literature; however, recent research (35) has indicated that organo-clays exhibit much promise for starch-based polymer nano-composites in improvement of the mechanical properties and stability over the unfilled compositions. More importantly, clay is environmentally friendly, naturally abundant, and economic. To realize the synergy of the biodegradability of the starch and PBAT, and the high strength and stability of the nano-scale clay, PBAT/MTPS/Clay nano-composites were prepared through the melt-intercalation method.

9.1.4 Starch – based Nano-Composites

Although the miscibility of silicates, including clay minerals, with organics and polymers has been known since the early 1950s, an industrial report of a nylon-6/montmorillonite (MMT) composite from Toyota has recently revitalized the field (36, 37). The nano-sized clays improved the moduli of the nylon composites to twice its original value, and also

increased the heat distortion temperature by 80°C. Giannelis et al. (38, 39) discovered that it is possible to melt-mix polymers with clays bearing cationic organic surfactants, eliminating the need for organic solvents or in situ polymerization schemes. Such melt-blending approaches generally yield similar concurrent enhancements of many materials properties by the nano-dispersion of inorganic silicate layers, which cannot be realized by conventional fillers; for example, simultaneously increasing tensile strength, flex modulus, and impact toughness, contributing a general flame retardant character (40), and affording a dramatic improvement in barrier properties (41 – 45).

On the basis of theoretical models, Balazs (46, 47) suggested that an increase in the length of the organic molecules tethered on clays is a promising approach to further promote dispersion of clay sheets in a polymer matrix. Toward this end, recent reports employing a variety of polymers (polystyrene (48), poly(methyl methacrylate) (49, 50), and poly(caprolactone) (51), epoxy matrices (52)) grafted on MMT surfaces observe varied extents of clay dispersion. Furthermore, subsequent annealing of these polymer bearing clays, or mixing them with the respective homopolymers, can lead to retention or collapse of the clay dispersion depending on the polymer (48 – 51). The differences in these responses were attributed to the specific polymer-clay interactions (53) in each case, indicating that where there exist strong interactions, the clay dispersions collapse; whereas, in those cases with weak polymer-clay interactions, the dispersions can be retained.

Clays have many attractive features in structure: active sites such as hydroxyl groups, Lewis and Bronsted acidity, exchangeable interlayer cations, and difference of SiO₄ tetrahedral sheet and Al₂(OH)₆ octahedral sheet in chemical stability. Moreover, clay

minerals are fine-grained materials with high surface area, and strong adsorption, giving the activation possibility.

Thus, polymer-layered silicate hybrids or nano-composites have been prepared from synthetic thermoplastics, thermosets and elastomers up to now. Very few studies have been done on starch-based biodegradable nano-composites, where the main challenge lies in tuning starch and the nano-clay architecture to achieve interactions (physical/chemical) between the clay and the polymer. Studies on biodegradable TPS-Polyester nano-composites so far have only improved solvent-resistance, thermal properties and modulus, but not strength and toughness (54, 55). This is due to the weak adhesion between the clay and the polymer even though clay is well-dispersed within the polymer matrix. To achieve good adhesion and wetting between starch and nano-clay, one could modify the starch architecture to introduce functional groups that favor stronger covalent or hydrogen bonding with nano-clay; or exchange the inorganic cations on the nano-clay with organic ions that would facilitate the incorporation of large starch molecules between the clay nano-sheets; or both. Rizvi and co-workers (56) have carried out studies on starch-PCL blends involving nano-clay, where no improvements in strength or break elongations were realized. They hypothesized that a more hydrophilic starch would form stronger hydrogen bonds with the clay surface and improve the adhesion between the two. They introduced carbonyl or carboxyl groups in the starch thorough peroxide oxidation. A slight improvement in properties was attained (tensile strength of ~ 10 MPa (1400 – 1500 psi), Break Elongations of ~ 600 – 900%), although, not enough to compete with the existing market.

This research aims at incorporating nano-scale clays in the PBAT-MTPS graft copolymer blends developed to enhance the mechanical, thermal and processing properties of the resulting product.

9.2 Materials and Equipment

Regular corn starch (un-modified) was obtained from Cargill-grade SMP 1100, with equilibrium moisture content of about 12 percent (w/w). Anhydrous glycerol [2136-03], 99.9% assay was obtained from J.T. Baker. Maleic anhydride or 2, 5 Furandione [108-31-6] was obtained from Sigma. Maleic acid was obtained from J.T. Baker. Lupersol 101 [78-63-7] was obtained from Aldrich Chemicals. All the above materials were used as obtained. Both pristine Na⁺ - MMT (Trade Name – Cloisite Na (d₀₀₁ = 11.7 Å)), with a cation – exchange capacity of ca. 0.926 mequiv/g; and an Octadecylammonium-modified MMT organophilic clay (Trade Name – Cloisite 30B (d₀₀₁ = 18.5 Å)), with an organic modifier (methyl, tallow, bis-2-hydroxyethyl, quaternary ammonium) concentration of 0.9 mequiv/g, were purchased from Southern Clay Products. Tallow comprises of about 65% C18 chains, ~30% C16, and ~5% C14 chains. The organic modifier for Cloisite 30B is shown in Figure 9.2.

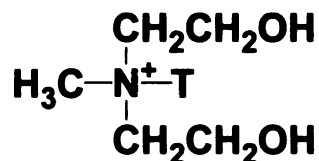


Figure 9.2 Methyl, tallow (T), bis-2-hydroxyethyl, quaternary ammonium

Cloisite® Na⁺ and Cloisite 30B are additives for plastics to improve various plastic physical properties, such as reinforcement, Heat Distortion Temperature (HDT), Coefficient of Linear Thermal Expansion (CLTE) and barrier.

BENTONE 111 is an organic derivative of a special smectite clay, while BENTONE 166 is an alkyl aryl ammonium hectorite clay, obtained from Elementis Specialties, with greatly improved dispersibility characteristics. They provide excellent mechanical strength, flame retardancy and highly improved gas barrier properties

A twin-screw co-rotating CENTURY ZSK – 30 extruder, having a length/diameter ratio (L/D) of 42 and a screw diameter of 30 mm, was used for the plasticization as well as the reactive blending chemistries. The extruder was electrically heated and cooled using circulating water. The auxiliary equipment included a water bath to cool the extrudate and a pelletizer to cut the strand into small pellets.

9.3 PBAT-Thermoplastic Starch (TPS) graft copolymers

In this section, experimental details on reactive extrusion processing of PBAT-TPS graft copolymers using maleic anhydride/maleic acid as the transesterification catalysts, along-with the characterization by Soxhlet extraction are outlined.

9.3.1 Synthesis of PBAT-TPS graft copolymers by reactive extrusion processing

The synthesis of PBAT-TPS graft copolymers was accomplished in a twin-screw co-rotating ZSK-30 extruder using maleic acid/anhydride as a trans-esterification catalyst. TPS was produced by plasticization of regular corn-starch using glycerol (20-wt %) as a plasticizer in the same extruder. Maleic acid was ground to a fine powder using a mortar

and pestle and pre-blended with the PBAT polyester before being fed to the feed port of the extruder. The concentration of maleic acid used was 1-wt% with respect to the total mass. Meanwhile, TPS (previously oven dried overnight at 75°C to remove any free moisture which might cause degradation of the PBAT backbone) was ground to a fine powder and fed using an external feeder to the feed port of the extruder. The feeder rates were adjusted accordingly to obtain a ratio of 70:30 (PBAT + Maleic acid): TPS. The temperature profile used was 15/95/125/145/160/165/165/165/150/145 from the feed throat to the die, and the melt temperature was 153°C. The screw speed employed was 150 rpm. The vent port was kept open for all studies to remove unreacted maleic acid and moisture. The extruded strand was cooled using a water bath and pelletized in line. The pellets were dried in an oven overnight at 75°C before being blown into a film.

9.3.2 Soxhlet Extraction Studies

PBAT-TPS graft copolymer was subjected to a Soxhlet Extraction to remove the unreacted PBAT using Dichloromethane (DCM) as the extraction solvent. Around 2-3 grams of the sample was accurately weighed into a cellulose extraction thimble (33 mm x 94 mm) and placed into the thimble holder. The evaporated solvent condensed into the thimble, containing the sample. The extraction was run for 24 hours. After extraction, the thimble along-with the sample was removed and dried to constant weight. FTIR and thermal analysis characterizations were conducted on the film sample obtained by solvent casting the extracted graft copolymer solution.

9.4 PBAT-Maleated thermoplastic starch graft copolymers

In this section, experimental details on maleation of starch using maleic anhydride/maleic acid in presence of glycerol plasticizer by reactive extrusion processing are outlined. Further, characterization techniques pertaining to analysis of MTPS are explained. Finally, experimental details pertaining to the synthesis and characterization of PBAT-MTPS graft copolymers are outlined.

9.4.1 Maleation of starch by reactive extrusion processing

Regular silver medal pearl corn-starch, obtained from Cargill Inc. was reactively modified using maleic anhydride/maleic acid in a twin-screw co-rotating CENTURY extruder with a screw diameter of 30 mm and a L/D ratio of 42. Maleic anhydride/acid (MA) was ground to a fine powder using a mortar and pestle and mixed with the starch (800 gm starch + [20 (2.5 wt %) /40 (5 wt %) /64 (8 wt %) gm] maleic anhydride/acid) using a kitchen blender for 15 minutes before being fed to the feed port of the extruder. Glycerol was mixed with 2,5-bis (tert-butylperoxy)-2,5-dimethylhexane (Lupersol 101) {200 gm glycerol + 1.6 gm Lupersol 101} and pumped to the extruder using a peristaltic pump. The relative rates of the starch/MA mixture to the glycerol/Lupersol 101 mixtures were maintained at 80:20. Vacuum (using water jets) was applied at the vent port to remove the unreacted maleic acid/water mixture. Due to the low viscosity of the extruded strand, MTPS was collected in aluminum pans and ground to a fine powder. Ground MTPS was stored in an oven at 50°C. The extrusion processing conditions were the same as outlined earlier in section 9.3.1 on the preparation of PBAT-TPS graft copolymers.

9.4.2 Synthesis of PBAT-MTPS graft copolymers by reactive extrusion processing

The synthesis of PBAT-MTPS graft copolymers was accomplished in a twin-screw co-rotating CENTURY extruder. MTPS was produced by reactive plasticization of regular corn-starch using MA modifier and glycerol (20-wt%) plasticizer as explained above. MTPS, previously oven dried overnight at 75°C, was ground to a fine powder and fed using an external feeder to the feed port of the extruder. The feeder rates were adjusted accordingly to obtain a ratio of 70:30 (PBAT: MTPS). The extruded strand was cooled using a water bath and pelletized in line. The pellets were dried in an oven overnight at 75°C before being blown into a film.

9.4.3 Soxhlet Extraction Studies

PBAT-MTPS graft copolymer was subjected to a Soxhlet Extraction to remove the unreacted PBAT using Dichloromethane (DCM) as the extraction solvent. The procedure was as explained in Section 9.3.2. FTIR and thermal analysis characterizations were conducted on the film sample obtained by solvent casting the extracted graft copolymer solution.

9.4.4 Fourier Transformed Infrared Spectroscopy (FTIR) Studies

FTIR analysis was conducted on samples of MTPS and the graft copolymers from 400 cm^{-1} to 4000 cm^{-1} using a Perkin Elmer Model 2000 FTIR. MTPS was extracted using THF in a Soxhlet extraction unit to remove the unreacted maleic anhydride and maleic acid, dried and ground to a fine powder. 1% MTPS was mixed with 99% KBr powder and pressed using a pellet maker to a fine transparent disk. This disk was directly put into

the sample holder in FTIR to obtain the spectrum. Films obtained by solvent casting the graft copolymer solution were directly introduced into the sample chamber to obtain the FTIR spectrum of the graft copolymer.

9.4.5 Thermal Analysis Studies

A high resolution Differential Scanning Calorimeter (DSC) 2920 from TA Instruments was used to determine the thermal transitions of the MTPS and the graft copolymer samples. Nitrogen was used as the purge gas at 50 ml/min. MTPS samples were heated to 200°C at the rate of 10°C per minute, cooled to -50°C and then reheated to 200°C. 2nd scan data was taken for analysis. The same procedure was followed for the graft copolymer samples.

A high resolution Thermal Gravimetric Analyzer (TGA) 2950 from TA Instruments was used to determine the degradation temperature of the MTPS and the graft copolymer samples. Air was used as the purge gas with the sample purge being 60 ml/min and the Nitrogen balance purge being 40 ml/min. The samples were heated to 550°C at the rate of 20°C per minute.

9.4.6 Intrinsic Viscosity Studies

The intrinsic viscosity of starch, TPS and the MTPS samples were determined using a Cannon Ubbelohde viscometer (size 0B) in DMSO solvent at 25°C.

9.4.7 Nuclear Magnetic Resonance (NMR) Studies

TPS and MTPS (after extracting the unreacted MA using acetone) were dissolved in deuterated dimethyl sulfoxide (DMSO-d₆) (on heating). ¹H-NMR spectra on the TPS and

MTPS were obtained using a Varian INOVA 300 MHz spectrometer using a 30° pulse. 24 scans were acquired for each sample.

9.4.8 Environmental Scanning Electron Microscopy (ESEM)

An environmental scanning electron microscope (Phillips Electroscan 2020) was used to observe the cryofractured surface of the resins as well as the surface morphology of the starch foams. The samples were submerged in liquid nitrogen and then fractured with a pestle in a mortar. They were then mounted on aluminum stubs, and the cryo-fractured surface was observed under the microscope to study mode of fracture.

9.4.9 Wide Angle X-ray Scattering

X-ray diffraction analysis was performed with a Rigaku Rotaflex Ru-200BH X-ray diffractometer operated at 45 KV, 100 mA with a nickel filtered Cu K_α radiation and a θ compensating slit. Data was acquired in 0.02° 2 θ , at the rate of 1°/minute. The basal spacing of the silicate layer of the nano-scale clay, d , was calculated using the Bragg's equation, $\lambda = 2d\sin\theta$ (λ (CuK_{α1}) = 0.15406 nm). Samples were used in the form of a powder or in the form a film as obtained by blown film extrusion. The samples were equilibrated in a constant environment room at 23 ± 1°C and 50 ± 2% RH for at least 72 hours before testing.

9.4.10 Blown Film Studies

Films of the graft copolymers made from both TPS and MTPS were made using a Killion single-screw blown film unit. The screw diameter was 25.4 mm with L: D ratio of 25:1.

The die inner diameter was 50.8 mm with a die gap size of 1.5 mm. The blown film processing conditions are shown in Table 9.1.

Table 9.1 Blown Film Processing Conditions for Polyester-Starch graft copolymers

	Die 3	Die 2	Die 1	Adaptor	Clamp Ring	Zone 3	Zone 2	Zone 1
Set (⁰ F)	70	350	355	360	360	395	395	300
Actual (⁰ F)	73	351	358	357	360	380	395	300

Melt (⁰ F)	364
Screw Speed (RPM)	12.4
FPM (ft/min)	5-6
Pressure (psi)	500-1000

9.4.11 Determination of the Mechanical Properties of the Films

Tensile properties of the films were determined using UTS Mechanical Testing Equipment Model SFM-20 fitted with a 100 lbs load cell. The crosshead speed was 20 inches per minute. Rectangular film samples, 4 inches x 1 inch dimension were conditioned at 23°C and 50% Relative Humidity for 48 hours before being tested according to ASTM D-882 testing.

9.5 Results and Discussion

The results of the various aspects of PBAT-TPS and PBAT-MTPS graft copolymers discussed in previous sections will be presented. Trans-esterification reaction chemistry leading to the synthesis of a graft copolymer will be explained. Soxhlet extraction results of PBAT-TPS graft copolymers along with the FTIR analysis and TGA results confirming the existence of a graft copolymer will be discussed. Mechanical properties of films, produced by blown film processing will be presented and discussed. Processing and characterization results of MTPS will be evaluated. Finally, results pertaining to synthesis and characterization of PBAT-MTPS graft copolymers will be discussed.

9.5.1 PBAT-TPS graft copolymers

9.5.1.1 Proposed Trans-esterification Reaction Chemistry in the Synthesis of PBAT-TPS graft copolymers

The proposed acid-catalyzed trans-esterification reaction chemistry is shown in Figure 9.3. Acid catalyzed esterifications cause significant degradation of the starch. In this particular case, it would be expected to cause hydrolysis of the polyester in addition to the starch.

9.

Th

T.

co

th

are

ext

Ho

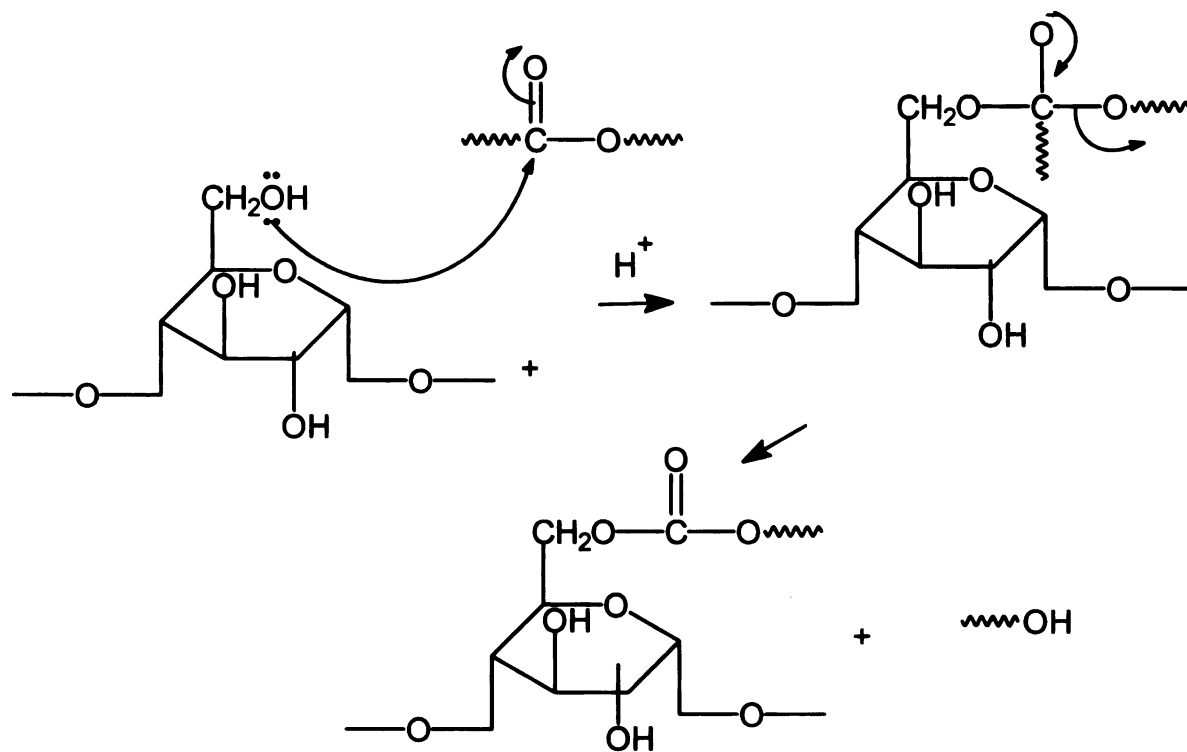


Figure 9.3 Proposed Acid-catalyzed trans-esterification chemistry in the synthesis of PBAT-TPS graft copolymers.

9.5.1.2 Proof of Grafting by Soxhlet Extraction

The aim of the extraction was to selectively remove the unreacted PBAT from the PBAT-TPS graft copolymers. However, after 24 hours of extraction, the graft copolymer was completely extracted out and the solution in the round-bottomed flask was murky. When this solution was cast, a transparent film was obtained. This proves that PBAT and TPS are covalently linked. It is this covalent bonding which makes the graft copolymer extractable in Dichloromethane (solvent wherein PBAT is soluble, but TPS is not). However, due to the insolubility of TPS in the solvent, the graft copolymer forms a

colloidal dispersion and not a clear transparent solution. The Soxhlet extraction results of PBAT-TPS graft copolymers are shown in Table 9.2. From Table 9.2, it is clear that when maleic acid is not used as a catalyst, no reaction occurs, which is confirmed by the fact that the amount of polyester (PBAT) extracted is close to the amount of polyester initially present in the blend. This proves that the TPS component in the blend is not attached covalently and only acts as particulate filler. However, for a PBAT/TPS/Maleic acid system, 97% of the material taken is extracted out, suggesting complete reaction and formation of covalent linkages between the ester functionalities in the PBAT backbone and hydroxyl groups in TPS.

Table 9.2 Soxhlet Extraction results of PBAT-TPS graft copolymers

System	Polyester (PBAT) initially present (gm)	Starch component (Granular starch or thermoplastic starch) initially present (gm)	Amount extracted (gm)	Percent extracted (%)
PBAT/TPS (70/30; w/w)	1.2075	0.5175	1.2595	73
PBAT/TPS/Maleic acid (70/29/1)	1.3812	0.5722	1.9074	97

9.5.1.3 Proof of Grafting by FTIR Analysis

The extracted PBAT-TPS graft copolymer solution was cast into a film and the FTIR spectrum is shown in Figure 9.4.

From Figure 9.4, it can be observed that the graft copolymer exhibits the carbonyl stretch peak at 1720 cm^{-1} , similar to pure PBAT and the extracted PBAT/TPS blend. Further, the ester C-O stretch at 1270 cm^{-1} is observed in the graft copolymer but not in TPS. The graft copolymer also exhibits a peak between $3200\text{-}3400\text{ cm}^{-1}$ corresponding to -OH stretch. This peak is also observed in TPS, but not in the other two. Moreover, primary alcohols peak ($1025\text{-}1060\text{ cm}^{-1}$) is seen in TPS and the PBAT-TPS graft copolymer, but not in the other two. All of the above data confirm the true existence of a graft copolymer. Finally, δ (O-H) bend of water at 1640 cm^{-1} is observed in TPS and not in any of the other materials.

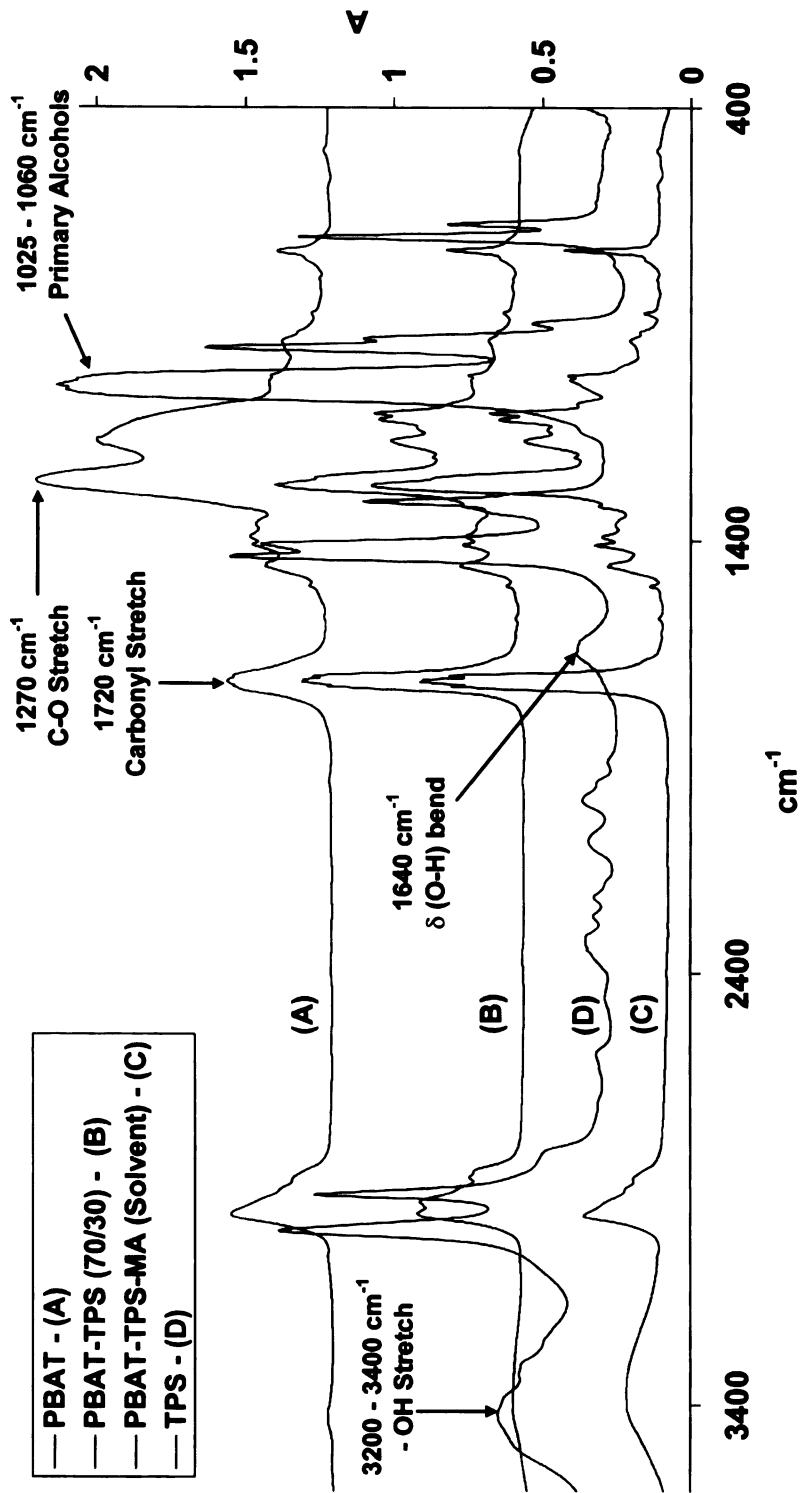


Figure 9.4 FTIR Spectrum of PBAT-TPS graft co-polymers

9.5.1.4 Proof of grafting by Thermal Gravimetric (TGA) Analysis

The TGA results of solvent cast films of extracted PBAT-TPS graft copolymers are shown in Figure 9.5 as shown below.

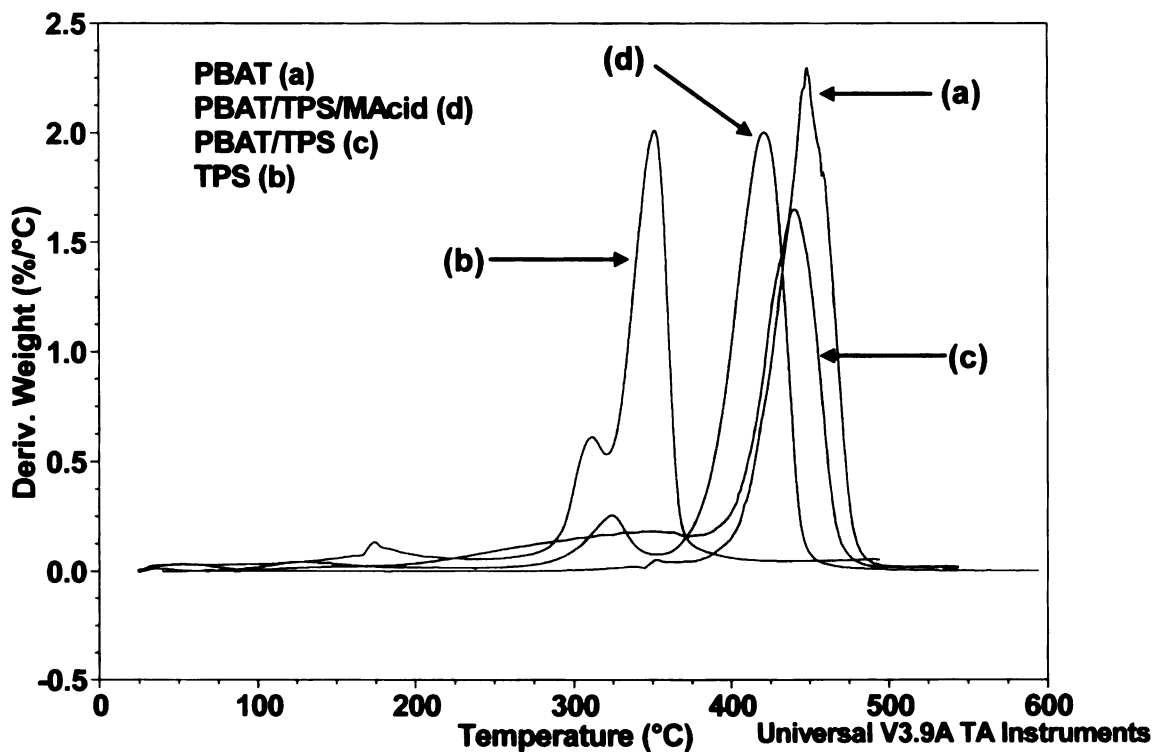


Figure 9.5 TGA Results of PBAT-TPS graft copolymers

From Figure 9.5, it is worthwhile to note that without the addition of maleic acid as a trans-esterification catalyst, i.e. for the PBAT/TPS blend, no degradation corresponding to starch is observed from the extracted portion, confirming the fact that only the unreacted polyester is extracted out. However, for the PBAT-TPS graft copolymer, starch

degradation along-with the polyester (PBAT) is evident. This confirms the existence of a graft copolymer wherein the PBAT polyester is covalently bonded to TPS.

9.5.1.5 Mechanical Properties Results

The tensile property results of PBAT-TPS graft copolymers in the Machine and Transverse directions are shown in Tables 9.3 and 9.4 respectively.

Table 9.3 Tensile Strength, Modulus of Elasticity, Break Elongation of PBAT-TPS Graft Copolymer (Machine Direction)

Entry	Sample	Tensile Strength (psi)	Modulus of Elasticity (psi)	Break Elongation (%)
1	PBAT	5600	20000	600
2	PBAT/TPS/MA (70/29/1)	980	6000	500
3	Low Density Polyethylene (LDPE)	2000	33000	450

Table 9.4 Tensile Strength, Modulus of Elasticity, Break Elongation of PBAT-TPS Graft Copolymer (Transverse Direction)

Entry	Sample	Tensile Strength (psi)	Modulus of Elasticity (psi)	Break Elongation (%)
1	PBAT	3000	8000	500
2	PBAT/TPS/MA (70/29/1)	900	5000	350
3	Low Density Polyethylene (LDPE)	-	-	-

It was observed from Tables 9.3 and 9.4 that the tensile strength values of PBAT-TPS graft copolymer, containing around 30% TPS, exhibited almost a six fold decrease as compared to pure PBAT polyester values. This reduction in tensile strength could be attributed to two reasons:

- Addition of TPS, which possesses poor properties
- Reduction in the molecular weight of PBAT due to acid hydrolysis, catalyzed by maleic acid.

The tensile strength values of the graft copolymer were lower than even LDPE values.

Moduli of elasticity results also followed the same trend as the tensile results. It was observed that the modulus values of the graft copolymer were lower than both LDPE and pure PBAT. Break elongation values of the graft copolymer were, however, slightly

higher than LDPE. This was probably due to the chemical covalent linkages, which enable stretching.

9.5.2 Maleated Thermoplastic Starch (MTPS)

This section presents the chemistry and results on reactive extrusion processing of MTPS followed by the subsequent characterization. Characterization techniques include FTIR, Thermal Analysis and Intrinsic viscosity measurements.

9.5.2.1 Proposed Starch Maleation chemistry

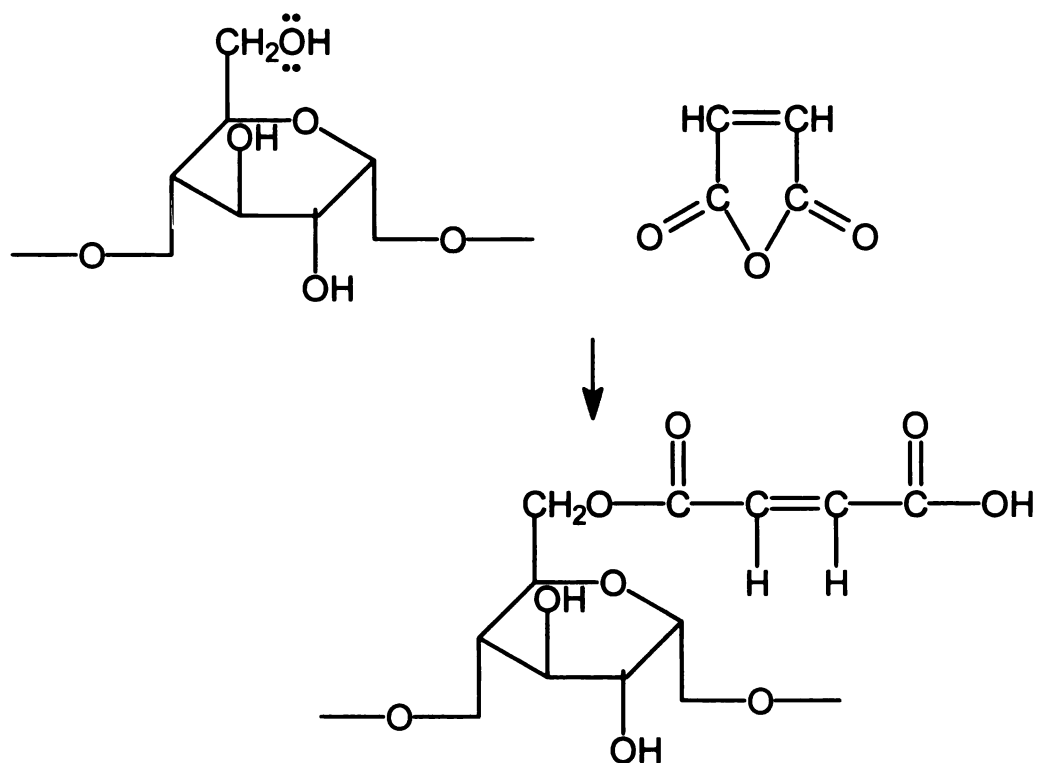


Figure 9.6 Proposed Chemistry for Maleation of starch using maleic anhydride

The maleation of starch using maleic anhydride is shown in Figure 9.6. Alternatively, maleic anhydride could react with water to form maleic acid, which could further react with starch to form the starch maleate. During the process of maleation, there is a reduction in the molecular weight of starch due to the hydrolysis of the starch backbone in the presence of maleic acid.

9.5.2.2 Results on reactive extrusion processing of MTPS

The reactive modification of regular corn- starch using maleic anhydride and maleic acid was accomplished in a twin-screw co rotating CENTURY extruder using glycerol as the plasticizer (20-wt%) and optional Lupersol 101 as a free radical initiator. When compared to regular TPS production, the value of torque in the synthesis of MTPS was very low (due to the reduction in molecular weight) due to the acid hydrolysis of starch in the presence of maleic acid. This reduction in molecular weight lead to decrease in melt viscosity values of MTPS. Due to this, reactive maleation processing could be done at much higher throughputs as compared to the regular thermoplastic processing of starch. Moreover, difficulties in regular corn- starch plasticization, such as, foaming at high throughputs or clogging near the die were prevented during the synthesis of MTPS. However, MTPS was difficult to pelletize due to its reduced viscosity and hence use of cooled rollers to convey the strand is recommended. These collected strands were then pulverized to form MTPS powder.

Nano-clay was introduced in the production of MTPS using two different techniques. In the first method, clay was mixed with the regular corn starch, and then fed into the feed-hopper of the extruder. In the other method, clay was mixed with glycerol in the required

amounts, and set for approximately 15 hours to induce some swelling in the clay, which would result in the separation of the clay galleries.

The MTPS, MTPS – nano-clay thus obtained were subsequently reacted with the aliphatic aromatic copolyester PBAT to develop reactive blends for film and foam-aid applications. Nano-clay was introduced to improve the mechanical properties and the water-vapor barrier of the PBAT-g-TPS/MTPS based products. The amount of clay added was so adjusted to maintain a final composition of 1% nano-clay in the PBAT-g-MTPS reactive blend. The formulations were made in such a way that the final nano-composite for the blown film application would have 70 parts by weight of PBAT, 30 parts by weight of MTPS, and 1 part by weight of nano-clay (introduced in the production of MTPS). In this way, the ratio of PBAT to starch would remain the same irrespective of the amount of clay added. Thus, the actual percent of starch or PBAT varied slightly.

9.5.2.3 Proof of reaction of maleic anhydride and maleic acid onto starch by FTIR

Analysis

MTPS samples made using maleic anhydride and maleic acid were extracted in THF solvent. Samples from the thimble and solvent (after evaporation of THF) were analyzed. FTIR results of MTPS samples using maleic acid and maleic anhydride are shown in Figures 9.7 and 9.8 respectively.

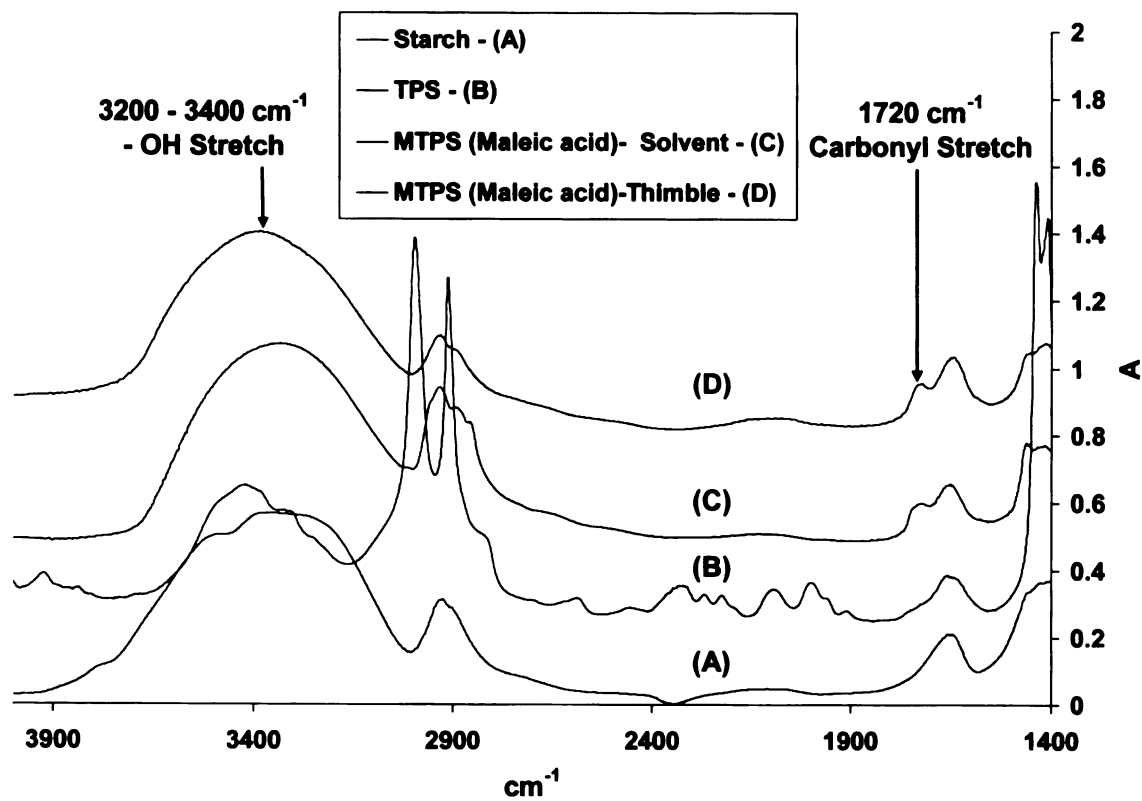


Figure 9.7 FTIR results of MTPS samples using maleic acid modifier

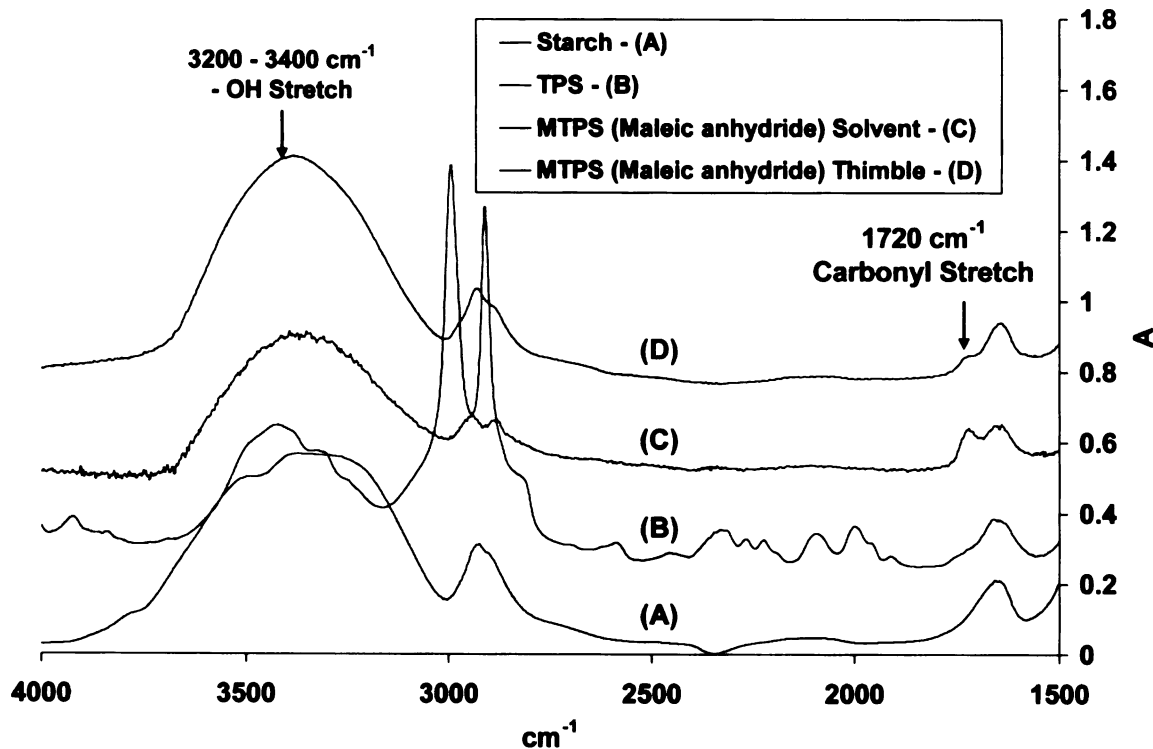


Figure 9.8 FTIR results of MTPS samples using maleic anhydride modifier

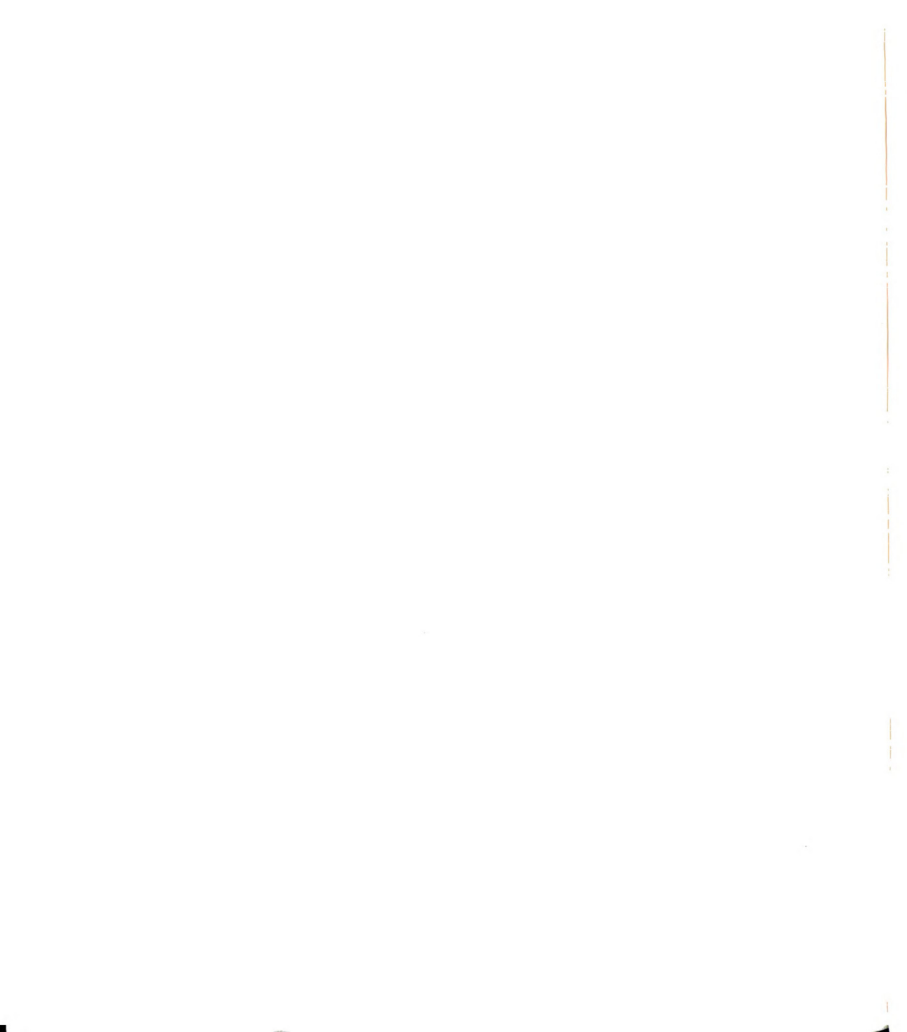
From Figure 9.7 and Figure 9.8, it could be observed that samples from the thimble and the solvent exhibited the carbonyl stretch peak at 1720 cm^{-1} . This was not observed in either the pure granular starch or TPS. This proved that the maleic acid and maleic anhydride were covalently linked to the starch backbone. Moreover, from Figure 9.8, since the MTPS samples showed no peaks at 1780 cm^{-1} corresponding to ring anhydride, it is suggested that the maleic anhydride ring was open. This is expected due to the presence of moisture during extrusion. Further, -OH stretch peak between $3200 - 3400 \text{ cm}^{-1}$ was observed in all the four samples.

9.5.2.4 Thermal Analysis Results

DSC results of MTPS are shown in Figure 9.9. From Figure 9.9, it can be observed that no melting for starch was observed. This is evident as starch degraded before it melted. However, plasticizers in the presence of heat and shear break the hydrogen bonds in starch and destroy the crystalline nature. Thus, a broad melting endotherm was observed in TPS, while two sharp melting endotherms were observed in MTPS. This was attributed to the maleation of starch leading to segments having slightly different melting characteristics. The melting temperatures of MTPS were around 153°C MTPS and were around 10°C higher than TPS. TGA results are shown in Figures 9.10 and 9.11.

From Figure 9.10, it can be observed that TPS and MTPS were both more stable than starch. Also, MTPS showed a slightly higher thermal stability than TPS. At a temperature of approximately 350°C, while 66% of TPS had degraded respectively, only 58% of MTPS had degraded. Further, TPS and MTPS showed additional degradation due to glycerol.

From Figure 9.11, it can be observed that all the MTPS samples showed the derivative peak for the degradation of glycerol. Further, MTPS samples modified with 5 and 8% maleic acid showed two peaks in the derivative curve for the degradation of starch as opposed to one peak shown by MTPS modified with 2.5% maleic acid. This was due to the fact that increased maleation lead to the development of fractions having varied degradation characteristics.



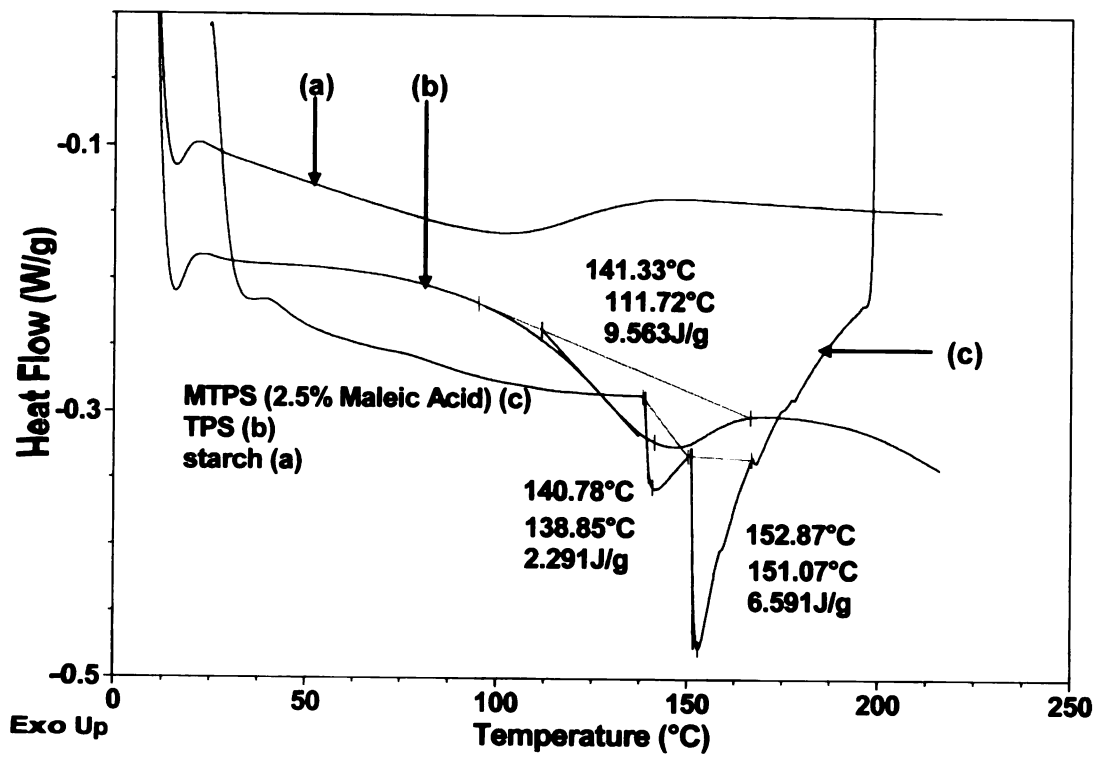


Figure 9.9 DSC Results of MTPS samples

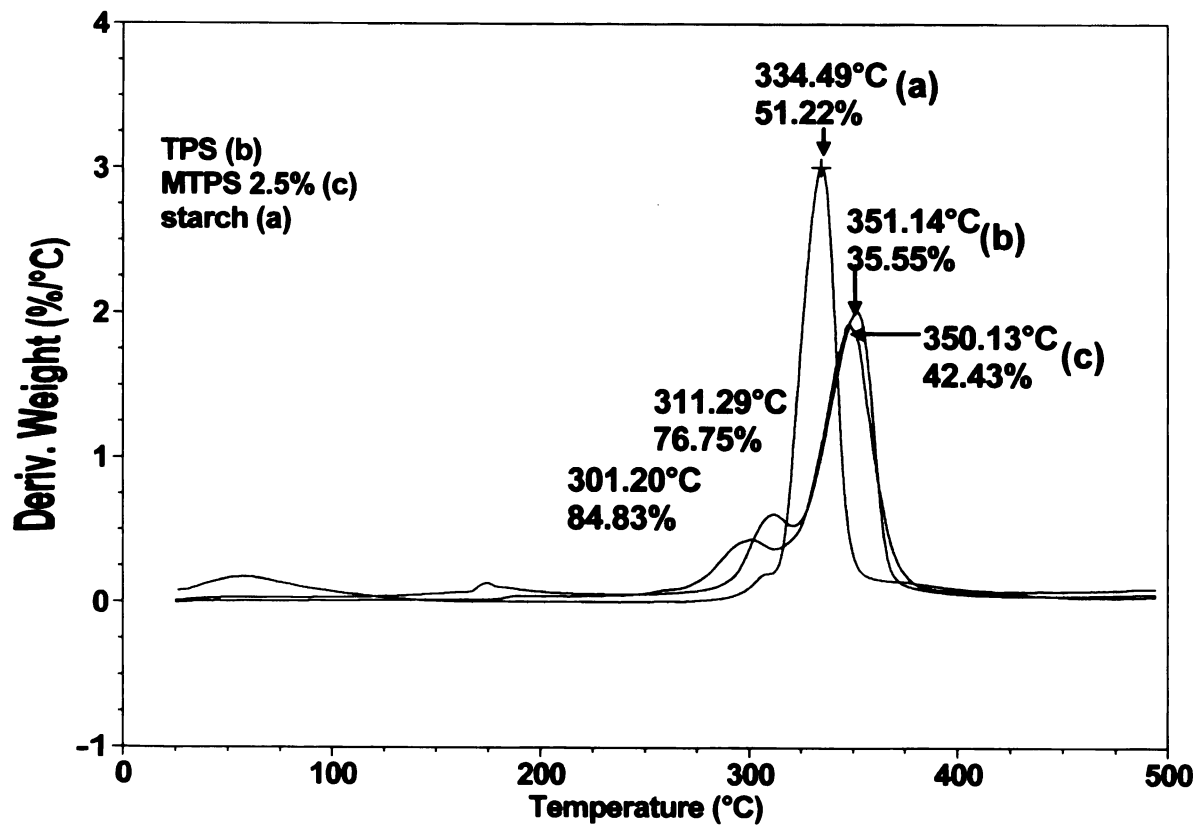


Figure 9.10 TGA Results of MTPS samples

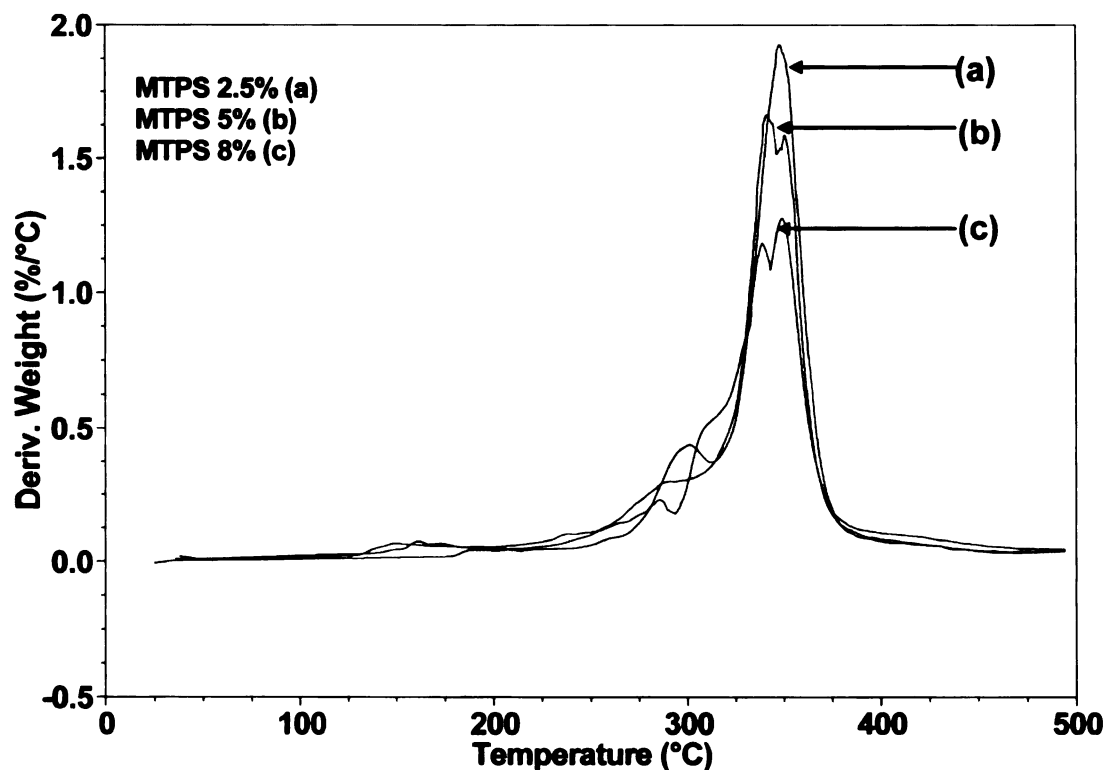


Figure 9.11 TGA Results of MTPS samples modified with 2.5%, 5% and 8% maleic acid

9.5.2.5 Intrinsic viscosity Results

The **intrinsic** viscosity of starch, TPS, MTPS (2.5% maleic anhydride), MTPS (2.5% maleic anhydride, 0.1% Lupersol 101), MTPS (5% maleic anhydride) and MTPS (8% maleic anhydride) were determined in dimethyl sulfoxide (DMSO) solvent and are shown in Figures 9.12 to 9.17 respectively. The intrinsic viscosity of starch (Figure 9.12) was

around 1.6 dl/g while that of TPS (Figure 9.13) reduced to 1.2 dl/g. However, on maleation using 2.5% maleic anhydride, the intrinsic viscosity of MTPS (Figure 9.14) drastically dropped to 0.27 dl/g. This reduction is attributed to a decrease in molecular weight due to the hydrolysis of starch in the presence of maleic acid at the α -1, 4 linkage point. The intrinsic viscosity further reduced to 0.24 dl/g in the presence of 5% MA (0% L101) (Figure 9.15), and 0.18 dl/g with 8% MA (0% L101) (Figure 9.16). However, on addition of Lupersol 101, the intrinsic viscosity (Figure 9.17) slightly increased back to 0.32 dl/g. This increase can be attributed to cross-linking reactions taking place, increasing the molecular weight slightly.

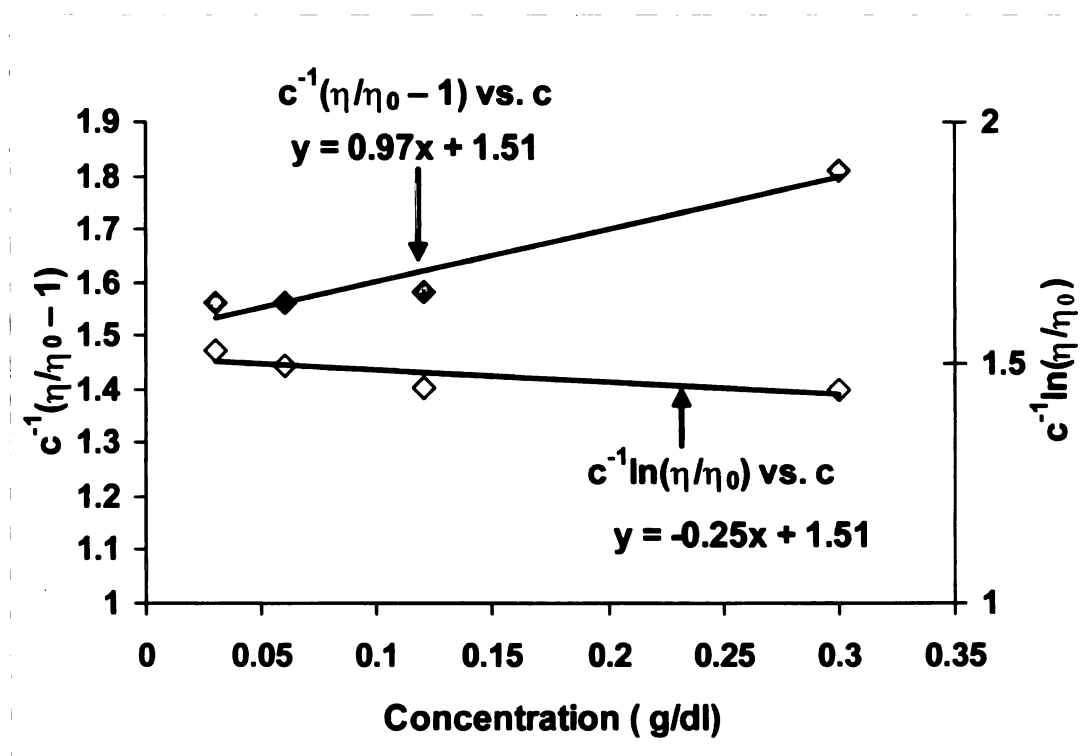


Figure 9.12 Intrinsic viscosity of regular corn starch

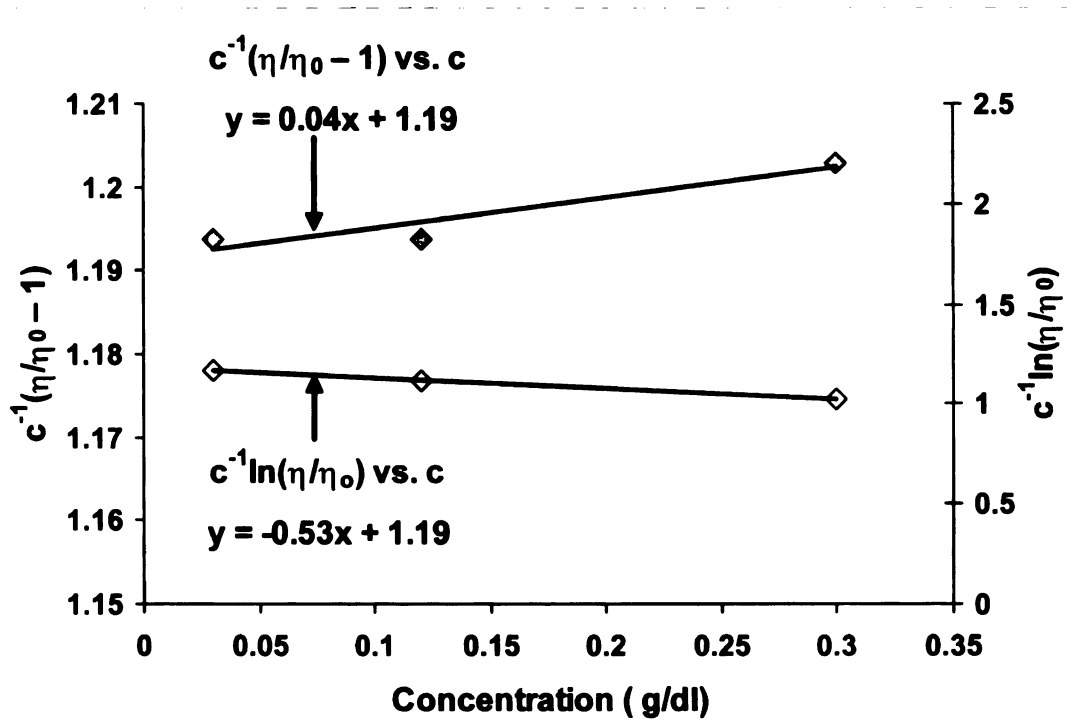


Figure 9.13 Intrinsic viscosity of TPS

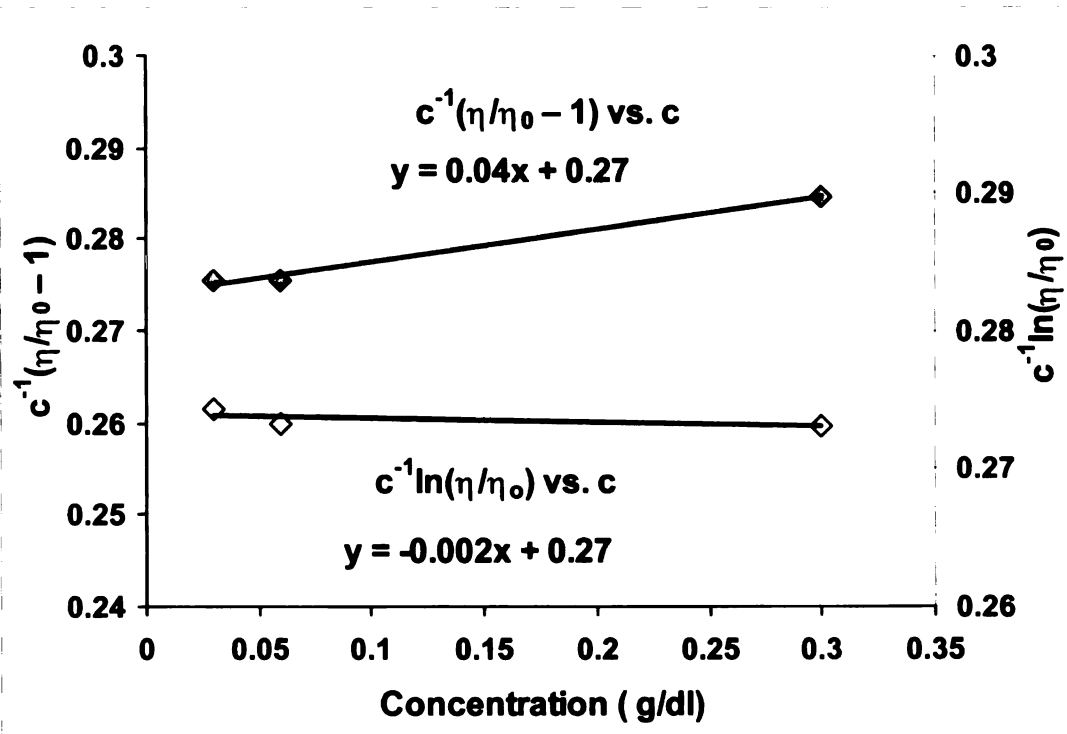


Figure 9.14 Intrinsic viscosity of MTPS (2.5% Maleic anhydride)

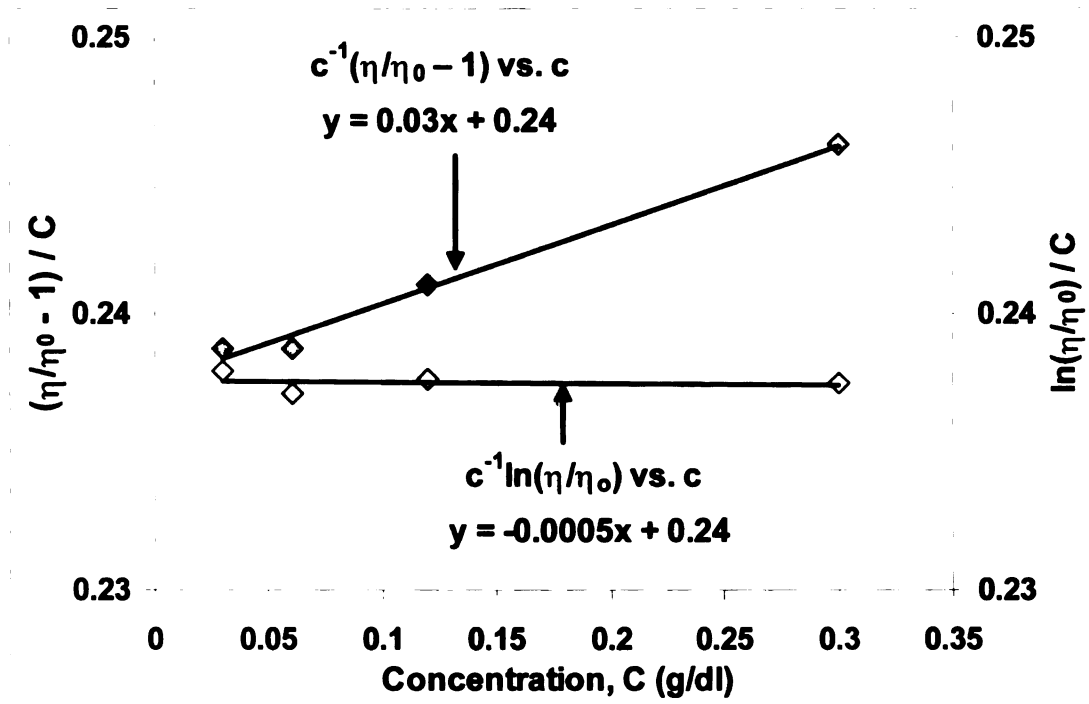


Figure 9.15 Intrinsic viscosity of MTPS (5.0% Maleic anhydride)

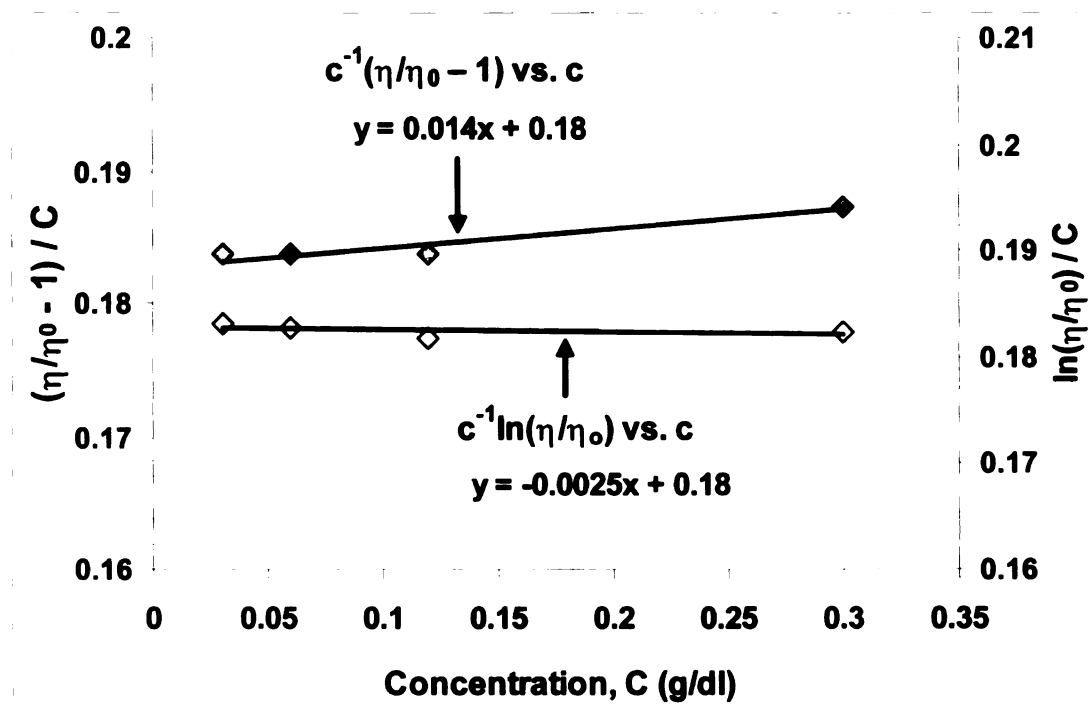


Figure 9.16 Intrinsic viscosity of MTPS (8.0% Maleic anhydride)

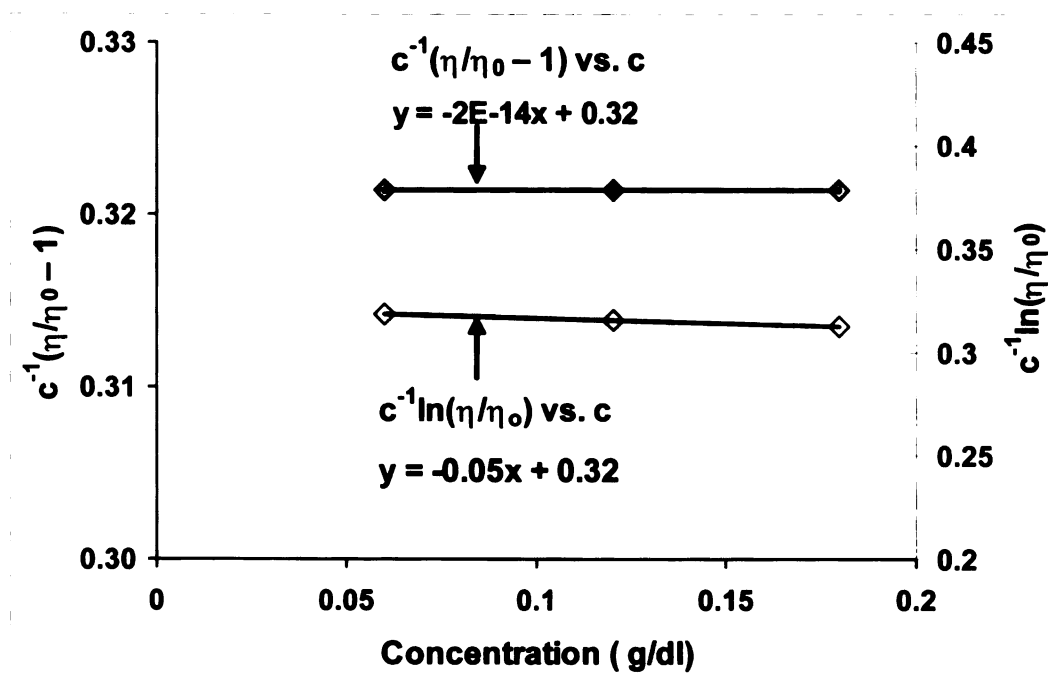


Figure 9.17 Intrinsic viscosity of MTPS (2.5% Maleic anhydride and 0.1% L 101)

9.5.2.6 NMR Results of TPS and MTPS in (DMSO-d₆)

TPS and MTPS (after extracting the unreacted MA using acetone) were dissolved in deuterated dimethyl sulfoxide (DMSO-d₆) (on heating). NMR spectra for TPS and MTPS are shown in Figures 9.18 and 9.19. the anhydroglucose equatorial band could be seen at about 5.1 ppm. MTPS exhibited two new bands at 5.3 ppm and 6.4 ppm due to the two non-equivalent protons from C=C of the mono-substituted maleate (only one carboxyl end-group has reacted with the starch hydroxyl), while the band at 6.1 ppm was due to the two equivalent protons on the C=C of the di-substituted maleate (both the carboxyl end-groups of the maleic acid entity have reacted with the starch hydroxyls).

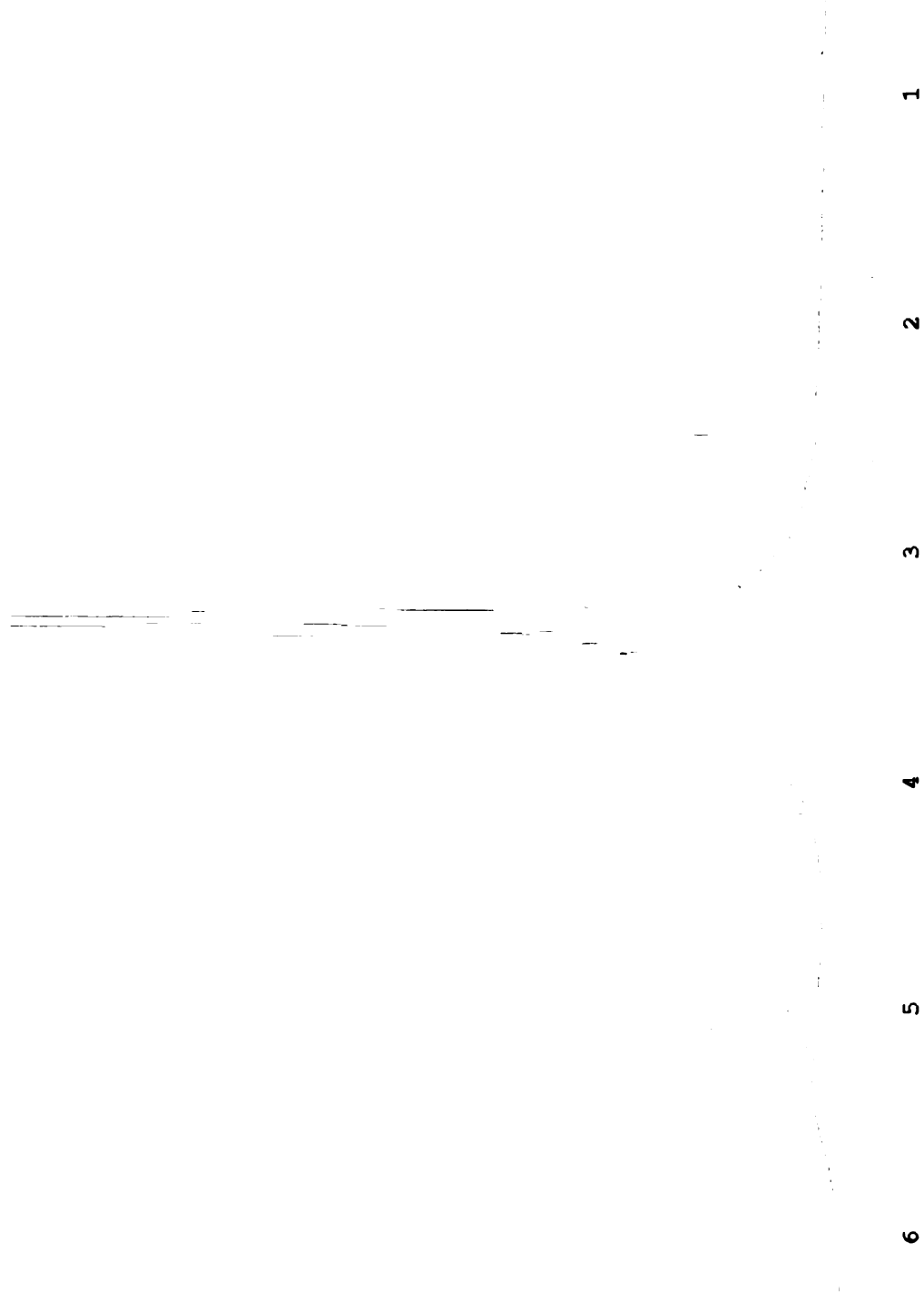


Figure 9.18 NMR Spectrum for Thermoplastic Starch (TPS)

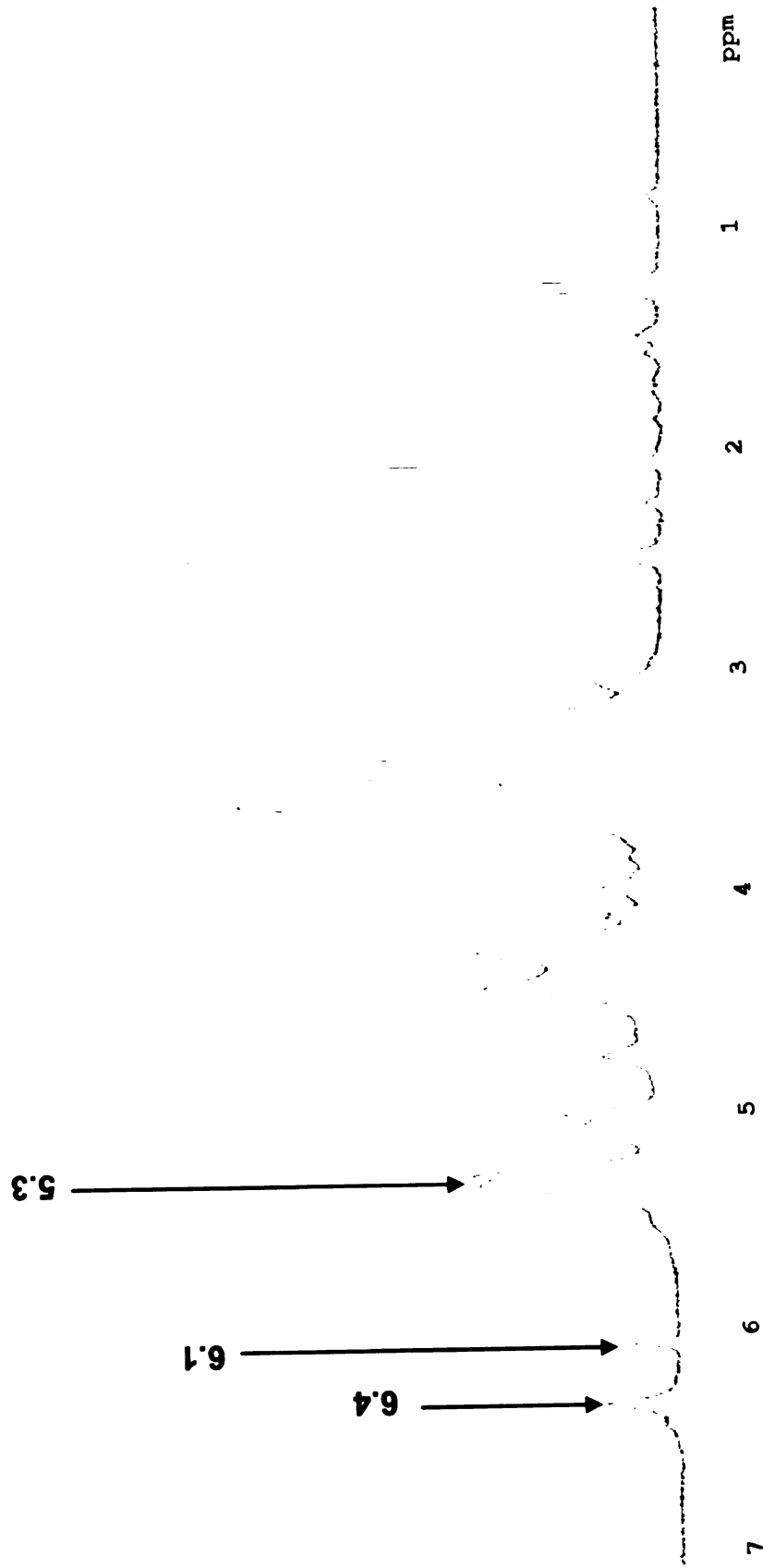


Figure 9.19 NMR Spectrum for Maleated Thermoplastic Starch (MTPS) using 8% MA

9.5.3 PBAT-MTPS graft copolymers (unfilled & nano-clay filled)

MTPS produced as described in the previous section would be reactively blended with the aliphatic-aromatic copolyester PBAT to form a PBAT-g-MTPS copolymer using the grafted maleic acid moiety or the unreacted maleic acid as the transesterification catalyst. This graft copolymer would be used for blown-film applications as well as a functional aid in the production of starch-based foams. MTPS-nanoclay produced would also be reactively blended with PBAT to form nanoclay-filled PBAT-g-MTPS, with improved mechanical, thermal and water-vapor barrier properties. Trans-esterification reaction chemistry leading to the synthesis of PBAT-MTPS graft copolymers will be discussed in this section. The extraction results of PBAT-MTPS graft copolymers will be presented. FTIR analysis of films, produced by solvent casting the extracted graft copolymer solution will be evaluated to confirm reactivity. Other characterization techniques such as Differential Scanning Calorimetry (DSC) and Thermal Gravimetric Analysis (TGA) will be presented. Synthesis of blown films of PBAT-MTPS graft copolymers and the effect of varying blown film pressures for different materials will be discussed. Further, mechanical properties of films made with the graft copolymers will be discussed in this section.

9.5.3.1 Proposed Trans-esterification Reaction Chemistry in the synthesis of PBAT-MTPS graft copolymers

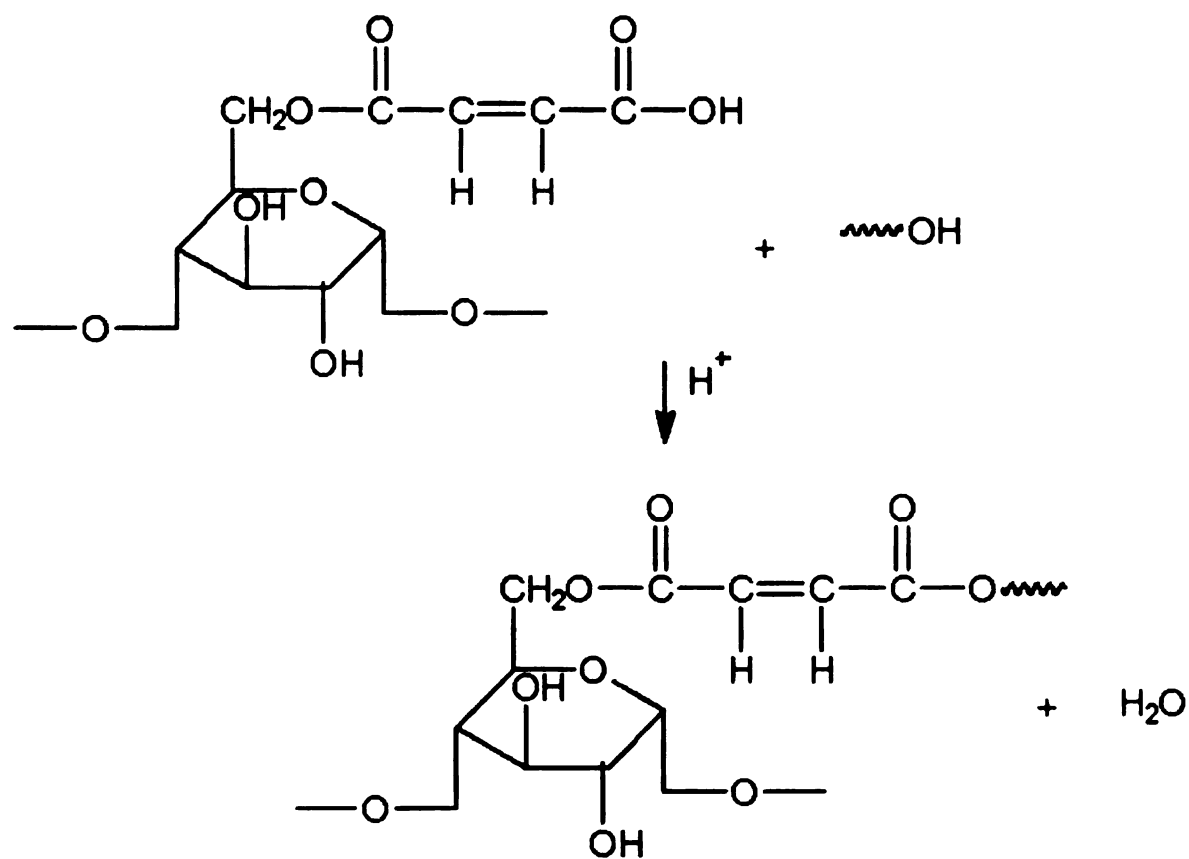


Figure 9.20 Proposed Trans-esterification reaction chemistry in the synthesis of PBAT-MTPS graft copolymers.

Chemistry in the synthesis of PBAT-MTPS graft co-polymers is exactly similar to the one showed in Figure 9.2. However, a further trans-esterification reaction between MTPS and the hydroxy terminated polymer formed is possible and is shown in Figure 9.20.

9.5.3.2 Proof of grafting by Soxhlet Extraction

As explained in section [9.5.1.2](#), the aim of the extraction was to selectively remove the unreacted PBAT from the PBAT-MTPS graft copolymers. The Soxhlet extraction results of PBAT-MTPS graft copolymers are shown in Table 9.5. As seen from Table 9.5, almost complete extraction was achieved for PBAT/MTPS (70/30 and 60/40) graft copolymers. When this solution was cast, a transparent film was obtained. This proved that PBAT and MTPS were covalently linked making the graft copolymer extractable in Dichloromethane (solvent wherein PBAT is soluble, but TPS is not). However, due to the insolubility of MTPS in the solvent, the graft copolymer formed a colloidal dispersion and not a clear transparent solution. However, for the 50/50 and 40/60 blends, only 47% and 38% respectively (close to the respective PBAT amount) were extracted out. This was probably due to the fact that an inversion in phase morphology was obtained. Thus, the reaction was also dependent on the relative amounts of the polyester and MTPS phases present. Also, from Table 9.5 (Row 6), it is clearly seen that when TPS was used instead of MTPS, there was very minimal or no reaction taking place. This suggested that the reaction between the hydroxyl groups in starch and the ester functionalities in PBAT occurred only in the presence of a trans-esterification catalyst such as maleic acid.

Table 9.5 Soxhlet Extraction results of PBAT-MTPS graft copolymers

No.	System	Polyester (PBAT) initially present (gm)	Starch component (TPS or MTPS) initially present (gm)	Material extracted (gm)	% Extracted
1	PBAT/MTPS (70/30;w/w)	1.3510	0.579	1.8878	98
2	PBAT/MTPS (60/40;w/w)	1.0682	0.7122	1.7010	96
3	PBAT/MTPS (50/50;w/w)	0.7998	0.7998	0.7503	47
4	PBAT/MTPS (40/60;w/w)	0.8639	0.5759	0.5513	38.2
5	PBAT/MTPS (70/30;w/w) [0.1% Lupersol 101]	1.9018	0.8150	2.6530	98
6	PBAT/TPS (70/30;w/w)	1.2075	0.5175	1.2595	71

9.5.3.3 Proof of grafting by FTIR Analysis

The extracted PBAT-MTPS graft copolymer solution was cast into a film and the FTIR spectrum is shown in Figure 9.21.

From Figure 9.21, it can be observed that the PBAT-MTPS graft copolymer exhibits the carbonyl stretch peak at 1720 cm^{-1} , similar to pure PBAT. Further, the ester C-O stretch at 1270 cm^{-1} is observed in the graft copolymer but not in granular corn starch. The graft copolymer also exhibits a peak between $3200\text{-}3400\text{ cm}^{-1}$ corresponding to -OH stretch. This peak is also observed in corn starch, but not in the other two. Moreover, primary alcohols peak ($1025\text{-}1060\text{ cm}^{-1}$) is seen in corn starch and the graft copolymers but not in PBAT. All of the above data confirm the true existence of a graft copolymer. Finally, δ (O-H) bend of water at 1640 cm^{-1} is observed in starch and not in any of the other materials.

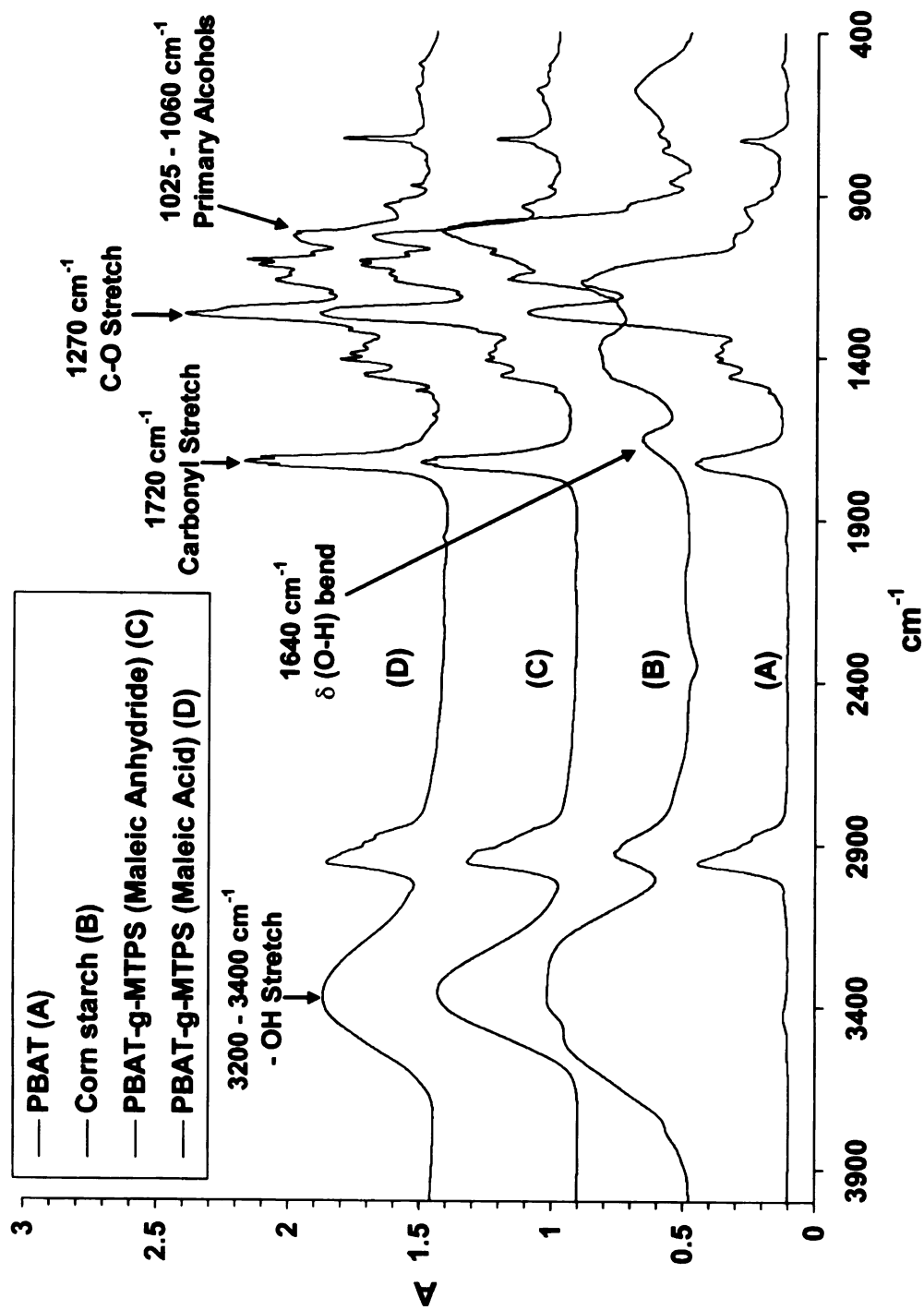


Figure 9.21 FTIR Results of PBAT-MTPS graft copolymers

9.5.3.4 Proof of grafting by Thermal Analysis

DSC and TGA experiments were carried out on solvent cast film samples of the extracted PBAT-MTPS graft copolymer. The results are shown in Figures 9.22 and 9.23 respectively.

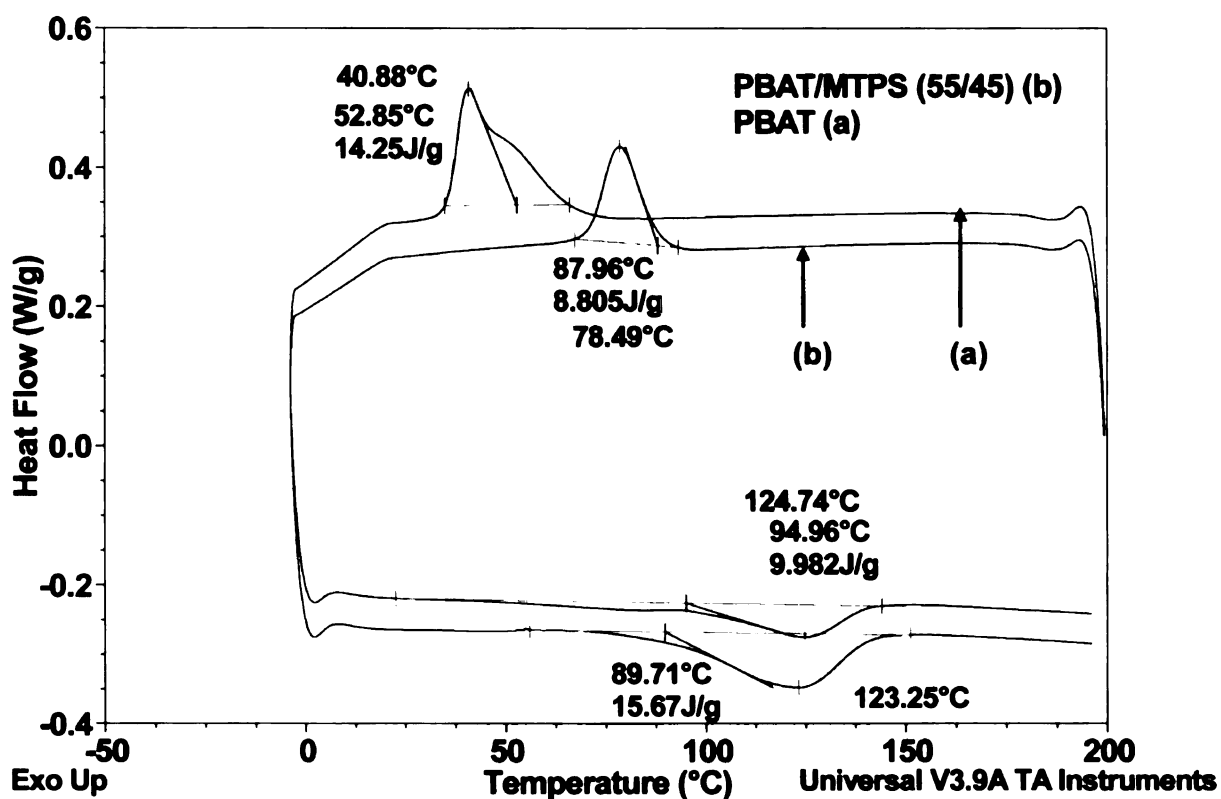


Figure 9.22 DSC Results of PBAT-MTPS graft copolymer

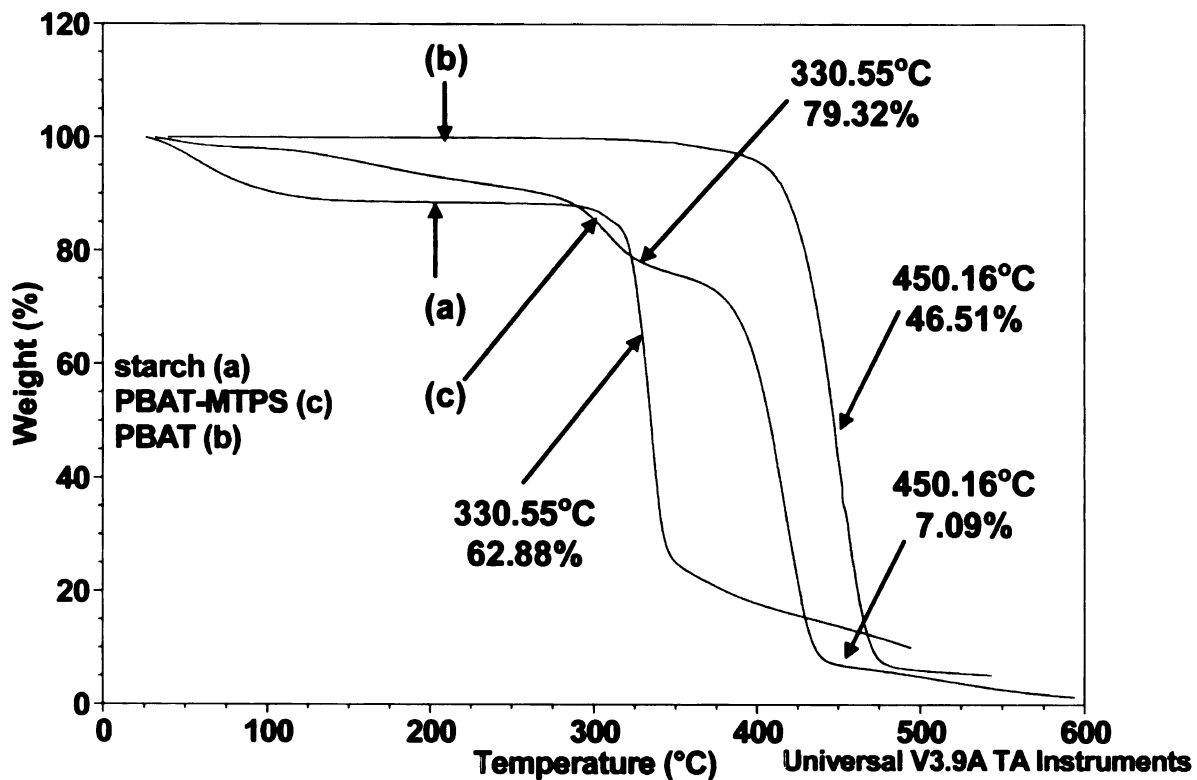


Figure 9.23 TGA Results of PBAT-MTPS graft copolymer

From Figure 9.22, it can be observed that the melting temperature of the PBAT-MTPS graft copolymer is very similar to pure PBAT. However, crystallinity of the graft copolymer reduces as evinced by the area under the melting peak. Thus, the area under the melting peak for pure PBAT is 15.67 J/g while that of PBAT-MTPS graft copolymer is 9.98 J/g. This is expected as the incorporation of starch into the PBAT matrix breaks the orderliness of PBAT bringing down the crystallinity. Moreover, peak crystallization temperature of the graft copolymer (78.49°C) is higher than that of pure PBAT (40.88°C).

This is due to the presence of impurities such as catalyst residues, which act as nucleating agents that fasten the crystallization process.

From Figure 9.23, it is seen that PBAT-MTPS graft copolymer exhibits two degradations; one corresponding to the starch and the other corresponding to PBAT. This further confirms that MTPS is chemically grafted onto PBAT. Further, at a temperature of 330°C, while ~ 80% of the graft copolymer is un-degraded, only 63% of starch is left behind. This is evident as MTPS is more stable than pure granular starch. However at 450°C, while 46% of PBAT is left behind, only 7% of the graft copolymer is left behind.

9.5.3.5 Blown Film Processing Results of PBAT-MTPS graft copolymers

Blown films of the graft copolymers were made using a Killion single screw blown film unit. Temperature profile in the blown film unit, melt pressure, draw rates and blow up ratio are some of the important processing parameters that need to be considered. Melt temperatures greater than 400°C made the bubble raise process difficult. Hence melt temperatures below 350°C were used. At very low (less than 5 ft/min) and very high (greater than 6.5 ft/min) draw rates; the films were either too thick or too thin respectively. This made the bubble unstable, causing it to collapse. Hence, draw rates around 5-6 ft/min were used. Blow up ratio was calculated to be around 2.5-3, similar to LDPE film processing. Blow up ratios higher than 3 led to necking issues during blown film processing, causing the bubble to break and collapse.

9.5.3.6 Mechanical Property Results of PBAT-MTPS graft copolymers

The mechanical properties of PBAT-MTPS graft copolymers (without nano-scale clays); (MTPS was produced using varying maleic anhydride contents in section 9.5.2.2) are tabulated below (Table 9.6). The MTPS was produced using 2.5, 5 and 8 wt% of MA with respect to the weight of the starch used.

Table 9.6 Tensile Strength, Modulus of Elasticity (MoE), Break Elongation of PBAT-MTPS Graft Copolymer (Machine Direction)

Entry	Sample	Tensile Strength (psi)	MoE (psi)	Break Elongation (%)
1	PBAT	5600	20000	600
2	PBAT/TPS/MA (70/29/1)	980	6000	500
3	PBAT-g-MTPS (PBAT:MTPS::70:30) (MTPS with 2.5% MA)	2350	11250	695.5
4	PBAT-g-MTPS (PBAT:MTPS::70:30) (MTPS with 5% MA)	2388.2	11269	699.0
5	PBAT-g-MTPS (PBAT:MTPS::70:30) (MTPS with 8% MA)	2351.5	11334	734.3
6	Low Density Polyethylene (LDPE)	2000	33000	450

Table 9.7 Tensile Strength, Modulus of Elasticity (MoE), Break Elongation of PBAT-MTPS Graft Copolymer (Transverse Direction)

Entry	Sample	Tensile Strength (psi)	MoE (psi)	Break Elongation (%)
1	PBAT	3000	8000	500
2	PBAT/TPS/MA (70/29/1)	900	5000	350
3	PBAT-g-MTPS (PBAT:MTPS::70:30) (MTPS with 2.5% MA)	2110	9900	680
4	PBAT-g-MTPS (PBAT:MTPS::70:30) (MTPS with 5% MA)	2146	10100	675
5	PBAT-g-MTPS (PBAT:MTPS::70:30) (MTPS with 8% MA)	2128	10060	677
6	Low Density Polyethylene (LDPE)	-	-	-

It was observed from Tables 9.6 and 9.7 that the tensile strength values of the graft copolymer were almost half as compared to PBAT (Tables 9.6 and 9.7, Entries 3 – 5). However, the values, though slightly, were higher than LDPE values. The tensile strength of PBAT-TPS graft copolymer using maleic acid/anhydride as the transesterification catalyst was the least (Tables 9.6 and 9.7, Entry 2). It was observed that the melt pressure decreased on increasing the MTPS weight fraction in copolymer. This was attributed to a

reduction in the molecular weight (maleic acid catalyzed acid hydrolysis) of PBAT on reaction with MTPS. The melt pressure was the least for the PBAT-TPS graft copolymer and was lower than PBAT-MTPS graft copolymer for the same TPS and MTPS weight fractions. This was attributed to the increased reactivity of MTPS with PBAT as compared to TPS, leading to stronger covalent linkages and increases melt pressures. This was probably due to the fact that complete homogenization was not achieved in the melt phase due to the high viscosity of the TPS melt, which resulted in a high viscosity ratio between the PBAT and the TPS in the reactive blend. This would result in a coarse phase morphology, and hence, poor properties. The effect of phase morphology on the viscosity ratio is explained in Chapter 7, Section 7.1.1 (Figure 7.1). Since complete homogenization might not have been achieved, the probability of the grafting reaction occurring is lower than that in the PBAT-MTPS blends. The MTPS produced had a much lower melt viscosity than that of TPS, which would result in a viscosity ratio of MTPS to PBAT to be closer to 1, and thus provide more homogeneous blends. Also, blends with finer phase morphologies would be achieved.

Scanning electron micrographs of the base polyester, and its blends with granular starch, TPS (with and without maleic acid) and MTPS were observed to study their phase morphology. Figures 9.24 – 9.28 show the scanning electron micrographs of the cryo-fractured samples of PBAT, PBAT-granular corn starch blend, PBAT-TPS blend, PBAT-*g*-TPS (using maleic acid), and PBAT-*g*-MTPS respectively.

Figures 9.25 and 9.26 exhibit the well-known incompatibility between the starch and PBAT in the form of a distinct interface between the two phases. The granular starch particles are obvious in Figure 9.25, and are of the order of 10- 30 microns in size. The

immiscibility in the PBAT-TPS blends (Figure 9.26) is evident from the phase separation occurring between the PBAT and the TPS phases. In both these cases, the fracture occurs at the interface between the starch and the PBAT phases. However, the dispersion of starch in the polyester matrix is improved in its plasticized form as opposed to in its granular form.

Figure 9.27 shows the cross-section of the PBAT-*g*-TPS using maleic acid catalyzed transesterification. There is an improvement in the phase compatibility between the PBAT and TPS phases due to the grafting reaction occurring in the melt phase. An amphiphilic graft copolymer was obtained with a hydrophobic PBAT end and the hydrophilic starch end.

In Figure 9.28, however, it was observed that the formation of a uniform blend is obtained. In addition to the grafting reaction taking place between the PBAT and MTPS in the presence of the unreacted maleic acid/anhydride, the miscibility between the two phases is also improved due to the matching of viscosities of the participating melts. This viscosity matching leads to a finer morphology of the dispersed phase (MTPS) in the continuous PBAT matrix leading to an increased surface area for the grafting reaction.

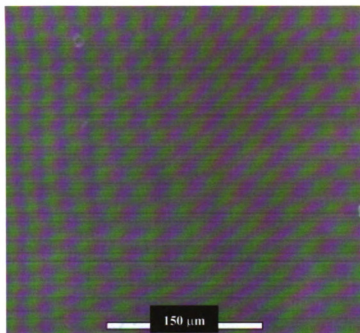


Figure 9.24 Electron Micrograph of the aliphatic-aromatic copolyester PBAT

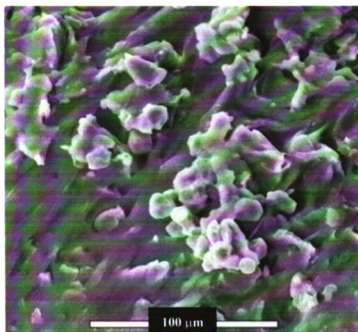


Figure 9.25 Electron Micrograph of the PBAT-Granular Starch blend

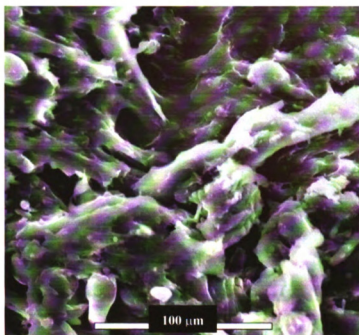


Figure 9.26 Electron Micrograph of the PBAT-TPS blend

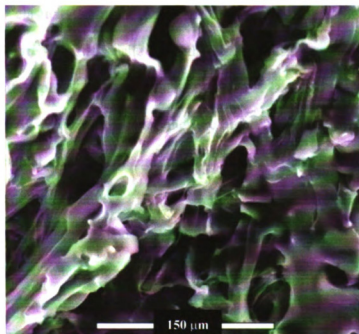


Figure 9.27 Electron Micrograph of PBAT-g-TPS (Maleic Acid catalyst)

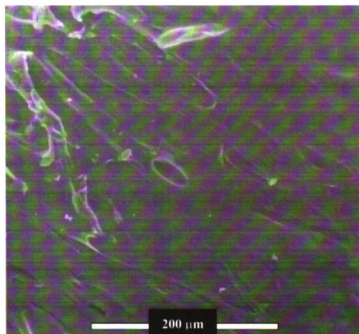


Figure 9.28 Electron Micrograph of PBAT-g-MTPS

The modulus of elasticity values (Tables 9.6 and 9.7) of the graft copolymers also followed the same trend as the tensile strength values. Thus, the modulus of elasticity of PBAT-MTPS graft copolymer is lower than pure PBAT. Break elongation values, on the other hand, of PBAT-MTPS graft copolymer are higher than pure PBAT. This could be attributed to chemical covalent linkages present in the graft copolymer, permitting the elongation of the polymer chains.

It is observed from Tables 9.6 and 9.7 (Entries 3 – 5) that increase in the maleic acid content in MTPS lead to an insignificant change in the tensile strength value. The MTPS produced using higher amounts of maleic acid/anhydride were also expected to have higher amounts of unreacted maleic acid. This unreacted acid could lead to the hydrolysis and, hence, the degradation of the PBAT backbone in the subsequent reactive blending step. It could also lead to an increased chemical reactivity between PBAT and MTPS. In

the production of MTPS, most of the unreacted maleic acid is removed in the vent port of the extruder, during the reactive maleation of starch, and does not get transferred to the next stage of processing. Thus, despite the expected degradation of the PBAT backbone in the presence of increased amounts of maleic acid, the retention of tensile strength value is purely attributed to increased maleation and hence increased chemical reactivity. All the values for the PBAT-g-MTPS copolymer were higher than that for LDPE. The modulus of elasticity values follows the same trend as the tensile strength values. All the values observed were, however, lower than LDPE.

Break Elongation values of the PBAT-g-MTPS graft copolymers were much higher than either pure PBAT or LDPE. Moreover, on increasing maleic acid content in MTPS, the break elongation values increase, though not appreciably. This is again attributed to the enhanced chemical reactivity between PBAT and MTPS.

The tear and puncture properties of PBAT-MTPS (70/30) graft copolymer (MTPS produced using 2.5% maleic acid/anhydride) are explained in Table 9.8 and compared with PE values.

**Table 9.8 Tear and Puncture properties of PBAT-MTPS (70/30) graft
copolymer**

Material	Thickness (in)	Tear (g)	Tear (g)	Puncture	Puncture
		MD	CMD	Max. (lb _f)	Ext. (in)
		ASTM D	ASTM D	ASTM F	ASTM F
		1922	1922	1306	1306
LDPE	0.0010- 0.0015	100-300	-	1.5-3.0	-
PBAT-MTPS (70/30) graft copolymer	0.0010- 0.0015	767.7	802.7	1.52	0.62

It could be observed from Table 9.8 that the tear and puncture properties of PBAT-MTPS (70/30) graft copolymer were comparable or better than LDPE. Tear and puncture are ‘energy related’ properties and hence related to the crystallinity of the polymer. Hence, an improvement in the tear and puncture properties of the graft copolymers, as compared to LDPE, could be attributed to reduced crystallinity. This makes these films a good replacement for LDPE in applications such as lawn and leaf compost bags, retail carryout bags etc.

9.5.3.7 Mechanical Property Results of PBAT-MTPS graft copolymers using Nano-scale Clays

The following Table 9.9 displays the mechanical properties of the PBAT-*g*-MTPS copolymers obtained using MTPS (produced using 8% maleic acid/anhydride). Nano-clay was introduced to improve the mechanical properties and the water-vapor barrier of the PBAT-*g*-MTPS based products. The amount of clay added was so adjusted to maintain a final composition of 1 wt% (based on the total weight) nano-clay in the PBAT-*g*-MTPS reactive blend.

Table 9.9 Tensile Strength, Modulus of Elasticity (MoE), Break Elongation of PBAT-*g*-MTPS Copolymer using 1 wt% Nanoclay (Machine Direction)

No	Sample	Tensile Strength (psi)	MoE (psi)	Break Elongation (%)
1	PBAT	5600	20000	600
2	PBAT- <i>g</i> -MTPS (PBAT:MTPS::70:30) (MTPS with 8% MA)	2351.5	11334	734.3
3	PBAT- <i>g</i> -MTPS (PBAT:MTPS::70:30) (MTPS with 8% MA) (1% Cloisite Na ⁺)	3788	18817	698.4
4	PBAT- <i>g</i> -MTPS (PBAT:MTPS::70:30) (MTPS with 8% MA) (1% Cloisite 30B)	4636.9	21723	800
5	PBAT- <i>g</i> -MTPS (PBAT:MTPS::70:30) (MTPS with 8% MA) (1% Bentone 111)	4666.6	19822	721
6	PBAT- <i>g</i> -MTPS (PBAT:MTPS::70:30) (MTPS with 8% MA) (1% Bentone 166)	3634.4	17533	642.2

It is worth noting that the tensile strengths of the nano-clay filled reactive blends, wherein the clay was not subjected to swelling in glycerol, were in the range of 3000 – 3500 psi, while the break elongations were ~600 – 650%, for all the four types of nano-clays used, and are not reported. The properties reported in Table 9.9 for the PBAT-*g*-MTPS reactive blends involve nano-clay that was subjected to the swelling pre-treatment.

From Table 9.9, it could be observed that the mechanical properties of the clay-filled nano-composites improve substantially on the introduction of 1 wt% of either nano-clay.

In order for the polymer to completely adhere and intercalate the clay or organo-clay tactoids, matching of the surface polarities of the polymer and the clays is crucial (58).

Polar-type interactions are critical for the formation of intercalated or exfoliated nano-composites via polymer melt intercalation (59). Thus, the hydrophilic Cloisite Na⁺ would be expected to be more thermodynamically compatible with the hydrophilic MTPS. It is expected that the moderate surface polarity of Cloisite Na⁺ is responsible for the formation of an intercalated (discussed in the following WAXS section) MTPS-Cloisite Na⁺ nano-composite. The Na⁺ cation renders the proper hydrophilicity and compatibility with the MTPS, which in turn favors intercalation. Also, the lower molecular weight MTPS (as compared to TPS) would be capable of penetrating the clay galleries resulting in intercalation or exfoliation of the nano-clay platelets. However, due to the hydrophobic nature of the PBAT copolyester, the nano-scale clay would be localized in the dispersed MTPS phase, not leading to a complete exfoliation of the dispersed clay. The tensile strength of the Cloisite Na⁺ filled PBAT-*g*-MTPS was ~ 3800 psi, much higher than that for the original PBAT-*g*-MTPS. An improvement in the modulus of the Cloisite Na⁺ filled PBAT-*g*-MTPS could be attributed to the creation of a three-dimensional network

of inter-connected long silicate layers, strengthening the blend through mechanical percolation (60).

The tensile strength of the PBAT-g-MTPS reactive blends, however, increased to about twice its original strength in the presence of 1 wt% of Cloisite 30B and Bentone 111. Tensile Strength as high as 4650 psi was obtained in the presence of 1% Cloisite 30B. Cloisite 30B, being more hydrophobic as compared to Cloisite Na⁺, one would expect poorer results from the MTPS-Cloisite 30B nano-composite. However, the quaternary ammonium ion present within the clay galleries also bears two hydroxyethyl groups which would be thermodynamically compatible with the maleic acid moiety grafted onto the starch backbone in the MTPS. Besides, the organo-clay Cloisite 30B, possessing methyl, tallow bis-2-hydroxyethyl ammonium cations, seemed to delaminate more effectively in the presence of the polyester PBAT. This may be due to better thermodynamic compatibility of PBAT with the less hydrophilic Cloisite 30B. The elongation at break also improved significantly (~ 800%) upon the addition of Cloisite 30B to the PBAT-g-MTPS. This enhancement in elongation could be attributed to the addition of Cloisite 30B, and a better gelatinization and modified crystalline structure of the extrudate. The dispersed Cloisite 30B presented a more tortuous path for the starch plasticizer (glycerol) to leach out of the blend (similar to the gas diffusion model proposed by Yano et al. (61)). This had a two-fold effect of lowering the gelatinization temperature for the MTPS, as well as decreasing the viscosity of the PBAT-g-MTPS blend. The more amorphous reactive blend (also from the DSC results showed earlier) thus obtained would undergo a viscoelastic deformation rather than fail through brittle fracture. An increase in the modulus of elasticity (21723 psi) was also observed similar to

that in the case of Cloisite Na⁺. Usually, the tensile strength and the modulus increase with an increase in the blend crystallinity. In this case, the enhancement in these properties was most probably due to the enhanced interfacial area of the Cloisite 30B, thus leading to nano-scale reinforcing of the blend.

BENTONE 111, an organic derivative of a special smectite clay, also rendered tensile strength as high as 4670 psi to the PBAT-g-MTPS, with an enhanced modulus of 19822 psi. These results were similar to those observed using Cloisite as the nano-scale reinforcing clay; whereas BENTONE 166 provided tensile strengths as high as 3650 psi, with a modulus of ~ 17500 psi, but lower elongations of ~ 650% as compared to those of the unfilled PBAT-g-MTPS reactive blend. This was probably due to the fact that BENTONE 166, which is an alkyl aryl ammonium hectorite clay, was devoid of the hydroxyethyl groups responsible for the compatibility with the maleic acid moiety of the MTPS, resulting in slightly inferior properties as compared to those obtained using Cloisite 30B and BENTONE 111. The following section on the Wide Angle X-Ray Diffraction patterns of the nano-composites reveals more explicit details on the intercalation and exfoliation of the clay platelets occurring in the reactive blends.

9.5.3.8 Wide Angle X-Ray Scattering (WAXS)

9.5.3.8.1 X-ray Diffraction Patterns on Regular Corn Starch, TPS, PBAT, MTPS and PBAT-g-MTPS

X-ray diffractogram of regular corn starch and plasticized starch is shown in Figure 9.29. Native starches are biosynthetically assembled as semi-crystalline granules. The type of native, crystalline structure, labeled as A-, B- or C- type, depends on the starch source.

As shown in Figure 9.29 (a), two single peaks at 14.8° and 22.6° and the double peak corresponding to 16.6° and 17.7° is characteristic of A type crystals observed in starches from grains (as in corn). B-starches are found in tuberous plants (as in potato), while the C-type structure is more rare and is thought to be an intermediate form occurring in some plant sources such as pea starch (62). Native A- and B- type crystal lattices consist of double helical, six-fold structures. The difference between the A-type and B-type crystallinity is the packing density of the double helices in the unit cell (63).

TPS that has been prepared by kneading, extrusion, compression molding, or injection molding of several native starches with glycerol as a plasticizer, may exhibit two types of distinguished crystallinity directly after processing.

- 1) Residual Crystallinity: native A-, B-, or C-type crystallinity caused by incomplete melting of starch during processing.
- 2) Processing-induced Crystallinity: amylose V_H -, V_A -, or E_H - type crystallinity which is formed during thermo-mechanical processing.

The amount of residual crystallinity is related to processing conditions like processing temperature and applied shear stress. The composition of the mixture indirectly influences the amount of residual crystallinity. Lower amounts of glycerol reduce residual crystallinity. The effects are attributed to an increase in the melt viscosity at decreasing plasticizer content, which cause an enhancement of the shear stresses on the melt (64). Processing-induced crystallinity, also influenced by processing parameters, is caused by the fast recrystallization of amylose into single-helical structures. An increase in the screw speed during extrusion or increasing residence time during kneading causes an increase in the single-helical type of crystallinity (64). Several V-type structures have

been reported for low and medium moisture starch food products such as bread and several extrusion cooked starch products (65 – 67).

Residual A-type crystallinity was observed in TPS ($\sim 17^\circ$) (Figure 9.29b), though diminished, dependent on the native crystal structure. These structures occur when the energy input is lower than necessary to completely melt the native crystals. By X-Ray diffraction, three processing-induced crystal structures of single-helical amylose type (V_H , V_A , or E_H) have been observed in TPS materials (64). On plasticization, the new processing-induced characteristic crystalline starch peaks were observed at 13.2° and 20.5° . By comparison of the diffraction data of TPS with those in literature, the diffraction pattern observed was assigned to the V_A structure. Its lattice is indexed as an orthorhombic unit cell with the dimensions: $a = 13.0$, $b = 22.5$, $c = 7.9 \text{ \AA}$ (68).

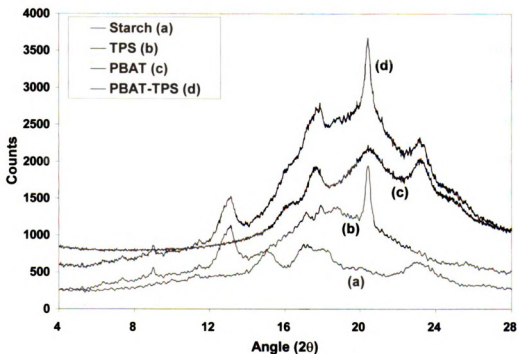


Figure 9.29 X-Ray diffractogram results of starch, TPS, PBAT, PBAT-TPS

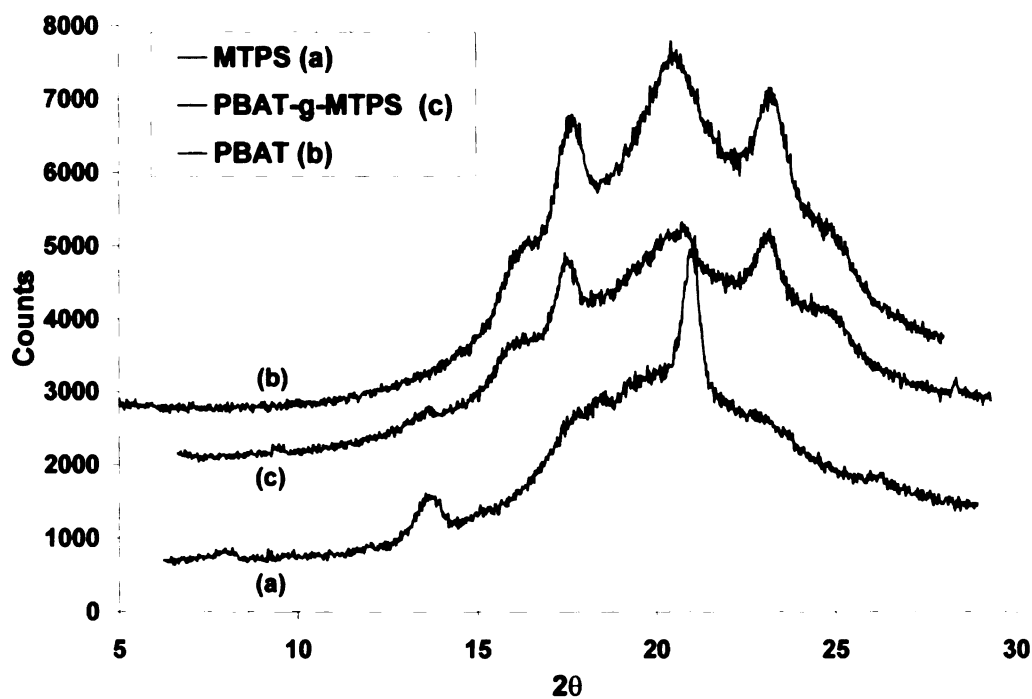


Figure 9.30 X-Ray diffractogram results of MTPS and PBAT-g-MTPS

The V_A lattice has more contracted amylose helices and contains less water than the hydrated V_H lattice ($a = 13.65$, $b = 23.7$, $c = 8.05$ Å) (69). These unit cell dimensions are based on fiber XRD patterns. These new peaks obtained are evidence of crystalline domains formed by retrogradation of the amorphous chains. Figures 9.29 (c) and (d) show the XRD patterns for PBAT and the PBAT-TPS blend respectively. It could be observed that the crystallinity from the TPS was not completely disrupted in the PBAT-TPS blend. This was probably due to the fact that the polyester and TPS were incompatible and phase separated giving their individual patterns in the blend.

Figure 9.30 (a) shows the X-ray diffraction pattern of the MTPS. It was observed that the residual crystalline peaks from the native starch crystals at $\sim 17^\circ$ were absent, suggesting that the inherent granular, crystalline structure of the native corn starch was completely disrupted. Since the MTPS had a lower shear viscosity, the energy input in the extruder

was sufficient to completely melt the native crystals. However, the processing-induced crystallinity of type V_A -caused by the fast recrystallization of amylose into single-helical structures is retained, and is observed in the form of individual peaks at 13.5° and 20.8° . Figure 9.30 (b) shows the X-ray diffraction pattern observed on the PBAT film obtained by blown-film extrusion. Figure 9.30 (c) shows the X-ray diffractogram of the PBAT-*g*-MTPS reactive blend. It was observed that the processing-induced crystalline structure present in MTPS was disrupted in the PBAT-*g*-MTPS reactive blend suggesting the grafting reaction/homogenization (with no phase separation) of the MTPS in the polyester continuous phase. The peaks obtained in the X-ray diffraction pattern at 17.5° , 20.5° and 23.2° were due to the semi-crystalline PBAT.

9.5.3.8.2 X-ray Diffraction (XRD) Patterns on Nano-Clay filled TPS, MTPS and PBAT-*g*-MTPS

WAXS has provided information about the short-range order of the molecular constituents in the polymer blends and the exfoliation process. It is generally thought that the polymer enters the organo-clay galleries and forces apart the platelets (intercalation). As more polymer chains enter the gallery, the platelets become disordered, thus causing broader peaks, and a wider distribution of such peaks.

The films produced from the nano-composite blends were examined using the WAXS. The XRD results obtained using TPS-Cloisite 30B, and TPS-Cloisite Na nano-composite were similar to those observed by Park et al. (54), and have not been reported. Intercalated hybrid structures were obtained in both these composites, wherein the peak at about 8° for Cloisite Na had shifted to about $4 - 4.5^\circ$ in the TPS-Cloisite Na

composite, while the peak corresponding to Cloisite 30B at about 5° had shifted to about 4.5° for the TPS-Cloisite 30B composite. Figures 9.31 – 9.34 show the diffraction patterns obtained using four different nano-scale clays: Cloisite Na^+ , Cloisite 30B, BENTONE 111, and BENTONE 166 respectively.

Figure 9.31 shows that the peak around 8° of the Cloisite Na^+ had shifted to $4.5 - 5^\circ$ for the MTPS-Cloisite Na^+ nano-composite, and further to $4 - 4.1^\circ$ for the PBAT-g-MTPS-Cloisite Na^+ film, indicating the intercalated hybrid structures.

Figure 9.32 shows that the peak around 5° of the Cloisite 30B had shifted to $4.2 - 4.3^\circ$ for the MTPS-Cloisite 30B nano-composite, and an extremely diminished shoulder was obtained at about $3 - 3.2^\circ$ for the PBAT-g-MTPS-Cloisite 30B film. This might suggest exfoliation of the organo-modified clay in diminutive amounts in the PBAT-g-MTPS matrix. The organo-clay seemed to delaminate more effectively in the presence of MTPS. The organic constituents of organoclay consisted of hydroxyethyl groups, which may be more thermodynamically compatible with the carboxylic acid groups present on the MTPS and explain such a trend. The significant increase in the tensile properties could be attributed to the exfoliation of the platelets, and the retention of the plasticizer.

Figure 9.33 corresponds to the results obtained using the nano-clay BENTONE 111. It could be observed that although the diffraction peak due to the nano-clay at 4.6° had almost diminished in the MTPS-Bentone 111 nano-composite (Figure 9.31 (b)). However, a very small shoulder was observed at $\sim 4.7^\circ$ probably due to some agglomeration of clay platelets, which is quite possible under the shear and extensional flows existing in the extrusion operations. No significant peaks were observed in the

Bentone 111 filled PBAT-*g*-MTPS suggesting complete exfoliation, thus confirming the superior mechanical properties observed earlier.

Figure 9.34 shows the diffraction patterns obtained using Bentone 166 as the nano-scale reinforcing filler. The peak due to the Bentone 166 at about 3.2° was shifted to about 2.7° in the form of a diminishing shoulder suggesting some intercalation in the MTPS-Bentone 166 nano-composite. This was expected knowing that Bentone 166 is a less hydrophilic, alkyl aryl ammonium hectorite clay, which would be incompatible with the starch. However, in the presence of the polyester PBAT, the peak vanishes probably due to the compatibility of the organic constituents with the hydrophobic PBAT.

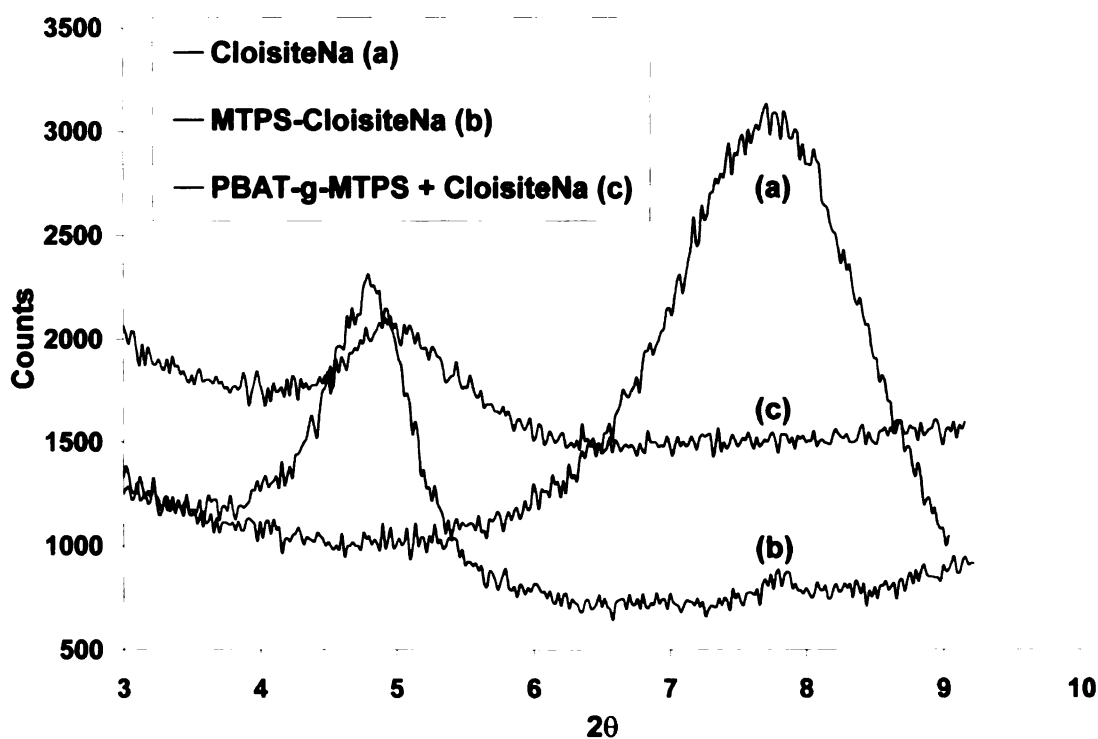


Figure 9.31 X-Ray diffractogram results with Cloisite Na⁺

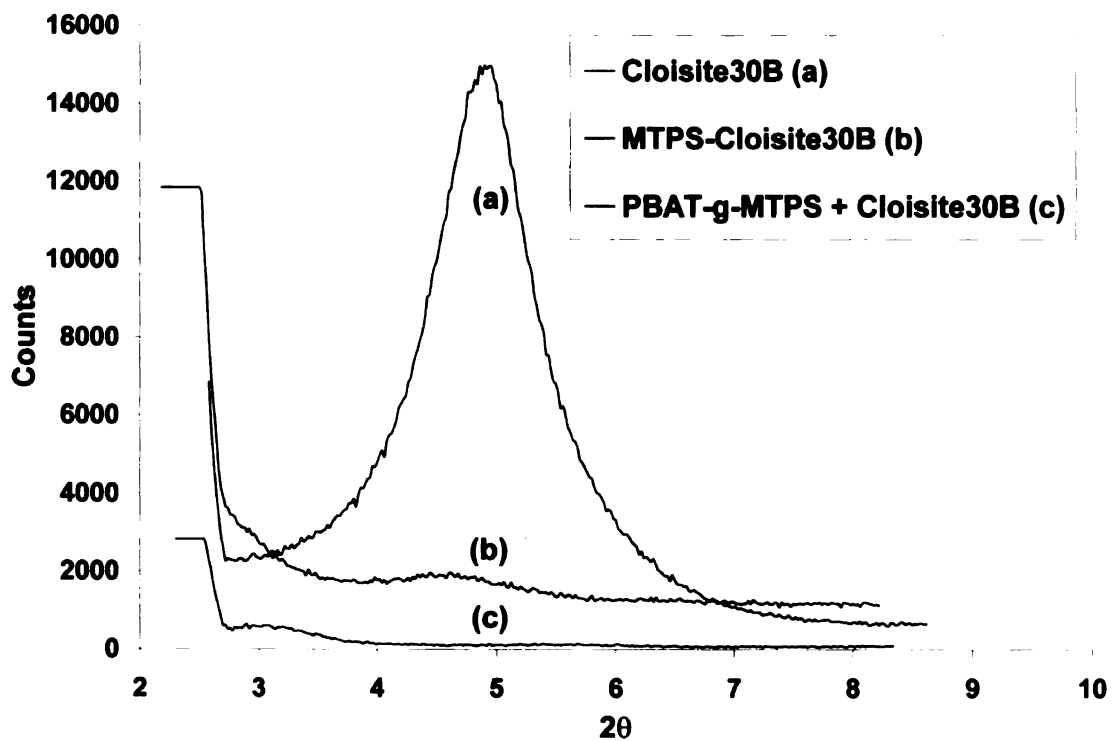


Figure 9.32 X-Ray diffractogram results with Cloisite 30B

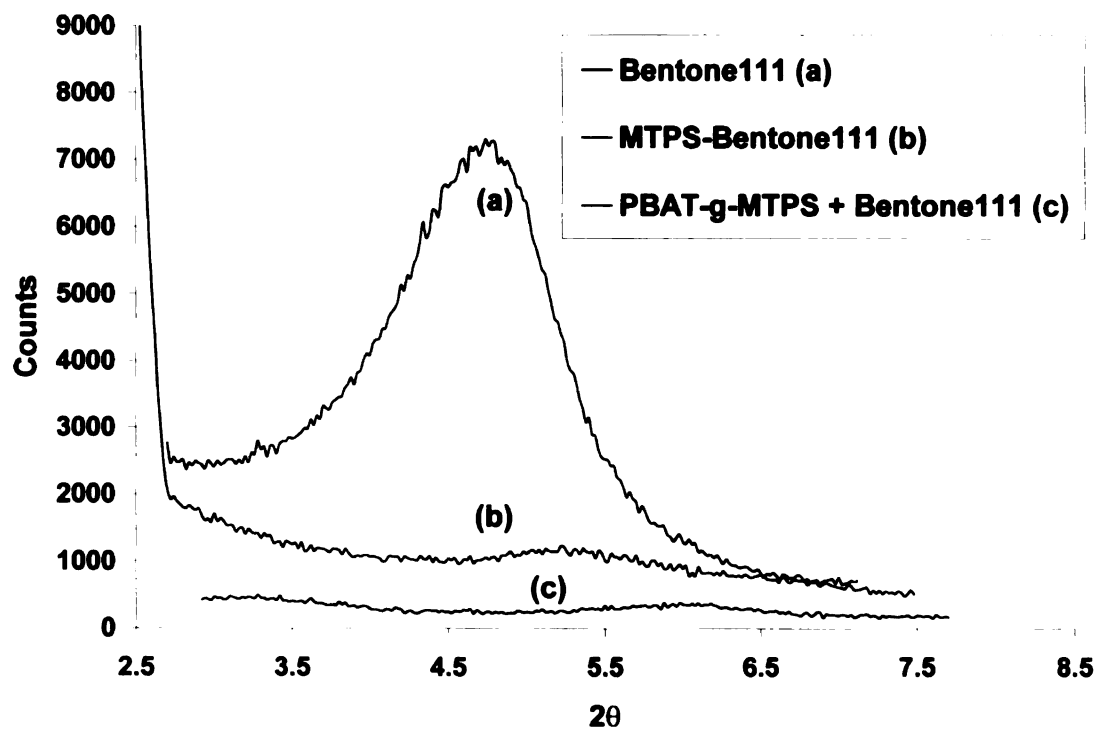


Figure 9.33 X-Ray diffractogram results with Bentone 111

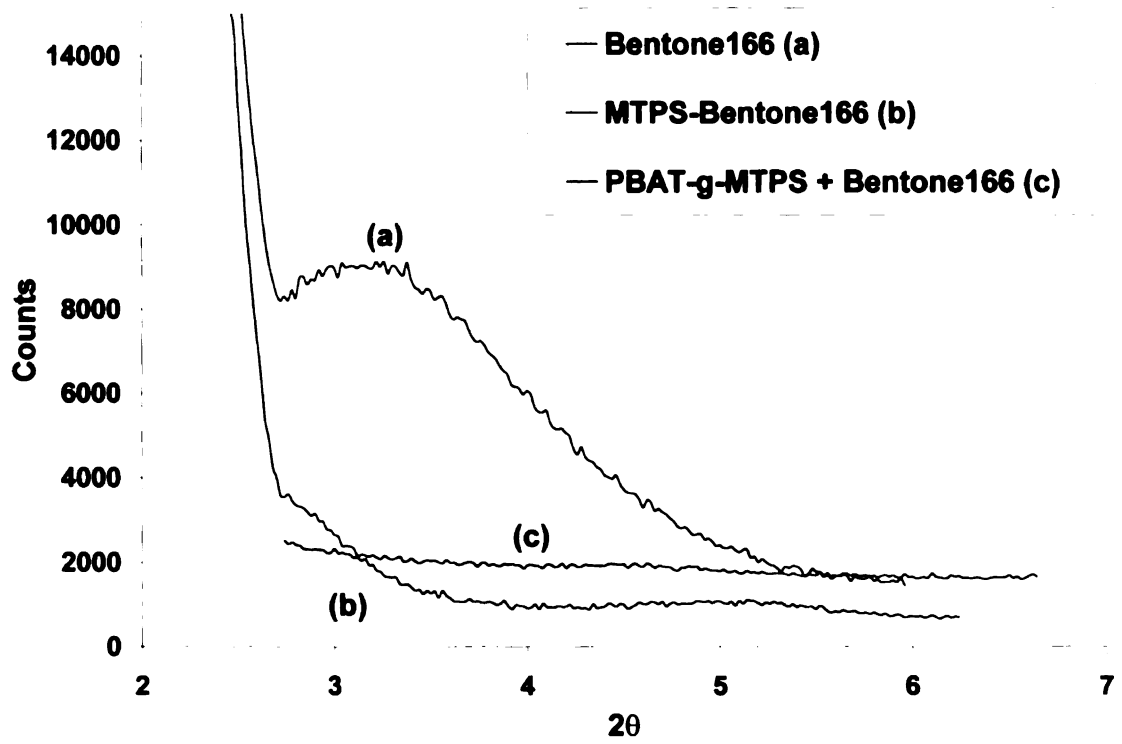
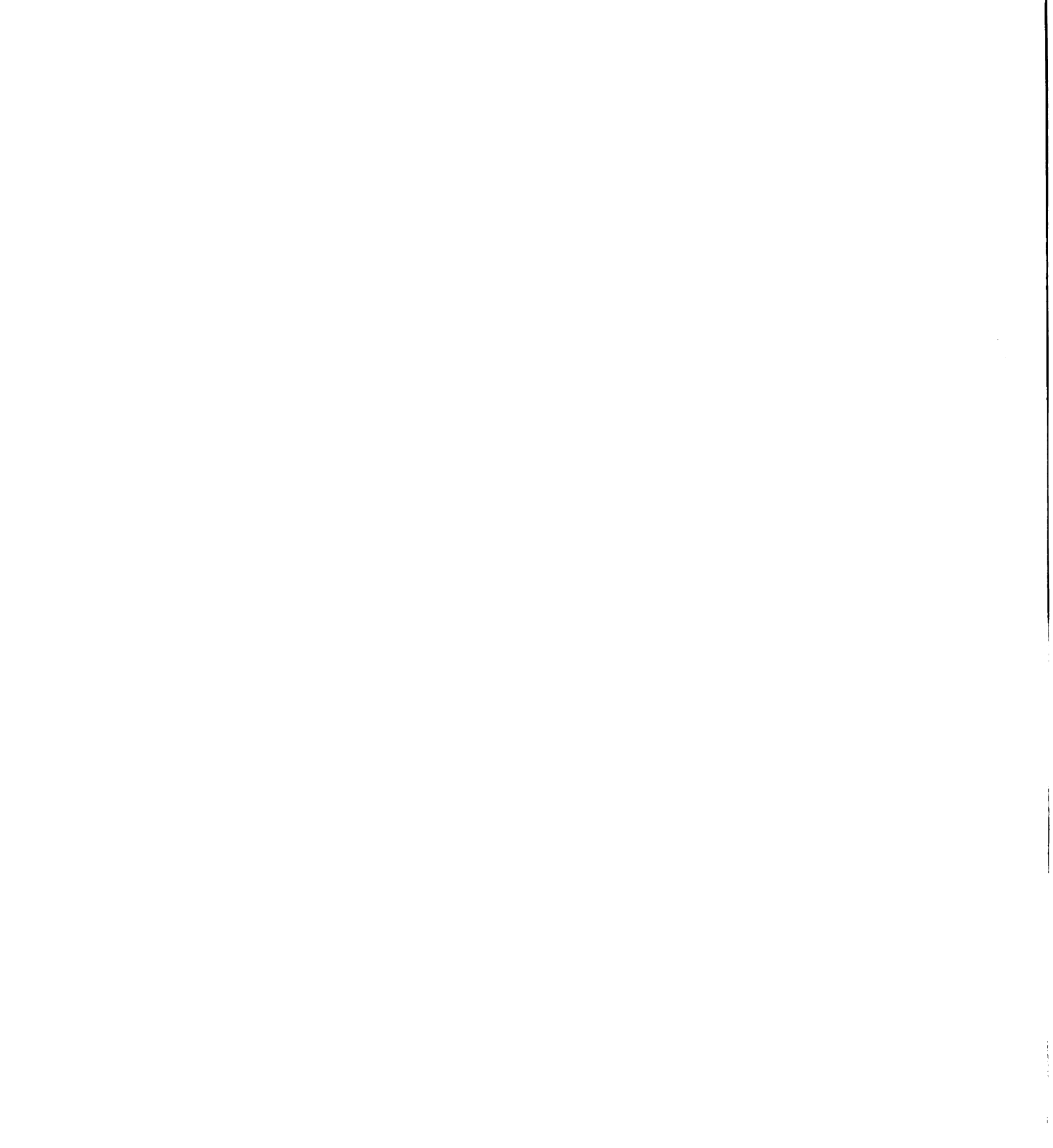


Figure 9.34 X-Ray diffractogram results with Bentone 166



9.6 Density, Expansion Ratio (ER) and Specific length (SL) of Starch foams

In this particular invention, the amphiphilic, biodegradable starch polyester graft co-polymer (PBAT-*g*-MTPS) has been used as a compatibilizer between the hydrophilic starch phase and the hydrophobic polyester phase to give improved physico-mechanical properties of starch foams using PBAT as a functional aid. The densities, expansion ratios and the specific lengths of the starch foams (control) are shown in Table 9.10, while those using different amounts of the compatibilizer (PBAT-*g*-MTPS) between starch and the PBAT are shown in Table 9.11. The improvement in properties is marginal when the starch polyester graft co-polymer is used directly as a functional aid, but it is substantial when the PBAT-*g*-MTPS co-polymer is used as a compatibilizer between the starch and the polyester.

Examples of foams using PBAT-*g*-MTPS as compatibilizer:

1. MTPS was made using 80% regular cornstarch, 20% glycerol and 2.5% MA (w/w of starch). 30% MTPS (w/w) was trans-esterified with 70% PBAT (w/w) to form PBAT-*g*-MTPS, which would be used as a compatibilizer between starch and PBAT in foams. (95% by weight hydroxypropylated high amylose corn starch + 4.5% by weight of PBAT + 0.5% by weight of PBAT-*g*-MTPS) were pre-mixed and then fed to a Century ZSK-30 co-rotating twin-screw extruder, and then extruded in the form of cylindrical foam shapes, using water as the plasticizing as well as the blowing agent.
2. MTPS was made using 80% high amylose cornstarch, 20% glycerol, 5% MA (w/w of starch), and 0.25% organic peroxide Luperox 101 (w/w of starch). 20%

MTPS (w/w) was trans-esterified with 80% PBAT (w/w) to form PBAT-g-MTPS, which would be used as a compatibilizer between starch and PBAT in foams. (95% by weight hydroxypropylated high amylose corn starch + 4.5% by weight of PBAT + 0.5% by weight of PBAT-g-MTPS) were pre-mixed and then fed to a Century ZSK-30 co-rotating twin-screw extruder, and then extruded in the form of cylindrical foam shapes, using water as the plasticizing as well as the blowing agent.

3. MTPS was made using 80% regular cornstarch, 20% glycerol and 2.5% MA (w/w of starch). 50% MTPS (w/w) was trans-esterified with 50% PBAT (w/w) to form PBAT-g-MTPS, which would be used as a compatibilizer between starch and PBAT in foams. (95% by weight regular corn starch + 4.0% by weight of PBAT + 1.0% by weight of PBAT-g-MTPS) were pre-mixed and then fed to a Century ZSK-30 co-rotating twin-screw extruder, and then extruded in the form of cylindrical foam shapes, using water as the plasticizing as well as the blowing agent.
4. MTPS was made using 80% regular cornstarch, 20% glycerol and 2.5% MA (w/w of starch). 40% MTPS (w/w) was trans-esterified with 60% PBAT (w/w) to form PBAT-g-MTPS, which would be used as a compatibilizer between starch and PBAT in foams. (95% by weight waxy corn starch + 4.0% by weight of PBAT + 1.0% by weight of PBAT-g-MTPS) were pre-mixed and then fed to a Century ZSK-30 co-rotating twin-screw extruder, and then extruded in the form of cylindrical foam shapes, using water as the plasticizing as well as the blowing agent.

For example, the foams obtained from examples 1 and 2 below (Table 9.11) have 35-37% lower densities and 31-32% higher resilience as compared to the hydroxypropylated high amylose corn starch foam (entry 1 of Table 9.10), and 19-22% lower densities and 8-10% higher resilience as compared to hydroxypropylated high amylose starch foam with 5% PBAT (entry 5 of Table 9.10).

The foam obtained from example 3 (Table 9.11) has 28-30% lower density and about 200-225% higher resilience as compared to the regular cornstarch foam (entry 3 of Table 9.10), and 18-20% lower density and 12-15% higher resilience as compared to regular cornstarch foam with PBAT (entry 6 of Table 9.10).

The foam obtained from example 4 (Table 9.11) has 25-30% lower density and about 145-150% higher resilience as compared to the waxy corn starch foam (entry 4 of Table 9.10), and 15-18% lower density and 15-18% higher resilience as compared to waxy corn starch foam with 5% PBAT (entry 7 of Table 9.10).

Foams were extruded using the same principle, but using PCL as the aliphatic biodegradable polyester. PCL-*g*-MTPS was also used as the compatibilizer between starch and PCL, and an improvement in physico-mechanical properties was achieved.

The amphiphilic starch polyester graft co-polymers retain their biodegradability. The water resistance of the starch and modified starches is improved by graft copolymerization with high molecular weight biodegradable polyesters, especially with semi-crystalline polyesters such as PCL or PHB/V, and similar biodegradable polyesters.

Figure 9.35 below shows the ESEM of the starch foam surface using hydroxypropylated high amylose corn starch, 4.5% PBAT and 0.5% PBAT-*g*-MTPS, which is used as the compatibilizer between the starch and PBAT.

Table 9.10 Physico-Mechanical Properties of Starch-based foams (Control).

Entry	Formulation	Density (kg/m ³)	Expansion Ratio	Specific Length (cm/gm)	Resiliency (%)
1	Hydroxypropylated high amylose corn starch (control)	30.2	39.6	14.6	69.8
2	High Amylose corn starch (control)	35.7	35.6	13.8	60.5
3	Regular corn starch (control)	45.8	23.3	16.4	21.9
4	Waxy corn starch (control)	42.4	28.6	14.4	31.5
5	Hydroxypropylated high amylose corn starch + 5% (w/w) PBAT	24.2	46.7	15.5	84.3
6	Regular corn starch + 5% (w/w) PBAT	40.9	24.5	17.4	62.5
7	Waxy corn starch + 5% (w/w) PBAT	36.4	32.0	15.0	67.5

Table 9.11 Physico-Mechanical Properties of Starch-based foams (using PBAT-*g*-MTPS as compatibilizer).

Entry	Formulation	Density (kg/m ³)	Expansion Ratio	Specific Length (cm/gm)	Resiliency (%)
1	Foam from Example 1 (Compare with Entries 1 & 5 of Table 9.10.)	19.4	51.9	17.3	91.8
2	Foam from Example 2 (Compare with Entries 1 & 5 of Table 9.10.)	19.0	47.0	19.5	91.6
3	Foam from Example 3 (Compare with Entries 3 & 6 of Table 9.10.)	32.9	30.6	17.4	71.0
4	Foam from Example 4 (Compare with Entries 4 & 7 of Table 9.10.)	30.3	36.6	15.8	78.0

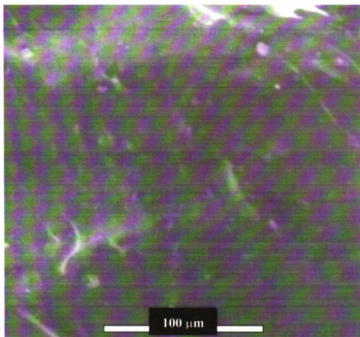


Figure 9.35 ESEM on starch foam surface from Example 1.

9.6.1 Moisture Sorption Analysis

The normalized steady state weight gains and dimensions of the starch foam samples on moisture sorption are listed in Table 9.12. The hydrophobic properties of the starch foams using PBAT (70) and MCO-g-PBAT as functional aids, and using MA-g-PBAT (71) as a compatibilizer between PBAT and starch have been reported in our previous work. The control hydroxypropylated high amylose cornstarch foams gained up to 13% of their original weight, and lost about 50% of their dimensions on moisture sorption. However, in the presence of PBAT, it was observed that PBAT migrated to the surface, which was evident from the scanning electron micrograph of the starch foam surface in Figure 7.10, thus providing a finer and a more stable surface preventing the rapid loss of moisture

through the surface, as discussed in Chapter 7, Section 7.4.6. The steady state weight gain was about 9.3 – 9.5% of the original weight of the foam samples on addition of PBAT, but dimensional stability increased significantly.

Table 9.12 Normalized Steady State Weight Gains and Dimensions of Starch Foams on Moisture Sorption

No.	Processing Aids	Normalized Steady State Weight Gain, $\left[\frac{W - W_0}{W_0} \right]$ (± 0.032)	Normalized Steady State Diameter, $\left[\frac{D}{D_0} \right]$ (± 0.041)	Normalized Steady State Length, $\left[\frac{L}{L_0} \right]$ (± 0.046)
1	None	0.13	0.56	0.50
2	5% pure polyester (PBAT)	0.094	0.79	0.81
3	(0.5% PBAT-g-MTPS + 4.5% PBAT) blend (Foam from Example 1 above)	0.06	0.85	0.84

The loss of radial and longitudinal dimensions decreased from 50% to about 20% respectively with an increase in the PBAT content. This could imply that most of the PBAT in the foam samples manifested at the surface and not in the core. Thus, the core of these samples continued to absorb as much moisture as it used to.

The results from Table 9.12 indicated that the foams using PBAT-g-MTPS as a functional aid affected the dimensional stability of the starch foams slightly (as compared to the starch foams using PBAT). However, the normalized equilibrium weight gain

reduces from ~ 9.3 – 9.5% to ~ 6 %. This suggested that the compatibility between starch and PBAT might have been improved, since most of the polymer does not manifest at the surface as it did earlier on phase separation.

9.7 Conclusions

PBAT-g-TPS copolymers were produced by reactive extrusion processing using maleic anhydride or maleic acid as a trans-esterification catalyst. The graft copolymer was completely extractable in Dichloromethane using a Soxhlet extraction technique. On solvent casting the extracted polymer solution, a transparent film was obtained. In the absence of maleic acid, only the polyester was extracted out. These results confirmed that PBAT and TPS were covalently linked, as opposed to a simple physical blend. FTIR results of PBAT-g-TPS copolymer, showing the carbonyl stretch at 1720 cm^{-1} , ester C-O stretch at 1270 cm^{-1} and the -OH polymer stretch at $3200\text{-}3400\text{ cm}^{-1}$ confirm the true existence of a graft copolymer. Tensile strength and modulus of elasticity of the graft copolymer were lower as compared to LDPE.

Regular granular cornstarch was maleated in a twin-screw co-rotating extruder using maleic anhydride or maleic acid modifiers in the presence of glycerol as the plasticizer and optional free-radical initiator such as Luperox 101. Due to the low viscosity of MTPS, reactive maleation can be done at much higher throughputs as compared to the regular thermoplastic starch (TPS) production. The reactive maleation process prevents problems during TPS production such as clogging of the thermoplastic starch melt and foaming at the die. Carbonyl stretch peak at 1720 cm^{-1} , observed for the extracted MTPS sample (made using both maleic anhydride and maleic acid modifier), confirms

reactivity. Differential Scanning Calorimetry (DSC) results of MTPS samples exhibit melting endotherms, not present in regular granular starch. NMR studies on the MTPS (after extraction of unreacted MA) confirmed the presence of the vinyl species grafted onto the starch backbone; although, more work needs to be done to clarify the reaction mechanism and the degree of substitution.

PBAT-*g*-MTPS copolymers were produced by the reactive extrusion processing of PBAT and MTPS. PBAT/MTPS (70/30 and 60/40; w/w) graft copolymers was completely extractable in Dichloromethane using a Soxhlet extraction technique. On solvent casting the extracted polymer solution, a transparent film was obtained. This reaction leading to the formation of a graft copolymer is dependent on the relative amounts of PBAT and MTPS present. FTIR results of PBAT/MTPS (70/30; w/w) graft copolymers (solvent cast films after extraction in Dichloromethane) made using both maleic anhydride and maleic acid, show the carbonyl stretch at 1720 cm^{-1} , and the -OH polymer stretch at $3200\text{-}3400\text{ cm}^{-1}$ confirming the true existence of a graft copolymer.

Nano-scale reinforcing clay was introduced in the PBAT-*g*-MTPS copolymer to improve its mechanical, thermal and barrier properties. High performance formulations having superior tensile strength (5000 psi) and break elongations (>800%) were obtained. These properties were attributed to the exfoliation achieved in the nano-clay as observed from the WAXS results. Transmission electron microscopy would be used as a tool to confirm the findings from the WAXS experiments. The above results indicate that on using the PBAT-*g*-MTPS as a compatibilizer between starch and PBAT yield starch based foams with much lower densities and improved mechanical properties such as resilience or spring index.

9.8 References

- 1) Griffin, G. J. L. Chemistry and Technology of Biodegradable Polymers, Blackie Academic and Professional, 1992.
- 2) Pranamuda, H., Tokiwa, Y., Tanaka, H. Journal of Environmental Polymer Degradation, 4, 1, 1996.
- 3) Ramsay, B. A., Langlade, V., Carreau, P. J., Ramsay, J. A. Applied and Environmental Microbiology, 59, 1242, 1993.
- 4) Wittwer, F., Tomka, I. US Patent 4,673,438, 1987.
- 5) Lay, G., Rehm, J., Stepto, R. F., Thoma, M., Sachetto, J-P., Lentz, D. J., Silbiger, J. US Patent 5,095,054, 1992.
- 6) Tokiwa, Y., Takagi, S., Koyama, M. US Patent 5,256,711, 1993.
- 7) Bahr, K-H., Fitton, M. G., Koch, H. US Patent 5,275,774, 1994.
- 8) Stepto, R. F. T., Tomka, I., Dobler, B., Pyrah, K. US Patent 5,382,611, 1995.
- 9) Stepto, R. F. T., Tomka, I., Thoma, M. US Patent 5,405,564, 1995.
- 10) Wiedmann, W., Strobel, E. Starch, 43, 138, 1991.
- 11) Shorgen, R. L., Fanta, G. F., Doane, W.M. Starch, 45, 276, 1993.
- 12) Forssell, P., Mikkila, J., Sourtti, T. J.M.S. Pure Applied Chemistry, A33, 703, 1996.
- 13) Narayan, R. Polymeric Materials from Agricultural Feedstocks, In: Polymers from Agricultural Coproducts, Ed., Fishman, M.L., Friedman, R.B. and Huang, S.J. American Chemical Society Symposium Series, American Chemical Society, Washington, DC, 575, 2, 1994.
- 14) Van Soest, J. J. G., Benes, K., D. de Witt, Polymer, 37, 3543, 1996.
- 15) Bastioli, C., Bellotti, V., Montino, A., Tredici, G., Lombi, R., Ponti, R. U.S. Patent 5,412,005, 1995.
- 16) Bastioli, C., Bellotti, V., Del Giudice, L., Lombi, R., Rallis, A., Del Tredici, G., Montino, A., Ponti, R. US Patent 5,288,765, 1994.
- 17) Bastioli, C., Bellotti, V., Del Giudice, L., Del Tredici, G., Lombi, R., Rallis, A., US Patent 5,262,458, 1993.

- 18) Bastioli, C., Bellotti, V., Del Tredici, G., Montino, A., Ponti, R. US Patent 5,462,980, 1995.
- 19) Bastioli, C., Romano, G., Scarati, M., Tosin, M. US Patent 5,512,378, 1996.
- 20) Fanta, G. F., Bagley, E.B. Encyclopedia of Polymer Science, John Wiley & Sons; New York, 1970.
- 21) Fanta, G. F. Block and Graft Copolymers- Vol I, John Wiley & Sons; New York, 1973.
- 22) Otey, F. H., Westhoff, R. P., Doane, W.M. Industrial Engineering Chemistry Products Research Development, 19, 592, 1980.
- 23) Otey, F. H., Westhoff, R. P. Industrial Engineering Chemistry Products Research Development, 23, 284, 1984.
- 24) Otey, F. H., Westhoff, R. P., Doane, W.M. Industrial Engineering Chemistry Products Research Development, 26, 1659, 1987.
- 25) Bloembergen, S., Narayan, R. US Patent 5,462,983, 1995.
- 26) Tomka, I. US Patent 5,314,934, 1994.
- 27) Bastioli, C., Bellotti, V., Montino, A., Del Tredici, G., Lombi, R., US Patent 5,234,977, 1993.
- 28) Narayan, R., Dubois, P., Krishnan, M. US Patent 5,540,929, 1996.
- 29) Whistler, R. L. Advanced Carbohydrate Chemistry, 1945.
- 30) Mark, A. M., Mehlretter, C. L. Die Starke, 24, 1972.
- 31) Caldwell, C. G., Hills, F. US Patent 2,461,139, 1949.
- 32) Caldwell, C. G., Hills, F., Wurzburg, O. B. US Patent 2,661,349, 1953.
- 33) Kovats, L. P. US Patent 3,732,207, 1973.
- 34) Tomasik, P., Wang, P., Jane, J. Starch, 47, 96, 1995.
- 35) De Vlieger, J. J. Biodegradable Nanocomposites in Proceedings of the Food Bio-Packaging Conference, Denmark, August 20 – 22, 2000.

- 36) Usuki, A., Kojima, Y., Kawasumi, M., Okada, A., Fukushima, Y., Kurauchi, T., Kamigaito, O. Journal of Materials Research, 8, 1179, 1993.
- 37) Kojima, Y., Usuki, A., Kawasumi, M., Okada, A., Fukushima, Y., Kurauchi, T., Kamigaito, O. Journal of Polymer Science, Part A: Polymer Chemistry, 31, 1983, 1993.
- 38) Vaia, R. A., Ishii, H., Giannelis, E. P. Chemistry of Materials, 5, 1964, 1993.
- 39) Giannelis, E. P., Krishnamoorti, R., Manias, E. Advanced Polymer Science, 138, 107, 1999.
- 40) Gilman, J. W., Jackson, C. L., Morgan, A. B., Harris, R. Jr., Manias, E., Giannelis, E. P., Wuthenow, M., Hilton, D., Phillips, S. Chemistry of Materials, 12, 1866, 2000.
- 41) Xu, R., Manias, E., Snyder, A. J., Runt, J. Macromolecules, 34, 337, 2001.
- 42) Vaia, R. A., Vasudevan. S., Krawiec, W., Scalon, L. G., Giannelis, E. P. Advanced Materials, 7, 154, 1995.
- 43) Strawhecker, K. E., Manias, E. Chemistry of Materials, 12, 2943, 2000.
- 44) Strawhecker, K. E., Manias, E. Chemistry of Materials, 15, 844, 2003.
- 45) Strawhecker, K. E., Manias, E. Macromolecules, 34, 8475, 2001.
- 46) Balazs, A. C., Singh, C., Zhulina, E. Macromolecules, 31, 8370, 1998.
- 47) Kuznetsov, D. V., Balazs, A. C. Journal of Chemical Physics, 113, 2479, 2000.
- 48) Beyer, F. L., Tan, N. C. B., Dasgupta, A., Galvin, M. E. Chemistry of Materials, 14, 2983, 2002.
- 49) Huang, X. Y., Brittain, W. J. Macromolecules, 34, 3255, 2000.
- 50) Okamoto, M., Morita, S., Taguchi, H., Kim, Y. H., Kotaka, T., Tateyama, H. Polymer, 41, 3887, 2000.
- 51) Messersmith, P. B., Giannelis, E. P. Journal of Polymer Science, Part A: Polymer Chemistry, 33, 1047, 1995.

- 52) Lan, T., Pinnavaia, T. J. Chemistry of Materials, 6, 2216 – 2219, 1994.
- 53) Vaia, R. A., Giannelis, E. P. Macromolecules, 30, 7990, 1997.
- 54) Park, H-M., Lee, W-K., Park, C-Y., Cho, W-J., Ha, C-S. Journal of Materials Science, 38 (5), 909-915, 2003.
- 55) Fischer, H. R., Fischer, S. European Patent 1134258, 2001.
- 56) McGlashan, S. A., Halley, P. J. Polymer International, 52, 1767-1773, 2003.
- 57) Kalambur, S. B., Rizvi, S. S. H. Polymer International, 53, 1413 – 1416, 2004.
- 58) Lebaron, P. C., Wang, Z., Pinnavaia, T. J. Applied Clay Science, 15, 11, 1999.
- 59) Vaia, R. A., Giannelis, E. P. Macromolecules, 30, 8000, 1997.
- 60) Lan, T., Kaviratna, P. D., Pinnavaia, T. J. Chemistry of Materials, 6, 573, 1994.
- 61) Yano, K., Usuki, A., Okada, A. Journal of Polymer Science, Part A: Polymer Chemistry, 35, 2289 – 2294, 1997.
- 62) Sarko, A., Wu, H. –C. H. Starch, 30, 73, 1978.
- 63) Imberty, A., Buleon, A., Tran, V., Perez, S. Starch, 43, 375, 1993.
- 64) Van Soest, J. J. G. Starch Plastics: Structure-Property Relationships, PhD Thesis, University of Utrecht, 1996.
- 65) Lai, L. S., Kokini, J. L. Biotechnology Progress, 7, 251, 1991.
- 66) Chinnaswamy, R., Hanna, M. A., Zobel, H. F. Cereal Foods World, 34, 415, 1989.
- 67) Riisom, T., Krog, N., Erikson, J. Journal of Cereal Science, 2, 105, 1984.
- 68) Winter, W. T., Sarko, A. Biopolymers, 13, 1447, 1974.
- 69) Zobel, H. F., French, A. D., Hinckle, M. E. Biopolymers, 5, 837, 1967.
- 70) Nabar, Y., Draybuck, D., Narayan, R., Journal of Applied Polymer Science, In Review.
- 71) Nabar, Y., Raquez, J-M., Dubois, P., Narayan, R., Biomacromolecules, In Press.

REACTIVE EXTRUSION OF BIODEGRADABLE MA-*g*-PBAT-TALC COMPOSITES

10.1 Abstract

New biodegradable poly(butylene adipate-*co*-terephthalate) (PBAT)-talc composites were prepared through reactive extrusion. In the first step, the polyester backbone was reactively modified through free-radical grafting of maleic anhydride; to react the anhydride with the hydroxyl functions from the lateral surface of talc in the second step. The hypothesis was to improve the interfacial adhesion between PBAT and talc. The resulting MA-*g*-PBAT from the first step was then reactively melt-blended with talc using Tin (II) Octoate ($\text{Sn}(\text{Oct})_2$) and 4 - Dimethyl aminopyridine (4-DMAP) as esterification catalysts. The interfacial adhesion between MA-*g*-PBAT and talc was improved as evidenced by scanning electronic microscopy and selective extractions of the polyester part from the composite. It resulted that the tensile properties for the blown films prepared from these resulting composites were considerably improved as compared to those of the simple melt-blend of PBAT-talc. Extrapolation to a one-step reactive extrusion process was successfully carried out. The *in situ* chemical modification of PBAT-talc composites allowed preparing compositions involving up to 60 wt% talc. Interestingly, the best composition regarding the improvement of tensile properties was achieved by melt-blending the reactively modified composite containing 60 wt%-talc (referred to as the masterbatch), with 50 wt% plain PBAT. Such approach allowed to

retain the superior mechanical strength of PBAT (added to the masterbatch) by preventing it from undergoing undesirable reactions such as β -scissions from MA and transesterification reactions from esterification catalysts that were present during the reactive extrusion process, as well as a thermal extrusion history.

PBAT-talc, as well as these high performance resins developed, were also employed as functional aids in the starch-based foam process using hydroxypropylated high amylose corn starch. The resulting foams with enhanced properties had densities as low as 17.5 kg/m^3 , and spring indices as high as 97% in certain cases.

10.2 Introduction

The recent environmental regulations, societal concerns and growing environmental understanding throughout the world have triggered renewed efforts in plastic industry to develop new products and processes compatible with our environment. In this respect, the design of biodegradable plastics using performing synthesis processes represents an appropriately eco-efficiency approach to enhance the environmental quality of many products, e.g. by minimizing the waste disposed in landfills. Recently, BASF has marketed a novel biodegradable poly(butylene adipate-*co*-terephthalate) (PBAT) trademarked Ecoflex[®] (1). This aliphatic-aromatic (co)polyester is prepared by polycondensation reaction from adipic acid, 1,4-butanediol, and more especially terephthalic acid (aromatic ring), wherein its role is to reinforce the copolyester structure. It is worth pointing out that the maximum amount of terephthalic acid must be less than 40wt-% (of the total di-acid) in order to retain the biodegradability of the copolyester. Interestingly, the melting ($105\text{-}115^\circ\text{C}$) and glass transition temperatures (-20°C) of

copolyester offers a good compromise between its processing and use temperature. In addition, PBAT has a tensile strength of 5200 - 5600 psi with a break elongation close to 600% (in the machine direction), comparable to those of HDPE (2). In this respect, PBAT can be useful for packaging applications such as food films. Unfortunately, the use of these biodegradable thermoplastic (co)polyesters as bulk materials is still restricted by their relatively high cost, and poor mechanical properties in some cases compared to commodity plastics such as polyethylene and polypropylene. Combination of these biodegradable polymers with cheap inorganic fillers such as talc provides a useful way for reducing the cost, and for optimizing the properties of biodegradable thermoplastic polyesters as well (3 – 5). Developing a melt-blend with satisfactory overall physico-mechanical behavior will depend on the ability to control interfacial tension to generate a small-dispersed phase size and strong interfacial adhesion. It is of prime importance to achieve high-performance mechanical properties for the final material. Typically, functional groups such as isocyanate, amine, anhydride, carboxylic acid, epoxide and oxazoline are introduced through a fast reactive extrusion process, and then combined with their respective suitable reactive functions, such as hydroxyl-isocyanate, amine-anhydride, amine-epoxide, amine-lactam, amine-carboxylic acid and amine-oxazoline (6). Such functionalization of polymer matrix can reduce the interfacial tension, strengthening the interfacial adhesion and minimizing the coalescence (7). Reactive extrusion technique has proved to be an effective way to introduce a variety of functional groups onto the surface of natural polymers (8, 9). Maleic anhydride (MA) was first used as a monomer to graft onto non-biodegradable polymers such as polyethylene, polypropylene and other polymers (10, 11). Earlier results from research conducted by

Bhattacharya and co-workers (12 – 22) on maleation of biodegradable polymers such as PCL, PBSA, poly(butylene succinate) (PBS) and Eastar Bio[®] co-polyester; and by Narayan and co-workers (23, 24) on maleation of PLA indicate that blends of anhydride functional polymers and starch as a natural filler could lead to products with useful end properties.

In this respect, the paper aims at studying the reactive melt-blending of PBAT with a natural filler through reactive extrusion process, yielding the preparation of blown films having interesting mechanical properties, as ultimate objective. In this study, talc was utilized as a natural filler. Although the basal surface of talc is composed of chemically inert magnesium silicate layer, its lateral surface exhibits some hydroxyl functions, capable of forming strong covalent bonds with suitable chemical groups such as anhydride functions. In a first step, PBAT chains were chemically modified through free-radical grafting of MA onto the polyester backbone. We have studied and reported the maleation of PBAT to form MA-g-PBAT in our earlier work (25). MA-g-PBAT obtained using 3% MA and 0.5% free radical initiator was chosen for this study, since it had sufficient MA grafted on the PBAT backbone, as well as appreciable melt strength (25). These MA-g-PBAT chains were then reactively melt-blended with talc via esterification reactions between the MA grafted onto the polyester backbone and hydroxyl functions from the lateral surface of talc. The effect of tin(II) octoate and 4-dimethylaminopyridine (4 – DMAP) was also studied as esterification catalysts. The molecular characteristics of the resulting composites as well as their physical and morphologic properties were determined, and compared to ones of a simple PBAT-talc melt-blend. Finally, these results were extrapolated to a one-step reactive extrusion process. Such a reactive

extrusion is highly desirable for economics reasons to prepare a composite material at low cost-production.

10.3 Experimental Section

10.3.1 Materials

Poly(butylene adipate-*co*-terephthalate) (PBAT) having a molecular weight of 43,510 g/mol and a polydispersity index (M_w/M_n) of 2.30 under the trade name Ecoflex FBX 7011 was purchased from BASF Corporation, and used as received. 2,5-dimethyl-2,5-di-*(tert*-butylperoxy) hexane (Lupersol 101), maleic anhydride (MA), and 4-dimethylaminopyridine (4-DMAP, 99+%) were provided by Sigma-Aldrich Chemical Company (Milwaukee, WI), and used as received. Talc having a particle size of ca. 6 μm under the trade name Luzenac 20M00S was provided by Luzenac Europe, and dried at 120°C overnight before use. Tin(II) octoate ($\text{Sn}(\text{Oct})_2$, 90+%) were provided by Alfa Caesar, and used as received.

10.3.2 Experimental Procedure

10.3.2.1 Maleation of PBAT Chains

1000g of PBAT, 30g of MA (3% by weight of PBAT) and 5g of Lupersol 101 (0.5% by weight of PBAT) were hand-mixed, and fed together to a Century ZSK-30 co-rotating twin screw extruder at a feed rate of 100 g/min. This composition was pre-determined based on our earlier studies (25). Barrel and die temperatures were maintained via ten electrical/cooling devices the temperature profile as follows: 20/125/145/165/185/185/185/185/185/180°C from the barrel section just after the feed

throat to the die, with a melt temperature of 184°C – 188°C. The screw diameter was of 30 mm, and the length-to-diameter ratio of 42:1. The screw speed was 150 rpm resulting in a mean residence time of about 4-5 minutes. The strand was extruded through a mono-hole die having a nozzle opening of 2.7 mm in diameter, cooled down into a water-bath, and pelletized downstream. The extent of maleation for samples grafted with MA was determined by a potentiometric back titration using the Automatic Titroline Alpha Titration system, according to Johnson and Funk's method (26). The unreacted MA was removed by drying the samples at 85°C under vacuum. After dissolution of approximately 1g of the dried crude sample in about 20 mL of chloroform-methanol (3:2), 2 mL of morpholine solution (0.05N in methanol) was added to react with the anhydride functions. The mixture was allowed to react for about 10 minutes. The samples were then titrated against 0.01N HCl. The HCl solution was initially standardized using a known KOH standard. The morpholine solution was also titrated against 0.01N HCl to obtain a blank reading. Under these conditions, the MA-grafted polymer was completely soluble, and did not precipitate during the titration. A 0.94 wt% of grafted MA on the PBAT backbone was calculated as follows:

$$\% \text{ MA grafted} = (V_{mor} N_{mor} - V_{HCl} N_{HCl}) \times \frac{98.06 \text{ g/mol}}{W_{sample}} \times 100 \quad (10.1)$$

Where V is the volume (liters); N is the normality (mol/equivalent); and W_{sample} is the weight of MA-g-PBAT in grams.

10.3.2.2 Reactive Melt-blending of MA-g-PBAT chains with Talc.

700g of MA-g-PBAT, 300g talc and 3.5g of the esterification catalyst (either Sn(Oct)₂ or 4-DMAP) were hand-mixed, and fed together to a Century ZSK-30 co-rotating twin screw extruder at a feed rate of 100 g/min. The temperature profile and screw speed were described heretofore. The strand was extruded through a mono-hole die having a nozzle opening of 2.7 mm in diameter, cooled down into a water-bath, and pelletized downstream. The grafting efficiency was gravimetrically determined by selective extraction of the polyester part from PBAT-talc composites as follows: solubilization of the composites in chloroform (Sigma-Aldrich, 99.9+%), separation of the supernatant containing the polyester fraction through ultracentrifugation at 4000 rpm for 1 hour, and evaporation of chloroform until reaching a constant weight.

10.3.2.3 One-Step (*In Situ*) Reactive Extrusion Process

700g of PBAT, 21g of MA (3% by weight of PBAT), 3.5g of Lupersol 101 (0.5% by weight of PBAT) and 300g of talc were hand-mixed, and fed together to a Century ZSK-30 co-rotating twin screw extruder at a feed rate of 100 g/min. Sn(Oct)₂ was pumped at a feed rate of 0.35 g/min (0.5% by weight of PBAT), at an inlet port 20D downstream of the feed port. The screw diameter was of 30 mm, and the length-to-diameter ratio of 42:1. Barrel and die temperatures were maintained by means of ten electrical/cooling devices as described heretofore. The screw speed was 150 rpm resulting in a mean time residence of about 4-5 minutes. The strand was extruded through a mono-hole die having a nozzle opening of 2.7 mm in diameter, cooled down into a water-bath, and pelletized

downstream. The grafting efficiency was gravimetrically determined as described heretofore.

10.3.2.4 Blown films

The reactively modified PBAT-talc composites were extruded into films a Killion single-screw blown film unit. The screw diameter was 25.4 mm with a length-to-diameter ratio of 25:1. The die inner diameter was 50.8 mm with a die gap size of 1.5 mm. The blown film processing conditions are shown in Table 10.1. The screw speed was maintained at 16 rpm. Blown films processing was carried out at a pressure of ~ 2000 psi, with a melt temperature of 150°C -160°C.

Table 10.1 Temperature profile used for blown films

Zone	1	2	3	Clamp	Adaptor	Die1	Die 2	Die 3	
				Ring					
T(°C)	150	150	150	135	130	125	125	25	

10.3.2.5 Molecular Characteristics and Mechanical Properties of Composites

PBAT-Talc

Size Exclusion Chromatography (SEC) of PBAT and MA-g-PBAT samples was performed in THF (Labscan, 99%) at 35°C using a Polymer Laboratories (PL) liquid chromatograph equipped with a PL – DG802 degazer, an isocratic HPLC pump LC 1120 (flow rate = 1ml/min), a Basic-Marathon Autosampler, a PL-RI refractive index detector

and three columns: a guard column PL gel 10 μm and two columns PL gel mixed-B 10 μm . Molecular weights and molecular weight distribution were calculated with reference to a polystyrene calibration.

Tensile properties of the films were determined using UTS Mechanical Testing Equipment fitted with a 100 lbs load cell. The crosshead speed was 20 inches per minute. Rectangular film samples, 4 inches x 1 inch dimension cut along the machine direction were conditioned at $23^{\circ}\text{C} \pm 2^{\circ}\text{C}$ and $50\% \pm 5\%$ Relative Humidity for 40 hours according to the ASTM D – 618 (27), before being tested for their mechanical properties according to ASTM D-882 testing (28).

A Ray-Ran Melt Flow Indexer was used to characterize the melt viscosity of PBAT-talc composites at standard conditions of 190°C and a 2.16 kg load, according to ASTM D – 1238 (29).

A high resolution Thermal Gravimetric Analyzer (TGA) 2950 from TA Instruments was used to determine the composition of talc from PBAT-talc composites. Nitrogen was used as the purge gas with the sample purge being 60 ml/min and the balance purge being 40 ml/min. The sample was heated to 600°C at the rate of 10°C per min. A modulated DSC 2920 from TA Instruments was used under nitrogen flow. To erase any prior history, the samples were first heated to 200°C at a heating rate of $40^{\circ}\text{C}/\text{min}$, kept isothermal for 1 minute, and then cooled down to -70°C at a cooling rate of $10^{\circ}\text{C}/\text{min}$. The crystallization temperature was recorded during the cooling step. The samples were then reheated to 200°C at a heating rate of $10^{\circ}\text{C}/\text{min}$ to determine the melting temperature and enthalpy of PBAT-talc composites.

10.4 Results and discussion

10.4.1 Preparation of compatibilized PBAT-talc composites

In an attempt to produce reactive functional groups on the polyester, for improving the interfacial adhesion between talc and the polyester, poly(butylene adipate-*co*-terephthalate) copolyester (PBAT) was chemically modified by free-radical grafting of maleic anhydride (MA) onto PBAT through reactive extrusion according the proposed mechanism (24) (Figure 7.3). It is worth noting that some authors proposed an end-chain grafting mechanism, involving the insertion through the aliphatic dicarboxylic acid units of the copolyesters (22). In practice, the maleation of PBAT was carried out in the presence of 3 wt% MA, and 0.5wt% Lupersol 101 as free-radical initiator through reactive extrusion at only one process temperature, i.e. 185°C, a temperature high enough to avoid the homopolymerization of maleic anhydride. It is worth noting that the temperature does not significantly affect the grafting percentage of MA onto the polyester backbone, as observed by our earlier studies (23, 24). The MA content for the resulting chemically modified PBAT, so-called MA-*g*-PBAT, was 0.94wt% by PBAT as determined by the potentiometric back titration as described earlier. The MA-*g*-PBAT was then melt-blended with 30 wt-% talc through a second reactive extrusion process. To promote the esterification reactions between the MA functions grafted onto the polyester backbone and the hydroxyl functions from talc, tin (II) octoate ($\text{Sn}(\text{Oct})_2$) and 4-dimethylaminopyridine (4-DMAP) were studied as esterification catalysts. Table 10.2 reports the molecular parameters of the MA-*g*-PBAT-talc composites (as obtained from a two – step reactive extrusion process) together with those of a simple PBAT-talc melt-blend. The talc content of composites was confirmed by thermogravimetric analysis

within an error less than 3 wt%. The grafting efficiency of the MA-*g*-PBAT onto talc particles was determined by selectively recovering the polyester part of the composite, after solubilization of the composite in chloroform, separation of the polyester fraction (supernatant) through ultracentrifugation at 4000 rpm for 1 h, and evaporation of chloroform. For the sake of comparison, these results have been compared to the simple melt-blended PBAT-talc.

Figure 10.1 shows the proposed reaction mechanism for the reaction of the grafted MA on the PBAT backbone with the silanol functionalities on the talc particles (Si – OH) using Sn(Oct)₂ as the transesterification catalyst. Figure 10.2 shows the proposed reaction mechanism for the reaction of the grafted MA on the PBAT backbone with the silanol functionalities on the talc particles using 4-DMAP as the transesterification catalyst.

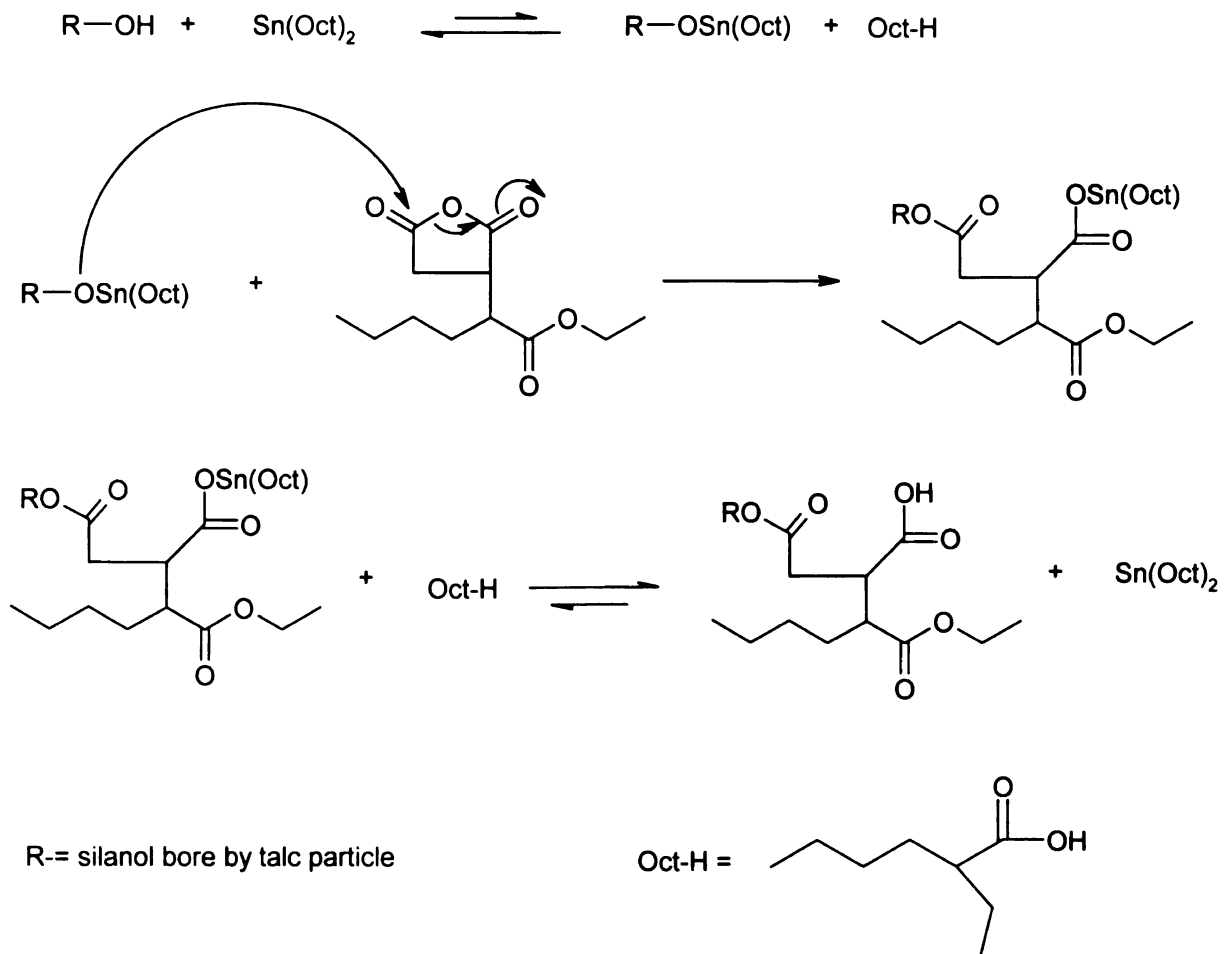


Figure 10.1 Proposed mechanism for the esterification reaction between silanol coming from talc (R-OH) and grafted-maleic anhydride polyester chains catalyzed by tin octoate

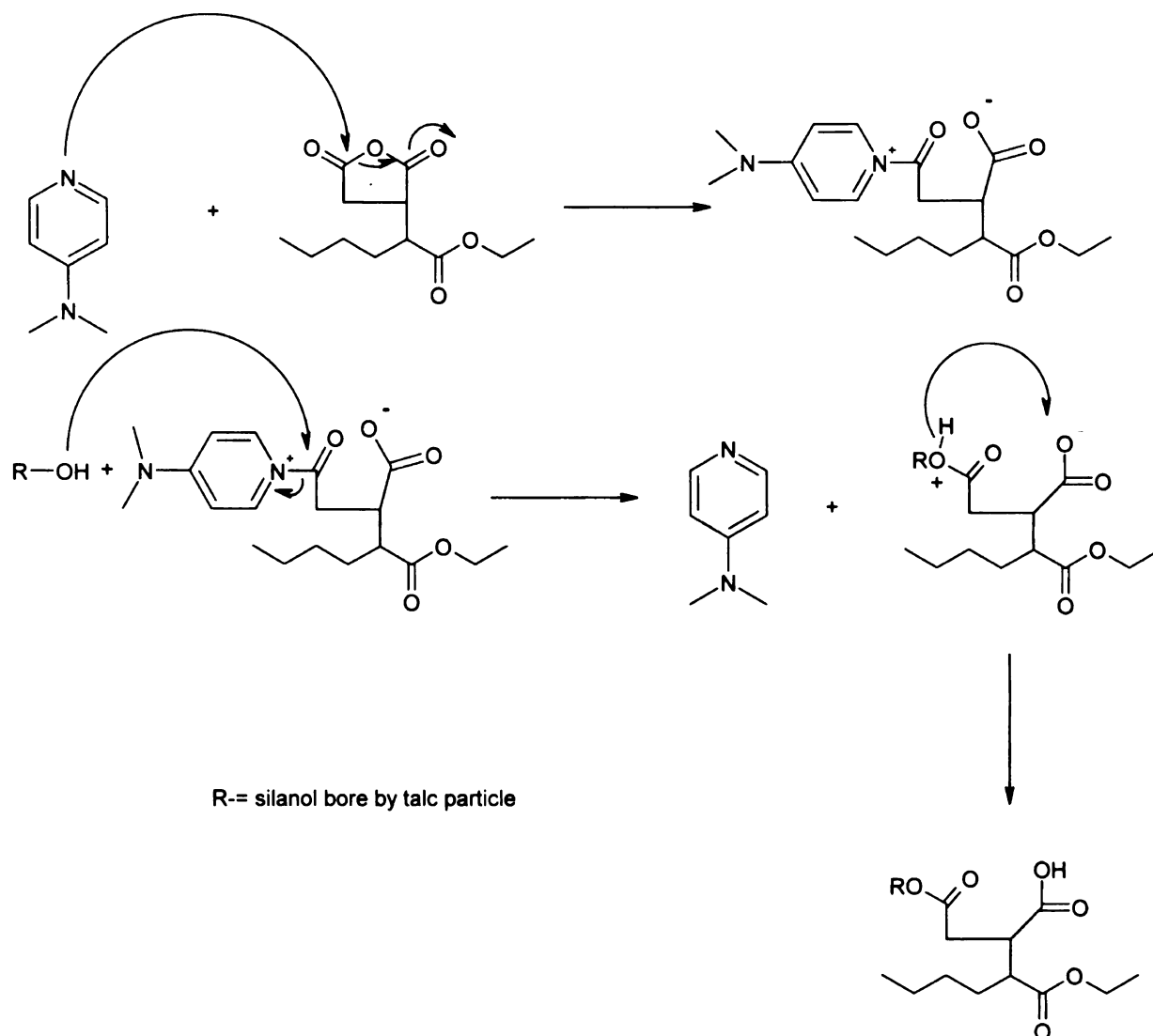


Figure 10.2 Proposed mechanism for the esterification reaction between silanol coming from talc (R-OH) and grafted-maleic anhydride polyester chains catalyzed by 4-Dimethylamino pyridine (4 – DMAP). NB: the positive charge bore by 4-dimethylaminopyridine is stabilized by resonance (resonance forms not shown here)

Table 10.2 Effect of esterification catalysts (Sn(Oct)₂ and 4-DMAP) on the Melt-Flow Index (MFI) of MA-g-PBAT-talc composites, and the weight fraction, number-average molecular weight (M_n), and molecular weight distribution (M_w/M_n) of their recovered polyester part, as prepared through a two-step reactive extrusion process.

Entry	Polyester Precursor	Catalyst	Catalyst weight % ^b (wt%)	MFI (g/10 min) ^c	Extracted Polyester		
					Recovered Polyester (wt%) ^d	M _n ^e	M _w /M _n ^e
1 ^a	PBAT	-	-	3.89	72	41,660	2.63
2	MA-g-PBAT	-	-	1.73	73	37,520	3.16
3	MA-g-PBAT	Sn(Oct) ₂	0.5	23.32	78	24,280	2.45
4	MA-g-PBAT	Sn(Oct) ₂	1	17.36	77	20,080	2.44
5	MA-g-PBAT	4-DMAP	0.5	8.23	73	36,340	2.60
6	MA-g-PBAT	4-DMAP	1	16.04	74	33,390	2.55

a) Simple PBAT-talc melt-blend.

b) Weight Fraction of Catalyst (by PBAT).

c) Melt-Flow Index determined at 190°C using a 2.16 kg load (ASTM D-1238).

d) Weight Fraction of the polyester recovered after solubilization of composites in chloroform, ultracentrifugation at 4000 rpm for 1 h, separation of the supernatant (polyester part), and evaporation of chloroform until reaching a constant weight.

e) Determined by SEC in THF at 35°C with respect to a polystyrene calibration

As far as the composites prepared in the absence of catalyst are concerned, the MFI of MA-*g*-PBAT-based composites was surprisingly lower than one of the simple melt-blend (entries 1 – 2, Table 10.2). This decrease of MFI is adequately related to an increase of the melt-viscosity for the maleated-PBAT-talc composites. This may suggest that even though the melt-viscosity of maleated-PBAT was lower than that of PBAT, as seen in our previous work (25), an effective compatibilization of the maleated-PBAT chains with the talc particles would offer a restriction to the flow through the capillary die due to the formation of a network between polyester chains and talc particles. It is also possible that in addition to the grafting reactions of MA onto the polyester backbone free-radically initiated by Lupersol 101, the peroxide could also promote branching reactions within the polyester, as a consequence, the (micro-) gelification of polyester chains, and thus the increase of melt-viscosity of MA-*g*-PBAT. Besides the cross-linking reactions, undesirable β -scission reactions had occurred during the maleation process as well (Figure 7.5). Such reactions decreased the molecular weight of polyester as attested by the decrease of M_n from 41,660 to 37,520 g/mol after maleation, for the polyester part recovered from composites, as prepared in the absence of catalyst (entries 1 – 2, Table 10.2). It is worth noting that the molecular parameters (M_n and M_w/M_n) of PBAT and MA-*g*-PBAT after and before extrusion were identical, highlighting the limited presence of thermal and/or hydrolytic degradations during their melt-blending with talc (see experimental part).

When any esterification catalysts were used for preparation of composites (entries 3 – 7, Table 10.2), the MFI of composites increased with increasing the catalyst concentration, i.e. their melt-viscosity, even their M_n and M_w/M_n for the extracted polyester part,

decreased. Such decrease of molecular parameters, more pronounced in the case of $\text{Sn}(\text{Oct})_2$, is attributed to the occurrence of inter- and intramolecular transesterification reactions. Indeed, in addition to their action as esterification catalyst, $\text{Sn}(\text{Oct})_2$ and 4-DMAP can also promote the intramolecular and intermolecular transesterification reactions. The intramolecular transesterification reactions yield the decrease of M_n through back-biting reactions, whereas the intermolecular ones rearrange polyester chains to yield the most probable molecular weight redistribution (M_w/M_n close to 2).

The most striking feature is that the amount of extracted polyester is quite higher, more particularly in the case of composites prepared in the presence of catalysts, compared to that of the simple melt-blend PBAT-talc. For example, the weight fraction of extracted polyester was 72 wt% for the simple PBAT-talc melt-blend, and 78 wt% for the composite maleated PBAT-talc prepared in the presence of $\text{Sn}(\text{Oct})_2$ (entries 1 and 3, Table 10.2). This attests that some MA-g-PBAT chains were grafted onto the surface of talc, probably through the formation of ester bonds between hydroxyl functions from talc, and MA from the MA-g-PBAT chains. As a consequence, talc particles so-grafted onto polyester chains were stripped off into the supernatant (polyester part) during the extraction step. It is worth noting that traces of talc in the extracted polyester fraction were confirmed by thermogravimetric analyses. Interestingly, the grafting of MA-g-PBAT chains onto talc particles was able to improve the interfacial adhesion between both the partners, and therefore the mechanical properties of resulting composites. This improvement of mechanical properties will be discussed hereafter.

10.4.2 Mechanical properties of maleated PBAT-talc composites

Table 10.3 reports the tensile properties of films obtained from these resulting composites prepared through a two-step reactive extrusion process (see Table 10.2), together with the simple PBAT-talc melt-blend, in the machine direction. It is worth noting that the tensile properties of films in the transverse direction exhibited a similar trend and are reported in Table 10.4.

By comparison to the simple PBAT-based and MA-g-PBAT composites, it was quite surprising that all the tensile properties were improved with the catalytic grafting of maleated PBAT onto the talc surface (entries 3 – 7, Tables 10.3 and 10.4). More particularly, the increase of Young's modulus, tensile and yield stress were significant. The remarkable increase of Young's modulus for the maleated PBAT-based composites prepared in the presence of any esterification catalysts is quite surprising since the talc weight fraction was identical for the simple melt-blend and MA-g-PBAT composites, i.e. 30 wt%. A possible explanation may be related to catalytically promoted-grafting of the maleated-PBAT onto the talc surface that could increase the volume of dispersed particles, e.g. through crystallization, forming micro-particles of talc wrapped by the maleated PBAT chains. It could result an increase of volume fraction for the talc particles yielding a tougher material and, thus, a higher Young's modulus.

In addition, retaining high toughness, the MA-g-PBAT-talc composites prepared using the catalysts exhibited tensile and yield stress values, twice compared to that of the simple melt-blend.

**Table 10.3 Tensile Properties (Machine Direction) of blown films
derived from the melt-blends prepared containing 30 wt% in talc
(see Table 10.2)**

No	Nature of		Young's modulus (psi)	Yield Stress (psi)	Tensile Stress (psi)	Break Elongation (%)
	Melt- Blend	Catalyst ^{b)}				
1 ^{a)}	PBAT	-	17004	1838.7	2058.9	600
2	MA-g- PBAT	-	15951	2695.4	2725.8	462
3	MA-g- PBAT	0.5 wt% Sn(Oct) ₂	32990	3942.4	3952.2	635
4	MA-g- PBAT	1.0 wt % Sn(Oct) ₂	27890	3737.4	3747.0	500
5	MA-g- PBAT	0.5 wt % 4-DMAP	33720	2817.1	3201.8	480
6	MA-g- PBAT	1.0 wt % 4-DMAP	39320	2981.4	3369.4	610
7	MA-g- PBAT	2.0 wt % 4-DMAP	34165	4192.5	4205.0	470

a) Non-compatibilized simple melt-blend

b) Weight fraction in catalyst by PBAT

**Table 10.4 Tensile Properties (Transverse Direction) of blown films
derived from the melt-blends prepared containing 30 wt% in talc
(see Table 10.2)**

No	Nature of		Young's modulus (psi)	Yield Stress (psi)	Tensile Stress (psi)	Break Elongation (%)
	Melt- Blend	Catalyst ^{b)}				
1 ^{a)}	PBAT	-	17225	1389.8	1528.2	300
2	MA-g- PBAT	-	17283	2326.7	2330.2	510
3	MA-g- PBAT	0.5 wt% Sn(Oct) ₂	25590	3287.5	3297.7	630
4	MA-g- PBAT	1.0 wt % Sn(Oct) ₂	31551	2978.5	2990	380
5	MA-g- PBAT	0.5 wt % 4-DMAP	29910	2401.0	2712	415
6	MA-g- PBAT	1.0 wt % 4-DMAP	22300	2326.1	2423.7	460
7	MA-g- PBAT	2.0 wt % 4-DMAP	30500	3424.5	3435.4	665

a) Non-compatibilized simple melt-blend

b) Weight fraction in catalyst by PBAT

For the break elongation in the machine direction, the MA-g-PBAT-talc composites prepared in the absence of catalyst (entry 2, Table 10.3) exhibited a lower break elongation, as compared to that of the simple melt-blend. This reduction of break elongation for the maleated PBAT-talc composites was probably due to the formation of some (micro-) cross-linking through free radical reactions (*vide supra*) during the maleation process of PBAT chains. Interestingly, when catalysts were used, the break elongation for the resulting maleated-PBAT composites (entries 3 – 7, Table 10.3) increased, and could reach, in some cases, a values higher than that of the simple PBAT-talc melt-blend (> 600 %). However, in the transverse direction, the modified composites exhibited a much higher break elongation as compared to the simple PBAT-talc blend, in some cases (Entries 3 and 7, Table 10.4) the value being ~ 650% as compared to 300%. A plausible explanation for this enhanced elongation in the transverse direction could be the formation of chemical/physical linkages (grafts) between the polyester chains and the talc particles, resulting in the formation of a network, which would permit higher elongations in the cross (transverse) direction (Entries 2 – 7, Table 10.4) as well, and at the same time, restricting the extension of the PBAT chains in the machine direction to some extent (Entries 2 – 7, Table 10.3).

These improvements in the tensile properties may be explained to the enhancement of interfacial adhesion between talc and polyester matrix as derived from the maleation process, and involving the esterification catalysts, as evidenced by scanning electronic microscopy (SEM) images of cryofractured surfaces of the resin pellets (Figure 10.3).

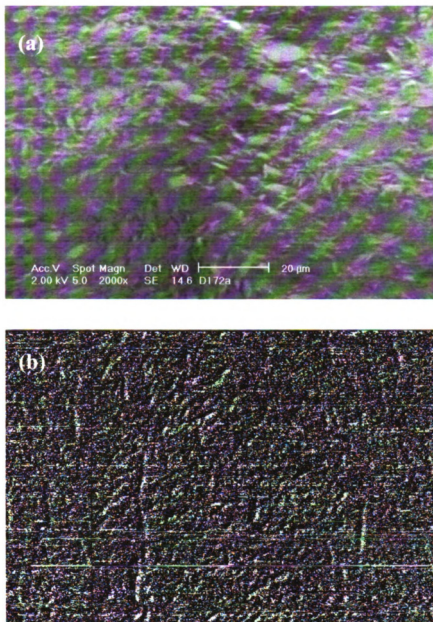
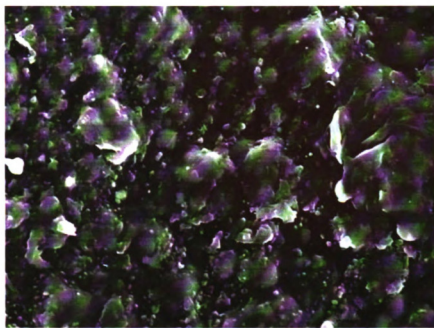


Figure 10.3 SEM Images of cryofractured surface of (a) a simple PBAT-talc melt-blend and (b) MA-*g*-PBAT-based composites prepared in the presence of 1wt% in Sn(Oct)₂ (entries 1 and 4, Table 10.2).

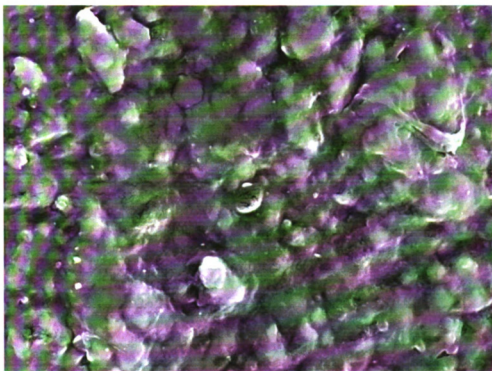
Examination of the cryofractured surface of the simple melt-blend revealed the presence of voids around the filler surface (in the form of platelets), in the polyester matrix, attesting for the poor adhesion between both the partners (Figure 10.3 (a)). These voids can be explained by the propagation of fracture stress via an equatorial location, with some talc particles stripped off from the fractured surface. In contrast, Figure 10.3 (b) confirms the very good adhesion between MA-g-PBAT and talc as created through catalytically promoted grafting of MA-g-PBAT onto talc. As the fracture stress propagated through the matrix mainly, the micro-particles of talc had remained embedded in the polyester matrix.

Also, Figure 10.4 shows the scanning electron micrographs of the ruptured film surfaces for the simple PBAT-talc blend (Figure 10.4 (a)), and the MA-g-PBAT-based composites prepared in the presence of 1wt% in $\text{Sn}(\text{Oct})_2$ (Figure 10.4 (b)). Similar to the results obtained from Figure 10.3, good adhesion between the talc and the polyester chains (wetting of the talc particles by the MA-g-PBAT) in the presence of a catalyst was evident from Figure 10.4. A sharp boundary exists between the talc particles and the polyester phase in Figure 10.4 (a), while a diffused interface suggesting improved adhesion in the presence of $\text{Sn}(\text{Oct})_2$ was observed in Figure 10.4 (b).

Actually, we may expect the formation of ester bonds between the MA grafted onto polyester backbone with the hydroxyl functions from talc for MA-g-PBAT-talc composites, as evidenced by SEM analyses, and selective extraction of the polyester from the composite. However, the authors do not have direct evidence for the formation of such ester bonds, and further investigation will be carried out by XPS experiments for evidence of these ester bonds.



20 μm



20 μm

Figure 10.4 SEM Images of ruptured films of (a) PBAT-talc melt-blend (b) MA-g-PBAT-based composites prepared in the presence of 1wt% in $\text{Sn}(\text{Oct})_2$

10.4.3 *In situ* chemically modified PBAT-talc composites prepared through One-Step Reactive Extrusion Process

In situ chemically modified PBAT-talc composites were prepared through a one-step reactive process. Such a single-step process is highly desirable for economic reasons, allowing the low cost production of a product to compete with the commodity polymers. Practically, the PBAT was hand-mixed with 0.5 wt% (of PBAT) free radical initiator, 3 wt% (of PBAT) MA, and different talc contents (20/30/40/50 wt %), in that order. The mixture was introduced using a feed rate of 100g/min into a co-rotating twin-screw extruder. Sn(Oct)₂, as esterification catalyst was pumped through peristaltic pump at the required rate (0.5/1/2 wt% of PBAT) through a downstream port as illustrated in Figure 10.5.

Talc/PBAT/MA(3wt%)/Peroxide(0.5wt%)

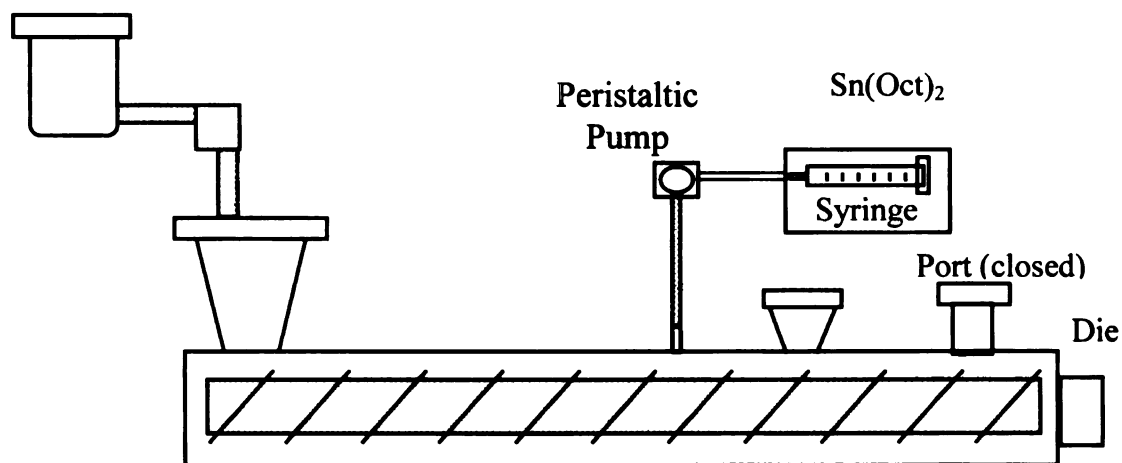


Figure 10.5 Schematic representation the extruder using for the single-step process

Table 10.5 reports the molecular parameters of the resulting composites prepared with different talc contents, as well as different catalyst contents. It is worth noting that an *in situ* chemically modified MA-g-PBAT-talc composite with 60 wt% talc was prepared and melt-blended with plain PBAT (in the ratio of 50:50) in order to achieve a final 30 wt% talc composition (entry 8, Table 10.5). For the sake of comparison, the molecular parameters of a simple PBAT-talc melt-blend, and an *in situ* chemically modified MA-g-PBAT-talc composite prepared in the absence of catalyst were also reported (entries 1 – 2, Table 10.5). The experimental talc composition matched with the measured one within less than a 2 wt% error, as checked by thermogravimetric analysis. The polyester fraction was extracted according to the procedure aforementioned, and its molecular parameters are also reported in Table 10.5.

In perfect agreement with our previous results, PBAT chains was efficiently grafted onto talc particles through the Sn(Oct)₂-promoted one-step reactive extrusion process, as attested by the extracted polyester fraction which was higher than that of the initial polyester composition (entries 3 – 7, Table 10.5).

Quite surprisingly, the MFI of the *in situ* chemically modified PBAT-talc composite prepared in the absence of catalyst, as well as the M_n for its extracted polyester part was almost comparable to those of the simple melt-blend (entries 1 – 2, Table 10.5).

This is in quite contrast to the maleation effect on the molecular parameters of PBAT chains, as observed for the composites prepared through the aforementioned two-step reactive extrusion (Section 10.4.1).

**Table 10.5 Molecular Characteristics of PBAT-talc melt-blends
prepared by direct reactive extrusion process – [One Step] (in the
presence of 3.0 wt% MA and 0.5wt% in peroxide)**

Entry	Polyester Composition (wt%)	Catalyst	Weight fraction in catalyst ^{b)} (wt%)	MFI (g/10 min) ^{c)}	Extracted Polyester		
					Polyester fraction (wt%) ^{d)}	M _n ^{e)}	M _w /M _n ^{e)}
1 ^{a)}	70	-	-	3.89	72	41.660	2.63
2	70	-	-	4.37	74	47.190	2.21
3	70	Sn(Oct) ₂	1	35.65	75	18.920	2.33
4	80	Sn(Oct) ₂	1	30.65	83	13.950	2.54
5	60	Sn(Oct) ₂	1	20.35	69	15.230	2.66
6	52	Sn(Oct) ₂	1	12.60	77	25.400	2.29
7 ^{f)}	40	Sn(Oct) ₂	1	0.38	49	23.490	3.06
8 ^{g)}	70	Sn(Oct) ₂	0.5	8.28	73	41.330	2.22

- a) Simple melt-blend (non-compatibilized – in the absence of MA)
- b) Weight fraction in catalyst with respect to the total mass in PBAT
- c) Melt-Flow Index (MFI) determined at 190°C using a 2.16 kg weight
- d) Weight fraction in polyester recovered after ultracentrifugation at 4000 rpm for 60 minutes.
- e) Determined by SEC in THF at 35°C according to a polystyrene calibration
- f) Preparation of maleated PBAT-Talc Masterbatch containing 60wt% in talc
- g) Redispersion of masterbatch into a plain PBAT matrix to reach 30wt% in talc

Such behavior can be explained by the presence of talc, which “diluted” the total concentration of MA and peroxide used for the one-step reactive extrusion process. Consequently, the incidence of β -scission reactions as well as the branching reactions (due to peroxides) was lessened. The dilution effect for the *in situ* chemically modified MA-g-PBAT-talc composites on the occurrence of undesirable transesterification reactions as promoted by $\text{Sn}(\text{Oct})_2$, could be observed. This was supported by the increase in M_n for the polyester fraction extracted from the *in situ* chemically modified composites with increased talc content (entries 3 – 7, Table 10.5). For instance, M_n (M_w/M_n) was 13,950 g/mol (2.54) for a 80 wt% PBAT content, and 23,490 g/mol (3.06) for a 40 wt% PBAT content (entries 3 and 7, Table 10.5). The MFI of chemically modified PBAT-talc composites also decreased, i.e. their melt-viscosity increased, with increased talc content (entries 3 – 7, Table 10.5).

Whereas the M_n and M_w/M_n of their extracted polyester fraction were identical, the melt-viscosity (inversely proportional to MFI) of the melt-blend prepared from masterbatch and plain PBAT was surprisingly lower, as compared to those of the simple PBAT-talc melt-blend (entries 1 and 8, table 10.5). Such a behavior suggests the desegregation of talc micro-particles, and their better dispersion within the polyester matrix for the masterbatch-based melt-blend. In addition to the improvement of the interfacial adhesion between the talc micro-particles and polyester, the $\text{Sn}(\text{Oct})_2$ -promoted one-step reactive extrusion process allowed to prepare a masterbatch (using 60 wt% talc), in which the steric volume of talc micro-particles grafted onto PBAT chains, and, thus, the resistance of materials to flow through the capillary die used for MFI analyses was reduced.

10.4.4 Tensile properties of compatibilized melt-blends prepared through a one-step reactive extrusion process.

Table 10.6 reports the tensile properties in the machine direction of blown films derived from the *in situ* chemically modified PBAT-talc composites, and the simple PBAT-talc melt-blend. It is worth noting that the tensile properties for the sample containing 60 wt% in talc were not reported since it was practically impossible to blow films due to its high toughness. The tensile properties of films in the transverse direction exhibited a similar trend (Table 10.7).

In perfect agreement, all the tensile properties of resulting blown films derived from the *in situ* chemically modified PBAT-talc composites were significantly improved, as compared to that of the simple PBAT-talc melt-blend (entries 1, 2, 4, 7, 8 and 9, Table 10.6). Particularly, a considerable increase in the Young's modulus of the *in situ* chemically compatibilized composites with increased talc content was observed (Entries 3 – 6, Table 10.6). It is worth noting that their yield and tensile strengths were almost constant with increased talc content, suggesting that the entanglement of the polyester chains, responsible for these values, did not change after the $\text{Sn}(\text{Oct})_2$ -promoted one-step reactive extrusion process. This could be attributed to the good adhesion obtained between the polyester and talc, as a result of which an appreciable drop in tensile values with increasing talc contents was not obtained. However, a decrease in break elongations was observed with increasing talc contents for the *in situ* chemically modified composites, suggesting more brittle materials with a high modulus of elasticity.

Also, it was observed that a lower catalyst ($\text{Sn}(\text{Oct})_2$) loading resulted in improved mechanical properties (Entries, 4, 7 – 8, Tables 10.6 and 10.7). This observation was

logical since the presence of increased amounts of $\text{Sn}(\text{Oct})_2$ resulted in further degradation of the polyester backbone, resulting in poorer tensile strengths and lower break elongations. Thus, 0.5 wt% (of PBAT) $\text{Sn}(\text{Oct})_2$ provided better mechanical properties. However, with the current set-up, low flow rates of catalyst could not be maintained for longer times and, hence, 1 wt% (of PBAT) $\text{Sn}(\text{Oct})_2$ was used for other studies.

The most striking feature is that the break elongations in the machine direction for the *in situ* chemically modified composites containing 30 wt% was remarkably superior to one of simple melt-blend. This is in contrast to the trend reported on MA-g-PBAT-talc composites prepared through the aforementioned two-step reactive extrusion (Section 10.4.2). This can be explained by the dilution effect of talc for the *in situ* chemically modified composites, reducing the incidence of cross-linking reactions, which are responsible for the decrease in break elongation. Interestingly, the best composition regarding the improvement of tensile properties was achieved by melt-blending the master-batch (containing 60 wt% talc) with plain PBAT (in the ratio of 50:50). This improvement can be adequately explained by the partial conservation of the polyester matrix. Such approach allowed to retain the superior mechanical strength of PBAT (added to the masterbatch) by preventing it from undergoing undesirable reactions such as β -scission from MA and transesterification reactions from esterification catalysts that were present during the reactive extrusion process, as well as a thermal extrusion history (entry 9, Tables 10.6 and 10.7).

**Table 10.6 Tensile Properties (Machine Direction) of Blown films
derived from PBAT-talc composites compatibilized through the
one-step reactive extrusion process (see entries 1-6 et 8, Table 5)**

Entry	Nature of melt-blend	Talc Composition (wt%) ^{d)}	Young's modulus (MPa)	Yield stress (MPa)	Tensile stress (MPa)	Break Elongation (%)
1 ^{a)}	Simple melt-blend	30	17004	1838.7	2058.9	600
2 ^{b)}	Maleation	30	26650	3126.7	3137.8	535
3	Maleation + 1% Sn(Oct) ₂	20	23675	3508.3	3513.9	670
4	Maleation + 1% Sn(Oct) ₂	30	31450	3901.5	3962.6	630
5	Maleation + 1% Sn(Oct) ₂	40	48311	3255	3815	440
6	Maleation + 1% Sn(Oct) ₂	48	53912	3260	3500	260
7	Maleation + 0.5% Sn(Oct) ₂	30	31765	4115.8	4117.3	645
8	Maleation + 2% Sn(Oct) ₂	30	23212	2475.6	2560	330
9 ^{c)}	Via masterbatch	30	50640	5265	5280	740

a) Simple melt-blend

b) Composite prepared through maleation without catalyst

c) Obtained by redispersion of « masterbatch » (see. entry 8, Table 5)

d) Weight fraction in talc determined by thermogravimetric analysis

**Table 10.7 Tensile Properties (Transverse Direction) of Blown films
derived from PBAT-talc composites compatibilized through the
one-step reactive extrusion process (see entries 1-6 et 8, Table 5)**

Entry	Nature of melt-blend	Talc Composition (wt%) ^{d)}	Young's modulus (MPa)	Yield stress (MPa)	Tensile stress (MPa)	Break Elongation (%)
1 ^{a)}	Simple melt-blend	30	17225	1389.8	1528.2	300
2 ^{b)}	Maleation	30	29780	2650	2810	480
3	Maleation + 1% Sn(Oct) ₂	20	23660	3635	3645	700
4	Maleation + 1% Sn(Oct) ₂	30	30970	2960	3120	530
5	Maleation + 1% Sn(Oct) ₂	40	52000	3317.8	3560	240
6	Maleation + 1% Sn(Oct) ₂	48	53371	2960	3150	230
7	Maleation + 0.5% Sn(Oct) ₂	30	32980	3980	4030	580
8	Maleation + 2% Sn(Oct) ₂	30	23880	2010	2070	195
9 ^{c)}	Via masterbatch	30	44300	4831	4850	665

a) Simple melt-blend

b) Composite prepared through maleation without catalyst

c) Obtained by redispersion of « masterbatch » (see. entry 8, Table 5)

d) Weight fraction in talc determined by thermogravimetric analysis

10.4.5 Thermal properties of *in situ* chemically modified PBAT-talc composites

Differential scanning calorimetry (DSC) analyses were carried out on the *in situ* chemically modified PBAT-talc composites containing different talc content, as compared to that of pristine PBAT. These data were recorded after erasing any prior thermal history of samples at 200°C for 1 min., and then cooling down at a cooling rate of 10°C/min up to -70°C, and heating to 200°C at a heating rate of 10°C/min under nitrogen flow (Table 10.8). The maximum temperature for the crystallization peak, as obtained during the cooling step, was also reported. The melting enthalpy of samples was normalized for a 100% polyester composition.

From Table 10.8, talc revealed to behave as a nucleating agent, as attested by the shift of crystallization temperature (T_c) to highest values, as compared to that of pristine polyester. The nucleating effect of talc onto the crystallization polyester decreased with the talc content probably due to the agglomeration of talc particles at higher talc contents. For instance, T_c passed from 110.4°C for the 20 wt% talc *in situ* chemically modified composite to 101.6°C for the 60 wt% talc one (entries 2 and 6, table 10.8).

Beside the nucleating effect of talc on T_c , increasing talc content also increased the glass transition (T_g) of *in situ* chemically modified composites. This suggests that the resulting material were getting tougher with talc content, in perfect relation to the trend observed for the Young's modulus of these *in situ* chemically modified composites at different talc content.

Finally, the melting temperature (T_m) and enthalpy (ΔH_m) were not affected by increased talc content. It is worth noting that even though the T_m of all *in situ* chemically modified composites was identical, the melting enthalpy was below of this of pristine PBAT,

suggesting that the polyester crystal size was reduced due to the presence of talc micro-particles.

Table 10.8 DSC data of plain PBAT matrix and composites at different talc loading.

Entry	Talc Composition (wt%)	Nature	T _c (°C)	T _g (°C)	T _m (°C)	ΔH _m (kcal/mol)
1	-	PBAT	25.6	-27.4	121.0	17.23
2	20	Maleation + 1% Sn(Oct) ₂	110.4	-36.2	125.5	11.1
3	30	Maleation + 1% Sn(Oct) ₂	109.0	-37.1	127.2	10.6
4	40	Maleation + 1% Sn(Oct) ₂	108.9	-34.3	125.4	11.5
5	48	Maleation + 1% Sn(Oct) ₂	107.6	-33.6	125.5	11.0
6	60	Maleation + 1% Sn(Oct) ₂	101.6	-31.0	124.8	12.51

10.5 Starch Foam Extrusion using PBAT-talc blends

The extrusion of hydroxypropylated high amylose starch foams using PBAT in the absence/presence of compatibilizers has been studied in the previous Chapters 7 – 9. However, instead of using PBAT as the functional aid, a blend of PBAT-talc, which was used as a film blend, (as explained in the previous sections) was used as a functional aid in the processing of starch foams due to the following reasons:

1. Better dispersion of the nucleating agent (talc) in the melt.
2. Increasing the viscosity of the functional aid (due to the presence of talc) for improved blending purposes (viscosity difference between plastic starch and PBAT-talc is lower than that between plastic starch and PBAT). Lower the viscosity difference better are the blend properties. The PBAT-talc blend had a Melt Flow Index (MFI) of 3.9-g/10 min as compared to 5.8-g/10 min for PBAT, thus indicating an increase in viscosity. A finer morphology would be obtained which can be explained by viscosity matching effect. Typically, the size of the dispersed phase (PBAT-talc blend, in this case) in a blend is lowest when the viscosity ratio approaches unity.
3. Reduction in cost.

The physico-mechanical properties of the hydroxypropylated high amylose starch foams using PBAT-talc blends are shown in the following Table 10.9.

**Table 10.9 Physico-Mechanical Properties of Starch foams using
PBAT-talc blend.**

No	Functional Aid	Unit Density (kg/m ³)	Radial Expansion ratio	Specific Length (cm/gm)	Compressive Strength (Pa)	Resiliency (%)
1	None	30.2	39.7	14.6	4.36 E+05	69.8
2	5% PBAT	24.2	46.7	15.5	4.02 E+05	84.3
3	5% PBAT-talc (70:30)	22.0	40.9	19.5	3.42 E+05	92.3

It was observed from the above data that the unit density of the starch foams obtained using PBAT-talc as the functional aid was approximately 22 kg/m³ as compared to 24.2 kg/m³, which was the density of the starch foams obtained using PBAT as the functional aid. Also, the resiliency of the starch foams increased up to 92.3% for the starch-based foams using PBAT-talc, as compared to 84% realized using PBAT as the functional aid. This is probably due to a more uniform cross-section of the foams obtained, due to uniform dispersion of the nucleating agent (talc), as evident from the picture below. A finer and better cell structure was obtained (Figure 10.6). Figure 10.6 (a) shows the foam cross-section obtained using 5% PBAT, while Figure 10.6 (b) shows the foam cross-section obtained using 5% PBAT-talc. Also, better melt mixing could have been attained due to a reduction in the viscosity difference between the plastic starch and the functional aid. The increase in viscosity helps in developing increased die pressure, which helps in improved foaming.

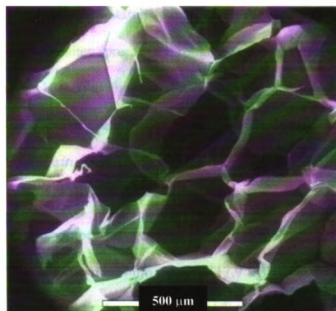
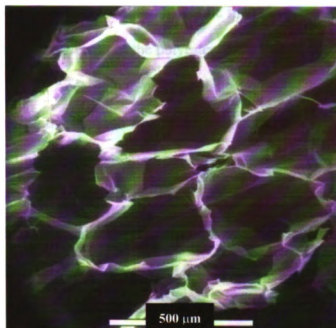


Figure 10.6 SEM of the cross-section of starch foams using (a) – 5% PBAT, (b) – 5% PBAT-talc blend.

However, the incorporation of these cheap inorganic fillers in the polyester matrix results in a decrease in the tensile strength of the polyester (5500 – 6000 psi for PBAT and 2000 psi for PBAT-talc blend). According to results obtained on polyethylene foams by Auger et al (30), a polymer with increased tensile strength would provide a foam with lower compression set and higher compression strength, resulting in improved resiliency, and further lower densities.

The tensile strength and elongation of the PBAT-talc blends were improved by increasing the compatibilization between talc and PBAT, by carrying out grafting chemistries between the Si-OH functions on the talc surface and the polyester, as described in the previous sections.

Hydroxypropylated high amylose starch foams were produced using *in situ* chemically modified PBAT-talc composites (prepared through a one-step reactive extrusion process as explained in Section 10.4.3) as functional aids. The physico-mechanical properties of the starch foams (unit density, expansion ratio, specific length, compressibility, and resilience) using these *in situ* chemically modified PBAT-talc composites are shown in Table 10.10.

The maleated-PBAT-talc composites provided starch-based foams having densities in the range of 17.5 – 22 kg/m³. The minimum density (17.9 kg/m³) and maximum expansion ratio (46.9) was obtained using the maleated-PBAT-talc composite produced by melt-blending the master-batch (containing 60 wt% talc) with plain PBAT (in the ratio of 50:50) (Entry 9, Table 10.10). This is because the composite had excellent tensile strength and elongation to support cell growth and, thus, foam expansion. Besides, the

maleated-PBAT also had good compatibility with the hydroxypropylated high amylose corn starch used for the foaming operation.

All maleated-PBAT-talc composites, with the exception of those having either a higher (50%) talc content (Entry 6, Table 10.10) or a higher (2%) Sn(Oct)₂ content (Entry 8, Table 10.10), offered starch-based foams with densities of approximately 20 kg/m³. This was due to the fact that the maleated-PBAT-talc composite with a talc loading of 50% had poor elongation and high rigidity (high Young's modulus), thus resisting cell expansion. Also, the maleated-PBAT-talc composite with a higher catalyst concentration had a poor tensile strength resulting in cell rupture during foam growth.

It was observed that the physico-mechanical properties of the starch foams improved on using the *in situ* chemically modified PBAT-talc composites as functional aids.

The resiliency of the foam samples is listed in Table 10.10. The addition of PBAT improved the resiliency considerably from 69.7% to 84.2% at a PBAT content of 5% of the starch used. The maleated-PBAT-talc composites had superior tensile strengths and break elongations as well as were compatible with starch. The spring indices obtained were in the range of 82 – 95% using maleated-PBAT-talc composites (Table 10.10, Entries 2 – 8).

Table 10.10 Physico-Mechanical Properties of Starch foams using *in situ* chemically modified PBAT-talc composites (prepared through a one-step reactive extrusion process).

No	Functional Aid	Unit Density (kg/m ³)	Radial Expansion ratio	Specific Length (cm/gm)	Compressive Strength (Pa)	Resiliency (%)
1	Entry 1 from Table 10.6	22.0	40.9	19.5	3.42 E+05	92.3
2	Entry 2 from Table 10.6	20.9	44.1	19.0	3.36 E+05	94.1
3	Entry 3 from Table 10.6	20.4	44.1	19.4	3.29 E+05	94.9
4	Entry 4 from Table 10.6	20.4	44.5	19.2	3.33 E+05	94.8
5	Entry 5 from Table 10.6	20.6	44.9	18.9	3.40 E+05	86.7
6	Entry 6 from Table 10.6	21.3	45.1	18.2	3.44 E+05	82.2
7	Entry 7 from Table 10.6	19.7	46.0	19.3	3.32 E+05	95.1
8	Entry 8 from Table 10.6	21.8	40.2	20.0	3.37 E+05	89.7
9	Entry 9 from Table 10.6	17.9	46.9	20.8	3.20 E+05	96.8

The resilience provided by maleated-PBAT-talc composites having 50% talc was minimum (~ 82%) (Entry 6, Table 10.10), due to its low break elongations and high moduli of elasticity (high rigidity). The maleated-PBAT-talc composites having 40% talc also offered starch foams having a spring index of ~ 87% (Entry 5, Table 10.10), also due to its high rigidity and low break elongations. The starch foams obtained using the maleated-PBAT-talc composite prepared using 2% Sn(Oct)₂ also exhibited poorer resilience of ~87% due to its lower melt strength. In accordance with their superior melt strengths, break elongations and reasonable flexibilities, the maleated-PBAT-talc composites (Entries 2 – 4 and 7, Table 10.10) provided starch-based foams having resilience of approximately 95%. This was due to the fact that a functional aid having higher melt strength is capable of resisting cell rupture due to brittle fracture during compression. The maleated-PBAT-talc composite produced by melt-blending the master-batch (containing 60 wt% talc) with plain PBAT (in the ratio of 50:50) provided enhanced starch foams having resilience as high as 97% (competitive with the commercial polyethylene and polystyrene foams), in accordance with its extremely superior mechanical properties. These results obtained were in accordance with those observed in the case of polyethylene foams by Auger et al. (30).

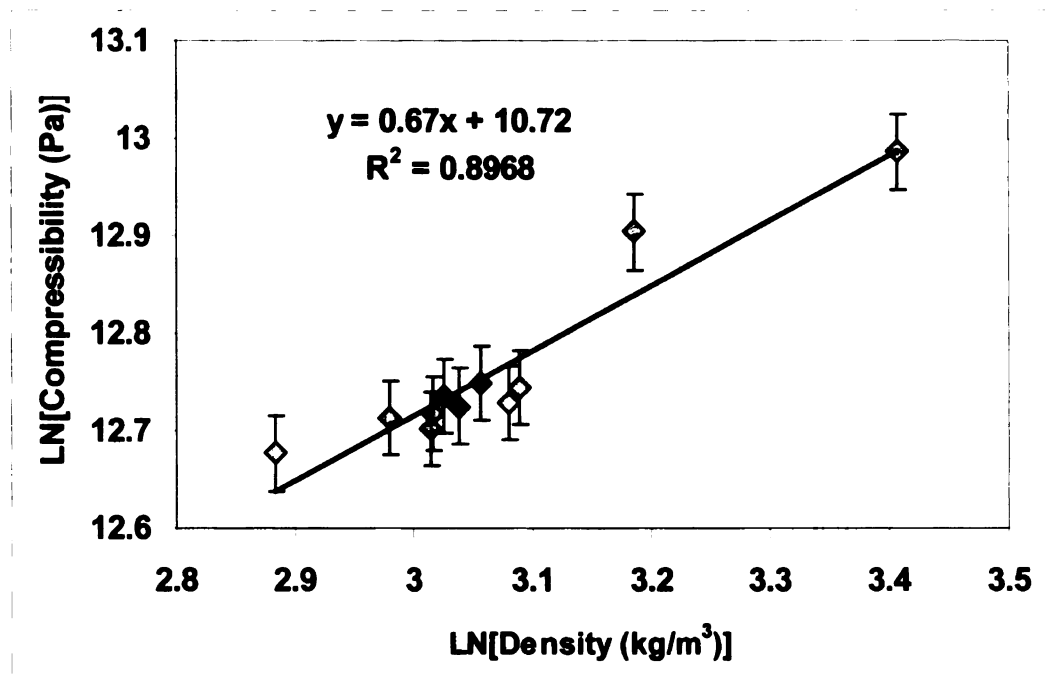


Figure 10.7 Logarithmic plot of Compressive Strength (Pa) as a function of foam density (kg/m³).

The regression line in Figure 10.7 was drawn and a slope of 0.67 was obtained ($n = 0.67$). A value of $n = 0.92$ was obtained by Willett et al. (31), while Hutchinson and co-workers (32) report exponents of 1.5 – 1.6 for compressive strengths of foams prepared from maize grits. The value of ‘n’ obtained was not in agreement with the value reported by Willett et al. However, this value is specific to the type of materials used as well as the extrusion system used for foaming.

10.6 Conclusions

Improvement of the interfacial adhesion between talc and PBAT was successfully achieved by free-radical grafting of MA onto the polyester backbone, and promoting using esterification catalyst, as carried out through reactive extrusion. It is of prime importance to develop biodegradable PBAT-talc composites having satisfactory physico-mechanical properties to be competitive with commodity polymers such as HDPE. In a first step, the polyester backbone was reactively modified through free-radical grafting of maleic anhydride, in order for the improvement of the interfacial adhesion between PBAT and talc to react together with the hydroxyl functions from the lateral surface of talc. The resulting maleated-PBAT was then reactively melt-blended with talc using $\text{Sn}(\text{Oct})_2$ and 4-DMAP as esterification catalysts. The interfacial adhesion between MA-g-PBAT and talc was so-improved as evidenced by scanning electronic microscopy and selective extractions of the polyester part from the composite. It resulted that the tensile properties for the blown films prepared from these resulting composites was considerably improved, as compared to those of the simple melt-blend of PBAT-talc.

Extrapolation to a one-step reactive extrusion process was successfully carried out. The *in situ* chemical modification of PBAT-talc composites allowed preparing compositions reaching up to 60 wt% talc. Interestingly, the best composition regarding the improvement of tensile properties was achieved by melt-blending *in situ* chemically modified PBAT-talc composite containing 60 wt%-talc with plain PBAT (in the ratio of 50:50). Such approach allowed to retain the superior mechanical strength of PBAT (added to the masterbatch) by preventing it from undergoing undesirable reactions such as β -scissions from MA and transesterification reactions from esterification catalysts that

were present during the reactive extrusion process, as well as a thermal extrusion history. Thermal properties of chemically modified PBAT-talc composites showed that talc behaved as a nucleating agent for the polyester chains.

To explain the improvement of the interfacial adhesion between talc and PBAT, a more thorough X-Ray Photoelectron Spectra (XPS) study will be carried out in order to attest for the formation of chemical bonds between both partners. A morphological study will be also carried out in order to determine the influence of compatibilization process on the size, the distribution of micro-particles as well as the dispersion homogeneity within the polyester matrix. The diffusion of different gases and vapor barrier properties will be also studied. We envision to expand the compatibilization process to other biodegradable polymers such as poly(ϵ -caprolactone) and other talc in function of their size and intrinsic nature (crystallinity, surface chemistry).

Additionally, hydroxypropylated high amylose corn starch-based foams were produced using the *in situ* chemically modified PBAT-talc composites (prepared through a one-step reactive extrusion process as explained in Section 10.4.3) as functional aids. The maleated-PBAT-talc composite produced by melt-blending the master-batch (containing 60 wt% talc) with plain PBAT (in the ratio of 50:50) provided enhanced starch foams having a density as low as 17.5 kg/m^3 , and resilience as high as 97% (competitive with the commercial polyethylene and polystyrene foams), in accordance with its extremely superior mechanical properties.

10.7 Current Research and Future Recommendations

Current research is focused on determining the thermal and hydrolytic stability of the films blown from the *in situ* chemically modified PBAT-talc composites prepared through a one-step reactive extrusion process (Entries 4 and 9, Tables 10.6 & 10.7). It is worth noting that for these stability experiments, the master-batch (containing 60 wt % talc) and the plain PBAT were hand-mixed in the ratio of 50:50, and directly subjected to blown-film extrusion. This further reduced a thermal extrusion history in the plain PBAT portion, providing higher mechanical properties. Earlier studies involved the melt-blending of the masterbatch and PBAT in the Century ZSK-30 TSE prior to blowing film from the collected resin in the Killion blown-film unit. The two stabilizers studied were discussed in the following section.

10.7.1 Stabilizers

The main purpose of using these stabilizers was to minimize the thermal/thermo-oxidative degradation of the polyester due to the residual catalyst ($\text{Sn}(\text{Oct})_2$). Thermal degradation in the presence of oxygen is characterized by a decrease in the molecular weight, and an increase in the carboxylic acid end-group concentration. The extent of thermal degradation is not only a function of temperature, but also depends heavily on the residual $\text{Sn}(\text{Oct})_2$ content. It is thought that the coordination of the metal ion to the carbonyl of the ester group leads to the polarization of the carbonyl, which favors the hydrogen abstraction in the cyclic transition state, and formation of a vinyl ester group (33).

10.7.1.1 ULTRANOX 626

ULTRANOX 626 phosphite (Bis(2, 4-di-*tert*-butylphenyl) pentaerythritol diphosphite) antioxidant (Figure 10.8) is a high performance solid organo-phosphite antioxidant that contains no more than 1.0% by weight Triisopropanolamine. It is a preventive type of antioxidant (34) which decomposes the hydroperoxides formed into the corresponding alcohols and gets transformed into a phosphate, without intermediate formation of free radicals. As a consequence, they prevent chain-branching resulting from the decomposition of the hydroperoxides into alkoxy and hydroxy radicals.

Also, the 'melt stabilization' effect of the phosphite has been attributed to the complexation/chelation of the transesterification catalyst $[\text{Sn}(\text{Oct})_2]$.

Molecular Formula: $\text{C}_{33}\text{H}_{50}\text{O}_6\text{P}_2$

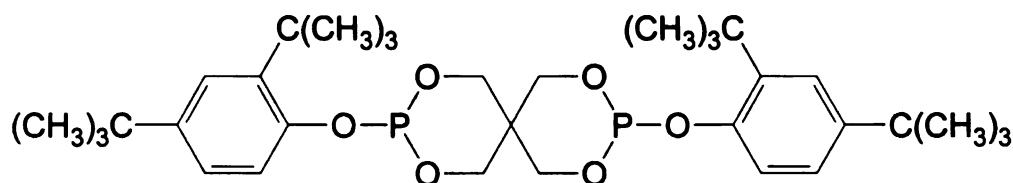


Figure 10.8 Structural Formula for ULTRANOX 626

10.7.1.2 Lupersol 101

2,5-dimethyl-2,5-di-(*tert*-butylperoxy) hexane (Lupersol 101) was also used as the stabilizer. The organic peroxide can undergo redox reactions with the tin(II) catalyst, reducing it to tin(0).

10.7.2 Experimental Protocol

The maleated PBAT-talc composites as obtained from the twin-screw reactive extrusion process were hand-mixed with the stabilizer in the required amounts, and then subjected to the blown film extrusion process. The amounts of Ultrinox 626 studied were 0.05%, 0.1% and 0.2% by weight of the polyester present in the composite. Blown films obtained with 0.05% and 0.1% (by weight of PBAT) of Lupersol 101 as the stabilizer were also studied. The films obtained with no stabilizer were used as the control. Thus, six formulations for each resin were obtained.

To study the thermal stability of the films, they were set in an environmental chamber and subjected to a temperature of 60°C, at a relative humidity of 50%. The mechanical properties of the films were determined (in the machine direction only) weekly, and the drop in properties was monitored.

10.7.3 Mechanical Properties as a Function of time

Table 10.4 displays the mechanical properties of the films obtained using the *in situ* chemically modified PBAT-talc composites prepared through a one-step reactive extrusion process, involving 30% talc (Entry 4, Table 10.6) over a period of 4 weeks. Table 10.5 shows the mechanical properties of the films obtained using the masterbatch (*in situ* chemically modified PBAT-talc composites with 60% talc) and the plain PBAT mixed in the ratio of 50:50 (Entry 9, Table 10.6).

It was observed that the effect of the residual catalyst was more pronounced on the films obtained using the *in situ* chemically modified PBAT-talc composites prepared through a one-step reactive extrusion process, involving 30% talc (Entry 4, Table 10.6). This is

logical because the PBAT (added to the masterbatch) does not undergo undesirable reactions such as β -scissions from MA and transesterification reactions from esterification catalysts that were present during the reactive extrusion process, as well as a thermal extrusion history. Also, based on these preliminary results, the organic peroxide seems to be a better thermal stabilizer, as compared to the phosphite. The drop in the tensile properties was minimum for the film samples involving 0.1% organic peroxide, while the films involving Ultrinox 626 exhibited properties lower than the control on thermal degradation. This is because; some phosphites and phosphonites are sensitive to hydrolysis. Besides the loss of the initial compound, the major drawback of hydrolysis of these antioxidants is the formation of acidic species that may lead to corrosion of machinery on processing and even to polymer discoloration. All aromatic phosphites of high purity that are inherently much more resistant to hydrolysis than alkyl or alkylaryl phosphites could be employed.

Also, a small amount of a base such as Triisopropanolamine is added to improve the storage stability of phosphites prone to hydrolysis.

It is worth noting that though there was a drop in the tensile strength and modulus for all the films tested, the break elongation values for all the films obtained using the masterbatch increased considerably. This type of a behavior was unforeseen, and it would be interesting to determine the responsible factors.

The thermal stability of these films could also be studied at a higher temperature ($\sim 80 - 90^\circ\text{C}$), the drop in tensile properties could be recorded, and probably, an Arrhenius relationship could be obtained, which would relate the mechanical properties of the films to the storage temperature. Once the relationship is developed, it would be possible to use

it to extrapolate the results to storage conditions (room temperature), and determine the shelf life of the film products.

The film samples subjected to the accelerated thermal degradation (60°C, 50% RH), and collected every week for the mechanical properties, would also be characterized for their molecular weights. After solubilization of the composite in chloroform, the polyester fraction (supernatant) would be separated through ultracentrifugation at 4000 rpm for 1 h. The molecular weight of the polyester would be determined by GPC. The drop in molecular weight could also be determined by evaluating the acid number.

Table 10.11 Mechanical properties of the films obtained using the *in situ* chemically modified PBAT-talc composites prepared through a one-step reactive extrusion process, involving 30% talc

No	%	Stabilizer	0 days			7 days (60°C, 50% RH)			15 days (60°C, 50% RH)			21 days (60°C, 50% RH)		
			MoE (psi)	Tensile Strength (psi)	Break Elongation (%)	MoE (psi)	Tensile Strength (psi)	Break Elongation (%)	MoE (psi)	Tensile Strength (psi)	Break Elongation (%)	MoE (psi)	Tensile Strength (psi)	Break Elongation (%)
1	-		86089	4366	208	28268	1816.3	39	37792	2224	18.5	35775	2102	13
2	0.05% U		76713	4280	233.2	57008	2480	28	31692	2127	24	36236	1923	14
3	0.1% U		87510	4360	231.5	72775	2810	24.5	31626	2330	25.1	35827	2266	15.8
4	0.2% U		54926	4864	233.5	63790	2718	24	30849	2090	16	35246	2030	14.5
5	0.05% L		81373	4360	224	55703	2300	22	32683	2230	26	36043	1951	13
6	0.1% L		88426	4620	217	64675	2814	30	32130	2128	17.5	36203	2225	17.6

U – Ultranax 626

L – Lupersol 101.

MoE – Modulus of Elasticity

Table 10.12 Mechanical properties of the films obtained using the masterbatch (*in situ* chemically modified PBAT-talc composites with 60% talc) and the plain PBAT mixed in the ratio of 50:50.

No	%	Stabilizer	0 days			7 days (60°C, 50% RH)			15 days (60°C, 50% RH)			21 days (60°C, 50% RH)			29 days (60°C, 50% RH)		
			MoE (psi)	Tensile Strength (psi)	Break Elongation (%)	MoE (psi)	Tensile Strength (psi)	Break Elongation (%)	MoE (psi)	Tensile Strength (psi)	Break Elongation (%)	MoE (psi)	Tensile Strength (psi)	Break Elongation (%)	MoE (psi)	Tensile Strength (psi)	Break Elongation (%)
1	-		36054	6008.4	408	58781	5374	428	21741	3857	842.6	24201	3341.6	714.7	24227	3724.6	836.4
2	0.05% U		61740	5811	408.4	55815	4672	365	22630	3921.5	775	28144	3170	640	28582	2350	372
3	0.1% U		44877	5551	371	62212	4465	420	33900	3355	630	28809	2750	467.2	33727	2455	400
4	0.2% U		60570	5550	436	41470	4884	381	22550	3336	730	28376	3260	675	27276	3083	610
5	0.05% L		43156	5515	362	47457	4906	431	22202	4205	767	27123	3860	727	26408	3720	707
6	0.1% L		44511	5600	295	53981	5300	336	20989	4700	732	24675	4328	700	22940	4064	790

U – Ultrinox 626

L – Lupersol 101.

MoE – Modulus of Elasticity



10.8 References

- 1) http://www.basf.com/static/science_and_you.html
- 2) Gross, R. A., Kalra, B. Science, 297, 803 – 807, 2002.
- 3) Hu, G., Polymer Engineering and Science, 36, 676-684, 1996.
- 4) Haile, W. A., Dean, L. R., McConnell, R. L., Tincher, M. E., White, A. W., Buchanan, C. M. U.S. Patent 6,495,656, 2002.
- 5) Farge, H. M. J., Farge, J. M. L. U.S. Patent 4,795,801, 1989.
- 6) Smith M., March, J. March's Advanced Organic Chemistry, Wiley-Interscience, 5th Edition, New York, pp. 389 – 1506, 2001.
- 7) Tserki, V. Journal of Applied Polymer Science, 88, 1825 – 1835, 2003.
- 8) Doane, W. M., Swanson, C. L., Fanta, G. F. Emerging Technologies for Materials and Chemicals from Biomass. Rowell, R. M., Schultz, T. P., Narayan, R., Eds; American Chemical Society Symposium Series, American Chemical Society, Washington, DC, 476, 197, 1992.
- 9) Glassner, W. G. Wood Processing and Utilization, Kennedy, J. F., Phillips, G. O., Williams, P. A. Eds, Ellis Horwood Ltd., West Sussex, 163, 1989.
- 10) Sathe, S. N., Rao, G. S. S., Devi, S. Journal of Applied Polymer Science, 53, 239-245, 1994.
- 11) Vermesch, L., Groeninckx, G. Journal of Applied Polymer Science, 53, 1365-1373, 1994.
- 12) Vaidya, U. R., Bhattacharya, M. Journal of Applied Polymer Science, 52, 617-628, 1994.
- 13) Vaidya, U. R., Bhattacharya, M., Zhang, D. Polymer, 36, 1179-1188, 1995.
- 14) Bhattacharya, M., Vaidya, U. R., Zhang, D., Narayan, R. Journal of Applied Polymer Science, 57, 539-554, 1995.
- 15) Ramkumar, D. H. S., Bhattacharya, M., Vaidya, U. R., Hakkainen, M., Albertsson, A. C., Karlsson, S. European Polymer Journal, 32, 999-1010, 1996.
- 16) Ramkumar, D. H. S., Bhattacharya, M., Vaidya, U. R. European Polymer Journal, 33, 729-742, 1997.

- 17) John, J., Tang, J., Yang, Z., Bhattacharya, M. Journal of Polymer Science: Part A: Polymer Chemistry, 35, 1139-1148, 1997.
- 18) Mani, R., Bhattacharya, M. European Polymer Journal, 34, 1467-1475, 1998.
- 19) Mani, R., Bhattacharya, M. European Polymer Journal, 34, 1477-1487, 1998.
- 20) Mani, R., Tang, J., Bhattacharya, M. Macromolecular Rapid Communications, 19, 283-286, 1998.
- 21) Mani, R., Bhattacharya, M. European Polymer Journal, 37, 515-526, 2001.
- 22) Mani, R., Bhattacharya, M., Tang, J. Journal of Polymer Science: Part A: Polymer Chemistry, 37, 1693-1702, 1999.
- 23) Carlson, D. L. Dubois, P. Nie, L. Narayan, R. Polymer Engineering and Science, 38, 311, 1998.
- 24) Carlson, D. L., Nie, L., Narayan, R., Dubois, P. Journal of Applied Polymer Science, 72, 477-485, 1999.
- 25) Nabar, Y., Raquez, J-M., Dubois, P., Narayan, R., Biomacromolecules, In Review.
- 26) Johnson, J. B., Funk, G. L. Analytical Chemistry, 27, 9, 1955.
- 27) American Standard Test Methods, 2002. Practice for Conditioning Plastics for Testing. In: Annual Book of ASTM Standards. D – 618, 08.01, Philadelphia, PA.
- 28) American Standard Test Methods, 2002. Standard Test Method for Tensile Properties of Thin Plastic Sheeting. In: Annual Book of ASTM Standards. D – 882, 08.01, Philadelphia, PA.
- 29) American Standard Test Methods, 2002. Standard Test Method for Melt Flow Rates of Thermoplastics by Extrusion Plastometer. In: Annual Book of ASTM Standards. D – 1238, 08.01, Philadelphia, PA.
- 30) Auger, J., Nguyen, L. 'Using Polymer Characterization Techniques to predict LDPE resin suitability for extruded foam applications.' Second International Conference of Thermoplastic Foam, Society of Plastics Engineers, 139-148, October 24-25, 2000.
- 31) Willett, J. L., Shogren, R. L. Polymer, 43, 5935, 2002.
- 32) Hutchinson, R. J., Siodlak, G. D. E., Smith, A. C. Journal of Materials Science, 22, 3956-3962, 1987.

- 33) Zimmermann, H. Plaste, Kautsch., 28, 433, 1981.
- 34) Gugumus, F. Plastics Additives, 4th Edition, Gachter, R., Muller, H., Eds., Hanser/Gardner Publications, Inc., Cincinnati, 1 – 104, 1993.

SUMMARY AND CONCLUSIONS

Cylindrical starch foam shapes were produced on a small scale (~ 11-12 kg/hr) Werner Pfleiderer ZSK - 30 Twin Screw Extrusion (TSE) process using water, which functions as a plasticizer as well as a blowing agent. The properties of the starch foams depend on the type of starch used (hydroxypropylated high amylose corn starch, 70% amylose), the amount of water and additives (poly (hydroxy aminoether)) (PHAE) used, and extrusion conditions such as temperature and the screw configuration. PHAE offered the adhesion and durability of epoxy resins with the flexibility and processability of thermoplastic resins. PHAE was successful in imparting mechanical strength and toughness, cell integrity, weather and water resistance to the foam structure. The purpose of this work was to study the effects of the extrusion (melt) temperature, amount of water added and the screw configuration on the density of starch foams. The water externally added was varied from 3% to 12%, while the poly (hydroxy aminoether) (PHAE) content was varied from 3% to 15% of the starch used (on a wet basis). The foaming was carried out at melt temperatures in the range from 85°C to 145°C. A match of material properties with process engineering conditions was achieved to facilitate the control of expansion to a structure with valuable commercial properties. The effects of processing conditions on the foaming process were studied using a Werner Pfleiderer ZSK - 30 Twin Screw Extruder (TSE). The optimum temperature, blowing agent content, and PHAE content were determined. The density of the cylindrical foam extrudates obtained was 22-25 kg/m³. The screw configuration, temperature and pressure profiles, additives affected the

morphology, Expansion Ratio, resilience and compressibility of the product. The study of the influence of input variables such as the starch feed rate, screw speed, moisture content, and the PHAE feed rate on the process variables such as pressure, torque and the specific mechanical energy of the system was imperative for the steady state operation of the starch foam process for the optimized formulation developed above.

This starch-PHAE foam extrusion process was modeled as a Multiple Input Multiple Output (MIMO) process, and the dynamics of the process were studied as a response to step changes in the input variables such as starch feed rate, screw speed, moisture content and PHAE feed rate. The responses were modeled as first order responses with a time delay. The linearity of the process was determined over a range around the set-point, and the parameters defining the first order system such as Gain 'K', Time Constant ' τ ', and Dead time ' t_d ' were determined in the linear range. The transfer function models can then be used in a predictive computer control system for on-line fine-tuning of the operating conditions. This could ensure a consistently high quality product even when low frequency disturbances are present in the system. It was observed that the time constants and the dead times recorded for both the pressure and torque responses did not exhibit significant variation within each manipulated or control variable tested. Thus, the system displayed linear dynamic characteristics with respect to each manipulated variable. It was also observed that for the same step-input variations in the manipulated variables, the torque loading on the twin-screw extruder exhibited a faster response (lower dead time), and also reached a steady state sooner (lower time constant). The response in pressure was fastest to step-input variations in the moisture content followed by the screw speed and the starch and PHAE feed rates. The response in torque loading was also fastest to

step-input variations in the moisture content as well as the screw speed followed by the starch and PHAE feed rates. Thus, the moisture content and screw speed were the most destabilizing variables since they induce rapid responses in the process variables. The moisture content in the extruder was, hence, determined to be the most influential factor in the stability of the process followed by screw speed and starch feed rate. PHAE feed rate was the least significant variable.

Multiple step-input tests were carried out in order to determine the validity of the principle of superposition. The validity of the principle of superposition implied the linearity of the process in the domain tested. The hypothesis of linearity is an implicit and necessary prerequisite to most of the classical techniques of process control. A linear model was fit using STATEASE 'Design of Experiments 6.0' modeling software with Pressure (P), Torque and SME as the response data; and the Starch Feed Rate, Screw Speed, Moisture Content, and PHAE Feed Rate as the factors (manipulated variables). Multiple regression analyses showed a significant linear effect of the manipulated variables on the response variables.

Once the dynamics of the starch-based foam process, and the influence of the manipulated variables on the process and product variables were studied, it was necessary to determine the melt viscosity of the starch-PHAE plastic, which showed immense promise for the large-scale manufacture of starch-based foam sheets from the previously developed optimized formulation. This viscosity model was further used in the design of an annular die for the production of starch-PHAE foam sheets to be targeted for cushioning and insulation applications.

A bifurcated die was used for the determination of the viscosity model for the earlier optimized starch- PHAE based foam formulation to be scaled up for the production of starch foam sheets. A Power Law behavior was assumed, and the parameters in the Power Law model such as Consistency Coefficient 'K', and Flow Behavior Index 'n' were obtained as functions of temperature, moisture content, PHAE content and the Specific Mechanical Energy (SME) input to the extruder. The flow behavior index varied between a minimum of 0.11 (MC = 17.52%, T = 110°C, PHAE = 7%, Screw Speed = 250 rpm) to a maximum of 0.52 (MC = 50.15%, T = 110°C, PHAE = 7%, Screw Speed = 200 rpm). The variation in the flow behavior index was considerable with variations in moisture content (0.17 – 0.52 with MC = 17.5% - 50.15% respectively), while temperature, screw speed, and the PHAE content did not affect the value of 'n' significantly. The Consistency Coefficient varied between a minimum of 3208 Pa.sⁿ (MC = 50.15%, T = 110°C, PHAE = 7%, Screw Speed = 200 rpm) to a maximum of 140965 Pa.sⁿ (MC = 17.52%, T = 110°C, PHAE = 0%, Screw Speed = 200 rpm). The variation in the Consistency Coefficient was also substantial with variations in moisture content (107880 Pa.sⁿ – 3208 Pa.sⁿ with MC = 17.5% - 50.15% respectively), while temperature, screw speed, and the PHAE content did not affect the value of 'K' appreciably. An annular die was designed for the manufacture of starch foam sheets using the viscosity model developed for the starch-PHAE formulation (K=107880 Pa.sⁿ & n=0.17 at MC = 17.52%, T = 110°C, PHAE = 7%, Screw Speed = 200 rpm), which provided the best physico-mechanical properties. The density of the cylindrical foam extrudates obtained on the Century ZSK – 30 was 22-23 kg/m³. This annular die was then successfully

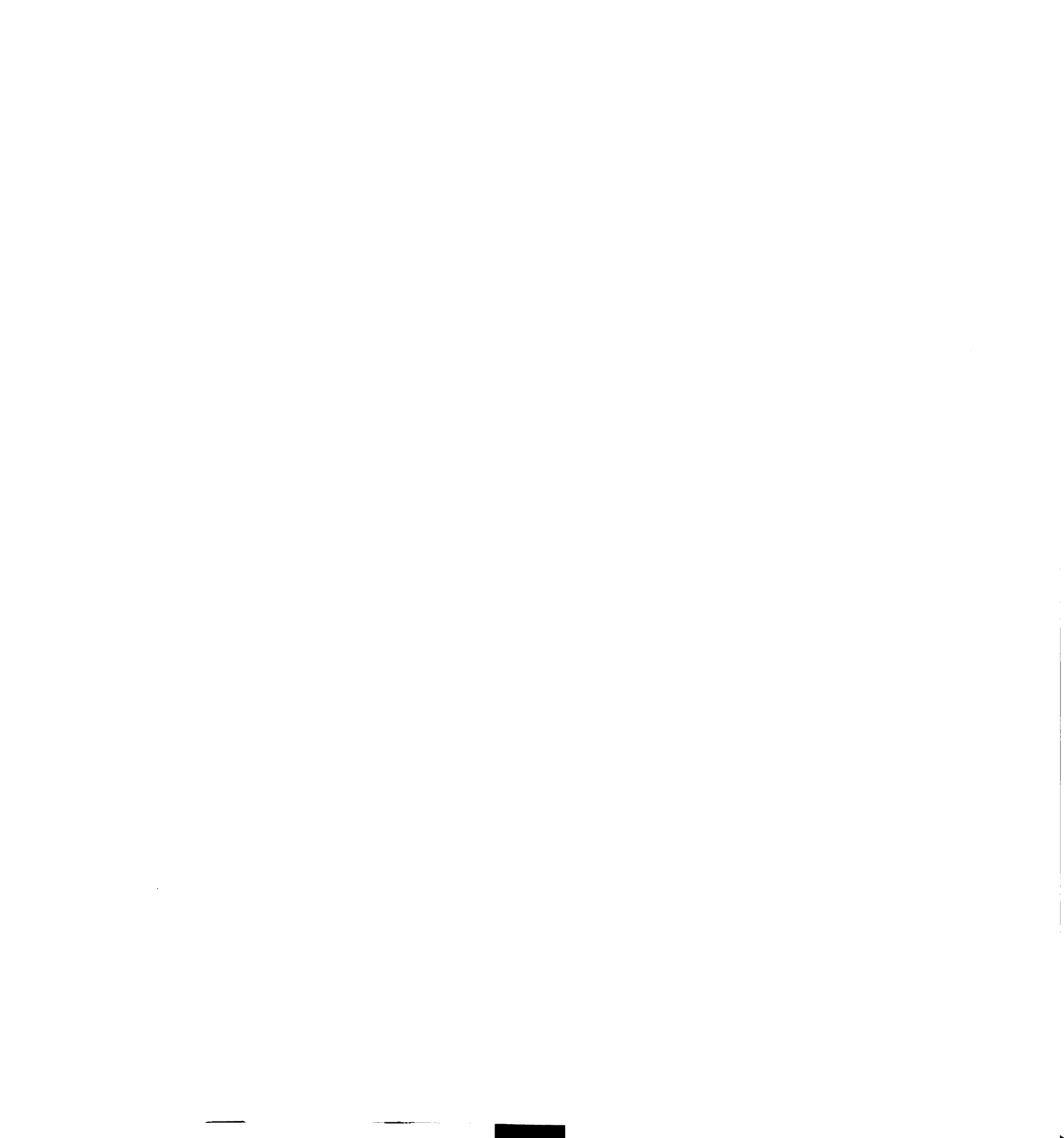
employed on an industrial scale (410-420 kg/hr) twin-screw food extruder, Wenger-80, to manufacture foam sheets. The density of the foam sheets was 27-30 kg/m³.

The results obtained on the Wenger TX – 80 were consistent with the results obtained on the laboratory scale ZSK – 30 twin-screw extruder. The extruded starch foam sheets provided excellent insulation properties. The R-values obtained suggested better insulation characteristics, as compared to expanded polystyrene, and efforts are in progress to enhance their thermal resistivity to make them comparable to polyurethane foams. Also, the dynamic cushioning data reveals that the starch foam sheets provided decent cushioning or shock absorption properties.

Due to the many types of cushions available and the parameters, which determine their behavior, the number of cushion curves required for a thorough account of the subject is immense. It was natural, therefore, to try to reduce the database to descriptive equations either by curve fitting or by solving the dynamics problem using a model of the cushion. Different models involving finite difference and finite element techniques were developed to predict the cushioning properties of the starch-based foam sheets produced as described in Chapter 4.

The solution to the three equations governing the drop/impact test, viz., force balance, energy balance, and the ideal gas law, was obtained using the finite difference method. Assuming that the finite difference method solves the system of differential equations accurately, the model seemed to consistently overestimate the G's for the 1" thick cushion. Also, for a 2" thick cushion, the model seemed to overestimate G's for low static loadings, and underestimate the deceleration for high loads.

The probable sources of error could be:



- i. The actual experimental cushion curves are in error by 10-15% (23) on average.
- ii. The 1-inch and 2-inch thick foams were actually 4 and 8 quarter inch corrugated sheets laminated together. Thus, the presence of voids between the laminated sheets might have added to the error.
- iii. The assumption made was that the foams under consideration were closed-cell foams. Thus, the possibility of mass transfer of air between the cushion and the surroundings was not considered. Starch foams are not completely closed-celled foams.
- iv. Also, at higher static loadings, it was possible that the some cell walls rupture increasing the open cell content, and thus deteriorating the cushioning performance. This leads to an underestimation of G-shock values by the finite difference formulation.
- v. Constant values for air properties were used.
- vi. The heat transfer coefficient, H , is known to be a function of temperature difference (13, 14). However, a constant value of $H = 11.84 \text{ BTU/hr/ft}^2/\text{°F}$ was used. H is also known to be accurate to within $\pm 50\%$.
- vii. The experimental error in reading the cushion curve must also be included in assessing the accuracy of the finite difference method.

The finite element method used was based on the finite difference method and, hence, provided results similar to those obtained using the finite difference method.

A different type of procedure was employed to predict the cushion curves of foam sheets, which utilized one of the conventional (experimentally determined) 'G vs. s' cushion curves for a specific drop height and cushion thickness. There were many advantages in

having a single relationship for cushion performance compared with many conventional cushion curves normally required.

1. Compactness of information.
2. The results may be used for a continuous range of drop heights and cushion thicknesses, whereas, the conventional cushion curves are limited to only those values published.
3. The results also provided information on the maximum cushion strain incurred in the impact, whereas, the conventional curves do not.
4. The cushion design was greatly simplified, since the database required as input information on the cushion performance had been drastically reduced, while its applicability to various drop conditions had been greatly increased.

It was no longer necessary to perform nearly as many drop tests on a new material to evaluate its dynamic performance since; a single G vs. s cushion curve was all that was required to generate all other cushion curves.

The study of starch-based foams using PHAE as the functional aid for imparting mechanical strength and toughness, cell integrity, weather and water resistance to the foam structure was concluded at this stage. As a summary, the study involved the development and optimization of the starch-based foams using PHAE on the laboratory-scale ZSK-30 twin-screw extruder (Chapter 2) followed by the investigation of the dynamics of the starch foam process (Chapter 3). A power-law shear viscosity model was developed for the starch plastic as a function of the moisture content, PHAE content, process temperature, and the specific mechanical energy input. This viscosity model was further used in the design of an annular die to be used on a manufacturing-scale Wenger

TX-80 twin-screw extruder to produce starch-PHAE foam sheets. These foam sheets were evaluated for their cushioning and insulation properties (Chapter 4), and a numerical simulation was developed in the sections above for the prediction of these cushioning properties of the starch foam sheets (Chapter 5). These starch-based foam sheets using PHAE that were developed and evaluated, have been commercialized by a local Michigan-based company, KTM Industries, and is currently used as protective packaging by Toyota for automotive parts such as windshields and bumpers, and by Sony for entertainment systems.

Chapter 6 dealt with the selection of a new biodegradable polymer, as an alternative to the currently used PHAE to develop new starch-based foam formulations. The objective was to develop new starch-based foam formulations possessing properties that were equivalent (if not better) to those obtained using the starch-PHAE formulation.

Hydroxypropylated high amylose cornstarch was extruded into foams using various functional aids such as PCL, PBAT, PVA, CA, Glyoxal and methylated pectin. The different formulations were successfully optimized to give foams with lowest densities. Some formulations with PVA and PBAT gave foams with densities lower than 25 kg/m^3 . The starch foams were subjected to a relative humidity of $95 \pm 5 \%$, and a temperature of $38 \pm 5 \text{ }^\circ\text{C}$ to determine the change in weight and dimensions on moisture sorption. The functional aids such as PVA, CA, MP and their combinations with glyoxal did not significantly affect the weight gain on moisture sorption. However, the weight gain could be reduced from about 13% for control starch to a minimum of about 9% for formulations involving PCL and PBAT. Also, the shrinkage in radial and longitudinal dimensions could be reduced from about 50% for control starch to about 12-20% for

certain formulations involving biodegradable polyesters, and to about 25-40% in formulations involving PVA, glyoxal, CA and pectin and combinations thereof. There is a possibility that most of the polyester migrates to the surface of the foams restricting the shrinkage of the starch foams, while the core continues to absorb as much moisture. Thus, the hydrophobic character of the starch-based foams in terms of its weight gain and dimensional stability on moisture sorption was improved considerably.

The aliphatic-aromatic co-polyester PBAT was the best candidate for melt-blending with starch to produce foams, by providing better physico-mechanical properties such as lower densities, better spring indices; and better hydrophobic properties such as improved dimensional stability on moisture sorption. Chapters 7, 8 and 9 focused on improving the compatibility between the starch and polyesters to improve the physico-mechanical as well as the hydrophobic properties of the starch-based foams. This would be done using reactive extrusion as a tool to chemically modify the starch or the polyester. The chemically modified entities would act as compatibilizers between the starch and the polyester.

The objective of the study from Chapter 7 was to manufacture starch foams in the presence of PBAT with better physico-mechanical and hydrophobic properties, wherein MA-g-PBAT was used as a compatibilizer between pristine PBAT and starch. Free-radical-initiated grafting of maleic anhydride (MA) onto poly (butylene adipate-co-terephthalate) (PBAT) backbone was achieved by reactive extrusion. The amount of MA grafted on the PBAT backbone was as high as 0.691% by weight. This grafted MA was sufficient to successfully compatibilize the polyester and starch. The maleation of the polyester proved to be very efficient in promoting strong interfacial adhesion with high

amylose cornstarch in starch foams by melt blending. The maleated polyesters had lower molecular weights as compared to the original polyester, resulting in their lower melt strengths. Hence, MA-*g*-PBAT by itself did not prove effective as a functional aid in the production of starch foams. However, when MA-*g*-PBAT was used as a compatibilizer between starch and PBAT, it reduced the density of starch foams (using PBAT) to $\sim 21 \text{ kg/m}^3$, and improved the resilience from 84% to as high as 95%. Also, the starch foams in the presence of PBAT, wherein MA-*g*-PBAT was used as the compatibilizer, exhibited improved hydrophobic properties in terms of lower weight gains on moisture sorption.

The maleation of vegetable oils has been studied in detail in some of our previous work (46). Free-radical-initiated grafting of maleated corn oil (MCO) onto PBAT to give MCO-*g*-PBAT was performed with a motive to reduce the chain scission in PBAT due to acid hydrolysis (due to MA) and, hence, prevent the reduction in melt strength due to degradation of the backbone. The maleation of the polyester using Maleated Corn Oil (MCO) to give MCO-*g*-PBAT was carried out in an attempt to improve the compatibility between PBAT and starch, without reducing the melt strength of the polyester.

In Chapter 8, the free-radical-initiated grafting of maleated corn oil (MCO) onto PBAT was performed with a motive to reduce the chain scission in PBAT due to acid hydrolysis and, hence, prevent the reduction in melt strength due to degradation of the backbone. The amount of MCO grafted on the PBAT backbone was as high as 0.42% by weight. The MCO-*g*-PBAT samples were compatible with starch and helped improve the resiliency of the starch foams. The spring indices obtained were in the range of 87 – 94% using MCO-*g*-PBAT with different grafting percentages. The resilience provided by MCO-*g*-PBAT using 5% MCO and 0.25% L101 was maximum (94%), probably due to

its grafting level and good mechanical strength. The graft polymers have sufficient melt strength to support expansion, since the amount of degradation is lower as compared to MPBAT. This is due to the presence of a lower number of anhydride groups, which result in the degradation of the PBAT backbone.

Chapters 7 and 8 dealt with the modification of PBAT by the introduction of reactive groups (anhydride) for enhanced compatibility with starch. Chapter 9 involved the modification of starch in order to improve the compatibility between the starch and PBAT. In this study, two novel methods were employed to achieve this compatibilization between starch and PBAT. The first method was to reactively graft a hydrophilic polymer such as starch onto the PBAT backbone using trans-esterification chemistry. The second method was to maleate starch to form maleated thermoplastic starch and then use the new maleated starch to form graft copolymers with PBAT.

PBAT-*g*-TPS copolymers were produced by reactive extrusion processing using maleic anhydride or maleic acid as a trans-esterification catalyst. The graft copolymer was completely extractable in Dichloromethane using a Soxhlet extraction technique. On solvent casting the extracted polymer solution, a transparent film was obtained. In the absence of maleic acid, only the polyester was extracted out. These results confirmed that PBAT and TPS were covalently linked, as opposed to a simple physical blend. FTIR results of PBAT-*g*-TPS copolymer, showing the carbonyl stretch at 1720 cm^{-1} , ester C-O stretch at 1270 cm^{-1} and the -OH polymer stretch at $3200\text{-}3400\text{ cm}^{-1}$ confirm the true existence of a graft copolymer. Tensile strength and modulus of elasticity of the graft copolymer were lower as compared to LDPE.

Regular granular cornstarch was maleated in a twin-screw co-rotating extruder using maleic anhydride or maleic acid modifiers in the presence of glycerol as the plasticizer and optional free-radical initiator such as Luperox 101. Due to the low viscosity of MTPS, reactive maleation can be done at much higher throughputs as compared to the regular thermoplastic starch (TPS) production. The reactive maleation process prevents problems during TPS production such as clogging of the thermoplastic starch melt and foaming at the die. Carbonyl stretch peak at 1720 cm^{-1} , observed for the extracted MTPS sample (made using both maleic anhydride and maleic acid modifier), confirms reactivity. Differential Scanning Calorimetry (DSC) results of MTPS samples exhibit melting endotherms, not present in regular granular starch.

PBAT-g-MTPS copolymers were produced by the reactive extrusion processing of PBAT and MTPS. PBAT/MTPS (70/30 and 60/40; w/w) graft copolymers was completely extractable in Dichloromethane using a Soxhlet extraction technique. On solvent casting the extracted polymer solution, a transparent film was obtained. This reaction leading to the formation of a graft copolymer is dependent on the relative amounts of PBAT and MTPS present (Does not hold true for more than 50% MTPS). FTIR results of PBAT/MTPS (70/30; w/w) graft copolymers (solvent cast films after extraction in Dichloromethane) made using both maleic anhydride and maleic acid, show the carbonyl stretch at 1720 cm^{-1} , ester C-O stretch at 1270 cm^{-1} and the -OH polymer stretch at $3200\text{-}3400\text{ cm}^{-1}$ confirming the true existence of a graft copolymer.

The above results indicate that on using the PBAT-g-MTPS as a compatibilizer between starch and PBAT yield starch based foams with much lower densities and improved mechanical properties such as resilience or spring index.

The extrusion of hydroxypropylated high amylose starch foams using PBAT in the absence/presence of compatibilizers has been studied in the previous Chapters 7 – 9. However, instead of using PBAT as the functional aid, a blend of PBAT-talc was used as a functional aid in the processing of starch foams to obtain a better dispersion of the nucleating agent (talc) in the melt. Also, an increase in the viscosity of the functional aid (due to the presence of talc) aids in improved blending (viscosity difference between plastic starch and PBAT-talc is lower than that between plastic starch and PBAT). Lower the viscosity difference better are the blend properties. A finer morphology would be obtained which can be explained by viscosity matching effect. Typically, the size of the dispersed phase (PBAT-talc blend, in this case) in a blend is lowest when the viscosity ratio approaches unity. An added advantage is the reduction in cost of the functional aid. It was observed that the unit density of the starch foams obtained using PBAT-talc as the functional aid was approximately 22 kg/m^3 as compared to 24.2 kg/m^3 , which was the density of the starch foams obtained using PBAT as the functional aid. Also, the resiliency of the starch foams increased up to 92.3% for the starch-based foams using PBAT-talc, as compared to 84% realized using PBAT as the functional aid.

A polymer with increased tensile strength would provide a foam with lower compression set and higher compression strength, resulting in improved resiliency, and further lower densities. The tensile strength and elongation of the PBAT-talc blends were improved by increasing the compatibilization between talc and PBAT, by carrying out grafting chemistries between the Si-OH functions on the talc surface and the polyester, Improvement of the interfacial adhesion between talc and PBAT was successfully achieved by free-radical grafting of MA onto the polyester backbone, and promoting

using esterification catalyst, as carried out through reactive extrusion. It is of prime importance to develop biodegradable PBAT-talc composites having satisfactory physico-mechanical properties to be competitive with commodity polymers such as HDPE. In a first step, the polyester backbone was reactively modified through free-radical grafting of maleic anhydride, in order for the improvement of the interfacial adhesion between PBAT and talc to react together with the hydroxyl functions from the lateral surface of talc. The resulting maleated-PBAT was then reactively melt-blended with talc using $\text{Sn}(\text{Oct})_2$ and 4-DMAP as esterification catalysts. The interfacial adhesion between MA-g-PBAT and talc was so-improved as evidenced by scanning electronic microscopy and selective extractions of the polyester part from the composite. It resulted that the tensile properties for the blown films prepared from these resulting composites was considerably improved, as compared to ones of the simple melt-blend of PBAT-talc.

Extrapolation to a one-step reactive extrusion process was successfully carried out. The *in situ* chemical modification of PBAT-talc composites allowed preparing compositions reaching up to 60 wt% talc. Interestingly, the best composition regarding the improvement of tensile properties was achieved by melt-blending *in situ* chemically modified PBAT-talc composite containing 60 wt%-talc with plain PBAT (in the ratio of 50:50). Such approach allowed to retain the superior mechanical strength of PBAT (added to the masterbatch) by preventing it from undergoing undesirable reactions such as β -scissions from MA and transesterification reactions from esterification catalysts that were present during the reactive extrusion process, as well as a thermal extrusion history. Thermal properties of chemically modified PBAT-talc composites showed that talc behaved as a nucleating agent for the polyester chains.

To explain the improvement of the interfacial adhesion between talc and PBAT, a more thorough X-Ray Photoelectron Spectra (XPS) study will be carried out in order to attest for the formation of chemical bonds between both partners. A morphological study will be also carried out in order to determine the influence of compatibilization process on the size, the distribution of micro-particles as well as the dispersion homogeneity within the polyester matrix. The diffusion of different gases and vapor barrier properties will be also studied. We envision to expand the compatibilization process to other biodegradable polymers such as poly(ϵ -caprolactone) and other talc in function of their size and intrinsic nature (crystallinity, surface chemistry).

Hydroxypropylated high amylose corn starch-based foams were produced using the *in situ* chemically modified PBAT-talc composites (prepared through a one-step reactive extrusion process as explained in Section 10.4.3) as functional aids. The maleated-PBAT-talc composite produced by melt-blending the master-batch (containing 60 wt% talc) with plain PBAT (in the ratio of 50:50) provided enhanced starch foams having a density as low as 17.5 kg/m³, and resilience as high as 97% (competitive with the commercial polyethylene and polystyrene foams), in accordance with its extremely superior mechanical properties.

RECOMMENDED PROJECTS

12.1 PBAT – Trimethoxy(vinyl)silane/Dimethoxy(vinylmethyl)silane – Talc blends

12.1.1 Introduction

New PBAT-talc composites were produced through reactive extrusion, following the same principle employed in Chapter 10. The PBAT backbone was reactively modified through free-radical grafting of Trimethoxy (vinyl) silane. Further, the objective of this study was to chemically react the methoxy (alkoxy) groups of the silane or the hydroxyl groups (resulting due to hydrolysis of the silane in the presence of moisture) with the hydroxyl functionality in the filler or with other such groups on adjacent polymer chains (with or without a condensation catalyst) to provide better filler-matrix adhesion and/or a tough, cross-linked matrix with improved mechanical properties and water repellency without sacrificing the flexibility and elongation.

Silane-Polyester graft copolymers can be melt cast or blown into transparent films with applications in the areas of lawn and leaf compost bags, agricultural mulch films, trash bags, regular carry out retail bags, food packaging etc.

US Patent 3,646,155 issued to Scott (1) relates to the cross-linking of polyethylene materials using an organofunctional silane as a cross-linking agent, which is grafted on to the polymer using a peroxide catalyst. The process as described in the patent also leads to a reduction in melt flow of the polymer leading to difficulties in processability in normal

equipment and significant reduction in elongation than the base material. Other US patents similar to the above work are US 4,117,195 (2), US 4,413,066 (3), US 4,514,539 (4), US 5,773,145 (5).

US Patent 5,880,195 issued to Kalinowski et al. (6) relates to the preparation of addition curable high tensile strength compositions starting with hydrosilanes and alkenyl functional polymer backbones. The process, though efficient, involved the use of very reactive hydrosilanes and use of polymers with unsaturations in their backbones, which are not very common. Also the hydrosilylation catalyst was very expensive, which required that extenders be added to the composition to reduce the cost, which in turn could lead to lesser property enhancements.

Use of trifunctional silanes in enhancing mechanical properties of thermosets has been discussed in the Japanese Patent Application 2003221446 (7); the main intention however was to produce highly cross-linked networks. The invention did not relate to manufacture of films, and also the mechanism of modification was the condensation reaction of end groups, and not a peroxide aided route as disclosed in the present work. Laminates using silane-grafted polypropylene and liquid crystal polyesters were discussed in the Japanese patent application 2001239539 (8). Production of fibers from waste polyesters and glass fibers is discussed in the Japanese patent application 2001040528 (9) – but the silane used as a coupling agent worked via a condensation mechanism and not by the peroxide route.

Thermoplastic polyurethanes have been modified using silane grafting agents (10). Their technique, however, was to use a condensation type reaction between an isocyanate grafting agent and an amino functional silane rather than a free radical peroxide induced

grafting which was the aim of the present work. Similar work is reported in literature (11) where the authors have grafted a vinylsilane on to a silicone rubber using an organic peroxide catalyst to improve compatibility with polyurethane.

DE 10111992 (12) discusses the use of silane grafting on polyolefins to make compatibilized blends with polyesters in the presence of a silane coupling agent- but in the invention, the focus was on grafting the polyolefin and not the polyester with the organosilane. Further the work did not mention about films, and is on manufacture of threads.

This present study deals with the improvement of the physico-mechanical properties of these silane-grafted filled polyester films by improving the compatibility between the filler and the polyester and chemical cross-linking between the silane groups. This graft co-polymer helps achieve the afore-mentioned objective by providing blends in a one-step extrusion process to give films with enhanced tensile strengths up to 6000 psi. Preliminary results based on the mechanical properties of the blown films have been discussed in this chapter, and future recommendations have been provided.

12.1.2 Experimental Section

12.1.2.1 Materials

Poly(butylene adipate-*co*-terephthalate) (PBAT) , 2,5-dimethyl-2,5-di-(*tert*-butylperoxy) hexane (Lupersol 101) were acquired as mentioned previously, and used as received. Talc having a particle size of ca. 6 μm under the trade name Luzenac 20M00S was provided by Luzenac Europe, and dried at 120°C overnight before use. Trimethoxy (vinyl) silane

(VTMOS) and Dimethoxy (methyl vinyl) silane (VMDMOS) were purchased from Gelest, Inc.

12.1.2.2 One-Step (*In Situ*) Reactive Extrusion Process

700g of PBAT was hand-mixed with 0.05/0.1/0.2 wt% (of PBAT) free radical initiator, 0.5/1/2 wt% (of PBAT) VTMOS/VMDMOS, and 300g of talc, in that order, and fed together to a Century ZSK-30 co-rotating twin screw extruder at a feed rate of approximately 150 g/min. The screw diameter was of 30 mm, and the length-to-diameter ratio of 42:1. Barrel and die temperatures were maintained by means of ten electrical/cooling devices as described heretofore. The screw speed was 150 rpm resulting in a mean time residence of about 4-5 minutes. The strand was extruded through a mono-hole die having a nozzle opening of 2.7 mm in diameter, cooled down into a water-bath, and pelletized downstream.

12.1.2.3 Blown films

The reactively modified PBAT-talc composites were extruded into films a Killion single-screw blown film unit. The description of the blown film unit and the extrusion conditions are described in Chapter 10, Section 10.3.2.4.

12.1.3 Results and Discussion

12.1.3.1 Mechanical properties of PBAT-silane-talc composites

Tables 12.1 and 12.2 report the tensile properties in the machine and transverse directions respectively, of blown films derived from the *in situ* silane-modified PBAT-talc composites, and the simple PBAT-talc melt-blend.

Using VT MOS (Entries 2 – 6, Table 12.1), it was observed that tensile strengths higher than 5000 psi in the machine direction could be achieved in some formulations (Entries 2 & 5, Table 12.1) with break elongations of 300 – 350%. Tensile strengths greater than 4000 psi and break elongations in the range of 150 – 300% were obtained from the remaining formulations (Entries 3, 4, & 6, Table 12.1). Thus, higher mechanical properties were obtained using lower contents of the free-radical initiator as well as of VT MOS. This was probably due to the fact that the low levels of branching would have occurred within the polyester chains due to the peroxide present. Also, the free-radically grafted silane would have induced low levels of branching. The branching in the polyester matrix due to the silane could be due to the curing of the methoxy groups with other methoxy groups from the grafted silane, as well as the curing of the grafted methoxy groups with the lateral hydroxyl groups possessed by the talc filler. This branching would effectively improve the tensile strength of the resulting composite, but result in a decrease in break elongations due to the formation of a network between the polyester and the filler (which would restrict the elongation of the polymer chains). Higher levels of peroxide or VT MOS would lead to increased branching (or possibly cross-linking) restricting the break elongations to very low values of 150 – 300%.

VMD MOS was used with an intention to reduce the branching due to the silane within the polyester chains, and to form a more flexible network with improved tensile strengths as well as elongations. VMD MOS is, however, more expensive as compared to VT MOS, and, thus, not economically feasible. The tensile strengths of the composites obtained using VMD MOS were approximately 4300 psi, with break elongations in the range of 430 – 480% (Entries 7 – 8, Table 12.1).

The tensile properties of the films in the transverse direction displayed a similar trend to those in the machine direction (Table 12.2).

Table 12.1 Tensile Properties (Machine Direction) of blown films derived from the PBAT-silane-talc blends

Entry	% Free Radical Initiator	Type and (% Amount of Silane)	Young's modulus (psi)	Yield Stress (psi)	Tensile Stress (psi)	Break Elongation (%)
1	-	-	17004	1838.7	2058.9	600
2	0.1	VTMOS (0.5)	56850	5795	5809.31	300.38
3	0.1	VTMOS (1.0)	54862	4627.2	4698.6	230.5
4	0.1	VTMOS (2.0)	50840	4009.21	4339.33	156.73
5	0.05	VTMOS (1.0)	47033	5106.6	5116.9	340.52
6	0.2	VTMOS (1.0)	49257	4317.75	4334.5	270.22
7	0.1	VMDMOS (1.0)	48006	4246.2	4288.5	469.2
8	0.1	VMDMOS (2.0)	49710	4259.54	4306.8	423.8

Table 12.2 Tensile Properties (Transverse Direction) of blown films derived from the PBAT-silane-talc blends

Entry	% Free Radical Initiator	Type and (% Amount of Silane)	Young's modulus (psi)	Yield Stress (psi)	Tensile Stress (psi)	Break Elongation (%)
1	-	-	17225	1389.8	1528.2	300
2	0.1	VTMOS (0.5)	50743	3321	3343.51	269.9
3	0.1	VTMOS (1.0)	57262	3690	3819.14	196.85
4	0.1	VTMOS (2.0)	51593	3242	3329	161.15
5	0.05	VTMOS (1.0)	47641	2991.58	3005.95	173.27
6	0.2	VTMOS (1.0)	52217	3650	3971.02	283.06
7	0.1	VMDMOS (1.0)	51553	3482	3509	426.3
8	0.1	VMDMOS (2.0)	53618	3732	3799	391.5

12.1.4 Recommendations for the PBAT-silane-talc composites

The results provided here are preliminary, and future work needs to be focused on the control of the grafting chemistry between the PBAT and the silanes.

It is also necessary to characterize the reactive blends in the absence of the filler to determine the gel content in the branched/cross-linked polyester matrix.

Lupersol 101 used herein is a symmetric free-radical initiator, whose fragments are equally capable of creating radicals, thus leading to the formation of radicals in the vicinity of each other; leading to the formation of short cross-links and thus poor

properties. An asymmetric organic peroxide like tert-butyl peroxalate could be tried instead, which would improve the grafting of the silane onto the polyester backbone, and minimize the cross-linking of the polyester chains due to the radicals generated by the peroxide.

The study of the rheology of the resulting composites is also crucial, since the formation of gels (in cases when cross-linking dominates over the grafting reaction) within the polyester matrix affects its flow in the within the extrusion system, as well as affects the mechanical properties of the polyester films. Depending on the size of the gels formed, they can lead to the rupture of the films under strain/tension (large gel size), or they can function as reinforcing deformable fillers within the polyester matrix leading to enhanced mechanical properties (similar to reinforcing ethylene-propylene rubbers in the propylene matrix).

Also, polycondensation catalysts such as dibutyl tin dilaurate (DBTDL) could be used for the curing of silanes, and its introduction through a “Masterbatch” is also worthwhile. This concept of the masterbatch could solve the problems with lower break elongations, while retaining the superior tensile strengths of the composites.

Similar to the principle followed earlier in Chapter 10, these composites with improved tensile strengths and enhanced elongations could be used as functional aids in the processing of starch foams.

12.2 Thermoplastic Starch (TPS) – based Nano-Composites

The interactions between starch and the alkali metal salts (NaCl, KCl, LiCl) were studied. Donovan and Mapes (13) showed that the interactions between salts and the molecular chains of starch are favorable when mixing, resulting in the release of water molecules that bind originally with salt ions, subsequently improving the gelatinization of starch. Oosten (14 – 16) hypothesized that the cations penetrate into the granular interior and form metal alcoholate with starch, followed by the release of H^+ into the water phase, the exothermic reaction of the released H^+ and OH^- to water and the gelatinization of starch catalyzed by the anions. In Oosten's hypothesis the anions, being the active gelatinizing agents, are proposed to be water-structure breakers and capable of rupturing the hydrogen bonds between starch molecules. However, this is not true for the BaF_2 system because both Ba^{2+} and F^- ions are water-structure makers ($\Delta n_{HB} = 0.01$ and 0.08 , respectively) (17). Being water-structure breakers is therefore not essential for the anions or solvated salt molecules enhancing the gelatinization. Other reactions, such as the electrostatic repulsion of the cations absorbed on starch, or other exothermic complexation reactions, may be responsible for their active gelatinizing effects. Secondly, the shear-thinning properties found for the starch blends with saturated $MgCl_2$, $CaCl_2$, $BaCl_2$, $CaBr_2$, CaI_2 , $Ca(NO_3)_2$, $Sr(NO_3)_2$ and $Ba(NO_3)_2$ solutions resembled those for the starch – sugar – water systems with plasticization effects (18, 19). Frequently, the plasticization effects are caused by a moderate quantity of free water and/or sugar co-solute molecules.

Ahmad et al. (20) also observed that the cations interact with the starch hydroxyl groups to disrupt the polymer chain aggregation, causing the peak gelatinization temperature and the modulus to decrease.

The hypothesis was to use an alkali metal salt such as NaCl, KCl or LiCl, wherein the cation would interact with the starch hydroxyls to form a complex, and further reduce the gelatinization temperatures rendering the starch more thermoplastic. Further nano-scale reinforcing clay possessing exchangeable cations could be introduced into this complexed thermoplastic starch, and an exchange between the cations on the complexed starch and those within the clay galleries could be expected. This might result in a novel nano-composite, with improved mechanical and barrier properties. To achieve this enhancement in properties, it is imperative that the clay galleries are exfoliated. Our preliminary results on thermoplastic starch using LiCl as the alkali metal halide indicate that exfoliation was attained. WAXS was used as the characterization tool. Figure 12.1 shows the X-ray patterns for the nano-clay (Cloisite Na⁺) as well as the exfoliated composite. The hydrophilic clay was used due to its higher compatibility with starch.

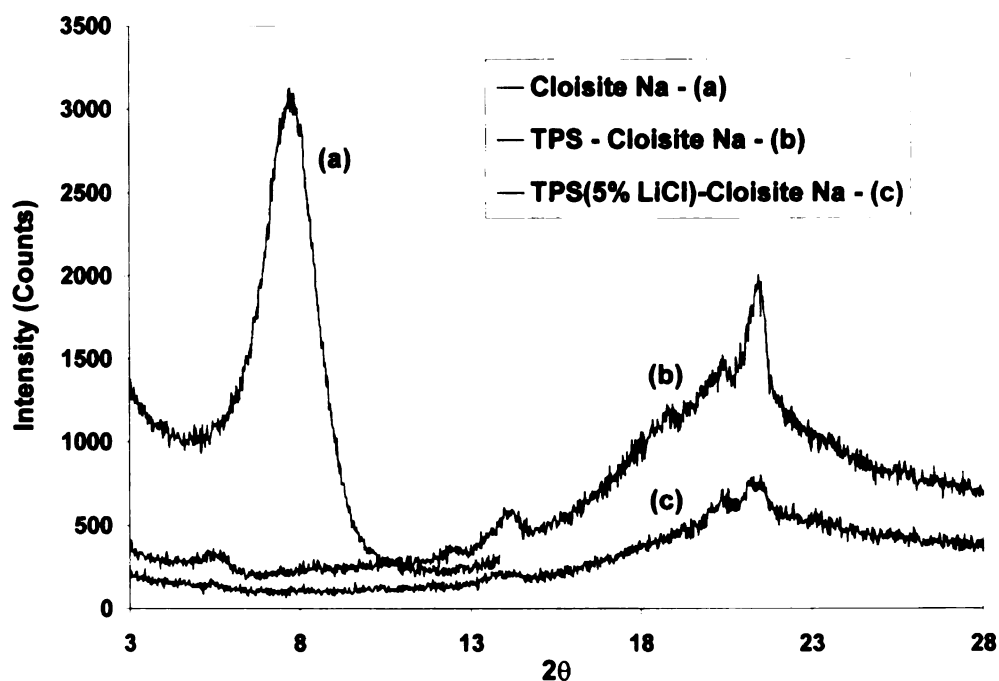


Figure 12.1 X-Ray Patterns for alkali salt modified TPS-clay nano-composite

Future work needs to be done to verify the complexation mechanism involved in the modification of TPS, as well as to establish the reason for the exfoliation of the clay galleries using this alkali salt modified thermoplastic starch. Transmission electron microscopy would be used as a tool to confirm the findings from the WAXS experiments. DSC studies could be carried out to determine the effect of the halide on the glass transition temperature of the TPS. Also, Dynamic Mechanical Analysis (DMA) could be used to study the change in the storage (G') and loss (G'') moduli of the nano-composites.

12.3 References

- 1) Scott, H. G. US Patent 3,646,155, 1972.
- 2) Swarbrick, P., Green, W. J., Maillefer, C. US Patent 4,117,195, 1978.
- 3) Isaka, T., Ishioka, M., Shimada, T., Inoue, T. US Patent 4,413,066, 1983.
- 4) Hatrich, G. A., Byron, S. J. US Patent 4,514,539, 1985.
- 5) Inoue, Y., Kuno, M., Fukui, T., Ohsawa, S. US Patent 5,773,145, 1998.
- 6) Kalinowski, R. E., Tomalia, M. K., Wolf, A. T. F. US Patent 5,880,195, 1997.
- 7) Japanese Patent Application 2003221446, 2003.
- 8) Japanese Patent Application 2001239539, 2001.
- 9) Japanese Patent Application 2001040528, 2001.
- 10) Dassin, S., Dumon, M., Mechin, F., Pascault, J-P. Polymer Engineering and Science, 42 (8), 1724-1739, 2002.
- 11) Maity, M., Khatua, B. B., Das, C. K. Journal of Elastomers and Plastics, 33(3), 211-224, 2001.
- 12) DE 10111992.
- 13) Donovan, J. W., Mapes, C. J. Starch/Starke, 32, 190 – 193, 1980.
- 14) Oosten, B. J. Starch/Starke, 34, 233 – 239, 1982.
- 15) Oosten, B. J. Starch/Starke, 35, 166 – 169, 1983.
- 16) Oosten, B. J. Starch/Starke, 42, 327 – 330, 1990.
- 17) Marcus, Y. Ion Properties, pp 1 – 30, 177 – 185, 199 – 208, 1997.
- 18) Chinachoti, P. Food Technology (Chicago), 134 – 140, 1993.
- 19) Lii, C. Y., Lai, V. M. F., Liu, K. F. Starch/Starke, 49, 346 – 354, 1997.
- 20) Ahmad, F. B., Williams, P. A. Journal of Agriculture and Food Chemistry, 47, 3359 – 3366, 1999.

MICHIGAN STATE UNIVERSITY LIBRARIES



3 1293 02956 2877